

Università degli Studi di Palermo

Dipartimento di Progetto e Costruzione Edilizia (DPCE)

Dottorato di Ricerca in Ingegneria Edile: Tradizione e Innovazione

Coordinatore: prof. Giuseppe Pellitteri

Ciclo XXII

Settore scientifico-disciplinare: ICAR 10 Architettura Tecnica

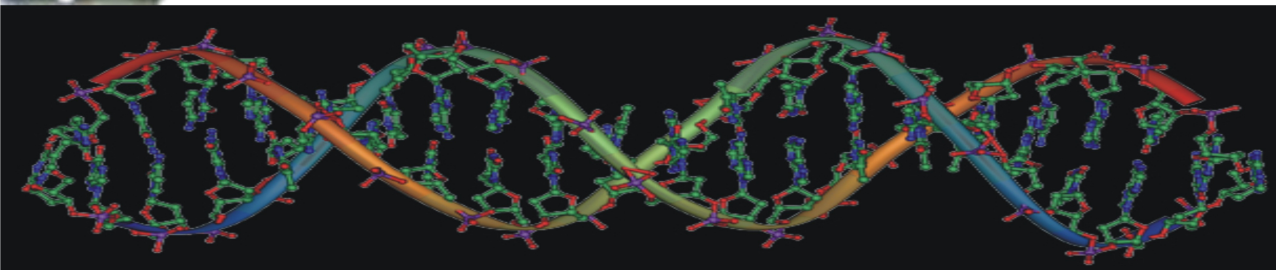


Nanotechnology in Construction



**Eng. Arch.
Manfredi Saeli**

Tutor: prof. Giovanni Fatta



Università degli Studi di Palermo

Dipartimento di Progetto e Costruzione Edilizia (DPCE)

Dottorato di ricerca in “Ingegneria Edile: Tradizione e Innovazione” – Ciclo XXII

Coordinatore: prof. Giuseppe Pellitteri

Nanotechnology in Construction

with two cases of study:

1. Thermochromic coatings for architectural glazing and
2. CNT-doped polyurea nanocomposite for large structure protection

PhD candidate: Eng. Arch. Manfredi Saeli

UniPA supervisor/Advisor: prof. Giovanni Fatta

UCL supervisor: prof. Ivan P. Parkin

Columbia supervisor: prof. Haim Waisman



**UNIVERSITÀ
DEGLI STUDI
DI PALERMO**

To hold an attitude is to take a stance
in a matter of controversy

(M. Billig, 1996)

ACKNOWLEDGEMENT

First of all, I would like to thank my PhD advisor at the University of Palermo, professor Giovanni Fatta, to have let me travel through this new field of scientific research, supporting and encouraging me every day.

Secondly, to my group of research and especially to ing. Tiziana Campisi.

A special thank to my supervisors at Christopher Ingold Laboratories, Chemistry Department, University College London (UCL), professor Ivan P. Parkin, and at Department of Civil Engineering and Engineering Mechanics, Columbia University, proff. Haim Waisman and Raimondo Betti for the great opportunity they have given to me, for their support, encouragement and appreciation.

I also wish to thank all the people I worked with during these three years of research:

- Dr. Clara Piccirillo and Dr. Russell Binions from Chemistry Department - UCL for having taught me the CVD and analysis techniques, for their help and advices from scientific and human point of view;
- Dr. Ian Ridley from the Barlett School of Graduate Studies - UCL who helped me in virtual modelling and for his availability;
- Dr. Geoffrey Hyett, Dr. Charlie Dunnill and Mr. Paolo Melgari from Chemistry Department - UCL for their advices;
- Mr. Adrian Brügger and Mr. Liming Li from the Carleton Laboratory - Columbia University for their assistance with tension tests;
- Mr. Kevin Reeves from UCL and Dr. Austin Joseph Akey from Columbia University for their invaluable assistance with electron microscopy.

I would like to acknowledge Università degli Studi di Palermo - Dipartimento di Progetto e Costruzione Edilizia (DPCE), Pilkington Glass, US Department of Homeland Security and H2CU - Honors Center of Italian Universities for financial support.

I would also like to acknowledge

- My PhD colleagues, with a special regard to Giuseppe Costa, for their help, support and for the moment spent together;
- All the professors of my PhD committee and especially those who gave me useful and practical advices;
- Arch. Federica Fernandez who encouraged me at the beginning of my adventure in nano;
- Prof. Patrizia Livreri from University of Palermo, director of the M.Sci “Nanotechnology for Cultural Heritage”;

- Prof. Nunzio Scibilia, Prof. Stefano Riva and Ing. Alessandro Busacca from University of Palermo for their support;
- Prof. Nicola Chiara from Columbia University for his useful advices and help as well as for the moment spent speaking about Sicily and Sicilian life;
- Prof. Christian Meyer, from Columbia University, department chair at the time I joined Columbia;
- Department staff of the Dipartimento di Progetto e Costruzione Edilizia (DPCE) from the University of Palermo;
- Department staff of the Chemistry Department from University College London;
- Department staff of the Department of Civil Engineering and Engineering Mechanics from Columbia University with particular regard to Mrs. Elaine MacDonald and Mrs. Christine Persaud;
- All the people I met in London and in New York whom I share my time.

To my parents, relatives and friends who have supported me every day.

TABLE OF CONTENTS

Acknowledgement	I
Table of contents	III
Introduction	XIII

SECTION 1

Nanotechnology and NanoArchitecture

1.	Introduction to Nanotechnology	
1.1	Introduction	1
1.2	Definition	2
1.3	Learning from nature – the Biometrics process	2
1.4	Historical background	4
1.5	Richard P. Feynman: the conceptual father of nanotechnology	10
1.6	Kim Erich Drexler: the nanoscale assemblers	11
1.7	Current research and general market developments	12
2.	Worldwide activities in Nanotechnology R&D	
2.1	Introduction	15
2.2	European activity on nanoscience and nanotechnology	17
2.2.1	European Union laws and regulations	18
2.2.2	The 6th Framework Programme: 2002 – 2006	19
2.2.3	The 7th Framework Programme: 2007 – 2013	20
2.3	USA National Nanotechnology Initiative (NNI)	21
2.4	Japan and Australasia	24
3.	Nanotechnology and Architecture: a new way of planning	
3.1	Introduction	25
3.2	Nanoarchitecture: new creativity and high performance buildings	25
3.3	Nanoarchitecture: Johansen visionary projects	28
3.3.1	The Metamorphic Capsule (1992)	28
3.3.2	The Air Quilt (1995)	29
3.3.3	The Molecular Engineered House for the year 2200 (2000)	30

3.4	The NanoHouse™, Australia	31
3.5	The NanoStudio™, USA	33
3.6	The Carbon Fibre Tower, USA	34
3.7	Laboratory for Visionary Architecture (LAVA) – Branded Towers	36
3.8	Shimizu TRY 2004 Mega-city Pyramid, Japan	38
3.9	NanoCity, India	40
3.10	Sylvia Leydecker: nanoapplication in interiors, Ger- many	42
4.	Nanomaterials: new materials in Construction	
4.1	Introduction	43
4.2	Nanotechnology R&D in Construction, a 2005 survey	43
4.3	Nanomaterials in Construction	45
4.4	Reports	46
5.	Nanotechnologies for glass-based materials	
5.1	Thin films for architectural glazing	47
5.1.1	Solar protection	47
5.1.2	Selective coatings: IR protection (Thermochromic coatings)	48
5.1.3	Selective coatings: UV protection	49
5.1.4	Anti-fogging coatings	50
5.1.5	Anti-reflective (or anti-reflection - AR) coating	51
5.1.6	Anti-fingerprints (or touch-proof)	53
5.2	Scratchproof and abrasion resistant coatings	55
6.	Nanotechnologies for cement-based materials	
6.1	Introduction	57
6.2	What has been done: a general overview	57
6.3	Use of nanoparticles	59
6.4	Nano-SiO ₂	60
6.5	Nanocement – cases of study	62
6.6	Carbon Nanotubes in concrete	63
6.7	Self-cleaning photocatalytic concrete	67
6.8	Water-proof cement	71
6.9	Anti-corrosion concrete	72
6.10	Self-compacting concrete	72
6.11	Future Developments	73
7.	Nanotechnologies for steel-based materials	
7.1	Worldwide steel production and usage in construction industry	75

7.2	Nano-research in steel for large structures	77
8.	Nanotechnologies for wood-based materials	
8.1	Macroscopic and microscopic characteristics	81
8.2	Nanostructure of carbonized wood	82
8.3	Wood surface modification and nanocomposites	83
9.	Nanotechnologies for quality and comfort	
9.1	Self-cleaning coatings	87
9.1.1	Introduction	87
9.1.2	Hydrophobic coatings – the Lotus-Effect ®	87
9.1.3	Hydrophobic coatings – production and use	90
9.1.4	Hydrophilic photocatalytic coatings – self-cleaning glass	92
9.1.5	Hydrophilic photocatalytic coatings – other applications	96
9.2	Easy-to-clean surfaces	98
9.2.1	Polysiloxanes and silane products	99
9.2.2	Other products on the market	100
9.3	Air-purifying materials: coatings, paintings and capsules	100
9.3.1	The indoor-air quality	100
9.3.2	Air-purifying glass	101
9.3.3	Fragrant capsules	101
9.4	Anti-bacterial materials	102
9.4.1	Efficiency of nanoparticles: activity, factors and mechanism	103
9.4.2	Silver antibacterial effect	104
9.5	Photocatalysis for antibacterial applications	105
9.6	Anti-graffiti coatings	106
9.7	Fire protection and detection	108
9.7.1	Fireproofing traditional materials	108
9.7.2	Innovation in cement and network detector	109
9.7.3	Glass-like coatings for panels	109
9.7.4	Fire-safety glass	110
9.7.5	Nano fire-proof paint	112
9.7.6	Bamboo nanocomposite for flame-retardant boards	113
9.8	Anti-icing materials	114
10	Nanotechnologies for energy control and saving	
10.1	Thermal regulation materials	117
10.1.1	Phase-change materials (PCM)	117
10.1.2	Nature of Phase-Change material	118

	10.1.3	Phase-Change material selection criteria	119
	10.1.4	Use of Phase-Change materials in construction	119
	10.1.5	Storing energy by PCM components in buildings	121
	10.1.6	Vacuum insulation panels	123
	10.1.7	Aerogel	125
10.2		Photocatalysis for comfort and energy control	128
10.3		Photovoltaic	128
	10.3.1	History, materials and photovoltaic effect	128
	10.3.2	Solar cells: the photovoltaic basis	130
	10.3.3	Solar cells: theory	131
	10.3.4	Thin-film solar cells	132
	10.3.5	Crystalline Silicon solar cells	132
	10.3.6	Nanocrystalline solar cells	132
	10.3.7	Carbon nanotubes in photovoltaic	133
	10.3.8	Worldwide and Italian financial incentives	134
	10.3.9	Building-integrated photovoltaics (BIPV)	136
	10.3.10	Transparent and translucent photovoltaic	137
	10.3.11	The solar Road-way: road-integrated photovoltaics	138

11 Nanotechnologies for sensing: overview on nanosensors and MEMs for buildings, civil structures and environmental monitoring

	11.1	Introduction	139
	11.2	Nanotechnology in sensing applications	141
	11.2.1	Sensors based on nanoparticles and nanoclusters	142
	11.2.2	Sensors based on nanotubes and nanowires	142
	11.2.3	Sensors based on nanostructures embedded in bulk material	143
	11.2.4	Sensors based on porous silicon	143
	11.2.5	Nanomechanical sensors	144
	11.2.6	Self-assembled nanostructures	144
11.3		Micro-electromechanical Systems (MEMS)	144
11.4		MEMS applications	146
	11.4.1	Pressure sensors	146
	11.4.2	Inertial sensors	147
	11.4.3	Radio Frequency sensors	148
11.5		Humidity sensors	148
11.6		Studies on wireless sensor network (WSNs) for civil large structure and infrastructure	149
11.7		Sensors for concrete structures temperature and internal humidity monitoring	152
11.8		Functional composite paints for monitoring applications	153

11.9	Nanosensors for energy and environment	154
11.9.1	Nanoparticle-based optical sensor	154
11.9.2	Nanoparticle-based electrochemical sensor	155
11.9.3	Magnetic-relaxation sensors	156
11.10	Gas detector: developing the electronic nose	156

12 Nanotechnologies for preservation and archaeology practise

12.1	The preservation of cultural heritage	159
12.2	Chemistry contribution to conservation science: the problem of reversibility	160
12.3	Wall painting cleaning	161
12.4	Ferroni-Dini method for structural consolidation of wall painting matrix and stones	163
12.5	Removing biological patina from monument surfaces: a new enzyme procedure	166
12.6	Preserving wood from acids: the Vasa case	169

13 Conclusions 171

SECTION 2

Thermochromic coatings for architectural glazing

University College London – Supervisor: Prof. Ivan P. Parkin

1. A brief introduction on glass

1.1	Introduction	173
1.2	Glass ingredients	173
1.3	Colour	174
1.4	Glass as a super-cooled liquid	174
1.5	A brief history of glass production	175
1.6	The behaviour of antique glass	178
1.6.1	The cathedral glass theory	178
1.7	Industrial manufacture: the float glass	179
1.8	Optical properties	180
1.9	Glass for architectural glazing	181
1.10	Physical principles: the electromagnetic spectrum	182
1.11	Glass energetic and physical properties	183
1.11.1	Transparency	183
1.11.2	Otherness	184

1.11.3	Transmittance of visible light	184
1.11.4	The energy balance	184
1.11.5	The green house effect	185
1.11.6	Enhanced glazing	185
1.12	Producing energy by means of the glass	185
1.12.1	Weather data	185
1.12.2	Solar gain	186
1.12.3	The microclimate	187
1.13	Enhanced coating for architectural glazing	187
1.14	Pilkington Glass (NSG Group) – A brief history of the company	188
2.	Thermochromic coating	
2.1	Introduction	191
2.2	Advanced glazing	191
2.3	Thermochromism	192
2.3.1	Hysteresis	192
2.4	Previous works	193
2.4.1	Vanadium (IV) Dioxide – VO ₂	193
2.4.2	Doping of Vanadium (IV) Dioxide	195
2.4.3	Tungsten-doped Vanadium (IV) Dioxide	195
2.4.4	Gold-doped Vanadium (IV) Dioxide	196
2.5	Gold nanoparticles and Surface Plasmon resonance (SPR)	196
2.6	Deposition using VO(acac) ₂ + HAuCl ₄ + Surfactant	198
3.	Theory on thin films and chemical vapour deposition	
3.1	Thin film	199
3.2	Thin film growth	199
3.3	Chemical vapour deposition (CVD)	201
3.4	Principles of CVD	202
3.5	Process principles and deposition mechanism	203
3.6	Fluid dynamics	204
3.7	Particles within the reactor	205
3.8	Advantages and disadvantages of CVD	207
3.9	Hybrid aerosol assisted and atmospheric pressure CVD (AA/AP CVD)	208
4.	Analysis Techniques	
4.1	Introduction	211
4.2	X-Ray Diffraction (XRD)	211
4.3	UV / visible / near IR Absorption Reflection Spectroscopy	213

4.4	Metal-to-semiconductor transition temperature (T _c)	213
4.5	Scanning Electron Microscopy (SEM)	213
4.6	Raman Spectroscopy	215
4.7	CIE Colour specification	215
5.	Results and Discussion	
5.1	Experiments 1: MVO _x , MAu and MVO _x Au	219
5.1.1	Reflectance and Transmittance of MVO _x , MAu and MVO _x Au	222
5.1.2	Hysteresis and T _c of MVO _x , MAu and MVO _x Au	224
5.1.3	Raman Spectroscopy of MVO _x , MAu and MVO _x Au	226
5.1.4	XRD of MVO, MAu and MVO _x Au	228
5.1.5	SEM/EDAX of MVO _x , MAu and MVO _x Au	230
5.1.6	Thickness of MVO _x , MAu and MVO _x Au	232
5.1.7	Colour of MVO _x , MAu and MVO _x Au	232
5.2	Experiments 2: use of surfactant - MVO _x AuT and MVO _x T	233
5.2.1	Reflectance and Transmittance of MVO _x AuT and MVO _x T	235
5.2.2	Hysteresis and T _c of MVO _x AuT and MVO _x T	237
5.2.3	Raman of MVO _x AuT and MVO _x T	238
5.2.4	XRD of MVO _x AuT and MVO _x T	239
5.2.5	SEM/EDAX of MVO _x AuT and MVO _x T	240
5.2.6	Thickness of MVO _x AuT and MVO _x T	242
5.2.7	Colour of MVO _x AuT and MVO _x T	242
6.	Thermochromic glass behaviour in a building model	
6.1	Introduction	243
6.2	Calculation of the model size	243
6.3	The experiment	245
7.	Energy model performance	
7.1	Introduction	249
7.2	The simulation program – Energy Plus™	249
7.3	Model	251
7.3.1	Geometry	251
7.3.2	Location – Weather data	252
7.3.3	Construction of the model - Materials	257
7.3.4	Construction of the model - Glazing	258
	7.3.4.1 Pilkington glazing	258
	7.3.4.2 Thermochromic glazing	267
7.3.5	Construction of the model - Internal conditions	269
	7.3.5.1 Light	270

	7.3.5.2 Casual gain	270
	7.3.5.3 Ventilation rate	270
	7.3.6 Run period	270
	7.3.7 Schedules	270
7.4	Running Energy Plus	270
7.5	Results	273
	7.5.1 Number of hours in the hot state	275
	7.5.2 Annual heating and cooling loads	277
	7.5.3 Artificial lighting loads	283
	7.5.4 Overall energy consumption	286
7.6.	Potential of thermochromic glazing	290
	7.6.1 Switching temperature	290
	7.6.2 Infrared hemispherical emissivity	294
8	Ideal thermochromic spectrum	
	8.1 Introduction	297
	8.2 Ideal thermochromic spectrum	297
	8.3 Varying d(T,R) through the IR region	302
	8.4 Varying d(T) through the visible region	308
11	Conclusions and further works	315

SECTION 3

Polyurea-based nanocomposite for civil applications

Columbia University – Supervisor: Prof. Haim Waisman

1.	Carbon Nanotubes (CNTs)	
	1.1 Introduction	321
	1.2 The discovery	321
	1.3 What a carbon nanotube is	322
	1.4 SWCNT and MWCNT	323
	1.5 Properties	324
	1.5.1 Strength	325
	1.5.2 Electrical properties	326
	1.5.3 Thermal properties	326
	1.6 Synthesis of CNT	326
	1.6.1 Arc discharge	326
	1.6.2 Pulsed laser vaporization/laser ablation	327
	1.6.3 Chemical vapour deposition (CVD)	328

1.7	Toxicity	329
1.8	CNTs producers	329
2	Polyurea: the material	
2.1	Introduction	331
2.2	Discovery and applications	331
2.3	Two systems in comparison: polyurea and polyurethane	334
2.4	Physical and chemical properties: state of art of the researches	335
3	CNT-doped polymers: state of art	
3.1	Introduction	339
3.2	Preliminary treatment of CNT	339
3.2.1	CNT purification	339
3.2.2	CNT functionalization	340
3.3	Dispersion of functionalized CNTs in the polymer	340
3.3.1	In situ polymerization	340
3.3.2	Solution processing	341
3.3.3	Melt mixing	341
3.4	CNT/polymer composite – state of art	341
3.4.1	Interfaces	341
3.4.2	Mechanical properties	343
3.4.3	Electrical properties	344
3.4.4	Thermal properties	344
3.5	CNT/Polyurea composite – state of art	344
4	Materials and specimen production	
4.1	Materials used	347
4.1.1	Carbon nanotubes	347
4.1.2	Polyurea	347
4.1.3	Tetrahydrofuran (THF)	348
4.2	Specimen production	348
5	Tension test	
5.1	Introduction	353
5.2	Elements of solid mechanics and some definitions	353
5.3	Apparatus and procedure	356
5.4	Calculations	358
5.5	Results and discussion – influence of THF	359
5.6	Results and discussion – influence of CNT	361
5.7	Results and discussion – tensile set	365

5.8	Results and discussion – load and unload test	366
5.9	Results and discussion – scanning electron micrograph (SEM) imaging	370
6	Deterioration and aging: discussion and results	
6.1	Introduction	373
6.2	Polymer aging	373
6.3	Accelerated aging testing – Theory	373
6.4	Aging conditions (New York City temperature)	374
6.5	Laboratory procedure	378
6.6	Discussion and results	378
6.7	Scanning electron micrograph (SEM) imaging	380
	References	383
	List of publications	405

INTRODUCTION

The history of nanotechnology began in 1959, when Richard Feynman in his famous lecture “There is plenty of rooms at the bottom”, proposed the concept of nanotechnology indicating that scientists should focus on understanding phenomena on a very small scale to complement the prevailing interest in “big science” at that time. Ever since, nanotechnology has been regarded as an emerging and multidisciplinary technology, introducing a new dimension to science and technology with the possibility of manipulating matter, atoms and molecules, at the nanometre level (*nano*-means one-billionth of a meter).

From the scientific point of view, “nanotechnology can be defined as referring to materials and systems with structures and components exhibiting novel and significantly improved physical, chemical and biological properties, as well as to the phenomena and processes enabled by the ability to control the material properties on the nano-scale size” (def. by: National Science and Technology Center, NNI, USA).

The nanotechnology emergence was enabled by the development of specialist instruments, which in turn facilitated the observation and manipulation of nanostructures at the atomic or molecular scale, as well as the discoveries of new nanomaterials. Nanotechnology also offered new opportunities in rapid development of miniaturization techniques (so-called top-down approach that includes methods to manipulate existing materials at the nanoscale through traditional lithography, cutting, etching or grinding techniques) and building macrostructures (so-called bottom-up approach that includes methods to create new materials at the nanoscale through chemical synthesis or self-assembly of particle molecules and their macrostructures). Nanoscience is widely seen as having huge potential to many areas of scientific research (such as physics, chemistry, material sciences, biology, engineering) and technological applications (such as healthcare and life sciences, energy and environment, electronics, communications and computing, manufacturing & materials) because of its nano-scale where the materials’ properties are significantly different from those of the same materials in bulk or macroscopic form. Therefore, nanotechnology involves understandings the interactions in the atomic or molecular scale and the capability to characterize and control materials using nano-tools.

Nanotechnology, which is both scientific and technical, is fundamental in making things (i.e. the construction, generation and growth of objects, devices and architecture) and has a highly multidisciplinary character, affecting multiple traditional technologies, scientific disciplines and industries.

In a certain way, it is possible to state that nanotechnology is still in an early stage of development as it is still very scientist-driven and thus largely exogenous to the economic system. On top of that, there are important ethical and regulatory issues to be debated. Further development will largely depend on the degree to which existing firms and industries are able to identify commercial applications. This will, in turn, depend on the degree to which the created scientific knowledge can be transferred from public sector research to the private sector.

Further, it should be remarked that nanotechnology is subject to a great deal of hype and partially unfounded expectations. It is therefore particularly important to highlight genuinely new issues and challenges that this emerging technology brings forward when discussing technology diffusion and commercialization of scientific knowledge.

The object of this thesis is the construction industry that is a sector of great economy activity though it often deals with coarse components and systems. In the last century, investments in research remained lower than in other industrial sectors thus advances were quite slower compared of other industrial sectors such as army, medicine, etc. Nowadays, nanotechnology seems to be a competitive route in achieving a real sustainable growth and innovation. Its scientific approach is essential if the potential for a new generation of materials, that are both of higher performance and more economically viable, is to be realised. Today there are interesting developments, based on nanotechnology, available on the market that can be applied to the construction industry. Many other (nano)technologies enable new developments: materials and products are fast emerging or already exist in bulky and expensive forms in other different industrial sectors, but a great deal of research should still be developed.

The aim of this research is to analyze the applications of nanotechnology, nanostructured materials and multifunctional/smart materials on construction components (energy, reinforcement, coatings, multifunctional materials and components, diagnostic, etc..) to investigate if, how and when these new high-materials could be produced and applied in order to improve buildings' performance in contrast to traditional techniques and materials that are available on the market.

The present research focuses on nanotechnology-based applications to construction and architecture and is divided in three main sections as follows:

1. **Nanotechnology and Architecture**, scientific developments and lots of possible applications to the construction sector are analyzed. New enhanced materials are already available on the market and lots of new researches are in progress worldwide to investigate new solutions to old or unsolved technical problems. Some of the possible applications of nanotechnology to the construction market are analyzed as well as the new concept of NanoArchitecture that is spreading out in architectural and engineering schools.
2. **Thermochromic coatings for architectural glazing**, hybrid aerosol assisted and atmospheric pressure chemical vapour deposition methodology has been utilised, to produce thin films of gold nano-particle vanadium dioxide nanocomposites for architectural glazing. Films were analysed by X-ray diffraction, scanning electron microscopy and X-ray photoelectron spectroscopy. Their op-

tical and thermochromic behaviour was also determined. Then, their energy performance was simulated by means of the software Energy Plus™ to understand how efficient thermochromic coatings could be if applied in different kind of buildings and in several climate conditions at different latitudes in the northern hemisphere in comparison to some products that are still on the market. Finally, some more computational simulations were performed to study an ideal thermochromic spectrum and to understand the limit of the technology.

This study was conducted at Christopher Ingold Laboratories, Chemistry Department, University College of London (UCL), London (UK) under the supervision of prof. Ivan. P. Parkin and with the collaboration of dr. Clara Piccirillo, dr. Russell Binions and dr. Ian Ridley.

3. **CNT-doped polyurea nanocomposite for large structure protection**, a polymer nanocomposite of polyurea matrix enhanced by different quantities of multiwalled carbon nanotubes intended for passive protection of civil structures has been produced. Several tensile and cyclic tests were performed in order to evaluate and characterise the mechanical behaviour of this new polymer-nanocomposite. Furthermore, the specimens were subjected to accelerated thermal aging to study their performance deterioration which is fairly unknown.

This study was conducted at Carleton Laboratory, Department of Civil Engineering and Engineering Mechanics, Columbia University, New York City (NY, USA) under the supervision of prof. Haim Waisman and prof. Raimondo Betti.

The acquisition of the knowledge on nanotechnology, nanostructured materials and multifunctional/smart materials in construction will allow to formulate a judgment on the real applicability and convenience on high technologies' usage in comparison to the traditional systems, consolidated by now in the practice.

SECTION 1

Nanotechnology and NanoArchitecture

1. INTRODUCTION TO NANOTECHNOLOGY

1.1 Introduction

Nanotechnology refers broadly to a field of applied science and technology whose unifying point is the possibility to control the matter on the molecular or atomic scale – generally 1 to 100 nanometres [nm] – and the fabrication of materials, devices and systems within that size range.

The prefix *nano* in the word *nanotechnology* means a billionth, 1×10^{-9} ; nanotechnology deals with everything having dimensions of the order of a billionth of a meter - the “nanometre”.

Nanotechnology is based on the recognition that particles less than the size of 100 nm impart to nanostructures built from them new properties and behaviour that strongly influence the macroscopic material (bulk) properties, with a significantly improvement in mechanical, optical, chemical, electrical, etc. properties, thus allowing to engineer their characteristics and performance.

The research area of nanotechnology is a highly multidisciplinary task, drawing from fields such as applied physics, materials science, chemistry, robotics to engineering and biology.

More generally, nanotechnology can be seen, in a certain way, as an extension of the existing sciences into the nanoscale, or as a recasting of existing sciences using newer and more modern applications.

Materials reduced to the nanoscale can suddenly show very different properties compared to what they usually show on a macroscale, thus enabling unique and novel applications. For instance, opaque substances become transparent (copper); inert materials become catalysts (platinum); stable materials turn combustible (aluminum); solids turn into liquids at room temperature (gold); insulators become conductors (silicon). A material such as gold, which is chemically inert at normal scales, can become a potent chemical catalyst at nanoscale. Much of the fascination with nanotechnology stems from these unique quantum and surface phenomena that matter exhibits at the nanoscale.

Examples of nanotechnology in modern use are the manufacture of polymers based on molecular structure or the design of computer chip layout based on surface science. Despite the great promise of numerous specific nanotechnologies such as quantum dots¹ and carbon nanotubes², there are real commercial applications such as suntan lotion, cosmetics, protective coatings for different applications, drug delivery and stain resistant clothing.

1 Quantum dots: a semiconductor whose excitons (imaginary particle representing the bond state of an electron) are confined in all three spatial dimensions. As a consequence their behaviour is between the bulk semiconductors and the discrete molecules.

2 Carbon nanotube: is an allotrope of carbon, it will be discussed in an other section of this thesis.

1.2 Definition

An exact definition of nanotechnology is quite difficult to determine and define so a couple of official statements will be reported.

The definition given by the American Nanoscale Science, Engineering and Technology (NSET) Subcommittee of the United States National Science and Technology Council (NSTC, White House), which coordinates the National Nanotechnology Initiative (NNI) is the following: “Research and technology development at the atomic, molecular or macromolecular levels, in the length scale of approximately 1-100 nanometre range, to provide a fundamental understanding of phenomena and materials at the nanoscale and to create and use structures, devices and systems that have novel properties and functions because of their small and/or intermediate size. The novel and differentiating properties and functions are developed at a critical length scale of matter typically under 100 nm. Nanotechnology research and developments includes manipulation under control of the nanoscale structures and their integration into larger material components, systems and architectures. Within these larger scale assemblies, the control and construction of their structures and components remain at the nanometre scale. In some particular cases, the critical length scale for novel properties and phenomena may be under 1 nm (e.g. manipulation of atoms at – 0.1 nm) or be larger than 100 nm (e.g. nanoparticle reinforced polymers have the unique feature at 200 ÷ 300 nm as a function of the local bridges or bonds between the nanoparticles and the polymer)”.

The definition given by the Bundesministerium für Bildung und Forschung³ (BMBF) summarizes nanotechnology as follows: “Nanotechnology refers to the creation, investigation and application of structures, molecular materials, internal interfaces or surfaces with at least one critical dimension or with manufacturing tolerances of (typically) less than 100 nanometres. The decisive factor is that the very nanoscale of the system components results in new functionalities and properties for improving products or developing new products and applications.”

1.3 Learning from Nature – the Biomimetics process

Nature has many objects and processes that work on a microscale to a nanoscale. Understanding these functions may help and guide to imitate and produce nanodevices and nanomaterials. Abstractions of design from nature are referred to as Biomimetics.

Billions of years ago, molecules began to organize themselves into complex structures that could support life with particular processes. Photosynthesis, for instance, uses solar energy to produce everything useful to a plant life. More particularly, molecules such as chlorophyll are light-harvesting and are arranged in a nano to a microscale into cells.

³ German Federal Ministry of Education and Research

Some live organs, as many bacteria, use chemical energy to survive or move. Their flagellum⁴, for exemplum, can rotate at over 10,000 revolutions per minute thanks to the proton flow caused by the electrochemical potential difference across the membrane.

The diameter of the bearing is about 20-30 nm with an estimated clearance of about 1 nm. Some biomedical systems have antiadhesion surfaces. Many plants' leaves (such as the Lotus leaf) are covered by a hydrophobic cuticle that repels water making their surfaces clean.

Geckos – wall-climbing lizards - can run on walls or stick to ceilings thanks to their soles that are covered with about half a million submicrometre keratin elastic hairs that are called setae, which are split into smaller nanostructures known as spatulae. Each hair is 30-130 μm long that can produce a tiny force of about 100 nN due to Van der Waals attraction and capillary interaction. Millions of hairs working together create a large adhesive force on the order of about 10 N with a pad area of approximately 100 mm^2 , which is sufficient to keep geckos firmly on their feet. Another exemplum of nanotechnology in the natural world is the Abalone shell. These molluscs construct super-tough shells with beautiful, iridescent inner surfaces. They do this by organizing calcium carbonate of crumbly schoolroom chalk into tough nanostructured bricks. For mortar, abalones concoct a stretchy goo of protein and carbohydrate. Cracks that may start on the outside rarely make it all the way through: the shell structure forces a crack to take a tortuous route around the tiny

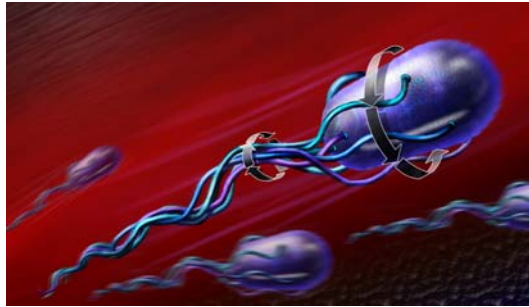


Fig. 1.1
Escherichia Coli cells use flagella to propel themselves.

Geckos – wall-climbing lizards - can run on walls or stick to ceilings thanks to their soles that are covered with about half a million submicrometre keratin elastic hairs that are called setae, which are split into smaller nanostructures known as spatulae. Each hair is 30-130 μm long that can produce a tiny force of about 100 nN due to Van der Waals attraction and capillary interaction. Millions of hairs working together create a large adhesive force on the order of about 10 N with a pad area of approximately 100 mm^2 , which is sufficient to keep geckos firmly on their feet. Another exemplum of nanotechnology in the natural world is the Abalone shell. These molluscs construct super-tough shells with beautiful, iridescent inner surfaces. They do this by organizing calcium carbonate of crumbly schoolroom chalk into tough nanostructured bricks. For mortar, abalones concoct a stretchy goo of protein and carbohydrate. Cracks that may start on the outside rarely make it all the way through: the shell structure forces a crack to take a tortuous route around the tiny

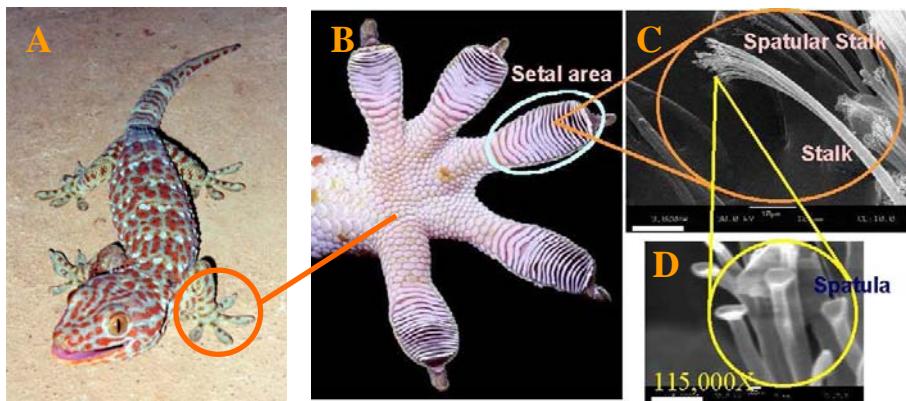


Fig. 1.2
Tokay gecko (A): foot-hair images. Foot bottom view (B); zooming into one of the stalks (C, bar indicates 10 μm), and zooming into spatulae and spatular stalks at the end of a stalk under SEM (D, bar indicates 300 nm). (source: Sitti M., Fearin R.S., *Synthetic Gecko Foot-Hair Micro/Nano-Structures for Future Wall-Climbing Robots*)

⁴ Flagellum: is a tail-like structure that project from the cell body of certain bacteria and functions in locomotions. It is made up of the protein flagellin and its shape is a 20 nanometres thick hollow tube.

bricks, which dissipates the energy behind the damage. Adding to the damage control is that stretchy mortar. As a crack grows, the mortar forms resilient nano-strings that try to force any separating bricks back together.



Fig. 1.3 a-b
Abalone shell: outside (left) and inside (right).

1.4 Historical background

It is not clear when humans first began to take advantage of nanosized materials but the first evidence of this use is an artwork from the IV century B.C. called the Lycurgus cup, nowadays resided in the British Museum in London. The cup, which depicts the death of King Lycurgus, is made from soda lime glass containing silver and gold nanoparticles that make the colour of the cup change from green to red as a light source is placed inside it.



Fig.1.4
Lycurgus cup.



Moreover, it was found out by Robert Curl Jr.⁵ that Indian craftsmen and artisans used nanotechnology extensively about 2000 years ago to make weapons and long lasting cave paintings even though they were completely unaware that they were practising carbon nano-techniques.

On the famous damascus blades - used in the sword of Tipu Sultan and Ajanta Paintings - scientists found carbon

Fig.1.5

Tipu sultan sword with mamluk (or ot-toman) damascus wateres steel blade.

nanotubes, cylindrical arrangements of carbon atoms first discovered in 1991 and now made in laboratories all over the world. Indian craftsmen used a unique smelting techniques to manufacture the damascus blades which led to nanotisation giving them a unique long-lasting edge. This technology was used to make wootz steel, a 'high-grade' steel that was highly prized and much sought after across several regions of the world over nearly two millennia.



Fig.1.6

Damascus blade (see next page for a detailed description).

⁵ Nobel laureate of Chemistry in 1996 with Richard Smalley and Harold Kroto for the discovery of carbon cage compounds, known as Fullerenes.

In the previous page, the four images of parts of a damascene sabre show what the blade is made of: carbon nanotubes that are responsible for the extraordinary strength and flexibility of the steel. (A) a Persian knife blade as we see it with the naked eye. (B) a close-up clearly showing the lighter carbide fields in the darker matrix of softer, low-carbon steel. The other two images were taken using electron microscopy: (C) a small part of a Damascene sabre was dissolved in hydrochloric acid revealing the presence of nanotubes, in this example a multi-walled carbon nanotube. The striped patterning is formed by a contrast between the layers of carbon. (D) cementite nanowire in a Damascene sabre encapsulated by a carbon nanotube, a leftover after dissolving the piece of sabre in acid. The scale in the bottom-right of the lower image measures 5 nm.

Wootz also had a high percentage of carbon, which was introduced by incorporating wood and other organic matter during fabrication. India, for ages, was a leading exporter of this steel which was used to make Persian daggers which were quite popular in Europe centuries ago.

The potential importance of clusters was recognized for the first time by the chemist Robert Boyle in his *Sceptical Chymist* - published in 1661 – where he criticizes Aristotle's belief that matter is composed by four elements: earth, fire, water and air. He suggested, instead, that tiny particles of matter combine in various way to form what he calls corpuscle. He wrote that “minute masses or cluster that were not easily dissipable into such particles that composed them”.

Photography, that was developed between the XIX and XX centuries, depends on production of silver nanoparticles sensitive to light. Photographic film is an emulsion of a thin layer of gelatine containing silver halides, such as silver bromide, and a base of transparent cellulose acetate. The light decomposes the silver halides into nanoparticles of silver that can be considered as the pixels of the image. In 1883 the American George Eastman, who would later start the Kodak Corporation, produced a film consisting of a long paper strip coated with an emulsion containing silver halides. He later developed this into a flexible thin film that could be rolled, which made photography accessible to many.

The first mention of some of the distinguishing concepts in nanotechnology (but predating use of that name) was in 1867 by James Clerk Maxwell when he proposed as a thought experiment a tiny entity, known as Maxwell's Demon, able to handle individual molecules.

In 1857 Michael Faraday published the paper *Philosophical Transactions of the Royal Society* which attempted to explain how metal nanoparticles affect the colour of church windows.

The first observations and size measurements of nano-particles was made during first decade of 20th century when Richard Adolf Zsigmondy made detail studies on gold sols and other nanomaterials with sizes down to 10 nm and less. He published a book in 1914 and he used ultramicroscope that employs *dark field* method for seeing particles with sizes much less than light wavelength. Zsigmondy was also the first who used the word *nanometer* explicitly for characterizing particle size. He defined

it as the million part of a millimeter (10^{-9} mm) and tried to develop the first system of classification based on the particle size in the nanometre range.

Then, have been many significant studies during the 20th century in characterizing nanomaterials and related phenomena. In the 1920s, Irving Langmuir and Katharine B. Blodgett introduced the concept of a monolayer, a layer of material one molecule thick. Langmuir won a Nobel Prize in chemistry for his work. In early 1950s, Derjaguin and Abrikosova conducted the first measurement of surface forces.



The “conceptual father” of the nanotechnology is the physicist and chemist Richard Feynman (1918 – 1988) who touched the topic in *There is a Plenty of Rooms at the Bottom*, a visionary lecture given on the 29th of December 1959 at a meeting of the American Physical Society. In his speech, Feynman speculated on the possibility and potential of nanosized materials envisioning etching lines, a few atoms wide, with beams of electrons. He proposed to manipulate individual atoms to make new small structures having very different enhanced properties such as circuits on the scale of nanometres that can be used as elements in more powerful computers. At the meeting, Feynman announced two challenges and he offered a prize of \$1000 for the first individuals to solve each one. The first

Fig. 1.7
Richard Feynman

challenge involved the construction of a nanomotor - which was achieved by William McLellan in November of 1960. The second challenge involved the possibility of scaling down letters small enough so as to be able to fit the entire Encyclopedia Britannica on the head of a pin, this prize was claimed in 1985 by Tom Newman.

Another area of activity in the 1960s involved electron paramagnetic resonance (EPR) of conduction electrons in metal particles of nano-dimensions referred to as colloids in those days. The particles were produced by thermal decomposition and irradiation of solids having positive metal ions and negative molecular ions such as sodium and potassium azide. Structural features of metal nanoparticles – such as the existence of magic numbers – were revealed in that period using mass spectroscopic studies of sodium metal beams.

In 1965 Gordon Moore observed that silicon transistors were undergoing a continual process of scaling downward, an observation which was later codified as Moore's law. Since his observation, transistor minimum feature sizes have decreased from 10 micrometers to the 45-65 nm range in 2007; one minimum feature is thus roughly 180 silicon atoms long.

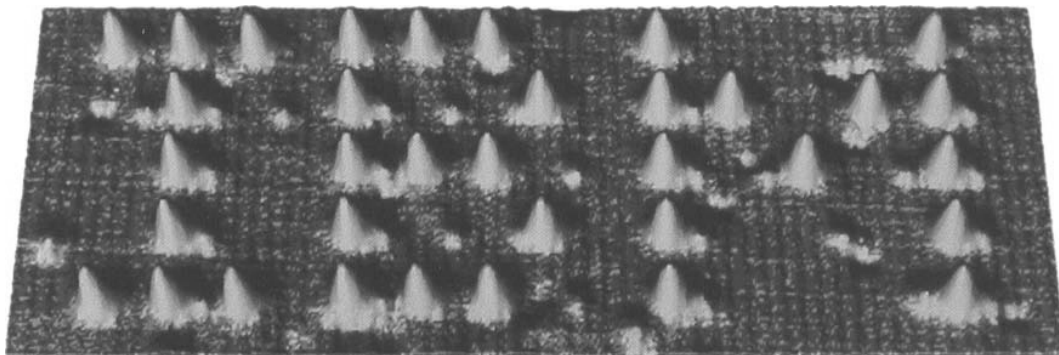


Fig. 1.8

The iconic image that caused a sensation in 1989: the letters IBM written out of 35 xenon atoms onto a nickel surface.

(source: Bhushan B., *Springer handbook of nanotechnology*)

Groups at Bell Laboratories and IBM in the early 1970s fabricated the first two-dimensional quantum wells that were made by a thin film growth technique that build a semiconductor layer one atom at a time. This work is considered as the beginning of the development of the zero-dimensional quantum dot.

The term "nanotechnology" was defined by Tokyo Science University Professor Norio Taniguchi in a 1974 paper (N. Taniguchi, "On the Basic Concept of 'Nanotechnology'," Proc. Intl. Conf. Prod. London, Part II, British Society of Precision Engineering, 1974.) as follows: "Nanotechnology mainly consists of the processing of separation, consolidation and deformation of materials by one atom or by one molecule". Also in 1974 the process of Atomic Layer Deposition, for depositing uniform thin films one atomic layer at a time, was developed and patented by Dr.

Tuomo Suntola and co-workers in Finland. However, it was not until the 1980s with the emergence of appropriate method of fabrication of nanostructures that a notable increase in research activity occurred and a number of significant developments resulted. For instance, in 1981 it was developed a method to make metal clusters using a high-powered focused laser to vaporize metals into a hot plasma and in 1985 this method was used to synthesize the fullerene⁶ (C_{60}).

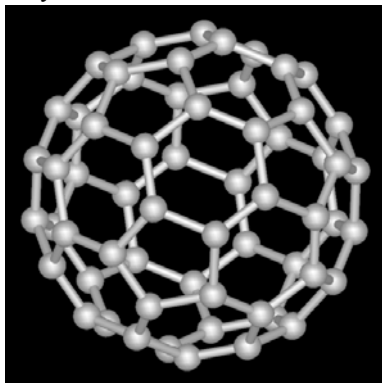


Fig. 1.9

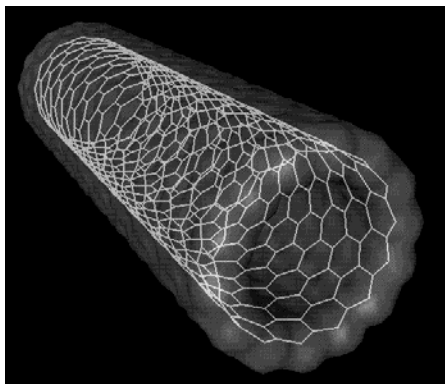
3D model of a Fullerene molecule.

G. K. Binning and H. Rohrer of the IBM Research Laboratory developed the Scanning Tunneling Microscope (STM) that, with the Atomic Force Microscope (AFM), provided new important tools for viewing, characterizing and atomic manipulation of nanostructures. Another important scientist was Dr. Kim Eric Drexler (n. 1955) who promoted the technological significance of nano-scale phenomena and devices through speeches and books such as: "*Engines of creation:*

⁶ Fullerenes: are a family of Carbon allotropes, molecules composed entirely of carbon in the form of a hollow sphere, ellipsoid, tube or plane.

the coming era of nanotechnology" (1986) and "*Nanosystems: Molecular Machinery, Manufacturing, and Computation*" (1992). His vision of nanotechnology is often called "Molecular Nanotechnology" (MNT) or "molecular manufacturing". Drexler at one point proposed the term "zettatech" which never became popular.

The first observation of the conductance quantization was carried out in 1987 by B. J. van Wees and H. van Houten of the Netherlands and by D. Wharam and M. Pepper of Cambridge University.



In the 1990s, Iijima made carbon nanotubes⁷ which is, nowadays, one of the main fields of research and in 1991 Yablonovitch fabricated the first three-dimensional periodic photonic crystal possessing a complete bandgap. In 1996, in USA a number of Government Agencies led by the National Science Foundation commissioned a study to assess the current worldwide status of trends, research and development in nanoscience and nanotechnology. The recommendations led to a commitment

Fig. 1.10
3D model of a
Carbon Nanotube.

by the Government to provide major funding and establish a *National Nanotechnology Initiative* (NNI).

In 2004 Richard Jones wrote *Soft Machines - nanotechnology and life* which is a book about nanotechnology but written for the general reader and published by Oxford University. In this book he describes radical nanotechnology as a deterministic/mechanistic idea of nano engineered machines that does not take into account the nanoscale challenges such as wetness, stickiness, brownian motion, high viscosity (Drexler view). He also explains what is the soft nanotechnology or more appropriately biomimetic nanotechnology which is the way forward to design functional nanodevices that can cope with all the problems at nanoscale.

Nowadays, nanoscience is one of the most investigated and funded fields of research all over the world and governments of all the countries make new laws and regulations to increase the nanotechnology development.

At present, the practice of nanotechnology embraces both stochastic approaches (in which, for example, supramolecular chemistry creates waterproof pants) and deterministic approaches wherein single molecules (created by stochastic chemistry) are manipulated on substrate surfaces (created by stochastic deposition methods) by deterministic methods comprising nudging them with STM⁸ or AFM⁹ probes and causing simple binding or cleavage reactions to occur.

⁷ Carbon Nanotube (CNTs): are allotropes of carbon with a nanostructure that can have a length-to-diameter ratio greater than 1,000,000. These cylindrical carbon molecules have novel properties that make them potentially useful in many applications, as following discussed.

⁸ STM. Scanning tunneling microscope.

For the future, some means has to be found for MNT design evolution at the nanoscale which mimics the process of biological evolution at the molecular scale. Biological evolution proceeds by random variation in ensemble averages of organisms combined with culling of the less-successful variants and reproduction of the more-successful variants, and macroscale engineering design also proceeds by a process of design evolution from simplicity to complexity as set forth somewhat satirically by John Gall: "A complex system that works is invariably found to have evolved from a simple system that worked. [...] A complex system designed from scratch never works and can not be patched up to make it work. You have to start over, beginning with a system that works".

A breakthrough in MNT is needed which proceeds from the simple atomic ensembles which can be built with, e.g., an STM to complex MNT systems via a process of design evolution. A handicap in this process is the difficulty of seeing and manipulation at the nanoscale compared to the macroscale which makes deterministic selection of successful trials difficult; in contrast biological evolution proceeds via action of what Richard Dawkins has called the "blind watchmaker" comprising random molecular variation and deterministic reproduction/extinction.

1.5 Richard P. Feynman: the conceptual father of nanotechnology

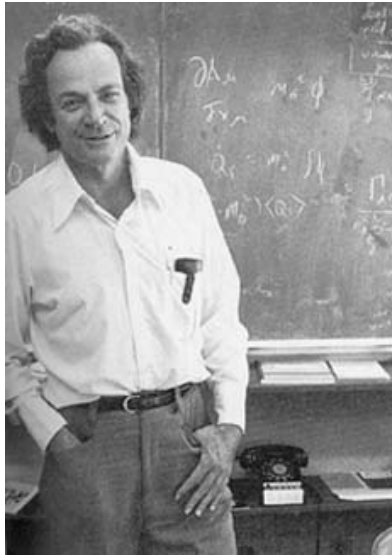


Fig. 1.11
R. Feynman.

Richard Feynman (New York, 11 May 1918 – Los Angeles, 15 February 1988) was one of the most famous American physicist and chemist. He is known for the path integral formulation of quantum mechanics, the theory of quantum electrodynamics, the physics of the superfluidity of supercooled liquid helium. For his contribution to the development of quantum electrodynamics he was awarded with the Nobel Prize in Physics in 1965, together with Julian Schwinger and Shin Ichiro Tomonaga.

In addition to his work in theoretical physics, he is considered the father of the term "nanotechnology" in his speech *There is a Plenty of Rooms at the Bottom*.

Feynman attended the Massachusetts Institute of Technology (MIT) where he got his bachelor's degree in 1939. After a course on

theoretical physics he was admitted to Princeton University where he received a Ph.D. in 1942. At Princeton, the physicist Robert R. Wilson encouraged Feynman to

participate to the Manhattan Project, the U.S. Army project at Los Alamos to develop the atomic bomb.

After the Second World War, Feynman followed Hans Bethe to Cornell University where he taught theoretical physics from 1945 to 1950. He had been called the “Great Explainer” for taking great care when giving explanations to his students and making complicated topics as the most accessible as possible.

He did his most significant works while at Caltech¹⁰, including research in:

- Quantum electrodynamics. He developed a functional integral formulation of quantum mechanics in which every possible path from one state to the next one is considered, the final path is a sum over the possibilities.
- Physics of the superfluidity of the supercooled liquid helium, where helium seems to display a lack of viscosity when flowing. Applying the Schrödinger equation to the question, he showed that the superfluid was displaying quantum mechanical behaviour observable on a macroscopic scale.
- A model of weak decay which showed that the current coupling in the process is a combination of vector and axial.
- Feynman diagrams, from his Ph.D. thesis. They are a device helping in conceptualizing and calculating interactions between particles and spacetime. From these diagrams Feynman could model all of physics in terms of those particle’s spin and the range of coupling of the fundamental forces.
- Quantum gravity. By analogy with the photon, that has spin 1, he investigated the consequences of a free massless spin 2 field, and he was able to derive the Einstein field equation of general relativity.

In the late 1980s Feynman played a crucial role in developing the first massively parallel computer.

1.6. Kim Erik Drexler: the nanoscale assemblers

K. E. Drexler (born on the 25th of April 1955 in Oakland, California) is an American engineer best known for popularizing the potential of molecular nanotechnology (MNT). Drexler holds three degrees from MIT. He received his S.B. in Interdisciplinary Sciences in 1977 and his S.M. in 1979 in Astro-Aerospace Engineering with a Master's thesis titled "Design of a High Performance Solar Sail System". In 1991 he earned a Ph.D. under the auspices of the MIT Media Lab (formally, the Media Arts and Sciences Section, School of Architecture and Planning). His Ph.D. work was the first doctoral degree on the topic of molecular nanotechnology and his thesis, "Molecular Machinery and Manufacturing with Applications to Computation", was published as "Nanosystems: Molecular Machinery, Manufacturing and Computation" (1992), which received the Association of American Publishers award for Best Computer Science Book of 1992. In 1986 Drexler and his wife, Christine Peterson, founded the Foresight Institute with the mission of "Preparing for nanotechnology" and in 2005 he joined

¹⁰ Caltech: California Institute of Technology

Nanorex, a molecular engineering software company based in Bloomfield Hills, Michigan, to serve as the company's Chief Technical Advisor.



Fig. 1.12
K.E. Drexler.
(source:
www.caltech.edu)

Drexler was very strongly influenced by ideas on Limits to Growth in the early 1970s. His response in his first year at Massachusetts Institute of Technology (MIT) was to seek out someone who was working on extraterrestrial resources. He found Dr. Gerard K. O'Neill of Princeton University, a physicist famous for a strong focus on particle accelerators and his landmark work on the concepts of space colonization. Drexler was involved in NASA summer studies in 1975 and 1976. Besides working summers for O'Neill building mass driver prototypes, he delivered papers at the first three Space Manufacturing conferences at Princeton.

The 1977 and 1979 papers were co-authored with Keith Henson, and patents were issued on both subjects, vapor phase fabrication and space radiators. During the late 1970s, he began to develop ideas about molecular nanotechnology (MNT). In 1979, Drexler encountered Richard Feynman's provocative 1959 talk *There's Plenty of Room at the Bottom*. The term nanotechnology was coined by the Tokyo Science University professor Norio Taniguchi in 1974 to describe the precision manufacture of materials with nanometer tolerances, and was unknowingly appropriated by Drexler in his 1986 book *Engines of Creation: The Coming Era of Nanotechnology* to describe what later became known as MNT. In that book, he proposed the idea of a nanoscale "assembler" which would be able to build a copy of itself and of other items of arbitrary complexity.

1.7. Current research and general market developments

According to several surveys, the market development in the field of nanotechnology is enormous and has got a huge potential. Nanotechnology applications may be found in the most of the aspects of our life: from medicine to industry, communication, transportation and, more important for our purpose, to architecture and construction.

Nanotechnology is the natural continuation of the miniaturization revolution that we have witnessed over the last decade. Especially the computer industry kept on pushing the limits of miniaturization, and many electronic devices we can see today, have nano features.

Not only universities and private research centres but also business enterprises and consultants, banks, industries and governments are active in this fast development. On the international arena, USA, Japan and Germany lead the field in America, Asia and Europe respectively. According to some Market Research Companies, the global market volume for nano-based products is about 500 billion US dollars in

2010 with a projected 2,6 trillion US dollars in 2014 as all business sectors will be influenced by nanotechnology.

Nowadays, nanotechnology plays a major role in many fields. Following there is a selection of the current applications:

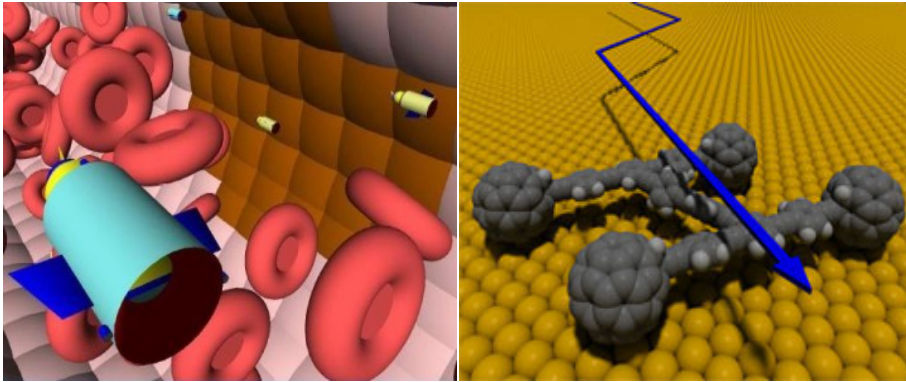


Fig. 1.13 a-b
 Left: nanorobot for medical applications.
 Right: space-filling model of a nano-car on a surface, using fullerenes as wheels.

- Cosmetic industry: skincare and haircare products are the spreadest products as well as decorative cosmetics.
- Air, space and automotive industry: in all these sectors new ultralight and ultrastrong materials are studied in order to improve vehicles performances speed and consumption. Nanostructured materials may be more stable and insulating for space travels and lighter with a high reduction in kerosene consumption. Modern cars already use of scratch-resistant and abrasion-resistant paints and mirrors may darken photochromically as the light changes or self-clean themselves.
- Medicine, life science and pharmaceuticals are helped by new treatments and agents. Tumour cells may be targeted directly without damaging the entire organism or new materials may cover surgery equipments to avoid fogging phenomena. Antibacterial catheters are studied to contribute to the reduction in infections in hospitals.
- Electronics. Reduction of sizes and new super-conductive materials help in creating new hyper-fast and super-small computers with new functionalities.
- Environmental technology. The use of nanotechnology is increasing in the energy consumption, climate protection, water recycling. Dirty water may be cleaned using photocatalysis or anti-reflecting coatings and new nanocomposite improve the photovoltaic system efficiency also reducing CO₂ emissions. Recycling may be improved with “debonding on command” materials and systems that may ease the separation of materials from one to another while “bond-on command” systems may contribute towards long-term adhesion between different components.

- Defence industry. New light and super-resistant materials may be use in the production of soldier clothing and equipment as well as new thin coating for military vehicles.
- Optics and light. New energy-efficient lighting systems are improving everyday to create a new concept of lighting the surrounding space and objects.
- Textile industry. The so-called smart textiles are equipped with additional functionality: self-cleaning water-repellent clothing and membranes may be use everyday changing our lifestyle.
- Sport and recreation. Ultra-light extra-robust sports equipments as suits, helmets, rackets and so on are already produced.

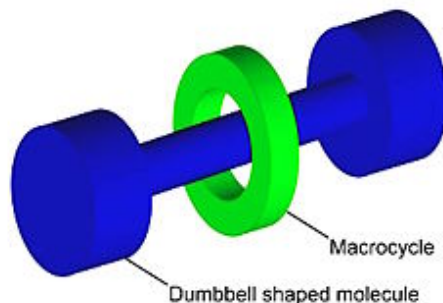


Fig. 1.14
Graphical representation of a rotaxane used as molecular switch.

The above-mentioned trends are just a few of the possible applications that nanotechnology may have in the market.

2. Worldwide activities in nanotechnology R&D

2.1 Introduction

In the early stage of nanotechnology development and diffusion, many expected benefits have not yet been fully accomplished. However, scientists and researchers in the scientific disciplines aggressively got involved in a relevant research as a parallel way to boost nanotech competitiveness through academic research, and corporations have been directing their R&D activities towards the exploration of nanotech opportunities.

Nowadays, nanotechnology is highly prioritized on the global scientific agenda. The most of the countries all over the world regard it as an interesting area of exploitation to material science and engineering, setting up national initiatives in order to prepare for the technological challenge. Research activities on nanoscience are continuously increasing as each government would like to have a strong and advanced leadership position in high-technology R&D. Several countries started national programme on nanotechnology between the mid-1980's and the mid-1990's and the overall investment has risen from around 200 million of euros in 1997 to around 1000 millions in 2003.

Volumes of scientific publications are a commonly accepted indicator of scientific performance in specific technological domains. They help illustrate the existing status and forecast future developments of a technology. The printed tables show the key trends and the respective involvement of European Union, United States of America, Asian countries including Japan in scientific & engineering research related to nanotech over the period of 1990–2004.

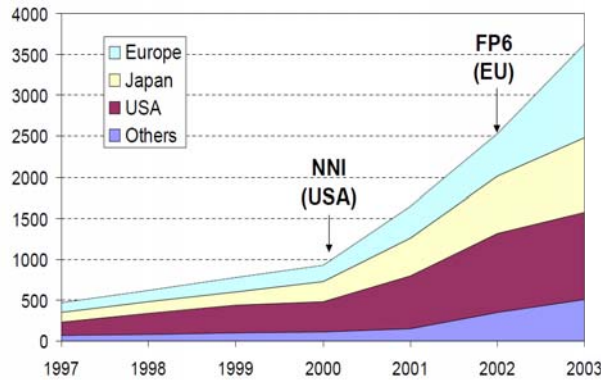


Fig. 2.1 Public expenditure [million of Dollars/Euros] on nanotechnology (source: European Commission).



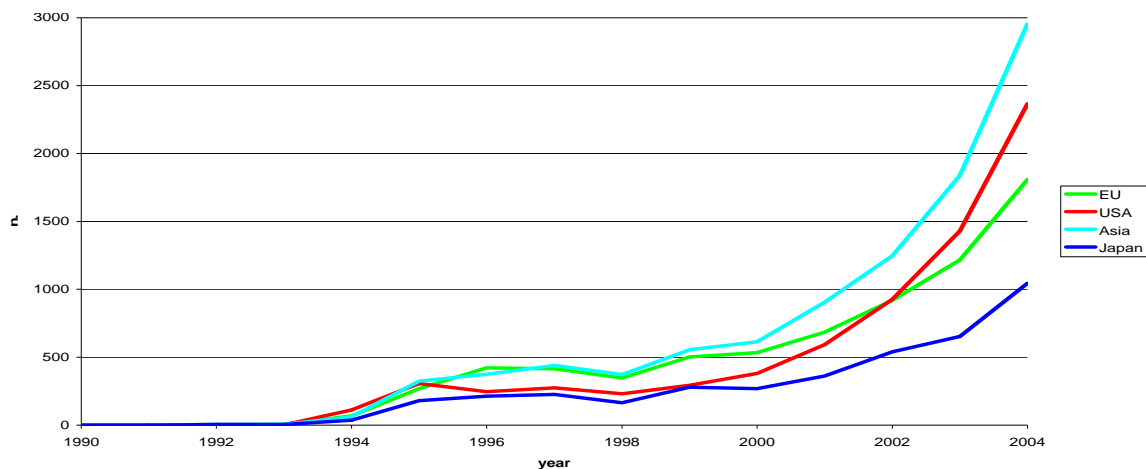
Fig. 2.2 Public expenditure [million of Dollars/Euros] on nanotechnology in 2003 (source: European Commission).

Table 2.1 (source: Elsevier COMPENDEX database)					
Overall volumes of scientific output over time related to nanotech					
Year	Total worldwide share	Total number by region			
		European Union	United States of America	Asia	Japan
1990	2	1	1	0	0
1991	1	0	1	0	0
1992	17	2	5	5	5
1993	19	7	2	6	4
1994	279	69	112	61	37
1995	1082	269	307	325	181
1996	1256	422	246	374	214
1997	1356	415	275	440	226
1998	1115	348	230	372	165
1999	1630	502	294	555	279
2000	1798	534	381	614	269
2001	2545	685	593	905	362
2002	3631	919	926	1247	539
2003	5137	1216	1430	1839	652
2004	8171	1808	2366	2953	1044
Tot		7197	7169	9696	3977

Fig 2.3

Worldwide scientific output over time related to nanotechnology (source: Elsevier COMPENDEX database)

Specific circumstances such as rates and levels of economic development, levels of education of the workforce, as well as specific industrial strengths and weaknesses, induce the differentiation in science and technology policies of the different countries, attempting to gain and maintain the leading edge in nanotechnology.



Shares of individual countries in EU also varied with particularly strong position of Germany, France, UK and Italy. Very slow advances are observed in nanotechnology research by other EU countries as illustrated in the figure below.

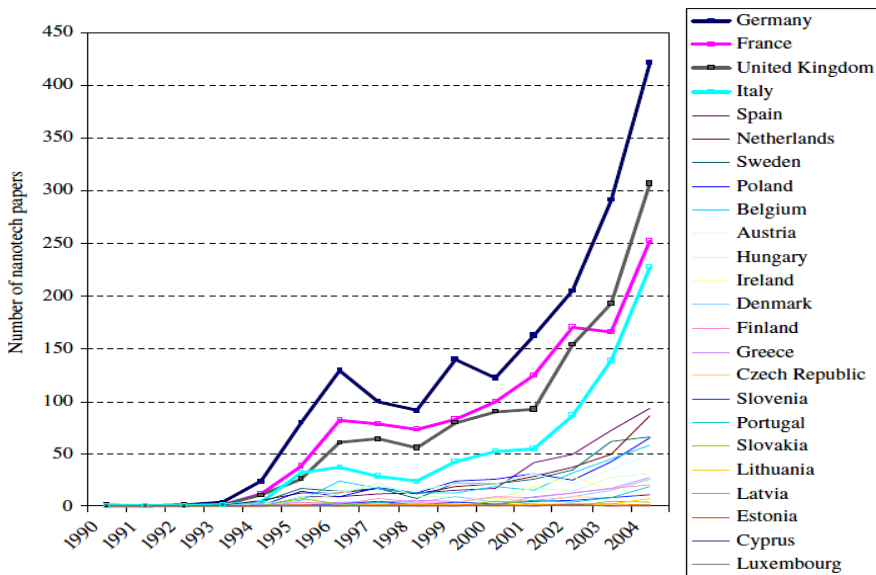


Fig 2.4
European scientific output over time related to nanotechnology (source: Elsevier COMPENDEX database)

Some studies showed that Asian countries play a very important role in the global nanotechnology research, accounting for approximately 40% of all scientific and technical articles worldwide. It demonstrated the dominant position of Japan and catching up processes of China in Asia; similarly Germany, France, UK and Italy in EU; which are becoming major players in this emerging technology area.

Nowadays, nanoscience and nanotechnology are objects of an intensive study and funding and all the governments try to develop new regulations to ensure a primary position in this field.

In the European Union the 6 Framework Programme identified nanotechnology as a primary area with 250 million Euro/year; in USA the National Nanotechnology Initiative (NNI) became a federal initiative with 220 million dollars funding; Japan started in 2003 with 800 million dollars. Many other countries, as China or South Korea, are active on nanotechnology research and everyday new researches are settled in.

2.2 European activity on Nanoscience and Nanotechnology

European Union feels that a strong R&D position in nanoscience needs to be translated into a real competitive advantage for European industry. The transformation of industry towards high-added value organisations necessitates real integrated ap-

proaches, either “vertical”, combining materials sciences, nanotechnologies and production technologies, or “horizontal”, combining multi-sectorial interests.

More particularly, European industrial production needs to move from resource-based towards knowledge-based more environment-friendly approaches, from quantity to quality, from mass produced single-use products to manufactured-on-demand multi-use. These changes are associated with radical shifts in the industrial structures, involving a stronger presence of innovative enterprises, with capabilities in networks and mastering new hybrid technologies.

2.2.1 European Union laws and regulations

During the past decade, a lot of laws and recommendations were studied and published to improve a higher interest towards nanoscience. Following, there are some of the most relevant European Union laws concerning nanotechnology:

- 2002, Council decision adopting a specific programme for research, technological development and demonstration¹;
- 2004, Communication from the Commission: Towards a European strategy for nanotechnology²;
- 2004, Conclusion of the Council of the European Union concerning the European strategy for nanotechnology³;
- 2005, Opinion of the European Economic and Social Committee on the Communication from the Commission: Towards a European strategy for nanotechnology⁴;
- 2005, Communication from the Commission to the Council, the European Parliament and the Economic and Social Committee: Nanoscience and Nanotechnologies: An action plan for Europe 2005-2009⁵;
- 20 June 2005, EU-US Declaration: Initiative to enhance transatlantic economic integration and growth⁶;
- 2006, European Parliament resolution on nanoscience and nanotechnologies: An action plan for Europe 2005-2009;
- 2006, Opinion of the European Economic and Social Committee on the Communication from the Commission to the Council, the European Parliament, and the Economic and Social Committee – Nanoscience and Nanotechnologies: An action plan for Europe 2005-2009;
- 2007, Opinion on the ethical aspects of nanomedicine from the European Group on Ethics in Science and New Technologies⁷;

1 2002/834/EC.

2 COM(2004) 338, 12.5.2004.

3 Doc. 12487/04 .

4 COM(2005) 243, 7.6.2005.

5 COM(2004) 338.

6 10305/05 (Presse 159).

7 EGE Opinion No 21, 17 January 2007.

- 2007, First Report on the implementation of the Nanotechnologies Action Plan for Europe 2005-2009⁸;
- 2008, Commission recommendation on a Code of conduct for responsible nanosciences and nanotechnologies research⁹;
- 2009, Second Report on the implementation of the Nanotechnologies Action Plan for Europe 2005-2009¹⁰.

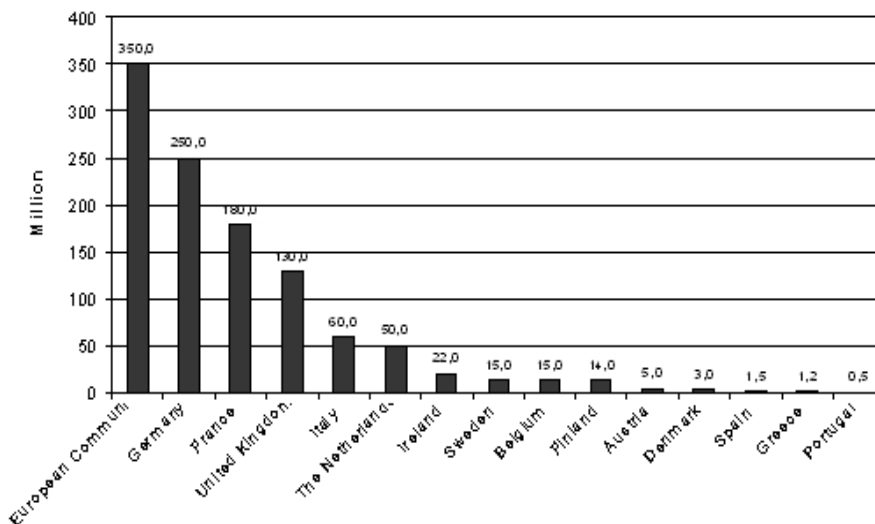


Fig. 2.5
Public expenditure [million of Euros] in Europe in 2003. (source: European Commission).

2.2.2 The 6 Framework Programme: 2002-2006

The sixth Framework Programme (FP6-NMP) started on the 30th September 2002 and ended on the 31st December 2006 providing 1429 million of Euros overall funding.

The primary objective of “Nanotechnologies and nanosciences, knowledge-based multifunctional materials and new production processes and devices” is to promote real industrial breakthroughs, based on scientific and technological excellence with 250 million of Euros per year funding

A radical breakthrough may be achieved through two complementary approaches: creation of new knowledge and new ways of integrating and exploiting existing and new knowledge.

The FP6 is structured in three main blocks of activities:

1. Focusing and Integrating Community Research;
2. Structuring the European Research Area;
3. Strengthening the foundations of the European Research Area.

8 COM(2009)607 final.

9 C(2008) 424 final.

10 COM(2009)607 final.

The “Nanotechnologies and nanosciences, knowledge-based multifunctional materials and new production processes and devices” is one of the seven thematic priorities laid down in the “Focusing and Integrating Community Research” programme of FP6.

2.2.3 The 7 Framework Programme: 2007-2013

The Seventh Framework Programme (FP7) started on the 1st January 2007 and it will expire on the 31st December 2013 providing a 3475 million of Euros funding.

The objectives of the FP7 research theme “Nanosciences, nanotechnologies, materials and new production technologies” are:

- to improve the competitiveness of European industry;
- to generate knowledge and ensure transformation from a resource-intensive to a knowledge-intensive industry;
- to generate step changes in knowledge;
- to implement decisive knowledge for new applications at the crossroads between different technologies and disciplines;
- to benefit both new, high-tech industries and higher-value, knowledge-based traditional industries;
- to enable technologies which impact all industrial sectors.

The main activities on nanoscience will focus on new materials and systems with pre-defined properties and behaviour. The main goals are:

- new knowledge of the interactions of atoms, molecules and their aggregations with both natural and artificial entities;
- the realisation of nano-structures, systems or materials;
- activities aiming at understanding or imitating the natural processes at nano-metric scale;
- processes for nano-fabrication, surface functionalization, thin layers, self-assembling properties;
- methods and processes for measuring and characterisation.

According to the new models of manufacturing industry, it is the materials themselves which are becoming the first step in increasing the value of products and their performance, rather than the processing steps themselves. Thus, research will focus on developing new advanced materials and surfaces with higher knowledge content, new functionalities and improved performance as they are increasingly critical for industrial competitiveness and for sustainable development.

A new approach to manufacturing is required for the transformation of EU industry from a resource-intensive to a sustainable knowledge-based industrial environment and will depend on the adoption of totally new attitudes towards the continued acquisition, deployment, protection and funding of new knowledge and its use, including towards sustainable production and consumption patterns.

One of the main activities sponsored by FP7 will focus on the exploitation of multidisciplinary research networks and of the convergence of the nano-, micro-, bio-, geo,

info-, optical and cognitive technologies to develop new added-value hybrid technologies, products and engineering concepts and the possibility of new industries.

The integration of new knowledge from nano-, materials-, and production-technologies will be supported in sectorial and cross-sectorial applications such as health, food, construction and building including cultural heritage, aero-space industry, transport, energy, chemistry, environment, information and communication, textiles, clothing and footwear, forest-based industry, steel, mechanical and chemical engineering, as well as in the generic subjects of industrial safety and measurement and testing.

It is widely recognized that the competitiveness of the industry of the future will largely depend on nanotechnologies and their applications that might accelerate the transformation of European industry.

The Programme supports research actions in the following areas:

- nanosciences and nanotechnologies;
- materials;
- new production technologies;
- integration of technologies for industrial applications.

Research activities carried out within this framework should respect fundamental ethical principles, including those which are reflected in the Charter of Fundamental Rights of the European Union.

2.3 USA National Nanotechnology Initiative (NNI)

As nanoscience has advanced, new discoveries are made and new nano-products are entering the international market, the governments attention towards these new high-technologies as a leading future economic growth for the countries is increasing continuously.

In November 1996 to coordinate and discuss the federal plans, programme and works on nanoscience, a group from several agencies was formed. In September 1998 the Interagency Working Group on Nanotechnology (IWGN) was established under the National Science and Technology Council (NSTC) and in August 1999 it completed its first draft of a plan for an initiative in nanoscale science and technology. In 2001 Clinton administration raised nanoscale science and technology to the level of a federal initiative, officially referring to as the National Nanotechnology Initiative (NNI). Subsequently, the IWGN was disbanded and the Nanoscale Science, Engineering and Technology (NSET) Subcommittee was established as a component of the NSTC's Committee on Technology (CT). The CT is composed of senior-level representatives from the federal government's research and development departments and agencies, and it provides policy leadership and budget guidance for this and other multiagency technology programs.

The NSET is responsible for coordinating the federal government's nanoscale research and development programs and includes representatives of departments and agencies currently involved in the NNI and Office of Science and Technology Policy (OSTP) officials. The National Nanotechnology Coordination Office (NNCO)

was also established to provide day-to-day technical and administrative support on federal nanotechnology activities for government organizations, academia, industry, professional societies, foreign organizations. The importance of a coordinated federal program for nanotechnology R&D was given greater recognition in 2003 with the enactment of the 21st Century Nanotechnology Research and Development Act (Public Law 108-153, Dec. 3, 2003).

Today the NNI consists of the individual and cooperative nanotechnology-related activities of 25 Federal agencies with a range of research and regulatory roles and responsibilities. Thirteen of the participating agencies have R&D budgets that are related to nanotechnology, with the reported NNI budget representing the collective sum of these. The NNI as a program does not fund research; however, it informs and influences the federal budget and planning processes through its member agencies.

Table 2.1 (source: www.nano.gov)
NNI Budget History by Agency (millions of dollars)

Agency	2001 Actual	2002 Actual	2003 Actual	2004 Actual	2005 Actual	2006 Actual	2007 Actual	2008 Actual	2009 Actual	2010 Proposed
DOD	125	224	220	291	352	424	450	460	464	379
NSF	150	204	221	256	335	360	389	409	505	423
DOE	88	89	134	202	208	231	236	245	362	351
DHHS (NIH)	40	59	78	106	165	192	215	305	311	326
DOC(NIST)	33	77	64	77	79	78	88	86	94	91
NASA	22	35	36	47	45	50	20	17	17	17
EPA	5	6	5	5	7	5	8	12	16	18
USDA(CREES)	-	-	1	2	3	4	4	7	7	12
DHHS(NIOSH)	-	-	-	-	3	4	7	5	5	5
USDA (FS)	-	-	-	-	-	2	3	6	3	3
DOJ	1	1	1	2	2	.3	2	-	-	-
DHS		2	1	1	1	2	2	3	9	12
DOT(FHWA)	-	-	-	-	-	1	1	1	3	3
TOTAL	464	697	760	989	1200	1351	1,425	1,554	1797	1640

Acronyms: **DHS** — Department of Homeland Security; **DOC** — Department of Commerce; **DOD** — Department of Defense; **DOE** — Department of Energy; **DHHS** — Department of Health and Human Services; **DOJ** — Department of Justice; **DOT** — Department of Transportation; **EPA** — Environmental Protection Agency; **FHWA** — Federal Highway Administration; **NASA** — National Aeronautics and Space Administration; **NIH** — National Institutes of Health; **NIST** — National Institute of Standards and Technology; **NSF** — National Science Foundation; **TSA** — Transportation Security Administration; **USDA** — U.S. Department of Agriculture.



Fig. 2.6
The 25 US federal agencies joining NNI.

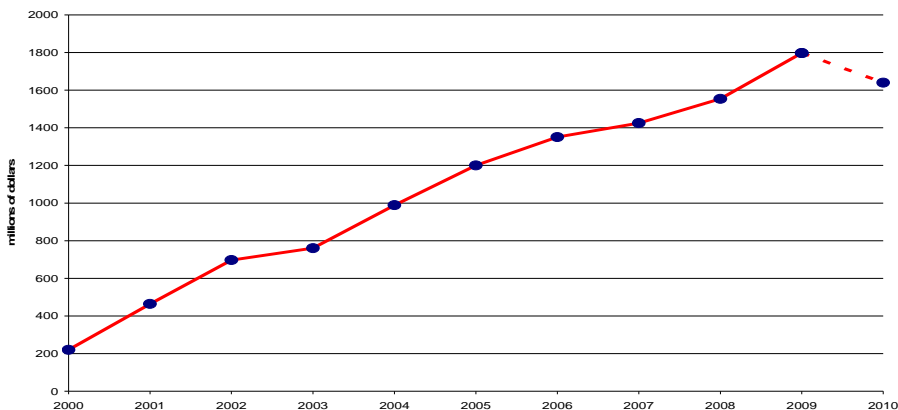


Fig. 2.7
Actual NNI budget
history. (source:
www.nano.gov)

2.4 Japan & Australasia

Japan has been investing in nanoscience since the 1980s and after USA is the biggest nanotechnology R&D spender worldwide. The Japanese government views the successful development of nanotechnology as one of the keys to the reinvigoration and sustainable success of the Japanese economy. Government agencies and large corporations are the main sources of funding for nanotechnology in Japan; small and medium-sized companies play only a minor role. Research activities are generally grouped in relatively large industrial, government, and academic laboratories.

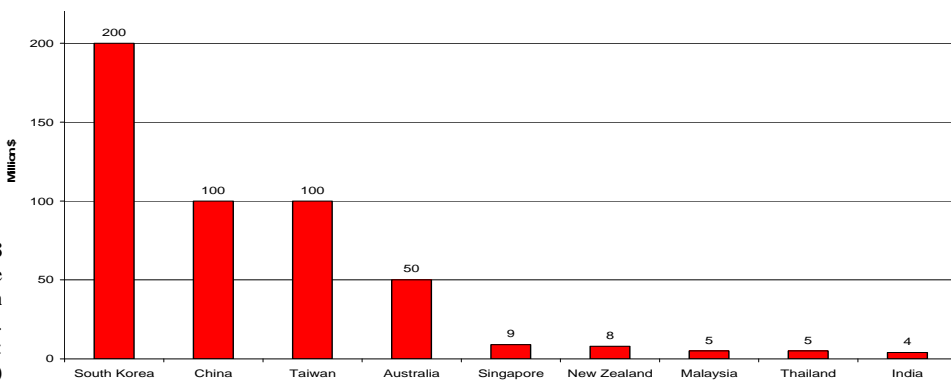


Fig. 2.8
Public expenditure
[million of dollars] in
Australasia in 2003.
(source:
www.nano.gov)

In response to the National Nanotechnology Initiative in the United States, the Japanese government set up an Expert Group on Nanotechnology under the Japan Federation of Economic Organizations (Keidanren) Committee on Industrial Technology. From 2001, Japan targeted nanotechnology as one of four priorities in science and technology budget. Anyway, all the other countries in Asia and Australasia set nanotechnology one of the primary trend of research increasing their public investment, as shown in the above graph.

3. Nanotechnology and Architecture: a new way of planning

3.1 Introduction

The use of nanotechnology in the construction sector is wide and varies from the early stages of planning to the final stages of finishing, especially in choosing the right materials with the correct and appropriate characteristics and behaviours that could better deal with external stimuli.

This new concept will not only reflect the design but also has a great influence in the methodology of thinking about architecture according to the new vast options that nanotechnology offers. In other words, in the construction sector nanotechnology is an enabling technology that may help to make other technological developments. When introducing a new technology to any field, it should be always examined at first all the possible benefits it could bring. In the case of application of nanotechnology to the construction sector, added value, additional functionality, as well as market demand with regard to product development are the most important aspects. Good design, in principle, is always based on demand, and in this way contributes to the evolution of both nanomaterials and the resulting nanoproducts. The use of nanotechnology is an ongoing demand for innovations as a result of the growing scientific cooperation between the different countries. More particularly, in the architectural planning process it is necessary to bring together the knowledge of many specialist planners. Generally, it is possible to say that independent of any factor nanotechnology can make a concrete contribution to the following areas:

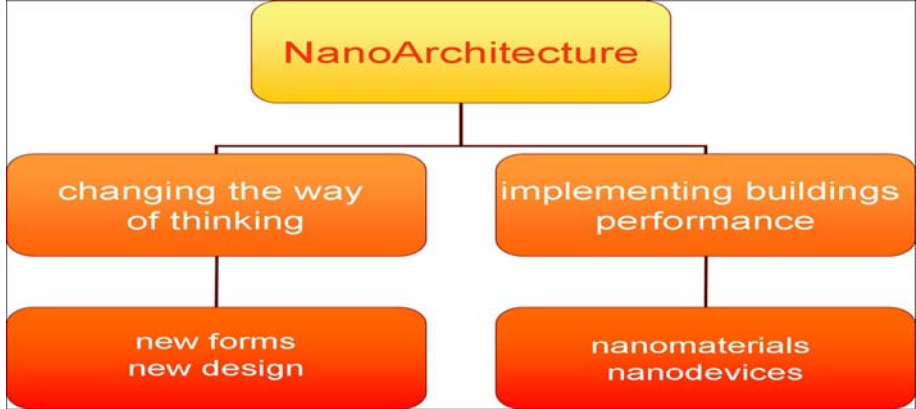
- optimization of existing products;
- reduction in weight and/or volume;
- reduction in the number of production stages;
- a more efficient use of materials;
- reduced need for maintenance and/or operational upkeep and/or protection;
- reduction in the consumption of raw materials and consequently a longer conservation of the primary resources;
- reduction of the waste of energy and reduction of the CO₂ emissions;
- greater economy;
- more comfort.

Nanotechnology may help architects and designers in finding and applying new customized materials with specific individual properties. From the client, or the user, point of view, the most realistic and sensible application focuses on aspects of aesthetics, functionality, economy and sustainability.

3.2 Nanoarchitecture: new creativity and high-performance buildings

In all the centuries, architects tried to find different and novel ways to use new technologies in architecture changing how a building is designed and built or look like. Thus, every day, new concepts of the surrounding space are developing. Nanoarchitecture, as a new contemporary architectural style of the 21st century, is revolutionizing the architectural world in many aspects as the way architects design buildings or,

most of all, the possibility to use new materials with new enhanced properties. Sub-atomic (nano) particles have been fascinating scientists since the first half of the 20th century and nowadays the study of the matter at the nano level is a new attractive believe that is accelerating worldwide the scientific research as matter at the nanoscale level may perform with new advanced functions.



A new concept in planning is spreading out, bringing us back to natural forms as natural structuring or branch systems usually establish suboptimal strength-to-weight ratio. Molecular-engineered buildings are expected to be 10% as massive as buildings today, resulting in entirely new systems of structuring and forming. Structure will be integrating with the building shell, walls and enclosure and construction materials will be seamlessly fused in a completely unified entity. In a certain way it is possible to say that nanotechnology will reshape the man-made environment.

Fig. 3.1 a-b

Left: Saldarini house known as “The dinosaur” or “The whale” and built in Baratti (Livorno, Italy) in 1962.

Right: the Atomium, built in 1958 for the Brussel’s World’s Fair designed by André Waterkeyn.



The notion of “growing architecture” was first proposed in 1961 by William Katavolos¹, and expanded by Vittorio Giognini² in “Early experiments in architecture using nature’s building technology” in 1977.

¹ William Katavolos. Professor at the Pratt Institute School of Architecture (Brooklyn, NY).

² Vittorio Giognini (Florence, 1926- 2010). Italian architect who spent his life in studying the relationship between architecture and biological systems.

It is well noted that “large plants and animals have vascular systems and intricate channels to carry material to molecular machinery working through their systems. In a similar way, artificial assembly systems could also employ this strategy to build a scaffold, then working through its volumes incorporating materials from the central source, in this case, the vat”.

Vat growth may be described through the process of accretion with atoms adhering to a base. At the scale of a building, there must be a linear or directional growth pattern: root, stem, rib, branches, nourished by a “fibro-vascular” distribution.

Taking inspiration from diamonds, a carbon made crystal, it will be possible to build large “carbon structures” of architectural scale with structural elements that will be produced by nanobots³ in any shape from dense to porous, from transparent, translucent to opaque. Nanotechnology may lead to lightweight, invisible structures that could perform a tremendous strength. Nanobots will produce clear sheets of diamond, a few millimetres thick, to form the exterior membrane of a building that could be opaque or, by electro-molecular realignment, could become translucent or transparent. This “morphability”, empowered by millions of controlled nanomotors, will alter the buildings main characteristics. Furthermore, protective nano-membranes may regulate light and air depending on external conditions. In warmer weather, the molecules respond by collapsing tightly, exhausting the air; for increased insulation the molecules expand into a thick foam with innumerable closed air spaces. Further advantages of morphable substances include such applications as interior room partitioning and adjustable, self-adaptive furniture that responds to position, attitude, and comfort requirements. The “seeds”, or coding device, will replace conventional specifications and construction procedures. In regards to ecological relationships, the seeds will contain all the instructions with feedback allowing the new building to respond to its immediate surroundings. The most extraordinary proposal is coordinating the artificial coding of a building with the DNA of a living environment. In other words, the building would be programmed to monitor its internal environment and adjust or alter its design to be in harmony, or symbiotic relationship, with the external space by means of millions of smart nanosensors. Frazier⁴ addresses the emerging field of “architectural genesis”. He approaches coding for architecture stating that “a building as, an artefact, is designed to interact and evolve with natural forces”. Frazier proposes “a new, computer-based technology for developing design models, not in physical form at this stage, but rather of inner logic. The computer model will be the expression of the equilibrium between the androgynous development of the architectural concept and the exogenous influences exerted by the environment”. These buildings may be considered self-organizing “will maintain stability by negative feedback interactions and promote their evolution in their employment of positive feedback”. The building knows its coding for development and may be considered an organism of artificial life and intelligence.

³ Nanobot: robot in nanoscale.

⁴ Owsley Brown Frazier (born 7th May 1935, Louisville, Kentucky (USA)) is an American philanthropist who founded the Frazier International History Museum.

The molecular building process is not biological, but mechanical; living cells are replicated by dividing, assembles replicate mechanically, by building others. As Drexler wrote: “the great difference is that nanotech use not living ribosome but robotic assemblers, not veins but conveyors belts, not muscles but motors, not genes but computers. Not cells dividing but small factories producing products and additional factories”. Assemblers are robots, or nanobots, with communicative powers that in collaboration can build anything they are programmed to build. They are organized by a main computer, into specialized building crafts that operate as part of a vast construction project. Mechanical assemblers are expected to employ a greater variety of tools and use them with greater force, control, and precision than ribosomes can in nature. Frazier envisions an architecture developed to this state as “literally part of nature, in which manmade and natural environments are to be considered each as parts of a global ecosystem”.

3.3 NanoArchitecture: Johansen visionary projects

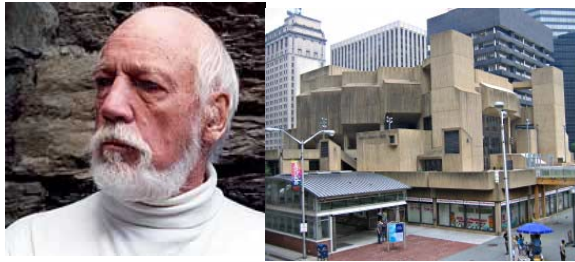


Fig. 3.2
Left: John Johansen.
Right: Morris Mechanic Theatre

The American architect John Mac Lane Johansen (born in New York, 1916) who studied under Walter Gropius at Harvard University, proposed some revolutionary projects based on molecular growth. In the early stages of this process,

small molecules survive only in a sealed vat where an entactic environment is assured. However, it is likely that these perishable molecules will build larger and more durable and they will withstand and survive in the external environment. This development from simple to complex molecules, from inside to outside the vat, is the critical and essential assumption of his proposal. One of his most important work is the Morris Mechanic Theatre built in Baltimore in 1967 but here, we will feature some of his works inspired by nanotechnology, magnetic levitation and bioengineering. Some of these projects were funded in part by a grant from the Graham Foundation for Advanced Studies in the Fine Arts.

3.3.1 The Metamorphic Capsule (1992)

The Metamorphic Capsule is an enclosure whose form, opacity and colour are controlled by electromagnetic fields. The suspension of an object in space by the application of electric forces has already been achieved in the laboratory. In this project, the surrounding field is formed by a system of nodes attached to a structural framework, with corresponding nodes placed on the outer surface of a fabric capsule place

within the field. Continuous air pressure from within is necessary to sustain the form of the capsule. The power of the attraction and repelling forces sent to each node determines the overall shape of the capsule. Changes in the

power sent to the nodes, or in the relative amounts of power sent to individual nodes, cause the capsule to undulate. Colour, degrees of opacity or transparency and other visual and audible stimuli can also be controlled. A serpentine levitator carries visitors around and through this shifting form. Movement of the individuals passing through the capsule can itself motivate visual effects. Brain waves that indicate the various moods are recorded and harnessed to prompt changes of light and sound. While not notably utilitarian, the capsule provides the experience of being swathed in a diaphanous, luminous, iridescent chamber in the timeless trading of the cave or womb.

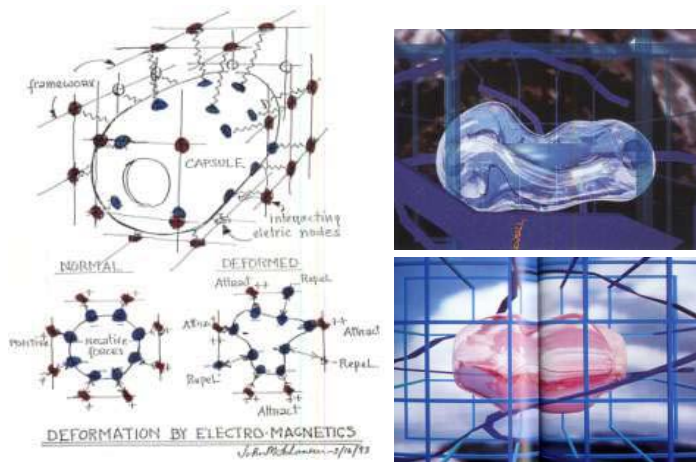


Fig. 3.3 a-b-c Left: deformation by Electro-Magnets Right: the Metamorphic Capsule. (source: Johansen John, *Nanoarchitecture: a new species of architecture*)

3.3.2 The Air Quilt (1995)

In this project, a quilt of spherical air chambers from malleable, habitable enclosures are clustered in two layers in a geometric pattern of hexagons and pentagons. An adaptive building that can adjust its interior volume by distorting the chambers into desired configuration. Distortion of the quilt surface is achieved by variable expansion and contraction of the two-layered air chambers.

Transferring air from the outer layer to the inner one results in a bending action and a convex form. Conversely, air passing from the inner strata out creates a concave form as seen from the interior. As with the Metamorphic Capsule, internal air pressure sustains the envelope by means of small air pumps, prompted by a computer system, power the air transference. By substituting helium gas for air, this structure would lift off and it could be tethered by cables to the ground. It could also be equipped with jet motors to lift and lower it, stabilize it against wind, and navigate it as well.

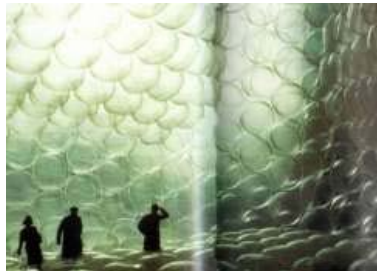


Fig. 3.4 Hexagon layers of the Air Quilt. (source: Johansen John, *Nanoarchitecture: a new species of architecture*)

3.3.3 The Molecular Engineered House for the year 2200 (2000)

The following is a diary created by the owner of a molecular-engineered house written during its construction. It is set in the year 2200.

Day 1: Excavation begins on site where assembly vats will be placed.

Day 2: Vats delivered to building site, along with selected chemicals and bulk materials in liquid form. The various materials are then pumped into the vats.

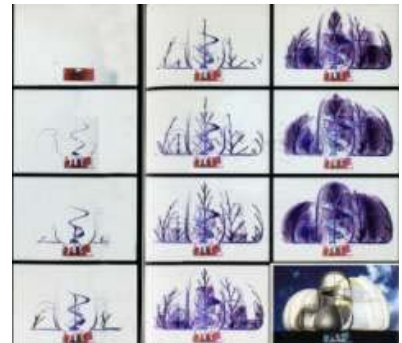
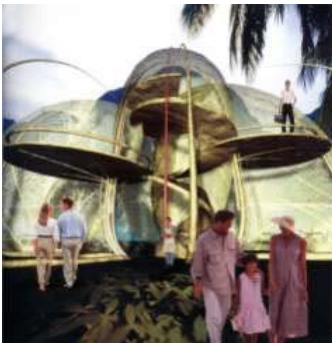
Day 3: The code developed from an architect's designs and then engineering and molecularly modelled, is ceremonially placed in the vat. We are amused that this code represents what long ago were the drawings, specifications, and strategies of construction management.

Day 4: Molecular growth, in the form of a vascular system, begins. This starts with roots stemming from the chemical composite. Reaching up and out of the vat to ground level, the roots form rudimentary "grade beams" extending horizontally to the edge of the house, where they curve upward to support the superstructure. Cross ribs connect the grade beams and form the ground floor platform.

Day 5: The cross of the superstructure starts with the development of primary exterior and interior vertical ribs. The infill of minor connecting ribs, "the lattice", also begins to develop. The lattices are of varied densities, and are programmed to meet stress requirements—being less dense and more open in pattern where door openings are specified, for example. Fine web work a membranes appear as protective enclosures an interior partitioning. A neural net works communicating via transmissions, and not pre-programmed, couples to the vascular system and begins operation.

Day 6: The upper platforms, supported by lateral brackets stemming from some the major structural ribs, are accessibly by a sprouting central spiral staircase. Exterior protective membranes conceal the interior. The molecules of the membranes link to create an unbroken fabric. The membranes provide openings for access that are prompted by two molecular activates first, the membranes are infused with electric current by a manual selector that induces the molecules to disengage and form the openings. Second, other molecules, acting as muscles at the opening edge, flex to draw the exterior membrane apart. We enter our house.

Fig. 3.5 a-b-c
Natural walls (left), exterior view (centre), diagrams of the days of the construction of the Molecular-engineered House (right).
(source: Johansen John, *Nanoarchitecture: a new species of architecture*)



Day 7: For the first time, we experience the space, ample for a small house. Ethereal light glows through the translucent membranes. With a signal, these membranes change from translucent to opaque to transparent, providing a view anywhere at any time desired. Our house is self-sufficient, functioning without dependence upon any outside public services. Solar power activates heating, cooling, recycling of wastes, and purifying of water. The vats and vascular system, vital to the growth of our house, remain and will convey additional material when repair or replacement is required. Interior finishes grow around us. "Body support," known previously as sofas, chairs, tables, and beds, are springing up from the floor, out from the wall ribs, and hanging from the arched vault – furniture as an extension of the structure itself. The floor, a "morphable topographic carpet," consists of resilient, molecular, spongy substance that is responsive to our every comfort, whim, or tactile experience.

Day 8: We return the next day to find our house more familiar. As a like "light modulator", the membrane responds to ever-changing conditions of the immediate environment to appear as cloudy, opalescent, gossamer, iridescent, and opaque. We have created an artificial, organic, protective cocoon.

Day 9: After six days of molecular growth, we move in. the house anticipates our changing needs, expanding the living space to form a small study, repartitioning the master bedrooms, rearranging and redesigned the "body supports", and extending the wheeled legs to a new site. This shape changes demonstrate the flexibility of the molecular engineering. In future years, if we cannot find a buyer for our house, we will demolish it, or more correctly, the house will demolish itself. The building growth operations will be recycled for future buildings.

3.4 The NanoHouse™, Australia

The NanoHouse™ Initiative was conceived in 2002 by Dr. Carl Masens at the Institute for Nanoscale Technology at the University of Technology, Sidney (UTS) with a multidisciplinary team that includes people from many institutions within Australia such as The Commonwealth Scientific Industrial Research Organization (CSIRO).

The NanoHouse was designed by the architect James Muir to illustrate what nanotechnologies are and how they work in a real building: for example, how the latest technology windows clean themselves, how tiles might resist build up of soap scum, or timber surfaces resist UV damage, etc.. The NanoHouse was planned to be as much of the house of the present as of the future incorporating products that already exist on the market. One of the main aim was achieving a good degree of flexibility to fit various environments and architectural needs. Furthermore, all components assemblies, subassemblies and building elements have also been coordinating to fit to standard shipping and trucking container sizes.

The NanoHouse has a radiative cooling paint as the outer surface of some of the roofing material: a metal roof coated with this paint will become a cooling element in a building rather than a source of unwanted heat gain. Other features are self-cleaning glass, cold lighting systems and the dye solar cell, a photovoltaic cell based



Fig. 3.6 a-b
NanoHouse logo
(top), system of the
windows (bottom)
(source:
www.nanoHouse.nl)



on titanium dioxide rather than silicon. It would be possible to construct a building with many more, larger windows than is currently viable, since heat can be kept out and UV photo-damage prevented. Reduction of the solar heat gain through windows reduces the need for cooling via air-conditioning, saving electricity. In certain parts of a building, solar thermal radiation is welcome, such as the exterior surface of a thermal mass. Even if it is surrounded with glass walls, the NanoHouse does not need any curtains. Glassy windows can be made almost opaque at the flick of a switch with suspended particle device (SPD) glass. It can be done manually with a switch, or automatically by attaching a sensing device and a controller, in much the same way street lights go on when it becomes overcast. The technology uses particles dispersed in a liquid or in droplets encapsulated in a thin plastic film. The particles align, allowing light to pass through when a charge is applied to a coating of electrically conductive transparent material. The particles return to random positions and block light when there is no charge. SPD glass can be used as substitute curtain for privacy. Other glass technologies are available to fill the insulation role of curtains. People are familiar with the use of dark colours to capture heat, but dark walls are ugly so, unsurprisingly, they rarely appear in house designs. There are nanotechnological solutions to the same problem: i.e. heat absorbent nano-particulate paints that are light-coloured in the visible part of the spectrum. Australian household applications utilizing nanotechnology extend beyond building materials and include clear sunscreens (Advanced Powder Technologies), supercapacitors for laptops and phones and smart paints.

Some of the types of technologies under consideration for inclusion in the house include:

- UV/IR filtering and reflecting windows for control of unwanted solar heat gain;
- self-cleaning TiO_2 coated glass;
- protective coatings for furniture offering UV protection;
- bottles, food containers etc. with tuned optical properties for the enhancement of shelf life of both containers and contents;
- cold lighting systems for the harvesting of daylight during the day and use with

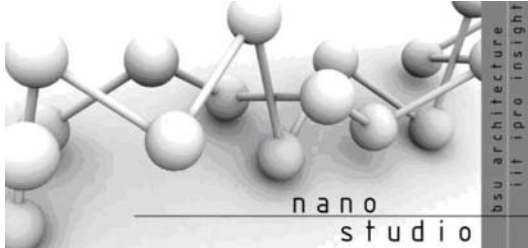
Fig. 3.7 a-b-c
Eastern computer
generated images of
the NanoHouse™.
(left and centre),
western image
(right). (source:
www.nanoHouse.nl)



ultra efficient bright white LED light sources;

- water quality control systems that remove pollutants from water, and clean effluent water;
- light coloured paints without glare and dark pigments for paints that do not retain heat.

3.5 The NanoStudio™, USA



In the NanoStudio, an interdisciplinary group of students from Ball University and Illinois Institute of Technology explore nanotechnology's potential impact on the built environment, as well as the social, ethical and environmental issues it raises.

The aim of the project is

designing buildings using nanomaterials including carbon nanotubes, quantum dot displays, and nanosensors to create new environments that are not limited by the constraints of traditional materials. The students' palette of materials included nanomaterials already developed in laboratories that are now working their way to market. These include transparent carbon nanotubes, nanosensors small enough to embed not only in building components but their users as well, and quantum dot lighting able to change the colour and opacity of walls and ceilings.

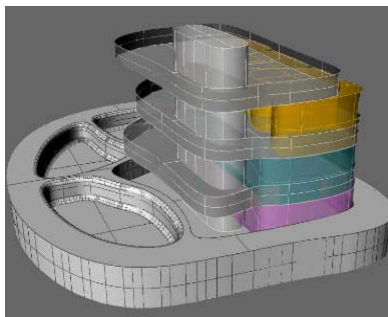
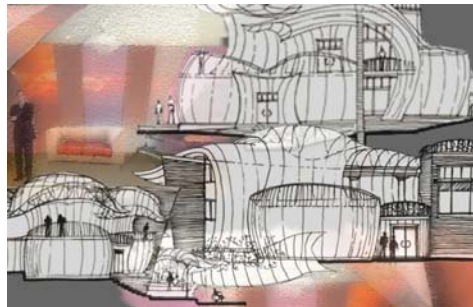
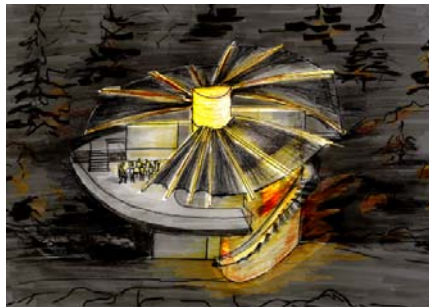


Fig. 3.8

NanoStudio logo.

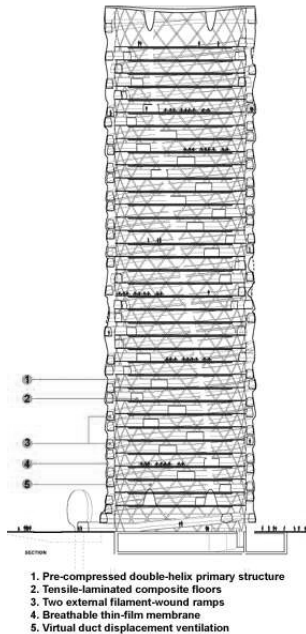
Fig. 3.9 a-b-c-d

Top left: vacation House, moveable walls and roof systems are made of a light nanowire paper that allows compact design and modifiable spaces. Quantum dots and nanosensors are incorporated to control lighting and built environment in a passive way.

Top right: NanoShell study.

Bottom: NanoSpa. The use of CNTs, nanosensors and nano-display screen technology in external envelope make people feel like they are in a different location depending on nanomaterials adaptability and changeability. (source: da-headley.iweb.bsu.edu /NanoStudio2)

3.6 The Carbon Fibre Tower, USA



The architect Peter Testa, with his partner Devyn Weiser and with the help of Arup New York designers, proposed in 2002 a prototype 40-story skyscraper made entirely of composite materials, mostly carbon fibre. According to Testa, whose firm Peter Testa Architects is located in Santa Monica, California, the willingness to use complex computer modelling tools will allow the design of new buildings, materials, and products that might transform the building industry. Although the materials seem well suited for architecture - in tension carbon fibre is five times stronger than steel - their use in buildings has been very rare. Testa, though, is convinced that (nano)composites will radically transform architecture during the next decade or two. His carbon skyscraper, which he likes to describe as a “woven building”, is designed to be not just less muscle-bound than the skyscrapers in which Americans work today but also more beautiful, environmentally friendly, and cheap to build. Testa’s carbon fibre tower is the product of ongoing research in computer-aided engineering and material science. But the basic form is not especially complex: a cylindrical building 40 stories high. Then picture that cylinder strung together by 40 carbon-fibre strands, about 1 inch (2,54 cm) wide and nearly 650 feet (198 m) long, that are arrayed in a helicoidal, or crosshatch, pattern. Filling in the structure between floors is an advanced glass substitute. A pair of ramps on the exterior of the building offers circulation and further stabilizes the structure. That, in simplified form, is Testa carbon tower.

Fig. 3.10
 Longitudinal section
 (top) and plane (bot-
 tom) (source:
 www.peter-
 testa.com)

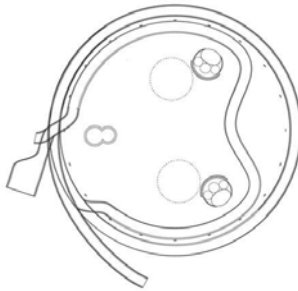
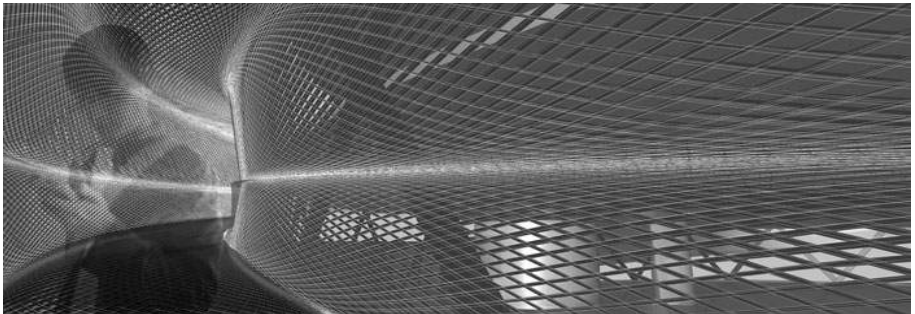


Fig. 3.11
 The primary structure
 would be woven from
 carbon fibre and all
 the components, in-
 cluding ramps lead-
 ing to a typical office
 floor, would be
 manufactured from
 composite materials.
 (source: www.peter-
 testa.com)



In the building there are no traditional materials such as concrete, steel or conventional glass but every major element, including the floors and the exterior ramps, is made of some kind of composite material. Amazingly important is the structural use of continuous carbon strands, which are woven to form a structure that distributes its loads over its entire surface.

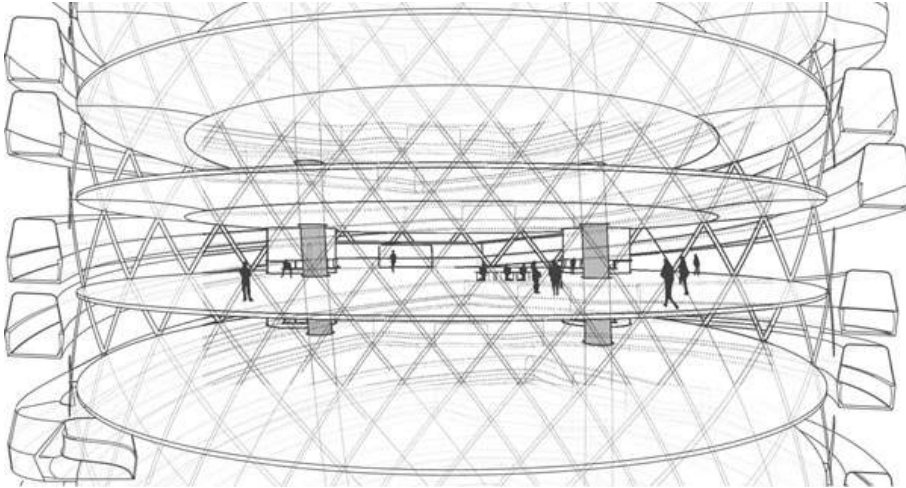


Fig. 3.12

Floors are accessed by elevators and by two perimeter ramps, that also help in distributing air and providing solar protection.

(source: www.peter-testa.com)

The tower aims to reconfigure all three central elements of contemporary skyscraper design: structure, circulation, and heating-and-cooling systems and taken together, the building's innovations open up the potential for what Testa calls a new "organic minimalist aesthetic" — a building whose surface and structure are one and the same. The 24 strands will be fixed into shape by something called a robotic pultrusion machine, which Testa envisions climbing up the structure like a spider and weaving the strands on the side of the tower as it is built. "You just bring a bundle of fibres and some plastic to the site, and then you manufacture the building right there", he says. "Each of the strands will have its own machine".

That method would offer obvious energy-saving advantages over traditional construction techniques, but there is another dramatic benefit as well.

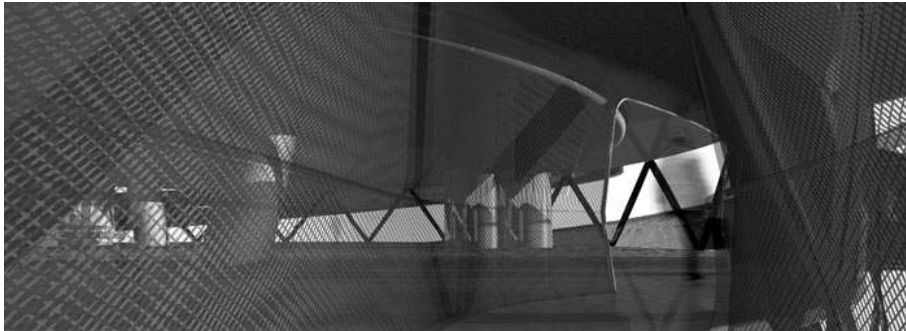


Fig. 3.13

Render image.

(source: www.peter-testa.com)



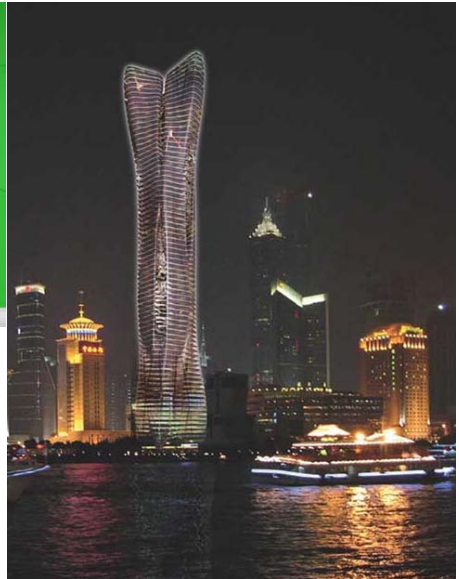
Fig. 3.14
Render image.
(source: www.peter-testa.com)

As Testa envisions it, this 40-story skyscraper won't need any vertical structural elements: no columns between floors, no central core. Air circulation would be handled through a pair of continuous open cylinders, or "virtual ducts", that run from the top of the building to the bottom and operate on the kind of displacement ventilation system that is already appearing in some European buildings. Three groups of elevators are distributed throughout the floor plan, instead of being crowded together at the core.

3.7 Laboratory for Visionary Architecture (LAVA) – Branded Towers



Fig. 3.15 a-b
Left: LAVA logo.
Right: Branded tower
render. (source:
www.l-a-v-a.net)



LAVA was founded by Chris Bosse and Tobias Wallisser in 2007 with the motto "Green is the new black". The founders think that architecture has always been, and always will be, the mirror of the society reflecting the current technology. In a certain way they want to reposition the role of man in the natural environment using the latest advances in computing and building technology.

The Branded Tower is a concept tower prototypical building that will be located at strategically chosen locations around the world. This tower is claimed by some to become the successor of the actual towers that dominate our cities. With intelligent systems and skins, it can react to the external influences such as air-pressure, temperature, humidity, solar-radiation and pollution.

To create a robust and light-weight structure new materials and technology will be used to harmonize the building to its surroundings.

Among the Branded Towers planned by LAVA, the Michael Schumacher Tower is a plan for an unprecedented series of branded towers featuring in seven cities

worldwide to mark Michael Schumacher's extraordinary feat of seven World Championship titles.

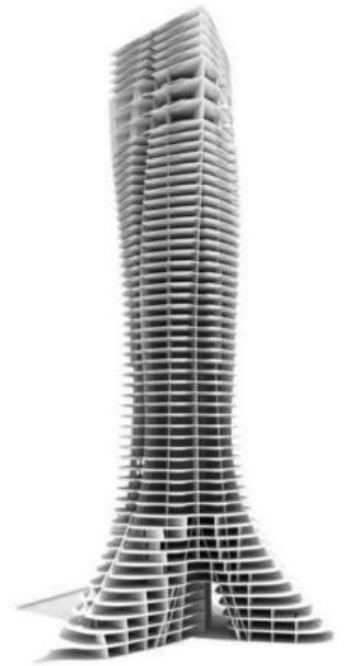
More particularly, the Michael Schumacher World Champion Tower was launched in Abu Dhabi using some new high-tech materials to create an intelligent building systems that will work together with the ergonomic design of the interior to make an efficient, seamless living environment. The 250 m high structure is located in Abu Dhabi's Central Business District on Reem Island and it is the first wharf tower in the world.

The ecological impact of the Abu Dhabi tower will be limited using the most conscientious and advanced methods available such as the followings:

- cogeneration of power;
- low to zero emissions from incineration of waste;
- central cooling and free cooling from the sea;
- photovoltaic cladding;
- sun shading to reduce heat load;
- high performance building management and maintenance systems.

Water efficient technology is an other important factor in the plans, with customisable settings for domestic usage as well as on-site water conservation measures.

Fig. 3.16 a-f
MSWC Tower renders with Abu Dhabi skyline. (source: www.mswct.com)



3.8 Shimizu TRY 2004 Mega-City Pyramid, Japan

The Shimizu TRY 2004 Mega-City Pyramid is a proposed project for construction of a massive pyramid over Tokyo Bay in Japan.

The masterplan was made by the Italian architect Dante Bini⁵ and sponsored by the Japanese Shimizu Corporation. If built, it would be the largest man-made structure in Earth's history (2004 m high) but, according to Discovery Channel, it would be complete only within the year 2110 as nowadays this structure is not feasible with current technology and resources. Engineering and some laws of physics do not allow for such structures to be built, due to complex issues such as basal water pressures to be delivered 2000 m up, as well as wind cross-shears on the structures inside the pyramid.

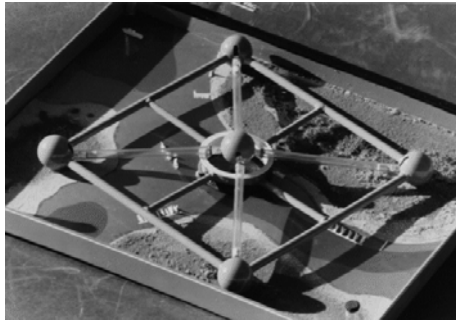


Fig. 3.17
Shimizu Mega-city
Pyramid foundation's
position over Tokyo
Bay. (source:
www.shimz.co.jp)

This pyramid would help answer Tokyo's increasing lack of space, although the project would only handle 1/47th of the Greater Tokyo Area's population. The structure would be about 14 times higher than the Great Pyramid at Giza, and would house about 750.000 people. The structure would be 730 meters above mean sea level (AMSL). The proposed structure is so large that it cannot be built with

currently available materials, due to their high weight. The design relies on the future availability of super-strong lightweight materials based on carbon nanotubes.

The dimensions are impressive: the foundation's perimeter would be 2004 m with an area of 8 square kilometres. The connected infrastructure would occupy an area of approximately 25 square kilometres while the gross building area is about 88 square kilometres of facilities layers of 146,4 m height each one, for 5 layers, the pyramid is 730m tall:

- layers 1 to 3: residential, offices, etc.
- layers 4 to 5: research, leisure, etc.

Its construction would be technically complicated as the pyramid structure would be composed of 204 smaller pyramids stacked eight high. The pyramid's foundation would be formed by 36 piers made of special concrete. Because the seismically active Pacific Ring of Fire cuts right through Japan, the external structure of the pyramid would be an open network of megatrusses, supporting struts made from carbon nanotubes to allow the pyramid to stand against and let through high winds, and survive earthquakes and tsunamis.

The trusses would be coated with photovoltaic film to convert sunlight into electricity and help power the city that will also be powered by pond scum or algae.

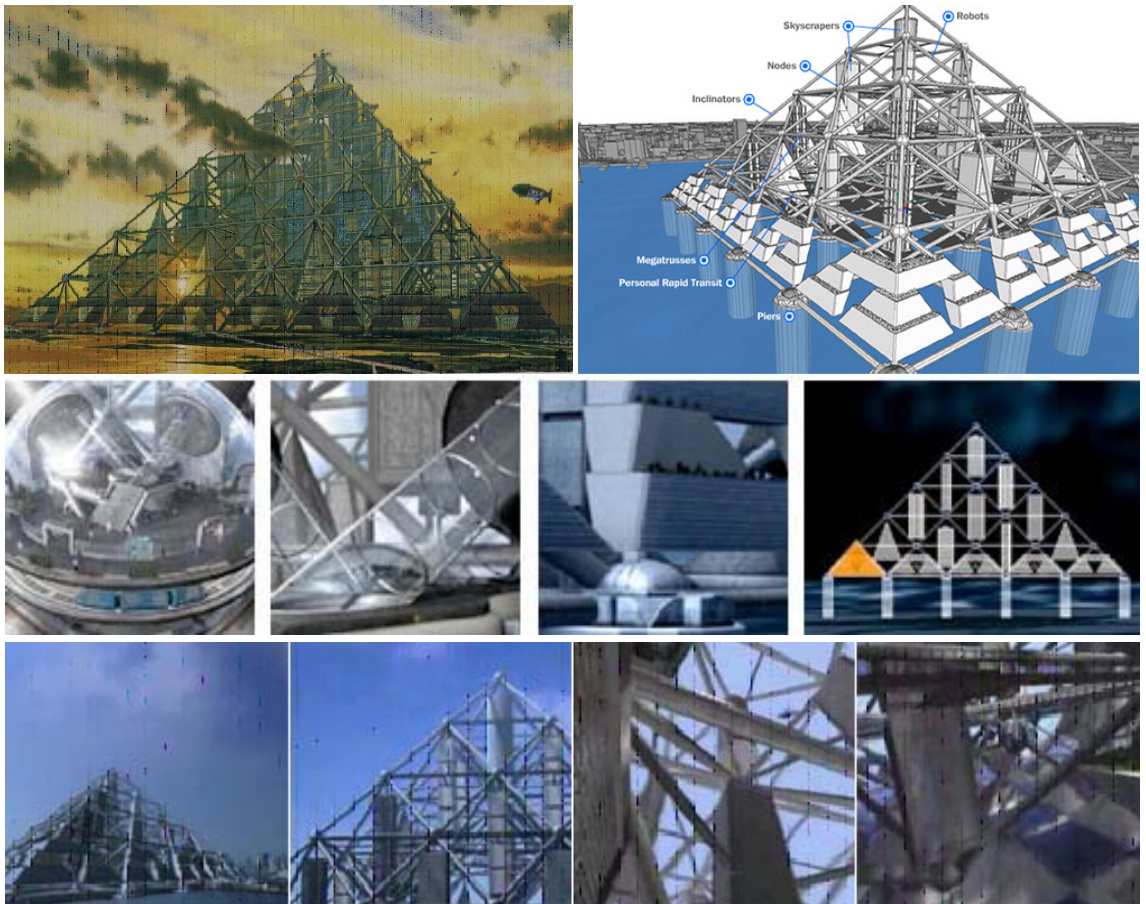
⁵ Dante Bini (born 1932) is an Italian architect, known as the architect of the pyramids due to the structure that he mostly studied and built. He is a pioneer in automated building construction systems and head of the Binisystems.

Large robots would assemble the truss structure, and air bladders would be used to elevate trusses above the first layer using a construction system proposed by Italian architect Dante Bini. Spheroid nodes at the connections between trusses would provide structural support and serve as transfer points for travellers.

The building would be zoned into residential, commercial and leisure areas. 50 km² would be given over to some 240.000 housing units, enough for 750.000 people. Each building would have its own energy resources (sun and wind). About 24 km² would be assigned to offices and commercial facilities intended to employ 800.000 people. The remaining 14 km² would be used for research and leisure purposes.

Australian Company, Straight Edge Tiling, have secured a contract for the internal tiling of the Pyramid. CEO Daiman Cartan met with construction engineer David Dimitric and lawyer Tavis Gorman in December 2007 to discuss innovative concepts regarding the huge task, as well as legal boundaries, to which an agreement was made.

Fig. 3.18 a-l Shimizu Mega-city Pyramid renders. (source: www.shimz.co.jp)



3.9 NanoCity, India

The NanoCity is a visionary project developed by the Haryana Government and Saabeer Bhatia of Hotmail fame as a joint venture near Panchkula. It has been designed by the Berkeley Group for Architecture and Planning (BgAP), University of California, Berkeley, to develop a sustainable city with world class infrastructure and to create an ecosystem for innovation leading to economy, ecology and social cohesion. NanoCity spans 4500 ha of flatland beyond the foothills of the Himalayas. More precisely, it is located about 25 km east of Chandigarh and just 200 km north of Delhi. NanoCity has been designed on three main principles:

- green-city: uses context as opportunity, promotes a lush and shaded climate-sensitive environment, encourages the expansion of local natural systems and advances ecologically intelligent and sustainable design. Half of the land will thrive as a green open space; the urban infrastructure will be ecologically intelligent and sustainable by outfitting the buildings with energy efficient systems based on new high-technologies and renewable energy sources.
- flex-city: creates an adaptable and evolving framework - based on nanomaterials - that is flexible over time, responds to changing needs and adjust to future uses and patterns of growth.
- complex-city: proposes a city of mixed use districts, encourages a dynamic sequence of neighbourhoods and open spaces, defined unique nodes of density and character linked by an efficient system of transportation and communication.

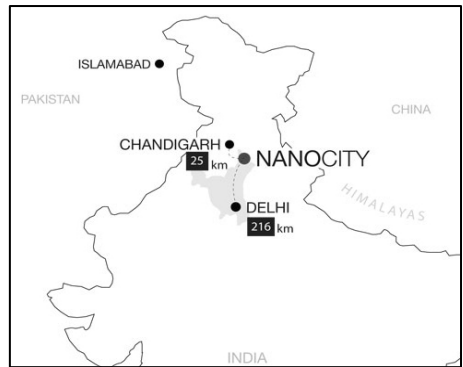


Fig. 3.19
NanoCity location.
(source:
www.nanocity.in)



Fig. 3.20
NanoCity master-
plan. (source:
www.nanocity.in)

Parks and open spaces help facilitate healthy living and create positive social environment that gives citizens a common sense of belonging. The urban structure has been developed as mixed-use buildings with the street level devoted to business and trade and the upper floors allocated for residential use thus creating a market of mutually complimentary and supportive services and activities.

The most attractive NanoCity claims are the sustainability and sustenance as the new town will preserve the naturally existing resources of the land and living nanomachine technology will provide NanoCity with the capacity to convert waste-water into odour-free drinking water. Half of the energy used in the city will come from renewable sources: wind, solar and photovoltaic technologies. Buildings will use climate responsive design techniques or new energy-saving materials such as sun shading, cross ventilation, direct evaporative cooling or phase changing materials.



Fig. 3.21 a-b
NanoCity renders.
(source:
www.nanocity.in)



3.10 Sylvia Leydecker: nanoapplication in interiors, Germany

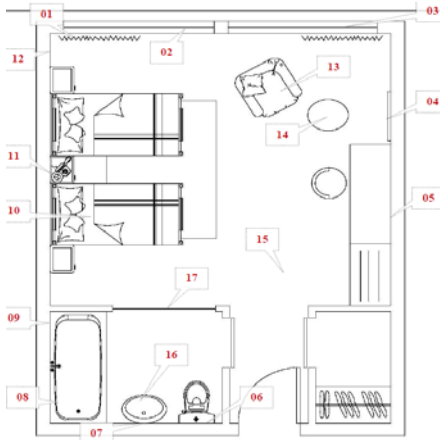


Fig. 3.22
Sylvia Leydecker.

Sylvia Leydecker is a German interior architect, leader of the Office 100% Interior in Cologne. She focuses her research on the application of nanotechnology in architecture trying to apply new nanostructured materials in her projects.

Below, two schematic plans for a hotel room and a bank branch room demonstrate her concepts in using nano-functions in interior design. The spaces are optimized through the strategic use of nanosurfaces with regard to aesthetic, economical and ecological concerns.

Leydecker is confident that although these new concepts are visionary, they could already be realized today in this or a similar form.

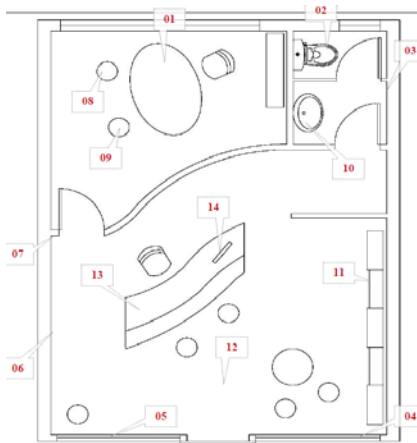


1	Curtains: air-purifying
2	Window: self-cleaning glass, photocatalytic, photochromatic or electrochromic
3	TV: antireflective
4	Wall-paint: air-purifying
5	WC: easy-to-clean
6	Sanitary-ware: anti-fingerprint
7	Mirror: anti-fogging
8	Bathtube & shower: easy-to-clean
9	Bathroom walls: nanoparticles ceramic walls
10	Bed: antibacterial
11	Light switches: antibacterial, non-stick
12	Upholstery: air-purifying
13	Glass-table: anti-fingerprint
14	Carpet: air-purifying
15	Frosted-glass: anti-fingerprints

Fig. 3.23

Nanostructured materials used in the interiors of a hotel room.

(source: Leydecker S., *Nanomaterials in architecture, interior architecture and design*)



1	Glass table: anti-fingerprints
2	WC: easy-to-clean
3	Walls: nanoparticles ceramic covering
4	Window: self-cleaning, photochromatic
5	Window: self-cleaning, photochromatic
6	Walls: nanoparticles ceramic covering
7	Switches and handles: anti-bacterial, non-stick
8	Chairs: dirt-repellent
9	Upholstery: air-purifying
10	Sanitaryware: anti-fingerprints
11	Screen: anti-reflective
12	Carpet: air-purifying
13	Counter: anti-fingerprint
14	Screen: anti-reflective

Fig. 3.24

Nanostructured materials used in the interiors of an office room in a bank branch.

(source: Leydecker S., *Nanomaterials in architecture, interior architecture and design*)

4. Nanomaterials: new materials in construction

4.1 Introduction

Nanomaterials are defined as those materials that have at least one dimension in the nanometre scale. At that scale, nanomaterials show dramatic changes and new properties that cannot be usually reported at the macroscopic scale. This new phenomenology often includes surface and interface phenomena, electronic confinement and quantum mechanics in general. The new generation of construction materials must be investigated within a scientific approach addressed to create multifunctional high performance materials and a more economically way of production. Furthermore, it must be said that far from being just a science and technology fashion, nanotechnology is a necessary path to achieve a real competitive and sustainable growth and innovation within the construction industry.

4.2 Nanotechnology R&D in Construction, a 2005 survey

In 2005, a selection of a 150 individuals and companies, representing researchers, engineers, architects and contractors from EU and worldwide were contacted for a survey in order to understand the state of knowledge, progress and applications of nanotechnology to the construction industry (source: EU commission).

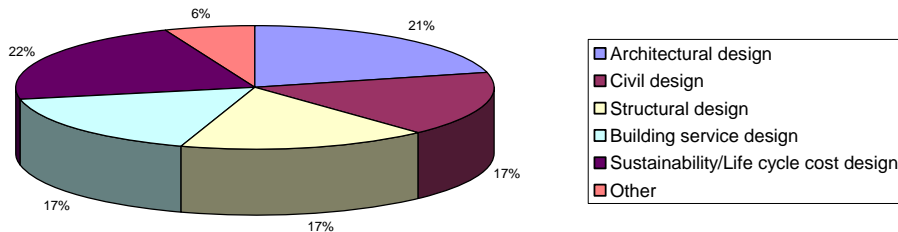


Fig. 4.1 Design area of the respondents.

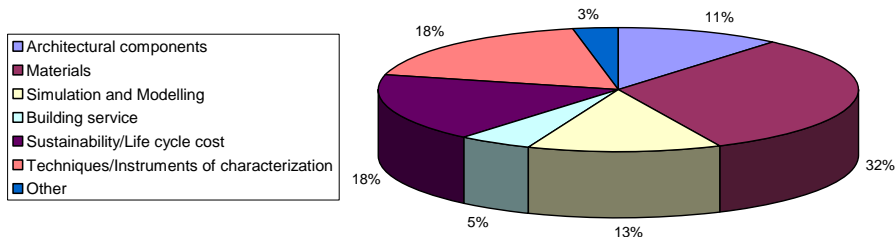


Fig. 4.2 Research area of the respondents.

A large majority of respondents stated that they are involved in research and many come from either universities or government bodies and are involved in design on several construction fields (fig. 4.1 and fig. 4.2). This is quite important as those who are in the research and management field are most likely to be knowledgeable of nanotechnology in construction.

Fig. 4.3
Knowledge of nanotechnology in general.

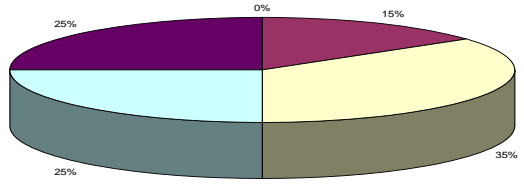
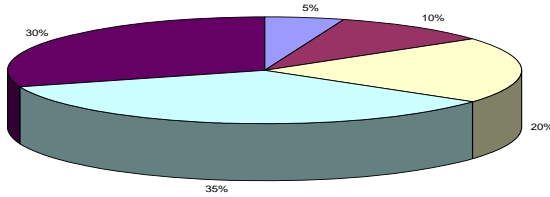


Fig. 4.4
Knowledge of nanotechnology in the construction field.



It's noteworthy that the majority of respondents stated that they have a good knowledge of nanotechnology (fig. 4.3) with direct applications to the construction field (fig. 4.4) as they are involved in this research sector. Only a few percentage of people (5 + 10 %) have a very little knowledge of this specific area.

Fig. 4.5
Kind of x-based materials that are object of research.

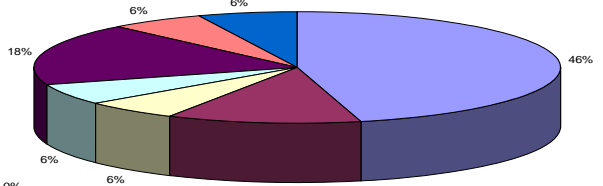
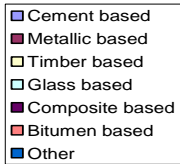
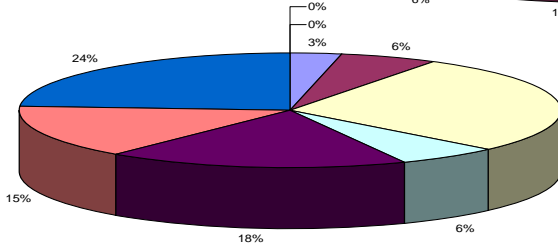
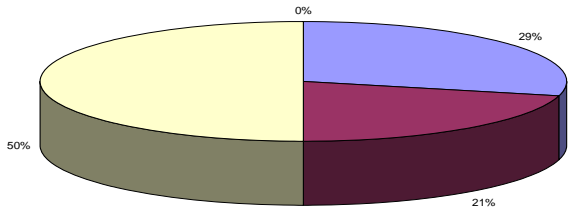
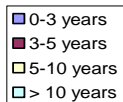


Fig. 4.6
The future about nanotechnology in building materials.



The most of the researches are focused on studying cement-based and metallic-based materials which seem to be the most sensible materials to nanoparticles incorporation research (fig. 4.5) but, in the future, the nanocomposite materials will probably lead the research (fig. 4.6) thanks to their advanced properties.

Fig. 4.7
How long new nanotechnologies will take to arrive on the construction market.



The last point that should be looked at is the number of years a new nanotechnology will take to arrive on the construction market, by researchers feelings. As it is possible to see from figure 4.7, in the previous page, research in the construction sector is at an early stage and the most of the studies are only at the beginning. Thus, new nanomaterials and nanoproducts will probably take a lot of ages before being ready to suit the markets requirements.

4.3 Nanomaterials in construction

The examination of worldwide nano-based activities related to the construction sector appears to indicate that a significant impact will be given by the following areas:

- understanding phenomena at nanoscale;
- new production techniques, tools and controls;
- nanostructured and nanocomposite modified materials;
- high-performance structural materials;
- special coatings, paints and thin films;
- multifunctional materials and components;
- smart materials, devices and sensors;
- integrated monitoring and diagnostic systems;
- energy saving devices.

One of the most ultimate and debated goal of nanotechnology is molecular manufacturing based on self-assembly or self-replicating nano-machines (thus the buildings that build themselves).

Generally speaking, it is possible to define the following sectors:

1. High-performance structural materials: the most significant example is perhaps the nanostructure modified steel reinforcement or the modified nanostructured concrete. Other applications are high strength ductile ceramics, glass and polymer nanocomposites.
2. Functional coatings and thin films: incorporating certain nanoparticles into transparent coatings and thin films may provide enhanced performance and additional functionalities. Nowadays, several composites have been produced and marketed for construction: self-cleaning, thermal/control energy saving, anti-reflection coatings for glass and windows, easy-to-clean and antibacterial coatings for work surfaces, more durable paints and anti-graffiti coatings.
3. Nano-fillers, additives and admixtures: this area is perhaps the most commercially developed/studied and the use of these nanoscale materials has been the basis for many current and potential applications in various industrial sectors such as electronics, healthcare, chemical, defence, energy, automobile, construction, etc.. Several nanoparticulate materials (e.g. TiO_2 , SiO_2 , CaCO_3 , etc.) have been widely used as fillers/additives in coatings, paints, adhesives and sealants. For example, carbon black nanoparticles have been added to rubber to increase wear resistance; nanoclay and nanotubes are increasingly used as rein-

forcement in high performance composites. Dispersion of amorphous nanosilica powder is produced as concrete admixture to improve segregation resistance for fresh self-compacting concrete or to enhance strength and durability of hardened concrete. Nano-particulate materials have also been used in environmental friendly anti-corrosion coatings for steel reinforcement and water-proofing admixtures for concrete. Furthermore, nanoparticles, carbon nanotubes and nanofibres help in developing new functional materials, devices and systems for construction and built environment.

4. Environment and Performance monitoring sensors: microscale sensors, devices and systems have already been used in construction and built environment to monitor and/or control the environment conditions such as temperature, humidity, gas noise etc. and the materials/structure performance such as stress, strain, vibration, pressure, corrosion, etc.. The nanotechnology approaches are not only enabling sensors/devices to be made much smaller, more reliable and energy efficient, but also opening up new possibilities beyond the reach of mere microscale manufacture.

Other new products and applications: many other nanotechnology enabled developments and materials/products are fast emerging or already exist in bulky and expensive forms in different industrial sectors. With the continuing reduction of size and affordability and improvement of performance, these products and developments are also likely to impact on construction process and the built environment in the short to medium term.

4.4 Reports

We are now going to analyze, in a more detailed way, a list of products and technologies that are already available on the construction market or some studies, researches and activities strictly related to construction and architecture.

All the materials and technologies analyzed will be grouped depending on the applications or on the main materials they could be used for.

In any case, this is not an exhaustive listing of all the nanomaterials available.

The main groups are:

1. Nanotechnologies for glass-based materials;
2. Nanotechnologies for cement-based materials;
3. Nanotechnologies for steel-based materials;
4. Nanotechnologies for wood-based materials;
5. Nanotechnologies for quality and comfort;
6. Nanotechnologies for energy control and saving;
7. Nanotechnologies for sensing;
8. Nanotechnologies for preservation and archaeology.

5. NANOTECHNOLOGIES FOR GLASS-BASED MATERIALS

5.1 Thin films for architectural glazing

5.1.1 Solar protection

Solar protection against heat gain from solar radiation is offered by two kinds of self-darkening glass: the electrochromic glazing and the photochromatic ones. Electrochromatic switchable glazing was previously available on the market but has since largely disappeared due to two main disadvantages: first, a constant electric current was necessary to maintain a darkened state and, second, large glass surfaces often exhibited optical irregularities.



Fig. 5.1
Electrochromic glazing in construction applications. (source: Leydecker S., *Nanomaterials in architecture, interior architecture and design*)

Nanotechnology has provided a new means of integrating electrochromatic glass in buildings. The primary difference to the earlier product is that a constant electric current is no longer necessary. A single switch is all that is required to change the degree of light transmission from one state to another.

Different levels of light transmission with various darkening effects are also possible, either as a smooth gradient or clearly differentiated, with a minimal electrical energy requirement and the switching process itself takes a only few minutes. Nowadays, the range of panel size currently available on the market, is relatively limited with a maximum size of 120 x 200 cm at present.



Fig. 5.2
Julbo-race USA
photochromic
sunglasses.

Photochromatic glazing is another solution for darkening glass panels. Here the sunlight itself causes the glass to darken automatically without any switching. This kind of technology is generally used in glass technology but producers are employing new advanced researches in this field.

5.1.2 Selective coatings: IR protection (Thermochromic coatings)

A thermochromic material changes its optical properties with changing temperature. More particularly, a thin film of thermochromic material might be used to create an intelligent window that may change its transmittance and reflectance properties in response to environmental changes in order to regulate the temperature within a room.

A suitable material would become more reflective – and therefore less transmitting – in the infrared (IR) region at higher temperatures. Hence, at low temperatures, in the transmitting state, solar thermal energy is allowed into the room to cause warming. At higher temperatures, in the reflecting state, the coating reflects most of the infrared solar energy whilst ideally transmitting as much visible light as possible.

These windows would be suited to geographical regions where the temperature may change dramatically during a day or over the year, such as most of Europe, Asia and North America.

A thermochromic film is therefore a type of advanced solar control coating that actively responds to a user's need.

By far the most promising candidate material for coating a thermochromic window is vanadium (IV) dioxide. VO_2 undergoes a metal-to-semiconductor transition at a critical temperature (T_c) changing from a transmitting state typical of a thin semiconductor film to a reflecting state typical of a metallic film. This change is a phase transition between rutile and monoclinic polymorphs, which is reversible in thin films of the material.

These kind of coatings will be widely discussed in section 2 of this thesis.

5.1.3 Selective coatings: UV protection

UV protection is in great demand in architecture as woods or coloured surfaces might change colour significantly when exposed to UV light.

Ultraviolet light is an electromagnetic radiation with an energy that varies between 3 eV and 124 eV and a wavelength that range from 10 nm to 400 nm.

The ISO 21348:2004 “Definitions of solar irradiance spectral categories” describes the following ranges within the UV spectral category:

Tab. 5.1 UV spectral range according to the draft ISO-DIS-21348			
Spectral sub-category	Abbreviation	Wavelength range l [nm]	Energy of photon [eV]
Ultraviolet A (black light)	UVA	400 – 315	3.10 – 3.94
Near	NUV	400 – 300	3.10 – 4.13
Ultraviolet B	UVB	315 – 280	3.94 – 4.43
Middle	MUV	300 – 200	4.13 – 6.20
Ultraviolet C (germicidal)	UVC	280 – 100	4.43 – 12.4
Far	FUV	200 – 122	6.20 – 10.2
Vacuum	VUV	200 – 100	6.20 – 12.4
Low	LUV	100 – 88	12.4 – 14.1
Super	SUV	150 – 10	8.28 – 124
Extreme	EUV	121 – 10	10.2 - 124

Many polymers used in construction are degraded by UV light. The problem appears as discoloration or fading, cracking and, sometimes, total product disintegration. The attack rate increases with exposure time and sunlight intensity. Furthermore, many pigments and dyes absorb UV and change colour, so paintings and textiles need extra-protection both from sunlight and fluorescent bulbs, two common sources of UV radiation. Common window glass provides some protection by absorbing some of the harmful UV, but valuable artefacts need an extra shielding.

UV protection may be achieved using both organic or inorganic materials with different kind of advantages and disadvantages. Furthermore, a prerequisite of protective coatings is that they are transparent so that the colouring and structure of the

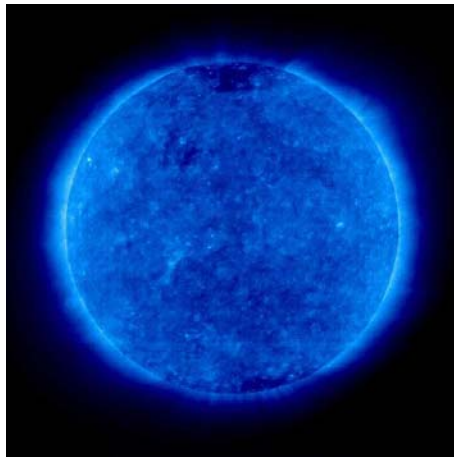


Fig. 5.3 False-colour image of the sun's corona as seen in deep ultraviolet by the Extreme Ultraviolet Imaging Telescope (source: NASA).

material beneath, usually glass, is preserved. Thus, the UV-absorbing particles must be smaller than 15 nm in size. Below this size they no longer scatter visible light and become effectively invisible. Larger particles, or the agglomeration of smaller particles to large aggregates, lead to a noticeable cloudiness in the formulation.

The organic methods that are usually used are of two kinds and employ additives. One method involves the use of UV absorbers that filter out the harmful rays in sunlight before they come into contact with the material itself. In this way they need to be deposited as an upper layer. The second approach uses free-radical scavengers that take effect at a later stage as they prevent the continued degeneration of an already damaged material. They react with the free-radicals that UV light forms and convert them to inert compounds. This kind of additive is typically impregnated in the material itself. The main disadvantages of both approaches is that neither is able to offer absolute protection and, furthermore, as they are organic, they are therefore themselves subject to a degree of degeneration through UV light. This means that their protective effect decreases over time not providing a durable and lasting protection in the long run.

A new means of UV protection using inorganic substances represents an innovation. Their primary advantage is that they do not themselves degenerate and, therefore, provide a lasting protective effect. Three compounds are particularly suited for this purpose: titanium dioxide (TiO_2), zinc oxide (ZnO) and cerium oxide (CeO). TiO_2 mainly absorbs the energetic UV-B rays leaving the UV-A spectral region unaffected; ZnO provides protection against both UV-A and UV-B rays; CeO absorbs UV rays as well as a part of the visible light resulting in a yellowish colouring.

5.1.4 Anti-fogging coatings

As soon as moisture condenses or settles on surfaces it forms many small droplets that combine clouding the surface itself. The phenomenon of condensation is the change in the phase of matter from the gaseous phase into liquid droplets or solid grains of the same element/chemical species. Upon the slowing down of the atoms/molecules of the species, the overall attraction forces between these prevail and bring them together at distances comparable to their sizes. Condensation on a window or on a mirror are typical examples of this phenomenon and the only way to maintain a clear view is heating the glazing continually making the moisture evaporate.



Fig. 5.4

Typical water condensation on a window. (source: Leydecker S., *Nanomaterials in architecture, interior architecture and design*)

By means of nanotechnology a permanent clear view is possible without the use/waste of electricity. More particularly, a thin film made by titanium dioxide, TiO_2 , could be applied to coat surfaces. Titanium dioxide, for instance, exhibits a high surface energy and therefore greater moisture attraction. On hydrophilic sur-

faces, moisture forms an ultra-thin film instead of water droplets so, though it still settles on the surfaces, it remains invisible. The film is transparent creating a fog-free clear appearance. In a building, the most sensitive surfaces attached by condensation are windows, glasses, mirrors, etc..

Anti-fog treatments were first developed by NASA during Project Gemini¹ to avoid helmet visors get dirty. In June 1966, during Gemini 9A the astronaut Eugene A. Cernan tested a NASA's first space suit discovering, during a space walk, that his helmet visors fogged.

The first patent for building applications is recorded in 1998 and nowadays, many industries produce these kind of coatings such as the Film Specialities, Inc. (USA).

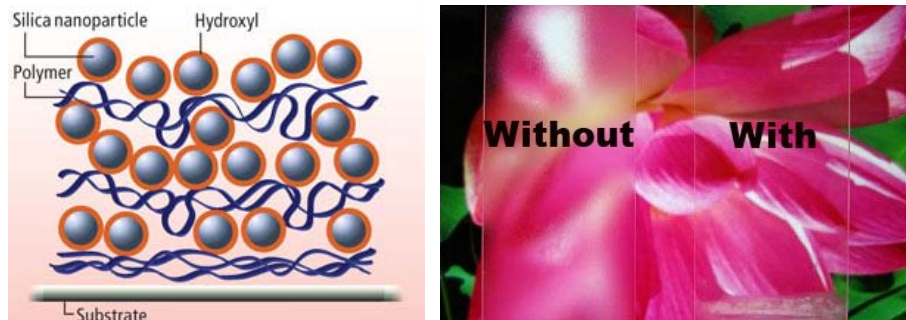


Fig. 5.5 a-b

Left: schematic representation of the technology developed at MIT. (source: Rubner M., Cohen B., MIT)

Right: the Defense Advanced Research Projects Agency (DARPA) is one of the major funders of the projects having a foggy windscreen.

Another method was discovered by Michael Rubner and Bob Cohen at the Massachusetts Institute of Technology (MIT) in 2005 (fig. 5.5). A glass-like nano-porous surface made by depositing alternating layers of a polymer called polyallylamine hydrochloride and silica nanoparticles contains tiny holes made by nanoparticles. The surface appears completely flat to the naked eye but is in fact super-hydrophilic. Moisture is drawn into the tiny pores thereby stopping water droplets from forming. A similar coating has been developed at the University of Queensland in Australia where a start-up, called XeroCoat, was made to bring the new product to the market. Anti-fogging sprays are effective as a temporary means of making surfaces appear clear but the effect does not last long and sometimes the application techniques are quite difficult and expensive.

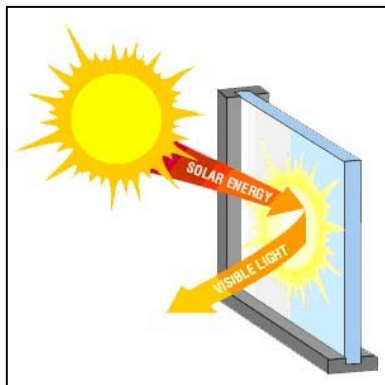
5.1.5 Anti-reflective (or anti-reflection - AR) coating

The transmission of light through transparent materials such as glass or plastic, which reflect some of the incident light, is reduced by the reflection of light rays. Plain glass, for instance, allows a maximum of 90% of incident light to pass through it. This phenomenon is caused by a change in the refractive index as light

¹ Project Gemini was the second human spaceflight program of NASA. It operated with 10 manned flights occurring between 1965 and 1966. Gemini missions included the first American spacewalk and new orbital maneuvers.

passes through two different media (e.g. glass and air). The decisive aspect is therefore the refractive index.

Fig. 5.6 a-b
Left: Scheme of a reflective glass.
Right: Anti-reflective glass installed in a building. It is possible to look outside the building, through the glass, without the inside being reflected on the glass



The use of anti-reflective glass to solve the problem of reflection is in itself nothing new, but traditional anti-reflective construction materials generally involve a complicated manufacture thus it is quite expensive. Transparent nanoscalar surface structures, where the particles are smaller than the wavelength of visible light, offer not only an innovative but also a cost-effective and efficient anti-reflective solution. Their structure consist of 30-50 nm large silicon-dioxide (SiO_2) balls. A single interference layer is applied by dipping the glass, or plastic, in the solution and functions across a broadband spectrum of light. The refractive index of the outer layer is very small and can be defined precisely, as can the thickness of the coating. A thickness of 150 nm is regarded as ideal. The ratio of reflected light is reduced from 8% to less than 1%.

In general, a nano-coating has a long lifespan and is more susceptible to dirt than normal glass. Furthermore, in comparison to conventional anti-reflective glass, a nanoscalar coating has a higher abrasion resistance, making it all in all well suited for everyday use.

Another cost-effective means of producing anti-reflective surfaces is the moth-eye² effect. The cornea of moths (fig. 5.7 a), which are active mostly at night, exhibit a structure that reduces reflections. The Fraunhofer Institute, directed by prof. Andreas Tünnermann, for Solar Energy Systems ISE, for Silicate Research ISC and for Applied Optics and Precision Engineering IOF in Jena (Germany) has developed a similar structure that can be impressed, or injection-moulded, onto glass (fig. 5.7 b, d). Using hot-process embossing, the visual transmission of glass can be increased to

² Moths' eyes surfaces are covered with a natural nanostructured film which eliminates reflections. This allows the moth to see well in the dark, without reflections to give its location away to predators. This kind of antireflective coating works due to the bumps size as they are smaller than the wavelength of visible light. The light sees the surface as having a continuous refractive index gradient between the air and the medium, which decreases reflection by effectively removing the air-lens interface.

over 98% and of plastics, such as acrylic glass, to over 99%. In addition to its anti-reflective function, dirt-repellent and anti-static properties can also be integrated.

A similar study was conducted by researchers from the Department of Physics and Mathematics at University of Joensuu, Finland. They have introduced an anti-reflective surface that provides significant reflection suppression below 0.45% for the visible wavelength band from wide angles (fig. 5.7 c). The design does not alter visual colour perception and it also repels water. Furthermore, the surface can be easily applied using high-precision, low-cost fabrication techniques.

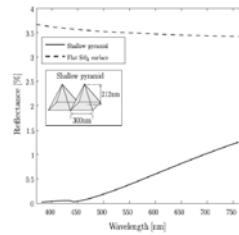
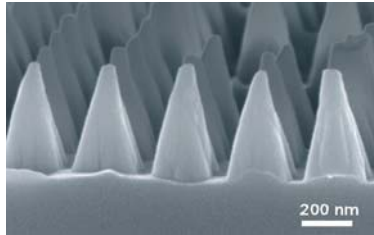
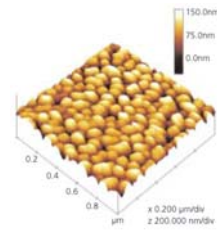
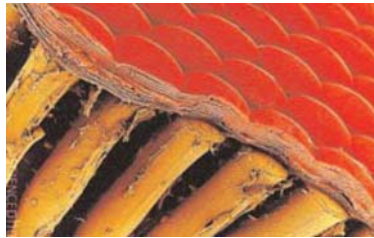


Fig. 5.7 a-d
Top left: Scanning Electron Micrograph (SEM) image of a moth's compound eye.

Top right: AFM image of a compound eye structure creating using a low-pressure plasma process. (source: Fraunhofer Institute)

Bottom left: Scanning electron micrograph of the nano-pyramid structures in silica fabricated in Finland.

Bottom right: Reflectances of the unpatterned silicon dioxide surface and shallow pyramid structure for normal incidence. (source: Fraunhofer Magazine, 2 (2005)).

5.1.6 Anti-fingerprints (or touch-proof)

Another big concern with architectural glazing, especially for interior applications, is that fingerprints show very clearly. Materials that are within easy reach are often touched, mostly because they have a related function, but sometimes just because they are there. This affect all the interiors as the appearance of cleanliness is desirable for aesthetic and hygienic reasons as well and steel and glass surfaces are particularly affected by repeated touching.



Fig. 5.8 a-b
Left: steel without and with an anti-fingerprint coating. Right: a sandblasted glass door.

An anti-fingerprints coating can offer a suitable solution for this matter and in some cases makes it possible to employ such materials. With the help of nano-anti-fingerprints coating, fingerprint marks are made practically invisible and imperceptible. The coating alters the refraction of the light in the same way the fingerprints have little effect. The light reflections on the coating make steel or glass surfaces appear smooth, giving the impression of cleanliness that users usually have to expect. On a careful examination, it is possible to see traces of fingerprints, but the improvement in comparison to normal uncoated surfaces is striking.

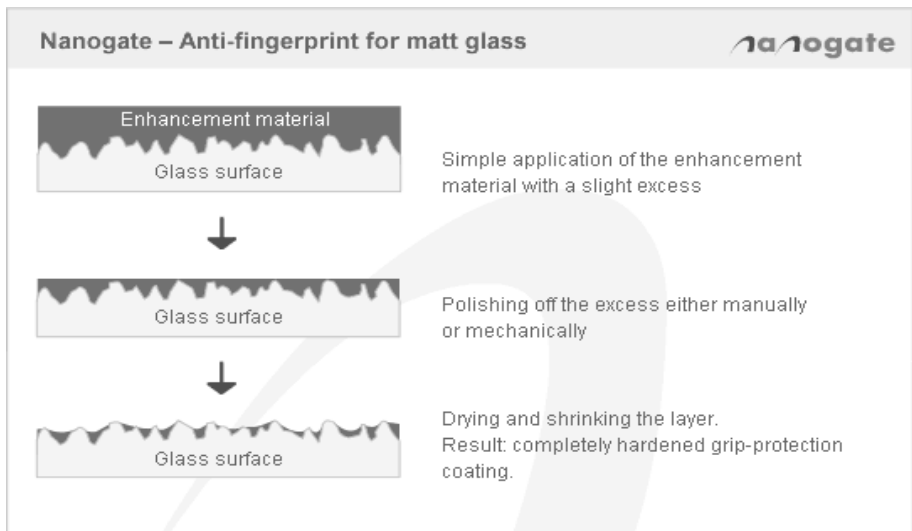


Fig. 5.9

The functional principle of a coloured protective coating retrofitted to a glass surface (source: NanoGate Technologie®).

Anti-fingerprint coatings are ultrathin and do not break after being deposited on the surface. This is extremely important with steel that is often re-shaped for the production of particular architectonic details.

Such coatings, not only reduce the impact of fingerprints but also of dust, especially on sandblasted surfaces. Unfortunately, at present the coating is not entirely transparent and cannot be used on clear glass.

An interesting facility management benefit is the reduction in cleaning costs. The coating is also effective for smaller surfaces where cleaning can be especially time-consuming. Typical trouble spots, such as surfaces around, door-knobs and grips, remain clean and look as good as when first installed.

A more recent innovation is a touch-proof coating that can also be used for colouring matt glass³ which is a quite expensive solution. A good cost-effective option is the use the nanocoating. The intensity of the colour depends on the roughness of the glass and the angle is looked at. The colour palette is currently limited to pastel colours and is quite resistant when exposed to UV light.

³ Coloured matt glass is usually achieved using coloured glass, silk screen printing or coloured foils in combination with laminated safety glass.

5.2 Scratchproof and abrasion resistant coatings

Scratch resistance is a desirable property for many materials and anti-scratch coatings may be applied to different materials such as wood, plastic, ceramics or metal.

The coating does not interfere with materials transparency or optical properties in general, but creates a permanent bond with the surface that reduces the appearance of hairline scratches. Though an anti-scratch coating is not 100% scratch-proof, it helps to prevent minor scratches that can easily happen to a regular surface.

There is no ideal coating developed, rather two basic principles apply: self-healing layers, which are less susceptible to scratching, or glass-like hard scratch-resistant layers, for which different companies offer specific products. In any case, the manufacture requires great care to achieve the desired level of transparency, which excludes the use of coarse additives.

Such coatings must, firstly, adhere to the surface they are deposited on and, secondly, be resistant against wear and abrasion; this is assessed by means of abrasion tests. The hard-variant of the scratch-resistant function is achieved through a glass-like nano-coating that is usually made of silicon dioxide. It noteworthy that scratch resistance does not mean protection from major mechanical impact such as scratches caused by keys, for instance.

For architectural applications, recently developed scratch-resistant stainless steel coatings are of particular interest and are available in transparent or coloured form.



Fig. 5.10
Scratched glass.

6. NANOTECHNOLOGIES FOR CEMENT-BASED MATERIALS

6.1 Introduction

Cement and steel are the largest consumed materials in the construction sector and are excellent candidates for manipulation and control at the nano-scale due to a very fast development of technologies available on the market. Nanotechnologies in civil engineering have been investigated for a long time by several groups of research of many countries for construction material applications in order to maximize the strength and the durability. Generally, it can be said that these new high technologies could help especially in the characterization of the materials at different scale levels (from the nano to the micro to the meso and, at the end, to a building component), in the development of new enhanced properties leading to new and useful building performance and in the development of sensors for measurement and testing. For instance, in 1992 the US Federal High Way Administration began partnership with American Iron and Steel Institute to develop a high performance steel for bridges using copper nanoparticles leading to microstructure changes that makes the steel tougher, easier to weld and more corrosion-resistance.

All the researches on new materials in construction, leading to the development of new enhanced materials, will probably lead to a new idea of design in architecture and engineering as buildings and infrastructures will take advantage of such stronger materials, ductile concrete and other advances, as well as multifunctional or smart materials thanks to the new understanding of basic materials structure-property relations.

6.2 What has been done: a general overview

Concrete is a porous material, ranging from air voids to nanometres scale pores produced by the cement-water chemical reaction. These nanoscale pores control the properties of the calcium-silicate-hydrate hydration product in the 1 to 100 nm which is the main glue and hold concrete together. Thus, concrete is, in some ways, a nanoscalar material.

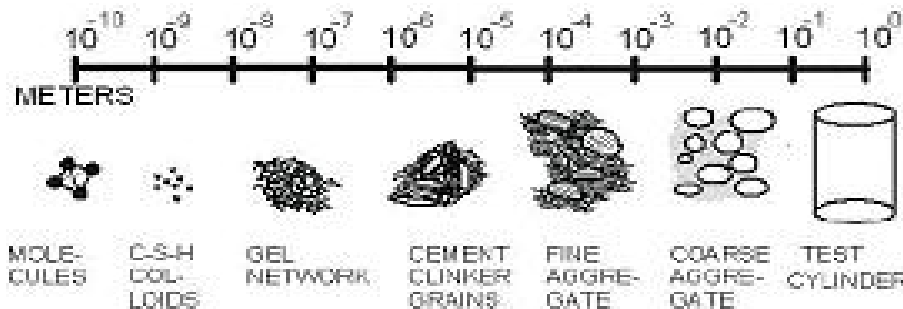
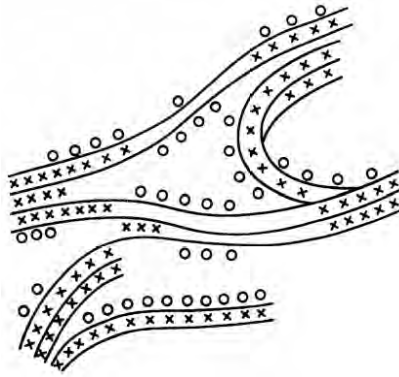


Fig. 6.1
Features of concrete at various scales (Livingston, 2005)

Fig. 6.2

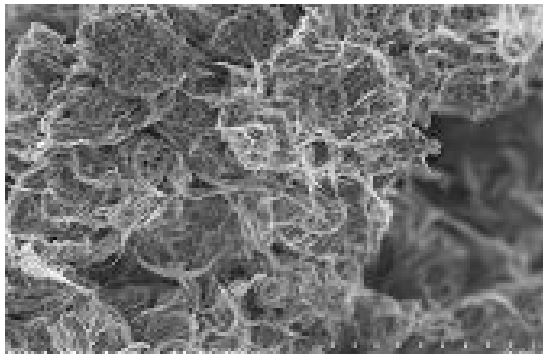
A model of the concrete structure: layers (lines), interlayer water molecules (crosses), adsorbed water molecules (circles). (source: Taylor, H.F.W., 1997)



Fundamentally, hydrated cement paste (HCP) is considered a nanomaterial. The structure of calcium silicate hydrate is much like a clay, with thin layers of solids separated by gel pores filled with interlayer and adsorbed water (fig. 6.2). This has a significant impact on the performance of concrete because HCP is sensitive to moisture movements, which can lead to shrinkage and consequent cracking if accommodation in element sizes are not made.

Better understanding of the extremely complex structure of cement-based materials at the nano-level should apparently result in stronger and more durable concrete. For example, de-icing chemicals could penetrate concrete's porous structure and oxidize the reinforcing steel thus causing cracking and deterioration to the structure. The addition of nano-silica fume to concrete mixes is being recognized as a big improvement in durability of concrete structures exposed to de-icing salts. Silica fume additive operates at a nanoscale and makes a more durable concrete. But if silica fume is added too much, the concrete will become brittle. There is a need to better understand quantitatively what takes place in the cement particle at a nanoscale level, which will lead to improved industry standards for mixing and curing concrete.

Plain concrete itself is a brittle material that is much stronger in compression than in tension. Various forms of reinforcement, typically in the form of rods or fibres, are added to concrete to compensate for its weakness in tension. Nano-engineered cement materials with nano-sized cementitious components, reaction modifier and reinforcing materials are under development and could result in concrete with greatly improved stress-strain behaviour and possibly possessing the range of newly introduced "smart" properties, such as electrical conductivity, light transmission, sensing abilities for temperature, moisture, and stress.

**Fig. 6.3**

Micrograph of nanotube on a small cement grain (Maker, 2003)

One of the most investigated areas in cement-based materials, is the application of carbon nanotubes to improve the mechanical performance of cement-carbon-nanotube composite for use in the construction industry. CNTs appear to be one of the strongest materials, even more resistant than steel. The research has shown that it is possible to distribute

CNT bundles across cement grains using an ethanol/sonication technique and the evidence of classical reinforcing mechanisms was observed in the composite materials.

Other researches include developing cementitious nanoparticles to improve cement hydration, creating new ways to control and time the release of cement admixtures, and the development of cement-polymer-based nanocomposites.

Engineered Cementitious Composites (ECC) are developed and reinforced by polymeric polyvinyl alcohol (PVA) fibre (see Fig. 6.4 left) through carefully micro-mechanical modelling fibre geometry, fibre/matrix interface and matrix properties. The key to achieve desirable performance of ECC is a proprietary nanoscale coating that controls the chemical bonding between reinforcing PVA fibres and the mortar matrix. This nano-enabled concrete is 500 times more resistant to cracking and makes concrete tough (Fig. 6.4 middle), and generally reduces infrastructure maintenance. The ECC already has been used to repair a bridge deck (see Fig. 6.4 right).



Fig. 6.4 a-c
 Left: PVA fibre with nanoscale coating (ScienCentral News, 2005);
 Middle: ECC suppresses cracking and becomes flexible (Imerito, 2005);
 Right: ECC is used to repair bridge deck (Kim, 2004).

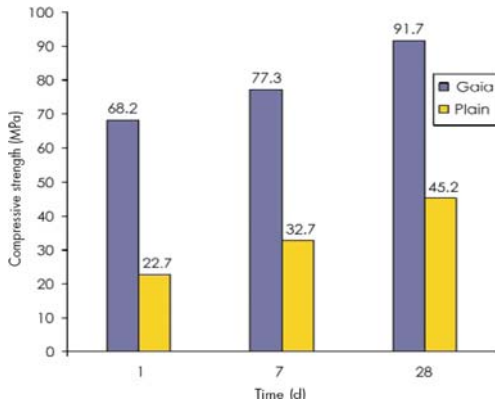
6.3 Use of nanoparticles

A lot of studies showed that adding nanoparticles to the cement matrix could improve its properties. Some of the particles investigated are: nanosilica, $\text{Ca}(\text{OH})_2$, CaCO_3 , TiO_2 , nanoclays, etc.. Their adding to the matrix showed great opportunities and advantages. As exemplum, a research focused on the compressive and flexural strengths of cement mortars that could be enhanced adding SiO_2 and Fe_2O_3 nanoparticles or organo-modified montmorillonites.

Researchers found out that nano-particles were uniformly dispersed in a cement paste and that they can accelerate the cement hydration due to their high activity. Additionally, the nano-particles will fill pores leading to an increased strength and better characteristics within the cement microstructure and the interface between the cement paste and aggregates in concrete. It was also found that nano- Fe_2O_3 exhibits a self-sensing of strain capability which can be useful for structural health monitoring. SEM study proved that the nano-iron-oxide and nanosilica particles filled the pores and decreased the content of calcium hydroxide within the hydration products. These effects resulted in the improvement of the mechanical properties of the cement mortars with nanoparticles and leading to increased early age and ultimate strength of high-volume fly-ash concrete. The developed concrete with nanosilica had a strength 81% higher compared with plain concrete. The 2-year strength of the developed concrete was 115.9 MPa, higher than the strength of reference Portland

cement concrete of ~ 103.7 MPa. It was also seen that nanosilica did not affect durability.

Fig. 6.5 a-b
Left: strength development of concrete with Gaia.
Right: effect of Gaia on the performance of concrete. (source: K. Sobolev, How nanotechnology can change the concrete world)



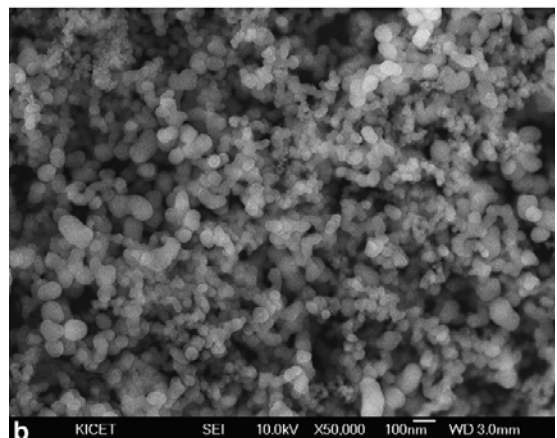
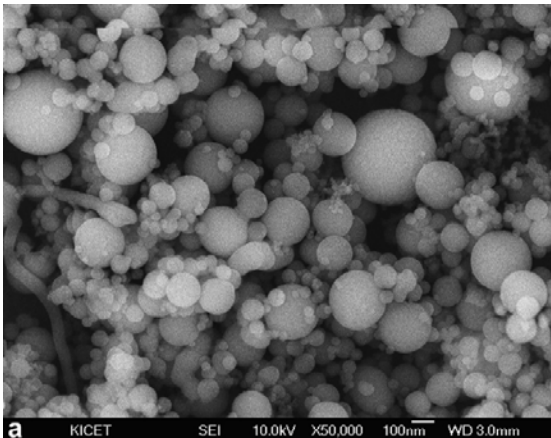
Mixture parameters	Plain	With Gaia
Cement type (EN-197)	II/A-P 42.5R	II/A-P 42.5R
Cement content (kg/m ³)	460	460
Admixture dosage (%)	1.3	
Air content (%)	2.7	1.1
Slump (mm)		
After 5 min	60	200
After 30 min	25	210
After 60 min	15	160
After 90 min		140
Ambient temperature (°C)	20	20
Compressive strength (MPa)		
At 1 d	22.7	68.2
At 7 d	32.7	77.3
At 28 d	45.2	91.7

One of the first commercial nano-admixtures for concrete, Gaia, was developed by Ulmen S.A. and Cognoscible Technologies. This product is available in liquid form that facilitates the satisfactory distribution of nanosilica particles in concrete (fig. 6.5).

6.4 Nano-SiO₂

Fig. 6.6 a-b
SEM imaging of: Silica fume (left), nano SiO₂ (right). (Source: Byung-Wan Jo, Characteristics of cement mortar with nano-SiO₂ particles).

Lots of studies had been conducted with cement plus SiO₂. The amorphous or glassy silica, is the major component of a pozzolan. In a cement mix, it reacts with calcium hydroxide formed from the hydration of calcium silicates. The rate of the pozzolanic reaction is proportional to the amount of surface area available for reaction. Therefore, it is plausible to add nano-SiO₂ of a high purity (99.9%) and a high Blaine fineness value (60 m²/g) in order to improve the characteristics of cement mortars.



A cement paste is composed of small grains of hydrated calcium silicate gels, nano-sized individual pores, capillary pores, and large crystals of hydrated products. Thus, there should be room for nano-phase materials to fill the pores of the cement paste. The amorphous or glassy nano-scale silica, which is the major component of a pozzolan, reacts with calcium hydroxides formed from the hydration of calcium silicates. The rate of the pozzolanic reaction is proportional to the value of Blaine fineness. Therefore, the nano-SiO₂ used was of particle form with 99.9% SiO₂, a particle size of 40 nm, and 60 m²/g Blaine fineness.

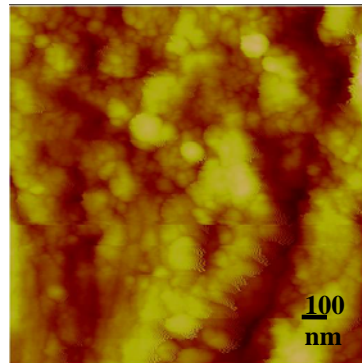
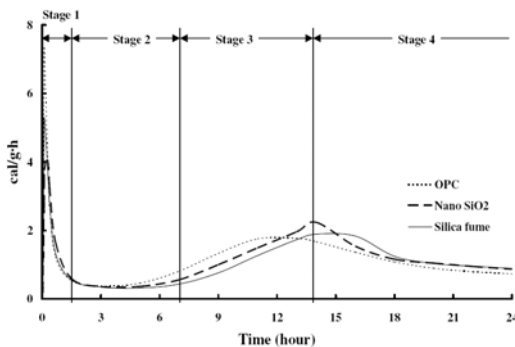


Fig. 6.7 a-b
 Left: Calorimetric curves of heat evolution.. (source: H.J.H. Brouwer, 2006)
 Right: atomic force microscopy of calcium silicate hydrate. (source: Shah, 2006)

A super-plasticizer is often added to ensure that no segregation would occur. The compressive strength resulted higher than that of control cement mortars and the microstructure revealed a dense and compact formation of hydration products and a reduced number of Ca(OH)₂ crystals. Furthermore, the addition of nano-SiO₂ increases the amount of heat evolved during the setting and hardening of the cement. However, a greater dosage of super-plasticizer retards the early hydration of the cement paste containing nano-SiO₂. Heat-treating is necessary to accelerate the early hydration and the pozzolanic reaction.

In conclusion, the idea is that adding nanoparticles to the concrete paste is possible to improve in a very good way concrete resistance properties such as strength and durability.

This improvement may be achieved since it was observed that at the nano-scale cement paste is full of nano-pores that usually remain empty with the traditional techniques of preparation. Filling in this gaps between the paste particle is the best way to have new enhanced properties.

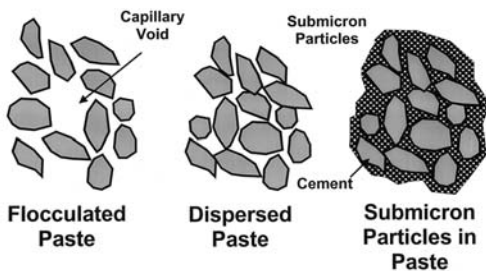


Fig. 6.8
 Scheme of cement paste structure.

6.5 Nanocement – cases of study

A study, conducted at the University of Delaware, focuses on synthesizing the components of Portland cement using nano-particles and comparing their properties to those of commercial cements. The technique of production used was the sol-gel method.

Tab. 6.1 materials used					
material	properties	C ₃ S	C ₂ S	C ₃ A	C ₄ AF
PEG	MW 3400 g/mol	4 g	4 g	4 g	4 g
Ca(C ₂ H ₃ O ₂) ₂	MW 158 g/mol	0,03 mol	0,02 mol	0,03 mol	0,04 mol
SiO ₂	variable	0,01 mol	0,01 mol	--	--
Al ₂ O ₃	MW 101,96 g/mol	--	--	0,01 mol	0,01 mol
Fe ₂ O ₃	MW 159,7 g/mol	--	--	--	0,01 mol
Water	deionized	15 mL	15 mL	15 mL	15 mL

Some important results came out: the compression tests revealed that Portland cement was able to withstand much more loading than the nano-cements and the over-aggregation of the particles created a weak zone in the form of voids and, as a result, low strength. Furthermore, the high water used for the nano-cements in order to have a good workability may also have contributed to a lower strength. Finally, the addition of gypsum is needed for the aluminate components to react with. This mineral, that is present in Portland cement, was not present in the nano-cement.

Other studies focused on the characterization of nanocement phases as the particle size of the starting materials affect the hydration process and so some key properties of the final material such as the setting time and the compressive strength.

A research, in particular, focused on an advanced procedure to characterize the nano-C₂S (nano-Belite), and nano-C₃S (nano-Alite) by Field Emission Scanning Electron Microscopy (FESEM) according to their high rate hydration behaviours. The products consist of aggregates that show a fine spherical and pure distribution of nano-C₂S (Fig. 6.9 a-b) and nano-C₃S (Fig. 6.10 a-b) with particle size < 200 nm. Characterization was performed before the beginning of the hydration process. It was showed that the tricalcium silicate offers new possibility in the industrial appli-

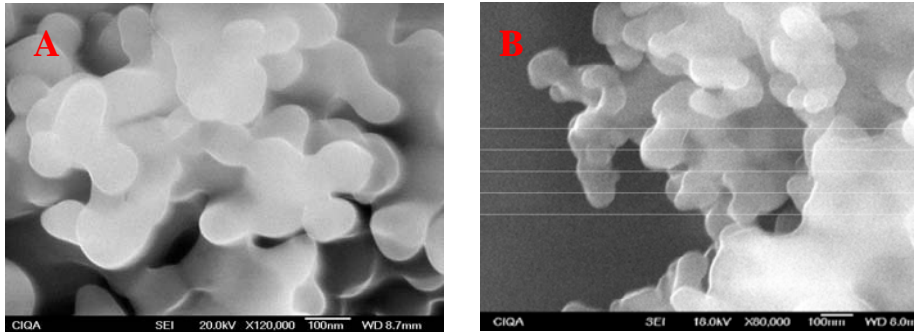


Fig. 6.9 a-b
FESEM imaging of:
(A) nano C₂S; (B)
nano C₃S.
(source: Y. Perera,
Characterization of
nano-cement phases
by field emission
scanning electron
microscopy (fesem))

cations as this material has been reported to be with some bioactive and hydraulic properties, which leads to spontaneous development on the strength (spontaneous consolidation) during its reaction with water.

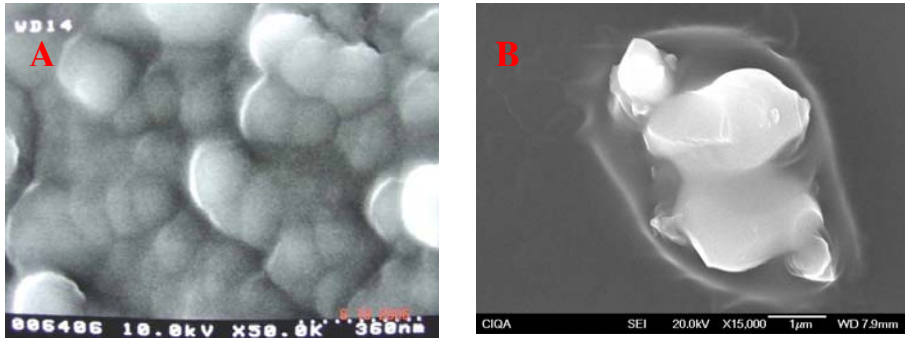


Fig. 6.10 a-b
FESEM imaging of:
(A) nano SiO₂; (B)
CSH gel production
during the hydration.
(source: Y. Perera)

6.6 Carbon Nanotubes in concrete

Carbon nanotubes (CNTs) are allotropes of carbon with a nanostructure that can have a length-to-diameter ratio greater than 1,000,000 and they are members of the fullerene structural family. These cylindrical carbon molecules have novel properties that make them potentially useful in many applications. Their main enhanced properties are: extraordinary strength, unique electrical properties, efficient conductors of heat. Nanotubes are categorized as single-walled nanotubes (SWNTs) and multi-walled nanotubes (MWNTs) where the distance between the layers is about 0.34 nm, which corresponds to the distance between the layers in crystalline graphite.

The nature of the bonding of a nanotube is described by applied quantum chemistry, specifically, orbital hybridization. The chemical bonding of nanotubes is composed entirely of sp² bonds, similar to those of graphite. This bonding structure, which is stronger than the sp³ bonds found in diamond, provides the molecules with their unique strength. Nanotubes naturally align themselves into "ropes" held together by Van der Waals forces. Under high pressure, nanotubes can merge together, trading some sp² bonds for sp³ bonds, giving the possibility of producing strong, unlimited-length wires through high-pressure nanotube linking (CNTs will be largely discussed in an other section of this thesis).

Tab. 6.2 Comparison of mechanical properties

Material	Young Modulus (TPa)	Tensile Strength (GPa)	Elongation at break (%)
SWNT	~1 (from 1 to 5)	13-53 ^E	16
MWNT	0.8-0.9 ^E	150	-
Stainless Steel	~0.2	~0.65-1	15-50

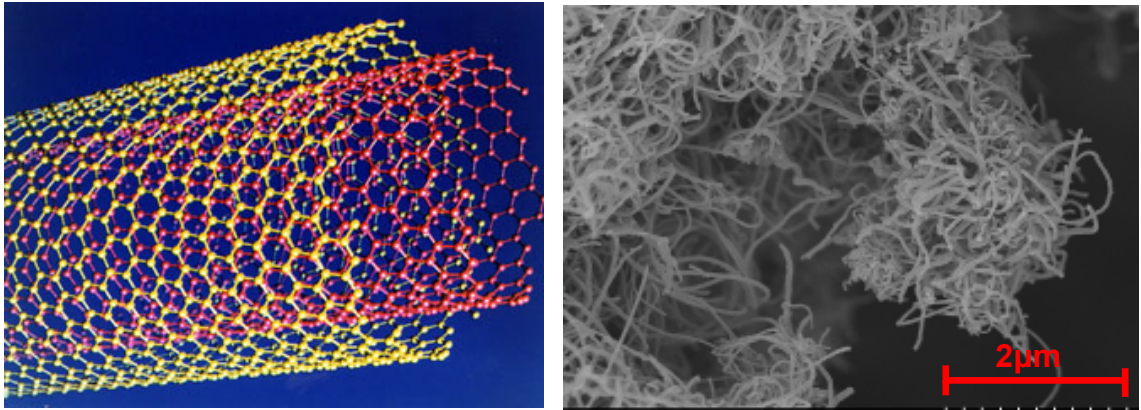


Fig. 6.11 a-b

Left: MWCNT $d = 10 \div 80$ nm.
(source: Shah, 2006)
Right: SEM images of MWCNTs

Lots of research had been conducted on CNT properties to enhance concrete performance. During one research, for instance, a technology for low-temperature carbon nanotube synthesis and patented in 2001 (Russian patent № 2169699) was used. The scanning electron microscope investigation showed that the obtained material is composed of fibre shaped agglomerations (length up to 10 mm) with a complex inner structure containing nanostructures of a cylindrical shape.

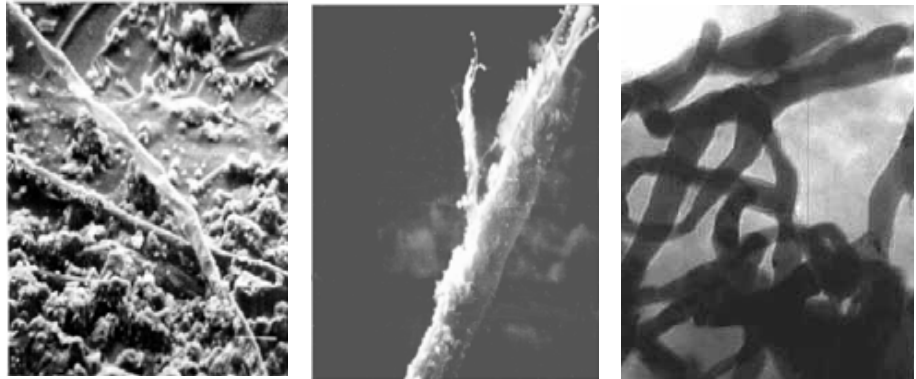


Fig. 6.12 a-b-c

Microstructure containing the new-growths:
Left: general view;
Middle: a fragment of cleaved fibre shaped;
Right: CNTs.
(Source: Yakovlev G. et al., Cement Based Foam Concrete Reinforced by Carbon Nanotubes)

The developed carbon nanotubes were used as a high-strength nanodispersive reinforcement in compositional crystallohydrated materials to improve the physico-mechanical properties of non-autoclave cement foam concretes. The amount of reinforcement phase in the mixture was 0.05 % based on the initial mass and the result was a decrease in heat conductivity up to 12 – 20 % and, in the same time, an increase of its compressive strength up to 70 %.

Tab. 6.3 Physico-mechanical characteristics of cement foam concrete						
n°	Amount of CNT, % based on the composition mass	Average density, kg/m ³	Compressive strength, MPa	Heat conductivity coefficient, λ, W/mK	Pore diameter, μm	Condition of wall pores
1	0	330	0,18	0,07	40-600	perforated
2	0,05	309	0,306	0,056	60-150	homogeneous

The main problem in working with dispersions of CNTs is that they tend to adhere together due to the Van der Waal forces, as it can be seen in the pictures below (fig. 6.14 a-b).

To obtain individual CNTs is often required the use of surfactant and ultrasonic energy. These methods could avoid them stick together within the dispersion. A very new tremendous discovery was done in 2008 by researchers of Nanocomp Technologies Inc. as they succeed in producing a 3-foot by 6-foot sheets of pure carbon nanotube material, where the SWCNT are aligned, continuous and 1 mm long. This discovery opened a big door to future advanced structural composites.

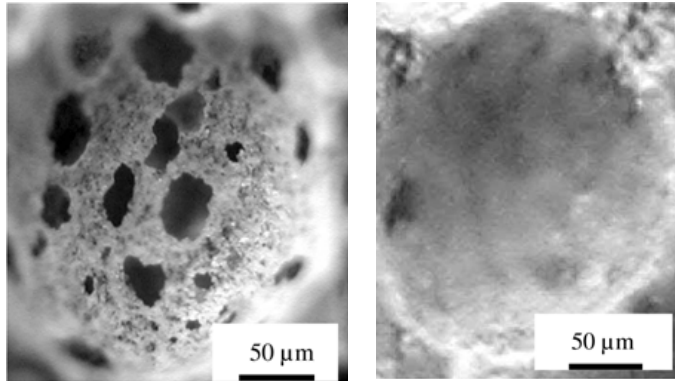
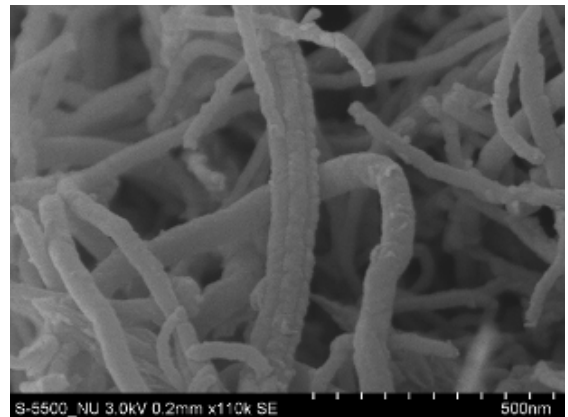
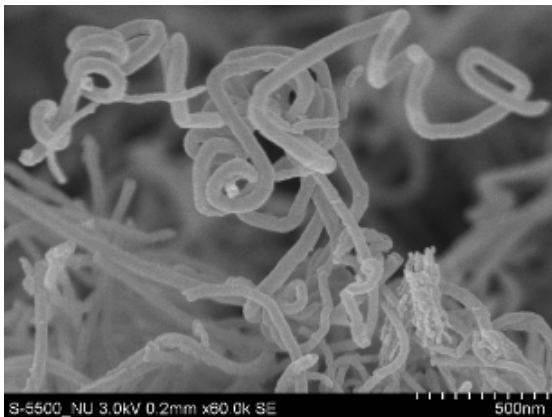


Fig. 6.13 a-b
Cement foam concrete microstructure: Left: without CNT, Right: with CNT. (Source: Yakovlev G. et al., Cement Based Foam Concrete Reinforced by Carbon Nanotubes)

Fig. 6.14 a-b
SEM images of poorly dispersed and stick together CNTs



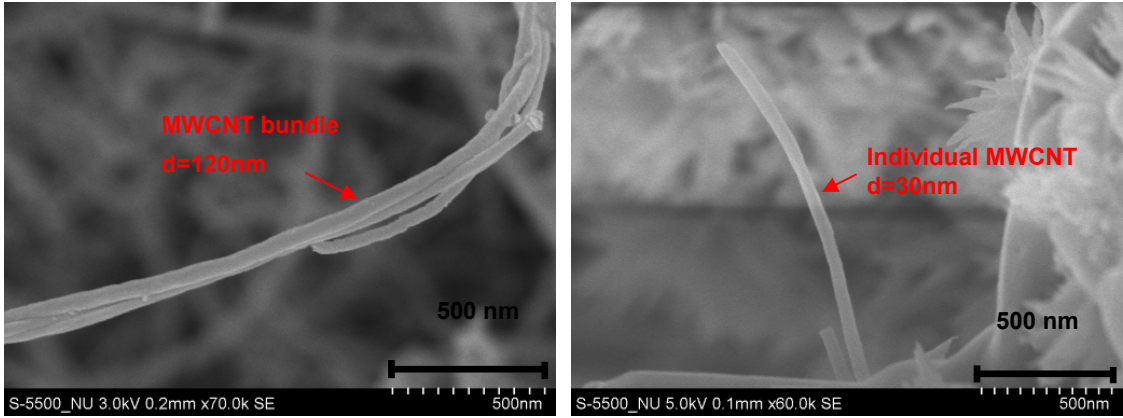


Fig. 6.15 a-b
SEM images of dispersed CNTs:
Left: without surfactant,
Right: with surfactant and sonication.

This CNT textile sheet may be easily incorporated into advanced concrete materials. To calculate the modulus of elasticity in concrete with a CNT reinforcement, a modelling approach should be performed. In some researches it was tried to calculate the Young's modulus modelling a nano-volume of concrete reinforced by a CNT bar, as can be seen in the images below, and analysing it by finite element approach.

Fig. 6.16 a-b
Left: Finite element calculations to determinate the Young's modulus.
Right: SWCNT-concrete composite volume element. (source: G. Rouainia, Evaluation of Young's modulus of single walled carbon nanotube reinforced concrete composite).

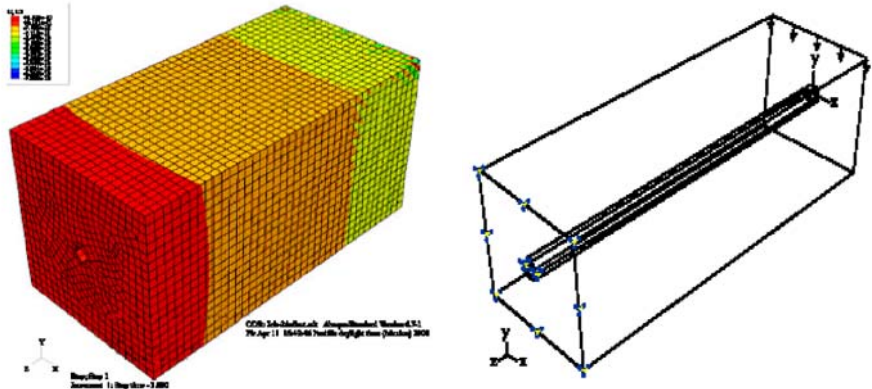
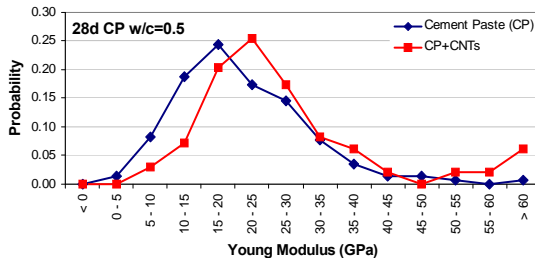


Fig. 6.17
Probability of the Young's modulus value.



Other researches calculated the probability of the value of the modulus. It was demonstrated that a CNT-reinforced concrete has a bigger probability to be higher.

Most of the researches conducted around the world by different groups showed that CNTs are a good additive to reinforce concrete structures, but a lot must be still done to lower the higher costs.

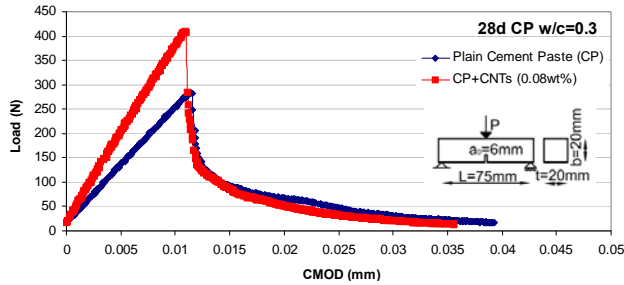


Fig. 6.18 Fracture properties of cement paste reinforced with CNTs.

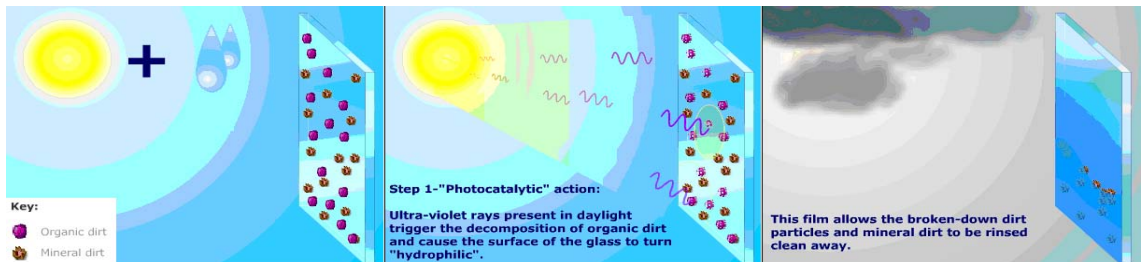
Tab. 6.4 Costs per Kg (\$) for the materials

Material	Cost per Kg [\$]	Dosage kg/m ³	Cost per m ³ of concrete [\$]
CNTs	150-2000	0,3-4	45-8000
Carbon fibres, 10-14 μm diam.	8-20	2	16-40
Carbon fibres, 7 μm diam.	55	2	110
Carbon nanofibres	350-700	2	700-1400
Graphite nanofibres	1730	2	3460
Steel fibres	1,7-5	30-160	51-800
PVA fibres	10-13	15	150-195
Polypropylene fibres	5-9	0.6-19	3-171

6.7 Self-cleaning photocatalytic concrete

This particular kind of concrete is hydrophilic and photocatalytic at the same time which means that it chemically breaks down dirt when exposed to light. The catalyst used is titanium dioxide (TiO₂) which is a very common semiconductor material that is also non toxic, chemically inert in the absence of light, inexpensive and relatively easy to deposit into thin films.

Fig. 6.19 Graphical scheme of a self-cleaning coating.



The self-cleaning properties of TiO_2 are governed by the absorption of ultra-violet light and the generation of electron-hole pairs. The band gap of bulk anatase TiO_2 is 3,2 eV, corresponding to a light of wavelength 390 nm, near ultraviolet (UV) light. A small proportion of the sunlight reaching earth exceeds 3,2 eV, so titania coatings

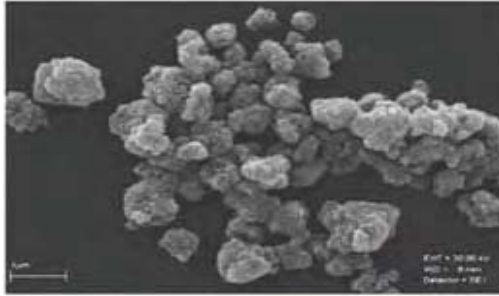


Fig. 6.20
 TiO_2 microparticle
made with nanocrystals.

can be solar activated. The most significant polymorphs of TiO_2 are rutile and anatase. The position of the conduction and valence bands relative to key red-ox potentials cause pure anatase to be very photoactive (photocatalytic and super-hydrophilic) while pure rutile is less so. Anatase TiO_2 is formed at temperatures exceeding

300 °C, but converts into rutile around 800 °C. The photocatalytic activity is tested by measuring the destruction of an organic compound on the surface and sunlight, or artificial UV light, is used to activate the coating. TiO_2 has shown itself capable of breaking down a wide variety of organic compounds, including long-chain carboxylic acids, chlorinated and fluorinated compounds and aromatic compounds.

Tab. 6.5 Published claims of some chemicals oxidized by photocatalysis	
Inorganic Compounds	NO_x , SO_x , CO_2 , NH_2 , H_2S
Organic Compounds	Alcohol, Acids, Alkene and Aromatic compounds (phenol, toluene...)
Chlorinated Organic Compounds	Chloro Alkans Dioxins, Chloro Benzene and Chloro Phenol
Pesticides	Triadimefon, Pirimicarb, Asulam, Diazinon, MPMC, Atrazine
Micro Organism	Bacteria, fungus and viruses

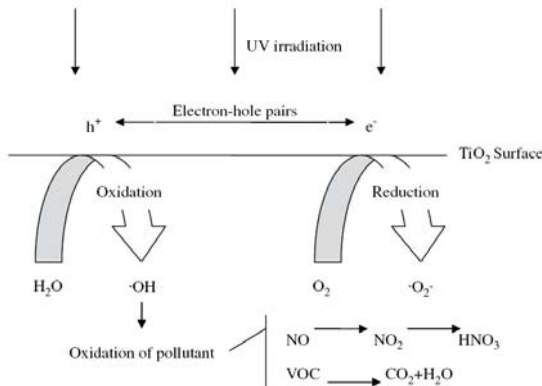


Fig. 6.21
Pollution removal
mechanism of TiO_2
photocatalysis.
(source: J. Chen et
al., Photocatalytic
construction and
building materials:
from fundamentals to
applications).

The use of photocatalysts together with building materials started from the early 1990s. The versatile function of TiO_2 , which can work both as photocatalytic materials and structural materials, has facilitated its application in exterior construction materials and interior furnishing materials, such as cement mortar, exterior tiles, paving blocks, glass and PVC fab-

ric. The air purifying reaction begins with the irradiation of light over TiO_2 . When TiO_2 absorbs a photon containing the energy equal to, or larger than, the band gap, an electron will be promoted from the valence band to the conduction band. The activation of the electrons results in the generation of holes (electron vacancy) in the valence band. In this reaction, h^+ and e^- are powerful oxidizing and reducing agents respectively. The electron-hole pairs may recombine in a short time, or take part in chemical reactions depending on reaction conditions and molecular structures of the semiconductors.

The strong oxidation power of h^+ enables it to react with water to generate the highly active hydroxyl radical (OH^\cdot) which is also a powerful oxidant. Most organic air pollutants can be degraded completely by either the hydroxyl radicals

or the holes themselves to innocuous final products (e.g. CO_2 and H_2O). In addition, the reducing power of the electrons can induce the reduction of molecular oxygen (O_2) to superoxide (O_2^-). It has been confirmed that the superoxide is almost as effective as the holes and hydroxyl radicals in the chain reactions for the breaking down of organic compounds. The de-pollution effect of photocatalytic cementitious materials has been demonstrated by many studies. Nitrogen oxides (NO_x) and volatile organic compounds (VOCs) have often been chosen by most studies as representative airborne pollutants due to their potential health risks and ability to generate photochemical smog. More particularly, the NO removal paving blocks made by waste materials and TiO_2 were evaluated by Poon and Cheung. They found that an optimum mix design which incorporated recycled glass, sand, cement and 10% TiO_2 achieved $4.01 \text{ mg h}^{-1} \text{ m}^{-2}$ NO removal.

It was reported that the air-cleaning capacity can be enhanced by increasing the surface area, reducing the air flow rate and increasing the turbulence of the pollutant in the test chamber. Motivated by the promising results of the laboratory scale investigation, several pilot projects have been carried out to verify the effectiveness of the photocatalytic cementitious materials in ambient environment. In Bergamo (Italy), a street in the city centre was re-paved by the photocatalytic concrete paving blocks (total area of about $12,000 \text{ m}^2$). Environmental monitoring was conducted on two locations: one was at the area where photocatalytic blocks were laid, and the other was at the extension of the road paved by normal bituminous concrete which was used as a reference. NO_x concentration was measured by chemiluminescence analyzers simultaneously on the two sites. A successive air monitoring campaign, lasting two weeks, showed an average NO_x abatement of 45% in day time (from 9 am

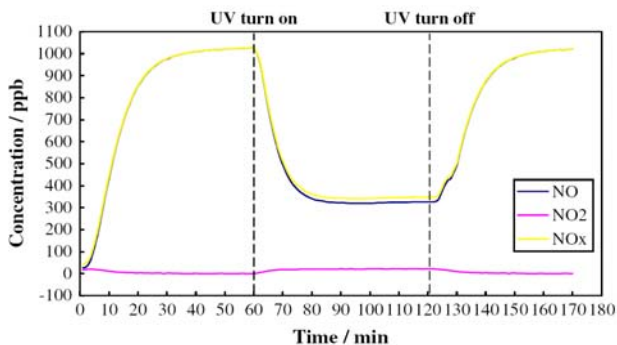


Fig. 6.22 NO_x removal results of photocatalytic paving block obtained in laboratory.

to 5 pm). Similar tests were conducted in other cities as Antwerp (Belgium) or Guerville (France). The most important studies and results on self-cleaning photocatalytic concrete are being made by the Italian company Italcementi Group that sells its products all over the world. TX Active® had been used in Italy by Richard Meier to build the Ara Pacis Augustae museum (fig. 6.23) and the Dives in Misericordiae church (fig. 6.24), both in Rome or the gateway of the Interstate 35 West Bridge over the Mississippi river in Minneapolis (fig. 6.25 left).

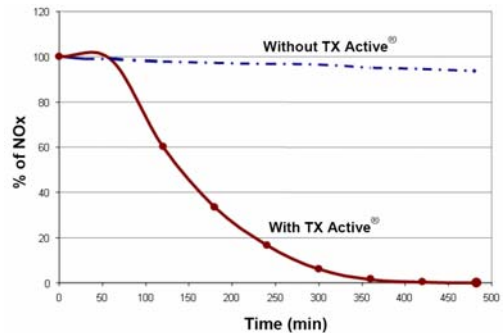
Fig. 6.23 a-b
Ara Pacis Augustae museum in Rome by Richard Meier.



Fig. 6.24 a-b
Dives in Misericordiae church in Rome by R. Meier.



Fig. 6.25 a-b
Left: The gateway of the re-opened I-35W Bridge in Minneapolis.
Right: Lab tests on TX Active® effectiveness in Indoortron test room, 35m³ (Italcementi Group).



Italcementi researchers calculated that in a large city such as Milan covering 15% of visible urban surfaces with products containing TX Active® would enable a reduction in pollution of approximately 50%. Laboratory tests have shown that just 3 minutes of exposure to the sun is sufficient to obtain a reduction in polluting agents of up to 75% while the tests carried out in recent years with applications in urban settings have shown a significant ability to reduce pollutants, between 20% and 70%, depending on atmosphere and light conditions (fig. 6.25 right).

Anyway, in some researches it was reported that there are still many unresolved problems when this technology is used in a real-life applications. It seems that the immobilization of TiO_2 by the construction materials can lead to significant loss of the photocatalytic activity. For instance, it was pointed out that TiO_2 -cement mixtures and red bricks containing TiO_2 were significantly less efficient than TiO_2 slurries in decomposing 3-nitrobenzenesulfonic. It is thought that the reduction of active surface and the presence of ionic species are the reasons for the catalytic activity loss. Other studies stated that the carbonation of the TiO_2 modified cements led to a noticeable loss in catalytic efficiency over several months because of the changes in cement surface structure. The report published by the Hong Kong Environmental Protection Department claimed that the photocatalytic activity of TiO_2 coated paving blocks decreased significantly after 4 months exposure in a downtown area due to the accumulation of contaminants on the block surface. This means that periodic servicing (washing or replacement) of the TiO_2 materials may be necessary to maintain the pollution reduction effect

6.8 Water-proof cement

Water-proofing of building materials has always been a problem due to their porous structure with several micro-cracks. The development in technology lead to the production of eco-friendly organo-silicon products to waterproof practically all the different kinds of building materials. The nanotechnology has ensured that service life of this approach will lead to a life cycles beyond 20 to 30 years at very economical cost. The size of the water molecule is 0.18 nm; the size of the pores in most of the building materials range from 5 to 200 nm; the size of most of the pollutants like acids, chlorides and sulphates would range between 1 to 2 nm. Even with the dense concrete and stones the pore size is much larger than water allowing easy entry with the hydrophilic nature of the building materials. On the market there are still two kind of water-proofing products: water repellent film formers (as acrylic paint or silicon polymers) and penetrants which can enter 3-5 mm deep in the substrate (as Silane, Syloxane, Siliconates, Acrylates, etc.).

Recently Zydex Industries in India has developed a waterproofing product called Zycosil that forms 4-6 nm size particles with a



Fig. 6.26

Lab test: the Rilem tube was affixed on the substrate surface and water was filled up to 5 ml mark. The drop in water level is observed over a 20-minute period. The hydraulic pressure generated on the surface was equivalent to 140 Km/hr wind driven rain. The water level did not drop for 24 hours for Zycosil treated cement block (on the right). The water of untreated cement blocks level dropped to about 2.5 ml mark after 20 minutes (on the left).

(source: P. Mehta, Nano Technology in Water Proofing of Building Materials).

service life of about 20-30 years. The tests performed by the industry showed that Zycosil treated samples of brick, concrete, cement sheet, plaster, Dholpur stone, etc., reduced water absorption rates by over 99%.

6.9 Anti-corrosion concrete

Large sums are used in research to ensure the durability of concrete structures, especially towards reinforcement corrosion. Much focus is placed on means of ensuring a long service life of cracked reinforced concrete structures as this seems to be the area of most concern. The effectiveness of the service life enhancing solutions is, however, difficult to evaluate basing on current service life models, as these models are not based on a detailed description of the corrosion process and do not take structural details and the presence of cracks and other defects into account. For a detailed evaluation of the impact of protective measures, models based on physio-chemical concepts are needed. Some study are trying to develop these models that should - besides a description of the electro-chemical corrosion process itself - include description of the structural detailing, the materials properties (including defects and cracks) as well as aging and deterioration.

6.10 Self-compacting concrete

The development of self-compacting concrete (SCC), also referred to as “self-consolidating concrete”, is one of the most important developments in the building industry. The incentive for the first development of this concrete in Japan came from

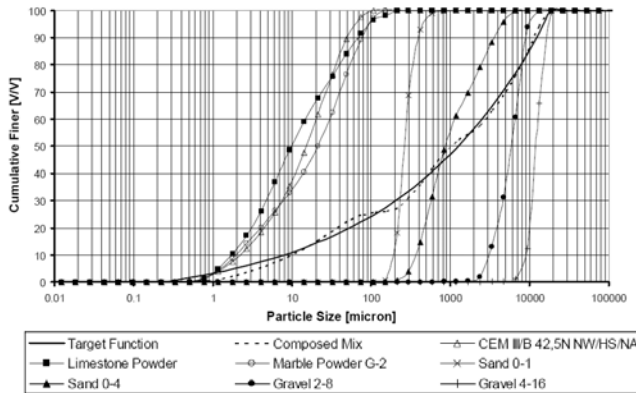


Fig. 6.27
PSD of a mix (dashed line) composed with the help of the new design concept. (source: H.J.H. Brouwer, 2006)

high-fluidity anti-washout underwater concretes developed in Germany during the 1970's. Ever since the pioneering work by R. F eret, it is known that the particle size distribution of the aggregates governs the workability and hardened properties of concrete mixes.

Lots of researches are studying the best packing approach and theoretical model that could enable the optimum use of nanoparticles in the mix design. Using both the new design concept based on the particle grading and the informations given by the determination of the water demands (less voids have to be filled with and on a smaller scale less void volume has to be filled with water; conversely, more water is available for lubrication), various SCC mixes have been produced and tested for their fresh and hardened concrete properties. The analysis of this information shows

a promising way of designing new kinds of SCC with improved qualities in regard to their workability, mechanical properties and durability. With lab experiments, an increase of the cement efficiency to values of 0.19 - 0.22 MPa per kg/m^3 was obtained.

6.11 Future Developments

Much progress in concrete science is to be expected in coming years by the adaptation of the new knowledge generated by the quickly growing field of nanotechnology.

The development of the following concrete-related nano-products can be anticipated:

- Catalysts for the low-temperature synthesis of clinker and accelerated hydration of conventional cements;
- Grinding aids for superfine grinding and mechanochemical activation of cements;
- Binders reinforced with nanoparticles, nanorods, nanotubes, nanodampers, nanonets or nanosprings;
- Binders with enhanced/nanoengineered internal bond between the hydration products;
- Binders modified by nanosized polymer particles, their emulsions or polymeric nanofilms;
- Biomaterials (including those imitating the structure and behaviour of mollusk shells);
- Cement-based composites reinforced with new fibres that contain nanotubes as well as with fibres covered by nanolayers (to enhance the bond and corrosion resistance or to introduce new properties, such as electrical conductivity);
- Next-generation super-plasticizers for total workability control and supreme water reduction;
- Cement-based materials with supreme strength, ductility and toughness;
- Binders with controlled internal moisture supply to avoid/decrease micro-cracking;
- Cement-based materials with engineered nanostructures and microstructures that exhibit supreme durability;
- Ecobinders modified by nanoparticles and produced with substantially decreased volume of Portland cement component (down to 10–15%) or binders based on the alternative systems (magnesia, phosphate, geopolymers and gypsum);
- Self-healing materials and repair technologies that use nanotubes and chemical admixtures;
- Materials with self-cleaning/air-purifying features based on photocatalyst technology

- Materials with controlled electrical conductivity, deformative properties, non-shrinking and low thermal expansion;
- Smart materials, such as temperature-, moisture- and stress-sensing or responding materials.

In the last few decades concrete has been made stronger and more durable. Concrete with compressive strengths up to 200 MPa are being used for super-tall buildings. High performance concrete is being used in transportation structures where enhanced durability is required for an aggressive environment. These improvements are only a little part of our better understanding of concrete at the micro-level. The next major development is an improved understanding at the nanolevel that, as many researches showed, will lead to enhanced concrete properties.

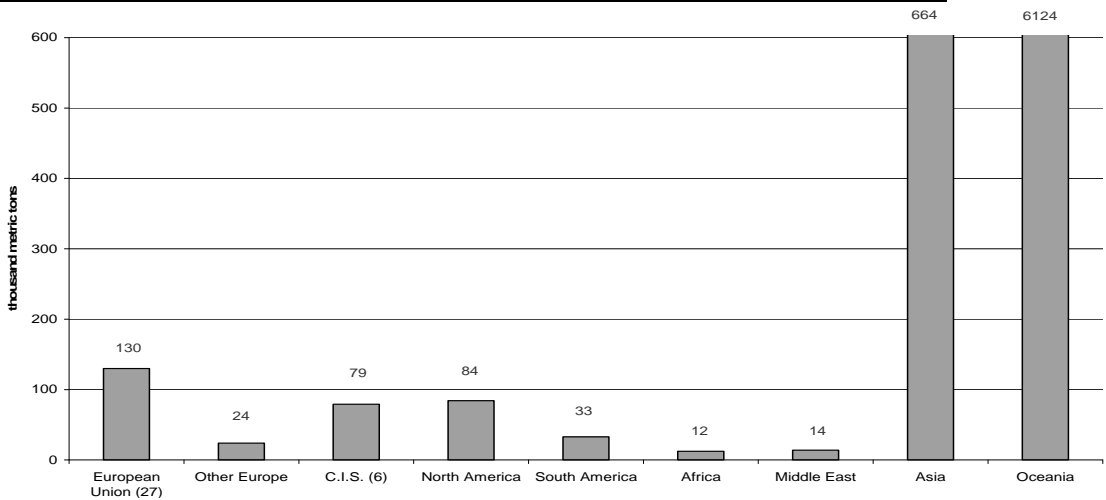
7. NANOTECHNOLOGIES FOR STEEL-BASED MATERIALS

7.1 Worldwide steel production and usage in construction industry

Steel has been widely available since the second industrial revolution in the late part of the XIX and early part of the XX century and has played a major part in the construction industry since that time. The World Steel Association reported for the 66 country affiliated a crude steel production of about 112 million metric tons (mmt) in September 2010. This is higher than September 2009.

Tab. 7.1 Worldwide steel production in 2010 (source: Worldsteel)										
Country	Jan	Feb	Mar	Apr	May	Jun	Jul	Aug	Sep [...]	Total
European Union (27)	13,62	13,31	15,55	15,42	16,51	15,18	13,79	12,25	14,29	- 130
Other Europe	2,42	2,17	2,54	2,69	2,87	2,89	2,645	2,90	2,93	- 24
C.I.S. (6)	8,56	7,87	9,21	9,25	9,59	8,60	8,70	8,71	8,71	- 79,2
North America	8,64	8,69	9,84	9,56	9,99	9,57	9,241	9,30	9,34	- 84,2
South America	3,70	3,38	3,67	3,52	3,70	3,63	3,667	3,90	3,68	- 32,8
Africa	1,35	1,22	1,38	1,38	1,44	1,32	1,401	1,46	1,40	- 12,3
Middle East	1,58	1,59	1,52	1,67	1,65	1,58	1,297	1,56	1,62	- 14,1
Asia	72,9	69,42	77,81	76,38	78,14	74,89	72,89	72,33	69,11	- 664
Oceania	676	594	682	647	687	688	736	744	670	- 6124

Fig. 7.1
Worldwide steel production in 2010 (source: Worldsteel).

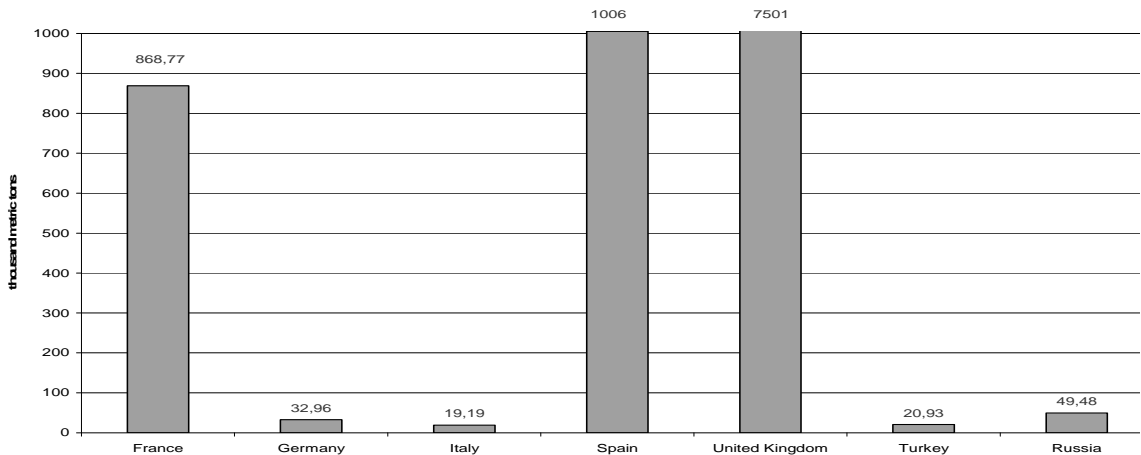


Nowadays, millions tons of steel are produced per year in the EU and studies on this material enjoys a healthy allocation of research funding.

Tab. 7.2 European steel production in 2010 (source: Worldsteel)

Country	Jan	Feb	Mar	Apr	May	Jun	Jul	Aug	Sep	Total
France	1,136	1,127	1,476	1,451	1,573	1,457	1,29	858	1,257	869
Germany	3,497	3,399	4,021	3,883	4,073	3,857	3,472	3,446	3,311	33
Italy	1,876	2,164	2,377	2,352	2,471	2,264	2,269	1,09	2,326	19,2
Spain	1,358	1,343	1,581	1,541	1,646	1,433	994	1,226	1,399	1006
United Kingdom	984	763	813	899	894	793	780	789	786	7501
Turkey	2,059	1,821	2,194	2,402	2,526	2,495	2,376	2,547	2,506	20,9
Russia	5,19	4,952	5,588	5,64	5,885	5,43	5,595	5,6	5,6	49,5

Fig. 7.2
European steel production in 2010
(source: Worldsteel).

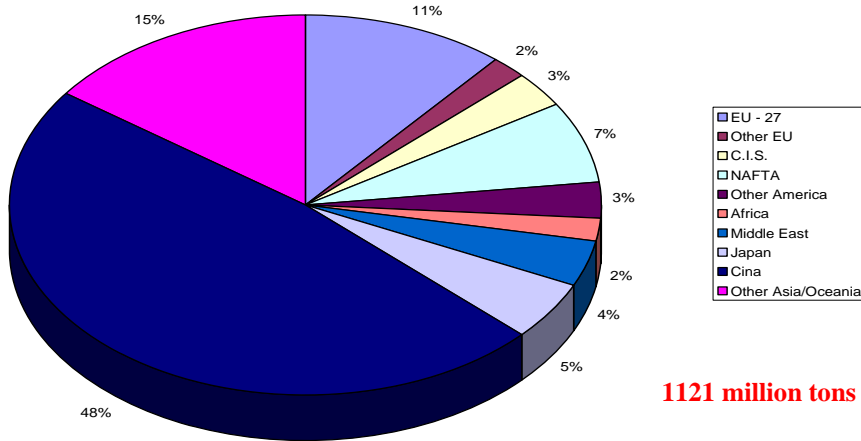


For several decades, automotive and construction industries have been the most important markets for steel companies. For instance, the global demand of automotive steels is currently estimated at around 90 million tons, which is approximately 13% of the total global market share.

Recently, worldwide consumption of finished steel is very large, especially of high strength steels (HSS) and stainless steel that have been dramatically increased.

To fulfil the increasing demand, steel companies have focused on the development of new high strength nano-enhanced steels.

In the graph in the next page (fig. 7.3), it is shown the steel quantity employed in the construction sector in 2009 according to World Steel Association.

**Fig. 7.3**

Worldwide apparent consumption of finished steel in 2009 (source: Worldsteel).

7.2 Nano-research in steel for large structures

The construction industry could benefit from the application of nanotechnology to steel and some of highly promising areas are currently under investigation or are even available today on the market. Generally speaking, the major efforts are employed to many applications to bridge and tall building constructions as the use of steel is larger in these areas and employs more technical and advanced requirements. The behaviour and performance of steels is intimately linked to their chemical and phase composition, structure and surface morphology. Only recently it has become possible to examine the morphology of solid surfaces at the nanoscale using some local probe techniques as the atomic force microscope (AFM). Correlations of AFM results with mechanical testing of steels were done for fatigue crack nucleation and examination and surface deformation at grain boundaries. AFM was also used for surface imaging. Traditionally, the trade off between steel strength and ductility is a significant issue for steel; the forces in modern construction require high strength, whereas safety and stress redistribution require high ductility especially in seismic areas. This has led to the use of low strength ductile materials in larger sizes than would otherwise be possible with high strength brittle materials and consequently it is an issue of sustainability and efficient use of resources. The use of stainless steel reinforcement in concrete structures has normally been limited to high risk environments as its use is cost prohibitive. However, a modified nano-structure that makes it corrosion resistant, for example, is a good alternative to conventional stainless steel, but at a lower cost. In the same way, adding some nanoparticles changes some characteristics of the original steel making it more and more resistant as well as more sustainable, with a big reduction in its use. Fatigue is a significant issue that can lead to the structural failure of steel subject to cyclic loading, such as in bridges or towers. This can happen at stresses significantly lower than the yield stress of the material and lead to a significant shortening of useful life of the structure.

The current design philosophy entails one or more of three limiting measures: a design based on a dramatic reduction in the allowable stress, a shortened allowable service life or the need for a regular inspection regime. This has a significant impact on the life-cycle costs of structures and limits the effective use of resources and it is therefore a sustainability as well as a safety issue. Stress risers are responsible for initiating cracks from which fatigue failure results.

A study has shown that the addition of copper nanoparticles reduces the surface unevenness of steel which then limits the number of stress risers and hence fatigue cracking. Advancements in this technology would lead to increased safety, less need for monitoring and more efficient materials use in construction prone to fatigue issues.

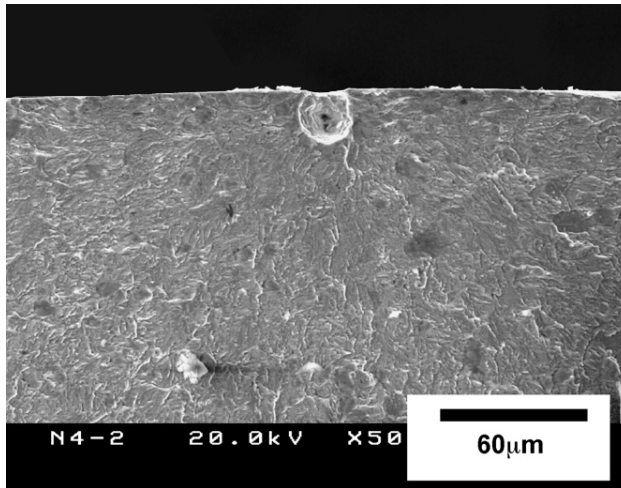


Fig. 7.4
SEM micrographs of
fracture surface
originating fracture.
(source: Chang-Min
Suha et. al., 2007)

Current research into the refinement of the cementite phase of steel to a nano-size has produced stronger cables. High strength steel cables are used in bridge construction as well as in pre-cast concrete tensioning; a stronger cable material would reduce the costs and period of construction, especially in suspension bridges as the cables are run from end to end of the span.

Sustainability is also enhanced by the use of higher strength cable as this leads to a more efficient use of materials.

High rise structures require high strength joints and this, in turn, leads to the need for high strength bolts. The capacity of high strength bolts is realized generally through quenching and tempering and the microstructures of such products consist of tempered martensite. When the tensile strength of tempered martensite steel exceeds 1.200 MPa even a very small amount of hydrogen embrittles the grain boundaries and the steel material may fail during use. This phenomenon, which is known as delayed fracture, has hindered the further strengthening of steel bolts and their highest strength has long been limited to somewhere around 1.000 to 1.200 MPa.

Research on vanadium and molybdenum nanoparticles has shown that they could improve the delayed fracture problems associated with high strength bolts. This is the result of the nanoparticles reducing the effects of hydrogen embrittlement and

improving the steel micro-structure through reducing the effects of the inter-granular cementite phase.

Welds and the Heat Affected Zone (HAZ) adjacent to welds can be brittle and fail without warning when subjected to sudden dynamic loading, and weld toughness is a significant issue especially in zones of high seismic activity. Weld and HAZ failures led to the re-evaluation of welded structural joints in the aftermath of the 1994 Northridge earthquake in the Los Angeles area and current design philosophy includes selective weakening of structures to produce controlled deformation away from brittle welded joints or the deliberate over-sizing of structures to keep all the stresses low.

Research currently under way, however, has shown that the addition of nanoparticles of magnesium and calcium makes the HAZ grains finer (about 1/5 the size of conventional material) in plate steel thus leading to an increase in weld toughness. This is a sustainability as well as a safety issue, as an increase in toughness at welded joints would result in a smaller resource requirement because less material is required in order to keep stresses within allowable limits.

Although carbon nanotubes are an exciting material with tremendous properties of strength and stiffness, they have found little application as an addition to steel as their inherent slipperiness makes them difficult to bind to the bulk material and they pull out easily, rendering them ineffective. In addition, the high temperatures involved in steel manufacture and consequently the effects of high heat on CNTs, presents a big challenge for their effective use as a composite component.

8. NANOTECHNOLOGIES FOR WOOD-BASED MATERIALS

8.1 Macroscopic and microscopic timber characteristics

Wood is a largely used material in construction from ancient times and its main characteristics are its anisotropic structure and non-homogeneous nature.

For technical purposes, only a stem without bark and pith is used. Cambium is a very thin layer of tissue containing the formative cells for the growth of the tree. Growth rings are visible in the cross-section of a stem as approximately concentric layers. When the conditions of the growth are nearly constant, as in tropical areas, the growth rings are not always distinct. In most species, a growth ring consists of early-wood and late-wood, with different structures of wood tissue. Usually around the 90% of the volume of soft-woods is comprised of cells called tracheids, which are parallel to the longitudinal axis of them. In soft-wood, tracheids serve for mechanical support and physiological needs. They consist of a cell lumen surrounded by a cell-wall and are usually 2-5 mm long with a 0,02-0,04 mm diameter. In hard-woods, the mechanical support is provided by some cells called of fibres, similar to the tracheids. Fibre are 1-2 mm long and 0,01-0,05 mm diameter.

Generally the fibres form at least 50% of the volume of hard-woods. Because mature wood cells are dead, even in the living tree, most cell lumina are empty and can be filled with water. Its cellular membrane, is composed of two different layers and small openings serve for communication between neighbouring cells. The primary wall is composed mainly of cellulose but, during the lignification process it receives large deposit of lignin. In the secondary wall there is about 10-20% of lignin. The wood tissue can be seen as reinforced concrete: cellulose represents the iron rods resistant to tensile forces, whereas lignin has the function of concrete, which is resistant to compression. The substance

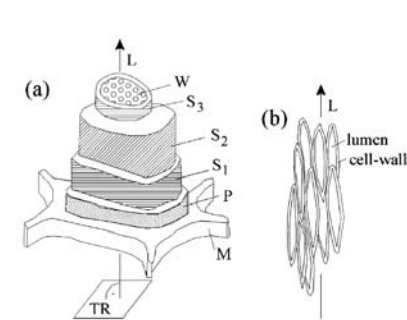


Fig. 8.2
Microscopic structure of tracheid or fibre. (a) cell-wall layers: M middle lamella; P primary wall; S_n layers of the secondary walls; W warty layer; (b) bundle of axially oriented cells. (source: Kopac, 2003)

that cements the cells together is called the middle lamella and it is mainly com-

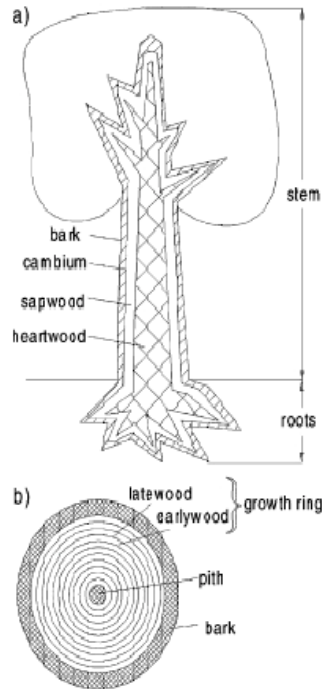


Fig. 8.1
Macroscopic structure of wood: (a) the main elements of the stem; (b) growth rings. (source: Kopac, 2003)

posed of lignin and some pectic substances. Wood is a high hygroscopic material and this affects its density and mechanical properties. Other factors are the structure of the wood, extractives and the chemical structure. Beside the differences in density between early-wood and late-wood, there is also variation in the density in the horizontal and vertical direction of the tree. Generally, in soft-woods and hard-woods, at each horizontal level of density increases with the distance from the pith, whereas in the vertical direction the density is higher at the foot than at the top of the tree. Other properties of wood which are strongly connected to its density are porosity and hardness.

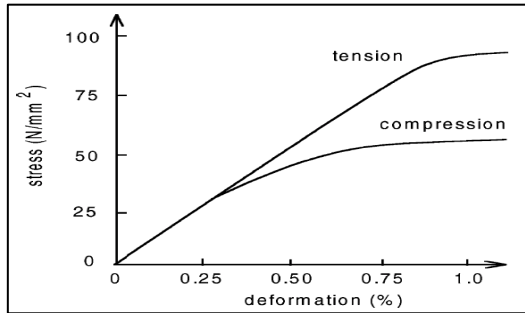


Fig. 8.3
Stress-deformation curves with the differences in tensile and compressive loading.
(source: Kopac, 2003)

From the mechanical point of view, wood is a viscous-elastic material; therefore relatively small elastic deformation can result in permanent plastic deformation if applied for a certain length of time. Usually the dependence of deformation on time is shown by creep curves.

8.2 Nanostructure of carbonized wood

The practice of converting wood into carbon to increase its resistance to degrading agents has existed for centuries. Carbonization of wood at high temperatures removes all carbohydrates, eliminating nutrient sources for microorganisms and insects. The resulting carbon is highly durable and is not subject to biological degradation. Studies performed in 1984 by F. Shafizadeh indicated that cellulose decomposes via two pathways when heated. The first pathway, which involves a reduction in the degree of polymerization, dominates at temperatures below 300 °C. The major decomposition products of this pathway are CO, CO₂, H₂O and solid carbon. The second pathway, which dominates at temperatures greater than 300 °C, involves cleavage of molecules and disproportionation reactions to produce a mixture of anhydro tar sugars and low molecular weight volatiles. There are considerable differences between the properties of carbons derived from cellulose and lignin when they are prepared at temperatures lower than 700 °C: cellulose carbon ablated faster at lower temperatures than lignin carbon. This difference in ablation properties decreased abruptly when the carbonization temperatures exceeded 700 °C. According to X. Xie, the difference in ablation properties was primarily due to the chemical structure of the materials, with the lignin carbon having fewer paraffinic structures than the cellulose carbon at lower carbonization temperatures. When wood fibre is heated in air at 250 °C there are readily visible changes, such as the colour change to dark brown or black as it is carbonized. However, changes can also occur at the nanoscale level. Heating wood and plant fibre in air at temperatures greater than 400

°C can result in a rapid ablation of the cellulose carbon derived from cellulose microfibrils. Under appropriate conditions, this can result in the formation of nanometer sized channels in the material that can act as template for carbon nanotubes production.

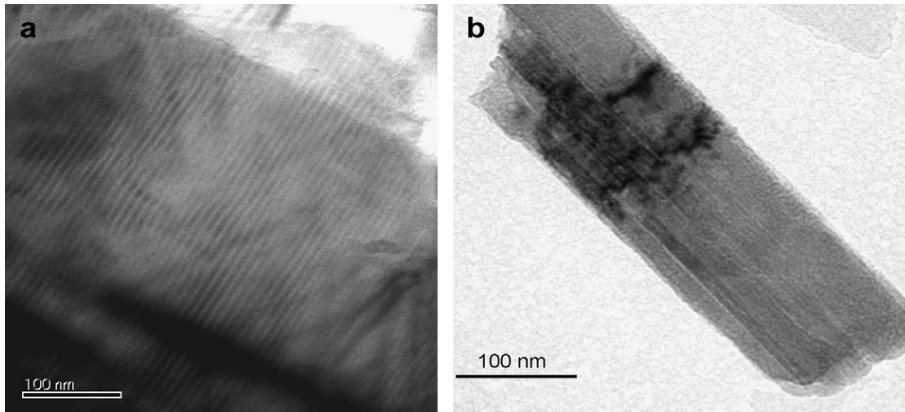


Fig. 8.4 Scanning electron micrograph of nano-channels in plant fibres undergoing oxidative carbonization at lower temperatures followed by oxidation at higher temperatures. a) wood fibre; b) bamboo fibre. (source: American Scientific Publishers, 2009).

8.3 Wood surface modification and nanocomposites

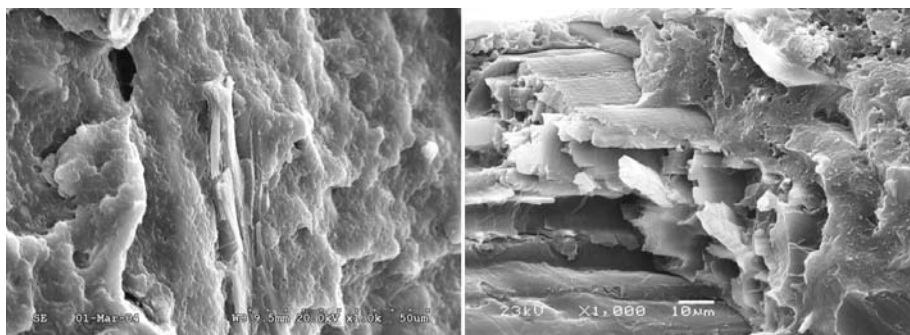
Architectural coatings are usually used to enhance the durability of wood, especially in exterior environment, designated to construction or decorative purpose. Those coatings are exposed to stressing factors (internal or external) such as solar radiation, humidity, temperature, oxygen, bacterial and fungus attack, freezethaw cycles, dirt and others chemical and mechanical factors due to pollution and continuous usage. The durability of wood coatings refers to loss of strength, embrittlement, discoloration, loss of adhesion, chalking, loss of gloss and environmental etching. It is still problematic for outdoor coatings to fulfil the guarantee periods expected by the users. Well-known, inorganic and organic UV absorbers that increase the polymer stability are often used in coatings formulation. Inorganic UV absorbers for exterior applications offer the most effective UV protection in the long-term because they do not decompose and do not migrate in coating during weathering. Beside the UV-shielding properties, ZnO and TiO₂ nanoparticles are known to improve thermal stability and wear resistance of polymers and increase the refractive indices of transparent polymers as well as antimicrobial and bactericide activity. All those beneficial properties require an homogeneous dispersion of the nanoparticles combined with a good stability during storage and drying of the coating.

Over the past years, the use of thermoplastic composites has experienced a dramatic growth in applications for building materials as well as automobiles and packaging industries. The lignocellulosic fibres, for instance, offer a combination of attractive properties such as low density, high specific strength and modulus, renewability, biodegradability, wide availability, and low cost, which make them alternatives to traditional synthetic fibres or protective coatings, in many applications.

However, some constraints do exist for the use of wood thermoplastic composites: low thermal stability that restricts the allowable processing temperature and hydrophilic nature that makes them difficult to process in many hydrophobic thermoplastics. Today, the production of polymer composites reinforced with wood is an established technology and many studies on nanocomposites were published in the last decade. Thermoplastic polymers like polyolefins (PP and PE), polyurethanes, polyimides and nylons are among the most studied matrices from the 80's. In many cases, fillers and coupling agents are added in polymers to enhance properties. The most used fillers are aluminium oxide (Al_2O_3), clay, calcium carbonate (CaCO_3), silica (SiO_2) and titanium dioxide (TiO_2). Studies generally showed that their addition in polymers is often related to a great improvement of mechanical properties.

Fig. 8.5

Scanning electron micrographs taken from the broken surfaces of tensile specimens. Wood content: 20 wt.% (left) 0.05 maleated polypropylene/wood ratio and (right) 0.5 wt.% Cellulose palmitate. (source: L. Dányádi, 2010)

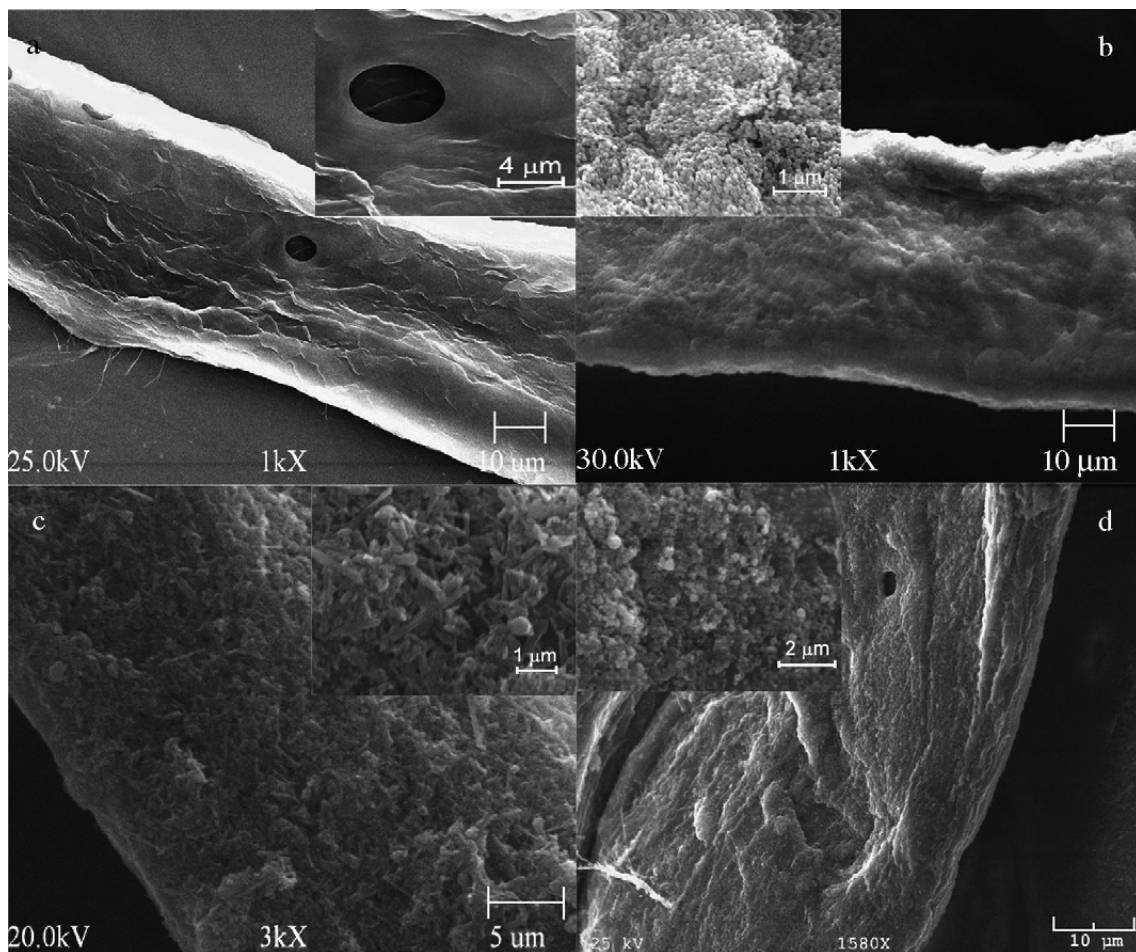


Improved scratch and impact resistance, Young's modulus, modulus of rupture are among the most researched properties for wood thermoplastic nanocomposites. Flame, fire and moisture resistance seem to be improved by clay introduction and exfoliation in thermoplastic polymers. In order to achieve the required combination of properties, interfacial interactions are often modified in these composites. Interfacial adhesion can be changed by the chemical or physical modification of the wood, by surface coating or by the introduction of a coupling agent, usually a functionalized polymer. The particles size of wood flour, routinely used for the reinforcement of plastics, is large and the particles easily debond during the loading of the composites that leads to the formation of large voids.

However, some problems of wood composites are not solve yet. They are aggregation, aesthetics or water absorption problems. Chemical modification is usually considerably more complicated than the simple addition of a component to the composite during homogenization. Surfactants can improve the processability and aesthetics of the product by decreasing interaction and friction among them, and they may decrease water absorption as well. Many efforts have been made to overcome these limitations and, in recent years, the layer-by-layer (LbL) self-assembly technique has been used for surface modification as it is possible to create thin films with a desired layer composition in a nanometre range, both on large surfaces and on microfibrils and cores, and can employ a great variety of substances including linear or

branched polyelectrolytes, nanoparticles and proteins. This technique involves the sequential adsorption of oppositely charged polyelectrolytes to the fibre surfaces. In literature, it is largely reported that many charged organic and inorganic nanoblocks have been used in this nanoassembly including globular protein, latex, SiO_2 , CeO_2 , ZrO_2 , TiO_2 , Fe_2O_3 , CdSe , Co , and Au nanoparticles as well as different types of clay, carbon and ceramic nanotubes thus changing the surface properties in a desired direction. The LbL modification method has largely been investigated in the field of paper science and successfully applied to cellulosic pulp fibres to enhance the properties of paper.

Fig. 8.6 (a) scanning electron micrographs of wooden virgin fibres coated with (b) four layers of SiO_2 nanoparticles, (c) halloysite clay nanotubes and (d) TiO_2 nanoparticles. (source Z. Lu, 2007)



9. NANOTECHNOLOGIES FOR QUALITY AND COMFORT

9.1 Self-cleaning coatings

9.1.1 Introduction

The technology of self-cleaning coatings has developed rapidly in recent years because of the wide range of possible applications. Their potential is huge and a lot of products are already on the market.

Basically, self-cleaning coatings can be divided into two categories:

1. hydrophobic coatings: characterised by rolling droplets of water that clean the surface;
2. hydrophilic coatings: characterised by sheeting water that carries away dirt with the additional property of chemically breaking down adsorbed dirt in sunlight.

Hydrophobicity and hydrophilicity depend on the contact angle¹ between water and the material surface.



Fig. 9.1
Contact angle:
left, hydrophobic
drop;
right, hydrophilic
drop.

9.1.2 Hydrophobic coatings – the Lotus-Effect®

Hydrophobic coatings are characterised by a high water contact angle so water forms almost spherical droplets that roll away on the surface carrying dust and dirt with them. Dirty water falling onto the hydrophobic coating is removed before it can evaporate. As a droplet rolls, an hysteresis develops in the contact angles at the advancing and receding three-phase interface between solid, liquid and gas. The requirements for a self-cleaning hydrophobic surface is a very high water contact angle $\theta_c \geq 160^\circ$. The theoretical description of contact angle arises from the thermodynamic equilibrium between the three phases: the liquid phase of the droplet (L), the solid phase of the substrate (S), and the vapor phase of the ambient (V). At equilibrium, the chemical potential in the three phases should be equal. It is convenient to frame the discussion in terms of the interfacial energies. We denote the solid-vapor interfacial energy as γ_{SV} , the solid-liquid interfacial energy as γ_{SL} and the liquid-vapor energy as γ , we can write an equation that must be satisfied in equilibrium, known as the Young Equation (eq. 9.1):

$$0 = \gamma_{SV} - \gamma_{SL} - \gamma \cos \theta_0 \quad (\text{eq. 9.1 Young Equation})$$

¹ The contact angle is the angle at which a liquid/vapour interface meets the solid surface. It is specific for any given system and it is determined by the interactions across the three interfaces.

where θ_0 is the equilibrium contact angle. The Young equation assumes a perfectly flat surface, and in many cases surface roughness and impurities cause a deviation in the equilibrium contact angle from the contact.

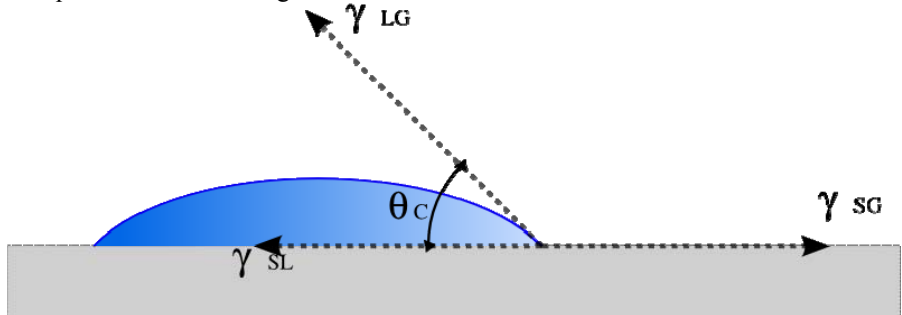


Fig. 9.2
Contact angle
scheme.

It is interesting to highlight that in nature there are several exempla of self-cleaning surfaces as a lot of plants use rolling droplets of water to keep clean.

More particularly, in the 1970s the botanist Wilhelm Barthlott, from the University of Heidelberg, observed this phenomenon on the Lotus leaves and on some other plants all over the world.



Fig. 9.3
Lotus effect in the
natural world.

What the plants have in common is a microscopically rough water-repellent surface that is covered with tiny knobbls or spikes so that there is a little contact surface for water to settle on. This phenomenon was described mathematically by Cassie and Baxter in the middle of the last century as explained above. Macro-sized droplets placed on a micron-textured surface finds it favourable to follow the contours of the surface, sinking down and spreading out. Therefore increasing the roughness of a

hydrophilic surface reduces the contact angle of a water droplet. On a rough hydrophilic surface the opposite occurs.

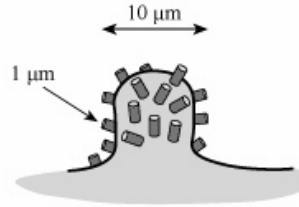
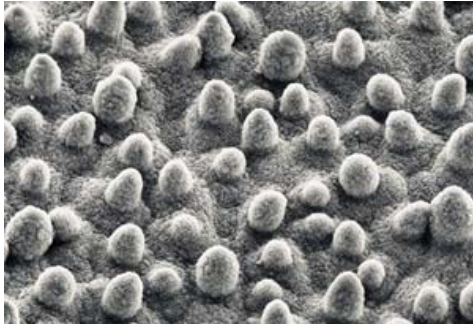


Fig. 9.4 a-b
 Electron micrographs of ultraphobic lotus leaf. Microscope observations reveal that the waxy surface of the lotus leaf is made of micron-sized bumps that are covered with nanoscale hair-like tubes. This two-fold structure traps air under any water drops that fall on the leaf, creating a surface that efficiently repels water. (source: Neinhaus, 1997)

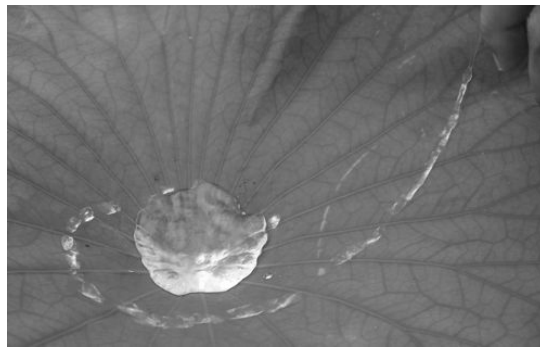
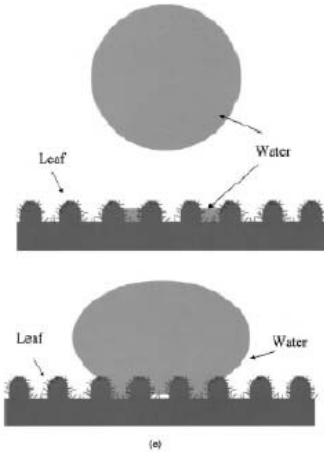


Fig. 9.5 a-b
 Left: Graphical representation of a water droplet on a Lotus leaf.
 Right: Natural Lotus-Effect ®.

It is important to notice that on the leaves, if some surfactants or other compounds are added to water, the hydrophobic effect is prevented. Nowadays, on the market there are some Lotus-Effect® products, such as the Lotusan self-cleaning painting by Sto, but they are well suited for surfaces that are regularly exposed to sufficient quantities of wa-

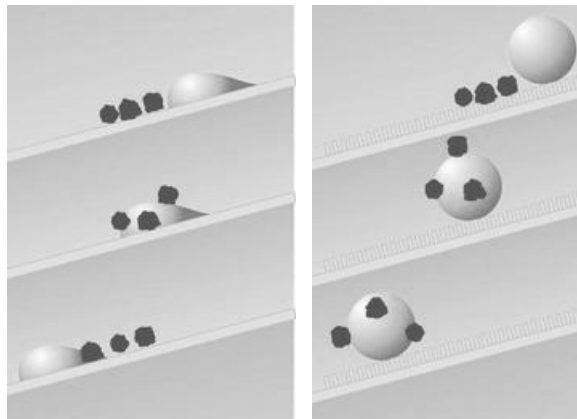


Fig. 9.6 a-b
 Schematic picture showing how Lotus-Effect ® works on a surface. On the left, as water droplets slip on a surface, dirt is simply lifted up and put down again. On the right, water droplets rolling on a hydrophobic surface, carry away dirt.

ter. Otherwise, small quantities of water leads to water droplet forming stains leaving the building façade even dirtier.

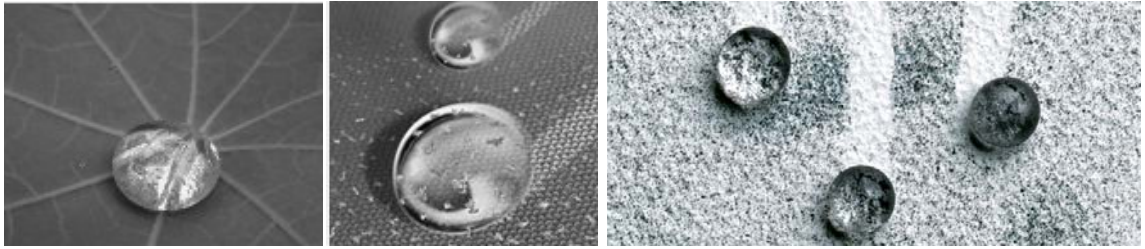


Fig. 9.7 a-b-c

Left: water droplet on Lotus leaf. Middle: trains of water on a leaf.

Right: in cases of insufficient quantity of water, droplets running off a building façade leave it even dirtier.

(source: Leydecker, 2009)

9.1.3 Hydrophobic coatings – production and use

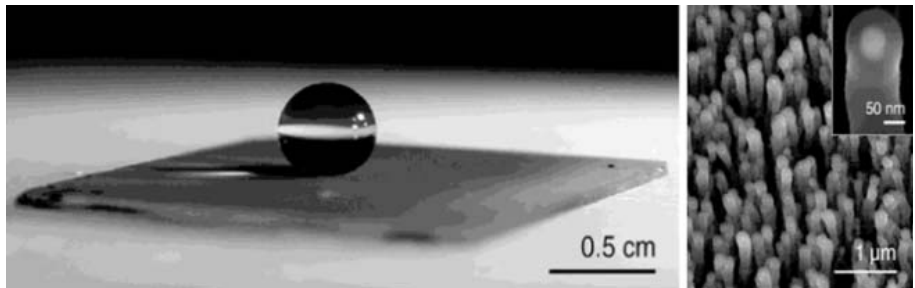
Several techniques are known for the micron-scale patterning of hydrophobic surfaces through the use of moulded polymers and waxes, by physical processing methods such as ion etching and compression of polymer beads, and by chemical methods such as plasma-chemical roughening. A way that was investigated is the production of a 2 mm thick film of vertically aligned carbon nanotubes (CNTs) via plasma enhanced chemical vapour deposition by Lau *et al.*. This technique grows CNTs by discharging a high voltage through an atmosphere of acetylene and ammonia. The result is a “forest” of vertically aligned CNTs, a surface highly textured on the micron scale. To induce ultraphobic behaviour, the CNTs must be rendered chemically hydrophobic, otherwise water will be simply absorbed by the texture. This was achieved by coating with a very thin layer of polytetrafluoroethylene (PTFE) via a second CVD process. This layer does not form a blanket on the surface but coats the length of the CNTs. The result is a highly textured surface with a hydrophilic coating with a contact angle value equal to 170° .

Fig. 9.8 a-b

Left: a drop of water resting on a PTFE coated carbon nanotube forest.

Right: an electron micrograph of the same ultraphobic surface.

(source: I.P. Parkin, 2004)



Processing a hydrophobic material is an expensive and time consuming technique and the coating produced are usually hazy and fragile materials. These facts prevented a widespread production and application.

One of the most used product, nowadays available on the market, is the self-cleaning paint StoCoat™ Lotusan® by Sto. It was successfully applied in the Ara Pacis Museum in Rome (Italy), planned by Richard Meier & Partners, to protect its white façade colour. The building, built on the bank of the Tevere river, was opened in 2006 to replace the old pavilion built in 1938 and protects the Ara Pacis Augustae.



Fig. 9.9
Rendering of the Ara Pacis Museum by R. Meier (Rome – Italy). (picture's copyright belongs to Comune di Roma, taken from: www.arapacis.it)



Fig. 9.10
Ara Pacis Museum by R. Meier (Rome – Italy). (picture's copyright belongs to Comune di Roma, taken from: www.arapacis.it)

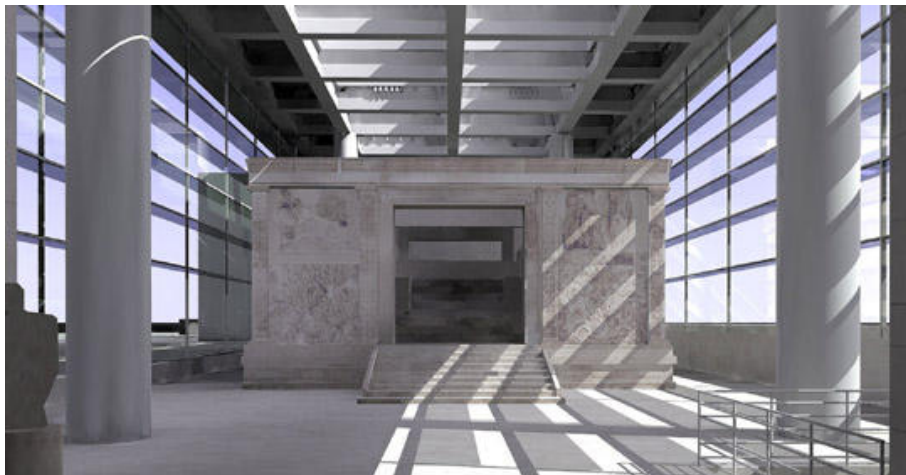


Fig. 9.11
Interior of the Ara
Pacis Museum by R.
Meier (Rome – Italy).
(picture's copyright
belongs to Comune di
Roma, taken from:
www.arapacis.it)

Other building were StoCoat™ Lotusan® by Sto was applied are, for instance, the following:



Fig. 9.12 a-b
Left: Playa del Mar
Condominiums, Ft.
Lauderdale, Florida
(USA).
Right: The Open
University hdq., Mil-
ton Keynes (UK).



9.1.4 Hydrophilic photocatalytic coatings – self-cleaning glass

The second class of self-cleaning surfaces differ from lotus effect coatings in that they are hydrophilic rather than hydrophobic. These coatings chemically break down dirt when exposed to light – a process known as photocatalysis – although it is the coating not the incident light that acts like a catalyst. The most used catalyst is titanium dioxide whose photocatalytic property was first discovered by Akira Fujishima² at the University of Tokyo, while working on his Ph.D. Under the supervision of Kenichi Honda³ he discovered the photocatalytic water decomposition (water

² Akira Fujishima was born in 1942 and from 2003 is Professor Emeritus at the University of Tokyo.

³ Kenichi Honda was born in 1925 in Tokyo. He was dean of the Faculty of Arts in 1994 and president of the University in 1996. In 1997 he received the designation as a “Person of Cultural Merit”, one of Japan’s highest honours.

photolysis) in the process in the TiO_2 surface later called Honda-Fujishima effect. Glazing is the largest commercialisation of self-cleaning coatings as they are used in architectural applications to create self-cleaning windows. These have been commercialized successfully by several companies, such as the NSG/Pilkington Glass⁴ or Saint Gobain Glass. Nowadays, all commercial self-cleaning windows are coated with a thin transparent layer of titanium dioxide, a coating that acts to clean the window in sunlight through two distinctive properties:

- photocatalysis causes the coating to chemically break down organic dirt absorbed onto the window;
- hydrophilicity causes water to form “sheets” rather than droplet – contact angles are reduced to very low value in sunlight (the coating becomes super-hydrophilic) – and dirt is washed away.

Both self-cleaning properties of TiO_2 are governed by the absorption of ultra-violet light and the generation of electron-hole pairs. The band gap of bulk anatase TiO_2 is 3,2 eV, corresponding to light of wavelength 390 nm, near ultraviolet (UV) light. A small proportion of the sunlight reaching earth exceeds 3,2 eV, so titania coatings can be solar activated.

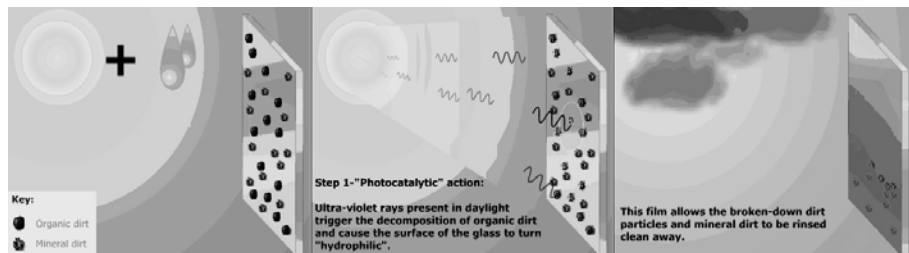


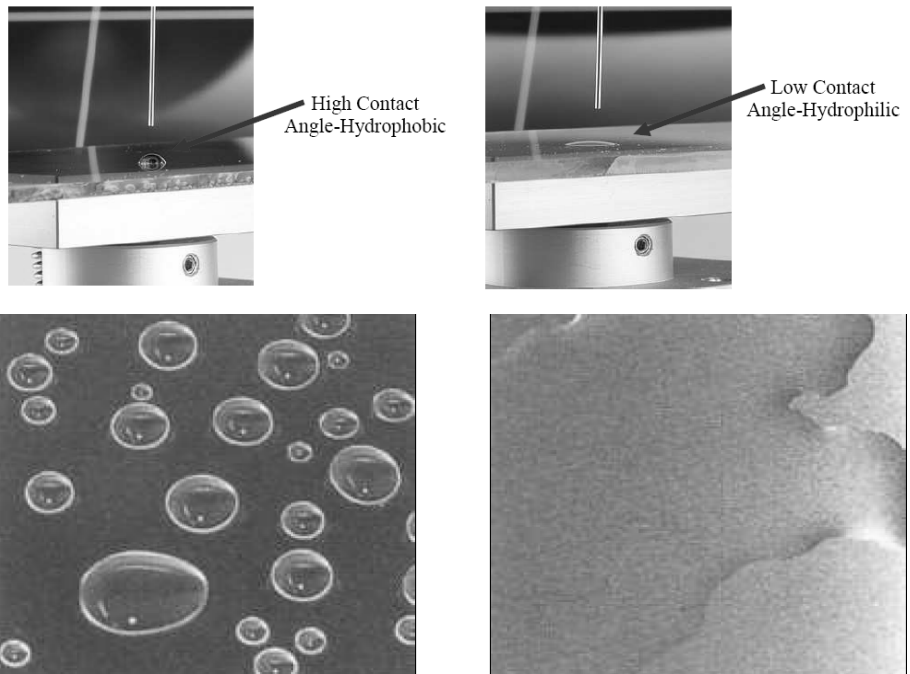
Fig. 9.13 a-b-c
Graphical scheme of a self-cleaning coating for glazing application work.

Titania has become the material of choice for self-cleaning windows, and hydrophilic self-cleaning surfaces in general, because of its favourable physical and chemical properties. Not only is titania highly efficient at photocatalysing dirt in sunlight and reaching the super-hydrophilic state, it is also non toxic, chemically inert in the absence of light, inexpensive and relatively easy to deposit into thin films.

The most significant polymorphs of TiO_2 are rutile and anatase. The position of the conduction and valence bands relative to key red-ox potentials cause pure anatase to be very photoactive (photocatalytic and super-hydrophilic) while pure rutile is less so. Anatase TiO_2 is formed at temperatures exceeding 300 °C, but converts into rutile around 800 °C. This temperature is a lot higher than the one usually found in a CVD process, although this temperature is exceeded on a float glass line. Titania films deposited by CVD tend to have small crystal sizes, with some commercial TiO_2 coatings have crystal sizes of 7-13 nm. The photocatalytic activity of a film is tested by measuring the destruction of an organic compound on the surface on the

⁴ Pilkington Glass was the first company announcing the development of a self-cleaning window in 2001, the Activ™.

film. Sunlight, or artificial UV light, is used to activate the coating, and IR, or UV spectroscopy, is used to quantify the destruction of the compound. TiO_2 has shown itself capable of breaking down a wide variety of organic compounds, including long-chain carboxylic acids, chlorinated and fluorinated compounds and aromatic compounds. Titania has a high refractive index and bulk TiO_2 is highly reflective. To achieve the high transparency required for windows, TiO_2 coatings must be under 50 nm thick so that the absorption of UV light is very low. Thicker films show significantly higher efficiency, and may be suitable for non-glazing applications.



There are a lot of self-cleaning glass already available on the market, such as the followings:

- Pilkington Active™ by Pilkington Glass (EU);
- Pilkington Active Blue™ (with solar control coating) by Pilkington Glass (EU);
- SGG Aquaclean™ (1st generation hydrophilic only, 2002) by Saint Gobain Glass (EU);
- SGG Bioclean™ (2nd generation, 2003) by Saint Gobain Glass (EU);
- SGG Bioclean™ Cool Lite ST (with solar control coating) by Saint Gobain Glass (EU);
- SunClean™ by PPG Industries (USA);
- Neat™ Glass by Cardinal Glass Industries (USA);

- Cleartect™ by Nippon Sheets Glass Co, Ltd. (Japan);
- Viewtec™ by Asahi Glass Co, Ltd (Japan).



Fig. 9.15 a-b
 Left: Pilkington Activ™ glass had been used in the MSV Arena Soccer Stadium, Duisburg, Germany.
 Right: Fergamma Offices, Mantova (Italy) – 2005, where SGG Bioclean™ glass produced by Saint Gobain had been used.

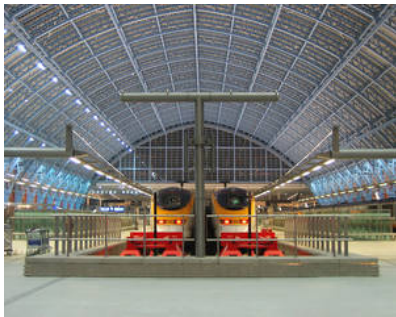


Fig. 9.16 a-b
 SGG Bioclean™ glass produced by Saint Gobain had been used in the arcades of S. Pancras Railway Station, London, UK (2007).



Fig. 9.17 a-b
 The Museum of Earth, New York (USA), where Pilkington Activ™ glass was used.



Fig. 9.18 a-b
In both these buildings Pilkington Active™ glass was used.
Left: the Chapel, Penge (UK).
Right : Hôtel de Région, Lille (France).



Fig. 9.19 a-b
Overground shelter in Veneto (Italy) where Pilkington Activ™ glass was used.



9.1.5 Hydrophilic photocatalytic coatings – other applications

Titanium dioxide has become the “gold standard” in photocatalytic hydrophilic coatings due to its high photoactivity and the ease of deposition. Aside from glazing applications, many other titania coated products have become available in the past years. Especially in Japan, where the photocatalytic properties of titania were first discovered, hundreds of companies produce self-cleaning products. Among the largest is TOTO Ltd, which manufactured several self-cleaning products with titania coatings for tiles, paints and textile, having registered about 270 patents.

Some products for architectural applications are:

- Selfclear™ by JFE Metal Products & Engineering Inc. (USA) - paint for external wall applications;



Fig. 9.20 a-b
Selfclear applications.

- Hydrotect™ by Deutsche Steinzeug Cremer & Breuer AG (EU) – metallic exterior tiles with anti-soiling property and interior ceramic tiles with antibacterial properties;



Fig. 9.21 a-b
Hydrotect application
Left: metallic antisoiling tiles.
Right: ceramic antibacterial tiles.

- SelfMax by Taiyo Kogyo Corporation (Japan) – film material for tent storage (Fig. 9.22 left);
- Skyclearcoat by Taiyo Kogyo Corporation (Japan) – film material for awnings (Fig. 9.22 right);
- Cleanmax by Taiyo Kogyo Corporation (Japan) - film material for buildings (Fig. 9.23 left);
- Ever Fine Coat by Taiyo Kogyo Corporation (Japan) – membrane for building (Fig. 9.23 right).



Fig. 9.22 a-b

Left: tent storage application.
Right: awnings application.



Fig. 9.23 a-b

Left: film material for big roofing.
Right: rendering image of the circular tensile membrane covering the children's playground in the Mannou National Government Park, Kagawa, Japan (2004).

An interesting application of TiO_2 , usually used to produce self-cleaning coatings on glass, is the cooling effect of evaporating water. This technology was experimented during the Expo 2005 in Japan when the windows, the canvas and the steel roofing of a trade fair pavilion were equipped with a photocatalytic TiO_2 coating and subjected to a constant stream of water. Due to the hydrophilic property of the surface, the water immediately formed a thin film, which evaporated quickly, absorbing in the process ambient warmth and thereby reducing the indoor temperature. Initial estimates suggest a potential energy reduction of between 10 % and 20 % in comparison to conventional air conditioning. In Japan, this effect is generally achieved by sprinkling water on the ground.

9.2 Easy-to-clean surfaces

Easy-to-clean surfaces (ETC) are water repellent smooth surfaces and they are often confused with self-cleaning glass due to their function. These surfaces have a lower force of surface attraction due to a decrease in their surface energy, resulting in reduced surface adhesion. This causes a water repellent effect so that water forms droplets and runs off. These surfaces are therefore hydrophobic and often oleophobic making them suitable for interior surfaces that require a high level of hygiene, as in bathrooms. Indeed, lots of applications could be found in ceramic sanitary installations or shower cubicle glazing. Anyway, each kind of material is suitable for this

kind of building application such as wood, metal, masonry or concrete as well as leather, facilitating the building management where cleaning costs represent a high proportion of maintenance costs. As a general rule, these coating should be applied on surfaces that are exposed to sufficient quantity of water and detergents must be used carefully to avoid damages. The treatment usually lasts from some months to a few years so it must be constantly renewed, that is why they are recommended for interior surfaces.



Fig. 9.24 a-b
 Left: Half coated stone after spraying with lacquer and cleaning with a high pressure cleaner with water.
 Middle and right: comparison of ceramic surfaces, middle, without ETC coating; right – with ETC coating.

9.2.1 Polysiloxanes and silane products

In any surface, there are lots of nano-porous between the crystals into which dirt and grease penetrate during normal use. With the coating process, thousands of crystals are deposited on the surface and enter the nano-porous creating a hydrophobic and smooth easy-to-clean surface, without changing the properties of the coating. Dirt stays on top of the surface and cannot go in between the above mentioned gaps. Polysiloxanes are the most common and one of the most important organosilicon polymers and the silanol, $\text{SiO}(\text{Me})_2$, is the key functional group in the synthesis of these polymers.

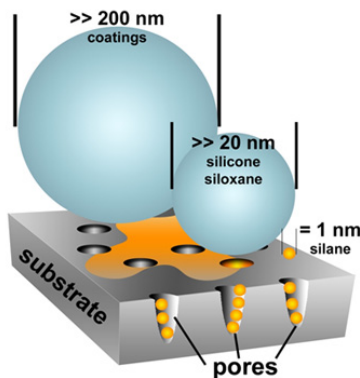


Fig. 9.25
 Comparison between 1nm sized silane particle and traditional coatings.

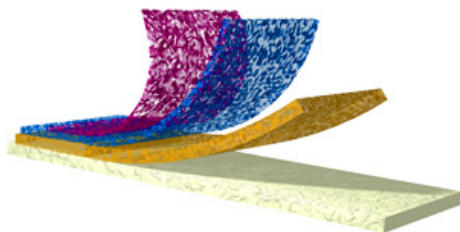


Fig. 9.26 a-b
 Stone with (left) and without (right) the Nanostone NS treatment.

Some products that are already available on the market, such as Nanostone NS produced by Nanoprotect Ltd., are supposed to perform up to eight years, providing a colourless, water-vapour permeable as well as hydro and oleophobic treatment on surfaces.

Fig. 9.27

CCFlex: four layer of ceramic wall covering that can be furnished with a functional easy-to-clean layer. From the latter: a flexible polymer, a coloured ceramic material, painting, ceramised top coat. It is produced by Degussa – Creavis technology and Innovation.



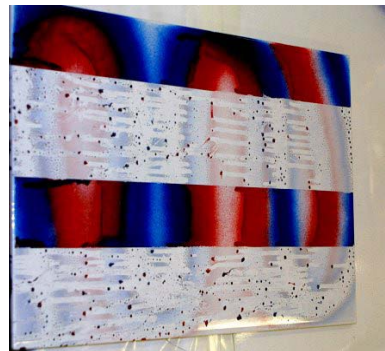
9.2.2 Other products on the market

An other product that presents a easy to clean coating is Steel enamel 3.5 mm produced by Kaldawei. It is a material used as surface finishing for bathroom accessories such as shower and bathtubs trays and it is guaranteed to remain resistant for 30 years. On the market there are also a great quantity of products available in bottles with sprayer or

in container that are supposed to create a easy-to-clean nanostructured coating on the surfaces. Some companies are: Percenta AG (Germany), Kälin & Co. AG (Switzerland), Nanosys (USA).

Fig. 9.28 a-b

Left: private residence in Erlembach (Switzerland) where the wood has been given a transparent hydrophobic treatment against rain and snow. The product used is Nanobois by Kälin & Co.. Right: Nanomers®. A easy to clean and antigraffiti coating on a ceramic tile produced by INM Leibniz – Insitut für Neue Materialien (Germany).



9.3 Air-purifying materials: coatings, paintings and capsules

9.3.1 The indoor air quality

The air-purifying properties of some nanomaterials are very important both for indoor as well as for outdoor environment. Though they are not able to completely purify the air, they help anyway in destroying pollutants and unpleasant odours. The indoor air quality is particularly important as people spend a lot of time inside buildings. Bad smells, pollutant or hazardous substances may influence a lot the way a person feels inside. Usually, the solutions used to deal with these problems are airing the rooms or using perfumes, but these methods have a limited effect. Nanotechnology may help in this way chemically decomposing pollutants and bad smells. To avoid the Sick Building Syndrome (SBS), lots of products are still on the market and

they can help in improving the air quality. To function in the best way, air-purifying surface area must be sufficient with regard to the volume of the room and must be exposed to air. For processes based on oxidative catalysis normal air circulation is sufficient while photocatalysis, for exemplum, requires daylight. The ability to reduce indoor air pollutants is therefore equally relevant for new as well as for existing buildings and lots of studies have been carried out on some different particles as nicotine, formaldehyde, ammonia, benzene and even fish odours. On the market it is still possible to find paintings or panels or textile with air-purifying properties. Anyway, it must be noted that the indoor air quality does also depend on oxygen content, relative humidity, temperature, ventilation, etc..



Fig. 9.29 a-b
RS Nano Air-purifying Panels by RS Nano Tech. These panels are impregnated with silver and titanium nanoparticles that makes them air-purifying and anti-bacterial up to 3 years. This company also produces tapestry with air-purifying anti-bacterial properties.

9.3.2 Air-purifying glass

An other way to improve the air quality is applying stained glass windows that are painted with gold. It was recently found out by a team of Queensland University of Technology that they purify the air when they are lit up by sunlight. For instance, numerous church windows across Europe are decorated with coloured glass by means of gold nanoparticles, they put together the beauty of the work of art along with “modern” discovered ability to destroy pollutant when energised by the sun. Often, in internal architecture air-purifying curtain materials can simultaneously be equipped with antibacterial properties and various products are already available on the market, with or without antibacterial combination.

9.3.3 Fragrant capsules

An other way to improve the air quality is affecting our subjective perception and our emotional response using minute fragrant capsules⁵. Fragrances are in a microcapsule and released in a controlled manner. The microcapsules exist in different forms with regard to their fillings that could be gaseous, solid or fluid and to the permeability of the container. The aroma function is initiated according to a “re-

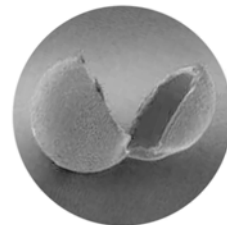


Fig. 9.30
Bayer micro-capsule.

⁵ The use of fragrances, whether natural or synthetic, should be regarded critically in the context of the rising incidence of allergies.

lease-on-demand” principle: the capsule, for instance, burst on mechanical contact when under pressure or when rubbed, releasing the fragrance contained within. These kind of capsules may be put in wall panelling or curtains or textile in general as carpets or even leather which have lost its typical smell due to the new processes of production. Usually, each individual microcapsule is about five micrometers in diameter and their shells are extremely fine, yet more stable than soap bubbles, transparent and highly elastic. The film surrounding the capsules is just a few nanometres thick and is usually made of polyurea. When the nano-film is subjected to pressure, it bursts like a balloon and releases its fragrant content.

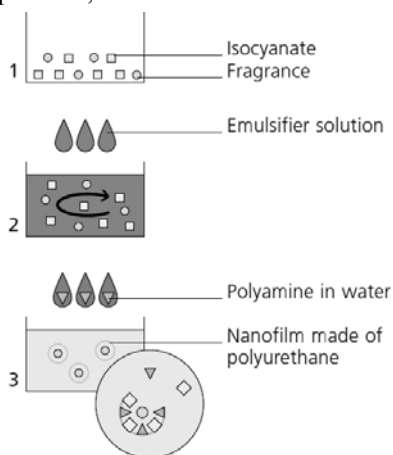


Fig. 9.31
Fragrance dispersion
into the capsules.

To get the fragrance into the capsule a particular process must be followed (fig. 9.31): the fragrance and the isocyanate, the water-insoluble polyurethane component, are mixed together by means of a mixer (1). The polyamine, which is the second polyurethane component, is then added to the aqueous solution (2). As the two polyurethane components are mixed together, they react on the surface of the micro-droplet forming a solid polyurethane nano-film containing the fragrance. The finely dispersed microcapsules float in the dispersion, which is then ready for spraying onto the relevant product.

Today, the microcapsules range in size from a few hundred nanometres to one millimetre. The capsules have to be small enough to penetrate into the material, but at the same time large enough to be trapped between the fibres.

9.4 Antibacterial materials

Improving hygienic standards in many parts of the world allow infectious diseases to be increasingly better controlled. Aside from contagion through contaminated air and direct contact with infected people or animals, contaminated objects play an important role in the spread of infectious diseases. Normal cleaning practices are mostly insufficient for elimination of bacterial or viral contaminants such as *Salmonellas*, *Campylobacteria*, *Escherichia Coli*, or noroviruses found up to 28% of the original contaminants to survive a visually thorough cleaning with detergents and disinfectants of surfaces contaminated by noroviruses. Thus, the hygienic properties of material surfaces are therefore important. In architecture, and especially in the interior practise, all surfaces are suitable candidates for antibacterial surface coatings, whether enclosing surfaces such as floors, walls and ceilings or furnishing. An antibacterial is anything that destroys bacteria or suppresses their growth or their ability to reproduce. Heat, chemicals such as chlorine, and antibiotic drugs have antibacterial properties. Many antibacterial products for cleaning and hand-washing

are sold today. Such products do not reduce the risk for symptoms of viral infectious diseases but, on the other hand, they show a potential contribution to reducing bacterial presence in buildings such as houses, hospitals, etc..

9.4.1 Efficiency of nanoparticles: activity, factors and mechanism

A large number of potential applications of nanotechnology have been developed in recent years. In the area of surface technology, nanoparticles have been used to prepare self-cleaning surfaces and to improve properties such as scratch and weathering resistance. Further, nanoparticles have been associated with improved antimicrobial properties, although their mode of action in this regard has not yet been thoroughly investigated. However, the possibility that nanoparticles may have adverse health effects in humans has not been ruled out. The antimicrobial activity of nanoparticles depends on many factors such as nanoparticles concentration. In the case of Ag^+ ions and metallic silver particles, the antimicrobial effect increases with increasing concentration. Yoon et al.⁶ observed a bactericidal effect on *Escherichia Coli* cultures only after the concentration of silver particles reached a certain level. However, no such minimum concentration was reported for copper particles.

Another factor is the particle type and dimensions depending on the bacteria to kill. Nanoparticle applications of different metals including silver, platinum and copper as well as metal oxides - such as MgO and TiO_2 - are described in literature. In a comparative study with silver and copper nanoparticles, copper showed a stronger antimicrobial effect than silver for *B. Subtilis* and *E. Coli*. The form of application is also important because it affects the bioavailability of biocides to microorganisms. Nanoparticles behave differently depending on whether they are embedded in a resin matrix or freely mobile in a dispersion, whether they are agglomerated or not, and whether molecules are adsorbed on their surface or not. A systematic comparison of the effects of individual factors such as particle size, concentration, and particle type is not possible based on the available literature. The effectiveness of nanoparticles also depends on the organism investigated, the form of application of the particles, and the mechanism of action. The biocidal mechanism can be both intracellular or extracellular. In the former case, the toxic effect results mainly from bonding to intracellular proteins or DNA. In the latter case, nanoparticles disrupt material transport chemically by attaching themselves to cell membranes, destroy the cell integrity in combination with other biocides, or cause mechanical damage to the cell wall. In a more detailed way, with an intracellular action nanoparticles fall approximately in the same size category with biomolecules and can therefore easily interact with them. For instance, the silver antimicrobial effect is partly due to nanoparticles binding to microbial DNA, which disrupts cell replication and thus hinders bacterial multiplication. Nanoparticles can also attach themselves to sulfhydryl (SH^{\cdot}) groups of enzymes which are important for metabolism. This disrupts electron transport, prevents cell respiration, and inactivates cells. A prerequisite is that the nanoparti-

6 K.-Y. Yoon, J.H. Byeon, J.-H. Park, J. Hwang, *Sci. Total Environ.* 373 (2007)

cles are taken up by the microorganisms. Nanoparticles should be released from an actively biocidal coating preferably continuously and in small amounts. In case of extracellular action, the disruption of cellular mass transport is due to the nanoparticles large surface area that allows more atoms to bind on their surfaces. This facilitates the adsorption of nanoparticles on bacterial cell walls, which changes the membrane properties of the bacterial shell, disrupting mass transport across the shell and, possibly, killing the bacterium itself. Nanoparticles are therefore well-suited for shuttling biocidal substances in the vicinity of the bacterial cell wall.

9.4.2 Silver antibacterial effect

The antimicrobial properties of silver have been known for more than 3000 years, and physicians have used this metal as disinfectant since the end of the XIX century. The primary difference between the current use of silver and that of the past is one of the scale. Previously, silver was used in its classic form as a metal alloy and was comparatively coarse in structure. The antibacterial effect of silver results from the

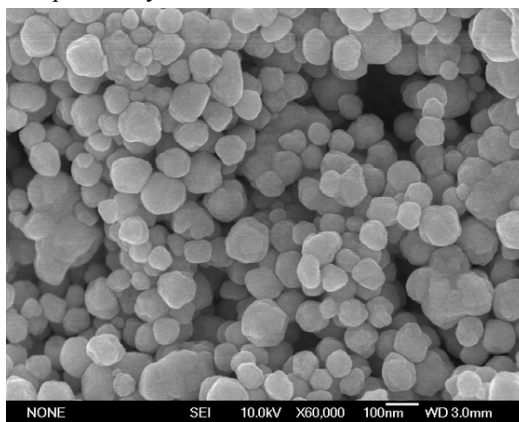


Fig. 9.32
SEM Micrograph
image of silver
nanoparticles.
(source:
www.azonano)

ongoing slow diffusion of silver ions. The very high surface area to volume ratio of the nanoparticles means that the ions can be emitted more easily and therefore kill bacteria more effectively. Bacteria have no chance of survival as the ions firstly hinder the process of cell division, secondly destabilize the cell membrane, walls or plasma and thirdly interrupt the enzyme's transport of nutrient. In this way, bacteria can be lastingly eradicated without the use of chemicals.

Furthermore, the antibacterial effect itself is also permanent. In addition, it is also advisable to equip surfaces with an anti-stick function to prevent the build-up of a bio-film of dead bacteria from which new bacteria could eventually grow. Silver nanoparticles not only reduce the need for chemical disinfectants but also reduce the amount of

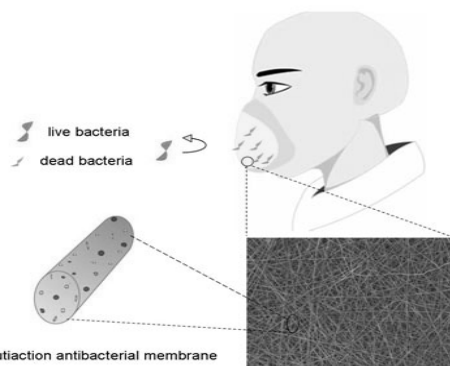


Fig. 9.33
Schematic illustration
of the use of multi-
action antibacterial
fibrous membranes as
protective face mask.

cleaning time necessary. Whether in the form of ultra-thin and invisible coatings or

materials to which the silver nanoparticles have been added, they represent an effective and unobtrusive bacterial killer, which, when employed, can sensibly offer significant benefits.



Fig. 9.34

Top: Housing Estate in Duisburg, Germany, 2004. The facades of the building were covered by mould that was very hard to eradicate (left and middle). A paint enhanced by silver nanoparticles was used to restore them, and 3 years later no mould infestation was seen (right).

Bottom: Operating theatre in Goslar (Germany) where floors and walls have been clad in silver photocatalytic tiles.

9.5 Photocatalysis for antibacterial applications

TiO₂ nanoparticles have many different applications due to their interesting polymorphable nature and particles action. The action of TiO₂, in its anatase form, is based on its semi-conductive properties and covers the gap between conductor and non-conductor bands from >3.2 eV. Since microorganisms are susceptible to UV light, UV irradiation has long been used for disinfection purposes thus photosensitizers boost the disinfecting effect considerably. The use of nanosized TiO₂ particles for destruction of microorganisms based on their photocatalytic effects has been known since the 1980s. The irradiation of TiO₂ with light at the wave length of 385 nm leads to formation of electron-gap pairs on the surface of TiO₂. This gap in the valence band is highly reactive, reacting with water molecules or hydroxyl ions adsorbed on the surface, producing singlet oxygen and hydroxyl radical species. The extra electron in the conductor band can reduce molecular oxygen to superoxide ion O₂⁻. The photocatalytically formed species are extremely reactive toward organic materials: on the one hand, they can destroy cell wall components of microorganisms, on the other hand, the oxidative elimination of organic impurities from the laminate surface deprives microorganisms of their nutrition source, hindering their growth. Such surfaces are called self-cleaning. Besides this purely photochemical mechanism of action, cells can also be deactivated as a result of their agglomeration onto TiO₂ particles. Individual particles can be taken up by cells and cause massive intracellular damage. An important advantage of photocatalysis lies in the inability of bacteria to become resistant to it. As long as photocatalysts are firmly anchored to

the matrix, they are not destroyed or washed off. Normally, small quantities are enough to obtain self-cleaning, microbe free, and chemical-free surfaces. Despite these attractive properties, a large number of application-technical problems remain to be solved before these technologies are commercially feasible. There are no established technologies in the market for the application of photocatalytic TiO_2 in laminate coating resins. The mixing of TiO_2 in melamine resin gives a coating matrix with a high nanoparticle content, which poses the danger of autocatalytic coating destruction. The cost of using expensive materials whose active components are readily consumed on the substrate surface is also prohibitive. Further, the effectiveness of the technology requires that sufficient light must be provided and that molecular oxygen and comparable reducible substances must be available. With pure TiO_2 films, normal ambient light conditions, together with a convective air supply, are sufficient to produce a photocatalytic effect. In contrast, the effectiveness of low concentrations embedded in a matrix remains to be shown. To avoid unduly high bulk concentrations, photosensitizers could be applied onto paper surface using an applicator roll or in water based buffer solution applied by spraying. It may be necessary to separate the photocatalytic layer from the melamine resin with a barrier layer, because a direct contact between catalyst and resin could result in autocatalytic resin destruction. Separation could be achieved by embedding TiO_2 in inert top coat systems based on sol-gel. However, the application of this technology would cancel out the real technological advantages of melamine films such as wear resistance, durability, and hardness.

9.6 Anti-graffiti coatings

Cleaning graffiti off buildings costs millions of dollars every year around the world.



Fig. 9.35
Saint Antonio's
Church in Pisa (Italy)
vandalized with graffiti.

Many cities have started anti-graffiti programs but vandalism is still a big problem.

Industries are attempting to develop coatings to prevent taggers from vandalizing public and private property for both new constructions as well as in building conservation. The coatings being developed can be the paint itself, or a clear coat added on top of existing paint or building facades.

Tab. 9.1 Annual expenses of graffiti cleaning in some places [US\$]	
Germany	Over 700 million
UK	1.5 billion
London	200 million
Los Angeles	140 million

Traditional anti-graffiti coatings are applied to surfaces to reduce the adhesion of graffiti. Unfortunately, they present two major disadvantages: first of all, the protective coating cannot be removed; secondly, it forfeits surfaces permeability. Nanotechnologies seem to have increased these coatings properties as they are highly effective and are used to make building materials water-repellent. Their extremely hydrophobic properties mean that graffiti can be removed more easily with appropriate detergents. Even porous and highly absorbent materials such as brick, lime sandstone, concrete and other similar materials can be protected efficiently using such nano-based coatings. Although the coating is effectively an impregnation, unlike other systems it does not close the pores of the material, allowing it to retain its vapour permeability. As the material remain permeable potential damage resulting from dampness is avoided. The ultra-thin nano-coating lines the capillary pores without closing them. More dense materials, such as compressed concrete, in general require less coating material.



Fig. 9.36

Top: Brandenburg gate in Berlin (Germany) is protected with an anti-graffiti coating since 1990.

Bottom: UEFA headquarter in Nyon (Switzerland), planned and constructed by Patrick Berger and Francis Goetschmann between 1993 and 1999, is fitted with anti-graffiti flooring to better remove chewing gum.



Furthermore, an anti-graffiti coating reduces dirt accumulation significantly, making the coating applicable for use on floor surfaces too, to clean chewing gum for instance. The effect of the impregnating coating is the result of several layers of molecules that are distributed evenly and have the same orientation. The upper layer fulfils a hydrophobic function, with a significantly reduced surface tension and molecular attraction; the lower layer ensures the entire coating adheres to the substrate it is applied to. The major problem is that the lower layer is not reversible once applied, so it cannot be removed. On the other hand, the appearance of the underlying surface remains unchanged, but variants with added coloured pigments are already available on the market.

9.7 Fire protection and detection

9.7.1 Fireproofing traditional materials

Fireproofing is a passive fire protection method to make materials, or structures in general, more resistant to fire. Fireproofing certification and rating are often compulsory in construction practice, especially for those buildings that are planned for a huge quantity of people at the same time.

The term *fireproof* does not necessarily mean that a building component cannot ever burn: it relates to measured performance under specific conditions of testing and



Fig. 9.37
Spray gypsum based
plaster fireproofing.

evaluation. Fireproofing does not allow treated items to be entirely unaffected by any fire, as conventional materials are not immune to the effects of fire at a sufficient intensity and/or duration. Some traditional materials used in construction are gypsum or cementitious or fibrous plaster. The industry considers gypsum-based plasters to be cementitious, even though these contain no Portland cement, or calcium alumina cement. Cementitious plasters that contain Portland cement have been traditionally lightened by the use of inorganic lightweight aggregates, such as vermiculite and perlite. Gypsum plasters have been lightened by using chemical additives to

create bubbles that displace solids, thus reducing the bulk density. Also, lightweight polystyrene beads have been mixed into the plasters at the factory in an effort to reduce the density, which generally results in a more effective insulation at a lower cost. Fibrous plasters, containing either mineral wool, or ceramic fibres tend to simply entrain more air, thus displacing the heavy fibres.

Other materials based on organic chemistry gained in popularity for a variety of reasons. In land-based construction, thin-film intumescent have become more widely used. Unlike their inorganic competitors, thin-film intumescent are installed

like paint. Thicker intumescent and endothermic resin systems tend to use an oil basis, usually epoxy, which, when exposed to fire, creates a thick smoke. Even though these products provide enough heat flow retardation towards the substrate, they tend to be banned from use inside of buildings because of the smoke they produce when subjected to fire, and are used mainly in exterior construction, such as LPG vessels, vessel skirts and pipe bridges in oil refineries, chemical plants and offshore oil and gas platforms.

9.7.2 Innovation in cement and network detector

Fire resistance of structures, and especially of steel, is often provided by a coating produced by a spray-on cementitious process, as stated in the previous section. Research into nano-cement has the potential to create a new paradigm in this area of application because the resulting material can be used as a tough, durable, high temperature coating. This is achieved by the mixing of carbon nanotubes with the cementitious material to fabricate fibre composites that can inherit some of the outstanding properties of the nanotubes, such as its strength. Polypropylene fibres also are being considered as a method of increasing fire resistance. This is a cheaper option than conventional insulation.

Furthermore, the use of processors in fire detection systems, which are built into each detector, head is fairly well established today. These improve reliability allowing better addressability and the ability to identify false alarms. The use of nanotechnology in the future through the development of nano-electromechanical systems (NEMS) could see whole buildings become networked detectors, as such devices are embedded either into elements or surfaces.

9.7.3 Glass-like coatings for panels

Flame-resistant lightweight building boards, sandwich elements made of straw and hemp, are a further interesting application in architecture. Originally developed for rapid construction in developing countries with special climatic needs, these panels can be also used nowadays for interiors and exhibition stands. By coating the product in a transparent covering of glass-like particles, it is possible to render it weatherproof and flame-resistant, despite the fact that it is made of natural, inherently easily flammable materials. The glass-like coating also serves as the adhesive and further flame retardant additives are not required. This technology is particularly interesting for corridors, foyers and meeting areas.

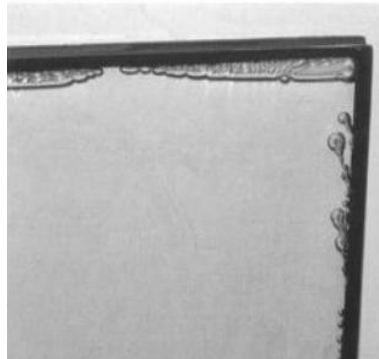


Fig. 9.38

A robust sandwich panel made of straw and hemp with a glassy coating that serves as bonding agent and is also fire-resistant.

When exposed to fire the product smolders and extinguishes.

9.7.4 Fire-safety glass

In Switzerland, the Interver Special Glass Ltd., in cooperation with the German Degussa, produces a safety glass of only 3 mm thick that provide more than 120 minutes of fire resistance against constant exposure to flames of a temperature of over 1000°C.

Depending on the desired duration of fire-resistance, Aerosil® is sandwiched between glass panes. Aerosil® is a pyrogenic silicic acid made by 7 nm large nanoparticles. These nanoparticles are highly reactive due to their large surface area that can be modified following the particles size. Standard products are generally between 90 and 380 m² per gram.

The main advantages of this technology is the very light weight of the glass, the slender construction, the good optical properties and the long duration of fire-resistance. In the event of fire, the fire-resistant layer expands in the form of an invisible foam preventing the fire from spreading and keeping escape routes accessible for users and firemen. Furthermore, it is also noise insulator and fulfils international testing criteria, norms and regulations and is certified for use around the world.

It is currently installed in Dubai's International Airport, the major aviation hub in Middle East, in the Terminal 3 that opened its doors on 14 October 2008, overtaking Beijing Capital International Airport's Terminal 3 as the largest terminal in the world.



Fig. 9.39
Dubai International
Airport, Terminal 3 –
render of the exterior.



Fig. 9.40 a-b
Dubai International
Airport, Terminal 3 -
exterior.



Fig. 9.41
Dubai International
Airport, Terminal 3 -
interior.

An other application was made at the beginning of the 1990s by the company Vetrotech Saint-Gobain International that conducted research into foaming silicate fire-resistant materials in fire-safety glazing.

The nanostructured fire-resistant mass, sold under the product name of “SGG Contraflam[®] fire safety glass”, is not affected by UV light and even thin layers offer fire retarding properties in excess of 120 minutes. In the event of a fire, the nanosilicate forms an opaque protective layer against the fire and heat radiation.

Tab. 9.2 SGG Contraflam [®] fireproofing performance	
Thickness [mm]	Integrity and insulation [min]
16	30
23	60
33	90
58	120

Fig. 9.42 a-b-c-d

Top left: German Post office headquarter in Bonn (Germany). Planned by Murphy e Jan, is entirely covered by SGG Contraflam® glazing.

Top right: The Cyberport project is being developed at Telegraph Bay in the Southern District of Hong Kong Island, on a 24 hectares of land reclaimed in 1989. The Cyberport is an important information infrastructural project that will provide first-class office accommodation for over 100 information technology and IT-related companies, a specially designed Cybercentre for over 50 commercial tenants of different trades and a deluxe international hotel that will have 176 rooms. It will all be built using SGG Contraflam® glazing.

Bottom left and right: Waverley Gate in Edinburgh (UK). A modern office complex, currently unoccupied. Planned by Hugh Martin Partnership, it was formerly the main Post Office.



9.7.5 Nano fire-proof paint

Nano fire-proof and flame retardant paints and coatings are the most studied and developed materials in building technology. New paintings are released everyday all around the world with increased properties and performances.

Researchers at the Department of Chemistry at the University of Warwick replaced the soap used to stabilize latex emulsion paints with nano-sized clay armour coating the polymer particles used in paints with a series of nanosized Laponite clay discs. These disks create a layer on the polymer latex group and they can be applied with presently available industrial paint manufacture equipment. Having a diameter of only 1 nanometre, the clay disks are individually small but extremely resistant as an ensemble. Laponite clay disks, in addition to being an efficient alternative to soap, can produce highly wear-resistant and fire proof paints. Tests revealed that the disks can burn away the polymer cores of the armoured particles within a closely packed sample, to produce a network of nanosized connected hollow spheres which provide an extremely useful surface area in a very small space.

In 2009, Australia's Commonwealth Scientific and Industrial Research Organisation (CSIRO) researchers, at the Materials Science and Engineering division, in Melbourne, developed tough fire-resistant coating materials called 'hybrid inorganic polymer system', or HIPS, which can withstand temperatures of over 1000 °C while current commercial coatings used on building materials and structures usually break

down at between 150-250 °C. HIPS coatings contain an inorganic geopolymer⁷ resin, and a small component of polymer additives that make HIPS not only fire-resistant but also blast- and acid-resistant and also strong, castable, sprayable, and extrudable.

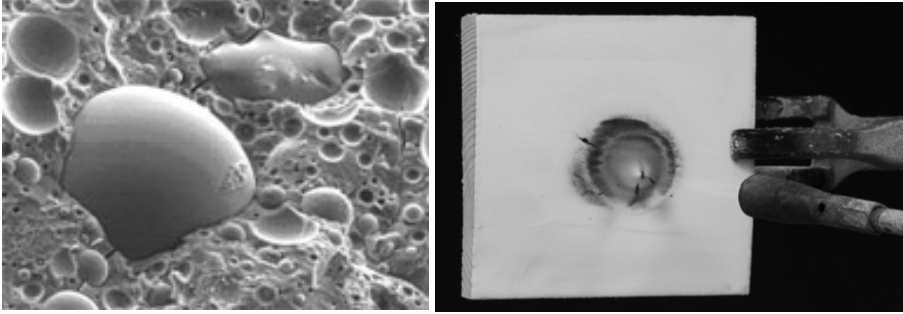


Fig. 9.43
Left: high magnification image of a geopolymer binder;
Right: HIPS coating.

9.7.6 Bamboo nanocomposite for flame-retardant boards

In U.S. Patent 7647957 (19 January 2010), Infinity Board, LLC (Seattle, WA) details a method of producing a virtually fireproof plywood from perennial grasses such as *Arundo Donax Ligneous*, various bamboo strains, or a blend of the materials. This is accomplished by first weaving the stalks of these plants into a mat and then layering these mats and binding each layer with any one of several commercial resins mixed with potash for the purpose of enhancing the board's fire retardant quality. The result is the formation of a finished product with structural board attributes and an exceptionally high flash point in relation to other manufactured board products made from forest materials.



Fig. 9.44
Arundo Donax Ligneous in a natural forest.

⁷ Geopolymer is a term covering a class of synthetic aluminosilicate materials with potential use in a number of areas, essentially as a replacement for Portland cement and for advanced high-tech composites and ceramic applications.

The combination of both structural board and dimensional lumber made from green materials utilizing this innovative method meets the objective of the inventors to provide a “total green” building system. These materials are ultimately designed as structural board and dimensional lumber products, but may also be used for other construction purposes which are non-structural in nature and in various other industries where they may be beneficial. Bamboo will provide a cost effective material superior in performance to wood for the manufacture of engineered building.

9.8 Anti-icing materials



Fig. 9.45
Iced roads and buildings.

Like most things, ice can be very dangerous if it forms on the roads, on rails or on buildings depending on the circumstances. At the University of Pittsburgh, an interesting study found out a way to reduce these dangers by developing a nanoparticle-based coating that can be easily applied to impede the building-up of ice on solid surfaces. More particularly, a team, led by prof. Di Gao, a chemical and

petroleum engineering professor, demonstrates the anti-icing capability of some super-hydrophobic surfaces made of nanoparticle-polymer composites. The anti-icing capability of these composites depends not only on their super-hydrophobicity but also on the size of the particles exposed on the surface. The critical particle sizes that determine the super-hydrophobicity and the anti-icing property are in two different length scales. In the experiments conducted, the team created different batches made of a silicone resin-solution combined with silica nanoparticles ranging in size from

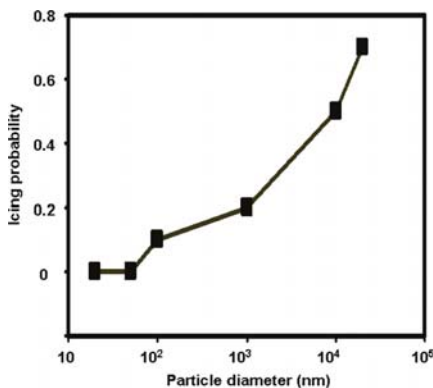


Fig. 9.46
Icing probability as a function of the particle size.

20 nanometres to 20 micrometres. They applied each variant to aluminium plates that were afterwards exposed to super-cooled water (-20 °C) to simulate freezing rain. They found that, although each compound containing silica bits of 10-or-fewer micrometers deflected water, only those with silica pieces less than 50 nanometres in size completely prevented icing. The minute surface area of the smaller fragments means they make minimal contact with the water. Instead, the water mostly touches the air pockets

between the particles and falls away without freezing. Though not all super-hydrophobic coatings follow the “Pitt recipe”, the researchers conclude that every type will have a different particle-scale for repelling ice than for repelling water. To

test its real world potential prof. Gao tested the coating with 50-nanometre particles outdoors in freezing rain. He painted one side of an aluminium plate and left the other side untreated. As can be seen in the picture below the treated side had very little ice, while the untreated side was completely covered. He produced similar results on a commercial satellite dish where the glossed half of the dish had no ice and the other half was encrusted.

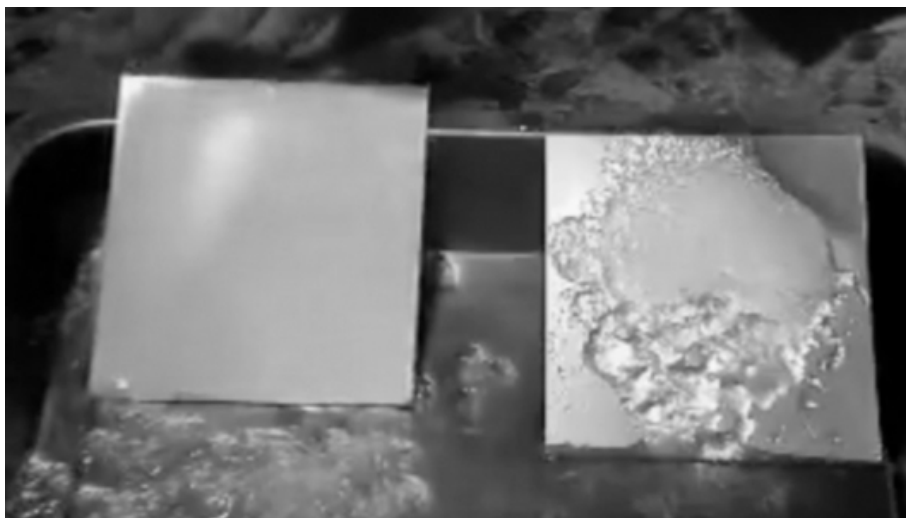


Fig. 9.47

The surface on the left coated by the super-hydrophobic coating is devoid of ice. The uncoated surface, on the right, is almost completely covered.

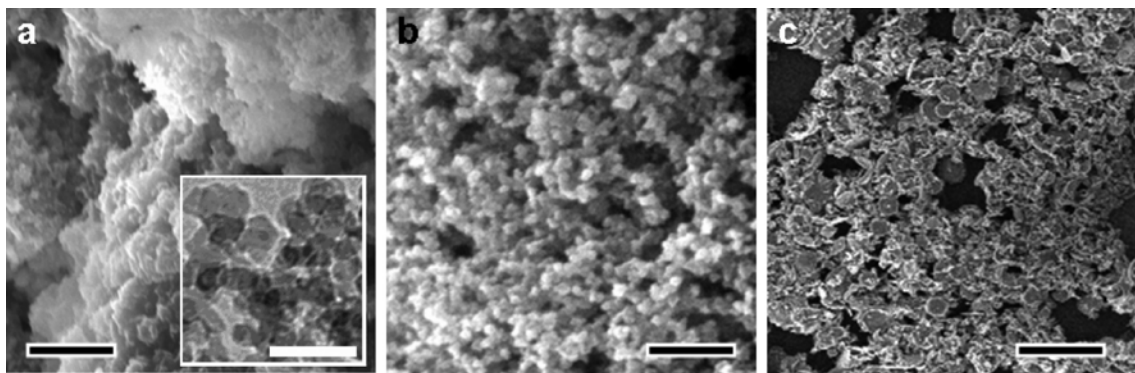


Fig. 9.48

Representative electron micrographs of particle-polymer composites. (a) particle-polymer composite made of 20 nm silica particles. Scale bar=1 μm . (Inset) Transmission electron microscopy image. Scale bar=50 nm. (b) particle-polymer composite made of 50 nm silica particles. Scale bar=1 μm . (c) particle-polymer composite made of 20 μm silica particles. Scale bar=100 μm . (source: Di Gao)

10. NANOTECHNOLOGIES FOR ENERGY CONTROL AND SAVING

10.1 Thermal regulation materials

10.1.1 Phase-change materials (PCM)

Regulating the building temperature consumes vast quantities of energy for both heating and cooling. In that process a great quantity of CO_2 is emitted whilst its reduction is recognized as a mean theme of concern for the countries worldwide.

Nanotechnology may significantly help in reducing the energy wasting with a large class of materials that could be used as heat storage, the phase change materials. For instance, in the USA up to 40% of all energy used is consumed by commercial or residential structures and nearly the 70% of that energy is spent on heating or cooling the buildings. According to the Oak Ridge National laboratories, the US Department of Energy (DOE) and others, the use of properly formulated PCM within the structures may reduce the energy load by between 40% to 60%.

Heat energy flows from a warmer to a cooler place and the amount of heat flow depends on the temperature difference between the two places and the conductivity of the heat flow path. Traditionally, we limit heat flow by placing more thermal resistance ("R" value) between the two temperature differences. Ordinary thermal insulation, such as fibreglass or cellulose, works by slowing down the rate at which heat energy flows from a warmer to a cooler area. On the contrary, a phase change material (PCM) do not change temperature during the heat flow, which is strictly related to a change of phase.

Generally, a PCM is a substance with a high heat of fusion¹ that, melting and solidifying at a certain temperature, is capable of storing and releasing large amounts of energy. Heat is absorbed or released as the material changes from solid to liquid and vice versa; thus, PCM are classified as latent heat storage units. PCM can be used as an effective means of regulating indoor room temperatures. Their good thermal retention can be used in both new and existing buildings as a passive means of evening out temperature fluctuations and reducing peak temperatures. A good example that illustrates the high thermal capacity of latent heat stored is an ice cube that begins to change to its liquid state at 0°C . Its liquid state also begins at 0°C but the energy required for this change of state is equivalent to that required to heat liquid wa-



Fig. 10.1
A typical sodium acetate heating pad. As the sodium acetate solution crystallises, it becomes very warm.

¹ The standard enthalpy of fusion also known as the heat of fusion or specific melting heat, is the amount of thermal energy that must be absorbed or evolved for 1 mole of a substance to change states from a solid to a liquid or vice versa. It is also called the latent heat of fusion or the enthalpy change of fusion, and the temperature at which it occurs is called the melting point.

ter from 0°C to 80°C. This latent thermal storage could be used for the insulation of buildings.

The use of PCM is not new. In ancient Baghdad, rooms were kept cool with the help of ice. During the XIX century, PCM have been used in many applications such as refrigerating transportation for rail and road and their properties were fairly known. In the 1940s, first attempts were made to use PCM in buildings in the USA, and in 1953 the first microcapsule was patented. In the 1980s, the NASA undertook, in companion with industry, basic research and development into PCM. In theory, PCM latent heat storage can be achieved through solid-solid, solid-liquid, solid-gas, and liquid-gas phase change. However, the only phase change used for PCM is the solid-liquid change and vice versa. Liquid-gas phase changes are not practical for use as thermal storage due to the large volumes or high pressures required to store the material when in gas phase. Liquid-gas transition have a higher heat of transformation than solid-liquid transitions. Solid-solid phase changes are typically very slow and have a rather low heat of transformation.

10.1.2 Nature of Phase-Change material

PCM could be organic, inorganic or eutectics. Each family has got different advantages and disadvantages, as follows:

A. Organic: paraffin (C_nH_{2n+2}) and fatty acids ($CH_3(CH_2)_nCOOH$)

❖ Advantages:

1. availability in a large temperature range;
2. freeze without super-cooling;
3. ability to melt congruently;
4. self nucleating properties;
5. great compatibility with conventional construction material;
6. no segregation;
7. chemically stable;
8. high heat of fusion;
9. safe and non-reactive;
10. recyclable.

❖ Disadvantages:

1. low thermal conductivity in solid state;
2. low volumetric latent heat storage capacity;
3. flammable.

B. Inorganic: salt hydrates (M_nH_2O)

❖ Advantages:

1. high volumetric latent heat storage capacity;
2. low cost and easy availability;
3. sharp melting point;
4. high thermal conductivity;
5. high heat of fusion;
6. non-flammable.

- ❖ Disadvantages:
 1. very high change of volume;
 2. super cooling phenomenon in solid-liquid transition;
 3. need nucleating agent.

C. Eutectics: organic-organic; organic-inorganic, inorganic-inorganic compounds

- ❖ Advantages:
 1. sharp melting point similar to the pure substance;
 2. high volumetric storage density.
- ❖ Disadvantages:
 1. physical properties are not well investigated as they are new to thermal storage application.

10.1.3 Phase-Change material selection criteria

PCM should be chosen carefully according to some criteria, below there are some of them:

- 1) Thermodynamics properties:
 - a) Melting temperature in the desired operating temperature range;
 - b) High latent heat of fusion per unit volume;
 - c) High specific heat, high density and high thermal conductivity;
 - d) Small volume changes on phase transformation and small vapour pressure.
- 2) Kinetic properties:
 - a) High nucleation rate to avoid super cooling of the liquid phase;
 - b) High rate of crystals growth.
- 3) Chemical properties:
 - a) Chemical stability;
 - b) Complete reversible freeze/melt cycle;
 - c) No degradation after a large number of cycles;
 - d) Non-corrosiveness, non-toxic, non-flammable and non-explosive.
- 4) Economic properties:
 - a) Low cost;
 - b) Large-scale availabilities.

10.1.4 Use of Phase-Change material in construction

In construction, PCM can be incorporated into different part of a building to improve its components' properties. The components include: the building envelope, interior and exterior walls and ceiling, the floor. Furthermore, the principles of latent heat storage can be applied to any porous building material, although current research has been primarily concerned with gypsum wallboard and concrete blocks. In any case, PCM may be dispersed into a wide range of building materials including wallboards, timber and brick. PCM for construction applications are invariably made from paraffin and salt hydrates. Minute paraffin globules with a diameter range from 2 nm to 20 nm are enclosed in a sealed plastic sheathing. These capsules can be in-

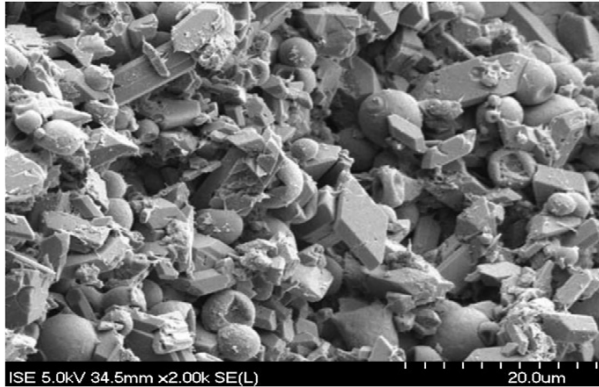


Fig. 10.2
SEM image of PCM micro-capsules in gypsum plaster. (source: Zhang et al., 2007)

and used to liquefy the paraffin. As the temperature rises, melting the waxy contents of the microcapsule, the paraffin changes from solid to liquid. The same principle also works in the other direction: rooms that are cooling down stay warm longer,

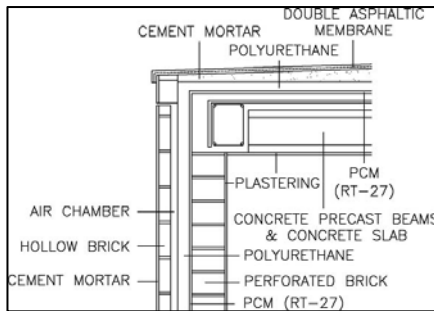


Fig. 10.3
Section of the constructive solution used for the conventional brick cubicles in Puigverd de Lleida (Spain). (source: Castell et al., 2010)

Fig. 10.4
Demonstration cubicles in Puigverd de Lleida (Spain). The structures were made by conventional bricks and alveolar bricks, enhanced by microencapsulated PCM, in order to study the thermal behaviour. (source: Castell et al., 2010)

while the molten paraffin gradually hardens, before losing warmth. The amount of energy that is taken up or released is considerable so that even a comparatively small mass has a large thermal retention capacity. Thus, temperatures inside buildings can be regulated. Energy is therefore stored latently as the material changes from one physical state to another, whether from solid to liquid or from liquid to gaseous. The latent warmth

or cold, that effectively fulfils a buffer function, can be used for temperature regulation. In this scenario, the switching temperature is the most important factor for building applications, as we will also see in the Thermochromic coatings section. The suboptimal switching temperature designed for construction is defined as 25°C; above this the indoor air temperature is generally regarded as being unpleasantly warm. Just for a comparison, depending on the PCM used, to regulate 5°C increase in temperature only 1 mm PCM is required in comparison to 10 – 40 mm of concrete.



egrated in a typical building material, whereby around 3 million such capsules fit in a single square centimetre. As PCM is able to take up energy (heat) without getting warm. It can absorb extremes in temperature, allowing indoor areas to remain cooler for longer, with the heat being retained in the PCM

For a comprehensive understanding of the potential PCM that can be applied in buildings, some of the suitable PCM are listed in the table below. Most of their melting points fall between 18 and 28°C, just the human comfort temperature range.

Tab. 10.1 PCM for building applications		
PCM	Transition point range [°C]	Heat of fusion [KJ/Kg]
CaCl ₂ • 6H ₂ O	24-29	192
Na ₂ S ₂ O ₃ • 5H ₂ O	40	210
CaCl ₂ • 6H ₂ O + MgCl ₂ • 6H ₂ O	23	--
Hexadecane	18	205-236
Heptadecane	22	214
Octadecane	28	244
Black paraffin	25-30	150
Emerest 2325 (butylstearate + butyl palmitate)	17-21	138-140
Emerest 2326 (butylstearate + butyl palmitate)	18-22	140
Butyl Stearate	19	140
1-dodecanol	26	200
Capric-lauric 45/55	21	143
Capric-lauric 82/18	19,1-20,1	147
Capric-lauric 61,5/38,5	19,1	132
Capric-myristic 73,5/26,5	21.4	152
Capric-palmitate 75.2/24.8	22.1	153
Capric-stearate 86.6/13.4	26.8	160
Peg 1000 + Peg 600	23-26	150.5
Propyl palmitate	19	186
RT 25	25	147

10.1.5 Storing energy by PCM components in buildings

Several PCM applications in buildings such as passive solar heating, active heating and night cooling are shown in the figure 10.5, in the next page. As previously mentioned, PCM incorporated in building envelopes (walls, roof or ceiling, floor, etc.) used for passive solar heating in winter can increase thermal capacity of light building envelopes, thus reducing and delaying the peak heat load and reducing room temperature fluctuation. Together with a solar collector system, a PCM building component can store more solar thermal energy during the day and discharge the heat during the night, thus maintaining good thermal internal comfort. With a heat pump, or under-floor electric heating system, PCM building envelopes can store heat with cheap electricity at night and then discharge heat during the day, thus decreasing the space-heating load. The shift of electrical consumption from peak periods to off-peak periods will provide a significant economic benefit.

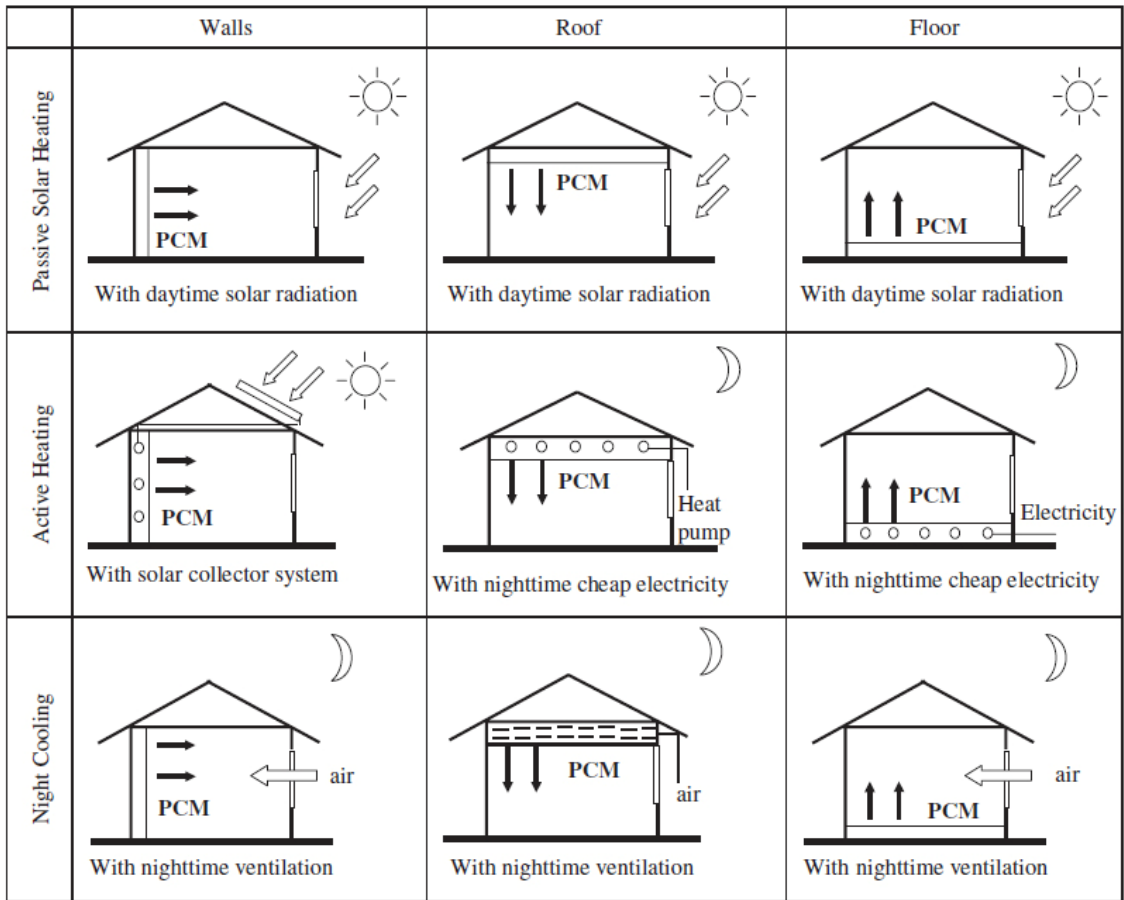
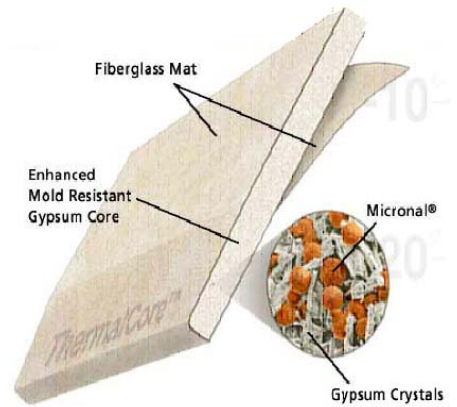
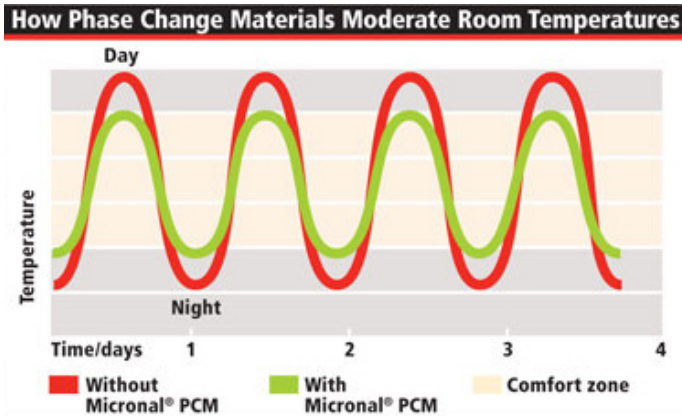


Fig. 10.5
Forms and effects of
PCM in a building
envelope (source
Zhang et al., 2007)

Another application is a night-time ventilation system with a PCM envelope for cooling storage. When the outdoor temperature is lower than the indoor air temperature, the ventilation system starts and the outdoor cooling can be stored in the PCM envelope such as a PCM ceiling or PCM walls, and then released during the day, which could decrease the cooling load of air-conditioning systems. The night-time cooling storage can be achieved by natural ventilation or by fan.

Lots of companies around the world already produce, or still test, new building components enhanced by PCM. For instance, the North Carolina company National Gypsum is testing drywall sheets called ThermalCORE™ that are plaster panels containing capsules that can absorb heat. These capsule, made by the giant BASF under the name of Micronal PCM, are microscopic acrylic capsule containing high-



purity paraffin wax that can be incorporated into a range of construction materials and are already available in some products in Europe.

10.1.6 Vacuum insulation panels

Vacuum insulation panels have existed since the 1950s, but were previously far too expensive for a economic use in construction. In recent years, intensive research has been undertaken to reduce the production costs and time significantly.

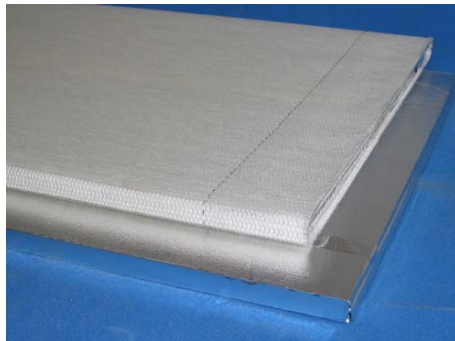


Fig. 10.6 a-b
Left: Study on a room temperature range with or without ThermalCORE & Micronal.
Right: ThermalCORE & Micronal.

Fig. 10.7 a-b
Left: Vacuum insulation panel with glass fibre textile as cover on top of blank panel.
Right: vacuum insulation panel for buildings.

Generally speaking, a vacuum insulation panel (VIP) consists of a gas-tight enclosure and a rigid core from which the air has been evacuated and is suited for providing thermal insulation with a thinner thickness than usual materials. In comparison to traditional materials such as polystyrene, the thermal conductivity is up to ten times lower. This results either in much higher levels of thermal resistance at the same insulation thickness or means that thinner insulation layers are required to achieve the same level of insulation. To make this technology work,



Fig. 10.8
Vacuum insulation forming a 90° bow.

as for thermos flasks, vacuum is created between the different layers that are made by a particular material with nano-scalar porosity of around 100 nm to withstand the pressure. Generally, the thickness of such panels ranges from 2 mm to 40 mm and they might be used for both new buildings and in conversion and renovation work. They can also be applied to walls as well as floors. The panels are constructed as follows: an enveloping skin made of plastic foil (often coated with aluminium) or of stainless steel or of glass fibres (see the figure 10.7 a in the previous page) encloses the fill material in a vacuum. The fill material take the form of a foam, powder or glass fibres and is always porous, resists pressure and can be evacuated. A hermetically weld-sealed ends protrude on each side and are usually folded back and stuck to the panel.

Flat evacuated insulation elements may also be bent to a cylindrical form. General objective of a recently finished EU project "VACI" was the development and refinement of methods to manufacture complex 3-dimensional curved vacuum insulation panels for different applications. The art of obtaining the desired shape lies in highly precise calculations of the cutting of the core material, which subsequently leads to the exact shapes required. It could be demonstrated that the vacuum insulation technique exhibited extremely low heat fluxes, thereby permitting a considerable reduction in insulation thickness. The objective of 60 mm vacuum insulation instead of 160 mm conventional insulation around pipes was actually improved even further. The total thickness of the vacuum insulation of about 50 mm has the same insulation performance as a conventional polyurethane foam insulation of 160 mm thickness. Thus the overall diameter of an insulated pipe is reduced from 520 mm to 300 mm. Application temperatures may vary between cryogenic conditions and temperatures of up to 90 °C. One of the biggest problems in using vacuum insulation panels is that to function correctly, it is imperative that the vacuum-enclosing skin is not pierced. Thus the panels must be used in standard dimensions as they cannot be cut to size. An other problem is that gaps between neighbouring panels must be minimised as far as possible to avoid cold bridges. Vacuum insulation panels are generally more expensive than conventional insulation materials and today are not necessarily conceived as a general replacement for conventional insulation. Their application is most suited to areas where thin layers are desirable or required and where space is limited and conventional solutions cannot be implemented. Vacuum insulation panels have already been successfully used in several buildings like the Sonnenschiff Centre in Freiburg, Baden-Württemberg in Germany that was completed in 2006 (fig. 10.9). In this building, vacuum insulation panels are used together with phase changing materials as latent heat storage systems for regulating indoor temperature. In Germany again, in 2004 it was built the first large building to be insulated entirely with vacuum insulation panels. It is a seven-storey mixed-use residential and commercial building in Munich (fig. 10.10 and fig. 10.11). There, the panels are also used in the roof terrace and window. These panels insulate 5 to 10 times better than comparable conventional types of insulation, allowing for much thinner walls on low energy buildings.



Fig. 10.9 a-b
Sonnenschiff Centre
in Freiburg (Germany).



Fig. 10.10 a-b
The building from the
Seitzstraße (Foto:
Sascha Kletzsch,
München).

10.1.7 Aerogel

Aerogel is a manufactured ultra-light aerated material with the lowest bulk density of any known porous solid material. It is derived from a gel - a foam - in which the liquid component has been replaced with a gas, usually simple air. The gas quantity varies between 95% and 99.9%, the remaining foam material is a glass-like material, silicon dioxide. This material is often used as thermal insulator and is also known as frozen smoke, solid smoke, solid air or blue smoke due to its translucent nature and the way light scatters in the material itself.

Aerogels were first developed in 1931 by



Fig. 10.11
Thermography of the
building showing a
lower temperature
where vacuum insula-
tion panels have been
placed (Copyright
ZAE Bayern, 2008).

Samuel Stephens Kistler². The current variant used in construction has been produced by the Canadian Cabot Corporation in Frankfurt am Main for several years. Today its spreader product is the brand “Nanogel”.

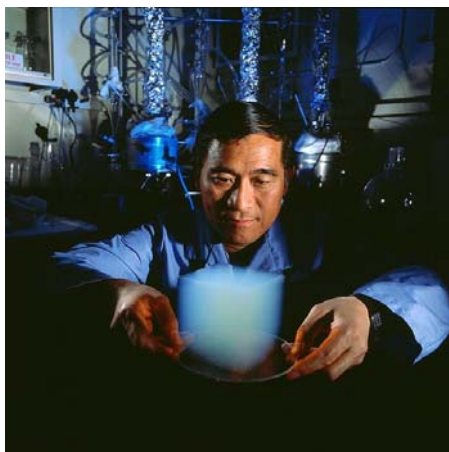


Fig. 10.12 a-b
Left: a 2.5 kg brick supported by a piece of aerogel weighing only 2 grams. (Nasa)
Right: Dr. Peter Tsou of NASA's Jet Propulsion Laboratory holding a sample of aerogel.



Fig. 10.13 a-b
Milwaukee Country Zoo, Wisconsin (USA), lions' den.

² Samuel Stephens Kistler (1900 – 1975) was an American scientist and chemical engineer, best known as the inventor of aerogels. The exact circumstances of the creation of the first aerogel are not well known. A popular story is that they resulted from a competition between Kistler and Charles Learned “to see if they could replace the liquid inside of a jelly jar without causing any shrinkage”. Kistler published a paper in *Nature* (Vol. 127, p. 741) titled “Coherent expanded aerogels and jellies”. In the early 1940s he started developing granular silica aerogel products under the trademark Santocel by Monsanto Company. Monsanto discontinued the line in 1970, probably due to the high cost of manufacture and competition from newer products.

Tab. 10.2 Nanogel by Cabot Corporation characteristics	
Thermal conductivity	9-12 mW/mK
Porosity	> 90% air
Size pores	20 – 40 nm
Surface area	750 m ² /g
Tap density	30/100 Kg/m ³
Oil absorption capacity	540g/100g
Specific heat capacity	0.7-1.15 KJ/Kg
Variety of particle sizes	5 micron – 4 mm

Aerogels are produced by extracting the liquid component of a gel through supercritical drying³. This procedure allows the liquid to be slowly drawn off without causing the solid matrix in the gel to collapse from capillary action. Despite their names, aerogels are a rigid, dry material and do not resemble a gel in their physical properties. The nanodimension is of vital importance for the pore interstices of the foam: the air molecules trapped within the nanopores of about 20 nm are unable to move due to the dendritic microstructure of the foam: spherical nanoparticles of average size 2-5 nm are fused together into clusters.

Aerogels are good thermal insulators due to the air trapped in their pores. They have usually got an extremely high thermal resistance which is expressed in a very low coefficient of thermal conductivity of just 0.018 W/mK. Because aerogels are translucent, they exhibit good light transmission. Direct sunshine is transformed into a glare-free soft light. The slight colour they show is due to Rayleigh scattering of the shorter wavelengths of visible light by the nanosized dendritic structure. This causes them to appear smoky blue against dark backgrounds and yellowish against bright backgrounds.

In addition to their thermal insulating properties, aerogel also act as a sound insulator according to the same basic principle. The air molecules immovably trapped in the nanopores of the aerogel stop sound waves from passing thorough the material. Several buildings around the world already use this material in façades or in interiors as, for instance, the Milwaukee Country Zoo in USA (fig. 10.13 and fig. 10.14), completed in 2005. In this zoo, a new form of translucent skylight manufactured by Kalwall Corporation plus nanogel was used obtaining a system with a U value of 0.11.



Fig. 10.14
Milwaukee Country
Zoo, Wisconsin
(USA).

³ Supercritical drying is a process to remove liquid in a precisely controlled way. As a substance crosses the boundary from liquid to gas it volatilizes. Thus the volume of the liquid decreases. As this happens, surface tension at the solid-liquid interface pulls against the structures that the liquid is attached to. Delicate structures tend to be broken apart by this surface tension as the interface moves by. To avoid this, the sample can be brought from the liquid phase to the gas phase without crossing the liquid-gas boundary.

10.2 Photocatalysis for comfort and energy control

An interesting application of TiO_2 ⁴, usually used to produce self-cleaning coatings on glass or other building components, is the cooling effect of evaporating water. This technology was first experimented during the Expo 2005 in Japan. The windows and the canvas as well as the steel roofing of a trade fair pavilion were equipped with a photocatalytic TiO_2 coating and subjected to a constant stream of water. Due to the hydrophilic property of the surface, the water immediately formed a thin film, which evaporated quickly absorbing – as a physical consequence – the ambient warmth and thereby reducing the indoor temperature. Initial estimates suggest a potential energy reduction of between 10 % and 20 % in comparison to conventional air conditioning. This effect is generally achieved by sprinkling water on the ground waiting until it evaporates.

10.3 Photovoltaic

This section on photovoltaic's theory and applications doesn't want to be a comprehensive study on the topic as it is very specific, technical and spread. It just wants to show what, in general terms, photovoltaic is and works, how it could be applied in buildings and how nanotechnologies may enhance its efficiency.

10.3.1 History, materials and photovoltaic effect

Photovoltaics are arrays of cells containing a solar photovoltaic material that converts solar radiation into direct current electricity. The term *photovoltaic* comes from



Fig. 10.15

The inventors of the Bell Solar Battery. From left, Gerald Pearson, Daryl Chapin, and Calvin Fuller, check devices for the amount of solar electricity derived from sunlight, here simulated by a lamp. (source: Perlin)

the Greek $\phi\omega\varsigma$ (*phōs*) meaning light, and *voltaic*, meaning electric, from the name of the Italian physicist Alessandro Volta⁵, after whom a unit of electro-motive force, the volt, is named. The *photovoltaic effect* was first recognized in 1839 by French physicist A. E. Becquerel⁶. However, it was not until 1883 that the first solar cell was built, by C. Fritts⁷, who coated the semiconductor selenium with an extremely thin layer of gold to form the junctions. The device was only around 1% efficient. Subsequently the Russian physicist A. Stoletov⁸

4 To know more about TiO_2 and photocatalysis look at Self-Cleaning coatings in “Nanotechnology for quality and comfort” section, pg. 87 of this thesis.

5 Alessandro Volta (1745 – 1827) was an Italian physicist known especially for the development of the first electric cell in 1800.

6 Alexandre Edmond Becquerel (1820 – 1891) was a French physicist who studied the solar spectrum, magnetism, electricity and optics. He is mostly known for his work in luminescence and phosphorescence. He is also credited with the discovery of the photovoltaic effect and the operating principle of the solar cell in 1839.

7 Charles Fritts was an American inventor credited with creating the first working solar cell in 1883.

8 Aleksandr Stoletov (1839 – 1896) was a Russian physicist, founder of the electrical engineering.

built the first solar cell based on the outer photoelectric effect (discovered by H. Hertz⁹ earlier in 1887). A. Einstein¹⁰ explained the photoelectric effect in 1905 for which he received the Nobel prize in Physics in 1921. R. Ohl¹¹ patented the modern junction semiconductor solar cell in 1946, which was discovered while working on the series of advances that would lead to the transistor. The highly efficient solar cell was first developed by Chapin, Fuller and Pearson¹² (fig. 10.15) in 1954 using a diffused silicon p-n junction. In past four decades, a remarkable progress has been made. Nowadays megawatt solar power generating plants have been built.

In general, the photovoltaic effect refers to photons of light knocking electrons into a higher state of energy to create electricity. The term photovoltaic denotes the unbiased operating mode of a photodiode in which current through the device is entirely due to the transduced light energy. Virtually all photovoltaic devices are some type of photodiode.

Nowadays, the materials used for photovoltaics include silicon in either monocrystalline¹³, polycrystalline¹⁴ or microcrystalline¹⁵ phase, cadmium telluride¹⁶ and copper indium selenide¹⁷/sulfide.

Due to the growing demand for renewable energy sources, the manufacture of solar cells and photovoltaic arrays has advanced dramatically in recent years. More specifically, its production has been increasing by an average of more than 20 percent each year since 2002, making it the world's fastest-growing energy technology.

9 Heinrich Hertz (1857 – 1894) was a German physicist who expanded the electromagnetic theory of light. He demonstrated the existence of electromagnetic waves by building an apparatus able to produce and detect VHF or UHF radio waves.

10 Albert Einstein (1879 – 1955) was a theoretical physicist. He is regarded as the father of modern physics and one of the most influential scientist of all time.

11 Russell Ohl (1898 – 1987) was an American engineer who is generally recognized for patenting the modern solar cell (U.S. Patent 2402662 “Light sensitive device” - 1946)

12 Daryl Chapin, Calvin Fuller and Gerald Pearson were three scientists who developed a high efficient solar cell by chance working for the A T&T at the Bell laboratories in 1952.

13 Monocrystalline silicon: in single crystal silicon, also called monocrystal, the crystal lattice of the entire sample is continuous and unbroken with no grain boundaries. Large single crystals are exceedingly rare in nature and can also be difficult to produce in the laboratory.

14 Polycrystalline phases are composed of a number of small crystals or crystallites. Polycrystalline silicon is a material consisting of multiple small silicon crystals. Single crystal silicon is used to manufacture most Si-based microelectronic devices as it can be as much as 99.9999% pure. Ultra-pure poly is used in the semiconductor industry, starting from poly rods that are five to eight feet in length. In microelectronic industry (semiconductor industry), poly is used both at the macro-scale and micro-scale (component) level.

15 Microcrystalline silicon, more often known as nanocrystalline silicon is a form of porous silicon. It is an allotropic form of silicon with paracrystalline structure. It is similar to amorphous silicon as it has an amorphous phase. The main application of this novel material is in the field of silicon thin film solar cells. The semiconductor industry is also investigating the potential for nanocrystalline silicon in the memory area.

16 Cadmium telluride (CdTe) is a crystalline compound formed from cadmium and tellurium. It is used as an infrared optical window and a solar cell material.

17 Copper indium gallium (di)selenide (CIGS), is a I-III-VI₂ compound semiconductor material composed of copper, indium, gallium, and selenium. The material is a solid solution of copper indium selenide and copper gallium selenide that is used as light absorber material for thin-film solar cells.

At the end of 2009, the cumulative global photovoltaic installations surpassed 21.000 megawatts. Such installations may be ground-mounted (and sometimes integrated with farming and grazing) or built into the roof or walls of a building, known as Building Integrated Photovoltaics (BIPV).



Fig. 10.16 a-b
Left: Solar Power Plant Madama Oliva in Carsoli (Aquila), 2008.
Right: Nellis Solar Power Plant at Nellis Air Force Base (USA).

10.3.2 Solar cells: the photovoltaic basis

A solar cell (fig. 10.17) is a device that converts the sunlight energy directly into electricity by the photovoltaic effect. Assemblies of cells are used to make solar panels, solar modules, or photovoltaic arrays. Solar cells produce direct current electricity from sun light, which can be used to power equipment or to recharge a battery. Solar cells are often electrically connected and encapsulated as a module. Photovoltaic modules often have a sheet of glass on the front (sun up) side, allowing light to pass while protecting the semiconductor wafers from the elements (rain, hail, etc.). Solar cells are also usually connected in series in modules, creating an additive voltage. Connecting cells in parallel will yield a higher current. Modules are then interconnected, in series or parallel, or both,



Fig. 10.17
Solar cell made from a monocrystalline silicon wafer.

to create an array with the desired peak DC voltage and current. The power output of a solar array is measured in watts or kilowatts. In order to calculate the typical energy needs of the application, a measurement in watt-hours, kilowatt-hours or kilowatt-hours per day is often used. A common rule of thumb is that average power is equal to 20% of peak power, so that each peak kilowatt of solar array output power corresponds to energy production of 4.8 kWh per day (24 hours \times 1 kW \times 20% = 4.8 kWh). To make practical use of the solar-generated energy, the electricity is most often fed into the electricity grid using inverters (grid-connected photovoltaic systems); in stand-alone systems, batteries are used to store the energy that is not needed immediately. Solar cells can also be applied to other electronics devices to make it self-power sustainable in the sun. There are solar cell phone chargers, solar bike light and solar camping lanterns that people can adopt for daily use.

Many currently available solar cells are configured as bulk materials that are subsequently cut into wafers and treated in a "top-down" method of synthesis (silicon being the most prevalent bulk material).

Other materials are configured as thin-films (inorganic layers, organic dyes, and organic polymers) that are deposited on supporting substrates, while a third group are configured as nanocrystals and used as quantum dots (electron-confined nanoparticles) embedded in a supporting matrix in a "bottom-up" approach. Silicon remains the only material that is well-researched in both *bulk* (also called wafer-based) and *thin-film* configurations.

10.3.3 Solar cells: theory

1. Photons in sunlight hit the solar panel and are absorbed by semi-conducting materials, such as silicon.
2. Electrons, which are negatively charged, are knocked loose from their atoms, allowing them to flow through the material to produce electricity. Due to the special composition of solar cells, the electrons are only allowed to move in a single direction.
3. An array of solar cells converts solar energy into a usable amount of direct current electricity.

More particularly, when a photon hits a piece of silicon, one of three things can happen:

- the photon can pass straight through the silicon — this (generally) happens for lower energy photons;
- the photon can reflect off the surface;
- the photon can be absorbed by the silicon, if the photon energy is higher than the silicon band gap value. This generates an electron-hole pair and sometimes heat, depending on the band structure.

When a photon is absorbed, its energy is given to an electron in the crystal lattice. Usually this electron is in the valence band, and is tightly bound in covalent bonds between neighboring atoms, and hence unable to move far. The energy given to it by the photon excites it into the conduction band, where it is free to move around within the semiconductor. The covalent bond, that the electron was previously a part of, now has one fewer electron — this is known as a hole. The presence of a missing covalent bond allows the bonded electrons of neighboring atoms to move into the hole, leaving another hole behind, and in this way a hole can move through the lattice. Thus, it can be said that photons absorbed in the semiconductor create mobile electron-hole pairs. A photon need only has greater energy than that of the band gap in order to excite an electron from the valence band into the conduction band. However, the solar frequency spectrum approximates a black body spectrum at ~ 6000 K, and as such, much of the solar radiation reaching the Earth is composed of photons with energies greater than the band gap of silicon. These higher energy photons will be absorbed by the solar cell, but the difference in energy between these photons and

the silicon band gap is converted into heat (via lattice vibrations — called phonons) rather than into usable electrical energy.

10.3.4 Thin-film solar cells

In 2002, the highest reported efficiency for thin film solar cells based on Cadmium Telluride (CdTe) is 18%, which was achieved by a research at Sheffield Hallam University, although this has not been confirmed by an external test laboratory. The US National Renewable Energy research facility, NREL, achieved an efficiency of 19.9% for the solar cells based on copper indium gallium selenide thin films, also known as CIGS. NREL has since then developed a robot that builds and analyzes the efficiency of thin-film solar cells with the goal of increasing the efficiency by testing the cells in different situations. These CIGS films have been grown by physical vapour deposition in a three-stage co-evaporation process. In this process In, Ga and Se are evaporated in the first step; in the second step it is followed by Cu and Se co-evaporation and in the last step terminated by In, Ga and Se evaporation again. Thin film solar has approximately 15% market-share; the other 85% is crystalline silicon. Most of the commercial production of thin film solar is CdTe with an efficiency of 11%. As of 28 April 2010, ZSW in Stuttgart have released a statement claiming they have created CIGS-based cells with a new record 20.1% efficiency.

10.3.5 Crystalline Silicon solar cells

The highest efficiencies on silicon have been achieved on monocrystalline cells. The highest commercial efficiency (22%) is produced by SunPower, which uses expensive, high-quality silicon wafers. The University of New South Wales has achieved 25% efficiency on monocrystalline silicon in the lab, technology that has been commercialized through its partnership with Suntech Power. Crystalline silicon devices are approaching the theoretical limiting efficiency of 29% and achieve an energy payback period of 1–2 years.

10.3.6 Nanocrystalline solar cells

Nanocrystalline solar cells, or quantum dot solar cells, are based on a silicon substrate with a coating of nanocrystals. A thin film of nanocrystals is obtained by a process known as spin-coating. This involves placing an amount of the quantum dot solution onto a flat substrate, which is then rotated very quickly. The solution spreads out uniformly, and the substrate is spun until the required thickness is achieved. Quantum dot based photovoltaic cells based around dye-sensitised colloidal TiO₂ films were investigated in 1991 and were found to exhibit promising efficiency of converting incident light energy to electrical energy. This was incredibly encouraging due to the low cost of materials in the search for more commercially viable/affordable renewable energy sources. A single-nanocrystal (channel) architecture in which an array of single particles between the electrodes, each separated by ~ 1 exciton diffusion length, was proposed to improve the device efficiency. Research on this type of solar cell is being conducted by groups at Stanford, Berkeley and the

University of Tokyo. Although research is still in its infancy and is ongoing, in the future quantum dot based photovoltaics may offer advantages such as mechanical flexibility (quantum dot-polymer composite photovoltaics) as well as low cost, clean power generation and an efficiency of 65%. Recent research in experimenting with lead selenide (PbSe) semiconductor, as well as with cadmium telluride (CdTe), which has already been well established in the production of "classic" solar cells. Other materials are being researched and tested as well.

10.3.7 Carbon nanotubes in photovoltaic

Organic photovoltaic devices are fabricated from thin films of organic semiconductors, such as polymers and small-molecule compounds, and are typically on the order of 100 nm thick. Because polymer based organic photovoltaics can be made using a coating process such as spin coating or inkjet printing, they are an attractive option for inexpensively covering large areas as well as flexible plastic surfaces. A promising low cost alternative to silicon solar cells, there is a large amount of research being dedicated throughout industry and academia towards developing organic photovoltaics and increasing their power conversion efficiency. Combining the physical and chemical characteristics of conjugated polymers with the high conductivity along the tube axis of carbon nanotubes provides a great deal of incentive to disperse CNTs into the photoactive layer in order to obtain more efficient organic photovoltaic devices. The interpenetrating bulk donor-acceptor hetero-junction in these devices can achieve charge separation and collection because of the existence of a bicontinuous network. Along this network, electrons and holes can travel toward their respective contacts through the electron acceptor and the polymer hole donor. Photovoltaic efficiency enhancement is proposed due to the introduction of internal polymer/nanotube junctions within the polymer matrix. The high electric field at these junctions can split up the excitons, while the single-walled carbon nanotube (SWCNT) can act as a pathway for the electrons.

Multiple research investigations with both multi-walled carbon nanotubes (MWCNTs) and single-walled carbon nanotubes integrated into the photoactive material have been completed. Enhancements of more than two orders of magnitude have been observed in the photocurrent from adding SWCNTs. However, even though CNTs have shown potential in the photoactive layer, they have not resulted in a solar cell with a power conversion efficiency greater than the best tandem organic cells (6.5% efficiency). But, it has been shown in most of the previous investigations that the control over a uniform blending of the electron donating conjugated polymer and the electron accepting CNT is one of the most difficult as well as crucial aspects in creating efficient photocurrent collection in CNT-based organic photovoltaic devices.

Therefore, using CNTs in the photoactive layer of organic photovoltaic devices is still in the initial research stages and there is still room for novel methods to better take advantage of the beneficial properties of CNTs.

10.3.8 Worldwide and Italian financial incentives

The political purpose of incentives policies for photovoltaic is to promote national energy independence, high tech job creation and reduction of CO₂ emissions.

Since 2004 the International Conference on Solar Photovoltaic Investments is settle to observe the financial investments around the world and to analyze the research state of art.

Following, two graphs show the photovoltaic implementation around the world (fig. 10.18) and in Italy (fig. 10.19). The total photovoltaic capacity in MkW is analyzed for different countries. They show the increasing governments interest on this topic.

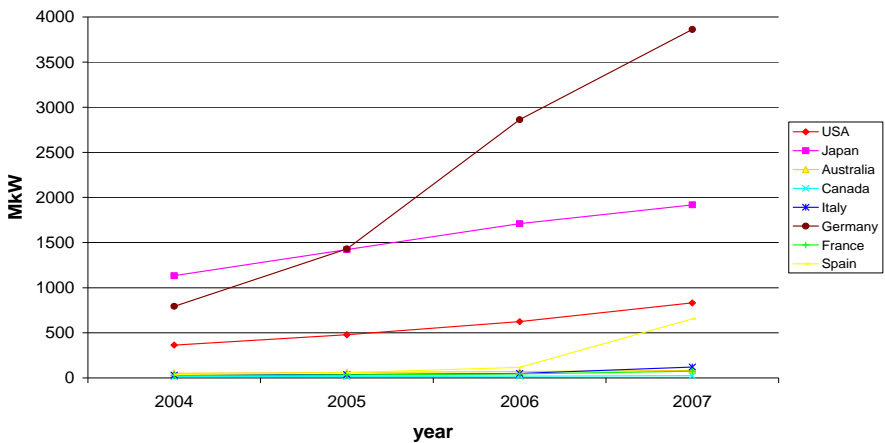


Fig. 10.18
Total photovoltaic capacity (MkW) around the world from 2004 to 2007.

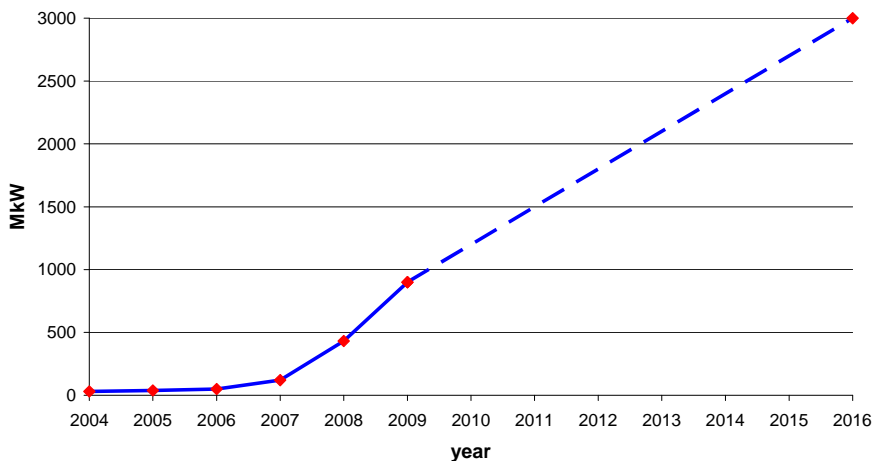


Fig. 10.19
Total photovoltaic capacity (MkW) in Italy from 2004 to 2009 with the 2016 prevision.

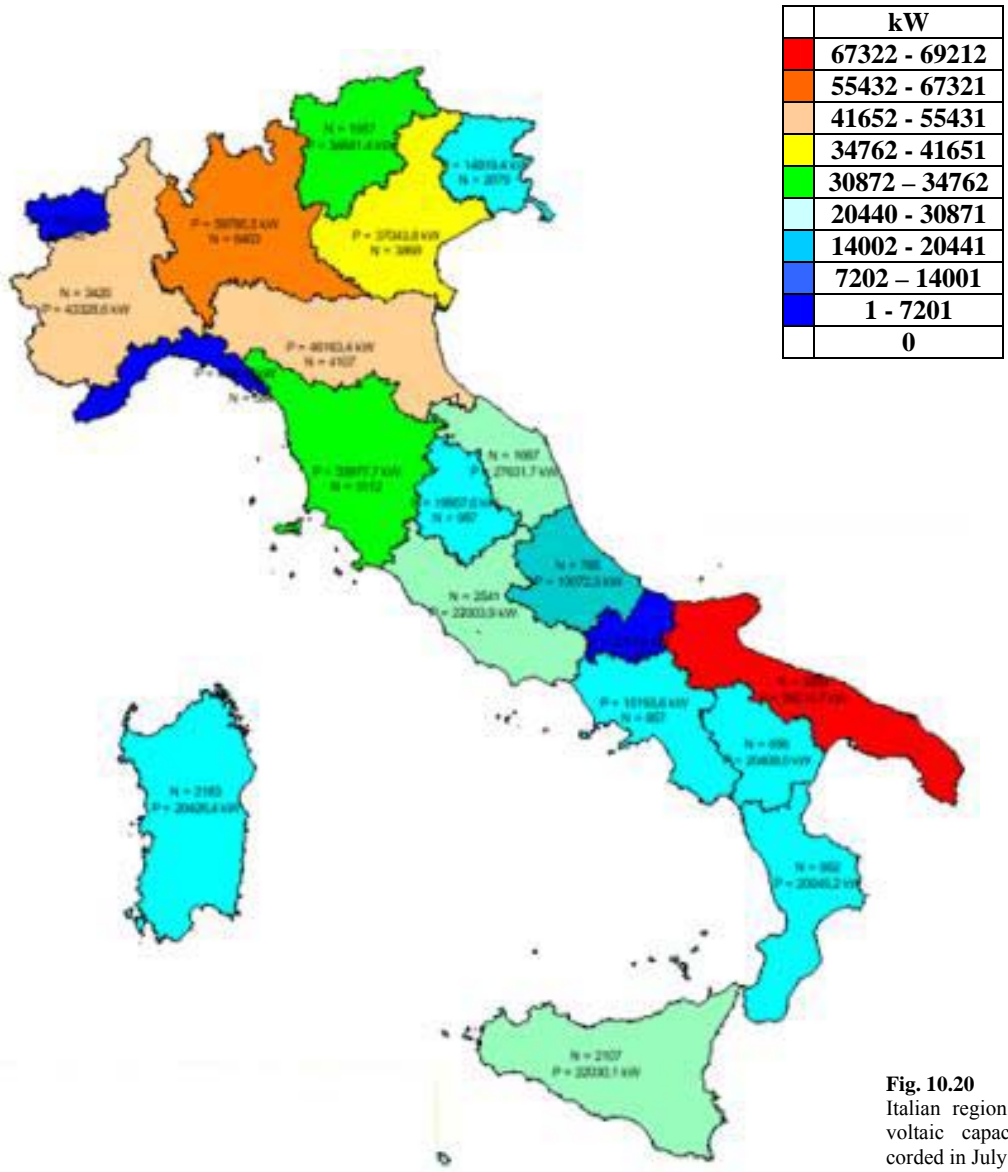


Fig. 10.20
Italian region photo-voltaic capacity recorded in July 2009

10.3.9 Building-integrated photovoltaics (BIPV)

Photovoltaics cells could be integrated in buildings elements to generate energy sufficient for the building's need. These systems are photovoltaic materials that are used to replace conventional building materials in parts of the building envelope such as the roof, skylights, or facades. They are increasingly being incorporated into the construction of new buildings as a principal or ancillary source of electrical power, although existing buildings may be retrofitted with BIPV modules as well. The advantage of integrated photovoltaics over more common non-integrated systems is that the initial cost can be offset by reducing the amount spent on building materials and labor that would normally be used to construct the part of the building that the BIPV modules replace. These advantages make BIPV one of the fastest growing segments of the photovoltaic industry.

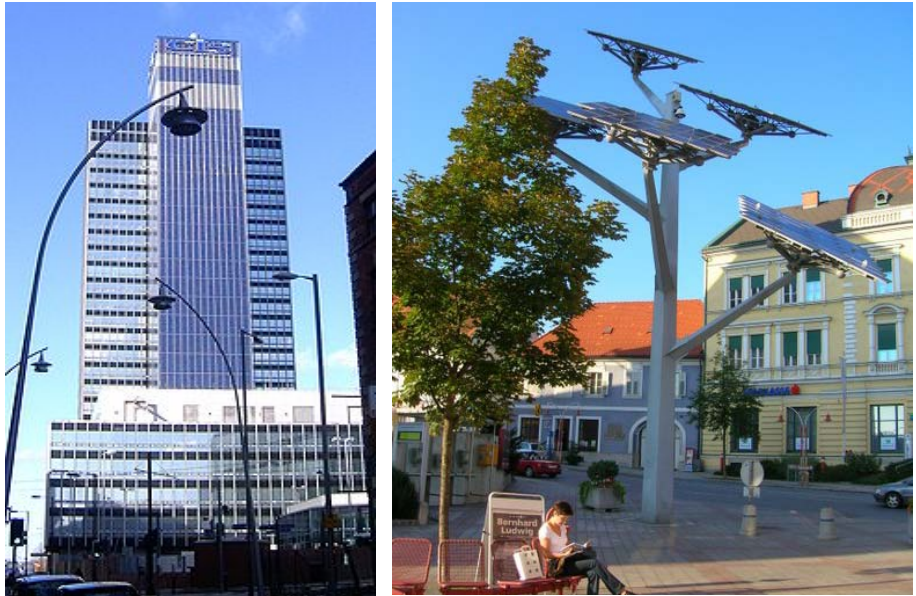


Fig. 10.21 a-b
 Left: CIS Tower in Manchester (UK) has three of its four sides completely clad in photovoltaic cells distributed in 7244 solar panels.
 Right: photovoltaic system tree in Styria, Austria.

PV applications for buildings began appearing in the 1970s. Aluminum-framed photovoltaic modules were connected to, or mounted on, buildings that were usually in remote areas without access to an electric power grid. In the 1980s photovoltaic module add-ons to roofs began being demonstrated. These PV systems were usually installed on utility-grid-connected buildings in areas with centralized power stations. In the 1990s BIPV construction products specially designed to be integrated into a building envelope became commercially available.

Building-Integrated Photovoltaic modules are available, today, in several forms, as follows:

1. Flat roofs: the most widely installed to date is a thin film solar cell integrated to a flexible polymer roofing membrane.
2. Pitched roofs: it extends normal roof life by protecting insulation and membranes from ultraviolet rays and water degradation. They could be modules shaped like multiple roof tiles or solar shingles that are modules designed to look and act like regular shingles, while incorporating a flexible thin film cell.
3. Façade: can be installed on existing buildings, giving old buildings a whole new look.
4. Glazing: (semi)transparent modules can be used to replace a number of architectural elements commonly made with glass or similar materials, such as windows and skylights.
5. Shading devices.
6. Winter garden: using transparent PV.
7. Art installation.

10.3.10 Transparent and translucent photovoltaic

Transparent solar panels use a tin oxide coating on the inner surface of the glass panes to conduct current out of the cell. The cell contains titanium oxide that is coated with a photoelectric dye. A module has been produced by the Austrian company Ertex Solar GmbH. Japan's National Institute of Advanced Industrial Science and Technology (AIST) as well as Konarka has also succeeded in developing a transparent solar cell that uses ultraviolet light to generate electricity but allows visible light to pass through it. Most conventional solar cells use visible and infrared light to generate electricity. In contrast, the innovative new solar cell also uses ultraviolet radiation. Used to replace conventional window glass, or placed over the glass, the installation surface area could be larger, leading to potential uses that take advantage of the combined functions of power generation, lighting and temperature control and could be applied in several non-conventional structures such as the tense-structures.



Fig. 10.22
Telecom Tower in Istanbul (Turkey) where photovoltaic modules in laminated safety glass were installed on the façade by Ertex Solar.



Fig. 10.23 a-b
In these the buildings photovoltaic modules in laminated safety glass were installed on the roof by Ertex Solar.
Left: family House in Thyrnau (Austria).
Right: WKÖ head-quarter (Geneva).

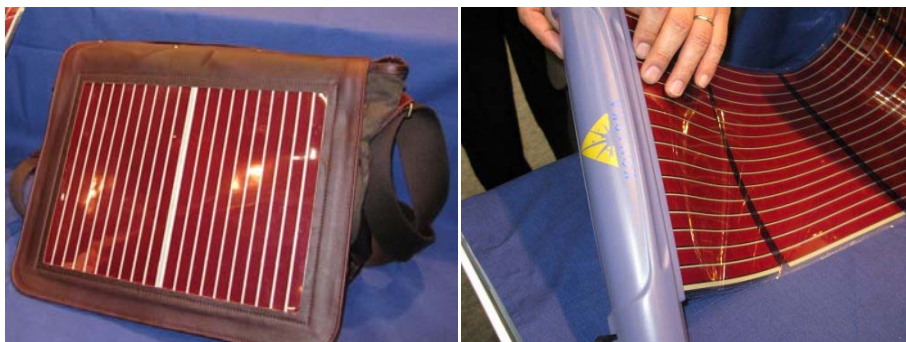


Fig. 10.24 a-b
Flexible photovoltaic
cell in a bag (left) and
in a scroll (right).

10.3.11 The solar Road-way: road-integrated photovoltaics

A solar roadway is a road surface that generates electricity by solar photovoltaics. One current proposal is for 4 x 4 m panels including solar cells and LED signage that can be driven on. The concept involves replacing highways, roads, parking lots, driveways, and sidewalks with such a system. The project was developed by an organization called Solar Roadways, run by Scott and Julie Brusaw in Idaho (USA) that was awarded a \$100000 research contract by the US Department of Transportation. Their idea spread out from the statement that a lot of people have trouble seeing the road lines at night, particularly when the oncoming headlights are blinding them or when it's raining.



Fig. 10.25
Solar Road-way.

On the contrary, a recent study in England showed that an illuminated highway could reduce by 70% night-time incidents. The panels they planned are composed from photovoltaic cells, LEDs and sensors. The cells will be used to power the device; LEDs will light up only when sensors will detect cars on its surface some metres ahead. In this way, there is no need to expend energy lighting desolate roads when no cars are traveling

and, furthermore, the LEDs can be customize by cities or town to meet their own unique needs. For instance, LEDs could move along with cars at the speed limit, warning drivers instantly when they are driving too fast or they will also be used to paint words right into the road, warning drivers of an animal on the road, a detour ahead, an accident, or construction work. Central control stations will be able to instantly customize the lines and words in real time, alleviating traffic congestion and making the roads more efficient as well as safer.

11. NANOTECHNOLOGIES FOR SENSING: OVERVIEW ON NANOSENSORS AND MEMS FOR BUILDINGS, CIVIL STRUCTURES AND ENVIRON- MENTAL MONITORING

11.1 Introduction

From time immemorial, human beings have been devising tools to help them obtain accurate measurement values of such things as weight, distance, temperature and humidity. Nowadays, measurement instruments are composed of three units: an input transducer that converts a non-electrical signal into an electrical signal; a processor that processes the electrical signal in some way, e.g., amplifies it or turns an analog signal into a digital signal; and an output transducer that converts the electrical signal into a signal that can either be perceived by one of our senses or can perform an action. Thus, a sensor could be defined as a system containing the transduction element, the interface circuitry, and the package.

Sensors make use of various kinds of effects, some of whom were already known in the 18th century. In 1821, T.J. Seebeck¹ discovered the effect used in thermocouples and E.H. Hall² discovered the effect that would later bear his name in thin gold foils in 1879. Many of such

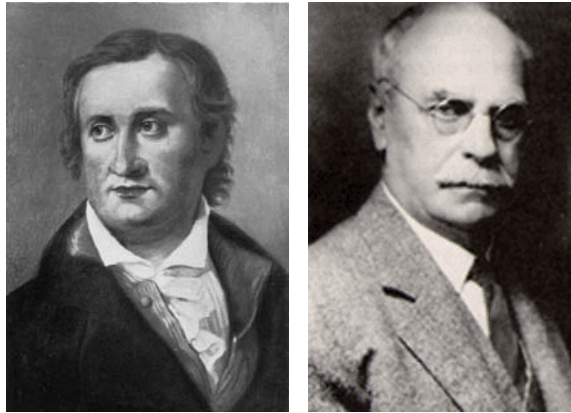


Fig. 11.1 a-b
Pictures of T. J.
Seedbeck (left) and
E. H. Hall (right).

effects can be used to convert energy as well as to construct sensors. For example, the Seebeck effect can be used to measure temperature differences between two spots in a furnace, but it can also be used as an energy source in, for instance, a paraffin lamp with thermoelectric converters that would enable Russian farmers in Siberia, who are not connected to any power station, to listen to Radio Moscow.

1 Thomas Johann Seebeck (9 April 1770, Tallin, Estonia – 10 December 1831, Berlin, Germany) was a physicist who in 1821 discovered the thermoelectric effect. He found that a circuit made from two dissimilar metals, with junctions at different temperatures, would deflect a compass magnet. More specifically, the temperature difference, produces an electric potential (voltage) which can drive an electric current in a closed circuit. Today, this effect is known as the Peltier–Seebeck effect.

2 Edwin Herbert Hall (7 November 1855, Gorham, Maine – 20 November 1938, Cambridge, Massachusetts) was an American physicist who discovered the "Hall effect" in 1879. The effect is a potential difference on opposite sides of a thin sheet of conducting or semiconducting material through which an electric current is flowing. The Hall effect is used in magnetic field sensors, present in a large number of devices.

Over the years, sensors have been fabricated in many different technologies: piezo-electric quartz crystals, II–VI compound photoconductors, and NiCr–CuNi thermocouples, just to name a few. But it is possible to say that their technology only really took off when pure germanium and, later on, silicon became available, around 1960.

Tab. 11.1 Major academic sensor programs, including starting year, location, and responsible faculty member.

Year	University	Institute	Location	Faculty
1965	Stanford University	CIS	Palo Alto	J.B. Angell
1968	Case Western Reserve University	MFL	Cleveland	W.H. Ko
1968	University of Twente	MESA	Enschede	P. Bergveld
1971	Tohoku University	VBL	Sendai	T. Matsuo
1972	Moscow Physics Eng. Inst.	MPhEI	Moscow	V.I. Vaganov
1973	UC Berkeley	BSAC	Berkeley	R.S. Muller
1974	Delft University of Technology	DIMES	Delft	S. Middelhoek
1974	University of Michigan	CIMS	Ann Arbor	K.D. Wise
1975	University of Linköping	S-SENCE	Linköping	I. Lundström
1976	MIT	MTL	Cambridge	S.D. Senturia
1978	University of Wisconsin	WCAM	Madison	H. Guckel
1981	Fudan University	–	Shanghai	M. Bao
1982	University of Neuchâtel	IMT	Neuchâtel	N.F. de Rooij
1983	University of Tübingen	IPC	Tübingen	W. Göpel
1985	K.U. Leuven	ESAT	Leuven	R. Puers
1987	T.U. Berlin	MAT	Berlin	E. Obermeier
1987	University of Tokyo	IIS	Tokyo	H. Fujita
1988	ETHZ	PEL	Zürich	H. Baltes
1990	T.U. of Denmark	MIC	Lyngby	J.W. Petersen
1991	Royal Institute of Technology	–	Stockholm	G. Stemme
1994	EPFL	IMS	Lausanne	R. Popovic

The sensor field has been, and continues to be known under a variety of names: transducers, sensors and actuators, micro-systems, micro-system technologies

(MST), and micro-electro-mechanical systems (MEMS). The current outpouring of various kinds of output transducers such as displays, micro-motors, micro-grippers, fluid micro-valves, fluid injectors, and light modulators, which are also fabricated in silicon, has given rise to a sub-field known as micromechanics.

Nowadays, thousands of institutes and industries all over the world have R&D programs in the field of sensors. A complete listing of these activities is therefore impossible.

11.2 Nanotechnology in sensing applications

Nanoparticles are used in a variety of fields and could also offer many advantages as nanosensors in rapid and high-throughput detection methods. The strong physical confinement of electrons or holes at the nanoscale makes nanoparticles attractive candidates for sensing. Furthermore, their small size gives them correspondingly large surface-to-volume ratios. When the size of the structure is decreased, this ratio increases considerably and the surface phenomena predominate over the chemistry and physics in the bulk.

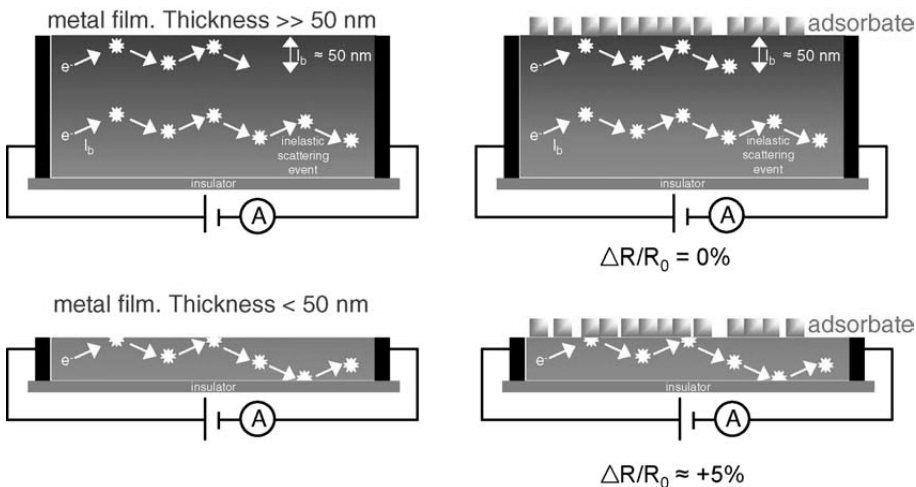


Fig. 11.2

Change in the measured property as a function of the thickness in resistive gas sensors. When the thickness is high (top left), the electrical resistance does not change because the inelastic scattering events in the bulk predominate (top right). When the thickness of the metal film is low (bottom left), the adsorbed target molecules can be detected by measuring the change in the electrical resistance (bottom right). (source: J. Riu et al., 2006)

Therefore, although the reduction in the size of the sensing parts and/or the transducer in a sensor is important in order to better miniaturize the devices, new sensor devices are built taking advantage of the phenomena that nanoscience deals with. New effects appear and play an important role that is often related to quantum mechanics and quantum mechanisms. Consequently, important characteristics and quality parameters of the nanosensors can be improved. For example, sensitivity can increase due to better conduction properties, the limits of detection can be lower, very small quantities of samples can be analysed, direct detection is possible without using labels, and some reagents can be eliminated. In addition, nanosensors have chemically tailored physical properties, which are directly related to their size, com-

position, and shape. Surface-modified nano-colloids, such as gold nanoparticles, quantum dots, magnetic nanoparticles and carbon nanotubes may have specific target-binding properties. Thus, the extremely small size and exceptional nanoscale properties make nanoparticles useful for new-generation sensor diagnostics.

Sensors have been classified according to multiple criteria but the most common way to group them considers either the transducing mechanism (electrical, optical, mass, thermal, piezoelectric, etc.), the recognition principle (enzymatic, DNA, molecular recognition, etc.) or the applications (environmental, food, medical diagnosis, etc.).

In this report we will briefly discuss some kinds of sensors and some specific applications to environment and large structure, dividing them on what they are made of. More particularly we will discuss:

- Sensors based on nanoparticles and nanoclusters;
- Sensors based on nanowires and nanotubes;
- Sensors based on nanostructures embedded in bulk material;
- Sensors based on porous silicon;
- Nanomechanical sensors;
- Self-assembled nanostructures.

11.2.1 Sensors based on nanoparticles and nanoclusters

Because of nanoparticles size, which is of the same order as the de Broglie wavelength associated with the valence electrons, nanoparticles behave electronically as zero-dimensional quantum dots with discrete energy levels that can be tuned in a controlled way by synthesizing nanoparticles of different diameters. For instance, nanoparticles have outstanding size-dependent optical properties that have been used to build optical nanosensors primarily based on noble metal nanoparticles for semiconductor quantum dots.

11.2.2 Sensors based on nanotubes and nanowires

Simple electronic devices including diodes, switches and transistors have recently been produced using carbon nanotubes. Several fields now take advantage of CNTs exceptional properties and, from the nanosensing point of view, the most interesting are:

- high length-to-radius ratio which allows a greater control over the unidirectional properties of the materials produced;
- they can behave as metallic, semiconducting or insulating material depending on their diameter, their chirality, and any functionalisation (or doping);
- they have a high degree of mechanical strength;
- their properties can be altered by encapsulating metals inside them to make electrical or magnetic nanocables or even gases, thus making them suitable for storing hydrogen or separating gases.

Recently, it was developed a CNT-based electrochemical nanosensor by demonstrating the possibilities of SWCNTs as quantum wires and their effectiveness in the development of field-effect transistors. Many studies have shown that although carbon nanotubes are robust and inert structures, their electrical properties are extremely sensitive to the effects of charge transfer and chemical doping by various molecules. The electronic structures of target molecules near the semiconducting nanotubes cause measurable changes to the nanotubes' electrical conductivity. Nanosensors based on changes in electrical conductance are highly sensitive, but they are also limited by factors such as their inability to identify analytes with low adsorption energies, poor diffusion kinetics and poor charge transfer with CNTs.

Several authors have used CNT sensing devices to detect a wide range of gases without functionalizing CNTs, which means that, since CNTs are sensitive to many surrounding compounds, there must be no interference if the gas of interest is to be reliably detected. The functionalization of CNTs is important for making them selective to the target analyte. Nanowires other than CNTs have also been used to build nanosensing devices, though to a lesser extent than CNTs.

11.2.3 Sensors based on nanostructures embedded in bulk material

Bulk nanostructured materials are solids with a nanosized microstructure whose basic units are usually nanoparticles. Several properties of nanoparticles are useful for applications in electrochemical sensors and biosensors but their catalytic behaviour is one of the most important as it was already discussed. Multilayers of conductive nanoparticles assembled on electrode surfaces produce a high porous surface with a controlled microenvironment. These structures could be thought of as assemblies of nanoelectrodes with controllable areas. For instance, platinum nanoparticles supported on materials such as porous carbon or noble metals such as gold are often reported to be relevant in the design of gas diffuse ion electrodes. Resistors are the basis for one of the simplest types of sensors. The electrical resistance of resistive sensors depends on the chemical species to which they are exposed. When chemiresistors are made of nanoparticles, or nanotubes, integrated into different organic matrices, their interaction with gases can be tailored and the selectivity and sensitivity of the sensor can be modulated. The high surface area of nanoparticles is suitable for immobilising molecules, polymers or biomaterial coatings that allow the generation of composite materials with tunable surface properties. For example, modifying metal nanoparticles with predesigned receptor units and assembling them on surfaces could lead to new electrochemical sensors with tailored specificities.

11.2.4 Sensors based on porous silicon

When a silicon wafer is placed as the anode of an electrochemical cell and a current is passed through it in the presence of an ethanolic solution of fluorhydric acid, some Si atoms are dissolved and the remaining film material, similar to a sponge, is known as porous silicon. The porous material is a complicated network of silicon threads, each with a thickness in the 2–5 nm range. The dimensions of the pores

range from a few nanometres to several microns. The result is a semiconductor material that displays an internal surface area-to-volume ratio of up to $500 \text{ m}^2/\text{cm}^3$. The extremely tiny pores give the material a strong luminescence at room temperature that is generally recognized to be due to quantum confinement effects. Light emission takes place mainly in the visible region of the electromagnetic spectrum. This emission has the unique property that the wavelength of the emitted light depends on the porosity of the material. For example, a highly porous sample ($> 70\%$ porosity) will emit at shorter wavelengths with green/blue light, while a less porous sample ($\approx 40\%$) will emit at longer wavelengths with red light. The luminescence of n -type porous silicon, for instance, is altered when molecules are incorporated into the porous layer. This property has led to the design of gas sensors whose qualitative response can be monitored by visually observing a change in colour.

11.2.5 Nanomechanical sensors

Mass sensitive transducers are the basis of different types of mechanical sensors such as quartz crystal microbalances and surface acoustic wave devices. The basic principle is that the resonance frequency changes when a mass is placed on the resonator. Although many applications are available, it is difficult to significantly improve their quality parameters at the macroscopic size. This can only be done when cantilever resonators are reduced to nanosize dimensions because the resonance frequency is proportional to the inverse of the linear dimension of the cantilever. Frequencies in the range of MHz are achieved in this way with cantilever sizes in the range of μm , and frequencies in the range of GHz can only be achieved at the nanometric scale. The change in the resonance frequency of the cantilever is proportional to the mass on the resonator.

11.2.6 Self-assembled nanostructures

The nanostructures explained so far have been developed following the top-down approach, thus starting with large-scale objects and gradually reducing its dimensions. Self-assembling tries to develop the nano and microstructures following the bottom-up procedure, i.e. from simple molecules to more complicated systems. Of the self-assembled structures, those using liposomes, polymerised lipid vesicles or pseudocellular membranes, are the most widely studied.

11.3 Micro-electromechanical Systems (MEMS)

Micro-electromechanical Systems, generally referred to as MEMS, has had a history of research and development over a few decades. Besides the traditional micro-fabricated sensors and actuators, the field covers micromechanical components and systems integrated or micro-assembled with electronics on the same substrate or package, achieving high-performance functional systems. MEMS are also referred to as micro-machines in Japan, or *Micro Systems Technology - MST* - in Europe. These devices and systems have played key roles in many important areas such as transportation, communication, automated manufacturing, environmental monitor-

ing, health care, defence systems, and a wide range of consumer products. MEMS are inherently small, thus offering attractive characteristics such as reduced size, weight, and power dissipation and improved speed and precision compared to their macroscopic counterparts.

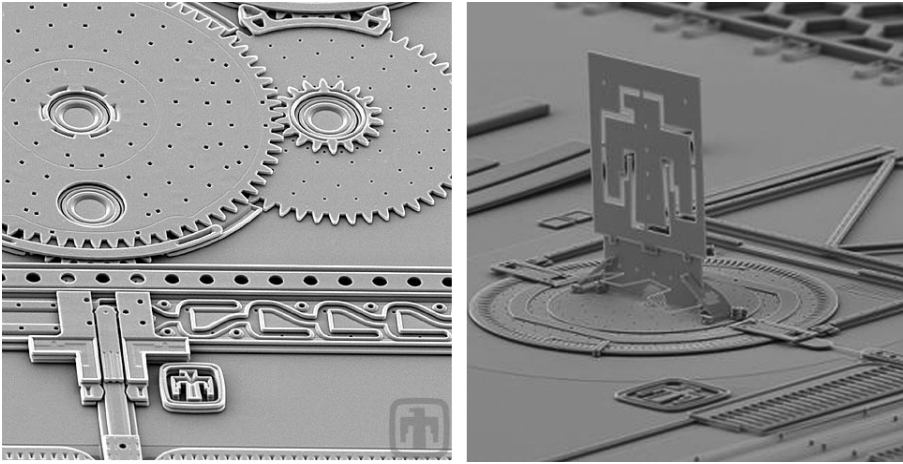


Fig. 11.3 a-b
MEMS devices:
Left: movement of sensor used in the Olympic torch to change light colours.
Right: a nanomotor.
(source: Bhushan, 2007)

The development of MEMS requires appropriate fabrication technologies that enable the definition of small geometries, precise dimension control, design flexibility, interfacing with microelectronics, repeatability, reliability, high yield, and low cost. Most MEMS devices exhibit a length or width ranging from micrometres to several hundreds of micrometres with a thickness from sub-micrometre up to tens of micrometres depending upon fabrication technique employed. A physical displacement of a sensor or an actuator is typically on the same order of magnitude.

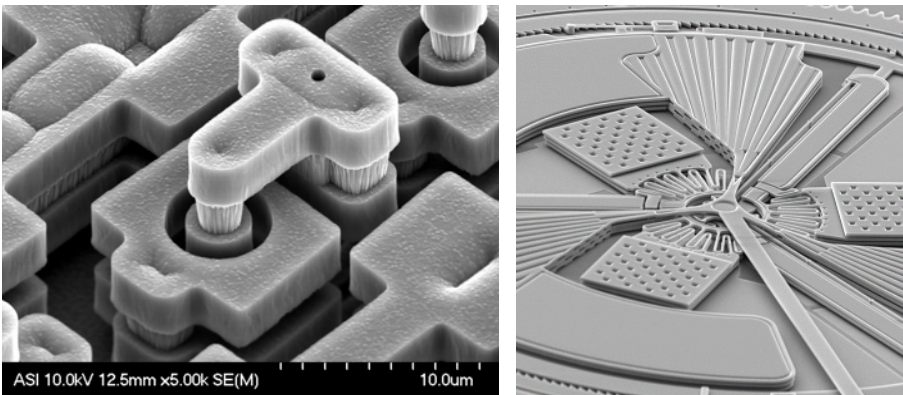


Fig. 11.4 a-b
MEMS devices:
Left: post style actuator.
Right: thermal actuator.
(source: Bhushan, 2007)

Fig. 11.5 a-b
MEMS devices:
Left: surface micro-
machined two-axis
micro-mirror.
Right: poly-silicon
surface micro-
machined vertical
torsion mirror.
(source: Bhushan,
2007)

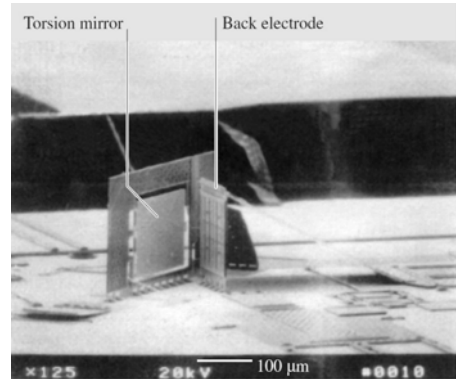
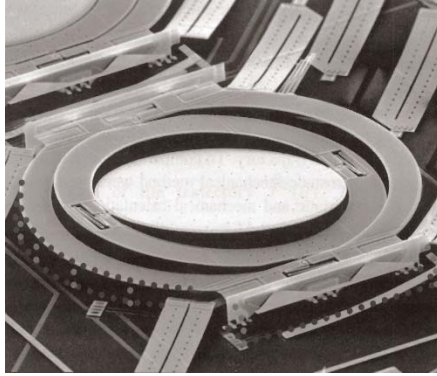
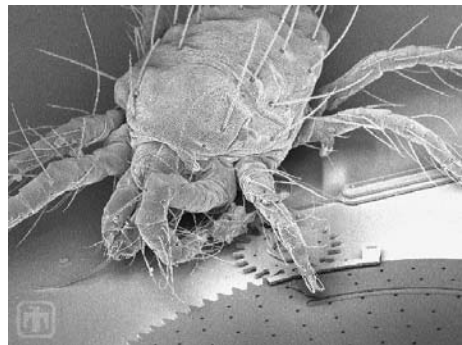
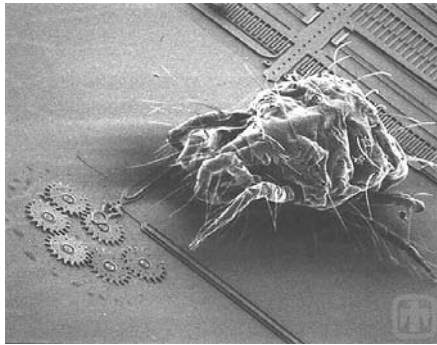


Fig. 11.6 a-b
Dimension compari-
son between MEMS
devices and dust
mites. (source:
Bhushan, 2007)



11.4 MEMS applications

MEMS devices are playing a key role in many areas of development. Microfabricated sensors, actuators, and electronics are the most critical components required to implement a complete system for a specific function. Microsensors and actuators can be fabricated by various micromachining processing technologies. In this section, a number of selected MEMS devices and studies are presented to illustrate some basic device operating principles and some future possibilities which MEMS will lead us to.

11.4.1 Pressure sensors

Pressure sensors are one of the early devices realized by silicon micromachining technologies and have become successful commercial products. The devices have been widely used in various industrial and biomedical applications. The sensors can be based on piezoelectric, piezoresistive, capacitive, and resonant sensing mechanisms. Silicon bulk and surface micromachining techniques have been used for sensor batch fabrication, thus achieving size miniaturization and low cost. For instance, the piezo-resistive effect in silicon has been widely used for implementing pressure sensors. A pressure-induced strain deforms the silicon band structure, thus changing

the resistivity of the material. The measurable pressure range for such a sensor can be from 10^{-3} to 10^6 Tor depending upon the design. An other kind of sensors are based on capacitive pressure. That is very attractive because they are virtually temperature independent and consume zero direct current power.

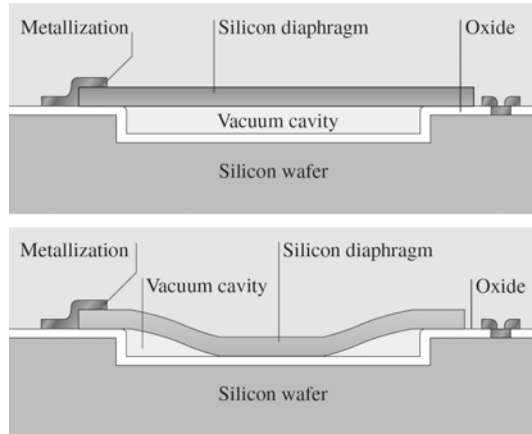
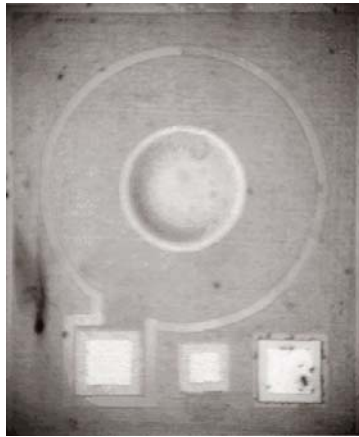


Fig. 11.7 a-b Image (left) and schematic cross-section functioning (right) of a capacitive pressure sensor. The device consists of an edge clamped silicon diaphragm suspended over a vacuum cavity. The diaphragm and substrate form a pressure dependent air gap variable capacitor. An increased external pressure causes the diaphragm to deflect towards the substrate, thus resulting in an increase in the capacitance value. (source: Bhushan, 2007)

11.4.2 Inertial sensors

Micro-machined inertial sensors consist of accelerometers and gyroscopes. These systems have been used in a wide range of applications such as automotive applications for safety systems. Inertial sensors, fabricated by micromachining technology, can achieve reduced size, weight, and cost, all which are critical for consumer applications. More importantly, these sensors can be integrated with microelectronic circuits to achieve a functional micro-system with ultra-high performance.

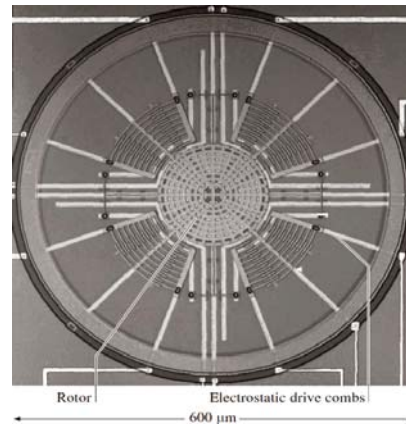
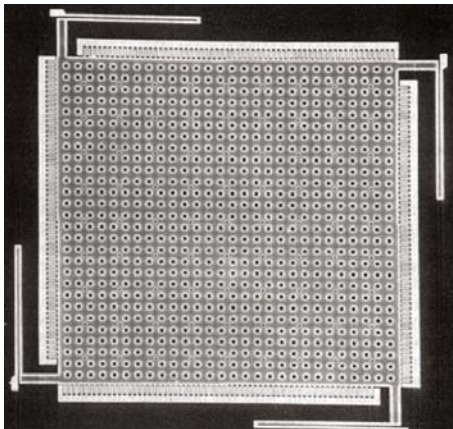


Fig. 11.8 a-b Scanning electron micrograph of (left) a polysilicon surface-micromachined z-axis accelerometer and (right) picture of a polysilicon surface-micromachined dual-axis gyroscope. (source: Bhushan, 2007)

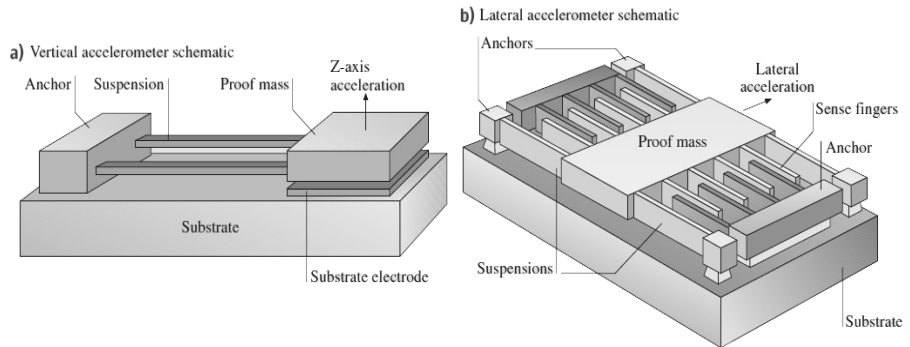


Fig. 11.9 a-b
Schematics of vertical (a) and lateral (b) accelerometer.
(source: Bhushan, 2007)

11.4.3 Radio Frequency sensors

The increasing demand for wireless communication applications, such as wireless data network, HVAC and humidity controller, security devices and all the systems that may be used for the building automation (domotics), motivates a growing interest

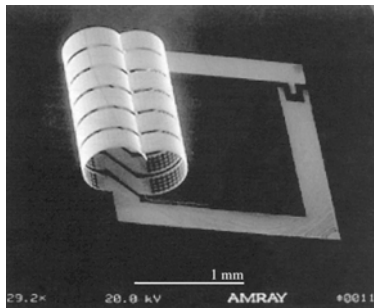


Fig. 11.10
Scanning Electron micrograph of a self-assembled out-of-plane coil inductor.
(source: Bhushan, 2007)

in developing miniaturized wireless transceivers with multi-standard capabilities. Such transceivers will greatly enhance the convenience and accessibility of various wireless services independent of geographic location. Miniaturizing current single-standard transceivers, through a high-level of integration, is a critical step towards building transceivers that are compatible with multiple standards. Highly integrated transceivers will also result in reduced package complexity,

power consumption, and cost. At present, most radio transceivers rely on a large number of discrete frequency-selection components, such as radio-frequency (RF) and intermediate-frequency (IF) band-pass filters, radio frequency voltage-controlled oscillators (VCOs), quartz crystal oscillators, solid-state switches, etc. to perform the necessary analogical signal processing.

11.5 Humidity sensors

Humidity sensors are used in a wide variety of applications, ranging from process and environmental monitoring, to the provision of feedback signals in gas sensors, household appliances, automotive control systems, Heating, Ventilation and Air Conditioning systems, materials structure monitoring and so forth.

In general, these micro-humidity sensors use vapor-absorbent films as sensing material. Their electric properties change when exposed to humidity and the magnitude of this change allows the value of the relative humidity to be determined. However, developing micro-sensors which exhibit a complete set of favourable characteristics such as good linearity, high sensitivity, low hysteresis and a rapid response time, is

quite problematic. Many researchers have exploited the high deflection sensitivity of cantilever structures to fabricate capacitive-type micro-humidity sensors. For example, a capacitive-type humidity sensor incorporating a silicon-based micro-cantilever was developed. The cantilever was suspended at a very small distance above a glass substrate and the relative humidity was determined by measuring the change in capacitance between the microstructure and the substrate as the micro-cantilever deformed as a result moisture absorption. The experimental results showed that the device had a good sensitivity but it lacked an adequate temperature compensation mechanism. Recently, in a capacitive-type humidity sensor with an integrated resistive temperature detector a polyimide layer was coated on the upper surface of the suspended micro-cantilever.

The device showed a good performance but the high bonding temperature - required to fabricate the composite cantilever structure - increases both the cost and the complexity of the fabrication process and therefore rendered the device inapplicable for low-cost sensing applications.

Anyway, lots of studies are in process as MEMS represent the most innovative solution to developing such kind of sensors.

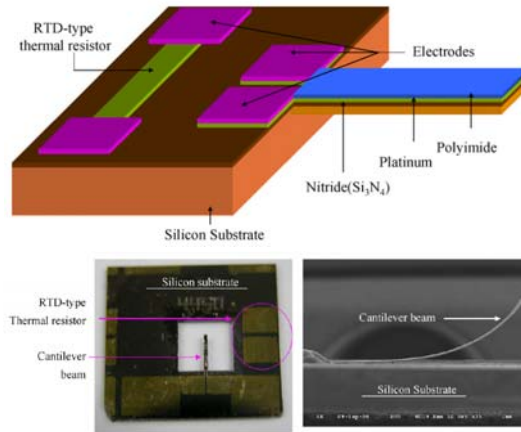


Fig. 11.11
Top: schematic of sandwiched cantilever with integrated thermal resistor, Bottom: humidity sensor chip top view (bottom-left) and side view (bottom-right). (source Chen L-T et al., 2008)

11.6 Studies on wireless sensor network (WSNs) for large civil structure and infrastructure

Large civil structure and infrastructure items such as bridges, highways, tunnels, etc. are expected to last for decades or even centuries. Unfortunately, over the course of their lifetimes, these structures slowly deteriorate depending on the weather conditions they are exposed to and the materials they are built of thus requiring timely maintenance. Traditionally, early detection of such deterioration is achieved by visual inspection, but they are time-consuming, expensive and therefore often infrequent. A effective alternative is equipping the infrastructural system with sensors that are permanently wired up to report back to a central system. The researchers goal is to develop a system for continuous long term monitoring of such infrastructure using wireless sensor networks (WSNs) which, compared to wired systems, are easier and cheaper to deploy and also offer the opportunity for straightforward expansion. Although many researches have been conducted on WSNs, experience papers reporting on real-world deployments are a minority: they include Mainwaring et al. who monitor seabirds' nesting environment and behaviour, Arora et al. who deploy a perimeter control WSN and Werner-Allen et al. who monitor an active vol-

cano, Krishnamurthy et al. who monitor equipment for early signs of failure, Kim et al. who monitor the structural health of the Golden Gate bridge, Barrenetxea et al. who deployed environmental monitoring networks over glaciers in the Alps, Stajano et al. who developed sensors for underground tunnel monitoring.

The main limit with these studies is that the most of the researches take place in laboratory setting and they are primarily concerned with monitoring vibration. Though other wireless sensors have been developed, including ones for acoustic emission detection in concrete structures and bridges, they have only been used in short-term test deployments.

Several groups have installed networks on actual civil engineering structures, such as the Golden Gate bridge (Kim et al.) or the Geumdang bridge (Lynch et al.); but, again, such monitoring has been relatively short-term and focused on vibration monitoring. There is a clearly wide gap between the WSN prototype that works in the lab and the one that works in the field attached to a real sensors, exposed to the inconsistencies and threats of a real environment, expected to stay up for months on end, required to be easy to deploy by a maintenance crew, robust to occasional failure of the hardware and software and so forth.



Fig. 11.12
Left: Golden Gate
bridge in San Fran-
cisco (CA, USA).
Right: Geumdang
bridge in Icheon, Ko-
rea.

It would be very nice if, one day, we could simply buy a commercial off the shelf WSN system and use it for monitoring our structures straight away. Unfortunately, though, the available commercial systems are typically only kits of building blocks and a non-trivial integration effort is required, together with the development of any missing parts, before arriving at a complete and usable monitoring solution.

If wireless sensor networks are to be used pervasively on civil infrastructure, they will be deployed by maintenance crew, not by academics or researchers, therefore, they must have some important requirements:

- Easy installation of the sensors. A few nodes can only be placed at specific locations: an inclinometer, for instance, that monitors whether a specific concrete panel is moving over time must be placed in specific positions. On the other hand, repeater nodes, as opposed to sensor nodes, can go essentially anywhere, so long as they enable communication: the location of a relative humidity or temperature sensor is not as critical. To evaluate the quantity of possible solu-

tions on where to put the nodes, it is essential to have a clear idea of what solutions should be considered as better than others.

- Radio connectivity is not always automatically guaranteed. Though it is possible to model the radio propagation environment, the geometrical complexity of the space would sometimes make it almost impossible to pinpoint regions of fading.
- Security of the resulting installation. It is quite common for technical people to elaborate very complicated designs for encryption of storage and communications for all nodes, before even knowing which assets the system owners consider valuable. Violating the integrity of sensor data might cause both false positives (a report of a problem where there is none) and false negatives (a report that all is fine, hiding an actual problem). Causing false negatives allows the deterioration to progress, to the point where pieces of the structure fall off; but this is hard for an attacker to exploit because they'd have to depend on deterioration occurring naturally as they would not be able to cause it to happen on demand. The ability to cause false positives, on the other hand, does not endanger the structure per se but forces the operator to waste resources in following up the alerts; eventually, it may cause the operator to ignore the WSN altogether, therefore effectively disabling it.

While integrity violations cannot easily result in physical damage to the structure being monitored, if the readings of the WSN are considered of any use and if denial of service through false alarms is to be prevented, then the end-to-end integrity of the readings must be ensured. This justifies employing cryptography in such scenarios. The requirements for battery life impose the use of symmetric cryptography rather than the more computationally expensive digital signatures. Another subtle and hidden way in which the addition of a WSN to a structure might introduce additional vulnerabilities is if by penetrating the WSN the attacker becomes able to infiltrate the back-end where the data is stored, analyzed and rendered and, depending on the quality of the internal isolation between subsystems, the rest of the computer system for that site.

- Good knowledge of large civil engineering installations problems. The original vision of WSNs for civil infrastructure of being stuck with glue or even scattered to the wind is not possible today and may never be possible. The reality is that the sensors must be packaged so that they will survive for years unattended. Furthermore, given the currently available technology, the size of the batteries alone makes the units too heavy and bulky to safely stick on with glue and dangerous to scatter to the wind.
- Data interpretation and presentation. One of the most important thing, studying and planning a sensor, is thinking about what is to be measured and why. Many times researchers install sensors because they are available rather than because they provide the data that is actually needed. If the data got are not the data needed, there is no point in putting that sensor on in the first place. With any monitoring system there are potentially a number of end-users, each hoping to

use the data in a different way. The first distinction is that there are those who are concerned with the data from the network and those who are concerned with the management of the network itself. These two groups want to know entirely different things. For example, network administrators want to know about the connectivity of the network, whereas civil infrastructure owners (or civil engineering researchers) are unconcerned with this as long as it works. There are also different levels of abstraction required for the data, as managers may only want to know when an action is required whereas engineers may require the complete data set for analysis. Unless the data is made available and presented in a way that is tailored to the user, it ends up being of no use to anyone.

11.7 Sensors for concrete structures temperature and internal humidity monitoring

Concrete is one of the most used materials in building practice but it shows several problems related to its durability and maintenance. Concrete properties (i.e., concrete strength, modulus of elasticity, creep, shrinkage, durability, etc.) mainly depend on the temperature and the dynamics of moisture transport in its matrix. The material properties change with the time and they are significantly influenced by the heat of hydration and moisture content in the concrete at early ages. Temperature and high moisture content can also promote deterioration processes of concrete structures. The deterioration mechanisms over time of concrete structures such as

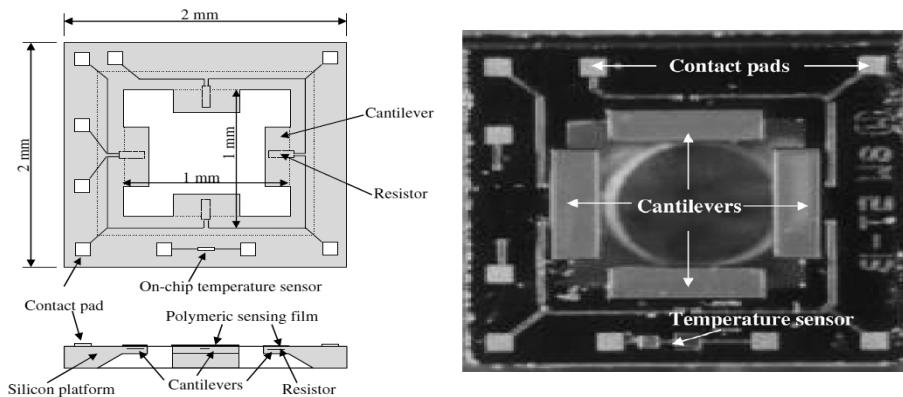


Fig. 11.13
Sensor chip for concrete: scheme (left) and manufacture (right). (Source: Alabama A&M University, Normal)

bridges, pavements and buildings are more related to moisture and temperature characteristics of these structures. Moisture from seawater, rain, soil, snow and flood is responsible for high chloride concentration transfer leading to corrosion of steel reinforcing rebars. Moisture transfer also promotes chemical deterioration and damaging processing. Therefore, a sensor system for continuous monitoring of internal RH and temperature is highly desirable both during construction and afterwards for its maintenance. When embedded into concrete, the sensor system can provide cru-

cial information about the curing process of the cement paste through the sensed temperature and internal humidity.

MEMS represent an innovative solution to current monitoring system, leading to wireless, inexpensive, durable, compact, and high-density information collection, processing and storage devices for structural health monitoring. Another advantage is that the small size of packaged MEMS sensors allows them to be embedded into concrete structures without compromising the geometry, weight or inherent properties of structures. Several studies are carried out in many universities and research centres and they are all dedicated to the fabrication of such desirable sensors.

11.8 Functional composite paints for monitoring applications

Paints are usually applied as films on structures surfaces in order to provide a protective and decorative layer. Recently, several studies focused on functional (or smart) paints that possess sensing capabilities. This kind of paints could be used as continuously distributed sensors for monitoring applications. Unfortunately, the currently available functional paints are very complex and expensive for spread and practical applications. For example, smart composite paints which are made of piezoelectric powder immersed in epoxy resin, must be coated with layers of electrodes and then poled using very high voltage to impart the sensing capability to the paint. Such a complex preparation processes make this type of paint extremely expensive. Furthermore, expensive charge amplifiers are necessary to monitor the capacitive output signals of the smart paint sensor. Alternatively, the pressure sensitive smart paints which modulate the light intensity through a repeatable chemical interaction of the sensing layer with atmospheric oxygen, require the use of an expensive photo-detector for interrogation of the paint.

Nowadays, lots of studies focus on carbon black composites as functional material. Some worked on deformation sensing with a composite that basically consists of electrically conductive carbon black aggregates embedded in a polymer matrix where the composite conductivity changes with the

applied mechanical deformation. Others focused on graphite filled polypropylene composites that show smart properties, such as a positive temperature coefficient of resistance and strain dependent conductivity. Some composites which are subject to uniaxial pressure were proposed for tensile strain and pressures sensors, others are capable of monitoring vibration and noise down to a quasi-static frequency of about 0 Hz. Accordingly, simple electrical circuits can be used to measure the changes in the current and voltage developed by the paint sensor. It is also important to mention that a functional paint can be easily applied to almost any structure, even of complex

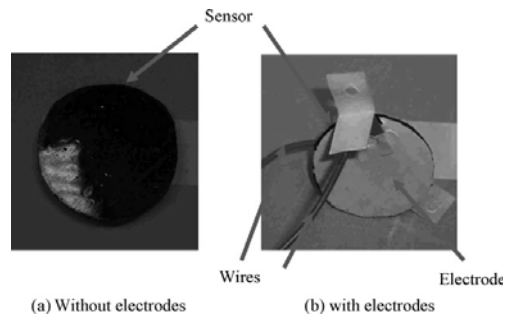


Fig. 11.14
Sample of a paint sensor. (source O.J. Aldraihem, 2009)

shapes, and can act as a continuously distributed sensor over very large areas of structural surfaces. In the future, paint sensors would be used in numerous applications ranging from monitoring infrastructures, payload fairings of launching vehicles, flexible space structures, as well as many other critical structures that are only limited by our imagination.

11.9 Nanosensors for energy and environment

Environmental pollution is a constant problem, since it affects human health and the sustainable development of both society and the economy. The presence of environmental toxins, heavy metals and organic pollutants, whether because of human or natural processes, is a serious environmental issue that has generated considerable scientific interest and public concern. Nanoparticle-based technology, that are used in a variety of fields, could be applied in the environmental diagnostic and detection in analyzing and improving air, water, and soil quality as different nanoparticles have specific optical, fluorescence and magnetic properties, and interactions between these properties give them great potential for environmental screening.

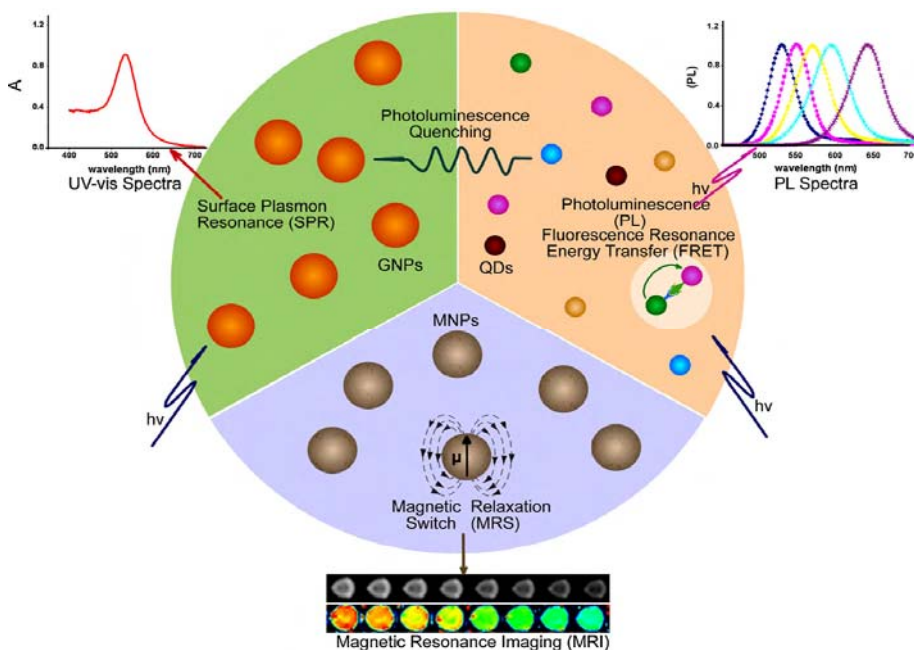


Fig. 11.15
Scheme of different properties of gold nanoparticles, quantum dots, and magnetic nanoparticles. (source: Wang L. et al., 2010)

11.9.1 Nanoparticle-based optical sensor

Optical sensors have been developed for the detection of toxins, heavy metals and other environmental pollutants. Gold nanoparticles present different colours, from red, to purple or blue, based on inter-particle reactions during aggregation, or disper-

sion of the nanoparticles aggregates. Other optical sensors are based on photoluminescence changes of quantum dots or dyes. Naturally occurring toxins, such as ochratoxin A, zearalenone, aflatoxin B1 and others are found as contaminants in cereals, cereal products, and coffee beans, and are considered to be teratogenic, mutagenic and immunosuppressive to animals and humans. Another class of toxins originating from *Bacillus Botulinus*, *Escherichia Coli*, or *Ricinus Communis* are found in animal tissue and plant which can be highly toxic and induce targeted damage to human body. Immunochromatographic strip assays combine chromatography technology with conventional immunoassays to provide a simple, low-cost and rapid tool for toxins diagnosis.

Environmental contamination by heavy metal ions is an ongoing concern through out the world. Heavy metal pollutants can exert serious adverse effects on the environment and also on human health. Thus, monitoring of aqueous heavy metal ions in environment becomes more and more important. For instance, some reported visual detection of Cu^{2+} by L-cysteine-functionalized gold nanoparticles in aqueous solution. In the presence of Cu^{2+} , the nanosolution changed from red to blue. This colorimetric nano-sensor allows rapid, quantitative detection of Cu^{2+} with a sensitivity of 10^{-5} M. Similarly, it was developed a system for the detection of mercury based on Hg^{2+} and Ag^+ where as the concentration of ions increases, their photoluminescence intensity decreases. Nanoparticles can be used to detect small molecules as well, such as hydrogen, carbon dioxide, nitrogen oxide, oxygen, and ammonium ions. Contamination with nitrite (NO_2^-) ions from chemical fertilizers, and from livestock and organic waste has been a problem through out the world. Gold nanorods can also be used as optical sensors, for example for the detection of bacteria. The presence of *Escherichia Coli* in the environment is a serious, ongoing worldwide health problem. It was produced a sensitive assay for this bacterium using an antibody-conjugated gold nanorod-based two-photon scattering technique that shows a detection limit of 50 colony formine unit (cfu)/mL.

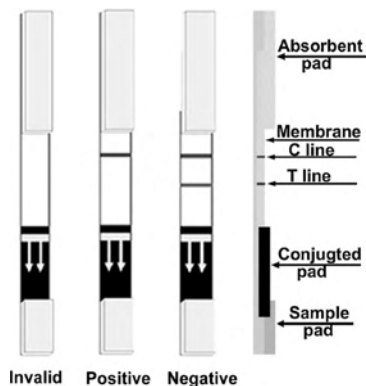


Fig. 11.16 Scheme of immunochromatographic strip assay. (source: Wang L. et al., 2010)

11.9.2 Nanoparticle-based electrochemical sensor

Electrochemical sensors are a rapidly growing area of research. The classic biosensor is enzyme-based, and the development of glucose sensors is still the largest area of research, and often used as a model system. Metal nanoparticles can be oxidized to form ions that are easily detected electrochemically. Electrochemical sensors have been widely investigated for use in environmental pollutants screens. For instance, an electrochemical sensor for copper ions was developed with a detection limit below 1 pM. Electrodes were first modified with gold nanoparticles, and then the gold

colloid surface was modified with cysteine for copper detection. Also single-walled carbon nanotubes (SWNTs) impregnating porous fibrous materials such as fabrics and papers, have been used to generate simple but high-performance biosensors.

11.9.3 Magnetic-relaxation sensors

Biocompatible magnetic relaxation switches methods are radio frequency-based, and, therefore, indifferent to light-based interference such as scattering, absorption or fluorescence in tissues or fluids. Magnetic relaxation switches technology has been used to detect analytes in different matrices, including in environmental toxin monitoring. For instance, it was developed a specific, highly sensitive and quantitative bacterial detection method based on these sensors that is expected to be able to identify and quantify bacteria in environmental samples. Due to the simplicity of the theory and easy operation magnetic relaxation switches assay, it may be a potential candidate for the rapid screening of environmental pollutants and may find a wider application; on the other hand, the equipment required is quite complex and expensive.

11.10 Gas detector: developing the electronic nose

Gas sensor technology was inaugurated when three pioneering gas detectors were developed in Japan: oxide semiconductor gas sensors for gas leakage alarms, solid electrolyte oxygen sensors for car emission control systems, and ceramic humidity sensors for automatic cooking ovens. These sensors, nowadays known as electric nose, demonstrated how dramatically important it is to monitor a specific gas species in situ, in real time and continuously. The applications includes: protecting environments, air quality control in HVAC system, safety/anti-terrorism, explosive gas (bomb) and hazardous pollutant gas detection in public area like airport, shopping centre, etc.. Other areas include odours detection in industries including food, drink, chemical, etc. applications in automobile and space, smart domestic applications and health cares.

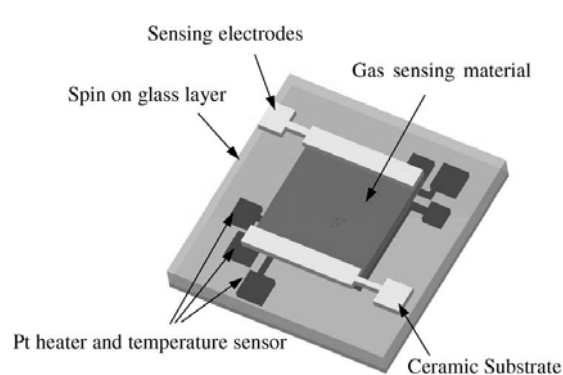


Fig. 11.17
Schematic gas sensor cell.

Currently various kinds of gases including reducing ones (methane, propane, carbon monoxide, ammonia, hydrogen sulfide, etc.) and adsorptive ones (oxygen, nitrogen dioxide, ozone, etc.) have been made detectable with gas sensors using semiconductors, electrolytes or catalytic combustion.

Yet, there are various new demands to gas sensors ranging from detecting volatile organic compounds at very

low concentrations (ppb levels) to constructing sensor network systems but there is no single gas detector existing that is 100% selective to a single chemical gas.

A desirable gas detection system can be described as followings: portable and corrosion resistant that is capable of being installed in hazardous areas, durable and operationally stable, simple and minimum needs in maintenance, enable for a minimally skilled person to operate and cost effective.

In the past a few decades, semiconductor metal oxide gas sensors have emerged as efficient gas detection tools. Compared to other gas sensing techniques such as conductive polymer, oscillating, electrochemical cell and fibre optical, semiconductor metal oxide gas sensors have advantages, such as more robust (up to 10-year-life time), less sensitive to environmental moisture and temperature, simple interface electronics, faster response time and fast recovery time. Furthermore, they have broader sensitivity than any other sensing technologies.

Therefore, semiconductor metal oxide gas sensor may represent the best sensing cells for chemical gas sensing electronic nose development.

12. NANOTECHNOLOGIES FOR PRESERVATION AND ARCHAEOLOGY PRACTICE

12.1 The preservation of cultural heritage

It's worldwide recognised that artworks - including not only buildings of historical and artistic value but also archaeological permanence, paintings, canvas or sculptures - must be protected and handed down to the next generations, for both a moral duty and because of laws and regulations. However, their conservation is not very easy and feasible to achieve due to many different factors that may cause damage. Nowadays, thousands of institutes and industries, especially in Italy and France, have a lot of R&D programs in the field of preservation and restoration. Nanotechnologies are slowly entering the restoration sector and new materials, instruments, technologies and techniques based on nanotechnology may be used in operations of preservation. Indeed, they may be applied in several technical applications as in diagnostic, for instance, to better understand the micro/nano-structure of both antique materials and degrading agents thus to find the better solution to specific problems. Thus will help operators finding the suboptimal solutions that constantly afflicts cultural heritage.

A complete listing of these activities is therefore impossible due to the vastness of the topic itself.

One of the most dangerous agent to the cultural heritage is the constant exposure to combined action of natural weathering and urban pollution that causes several damages to carbonatic materials: air pollution, soluble salts, bio-deterioration are the main causes of decay. The results of these phenomena are flaking of the surface layers, powdering, formation of small blisters and loss of large parts of the artefact.

In any case, the primary aim of any scientist is finding the correct choice of the right conservation procedure to be applied to every single case of study.

Nowadays, the preservation of cultural heritage attracts universal attention and new regulations focus on the application of new technologies in conservation, exhibition, storage and transport. To minimize the effects of aging, renovation and logistic operations, monitoring and controlling the micro-climate of the cultural object is crucial. Such aspect is well recognized in museums, for instance, where storage facilities, libraries, archives, galleries are planned in order to ensure the long-term preservation, safety and preventive conservation of artworks, antiques and archaeological collections. Among the most relevant environmental factors that affect the precious items, it is possible to mention the temperature, the relative humidity and the chemical environment. Furthermore, mechanical vibration and ultraviolet light exposure accelerate the damaging effects. Fluctuations in RH and temperature can cause several kinds of damage and deterioration such as dimensional change, chemical reac-



Fig. 12.1
A restoring operator who is cleaning statue surfaces.
(source: Servitec, 2009)

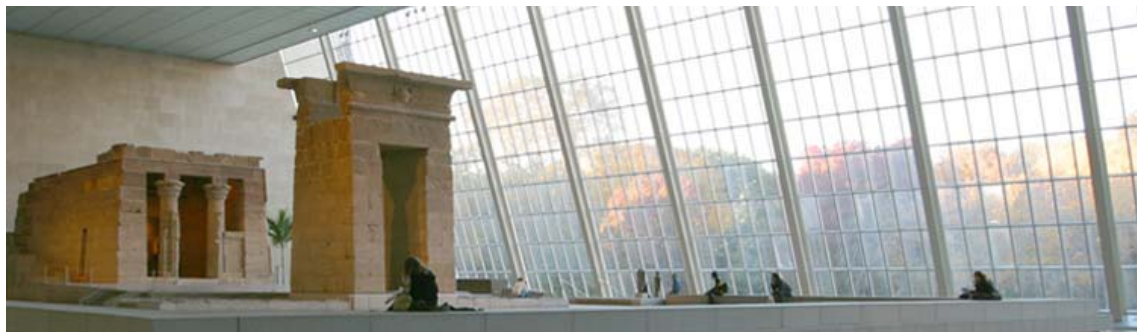


Fig. 12.2
The temple of Dendur. Metropolitan Museum of Art, New York City.

tivity and bio-deterioration of museum objects, which are often made of non-isotropic materials. Thus, continuous environmental monitoring and the assurance of stable conditions in the local environment of the artwork are necessary to preserve the items for long periods of time. A main goal of preventive conservation is to maintain the artworks and collections under basically constant levels of temperature



Fig. 12.3
Apollo Gallery, Musée du Louvre (Paris).

and RH. A precise control of these physical parameters is a strict requirement.

In this context, increasing recent interest in the field of cultural heritage points to a new generation of sensors tailored for applications in museums indoor environment¹.

12.2 Chemistry contribution to conservation: the problem of reversibility

The peculiarity of the research in cultural heritage resides in its high multidisciplinary nature. The co-operation between conservators and private/public institutions and experimentation is fundamental in the definition of the restoration procedures and innovative methodologies. During the last years, the contribution of scientists from different fields has radically grown up. Thus, the awareness of a work of art is no longer restricted to humanists and the contribution of chemists and physicists is becoming predominant for the prediction of the degradation insight and for the preservation of cultural heritage.

Nowadays, thanks to the contribution of chemistry we know how to address most of the degradation factors caused by chemicals in environments. The most of the interventions suggest the reinforcement of the porous structure and the consolidation of

¹ Sensors for environmental control are discussed in the previous section of this thesis.

the surface layer of a work of art that is usually the most precious. After cleaning and consolidation, protective treatments confer a longer lifetime to the artistic object. Restoration strives the opacity of the surface by minimizing the light scattering effects, and the protection of the surfaces strongly reduces the degradation from pollutants and water condensation. All the interventions directed to preservation of the historical meanings of the works of art are commonly designed as conservation treatments. In a strict sense, all the chemical treatments to preserve any work of art from damage and deterioration are the matter of conservators and scientists aiming to rescue the original materials. On the other hand, despite a common opinion, every restoration treatment should be considered as invasive. Conservators often have to remove chemicals from surfaces, such as fat, salts, varnishes, pollutants; this is, usually, done by chemicals or mechanical methods, which may also affect the substrate. Moreover, chemicals for consolidation and protection are used for improving the physico-chemical and mechanical features of the materials. These products are introduced within the porous structure of the original material, strongly modifying the original characteristics of the objects and making very hard the prediction of the lifetime of the restored materials. Some basic principles have been established, and accepted, by most conservators, in order to reach the best results in a restoration workshop.

Basically, three main points can be stressed out:

1. the treatment should be reversible so that at any time it should be possible to revert to the status before the treatment;
2. all the applied chemicals should ensure the maximum durability and the chemical inertness;
3. the chemicals used in the conservation treatment should be compatible with the substrate.

However, scientists know that reversibility does not exist. It follows that methods based on compatible materials should be preferred, so that the original features of the materials are slightly changed, or, at the best, they are not changed at all.

12.3 Wall painting cleaning

Restoration of wall paintings requires several complex operations: among these is the painting cleaning. Around mid 1980s, the wall paintings by Masaccio and Lippi in the Brancacci Chapel in Florence, considered one of the most important masterpieces of the Italian renaissance, were objects of an intense work of restoration with the removal of the hydrophobic impurities that covered their surface.

UV fluorescence investigations and preliminary cleaning tests revealed the presence of a patina from wax spots due to extinction of altar votive candles. This prompted to study systems to solubilise and extract wax from the porous matrix of the wall. Due to the thermodynamic stability and the detergency efficacy, oil-in-water microemulsions were the best candidates.



Fig. 12.4 a-b-c (top)
Brancacci chapel,
Florence. "San Pietro
che risana con l'ombra"
by Masaccio
(XV century). UV
fluorescence images
before (A) and after
(B) cleaning with w/o
microemulsions. (C):
image in visible light
after removal of the
hydrophobic impuri-
ties.



Fig. 12.5 a-b-c (middle)

Left: Brancacci chapel.

Centre & Right: frescoes in San Salvador church in Venice. Pre (left) and post (right) removal of Paraloid B72.

Fig. 12.6 (bottom)
Masaccio's frescoes in Brancacci chapel. Pre (left) and post (right) removal of wax spots.



The oil-in-water microemulsion ensured very low aggressiveness to the painted layer, due to the presence of water as a dispersing medium that remained in direct contact with the hydrophilic surface of the wall painting. Furthermore, water favoured the wetting of the wall and ensured the right contact time with the hydrophobic material to be removed. On the other side, the oil phase works as a nano-container where polymers can be solubilised and removed from the surface. The detergency depends on the huge surface of micelles or microemulsion nanodroplets where polymers can be solubilised. The microemulsion system was applied on the surface by proper equipment that ensured a continuous microemulsion flux by means of a pipette connected to a reservoir tank.

This methodology has been transferred to the removal of polymers applied to works of arts during conservation interventions. In the past, some conservation treatments performed using synthetic polymers have produced severe degradation of the surface of the works of art, as clearly evidenced by the poor conservation conditions shown by several masterpieces in different countries. Nowadays, it is possible to use some nano-systems, as micelle and microemulsions, specifically tailored for the removal of such products as Paraloid B72 (ethyl-methacrylate methyl-acrylate copolymer), Primal AC33 (ethyl-acrylate methyl-methacrylate copolymer), and Mowilith DM5 (vinyl-acetate n-butylacrylate copolymer) that produced devastating and completely unexpected degradation processes.

12.4 Ferroni-Dini method for structural consolidation of wall painting matrix and stones

At the International ICOM Conference in Amsterdam in 1969, prof. Enzo Ferroni, from University of Florence, and the conservator prof. Dino Dini proposed a new method for in situ consolidation of wall paintings. This method, known as *barium* or *Ferroni-Dini* method, was the first example of a chemical and structural consolidation technique for the restoration of wall paintings that underwent phenomena of salts' crystallization and/or sulphatation. The Ferroni-Dini method inverts the chemical reactions that produce the degradation of wall paintings, stabilizing the structure of the mortar and regenerating the binder of the painted layer, that is calcium carbonate. The method is based on the application of ammonium carbonate and barium hydroxide solutions on the painting surface so that they could penetrate the painting matrix, due to the nanosized dimensions, and react with it. The treatment eliminates the harmful gypsum that is formed by environmental pollution, and promotes the formation of new slaked lime, $\text{Ca}(\text{OH})_2$, formed in situ which acts as the

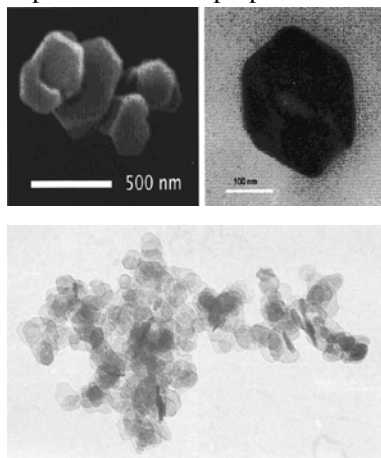


Fig. 12.7

Top left: SEM micrograph of $\text{Ca}(\text{OH})_2$ particles.

Top right: TEM micrograph of a single $\text{Ca}(\text{OH})_2$ showing the hexagonal habitus.

Bottom: TEM micrograph nanoparticles of $\text{Mg}(\text{OH})_2$. The nanoparticles average dimension is 120 nm. (source: Baglioni P. et al., 2009)

fresh binder, giving new setting for mortar with maximum physicochemical compatibility. The Ferroni-Dini method is at the moment one of the more powerful techniques available for frescoes matrix consolidation.

Its success depends on the salts' removal and, at the same time, on the reinforcement of the porous structure of the fresco painting due to the reduced dimensions, that are nanodimensions, of the material used.

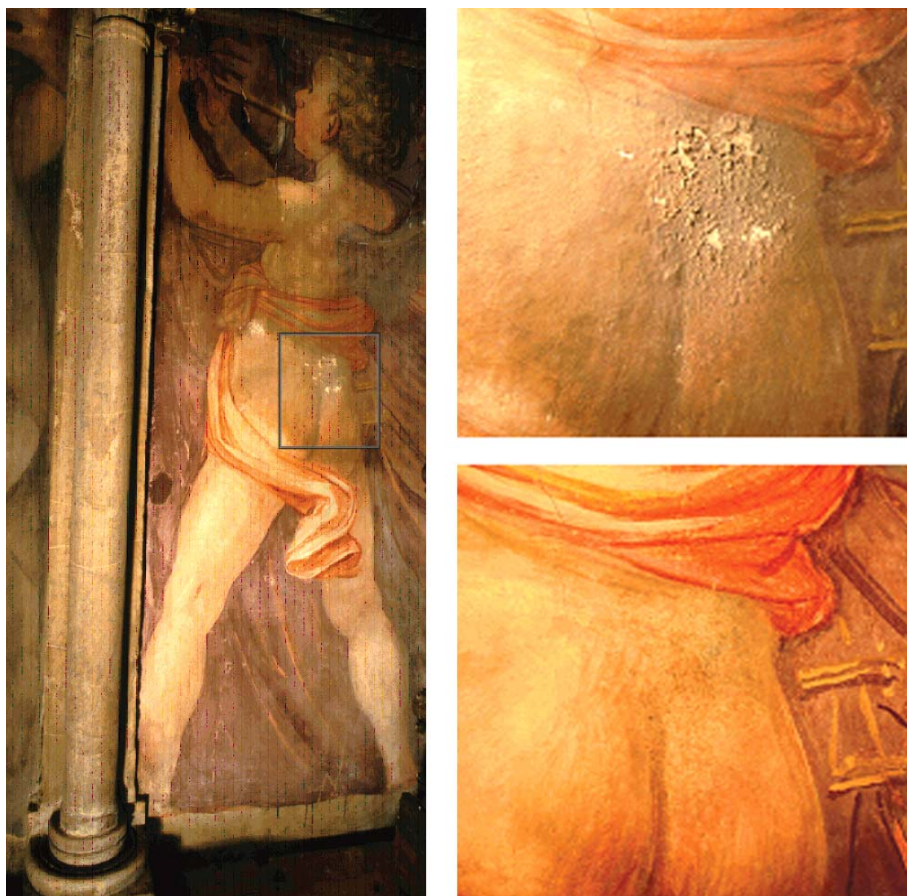


Fig. 12.8 a-b-c
Restoration of the
“Angeli Musicanti”
by Santi di Tito (XVI
century) in Santa
Maria del Fiore ca-
thedral in Florence
(Italy) with nanopar-
ticles of $\text{Ca}(\text{OH})_2$.

A few years later, after having performed the Ferroni-Dini method on the wall paintings by Beato Angelico in San Marco church in Florence, Ferroni and Dini realized that the consolidation treatment was performing much better with time. This finding convinced Ferroni that a large excess of barium hydroxide used during the application could be responsible for the slow and progressive transformation of calcium carbonate to calcium hydroxide, i.e. barium hydroxide generated new binder from

the calcium carbonate. The newly formed binder was considered to be responsible for the good consolidation, similar to a new setting process of lime, calcium hydroxide. Later, they proposed to apply calcium hydroxide in the form of nanoparticles for the consolidation of wall paintings synthesizing water-in-oil (w/o) micro-emulsion of $\text{Ca}(\text{OH})_2$. They obtained calcium sulfate nanoparticles with different shapes working with $[\text{SO}_4^{2-}]$ and $[\text{Ca}^{2+}]$ inside the aqueous pool of the w/o microemulsion. In the same way, the Dini-Ferroni method may be applied to consolidate any tuff stone in general. In the last 30 years, many conservators and restorers experimented polymeric resins as consolidating and protective agents for stone restoration; more particularly synthetic acrylic and vinyl polymers, organosilicone compounds and fluorinated materials were used for preserving historic and artistic monuments. Some of these materials act as protective agents while others induce consolidative effects on the substratum on which they are applied.

Anyway, they present a basilar disadvantage: they do not obey to the fundamental rule of physicochemical compatibility with the substrate and consequently cannot be considered as suitable for consolidating purposes. Inorganic consolidants have the great advantage of high compatibility with the constituting materials: according to the idea that the original binder for wall paintings and limestone is also their most effective consolidant, new methodologies are being studied.

Recently, a new class of composite materials is offered by layered polymeric nanocomposite systems, based on organic polymers and inorganic layered reinforcements consisting of organo-modified silicates whose layers are few nanometres thick. These systems show a great interfacial area per volume between the nanosheets and polymer, with higher properties compared to the unmodified organic resin. In particular, they exhibit higher chemical, thermal and mechanical resistance and reduced gas and vapour, without spoiling the optical properties of the polymeric matrix. Thus, they are more compatible to tuff materials, showing a deeper penetration. Reducing the average size of the consolidating particles to the sub-micrometric scale is critical in a satisfactory stone consolidant process in order to achieve a deeper penetration of the dispersion, a better stability and to avoid the formation of white glazing on the treated surface.

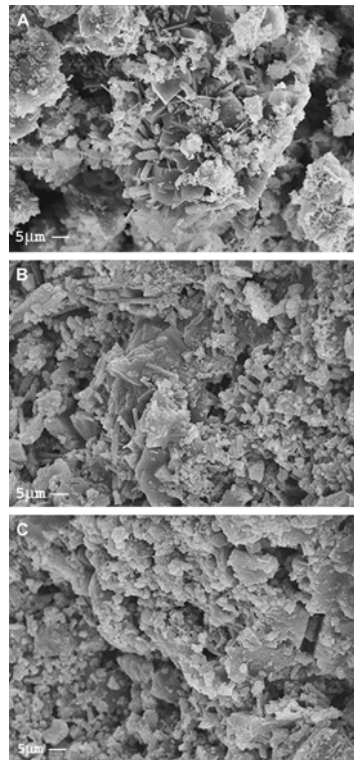


Fig. 12.9 a-b-c
SEM micrographs of Neapolitan yellow tuff samples. (A) untreated stone where rod-shaped phillipsite crystals are immersed in a matrix of pseudocubic chabazite crystals; (B) sample treated with a resin that soaks the surface layer of stone. The distribution and the morphology of the polymeric layer inside the tuff do not seem to be significantly affected by the presence of the organoclay; (C) sample treated with a nanocomposite system where a quite continuous polymeric layer coats the inner walls of the pores within the stone and links up the disaggregated parts one another. (source: Journal of Cultural Heritage 9 (2008), p.257-258)

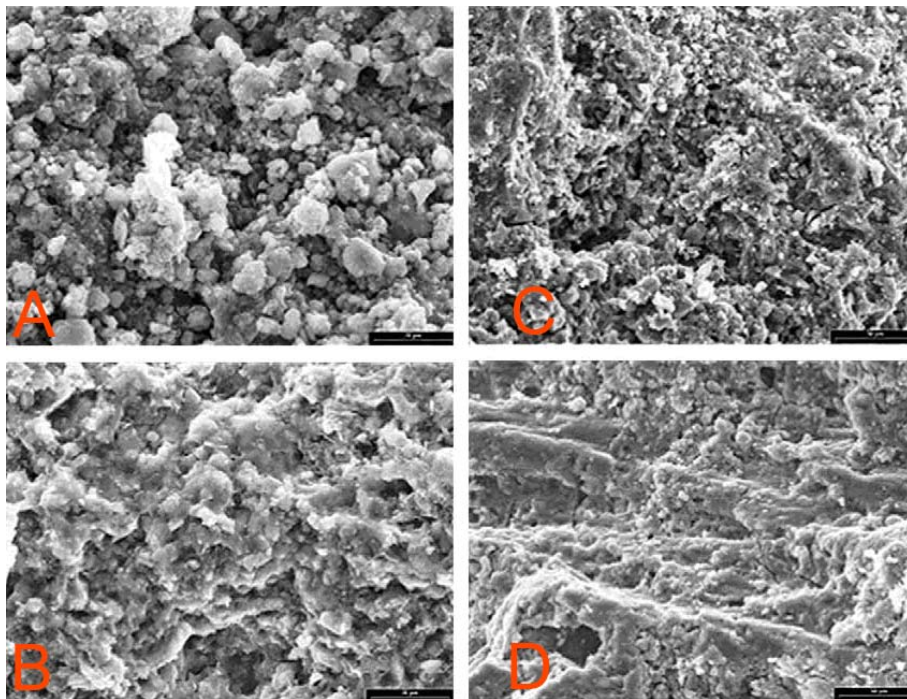
Researchers from the University of Florence achieved interesting results carried out some tests on two kinds of limestones, Gallina and Alberese stones, taken from historical buildings and consolidated in laboratory by nanophases of calcium hydroxide nanoparticles. Gallina stone is a soft calcareous sandstone, used for the façade of an historical building in Mantova, Italy. It showed evident powdering of the surface and brittleness. The second stone is a compact limestone coming from the bell tower of Santa Maria church in Impruneta, Florence, Italy. It was affected by flaking and powdering of the surface. The samples were immersed in the nanodispersion for 8 hours and the effectiveness of the conservation treatment was evaluated by performing SEM-EDX and water absorption analyses, as shown in the following images.

Fig. 12.10 a-b-c-d

SEM micrographs. Alberese stone: (A) untreated and (B) treated. Gallina stone: (C) untreated and (D) treated. Bar = 20 micron. Visual observations of the treated samples did not show any remarkable change in colour, while the re-cohesion of the surface was evident by touch. The comparison of SEM-EDX analyses performed on untreated and treated surfaces show that consolidated samples appeared more compact and with a higher Ca/Si ratio.

Furthermore, for both Alberese and Gallina stones, the consolidation treatment strongly affects the kinetics of capillary suction while the specific surface areas were slightly affected.

(Source: Journal of Cultural Heritage 7 (2006), pp. 111-113).



12.5 Removing biological patina from monument surfaces: a new enzyme procedure

In cultural heritage science, bacteria have been largely used to remove pollutant from surfaces. Among these the *Desulfovibrio Desulfuricans* to remove the black patina containing large amounts of sulphates or, similarly, the *Pseudomonas Stutzeri* to remove nitrates. On the other hand, it was observed that the metabolic products of these bacteria could chemically react with the substrata itself provoking several destabilization problems.

Other additional briofite such as musk, liverwort and vascular plants abundantly grow on the archaeological areas and on buildings when the environmental conditions, and the chemical composition of the substrata, show favourable results. Especially the briofite are able to accumulate the environmental particulate matter catalyzing the modification of the stones on the monument surfaces. All these highlight the negative role of the biological patina. These patina show different colours, thicknesses and different microstructures.

Several studies have been carried out to classify them with respect to their morphology (i.e., films, etching surfaces, crust), their petrography (i.e., grain dimensions, porosity, wettability) and the microflora colonization.

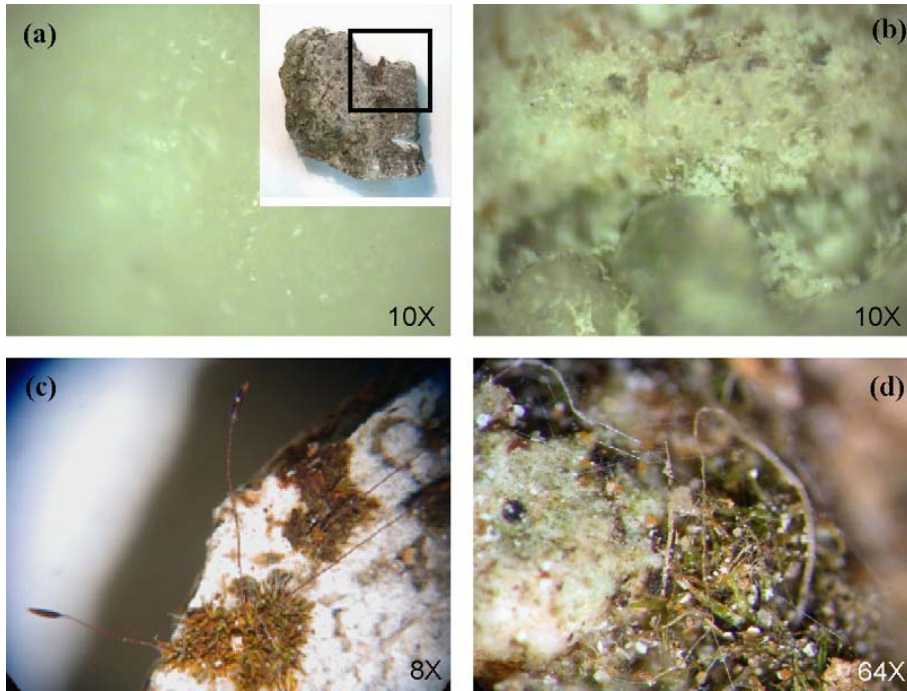
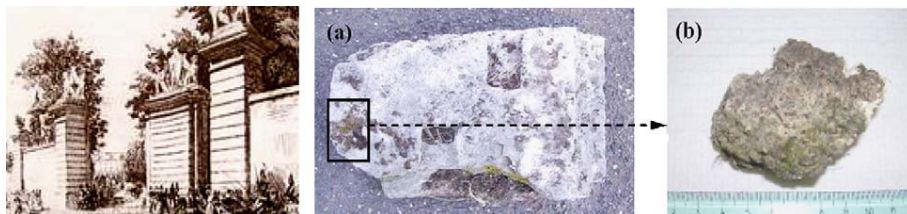


Fig. 12.11 a-b-c-d Morphological investigation of travertine stone: (a) control sample; (b) travertine sample during the biodeterioration process; (c) green biofilm composed of moss sporophytes and (d) gametophyte. (source: F. Valentini et al., 2010)

All these studies are necessary to plan the suitable strategy necessary to reach the cleaning efficiency, consolidation and preservation of the cultural heritage materials. Until now, several hydrolase enzymes have been widely used to remove the biological patina as some microorganisms are able to produce amylase, cellulase, lipase and protease that are able to modify the chemical composition of substrata. This helps in removing the biological patina and cleaning the surfaces. At the same time, they can induce the calcite production on the CaCO_3 substrata (i.e., bio-mineralization process).

A new study, performed in Villa Torlonia in Rome, focuses on the application of a new bio-cleaning procedure based on the glucose oxidase enzymes (i.e., GOx) to remove biofilms.

Fig. 12.12 a-b-c
Villa Torlonia in Rome: “Main Entrance” (1802–1806). Biological patina on travertine fragment. (source: Applied Surface Science 256 (2010), p. 6551).



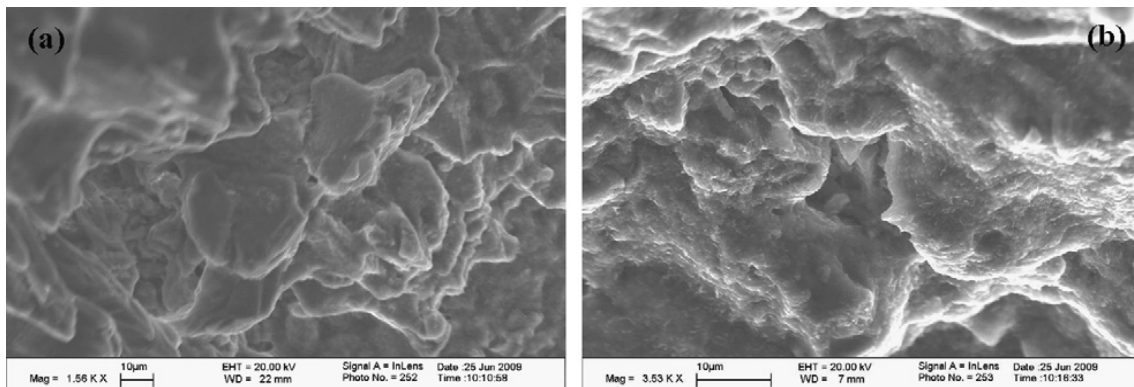
This particular enzyme is able to produce H_2O_2 from the catalytic reaction of the glucose. H_2O_2 represents a cleaning agent because of its oxidizing properties, resulting in a bleaching effect on these surfaces.

The analytical advantages of the GOx enzymatic approach, compared with the conventional chemical method concern the following:

- the possibility to control the peroxide concentration on these surfaces, removing the biofilm;
- the possibility to realise small amounts of the oxidizing agent, avoiding the etching of these stone materials;
- the possibility to gain better cleaning efficiency depending on the porosity of stone materials. In particular, substrata having the lowest porosity, strongly retain the H_2O_2 for longer time on their surface (avoiding its diffusion into the bulk), especially where the biopatinas strongly adhere.

The cleaning performances of GOx have also been compared with those obtained using the traditional chemical treatments based on the EDTA or $(NH_4)_2CO_3$ and with enzymatic treatment, performed with lipase. Also in this last case, the new bio-cleaning method results comparable to some others, such as the lipase treatment as confirmed by the SEM investigation shown in the following pictures.

Fig. 12.13 a-b
Micrograph of the travertine sample treated with GOx enzyme: presence of kaolinitic clay minerals.



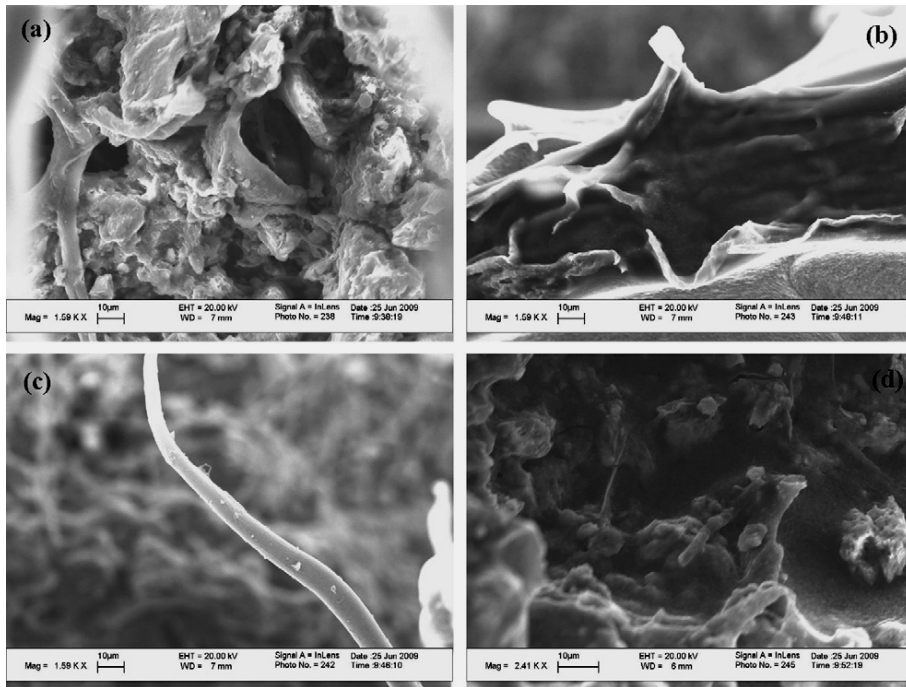


Fig. 12.14 a-b-c-d Micrograph images of travertine sample with a biological patina from Villa Torlonia in Rome: (a) external appearance of cyanobacterial cells encrusted in the stone; (b) adhered bacteria; (c) detail of microalgal filament grown in close contact with the underlying substratum; (d) a chaotic aggregate of smaller particles of various nature (source: Applied Surface Science 256 (2010), p. 6556).

12.6 Preserving wood from acids: the Vasa case

An other field where nanotechnologies have being applied with many interesting results is timber protection. Timber, along with stones, is a largely used material in the traditional worldwide construction practice and many monuments and historical buildings have wooden floors, roofs or pillars in their structure. One of the main problem related to this material is the acidity neutralization.

An acidic environment, indeed, catalyzes the cellulose hydrolysis making wood fibres losing their mechanical properties. By means of the nanometric dimensions of hydroxide nanophases it is possible to make less acid the environment and to exploit the dispersing means to reach a deep penetration through the fibres.

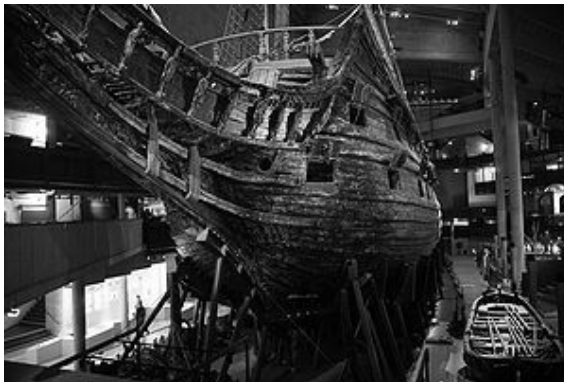


Fig. 12.15 Vasa in the bow at the National Maritime Museum in Stockholm.

The *Vasa* case shows how difficult it is preserving wooden structure from slow oxidation. *Vasa* (fig. 12.15 in the previous page) is a unique Sweden warship of the XVII century that sank during its maiden voyage in 1628 and was in surprisingly good condition after 333 years at the bottom of the sea.

Nowadays it is exhibited at the Stockholm National Maritime Museum where various experiments are conducted on some pieces of it to preserve its integrity. The more and more polluted waters of Stockholm port made no aerobic bacteria, that are usually responsible of underwater wood decomposition, live in that environment. On the other hand, some anaerobic bacteria survive and their action generated a lot of sulphurous compounds that stored in *Vasa* wood.

In 1961 it was exhumed, and its oak timber would have quickly deteriorated if the hull had been simply allowed to dry. It constituted an unprecedented conservation problem that was solved spraying polyethylene glycol (PEG) for 17 years, followed by 9 years of slow drying. Oxidation is still in progress and new studies with nanoparticle applications are trying to solve the acidity problems making a reservoir of alkaline compounds inside the wooden components.

13. Conclusions

In the first section of this thesis we investigated what nanotechnologies are and why they are so studied worldwide with thousands of different applications in many scientific and technological fields.

Nowadays, nanotechnology is highly prioritized on the global scientific agenda regarding it as one of the most relevant area of exploitation to material science and engineering. Thus lots of countries set up national initiatives, regulations and appoint funding to research.

In this section, we focused on the construction sector where nanotechnology seems to be a competitive route in achieving a real sustainable growth and innovation. Its usage in construction is highly wide and varies from the early stages of planning to the final stages of finishing, especially in choosing the right materials with the correct and appropriate characteristics and performances that could better deal with external stimuli.

The development of new materials has a great influence in the methodology of thinking about architecture according to the new vast options that nanotechnology offers. In other words, in construction nanotechnology is an enabling technology that may help to make other technological developments.

Nowadays, there are a lot of new products available, based on nanotechnology, that can be applied to the construction industry. The new generation of building materials must be investigated within a scientific approach addressed to create multifunctional high performance materials as well as more economically way of production. Nanotechnology may help architects and designers in finding and applying new customized materials with specific individual properties. From the client, or the user, point of view, the most realistic and sensible application focuses on aspects of aesthetics, functionality, economy and sustainability.

Within this scenario we analysed many new materials that are already available on the global market, discussing them in many dedicated reports. A complete listing is therefore impossible but the quantity of the products listed in the reports gives us an idea of what has been developing around our traditional view of architecture and construction.

This thesis is not intended to be a resolved work but, on the contrary, it is in continuous evolution as, everyday, new papers and patents are published as well as new materials are promoting on the global market.

From what we have discussed, it is possible to summarize that:

- nanotechnology is both scientific and technical and has a highly multidisciplinary character, affecting multiple traditional technologies, scientific disciplines and industries, among with the construction one;

- millions of dollars are spent every year in research in nanotechnology all over the world, both in publics and privates;
- hundreds of nanostructured products are already available on the construction market or are under investigation;
- hundreds of new patents and papers are published every year with a positive trend;
- enhanced new buildings are being designed worldwide imagining what it will be possible to build in a hundred years by means of this new class of advanced materials;
- architects, engineers, contractors as well as all the building operators, began to have a deeper knowledge of nanotechnology and began to apply nano-materials in their new building projects.

Far from being a science and technology fashion, nanotechnology is a necessary path to achieve a real competitive and sustainable growth and innovation within the construction industry.

Some of the main problems related to this field of research are:

- researchers high-specialization;
- high-tech laboratory and equipments (expensive, complicated, dangerous);
- materials high toxicity;
- laboratory materials still very expensive in bulk.
- often out-of-date construction operators way of thinking and difficulties in accepting new theories and applications.

SECTION 2

Thermochromic coatings for architectural glazing

1. NOTES ON GLASS FOR ARCHITECTURAL GLAZING

1.1 Introduction

The word “glass”, in the common sense, refers to a hard, brittle, transparent amorphous solid, such as the one used for windows.

In the technical sense, glass is an inorganic product of fusion which has been cooled to a rigid condition without crystallizing. Many glasses contain silica as their main component.

In the scientific sense, the term glass is often extended to all amorphous solids (and melts that easily form amorphous solids), including plastics, resins, or other silica-free amorphous solids.

The material glass plays an essential role in a lot of scientific fields and in industry. Its optical and physical properties make it suitable for many applications such as float glass in architecture, container glass, optics and optoelectronics materials, laboratory equipment, thermal insulator (glass wool), reinforcement fibre (glass-reinforced plastic, glass fibre reinforced concrete) and art.

1.2 Glass ingredients

From a chemical point of view, some principal oxides (SiO_2 , B_2O_3 , P_2O_5) and some modifiers oxides (Na_2O , K_2O , CaO) may be distinguished.

Glass has no long range order due to its amorphous structure of glassy silica (SiO_2), however there is local ordering with respect to the tetrahedral arrangement of oxygen (O) atoms around the silicon (Si) atoms.

The standard definition of a glass - or vitreous solid - is a solid formed by rapid melt quenching.

If the cooling down is sufficiently rapid (relative to the characteristic crystallization time) then

crystallization is prevented and instead the disordered atomic configuration of the super-cooled liquid, it is frozen into the solid state at the glass transition temperature T_g . Generally, the structure of a glass exists in a metastable state with respect to its crystalline form.

As in other amorphous solids, the atomic structure of a glass lacks any long range translational periodicity. However, due to chemical bonding characteristics glass possesses a high degree of short-range order with respect to local atomic polyhedra.

The glass used nowadays in architecture is the soda-lime one which is usually made of different specific compounds. In the labels in the next page, the main compounds and physical characteristics of this kind of glass are reported, according – for Europe - to the UNI EN 572:1996 part 1.

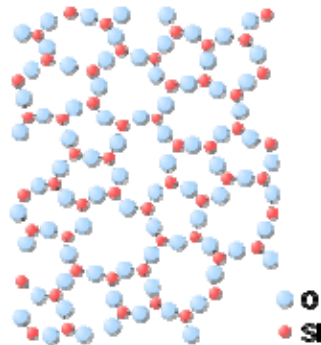


Fig. 1.1
Schematic glass structure.

Compound	Chemical formula	Percentage
Silica Oxide	SiO ₂	69-74 %
Calcium Oxide	CaO	5-12 %
Soda Oxide	Na ₂ O	12-16 %
Magnesium Oxide	MgO	0-6 %
Alluminium Oxide	Al ₂ O ₃	0-3 %

Characteristics	Symbol	Amount and unit
Density at 18 °C	r	2500 kg/m ³
Superficial sclerometric hardness		6-7 (Mohs scale)
Young's modulus at 20 °C	E	7 x 10 ¹⁰ Pa
Poisson's coefficient at 20 °C	μ	0,2
Heat capacity at 20 °C	c	0,72 x 10 ³ J/(kg K)
Coefficient of linear thermal expansion	a	9 x 10 ⁻⁶ K ⁻¹
Thermal Conductivity at 20 °C	λ	1 W/(m K)
Transition temperature	T _g	573 °C
Surface tension at ~1300 °C		315 mJ/m ²
Refractive index in the visible at 20 °C	n	1,5

1.3 Colour

Colour in glass is very important - especially in architecture and in other aesthetic applications – since it often leads to some different energy performance¹. Colours are usually obtained by the addition of coloring ions that are homogeneously distributed by precipitation of finely dispersed particles.

Ordinary soda-lime glass appears colorless to the naked eye when it is thin, although iron(II) oxide (FeO) impurities of up to 0.1 wt % produce a green tint which can be viewed in thick pieces or by means of scientific instruments. Further FeO and Cr₂O₃ additions may be used for the production of green bottles. Sulfur, together with carbon and iron salts, is used to form iron polysulfides and produce amber glass ranging from yellowish to almost black. Manganese dioxide can be added in small amounts to remove the green tint given by iron (II) oxide.

1.4 Glass as a super-cooled liquid

Glass is generally classified as an amorphous solid rather than a liquid since it displays all the mechanical properties of a solid body. Some scientists consider this

¹ For energy performance changes due to different colours in glass, refer to chapter 7 of this section – “Energy modelling performance”.

material as a liquid due to its lack of a first-order phase transition where certain thermodynamic variables such as volume, entropy and enthalpy are continuous through the glass transition temperature. However, the glass transition temperature may be described as analogous to a second-order phase transition where the intensive thermodynamic variables - such as the thermal expansivity and heat capacity - are discontinuous. Despite this, thermodynamic phase transition theory does not entirely hold for glass, and hence the glass transition cannot be classified as a genuine thermodynamic phase transition. Although the atomic structure of glass has almost the same characteristics of the structure of a super-cooled liquid, glass tends to behave as a solid below its glass transition temperature². The change in heat capacity at a glass transition and a melting transition of comparable materials are typically of the same order of magnitude indicating that the change in active degrees of freedom is comparable as well. Both in a glass and in a crystal it is mostly only the vibrational degrees of freedom that remain active, whereas rotational and translational motion becomes impossible explaining why glasses and crystalline materials are hard.

1.5 A brief history of glass production

The first form of glass usage recorded in history was the obsidian which is a naturally occurring glass. During the Stone Age, obsidian was used by many populations for the production of sharp cutting tools. Generally, archaeological evidence suggests that the first real glass, as we know it, was made in the coast areas of north Syria, Mesopotamia and Old Kingdom of Egypt. The earliest known glass objects, of the mid III millennium B.C., were beads, perhaps initially created as accidental by-products of metal-working slags or during the production of faience, a pre-glass vitreous material made by a process similar to glazing.

During the late Bronze Age in Egypt and Western Asia there was an explosion in glass-making technology: archaeological finds from that period include coloured glass ingots, vessels (often coloured and shaped in imitation of highly prized wares of precious stones) and the ubiquitous beads. The alkali source for Syrian and Egyptian glass was soda ash, sodium carbonate which can be extracted from the ashes of many plants, notably halophile seashore plants.

By the 15th century B.C. extensive glass production was occurring in Western Asia and Egypt. It is thought that the techniques and recipes required for the initial fusing of glass from raw materials were a closely guarded technological secret reserved for the large palace industries of powerful states. Glass workers in other areas therefore relied on imports of pre-formed glass, often in the form of cast ingots such as those found on the Ulu Burun shipwreck off the coast of Turkey.

Glass remained a luxury material, and the disasters that overtook Late Bronze Age civilizations seem to have brought glass-making to a halt. It picked up again in its

2 A super-cooled liquid behaves as a liquid but it is below the freezing point of the material and it will crystallize almost instantly if a crystal is added as a core.

former sites, in Syria and Cyprus, in the IX century BC, when the techniques for making colourless glass were developed. In ca. 650 B.C. the first glass receipt is reported. Instructions on how to make glass are contained in cuneiform tablets discovered in the library of the Assyrian king Ashurbanipal and tells that *glass is made with 60 parts of sand, 180 parts of seashore plants ash and 5 parts of clay*.

During the Hellenistic period many new techniques of glass production were introduced and glass began to be used to make larger pieces. Techniques developed during this period include “slumping” viscous (but not fully molten) glass over a mould in order to form a dish and “millefiori”³ technique, where canes of multi-coloured glass were sliced and the slices arranged together and fused in a mould to create a mosaic-like effect.



Fig. 1.2
Mergering oven for glass. Engraving from: Georgius Agricola (1494–1555), *De re metallica*, volume XII, Basilea, 1557.

According to Pliny the Elder, Phoenician traders were the first to stumble upon glass manufacturing techniques at the site of the Belus River while Georgius Agricola reported in *De re metallica* the following tale: "The tradition is that a merchant ship laden with nitrum being moored at this place, the merchants were preparing their meal on the beach, and not having stones to prop up their pots, they used lumps of nitrum from the ship, which fused and mixed with the sands of the shore, and there flowed streams of a new translucent liquid, and thus was the origin of glass".

This account is more a reflection of Roman experience of glass production, however, as white silica sand from this area was used in the production of Roman glass due to its low impurity levels.

It was the Romans who began to use glass for architectural purposes, with the discovery of clear glass. Cast glass windows, albeit with poor optical qualities, thus began to appear in the most important buildings in Rome and the most luxurious villas of Herculaneum and Pompeii. The plate glass, put without framework or with wooden or bronze one, usually had the dimensions of 30 X 50 cm and were 3-6 cm thick. Their production was carried on with a particular techniques called “straining and ironing” as the glass paste was fused on a plate and covered with sand.

During the Middle Age, glass production was strictly related to Church and Monastery buildings.

The main techniques of production were: the cylinder-blowing and the sphere-blowing. The spheres were swung out to form cylinders and then cut while still hot, after which the sheets were flattened.

Glass objects from the 7th and 8th centuries have been found in Venice. These form an important link between Roman times and the later importance of that city in the production of the material.

3 “Millefiori” is an Italian word meaning thousands of flowers.

Until the XII century, stained glass - glass to which metallic or other impurities had been added for coloring - was not widely used.



Fig. 1.3
Left: Roman cup from Cologne dated IV century A.D. Right: Medieval glazing in the church of Notre Dame, Les Andelys, France.

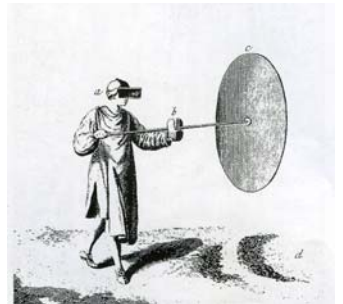
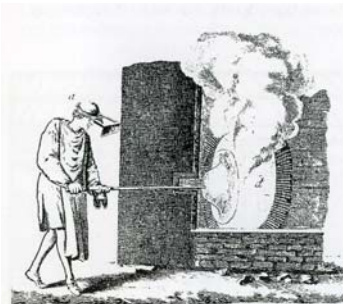
Between the XV and XVII centuries, the most famous production of artistic glass was reported in Venice, and, more particularly, in the isle of Murano. The glassmaking developed many new techniques and became the center of a lucrative glass export trade.

Venice glass was particularly clear and transparent due to a fine sand that was combined with soda ash obtained from the Levant, for which the Venetians held the sole monopoly.



Fig. 1.4
Left: A Millefiori pendant from Murano (Italy). Right: The modern technique of production in Murano.

Fig. 1.5 (bottom)
Plate glass production by means of the sphere-blowing technique. Engraving from Encyclopédie by Diderot and D'Alembert, 1773.



The clearest and finest glass is tinted using a small or large amount of a natural coloring agents that are ground and melted with the glass. More particularly, it was used to add sodium (to make the glass surface opaque), nitrate and arsenic (to eliminate bubbles) and colouring or opacifying substances.

In 1687, the French Bernard Perrot developed a new technique to produce glass: the fuse glass was strained on a hot smooth copper plate and then spread with a metallic roll until it became one plate. This glass plate was, then, worked with sand and water and, finally, polished with an iron oxide paste.

The real industrial revolution was due to the English Alastair Pilkington in 1959. He developed a technique called “float” to produced the float-glass which is nowadays one of the most used in buildings⁴.

1.6 The behavior of the antique glass

The observation that old windows are often thicker at the bottom than at the top is often offered as supporting evidence for the view that glass flows. It is then assumed that the glass was once uniform, but has flowed to its new shape, which is a property of liquid. In actuality, the likely reason for this is that when panes of glass were commonly made by glassblowers, the technique used was to spin molten glass to create a round, mostly flat and even plate that was then cut to fit a window. The pieces were not, however, entirely flat; the edges of the disk became thicker as the glass spun. When actually installed in a window frame, the glass would be placed thicker side down both for the sake of stability and to prevent water accumulating at the bottom of the window. Occasionally such glass has been found thinner side down or thicker on either side of the window's edge, as would be caused by carelessness at the time of installation.

Mass production of glass window panes in the early twentieth century caused a similar effect. In glass factories, molten glass was poured onto a large cooling table and allowed to spread. The resulting glass is thicker at the location of the pour, located at the center of the large sheet. These sheets were cut into smaller window panes with non-uniform thickness. Modern glass for windows is usually produced as float glass and has a very uniformity in thickness.

1.6.1 The cathedral glass theory

There is a theory, however, that explain the more thickness at the bottom edge and it is known as the “cathedral glass theory”. Some glasses have a transition temperature T_g close to - or below to - the room temperature. Such material’s behaviour depends upon the timescale during which the material is manipulated. If the material is hit it may break like a solid glass, but if the material is left on a table for a week – for example - it may flow like a liquid. This simply means that for the fast timescale its transition temperature is above room temperature, but for the slow one it is below. The shift in temperature with timescale is not very large however. To observe

⁴ The float-glass will be discussed in the paragraph 1.7. In this work all the glass panes used to carry on depositions were produced with this particular technique by the company Pilkington Glass UK.

window glass flowing as a liquid at room temperature, we would have to wait a very long time, maybe hundreds or thousands of years. Therefore it is safe to consider a glass as a solid material far enough below its transition temperature: Cathedral glass does not flow because its glass transition temperature is many hundreds of degrees above room temperature. Close to this temperature there are interesting time-dependent properties. One of these is known as aging. Many polymers that we use in daily life such as rubber, polystyrene and polypropylene are in a glassy state but they are not too far below their transition temperature so their mechanical properties may change over time.

1.7 Industrial manufacture: the float glass

A float glass is a sheet of soda-lime glass made by floating molten glass on a bed of molten tin. This method gives the sheet of glass uniform thickness and very flat and transparent surfaces. Nowadays, the float glass is the most produced for architectural glazing since this industrial manufacture leads to a highly standardized and optically transparent glass. The market is dominated by four main companies: Asahi Glass, NSG/Pilkington⁵, Saint-Gobain, and Guardian Industries. Other companies include PPG, Central Glass, Hankuk, Visteon, Cardinal Glass Industries.

In the float glass process, the raw materials are mixed in the correct quantities before passing into the furnace at 1500 °C. The molten glass is then fed onto a bath of liquid tin at a constant rate; the continuous band of glass then floats along the surface of the tin. The temperature is maintained constant at 1000 °C so that irregularities and defects melt as the glass proceeds along the tin. After a sufficient time, the glass is cooled to about 600 °C and on leaving the bath it is sufficiently hard to resist damage from the rollers that pass then the glass into the annealing line. The annealing removes some of the internal stresses within the glass so that it can be cut and shaped without incurring damage. The use of a molten metal bath allows extremely regular and flat glass, typically with less than 1 nm variation across the surface. By varying the temperature and speed at which the glass pass along the bath, a range of thicknesses can be achieved: in Europe, its characteristics are regulated by the UNI EN 572: 1996 part 2 and it is possible to find in the market the sheet's thickness showed in the table below:

Tab. 1.3 Thicknesses and tolerances of the float glass.	
Thickness [mm]	Tolerance [mm]
2 ÷ 6	± 0,2
8, 10, 12	± 0,3
15	± 0,5
19, 25	± 1,0

⁵ A brief Pilkington Glass history will be discussed in the next section since the glass substrate used in this work to deposit thin films was supplied by this company.

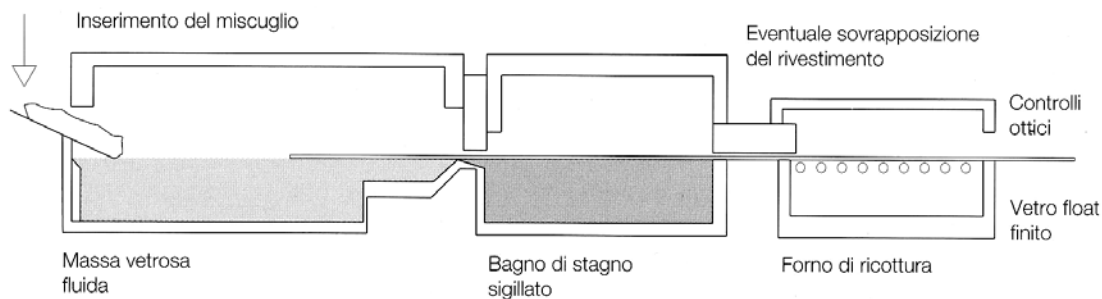


Fig. 1.6
Typical scheme of a
float glass production
line.

To prevent oxidation of the tin, the float bath is contained in a protective inert nitrogen atmosphere that is maintained constant since the molten glass itself often contains oxygen and sulphur compounds that may be evolved at the glass surface. Consequently, there is often about 10 % hydrogen added to the nitrogen atmosphere, which helps to cleanse the atmosphere of the more damaging impurities through reduction.

The process is fully automated with production lines about 500 m long that can operate continuously for 10-15 years producing about 6000 km of glass per year.

The resistance to sudden change of temperature is between 30 °C to 40 °C and adding some precursors makes it possible to improve the glass properties such as the optical ones: transmittance and reflectance, for instance.

Tab. 1.4 Minimum transmittance values for a transparent float glass to be appointed as a clear glass

Thickness [mm]	Minimum Transmittance [%]
2	0,89
3	0,88
4	0,87
5	0,86
6	0,85
8	0,83
10	0,81
12	0,79
15	0,76
19	0,72
25	0,67

1.8 Optical properties

Glass optical properties mostly depend on the colour and the coating deposited on it as well as the solar radiation used as base-line for the tests. In Europe, the normative followed to calculate a glass optical properties is the EN 410. The terrestrial radiation is used as reference radiation with air mass equal to 1, water vapour equal to

1,42 cm and quantity of ozone equal to 0,34 ppm. These parameters were defined by the Commission Internationale de l'Éclairage (CIE), within the CIE n. 26.

The electromagnetic distribution that is usually looked at for the tests are:

1. Ultraviolet (UV), between 280 and 380 nm;
2. Visible, between 380 and 780 nm;
3. Near InfraRed (NIR), between 780 and 2500 nm.

In the case of the float glass the radiations lower than 300 nm and higher than 2500 nm are not analyzed as they are completely absorbed by this kind of glass.

The most relevant optical properties are:

- Reflectance, is defined as the light flow that is directly reflected by the glass. It mostly depends on the rays incident angle and on the surface. In the tests, the rays perpendicular to the surface only are considered.
- Transmittance, is defined as the percentage of the light flow that is directly transmitted through the glass. This property depends on the incident angle as well.
- Energy absorption, is the amount of the Energy flux absorbed by the glass.
- Solar factor, indicates the amount of the solar Energy passing through the glass.
- Transmission factor, indicates the amount of radiation between 380 and 780 nm wavelength (visible light) that passes through the glass.
- Thermal transmittance (U value). The thermal conductivity of the glass is quite low due to its amorphous structure that lower the photons free average path⁶. When the temperature is high the thermal conductivity has an important role increasing a lot from the standard value at the environmental temperature.
- The emissivity of a material, usually indicated with the symbol ϵ , is the fraction of energy radiated by that material in comparison to the energy radiated by a black body at the same temperature of the material. In other words, it indicates the ability of radiating energy. A black body would have $\epsilon=1$ while every other object has $0 < \epsilon < 1$. The emissivity depends on some factors such as: the temperature, the emissivity angle, the wavelength, the surface of the object analyzed, even though it depends on the different points of the surface itself. For engineering applications, emissivity is considered equal through all a surface, this assumption is known as the grey body hypothesis.

1.9 Glass for architectural glazing

One of the most important characteristics of the glass used in building construction is that it lets the solar radiation in while keeping outside external climatic factors such as wind, rain and cold air. The solar rays can be used to heat the internal environment of a building due to the enhanced glass selectivity. The short waves such as visible light, can cross the glass plate while the long waves, the infra-red (IR), coming from the irradiated surfaces, are reflected and trapped inside the building. This particular behaviour makes glass a very interesting material in controlling the energy

⁶ Free average path is the average distance covered by a particle between two consecutive crashes.

passing through/in a building and it can be considered one of the most powerful materials in the energy saving problem.

1.10 Physical principles: the electromagnetic spectrum

The electromagnetic spectrum consists of radiations or, in other words, of electromagnetic waves that are characterized by means of wavelength and frequency. Wavelength and frequency are inversely proportional; the energy associated to the wave increases as the frequency. By means of our eyes we can see only a range of wavelength from 380 nm to 760 nm, that is usually called visible light. The shorter wavelength are UV ray, x-ray and γ -ray whose frequencies are bigger than visible light's one thus they are more energetic. Infrared-waves, radio-waves and micro-waves are characterized by a bigger wavelength than the visible light thus they are less energetic.

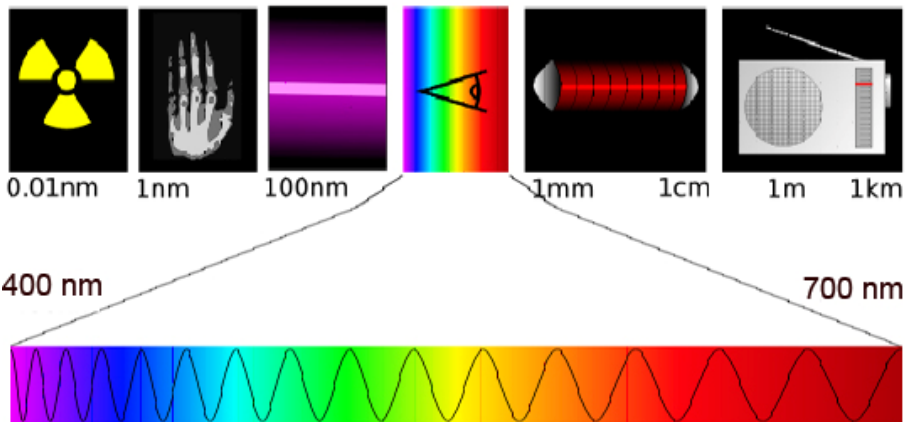


Fig. 1.7
Graphical scheme of the Electromagnetic Spectrum with the indication of the visible light.

The ultraviolet radiation ranges from 0.35 μm to 0.4 μm . X-rays are associated with radiation up to 0.006 μm and the γ range is beneath them.

On the other side, where wavelength is bigger, that is to say over the red, there is the infrared range from 0,7 μm to 0,4 mm.

This range of the spectrum is generally divided into four sections:

1. near infrared (NIR), between 0.78 μm and 2 μm ;
2. infrared, between 2 and 6 μm (short wave);
3. far infrared (FIR), between 6 and 15 μm ;
4. extremely far infrared, between 15 and 1000 μm , is mainly used in astrological studies.

Then it follows the microwave range, between 0,4 mm. and 100 cm, followed by the radio waves: the short one between 1 m and 100 m, the medium one between 200 m and 600 m, and the far over 600 m.

Tab. 1.5 Electromagnetic radiation with their characteristic parametre		
Electromagnetic radiation	Frequency	Wavelength
Radio wave	< 3 GHz	> 10 cm
Micro wave	3 GHz – 300 GHz	10 cm – 1 mm
Infrared	300 GHz – 428 THz	1 mm – 700 nm
Visible light	428 THz – 749 THz	700 nm – 400 nm
Ultraviolet	749 THz – 30 PHz	400 nm – 10 nm
X ray	30 PHz – 300 EHz	10 nm – 1 pm
g ray	> 300 EHz	< 1 pm

It is quite interesting to notice that only a few radiations are visible to human eyes, but the word “light” is used only for the visible range of the spectrum and its closer parts. The visible light of the spectrum is emitted by incandescent bodies. γ -rays result from the radioactive decay while the radio-waves may be produced by power drains that produce electromagnetic waves.

In the EN 410:2000, the solar radiation - in the building sector - is usually divided into three parts:

- Near UV → 0 – 380 nm;
- Visible light → 380 – 780 nm;
- Near IR → 780 – 2800 nm,

and the biggest percentages are: the visible light (47 %) and the IR (46 %). The sum of the incident radiation and the atmospheric absorption is about 1353 W/m^2 . One of the chemical compounds that mostly absorbs the solar radiation is the iron oxide (Fe_2O_3). It can be easily recognized from the green colour on the glass edges.

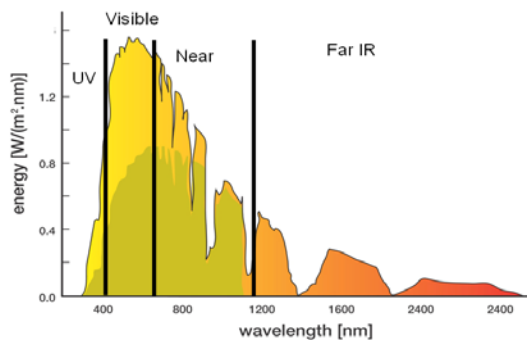


Fig. 1.8
Graphical scheme of
the Solar Radiation
Spectrum
(EN 410:2000).

1.11 Glass energetic and physical properties

1.11.1 Transparency

The word “transparency” means the possibility to see an object put behind the glass, crossing of the visible light, clearness and comprehensibility. The way light crosses a glass depends on some factors such as the radiation nature, the wavelength or the spectrum of the light source. In other words, a transparent object lets us see in a clear way what is behind it while, on the contrary, a translucent object lets radiation passing through it but the quality of the image received is not very clear and well-defined. The transmittance only defines the permeability to the radiation regardless of the quality of the image transmitted.

1.11.2 Otherness

The otherness defines how clear the edge of an image are as an object is looked through a plate glass. It also indicates the overall uniformity of the image and the presence of distortions.

1.11.3 Transmittance of visible light

The transmittance of the visible light is a very important factor that characterized a glass and the energy lighting consumption in a building as well as the dimensions of the windows. The glazing placement and the thermal reflection on the internal surfaces determinate the internal distribution of heat.

1.11.4 The energy balance

According to the laws of thermodynamics, we know that energy cannot be lost but only transformed from one kind to another. Considering this law, it is possible to find out a mathematical balance for each kind of radiation for every glazing of a building.

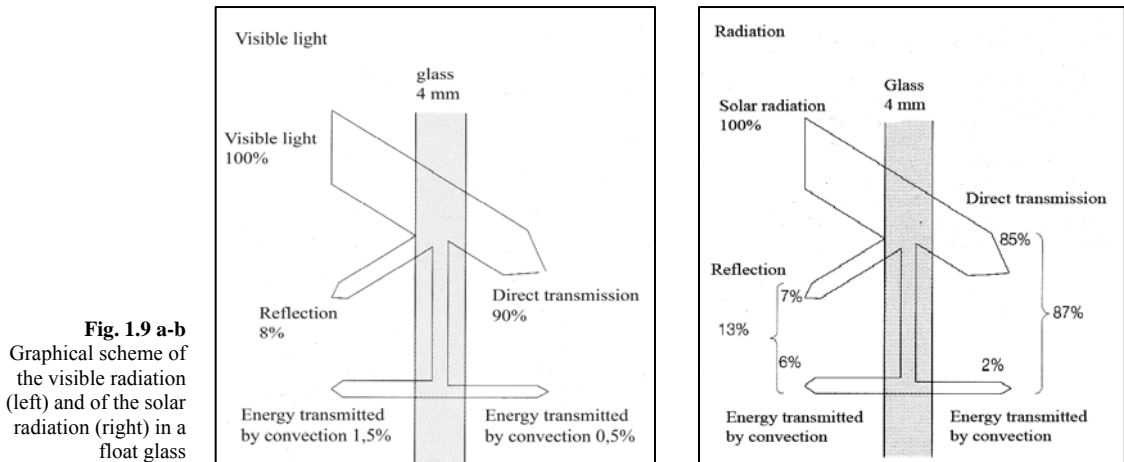


Fig. 1.9 a-b
Graphical scheme of the visible radiation (left) and of the solar radiation (right) in a float glass

The whole energy arriving to a glazing can be transmitted, reflected or absorbed by the glass itself or transformed in thermal energy that is spread again to the environment. In the images above (fig. 1.9 a-b) the energy balance between two glazing surfaces – external and internal – made of float glass 4 mm thick is shown. It can be noticed that the transmittance through the plates in the two cases is very different due to the different absorption and reflectance in the visible and solar spectra.

1.11.5 The green house effect

The green house effect is a particular phenomenon generated by the different way wavelengths are transmitted through a float-glass. A part of the solar gain passing through the glass pane of a window is absorbed by the glass itself, the transmitted

part is usually absorbed and reflected by the other internal surfaces. What influences a lot this phenomenon is the geometry and the placement of the object in the room we are analysing. Every body reached by solar radiation absorbs a part of it that is later transformed into thermal energy (blackbody radiation). This energy is spread in the environment and, as it reaches the glass, it is partially absorbed or transmitted and partially reflected again into the inside space. This makes the internal temperature becomes higher and higher. That is why we have to take care of this phenomenon that may create a lot of discomfort in a building if poorly planned.

1.11.6 Enhanced glazing

Usually to make glazing work in a particular way some particular coatings are deposited on their surface. These enhanced coatings are usually between 10 nm and 1 μm thick and are produced by a variety of technologies. The materials used to produce these coatings have particular properties that make the glass properties, such as the optical ones – transmittance or reflectance - or even the emissivity, change. Another important aspect is the film position on the glazing's surfaces to avoid a behaviour opposite to what we want to obtain. Usually, the materials used to produce these kind of films are copper (Cu), silver (Ag) or gold (Au), some semi-conductors, such as metal oxides, as the vanadium oxide (VO_2) used in this work to produce the thermochromic coatings. Some examples of enhanced glazing are the low emissivity glass (low-e), thermochromic glass or self-cleaning glass.

1.12 Producing energy by means of the glass

In architecture, the material “glass” is very important as it could define the external shape of a building. Not only it makes the light enter the internal environments but it also helps in heating the internal rooms letting the thermal radiation (IR) passing through it. Unfortunately, some factors - such as a wrong building plan - could lead to a massive and inappropriate usage of this material that might causes a high increase of the internal temperature. In those cases there must be found some new methods to move away or reuse this high thermal energy trapped in the building.

In the following paragraphs, we are going to look at the weather data to understand how they could be used to produce energy.

1.12.1 Weather data

The local weather conditions are very important to understand how and if energy can be produced at a particular latitude. They also contribute in the total energy balance of a building and will be considered in this work. Solar radiation, average temperature as well as its peaks, wind velocity, clouds and humidity are just some factors that must be looked at as well as the materials used to build a building with particular care to the glass nature.

In the central and south Europe four main different climatic conditions can be distinguished:

1. North European maritime climate: characterized by freezing winters with low solar radiation and warm summers;
2. Central European maritime climate: characterized by cold winters with low solar radiation and hot summers;
3. Continental climate: characterized by quite warm winters with high solar radiation and hot summers;
4. South European and Mediterranean climate: characterized by warm winters with high solar radiation and boiling summers.

Within these four macro-climates there are a lot of micro-climates - called regional climatic zones - that characterized every territory and are usually affected by some factors such as the topographic configuration, the local vegetation, the human interventions, etc.. To do a correct energetic evaluation some factors must be overtaken. Some of them are the followings:

- direct or indirect solar gain that depends on the seasons and on the geographical zoning;
- environmental temperature;
- velocity of the wind that makes surfaces cooling down.
- humidity.

1.12.2 Solar gain

The extra-terrestrial solar spectrum is filtered by the terrestrial atmosphere that prevents a big amount of ultra violet rays (UV) reach the ground of the earth. A typical solar spectrum is shown in figure 1.8 (pg. 183). Usually, in a beautiful day, no more than 1100 W/m^2 reach the ground; the other part of the solar radiation is reflected toward the space or transformed in thermal energy by the atmosphere compounds (ozone, water vapour and carbon dioxide – CO_2), and another part of it is spread towards the ground as visible light.

The percentage of solar radiation that is directly transmitted is called direct radiation. The sum of terrestrial radiation, direct radiation and diffused radiation is called global radiation. In Europe, the annual radiation sum over a horizontal surface varies from 980 KW h/m^2 for the city of Hamburg (Germany) to 1780 KW h/m^2 for the city of Almeria (Spain).

The glass transmittance usually depends on some factors such as the incident angle, the inclination and the direction of the surface in comparison to the radiation source, in our case the sun. As a consequence, the quantity and quality of energy passing through the glass vary a lot during one year. Nevertheless, the direct effect on the glass surfaces depends mostly on the daily trend during one year.

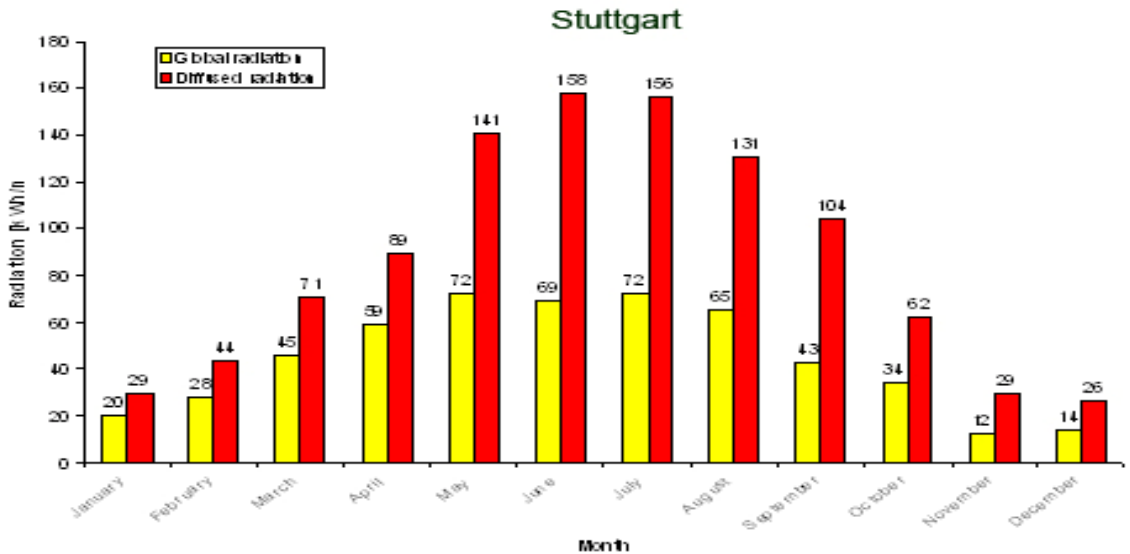


Fig. 1.10
Graphical scheme of
Global and Diffused
radiation over Stutt-
gart (Germany).

1.12.3 The microclimate

The yearly trend of the external air temperature depends on the yearly global radiation. The absence of clouds in the sky that hides a part of the radiation is particularly important to look at when we want to produce energy as we lose a big amount of the long radiation. During the winter, with the sun in a low position, the fluctuations of daily temperature are quite low; during the summer they are much bigger with a big improvement in the eventual energy production.

Even the buildings themselves are very important in influencing a microclimate. For instance, in a urban environment during the winter the lowest temperatures are about 4 K higher than the areas in the countryside; during the summer this difference can reach peaks of 10 K.

1.13 Enhanced coating for architectural glazing

The purpose of thin coating on glass surface is the modification of the spectrophotometric properties of the glass substrate. The properties of a coating cannot be considered separately from those of the glass substrate to which it is attached.

The UNI EN 1096 part 1:2000 defines the characteristics, properties and classifications of coated glass for use in building.

- Class A: the coated surface of the glass can be positioned on the outer or the inner face of the building;
- Class B: the coated glass can be used as monolithic glazing but the coated surface shall be on the inner face of the building;

- Class C: the coated glass shall be used only in sealed multiple glazing units and the coated surface should be facing into the unit cavity;
- Class D: the coated glass shall be incorporated into sealed units, with the coated surface facing into the unit cavity, as soon as they are coated;
- Class S: the coated surface of the glass can be positioned on the outer or the inner face of the building.

The coatings can be produced by means of different techniques that can be divided into two processes: chemical⁷ and physical⁸ film formation processes.

Within the chemical processes are the following:

- Wet chemical deposition: a mixture of a dissolved metal salt and a reducing compound is sprayed on to the glass surface. A reduction reaction takes place and fine grained metal is precipitated;
- Sol-Gel coating: solutions of metallo-organic-compounds are dip coated and pyrolytically transformed into suitable oxides;
- Chemical vapour deposition⁹: compounds in a vapour phase reacting chemically on the hot surface of the glass substrate;
- Spray coating: sprayed liquids reacting pyrolytically on the hot surface of the glass substrate;
- Powder coating: powders reacting chemically on the hot surface of the glass substrate.

Within the physical processes are the following:

- Evaporation: the material forming the coating is evaporated by heating and deposited on the glass surface;
- Sputtering: in a gas discharge, ions bombard a target causing sputtering of material which condenses on the glass surface.

1.14 Pilkington Glasses (NSG Group) – A brief history of the company

Pilkington Glasses is the largest glass manufacturer in the United Kingdom. It is based in St Helens. It was formerly an independent company listed on the London Stock Exchange but in 2006 it was taken over by the Japanese NSG.

The company was founded in 1826 as a partnership by members of the Pilkington and Greenall families. The venture used the trading name of “St Helens Crown Glass Company”. On the departure from the partnership of the last Greenall in 1845, the firm became known as “Pilkington Brothers” and in July 1894 the business was incorporated under the Companies Act 1862 as Pilkington Brothers Limited.

⁷ Chemical film formation process: processes where chemical reactions produce films on the glass from liquid, vapour or powder.

⁸ Physical film formation process: processes, under vacuum conditions, whereby material from a source are transferred as elements, compounds or ions. Their subsequent condensation on the glass surface produces the film. Chemical reactions can be associated with this process.

⁹ Chemical vapour deposition (CVD) is the technique used in this work to produce thin films.

Pilkington was floated as a public company on the London Stock Exchange in 1970 and it was for many years the biggest employer in the northwest industrial town. Between 1953 and 1957, Sir Alastair Pilkington and Kenneth Bickerstaff invented the float glass process which was discussed in the previous section.

Pilkington, with its subsidiary Triplex which it acquired in 1965, also became a major world supplier of toughened and laminated safety glass to the automotive and building industries.

During the 1960s and 1970s, the company used the flow of float royalties to invest in float glass plants in several countries including Argentina, Australia, Canada and Sweden; also to acquire major existing flat and safety glass producers and plants in USA, Germany and elsewhere.



Fig. 1.11
Pilkington headquarter (left) and logo (right).

In late 2005 the company received a takeover bid from the smaller Japanese company NSG. The initial bid and the first revised bid were not accepted, but on 16 February 2006 NSG increased its offer for the 80% it did not already own to 165 pence per share (£1.8 billion or \$3.14 billion in total) and this was accepted by Pilkington's major institutional shareholders, enabling NSG to compulsorily acquire the smaller holdings of other shareholders, many of them being existing and retired employees, who had not wished to support the takeover.

The combined company will compete for global leadership in the glass industry with the leading Japanese glassmaker Asahi Glass, which had around a quarter of the global market at the time of the deal. Pilkington had 19% and NSG around half that.

2. THERMOCHROMIC COATINGS

2.1 Introduction

The use of air-conditioning equipment, in order to maintain comfortable conditions inside buildings during the summer/winter months, is ever increasing in the whole world and consumes vast amounts of electricity. Nowadays, there is a concurrent increase in carbon dioxide emissions and of various other atmospheric pollutants created during the power generation. Signing specific papers and protocol, as the Kyoto Protocol, Governments are trying to limit carbon dioxide emissions into the atmosphere and the waste of energy in buildings.

The energy saving control is one of the most important aim of the international scientific research and a lot of groups of research of different universities, as the Prof. Ivan P. Parkin's one from the Department of Chemistry of the University College London (UCL), are studying solar control coatings that is a technology applicable to all the types of glazing – commercial or residential – to play an active role in improving the energy efficiency of the buildings.

Current coatings consist of an all out approach that is applicable to constant climates. If an environment is consistently hot, tinted glass or thin metallic coatings can be used to reflect solar heat and prevent it from entering the building, limiting the need for internal cooling. In a consistently cold environment, heat may be retained in a building by the use of a wavelength selective coating. These glasses are often transparent in the visible part of the spectrum but highly reflective in the infra red. This allows sunlight rays to enter into the building but prevents blackbody radiation and internally generated heat from escaping, consequently reducing heating requirements. However, coatings of either type typically produce only a marginal energy benefit in changeable climates such as northern and central Europe, the USA, Canada and Japan which usually have cold winters and hot summers.

2.2 Advanced glazing

Advanced glazing are very important in the new building construction market because they could help lower the total energy a building requires for its operation thus lowering the running cost and the CO₂ emitted in the atmosphere.

Switchable glazing can alter their optical properties like transmission, reflectance and absorption over the electromagnetic spectrum. The way it is done is by the use of special coatings, deposited on them, which is the phase changing material. This coating contains molecules that under an external influence can rotate or become aligned (or not), thus helping or obstructing the passage of radiation through them.

There are three different advanced glazing types sorted mainly by the way they are triggered to change their properties:

- Electrochromic glass: can change between two states under the effect of an electric field. Some types need power only during changing while others require a constant field to remain in one state.

- Photochromic glass: can change and become darker under direct sun radiation. It has found application in sunglasses that are lighter inside an enclosed space but become darker when the person goes out in the sunlight.
- Thermochromic glass: can change their physical properties or change colour, like becoming darker, above a certain surface temperature.

2.3 Thermochromism

Thermochromic glazing is a type of intelligent glazing whose optical properties of the coating change according to some external stimulus, like temperature, and are usually related to a structural phase change. More particularly, a thermochromic window is a device that changes its transmission and reflectance properties at a critical temperature (T_c). At this specific temperature the material undergoes a semiconductor to metal transition. At temperatures lower than T_c the window lets all of the solar energy that hits it through. At temperatures above T_c the window reflects the infra-red (IR) portion of solar energy.

In such a way thermochromic windows may help reduce air conditioning and heating costs leading to more energy efficient buildings.

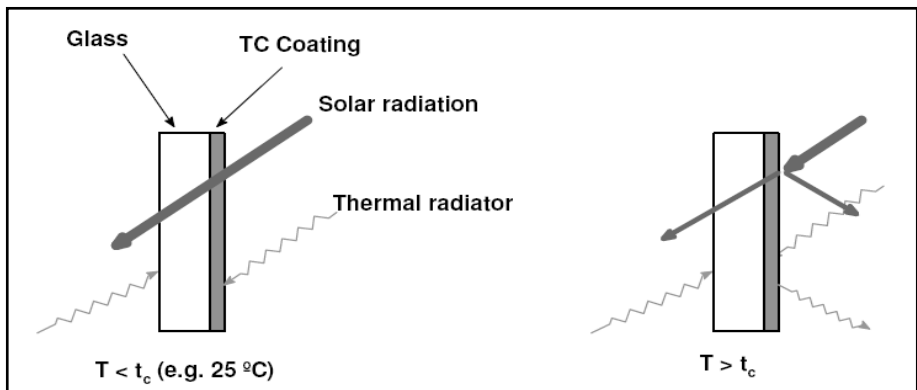


Fig. 2.1
Schematic demonstration of the application of thermochromic coating to advanced window glazing.
(source: Parkin 2008)

There is a lot of research being conducted around the world on thermochromic materials and especially glazing. Although some of them are very advanced, they are still in an experimental stage and are not available on the market.

2.3.1 Hysteresis

The transition from one phase to the other does not take place in a fraction of a degree but it requires a small margin. This margin is a few degrees (e.g. $\pm 4^\circ\text{C}$) wide and depends on the composition of the film and of its thickness. In this space the switching takes place gradually. To complicate matters even more, this switching follows a different route depending if the pane is heated up or cooled down. This phenomenon is called hysteresis.

It is more easily comprehensible in the following Figure 2.2.

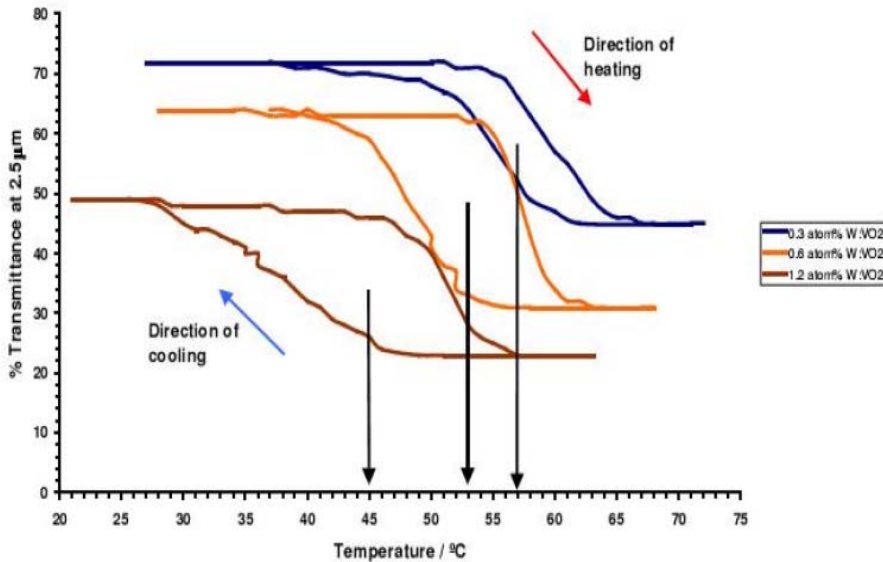


Fig. 2.2 Hysteresis curves for different thermochromic samples. (source: Manning T., PhD Thesis. University of London, 2004).

As we can see from the image above, the transmittance follows a different path during heating and cooling for every samples and this margin can be relatively narrow or wide. The width is attributable to several factors such as a variety of grain size, and/or crystallographic orientation. Ideally this hysteresis would be as small as possible to maximize the energy saving effect.

2.4 Previous works

This section describes the previous works conducted by Prof. Ivan P. Parkin, Dr. Russell Binions, Dr. Troy D. Manning and Dr. Clara Piccirillo who had worked on solar control coatings.

2.4.1 Vanadium (IV) Dioxide - VO₂

Vanadium (IV) Dioxide, researched by Prof. Parkin's group, displays thermochromic properties which show great promise for use in architectural glazing coatings.

The metal-to-semiconductor transition temperature (T_c) for a pure single crystal of VO₂ is 68 °C. That is one of its greater limit in building applications.

At temperatures below T_c the material is transparent in both the infra-red and visible part of the spectrum, thus allowing solar radiation to pass through the window, maximizing the heating effect of sunlight and black body radiation within the building. At temperature above T_c the coating is transparent in the visible but becomes reflective in the infra-red part of the spectrum. This prevent the thermal part of solar radiation from heating the building interiors.

The metal-to-semiconductor phase transition corresponds to a structural phase transformation from monoclinic to tetragonal (or rutile).

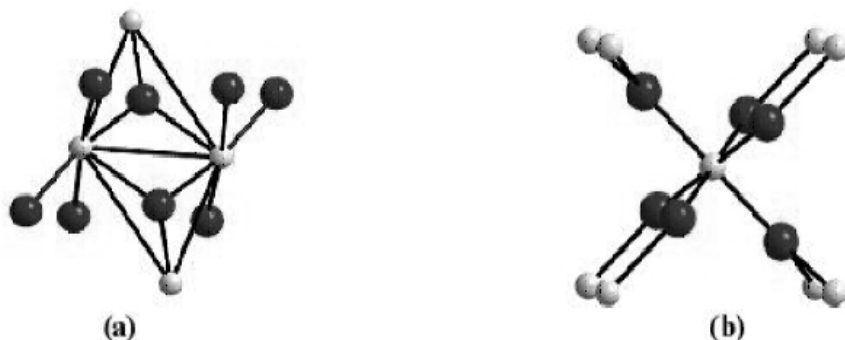


Fig. 2.3
Monoclinic (a) and tetragonal (b) phases of VO_2 .
(Source: Vernardou D., PhD Thesis, 2005).

This structural transition results in significant changes in optical properties and electrical conductivity. The rutile material is metallic and reflects a wide range of solar radiation, whereas the monoclinic phase is a semiconductor and generally optically transparent. The low temperature, monoclinic phase has unit cell parameters $a = 5,75 \text{ \AA}$, $b = 4,52 \text{ \AA}$, $c = 5,38 \text{ \AA}$ and $\beta = 122,60^\circ$. The structure involves $\text{V}^{4+} - \text{V}^{4+}$ pairing with alternate shorter (0,265 nm) and longer (0,312 nm) $\text{V}^{4+} - \text{V}^{4+}$ distances along the monoclinic a axis. The high temperature phase has a tetragonal rutile type structure, cell parameters $a = 4,55 \text{ \AA}$ and $c = 2,85 \text{ \AA}$, with equidistant vanadium atoms (0,288 nm) in chains of edge sharing $[\text{VO}_6]$ octaehdra.¹ On passing through the metal-to-semiconductor phase transition, the planes of Vanadium atoms in the monoclinic phase shift by 0,043 nm parallel to. This shift is sufficient to break the $\text{V}^{4+} - \text{V}^{4+}$ pairs to form a tetragonal phase allowing metallic conductivity.

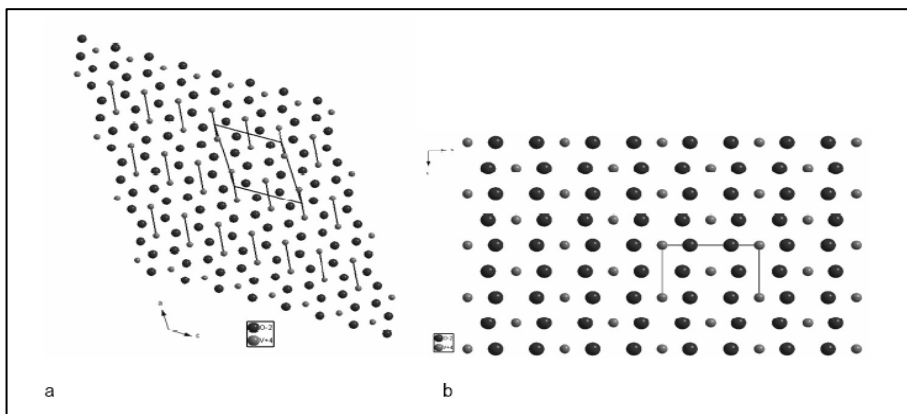


Fig. 2.4
Representations of the structures of (a) monoclinic VO_2 , with $\text{V} - \text{V}$ pairs indicated, and (b) tetragonal VO_2 , viewed along the b -axis of the unit cell. Oxygen atoms are the larger dots.

¹ Ivan P. Parkin, Russell Binions, Clara Piccirillo, Christopher S. Blackman and Troy Manning, *Thermochromic coatings for intelligent architectural glazing*.

On passing through the T_c , electrical conductivity and infra-red reflectivity increase dramatically but there is virtually no change in the visible region.

Vanadium precursor	$\text{VO}(\text{acac})_2$
Precursor concentration	$0,075 \text{ mol L}^{-1}$
Solvent	Ethanol
N_2 flow rate	$1,5 \text{ L min}^{-1}$
Deposition temperature	$500 - 550 \text{ }^\circ\text{C}$
Deposition time	1 min
Substrate	SiO_2 coated glass

2.4.2. Doping of Vanadium (IV) Dioxide

The introduction of dopants at low levels may influence the temperature (T_c) at which the metal-to-semiconductor transition occurs. It has been observed that high valence metal ions, such as tungsten (VI) or niobium (V), when doped into VO_2 decrease the metal-to-semiconductor temperature of vanadium (IV) dioxide. While low valence ions, such as aluminium (III) or chromium (III), were shown to increase the T_c . It has also been observed that dopant ions with an ionic radius smaller than V^{4+} , or that created V^{5+} defects (which were smaller than V^{4+}) increase the T_c temperature, while dopant ions with larger ionic radius than V^{4+} caused a decrease in the transition temperature². The direction and the magnitude of the change in the T_c are related to a number of factors such as dopant ion charge and size.

2.4.3. Tungsten-doped Vanadium (IV) Dioxide

Of the dopants investigated so far in single crystals thin film, tungsten (W) has been found to reduce the transition temperature of vanadium (IV) dioxide. VO_2 films containing about 2 atom % W have been shown to have a thermochromic transition temperature of about $25 \text{ }^\circ\text{C}$, suggested as the ideal transition temperature for intelligent window coatings.

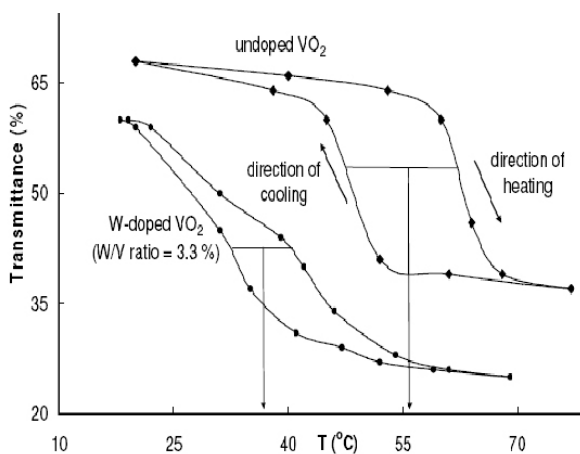


Fig. 2.5
Hysteresis behaviour of thin film of doped and un-doped vanadium (IV) dioxide prepared by aerosol-assisted chemical vapour deposition (AA-CVD). (source: Parkin 2008)

2.4.4 Gold-doped Vanadium (IV) Dioxide

Gold-doped VO_2 coatings have been produced by Aerosol Assisted Atmospheric Pressure CVD (AA/AP CVD) which will be discussed at length in section 3.

An other problem with a Vanadium Dioxide coating is the brown/yellow colour of the film that makes it unpleasant to the construction market, but using gold nanoparticles of the right size, the colour centre can effectively be turned to light yellow/green/blue. Gold nanoparticles have a surface plasmon resonance that is strongly absorbing, the frequency of which is strongly dependent on the dielectric properties of the host matrix and the size of the nanoparticles.

In this work, a hybrid technology, AA/AP CVD, has been used to deposit thin films of gold nanoparticle-doped vanadium (IV) dioxide from the CVD reaction of Vanadyl Acetylacetonate $\text{VO}(\text{acac})_2$ and Auric Acid (HAuCl_4) in methanol varying the different flow rates, as discussed in chapter 3 (CVD) and chapter 5 (Results and discussion).

2.5 Gold nanoparticles and Surface Plasmon Resonance (SPR)

In common with many other materials, some properties of gold, i.e. optical constants, melting point and chemical reactivity, change and become size dependent when the material is very finely divided.

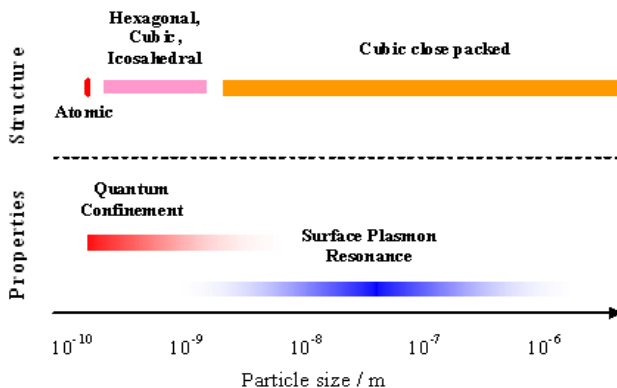


Fig. 2.6
Summary of structure and size dependent properties of gold at small particle sizes.
(source: Palgrave, PhD thesis, 2007)

Figure 2.6. shows some of the main properties of gold at different length scales, and the structures that the material adopts at those scales. A gold atom is approximately 2.7×10^{-10} m in diameter. Particles from this size, up to around 10^{-9} metres, show strong quantum confinement,

i.e. the quantisation of electronic energy levels, and can be usefully thought of as clusters of metal atoms. Clusters around 10^{-9} m in size have countable numbers of atoms, and certain 'magic numbers' of atoms lead to stable clusters. Above around 3×10^{-9} m, quantum confinement ceases, and the electronic structure of the material becomes much like the band structure of the bulk solid. At this point, the number of atoms in each particle becomes larger, and not easily countable. The crystal structure becomes cubic close packed, as found in the bulk solid, and each particle may be made up of more than one crystallite. This point is sometimes considered the boundary between gold clusters and gold colloids.

In the size interval 3×10^{-9} m to around 5×10^{-7} m, the optical properties of gold particles are dominated by surface plasmon resonance (SPR). Particle shapes can vary widely, and are determined by particle growth processes rather than gold atom packing. A very wide range of shapes can be produced. Above around 5×10^{-7} m in diameter, the SPR absorption is no longer significant, and particles behave as bulk gold.

The most prominent nanoscale property of gold in the size interval is surface plasmon resonance. A surface plasmon (SP) is a coherent and collective oscillation of free electrons at the boundary between a metal and an insulator. It is a multi-electron rather than a single-electron excitation involving all the free electrons at the metal surface. When no boundary conditions are imposed, and in the case of a perfect, defect-free metal, the oscillation frequency of the SP depends only on the dielectric properties of the two materials. When boundary conditions are imposed, the size and shape of the metal phase increasingly affect the SP frequency. Electromagnetic radiation can couple to the SP of a metal when the electric field of light oscillates at the resonant frequency of the SP. This phenomenon is known as surface plasmon resonance (SPR), and results in strong absorption of light at the resonant frequency.

Figure 2.7 shows the interaction of the electric field of light with a metal sphere. The oscillating electric field induces a resonant oscillation of the surface free electrons in the particle.

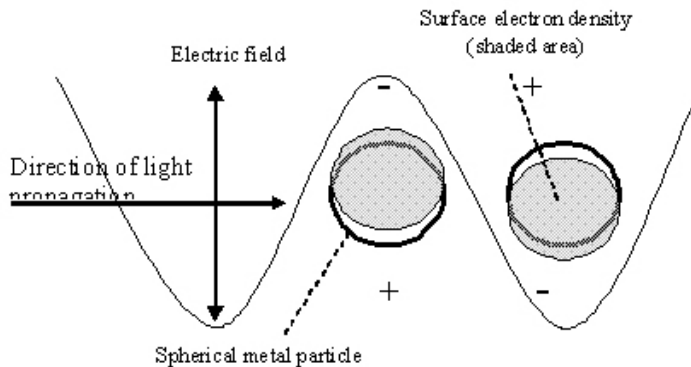


Fig. 2.7

Scheme to illustrate the excitation of a dipolar surface electron oscillation, or SPR, by the electric field of incoming light. The grey shading represents surface electron density. The frequency of the oscillation is equal to the frequency of the resonant light. The particle is much smaller than the wavelength of the incoming light, so is homogeneously polarised.

(source: Palgrave, PhD thesis, 2007)

The SPR shown in Figure 2.7 is dipolar as the oscillation is one-dimensional. Dipolar SP oscillations are induced when the particle size is much smaller than the wavelength of the exciting radiation, as in this case the particle experiences a near homogeneous polarisation.

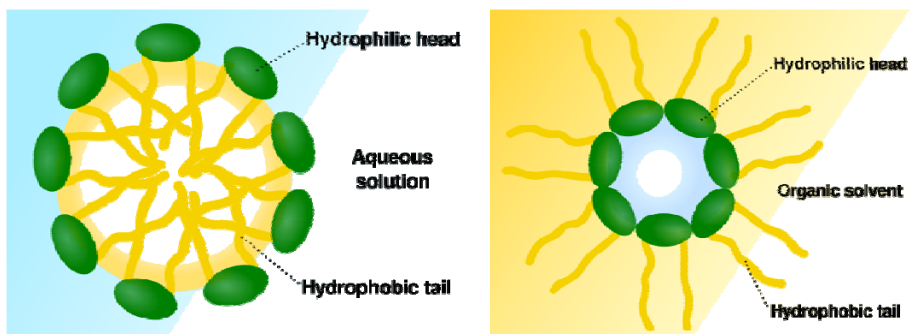
The frequency of SP oscillation corresponds to visible light for group 11 (coinage) metals and alkali metals in the sub-micron size regime. The optical properties of group 11 and alkali-metal nanoparticles above 10 nm in diameter are dominated by absorption caused by SPR, as other size-dependent effects, such as quantum confinement, are negligible in metal particles of this size. The extremely high reactivity of finely divided alkali metal particles has prevented detailed study of their optical properties; conversely, the chemical robustness of group 11 nanoparticles, especially gold particles, has allowed their extensive investigation.

2.6 Deposition using $\text{VO}(\text{acac})_2 + \text{HAuCl}_4 + \text{Surfactant}$

Gold-doped vanadium dioxide coatings showed various morphologies and optical properties; the particles showed a wide range of size and shape that can be controlled through the use of various stabilising agents.

The term *surfactant* is a blend of "**surface acting agent**". Surfactants are usually organic compounds that are amphiphilic, meaning they contain both hydrophobic groups (their "tails") and hydrophilic groups (their "heads"). Therefore, they are soluble in both organic solvents and water. Surfactants reduce the surface tension of water by adsorbing at the liquid-gas interface. They also reduce the interfacial tension between oil and water by adsorbing at the liquid-liquid interface. Many surfactants can also assemble in the bulk solution into aggregates. Examples of such aggregates are vesicles and micelles.

Fig. 2.8
Left: scheme of a micelle formed by phospholipids in an aqueous solution.
Right: scheme of an inverse micelle formed by phospholipids in an organic solvent.



The concentration at which surfactants begin to form micelles is known as the critical micelle concentration or CMC. When micelles form in water, their tails form a core that can encapsulate an oil droplet, and their (ionic/polar) heads form an outer shell that maintains favourable contact with water. When surfactants assemble in oil, the aggregate is referred to as a reverse micelle. In a reverse micelle, the heads are in the core and the tails maintain favourable contact with oil. Surfactants are also often classified into four primary groups; anionic, cationic, non-ionic, and zwitterionic (dual charge).

Thermodynamics of the surfactant systems are of great importance, theoretically and practically. This is because surfactant systems represent systems between ordered and disordered states of matter. Surfactant solutions may contain an ordered phase (micelles) and a disordered phase (free surfactant molecules and/or ions in the solution).

In this work depositions were carried out using TOAB (tetraoctylammonium bromide), a quaternary ammonium salt, that had been used as a surfactant for directing nanoparticle growth, as discussed in Chapter 5.

3. THEORY ON THIN FILMS AND CHEMICAL VAPOUR DEPOSITION (CVD)

3.1 Thin film

Thin films are thin material layers ranging from fractions of a nanometre to several micrometres in thickness. Deposition of thin film has been a subject of intensive study for almost a century and many methods have been developed and improved. The film deposition involves predominantly heterogeneous processes including heterogeneous chemical reactions, evaporation, adsorption and desorption on grown surface, heterogeneous nucleation and surface growth.

3.2 Thin film growth

Growth of thin film involves the processes of nucleation and growth on the substrate or growth surfaces. The nucleation process plays a very important role in determining the crystallinity and microstructure of the resultant films.

In the nanometre region, the initial nucleation process is even more important and it is a heterogeneous process. The size and the shape of initial nuclei are assumed to be solely dependent on the change of volume of Gibbs free energy, due to the supersaturation, and the combined effect of surface and interface energies. Many experimental observations revealed that there are three basic nucleation modes:

1. Island or Volmer-Weber growth (Fig. 3.1, a);
2. Layer or Frank-van der Merwe growth (Fig. 3.1, b);
3. Island-layer or Stranski-Krastonov growth (Fig. 3.1, c).

Island growth occurs when the growth species are more strongly bonded to each other than to the substrate, subsequent growth results in the island to coalescence to form a continuous film. The layer growth occurs where growth species are equally bound more strongly to the substrate than to each other. The island-layer growth is an intermediate combination of layer growth and island growth.

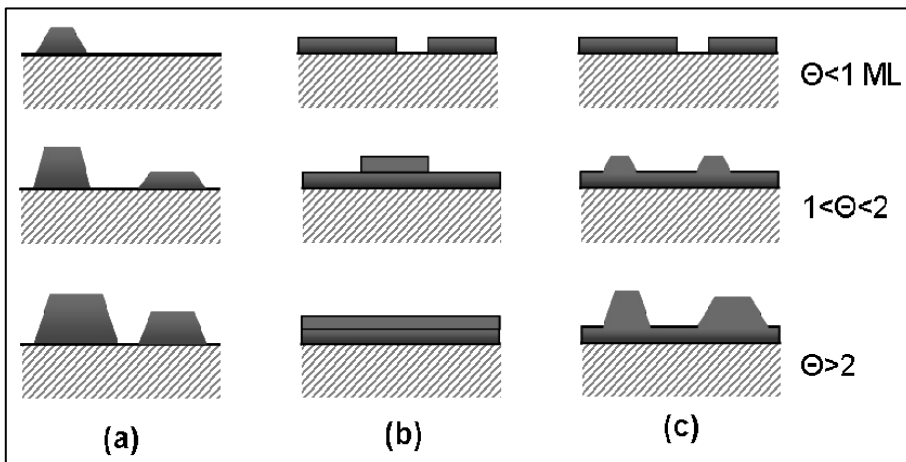


Fig. 3.1

Cross-section views of the three primary modes of thin film growth including (a) Volmer-Weber (VW: island formation), (b) Frank-van der Merwe (FM: layer-by-layer), and (c) Stranski-Krastonov (SK: layer-plus-island). Each mode is shown for several different amounts of surface coverage, Θ .

Determining the mechanism by which a thin film grows requires consideration of the chemical potentials of the first few deposited layers. A model for the layer chemical potential per atom has been proposed by Markov as:

$$\mu(n) = \mu_{\infty} + [\varphi_a - \varphi'_a(n) + \varepsilon_d(n) + \varepsilon_e(n)] \quad (\text{eq. 3.1})$$

where μ_{∞} is the bulk chemical potential of the adsorbate material, φ_a is the desorption energy of an adsorbate atom from a wetting layer of the same material, $\varphi'_a(n)$ the desorption energy of an adsorbate atom from the substrate, $\varepsilon_d(n)$ is the per atom misfit dislocation energy, and $\varepsilon_e(n)$ the per atom homogeneous strain energy. In general, the values of φ_a , $\varphi'_a(n)$, $\varepsilon_d(n)$, and $\varepsilon_e(n)$ depend in a complex way on the thickness of the growing layers and lattice misfit between the substrate and adsorbate film.

In the limit of small strains, $\varepsilon_{d,e}(n) \ll \mu_{\infty}$, the criterion for a film growth mode is dependent on $\frac{d\mu}{dn}$.

- VW growth: $\frac{d\mu}{dn} < 0$ (ad atom cohesive force is stronger than surface adhesive force)
- FM growth: $\frac{d\mu}{dn} > 0$ (surface adhesive force is stronger than adatom cohesive force)

SK growth can be described by both of these inequalities. While initial film growth follows a FM mechanism, i.e. positive differential μ , non-trivial amounts of strain energy accumulate in the deposited layers. At a critical thickness, this strain induces a sign reversal in the chemical potential, i.e. negative differential μ , leading to a switch in the growth mode. At this point it is energetically favorable to nucleate islands and further growth occurs by a VW type mechanism. It should be noted that a thermodynamic criteria for layer growth similar to the one presented above can be obtained using a force balance of surface tensions and contact angle.

Since the formation of wetting layers occurs in a commensurate fashion at a crystal surface, there is often an associated misfit between the film and the substrate due to the different lattice parameters of each material. Attachment of the thinner film to the thicker substrate induces a misfit strain at the interface given by $(a_f - a_s)/a_s$.

Here, a_f and a_s are the film and substrate lattice constants, respectively. As the wetting layer thickens, the associated strain energy increases rapidly. In order to relieve the strain, island formation can occur in either a dislocated or coherent fashion. In dislocated islands, strain relief arises by forming interfacial misfit dislocations. The reduction in strain energy accommodated by introducing a dislocation is generally greater than the concomitant cost of increased surface energy

associated with creating the clusters. The thickness of the wetting layer at which island nucleation initiates, called the critical thickness h_c , is strongly dependent on the lattice mismatch between the film and substrate, with a greater mismatch leading to smaller critical thicknesses. Values of h_c can range from sub-monolayer coverage to up to several monolayers thick. Figure 3.1 illustrates a dislocated island during SK growth after reaching a critical layer height. A pure edge dislocation is shown at the island interface to illustrate the relieved structure of the cluster. In some cases, most notably the Si/Ge system, nanoscale dislocation-free islands can be formed during SK growth by introducing undulations into the near surface layers of the substrate. These regions of local curvature serve to elastically deform both the substrate and island, relieving accumulated strain and bringing the wetting layer and island lattice constant closer to its bulk value. This elastic instability at h_c is known as the Grinfeld instability (formerly Asaro-Tiller-Grinfeld; ATG). The resulting islands are coherent and defect-free, garnering them significant interest for use in nanoscale electronic and opto-electronic devices. Such applications are discussed briefly later.

Finally, it should be noted that strain stabilization indicative of coherent SK growth decreases with decreasing inter-island separation. At large areal island densities (smaller spacing), curvature effects from neighboring clusters will cause dislocation loops to form leading to defected island creation.

3.3 Chemical vapour deposition

Chemical Vapour Deposition (CVD) involves the dissociation and/or chemical reactions of gaseous reactants in a activated (heat, light, plasma) environment, followed by the formation of a stable solid product.

The deposition involves homogeneous gas phase reactions, which occur in the gas phase, and/or heterogeneous chemical reactions which occur on/near the vicinity of a heated surface leading to the formation of powders or films, respectively.

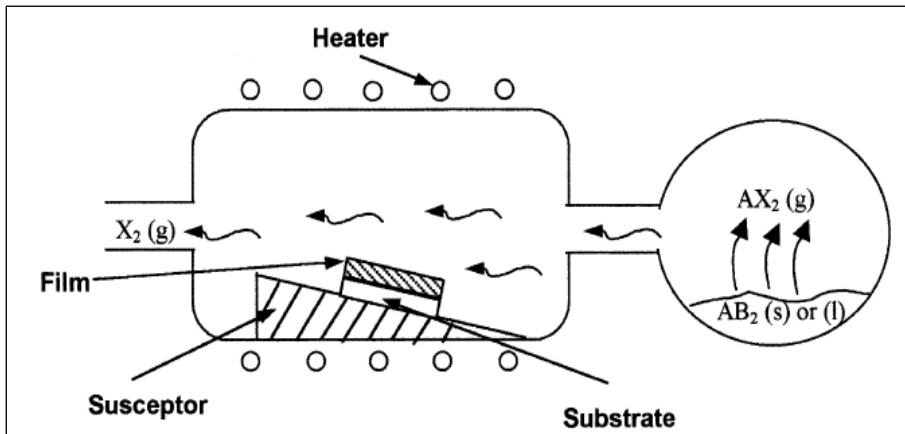


Fig. 3.2
Schematic diagram
of the CVD coating.
(source: Choy, 2003)

3.4 Principles of CVD

CVD is the deposition of a solid film from the gas phase via a chemical reaction. It is the chemical reaction that distinguishes CVD from other deposition mechanisms such as evaporation, sputtering and vapour transport, which are examples of physical vapour deposition (PVD). All types of CVD involve three basic processes: introduction of precursor to the gas stream, transport of precursor to the substrate and application of energy to cause a reaction.

A wide range of deposition techniques fall under the definition of CVD, and these differ in one or more of the following parameters:

- **Pressure.** CVD can be carried out at atmospheric pressure or under reduced pressure.
- **Precursor activation.** The chemical reaction of the precursors can be initiated by heat, light, RF plasma or another method.
- **Number of precursors.** Depositions can be made from a single precursor or multiple precursors (single, dual or multiple source CVD).
- **Precursor transport.** The precursor can be introduced to the gas phase by thermal vapourisation, liquid injection or through aerosol formation.
- **Type of reactor.** The reactor where the deposition takes place may be hot wall or cold wall and have a horizontal, vertical or rotating substrate.

Figure 3.3 shows a schematic of a horizontal bed cold wall CVD reactor, which is the type of reactor used in this work. The substrate lies horizontally on top of a heater. Gas enters the reactor and flows parallel to the substrate. At some point within the reactor, precursors react and form a film on the substrate. Since only the substrate is directly heated, a temperature gradient will exist in a cold wall reactor.

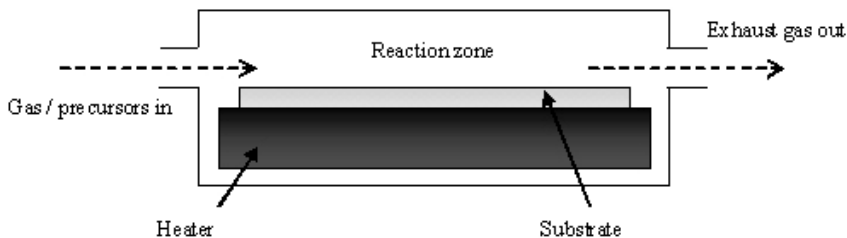


Fig. 3.3
A schematic of a horizontal bed cold wall CVD reactor. (source: Palgrave, PhD thesis, 2007)

In general, a CVD reactor consists of a reaction chamber equipped with a loadlock for the transport and placement of the substrate into the chamber, a substrate holder and a heating system.

The CVD reactor can be either a hot-wall or a cold-wall. A hot-wall reactor uses a heated furnace into which the substrate are placed for indirect heating; a cold-wall reactor, as the one reported in this thesis, has the substrate only heated, inductively or resistively.

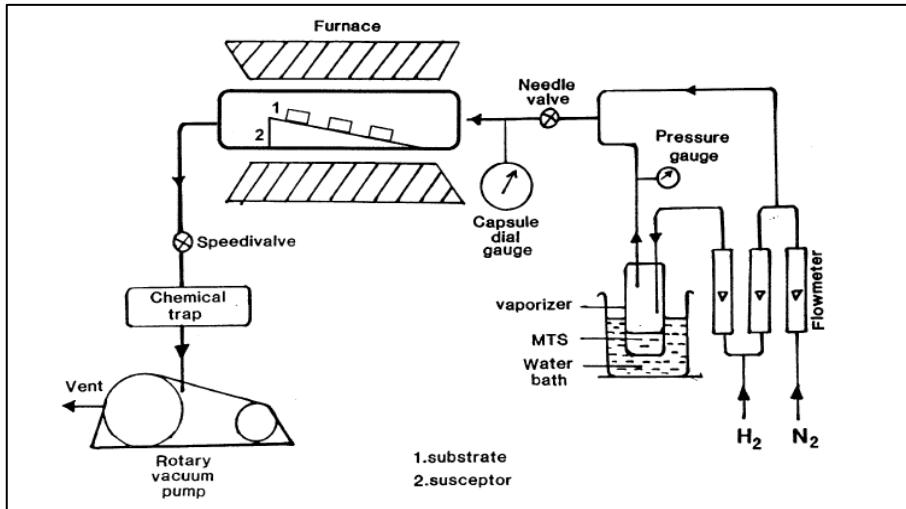


Fig. 3.4
Schematic diagram of a typical laboratory CVD equipment for coating's deposition. (source: Choy, 2003)

3.5 Process principles and deposition mechanism

In general, the CVD process involves the following key steps:

- (1) Generation of active gaseous reactant species.
- (2) Transport of the gaseous species into the reaction chamber.
- (3) Gaseous reactants undergo gas phase reactions forming intermediate species:
 - (a) at a high temperature above the decomposition temperatures of intermediate species inside the reactor, homogeneous gas phase reaction can occur where the intermediate species undergo subsequent decomposition and/or chemical reaction, forming powders and volatile by-products in the gas phase. The powder will be collected on the substrate surface and may act as crystallisation centres, and the by-products are transported away from the deposition chamber. The deposited film may have poor adhesion.
 - (b) at temperatures below the dissociation of the intermediate phase, diffusion/convection of the intermediate species across the boundary layer (a thin layer close to the substrate surface) occur. These intermediate species subsequently undergo steps (4)–(7).
- (4) Absorption of gaseous reactants onto the heated substrate, and the heterogeneous reaction occurs at the gas–solid interface (i.e. heated substrate) which produces the deposit and by-product species.
- (5) The deposits will diffuse along the heated substrate surface forming the crystallisation centre and growth of the film.
- (6) Gaseous by-products are removed from the boundary layer through diffusion or convection.
- (7) The unreacted gaseous precursors and by-products will be transported away from the deposition chamber.

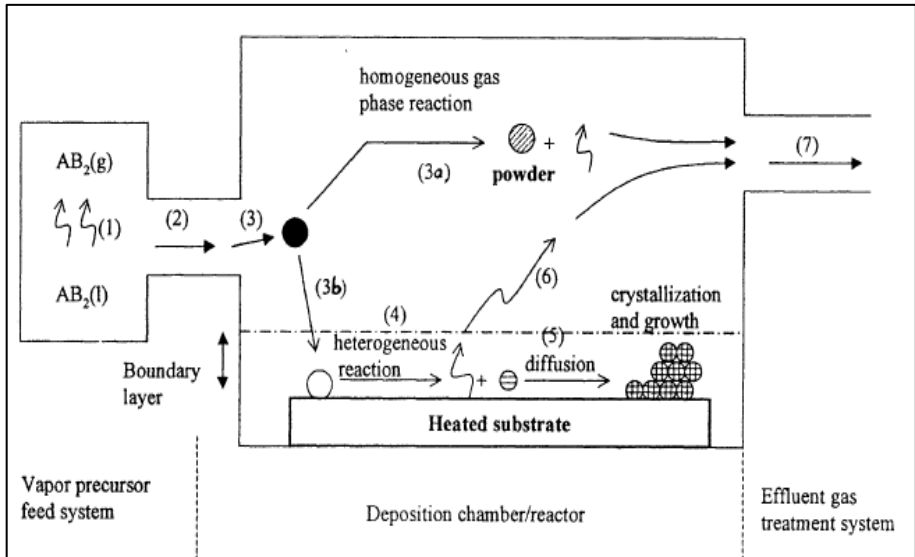


Fig. 3.5
A schematic illustration of the key CVD steps during deposition. (source: Choy, 2003)

3.6 Fluid Dynamics

The behaviour of a gas in motion is described by the equations of fluid dynamics. The motion of gas is an important consideration in CVD as it dictates the transport of reactants to the substrate. The Reynolds number (R_e) is a ratio of forces often used to characterize a fluid flow through a pipe.

The dimensionless Reynolds number is defined as:

$$R_e = \rho v L / \mu \quad (\text{eq. 3.2})$$

In equation 3.2, ρ = fluid density, v = mean fluid velocity, L = characteristic length of the pipe (typically the pipe diameter) and μ = fluid viscosity.

Two flow regimes can be defined: laminar and turbulent flow. In the laminar flow regime, the fluid flows in layers parallel to the direction of flow; in this regime, lateral motion within the fluid occurs only through diffusion. In contrast, turbulent flow is characterised by large scale vortices and eddies that cause significant lateral mixing of the fluid. Low values of R_e , caused by low viscosity, low velocity, small pipe diameter or high fluid viscosity result in laminar flow, while high values of R_e result in turbulent flow. The low densities of the carrier gases and the relatively low flow rates used in most forms of CVD mean that the flow is laminar.

Figure 3.6, in the next page, shows the velocity profile of a gas under laminar flow conditions. The gas enters the pipe at the left of the diagram with a constant velocity profile. Loss of momentum due to collisions with the stationary walls causes the velocity of the gas to decrease. The velocity of the layer of gas directly in contact with

the walls is assumed to be zero; this stationary layer is known as the static boundary layer. The layers of gas above the static layer are also progressively slowed, and the velocity profile becomes less uniform: profile II has a central core of uniform velocity, but profile III has no uniform portion. A profile such as III is known as fully developed laminar flow. A second boundary layer can be defined between regions of uniform and non-uniform fluid velocity, and is shown by dashed lines. This velocity boundary layer vanishes at III, although the static boundary layer remains throughout.

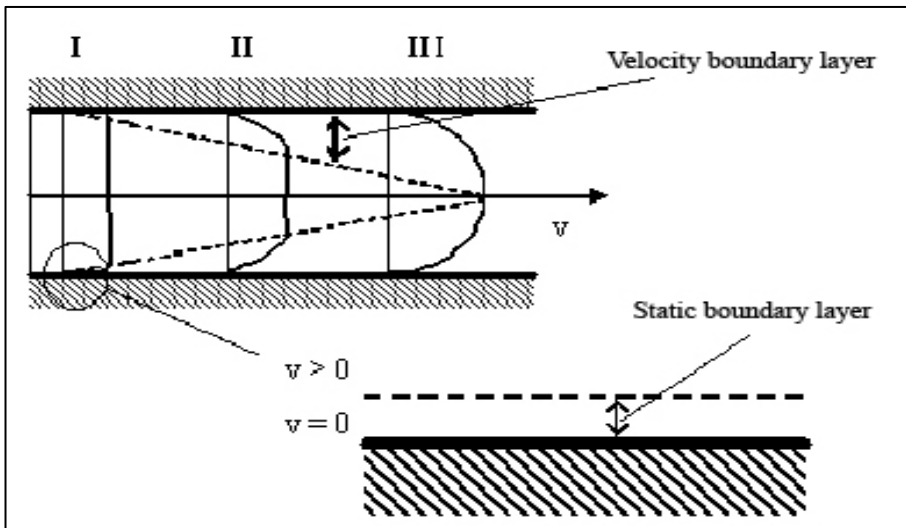


Fig. 3.6 Velocity profiles of gas in a laminar flow along a two dimensional pipe. The expanded section shows the static boundary layer next to the pipe wall. (source: Palgrave, PhD thesis, 2007)

3.7 Particles within the reactor

Within the CVD reactor, particles may be present in the gas flow. These may be solid particles present due to gas phase reaction of precursors, or the solid particles themselves may be the precursor. In general, gas phase particles are subject to a number of forces within the reactor.

Thermophoresis, also known as the Soret effect or thermal diffusion, is a force acting on particles (and also molecules) suspended in a fluid in the presence of a temperature gradient. The force can be regarded as arising from non-uniform bombardment of the particle by fluid molecules; this bombardment will be greater on the *hot side* of the particle, therefore this force is usually found to repel particles from a hotter surface and attract them to a colder surface; the term *thermophobic force* is used. However, under certain conditions, thermophoresis can act in the opposite direction, driving particles towards a hot surface; this is known as *thermophilic force*. The switch between thermophobic and thermophilic behaviour is not well understood. One factor that seems to be important is particle concentration. At very high particle concentrations, interactions between particles influence the thermophoretic effect, in

some cases causing thermophilic movement of particles. However, it is expected that at lower particle concentrations, as may be found in the gas phase of a CVD reactor, the thermophoretic effect will be thermophobic. The thermophoretic force is generally dependent on the size of the particle; larger particles experience larger forces. In cold wall CVD reactors, thermophoresis acts to prevent large solid particles being incorporated into the film, increasing film homogeneity and adherence. However, it has been shown that for nano-sized particles (diameter 50 nm and below) the magnitude of the thermophoretic force depends only very weakly on particle size. The second force to be considered is diffusion. Particle movement in a fluid, also known as Brownian motion, is an essentially random movement of particles due to instantaneously asymmetric bombardment by the molecules that constitute the fluid. Brownian motion is a significant consideration for nanoparticles suspended in a gas stream. The particle diffusivity in a gas, D , can be expressed as:

$$D = \frac{CkT}{d_p\mu} \quad (\text{eq. 3.3})$$

In equation 3.3, k is Boltzmann's constant, T is the absolute temperature, d_p is the particle diameter and μ is the gas viscosity. C is a factor which depends on pressure, and will be approximately constant at pressures close to atmospheric pressure. It can be seen from the above equation that particle diffusion is higher for smaller particles and at higher temperatures. Particles close to the substrate (or other reactor surface) may experience additional forces. Van der Waals force will be attractive between particle and surface. There may also be Columbic attraction or repulsion, depending whether the particle and surface are charged. Additionally, gas phase particles may be attracted to or repelled from particles already adsorbed onto the substrate, either electrostatically or due to steric factors. Steric repulsion may be caused by capping groups attached to either particle.

Figure 3.7 summarises the forces discussed in this section.

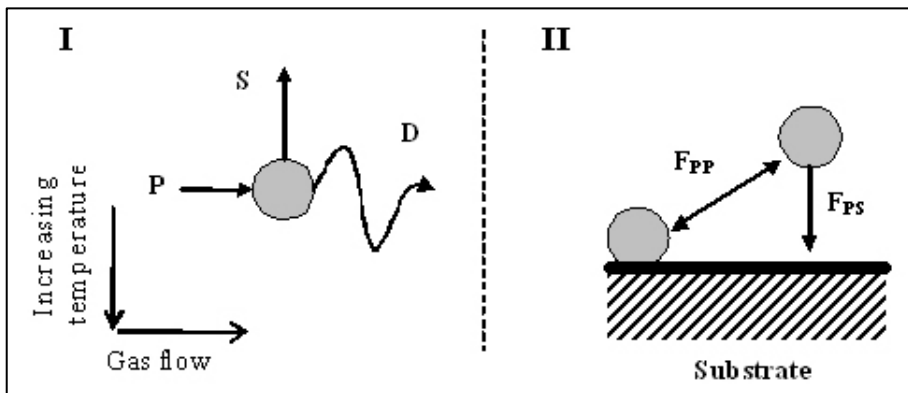


Fig. 3.7

Forces acting on particles suspended in the gas phase in a cold wall CVD reactor. Panel I illustrates a particle far from the substrate, and panel II shows a particle close to the substrate. S is the Soret (thermophoretic) effect acting as the expected thermophobic force, D is diffusion (Brownian motion) and acts in a random direction and varies with time. P is the force due to the flow of gas. F_{PP} is the attractive or repulsive force between two particles. F_{PS} is the attractive force between the particle and the substrate.

(source: Palgrave, PhD thesis, 2007)

As seen in figure 3.7, panel I, when a particle is far from the substrate, the only force that directs it towards the substrate in the laminar flow regime is diffusion. Equation 3.3 shows that diffusion is greater for smaller particles. Additionally the thermophoretic effect, which directs particles away from the hot substrate, is smaller for small particles (although the size dependence is weak for nano-sized particles). Thus smaller particles are more likely to be directed against the temperature gradient and towards the substrate in a cold wall CVD reactor. Close to the substrate (figure 3.7, panel II) there is attraction between the particle and substrate through Van der Waals interactions, although the thermophoretic effect will be greater due to a greater temperature gradient close to the substrate. The force between gas phase and adsorbed particles can be attractive or repulsive. In the case of an attractive inter-particle force, the resulting film is expected to be composed of aggregates of particles. In the case of a repulsive force, the film will consist of widely spaced particles. At high levels of coverage, these two types of film will become indistinguishable, as the entire substrate will be covered, and spacing between particles will not be measurable. In addition to the forces shown in figure 3.7, gravity and buoyancy will act on the particle. Gravitational settling is an important process for fluid phase particles, although for particles smaller than 1 μm in diameter gravitational force is small compared to the other forces discussed above.

In summary, deposition of nanoparticles onto a substrate is governed by competition between the thermophoretic effect, which is expected to be thermophobic, and particle diffusion. Since diffusion is greater and thermophoresis is smaller when the particle diameter is small, it is expected that small particles will migrate to the substrate faster than large particles. Since diffusion is a random process, it is as likely to direct the particles upwards away from the substrate as towards it. Therefore, even in the case where diffusion is much greater than thermophoresis and in an infinitely long two dimensional reactor, a statistical limit of 50% of the gas phase particles will migrate to the substrate. In practical cases, where thermophoresis is significant, the reactor is finite in length, and migration to the reactor walls is possible, the proportion of gas phase particles that reach the substrate will be much lower.

3.8 Advantages and disadvantages of CVD

Although CVD is a complex chemical system, it has some distinctive advantages as follows:

- (a) capability of producing highly dense and pure materials;
- (b) produces uniform films with good reproducibility and adhesion at reasonably high deposition rates;
- (c) ability to control crystal structure, surface morphology and orientation of the CVD products by controlling the CVD process parameters;
- (d) deposition rate can be adjusted readily;
- (e) reasonable processing cost for the conventional CVD technique;

- (f) flexibility of using a wide range of chemical precursors which enable the deposition of a large spectrum of materials;
- (g) relatively low deposition temperatures, and the desired phases can be deposited in-situ at low energies through vapour phase reactions, and nucleation and growth on the substrate surface.

However, the drawbacks of CVD include:

- (a) chemical and safety hazards caused by the use of toxic, corrosive, flammable and/or explosive precursor gases;
- (b) difficult to deposit multicomponent materials with well controlled stoichiometry using multi-source precursors because different precursors have different vapourisation rates;
- (c) the use of more sophisticated reactor and/or vacuum system by CVD variants tends to increase the cost of fabrication.

3.9 Hybrid aerosol assisted and atmospheric pressure CVD (AA/AP CVD)

Hybrid aerosol assisted (AA) and atmospheric pressure (AP) CVD methodology was utilized for the first time by prof. Ivan P. Parkin, Dr. Clara Piccirillo and Dr. Russell Binions (Christopher Ingold Laboratories, Department of Chemistry – University College London (UCL)) to produce thin film of gold nanoparticle-doped vanadium (IV) dioxide.

This hybrid technique showed great potential as the film characteristics were similar

to those produced by APCVD (good adhesion, uniformity and coverage) but with the versatility afforded by AACVD. Experiment had been conducted combining the AA and AP CVD system by adding the aerosol flow into the reaction chamber along with the atmospheric pressure reaction gas flow. The aerosol flow is composed of liquid droplets transported, using a nitrogen gas flow, to the reaction chamber where the solvent evaporates and the precursor is able to take part in surface reactions.

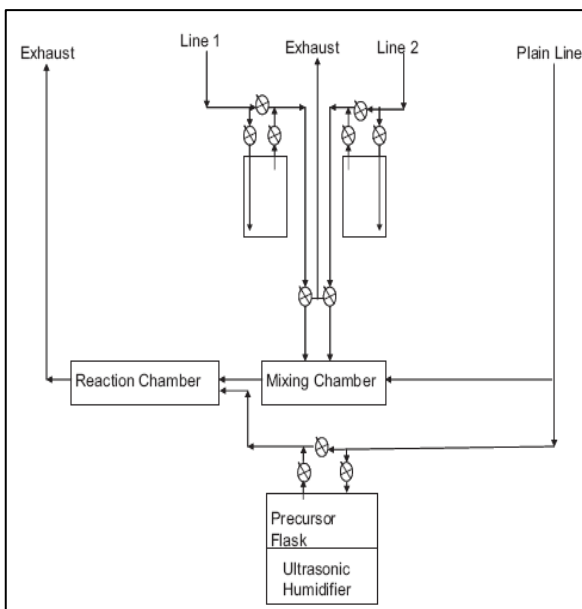


Fig. 3.8

Schematic of the AA/AP CVD set up. (source: Chem. Vap. Deposition 2008, 14)



One of the challenges of AACVD is to prevent aerosol droplet condensation prior to the introduction into the reactor. The two flows are introduced into the reaction chamber by means of a special manifold block containing two inputs, one for the APCVD flow and one for the AACVD. The routes through the block differed: the APCVD route has a baffle in the way of the flow, whereas the AACVD route does not. The two flows are introduced separately into the reaction chamber to reduce the likelihood of pre-reaction or disruption of the aerosol droplets. The APCVD flow is introduced above the AACVD flow relative to the substrate to suppress the effects of thermophoresis¹.

Fig. 3.9
AA/AP CVD reactor.



Fig. 3.10 a-d
Top left: AA/AP CVD used.
Top right: AA/AP CVD mixing chamber.
Bottom left: Reactor and Bubblers of the AA/AP CVD set up.
Bottom right: Ultrasonic aerosol.

¹ Thermophoresis had been observed previously with AACVD system and it is undesirable as it leads to deposition on the top plate of the reaction chamber and powdery, non-adherent films.

The AA/AP CVD reported in this thesis was carried out using a horizontal bed reactor of in-house design (see figure 3.10 top left).

The reactor consisted of an open ended quartz cylindrical tube, 60 mm in diameter and 160 mm in length. Within the tube were supports for a top plate and a carbon block containing a heating element and two thermocouples. Each end of the quartz tube was capped with a removable stainless steel end plate. Gas may enter through one of the plates via brass manifold, and leave at the opposite end via an exhaust port. The substrate was placed on the carbon block, and a top plate was placed parallel to the substrate and 10 mm above it. Both the substrate and top plate were 150 x 45 x 4 mm sheets of SiO₂ coated float glass cut from larger sheets supplied by Pilkington Glass Plc, which were cleaned using acetone and propan-2-ol and then dried in air prior to use. The substrate was placed on top of the carbon heating block at room temperature. The reactor was then sealed and heated to the desired temperature (525 °C). Only the substrate was directly heated, hence the reactor is known as a cold wall reactor. The precursor powder of VO(acac)₂ was contained within a metal bubbler (bubbler 1). The precursor solution of H₂O₂ in methanol was contained within a glass vessel with a thinned base, which allowed more rapid aerosol generation. A Vicks ultrasonic humidifier was used to generate the aerosol mist. The piezoelectric device contained within the humidifier functioned at 20 kHz. The nitrogen gas² was passed through flow meters and into the precursor flasks, driving the aerosol mist to the reactor through PTFE tubing while the powder to the reactor through a previous mixing chamber. The precursor mix passed through the brass manifold, designed to generate a uniform flow of gas across the width of the reactor, and entered the reactor between the substrate and the top plate. The exhaust was vented into a fume cupboard. The gas flow was continued until all the precursor mix had passed through the reactor, typically taking 10 to 30 minutes depending on the gas flow rate. Films were cooled to room temperature *in situ* under a flow of N₂, and after cooling were handled and stored in air. The brass manifold was routinely cleaned in an ultrasonic bath and by rinsing with organic solvents in order to avoid blockages.

² 2% O₂ in N₂ under pressure.

4. Analysis techniques

4.1 Introduction

Characterization of nanomaterials and nanostructures is largely based on the surface analysis technique and conventional characterization method developed for bulk materials.

This section describes the physical analysis techniques used to characterize the films deposited by hybrid Aerosol Assisted and Atmospheric Pressure Chemical Vapour Deposition (AA/AP CVD).

4.2 X-Ray Diffraction (XRD)

XRD is a very important experimental technique that is performed on polycrystalline powders or films. It gives information on the crystalline phases present, preferred orientation of the crystallites and crystallite size. It is a non destructive technique, it does not require elaborate sample preparation and it is very useful in characterizing nanoparticles. Light is diffracted from a set of periodic planes according to the Bragg law (eq. 4.1).



Fig. 4.1
XRD instrument.

The distance between Miller planes in crystalline materials is of the order of 10^{-10} m, therefore the wavelength of light which is diffracted from these planes corresponds to X-rays.

$$I = 2d \sin \theta \quad (\text{eq. 4.1})$$

where d is the space between atomic planes in the crystalline phase and I is the X-ray wavelength. The intensity of the diffracted X-rays is measured as a function of the diffraction angle 2θ and the specimen orientation. The diffraction pattern is used to identify the specimen's crystalline phases and to measure its structural properties. XRD was undertaken using a Bruker-Axs D8 (GADDS) diffractometer.

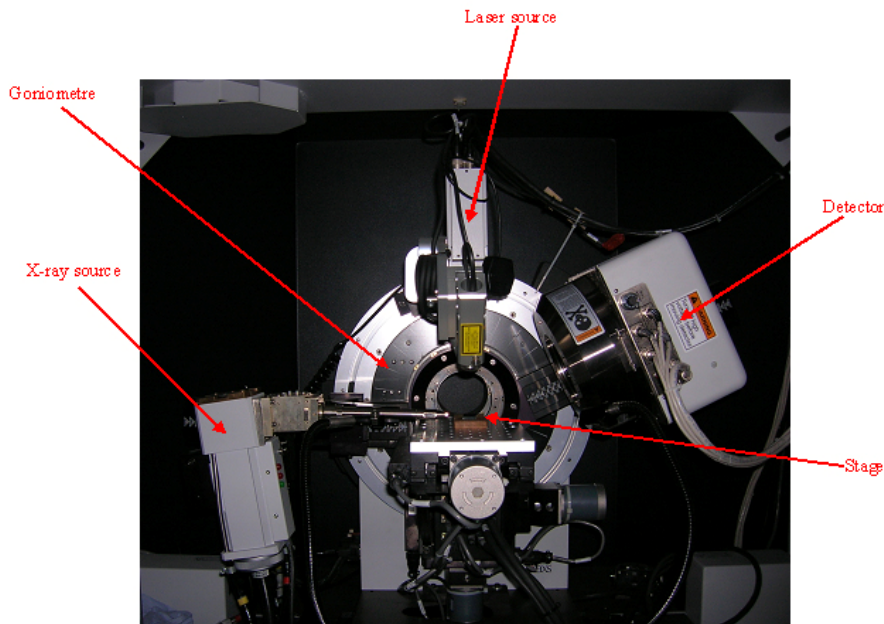


Fig. 4.2
XRD components.

This instrument uses a 2D area X-ray detector to record large sections of multiple Debye-Scherrer cones simultaneously. After collection, the data can be integrated to produce a standard one-dimensional diffractogram. The instrument uses a $\text{Cu K}\alpha$ X-ray source which is collimated such that only a small area of the sample (approximately 4 mm^2) is illuminated by the beam at any one time.

In this thesis to record diffraction peaks from the thin films, it was set: an angle from 1.5° to 25° ; detector angle 30° , collection time 1200 s (20 min), cathode current 40 mA, potential difference 40 kV.

The VO_2 main peaks appears at a 2θ value of around 27° and 37° . The Au [111] peak, appearing at a 2θ value of around 38.3° , was then integrated using a linear baseline to obtain the peak intensity. The intensity is dependent only on the molar amount of crystalline species within the illuminated volume.

4.3 UV / visible / near IR Absorption Reflection Spectroscopy

The absorption of UV, visible and near infra red light is an important property of nanoscale film, hence the recording of absorption/reflection spectra was an important characterization technique. Spectra were obtained using a Thermo Helios- α spectrometer with a resolution of 10 nm and a range of 300 – 2500 nm (300-860 nm: Visible; 860-2500 nm: IR). These analysis were performed on a UV WinLab L800/L900 produced by Perkin-Elmer.



Fig. 4.3
UV/IR Spectropho-
tometer.

4.4 Metal-to-semiconductor transition temperature (T_c)

An infrared spectrophotometer 298, produced by Perkin-Elmer, was used to search for T_c . The sample has been slowly warmed from environment temperature (~ 28 °C) to 120 °C and cool again down while the percentage transmittance through the film was measured. The data obtained were a hysteresis from which can be calculate the T_c as the mean point of the mean wideness of the curve.

4.5 Scanning Electron Microscopy (SEM)

SEM is an electron imaging technique used to record high resolution images of the sample surface. A high energy electron beam is focussed onto the sample surface and electrons emanating from the sample are collected; these can be divided into two types depending on their origin: backscattered electrons (bs) and secondary electrons (se). Backscattered electrons are incident electrons which have undergone elastic or inelastic scattering from the sample surface. The kinetic energy of backscattered electrons is usually lower than that of the incident electron beam due to one or more inelastic scattering events. The intensity of backscattered electrons depends strongly on atomic number, as scattering is more likely to occur from regions of high electron density. Regions with high electron density will backscatter more electrons, and so will appear brighter in backscattered electron images. For this reason, backscattered electron images, also known as compositional images, can be used to distinguish different elements or phases within composite materials.

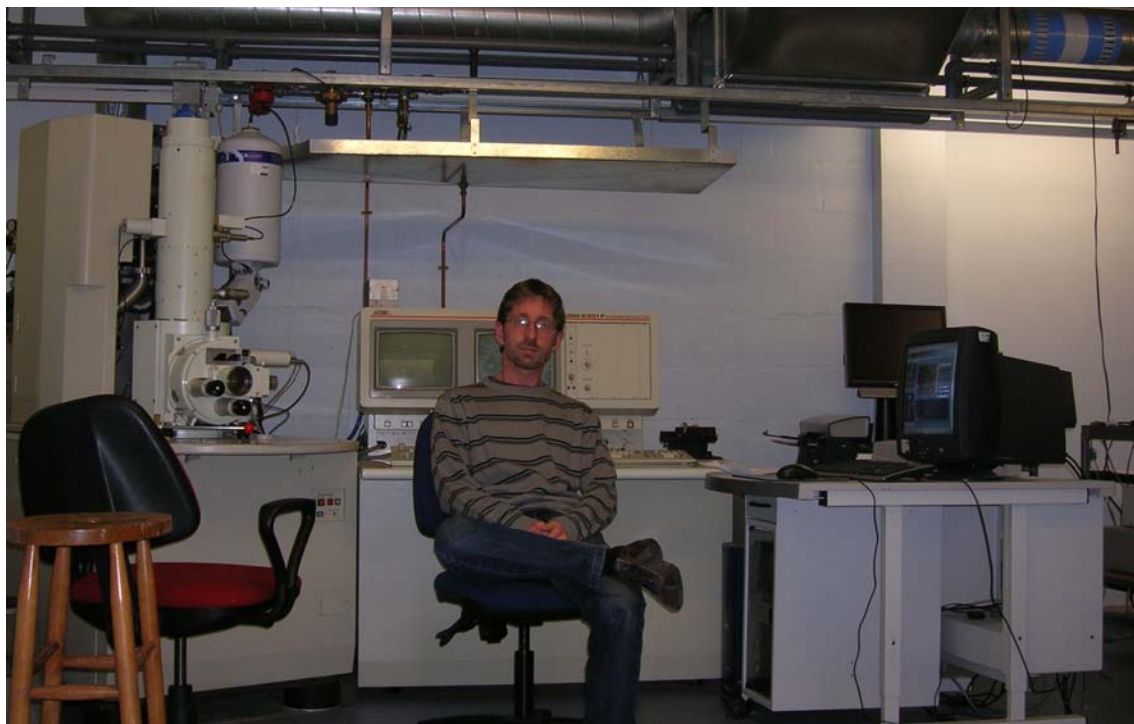


Fig. 4.4
Scanning Electron
Microscope at the
Archaeology De-
partment (UCL).

Secondary electrons are electrons ejected from the sample by the high energy incident electrons. The kinetic energy of secondary electrons is usually much lower than that of backscattered electrons, and this energy difference is the primary method of distinguishing the two types of electron emission. Because of their low kinetic energy, secondary electrons are easily recaptured by ionised atoms within the sample. Therefore secondary electrons escape only from the surface region of the sample. Secondary electron emission is strongly dependent on the surface morphology; highly curved or angled surfaces appear brighter in secondary electron images.

SEM analysis was performed on a JEOL 6301F instrument using a voltage of 20 kV, at 8 μA . Images were recorded and analysed using the SemAfore software. Samples were coated prior to analysis to enhance conductivity and reduce charging, which causes image distortion. A coating of gold is usually used for this purpose. Therefore a carbon coating was applied to the film surface. Samples were placed on a stainless steel stage.

Images were taken at different positions by moving the samples within the instrument; the position could be determined with an accuracy of 0.1 mm in this way.

4.6 Raman Spectroscopy

Raman spectroscopy is a vibrational technique that is characterized by an indirect coupling of high-frequency radiation, such as visible light, with vibrations of chemical bond. Raman spectroscopy is very sensitive to the lengths, strengths and arrangements of chemical bonds in a material, but less sensitive to the chemical composition. When the incident photon interacts with the chemical bond, the chemical



bond is excited to a higher energy state. Most of the energy would be re-radiated at the same frequency as that of the incident light, which is known as the Rayleigh scattering. A small portion of the energy is transferred and results in exciting the

Fig. 4.5
Raman Leica DMLM

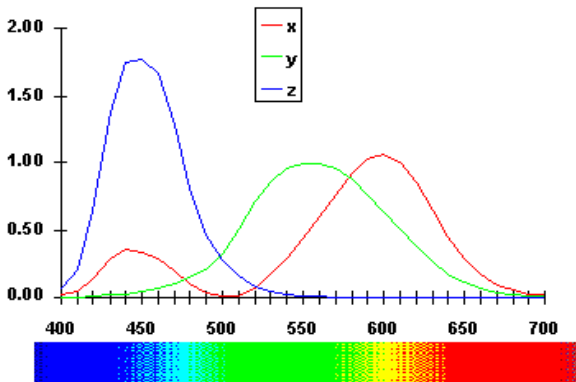
vibrational modes. The subsequent re-radiation has a frequency lower than that of the incident exciting light. The vibrational energy is deducted by measuring the difference between the frequency of the Raman line and the Rayleigh line.

In other words, it measures the frequency shift $\Delta\omega = \omega_{\text{phonon}} = |\omega_{\text{inc}} - \omega_{\text{scat}}|$ between the incident ω_{inc} and scattered ω_{scat} light frequencies when ω_{phonon} is an optical phonon mode vibration. The Raman effect is extremely weak and, thus, intense monochromatic continuous gas laser are used as the exciting light.

These analysis were performed on a Leica DMLM 50x.

4.7 CIE Colour specification

In 1931 the CIE (Commission Internationale de l'Eclairage) developed a system for



specifying colour stimuli using tristimulus values for three imaginary primaries. The basis of this system was the CIE 1931 standard observer: according to the trichromatic theory of colour vision an observer can match a colour stimulus with an

Fig. 4.6
Tristimulus values of the spectral colours CIE 1931 – 2° standard observer (source: www.cie.co.at)

additive mixture of three primaries. Therefore any colour stimulus can be specified by the amounts of the primaries that an observer would use in order to match the stimulus. The CIE standard observer resulted from experiments where observers were asked to match monochromatic wavelengths of light with mixtures of three primaries. The standard observer is in fact a table showing how much of each primary would be used (by an average observer) to match each wavelength of light.

The graph aside shows the colour matching functions for the CIE XYZ primaries. These are literally the relative amounts of the three primaries that an average observer would use to match a unit of light at each wavelength.

CIE XYZ tristimulus values can be calculated from the reflectance spectrum by the integration of the reflectance values $R(\lambda)$, the relative spectral energy distributions of the illuminant $E(\lambda)$, and the standard observer functions $x(\lambda)$, $y(\lambda)$, and $z(\lambda)$.

The integration is approximated by summation, thus:

$$\begin{array}{lll} X = 1/k \sum R(\lambda) E(\lambda) x(\lambda) & \text{(eq. 6.2)} & k = \sum E(\lambda) y(\lambda) \\ Y = 1/k \sum R(\lambda) E(\lambda) y(\lambda) & \text{(eq. 6.3)} & \text{where: and} \\ Z = 1/k \sum R(\lambda) E(\lambda) z(\lambda) & \text{(eq. 6.4)} & \lambda = \text{wavelength} \end{array}$$

The normalizing factor $1/k$ is introduced such that $Y = 100$ for a sample that reflects 100% at all wavelengths: recall that Y is proportional to the luminance of the stimulus. The introduction of this normalization is convenient since it means that relative, rather than absolute, spectral energy distributions for the illuminant can be used (thus the units in which they are expressed are unimportant).

There are perhaps two problems with the specification of colours in terms of tristimulus values and chromaticity space. Firstly, this specification is not easily interpreted in terms of the psychophysical dimensions of colour perception namely, brightness, hue, and colourfulness. Secondly, the XYZ system and the associated chromaticity diagrams are not perceptually uniform. The second of these points is a problem if we wish to estimate the magnitude of the difference between two colour stimuli.

The need for a uniform colour space led to a number of non-linear transformations of the CIE 1931 XYZ space and finally resulted in the specification of one of these transformations as the CIE 1976 ($L^* a^* b^*$) colour space.

In fact, in 1976 the CIE specified two colour spaces; one of these was intended for use with self-luminous colours and the other was intended for use with surface colours. These notes are principally concerned with the latter known as CIE 1976 ($L^* a^* b^*$) colour space or CIELAB.

CIELAB allows the specification of colour perceptions in terms of a three-dimensional space: the L^* -axis is known as the lightness and extends from 0 (black) to 100 (white); the other two coordinates a^* and b^* represent redness-greenness and yellowness-blueness respectively.

¹ Illuminant: is the specification for a potential light source different from light source which is a physical emitter of radiation

Samples for which $a^* = b^* = 0$ are achromatic and thus the L^* -axis represents the achromatic scale of greys from black to white.

The quantities L^* , a^* , and b^* are obtained from the tristimulus values according to the following transformations:

$$L^* = 116(Y/Y_n)^{1/3} - 16 \quad (\text{eq. 6.5})$$

$$a^* = 500[(X/X_n)^{1/3} - (Y/Y_n)^{1/3}] \quad (\text{eq. 6.6})$$

$$b^* = 200[(Y/Y_n)^{1/3} - (Z/Z_n)^{1/3}] \quad (\text{eq. 6.7})$$

where X_n , Y_n , and Z_n are the values of X , Y , and Z for the illuminant that was used for the calculation of X , Y , and Z of the sample, and the quotients X/X_n , Y/Y_n , and Z/Z_n are all greater than 0.008856 ².

The software used to calculate colour specification was: Optic 5 and Window 5 - by LBNL.

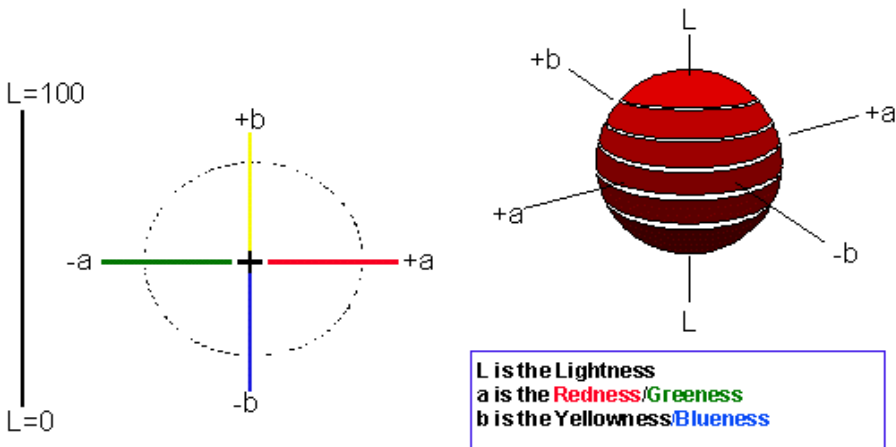


Fig. 4.7
3D Colour space.
(source:
www.cie.co.at)

² When any of the quotients are less than or equal to 0.008856 a slightly different set of equations is used.

5. RESULTS AND DISCUSSION

5.1 Experiments 1: MVOx, MAu and MVOxAu

In this work, the hybrid technology AA/AP CVD, in a 525°C cold wall reactor, has been performed to deposit thin film of gold nanoparticle-doped vanadium (IV) dioxide from the CVD reaction of Vanadyl Acetylacetonate VO(acac)₂ at 175°C and 40 mg of Auric Acid (HAuCl₄) in 25 ml of methanol, varying the three flow rates (plain, bubbler and aerosol), as shown in the following table:

Tab. 5.1				
Different flow rates [L min ⁻¹] used to carry on depositions				
N°	Plain	Bubbler	Aerosol	Total
Start point				
1	2	3	2	7
Vary flows				
2	1	3	3	7
3	2	2	3	7
4	3	1	3	7
5	4	1	2	7
6	4	2	1	7
7	5	1	1	7
8	1	4	2	7
9	2	4	1	7
10	1	5	1	7
11	3	3	1	7
12	1	2	4	7
13	2	1	4	7
14	1	1	5	7

With each condition, two samples (or sometimes three) have been produced to ensure that the technique can be considered reproducible. Each sample had been given a name, MVOxAu, followed by a number and a letter to identify the particular sample. The bottom plate only was used to characterize the films. For each couple, one sample, with the best in coverage and uniformity, was analyzed to examine its chemical and physical properties. Raman spectroscopy didn't show any features though these films are poor Raman scatters thus, it was not performed anymore.

To investigate the optical properties, tests on Reflectance and Transmittance (R/T) were performed on hot and cold samples showing various results, as well as tests to find out the metal-to-semiconductor transition temperature (T_c) that resulted to be quite low in comparison to the previous works: ~ 40°C. Scanning Electron Microscope (SEM) was used to take images (Low Resolution Secondary Electron imaging (se) and Backscattered Electron imaging (bs)) that showed a uniform surface deposi-

tion coverage with round nanoparticles and EDAX to take chemical quantitative spectra.



Fig. 5.1
HAuCl₄ in Methanol.



Fig. 5.2
Top right: HAuCl₄ in the bottles.
Bottom right: VO(acac)₂ powder.



Fig. 5.3
Left: Aerosol of HAuCl₄ in Methanol.
Right: Aerosol.



XRD has shown that VO_2 had been deposited but films seemed to not be very crystalline so some examples (MVOxAu2a; MVOxAu3c; MVOxAu4a; MVOxAu6a; MVOxAu9a; MVOxAu11a) have been annealed¹ in N_2 atmosphere. Unfortunately, no improvement in crystallinity was noticed and, furthermore, some examples have been oxidised becoming V_2O_5 .

The thickness of films was also calculated showing an average thickness between $100 \div 200$ nm but some films resulted to be less than 50 nm. There is, apparently, no direct relationship between the different flow rate conditions and the films' properties to formulate any kind of equation or law, since a great deal of variation is present. To compare the results obtained with the different precursors, films of VO_2 only, by AP CVD, and gold only, by AA CVD, had previously deposited and R/T tests on blank glass were performed.

One of the problems related to the use of these coatings in a building as architectural glazing is, not only their optical properties, but also their colour: vanadium (IV) dioxide coating is of a dark yellow-brown colour that, despite of its thermochromic behaviour, makes it unpleasant to use in windows; gold films are blue; gold-doped vanadium (IV) dioxide films are light yellow/green/blue with gold metallic reflex in reflected light.

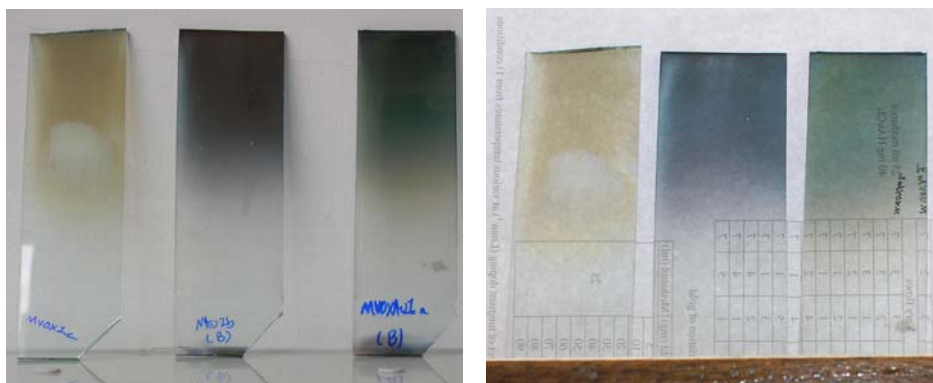


Fig. 5.4

Left: three different coatings in reflected light: from the left Vanadium (IV) Dioxide, Gold and Gold-doped Vanadium (IV) Dioxide.

Right: the same three different coatings in transmitted light: from the left Vanadium (IV) Dioxide, Gold and Gold-doped Vanadium (IV) Dioxide.

In the following pages there are reported some results of the analysis performed on the different coatings to show the differences between the various coatings' behaviours due to the initial flow rate conditions.

¹ Annealing: the name and inspiration come from "annealing" in metallurgy, a technique involving heating and controlled cooling of a material to increase the size of its crystals and reduce their defects (the primary type of which is the linear defect called a dislocation) and the internal stresses which they cause. The heat causes the atoms to become unstuck from their initial positions (a local minimum of the internal energy) and wander randomly through states of higher energy. The slow cooling gives them more chances of finding configurations with lower internal energy than the initial one.

5.1.1 Reflectance and Transmittance of MVO_x, MAu and MVO_xAu

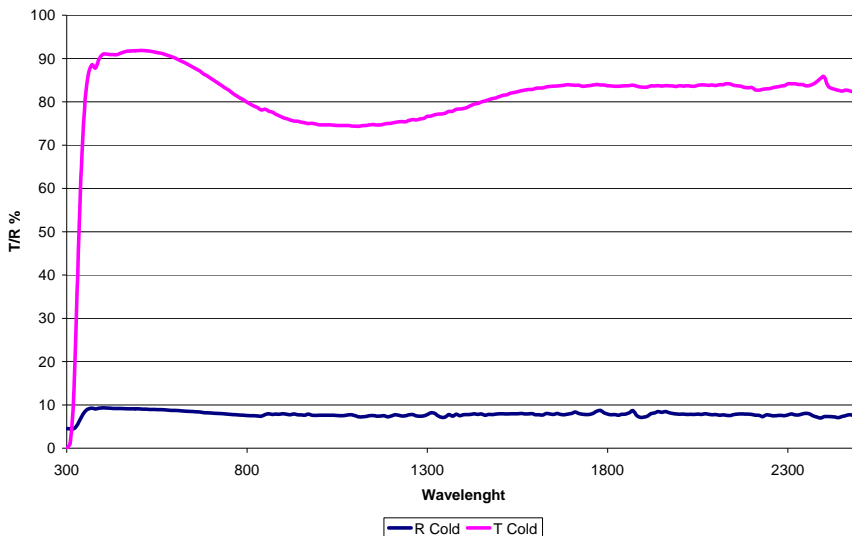


Fig. 5.5
T/R on a Blank
sample.

Transmittance and Reflectance of a blank sample² shows the characteristic behaviour of a common glass with a SiO₂ coating on just one side: a high transmittance and a very low reflectance in both visible and infrared range of the spectrum.

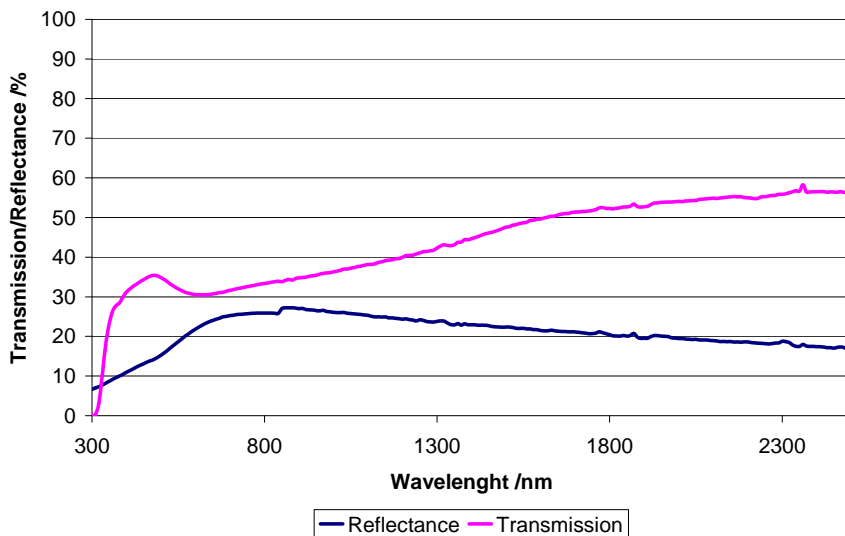
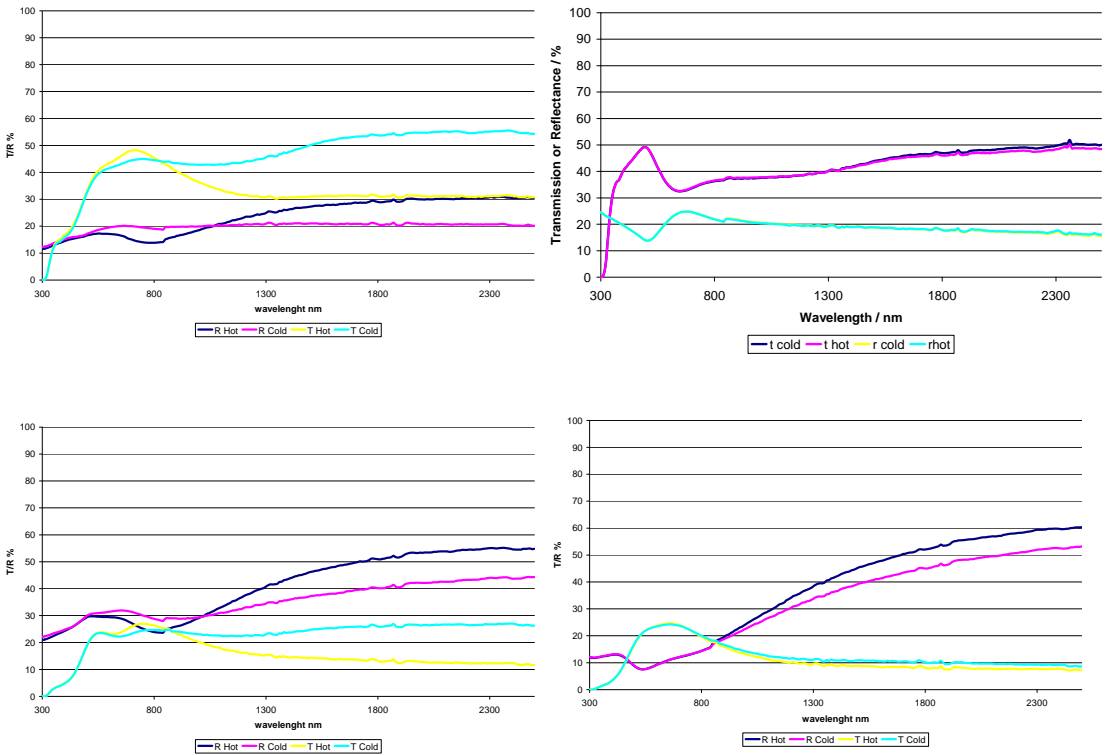


Fig. 5.6
T/R on Mau-2a, a
Gold coated sample.

² Blank sample: glass with SiO₂ layer only on it as it furnished from Pilkington Glasses.

A gold-film sample shows a typical metallic behaviour: a quite low reflectance, about 20 %, in the far IR and a higher one in the near IR and visible; a quite higher transmittance in the far IR, about 55 %, that lows toward the visible range. Below, there are some different graphs showing some behaviours of gold-doped vanadium (IV) dioxide coatings:

Fig. 5.7
Left: T/R on MVoxAu-2a;
Right: T/R on MVoxAu-3a



The film with the hugest switch between cold and hot Transmittance and cold and hot Reflectance is recognized to be the one with the best behaviour (MVOxAu9a) where there is a good mix of gold and vanadium in the coating. All the samples show that Transmittance is higher as the film is cold and lower as it is hot; Reflectance, on the contrary, is higher as the film is hot and lower as it is cold. This type of thermochromic behaviour makes them suitable for smart windows.

Sample MVOxAu3a (Fig. 5.7 right) shows almost no switch between the hot condition and the cold one, this fact shows that vanadium is almost absent in the film while there is a large amount of gold deposited in it.

Sample MVOxAu10a (Fig. 5.8 right) shows a very small switch that indicate, as the previous sample, that just a small amount of vanadium has deposited while there is a

Fig. 5.8
Left: T/R on MVoxAu-9a;
Right: T/R on MVoxAu-10a

large amount of gold; in these two samples thermochromic properties are not very evident.

Sample MVOxAu2a (Fig. 5.7 left) shows an opposite behaviour: there is a big switch between the hot state and the cold one that indicates a large amount of Vanadium in the coating but, the low values of both Transmittance and Reflectance in the far IR indicate that the quantity of gold is quite low.

Sample MVOxAu9a (Fig. 5.8 left) shows excellent optical properties because, even if the transmittance is quite low in the cold state, nevertheless there is quite big switch between the cold state and the hot one for both Transmittance and Reflectance that shows a good mix between vanadium (IV) dioxide and gold in the matrix with good thermochromic properties.

5.1.2 Hysteresis and Tc of MVOx, MAu and MVOxAu

Graphical procedure to calculate the Tc from the Hysteresis got from the test. The hysteresis' width (____ width in average switch) is calculated from the average value of the percentage transmittance (____ switch). The Tc (____ Tc) is calculated from the width's average value.

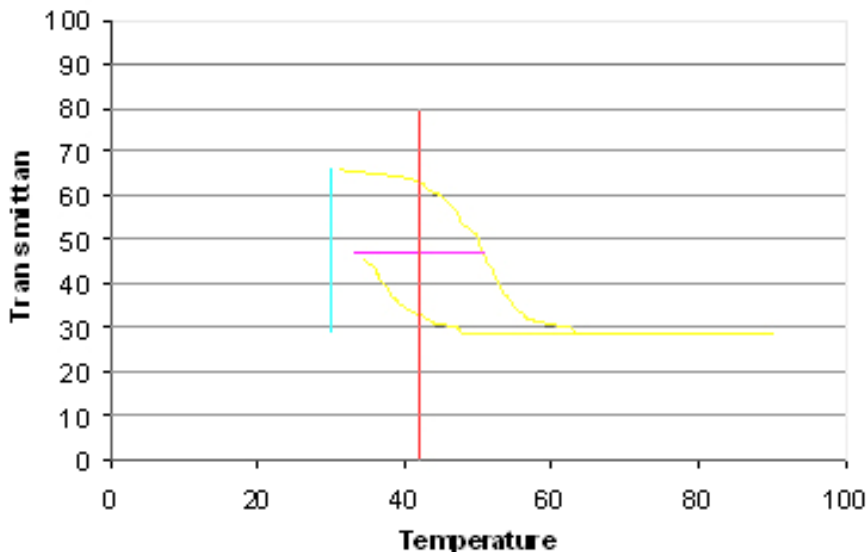


Fig. 5.9
Graphical procedure
to Calculate Tc from
the Hysteresis.

The graphs in fig. 5.10 show some different Hysteresis used to calculate the Transition Temperature (Tc) of Gold coating (Fig. 5.10 left) and Vanadium (IV) Dioxide coating (Fig. 7.10 right). The Gold film has got no Hysteresis as expected looking at the results of previous works; the second one shows a good Hysteresis from which a Tc of 42 °C has been calculated.

From the MVOxAu3c Hysteresis (Fig. 5.11 left) it has been calculated a transition temperature (Tc) of 42 °C with a switch of 17 %. This fact represents a very good

result considering that Vanadium (IV) Dioxide coatings usually show a $T_c \sim 68\text{ }^\circ\text{C}$ which is another big problem in the use of these coatings in architectural glazing because of the high switch temperature.

From the MVOxAu9a Hysteresis (Fig. 5.11 right) a transition temperature of $39\text{ }^\circ\text{C}$ with a switch of 19 % has been calculated. That is another point for the flow rate conditions of this particular sample. All the Hysteresis shown are not closed because of the procedure applied in the laboratory which displays some difficulties in cooling down the sample to the environmental temperature but if the test has been repeated from the same environmental temperature, an equal curve can be drawn with the same % transmittance at the beginning and at the end of the test. In theory, using a different apparatus, not available in this laboratory, it is possible to cool down the glass to the initial temperature to have a complete and closed Hysteresis.

The x-axis scale is $100\text{ }^\circ\text{C}$ in $20\text{ }^\circ\text{C}$ step; the y-axis is 100% in 20% step.

Fig. 5.10
Hysteresis of:
Left: MAu-2a
Right: MVox-1b

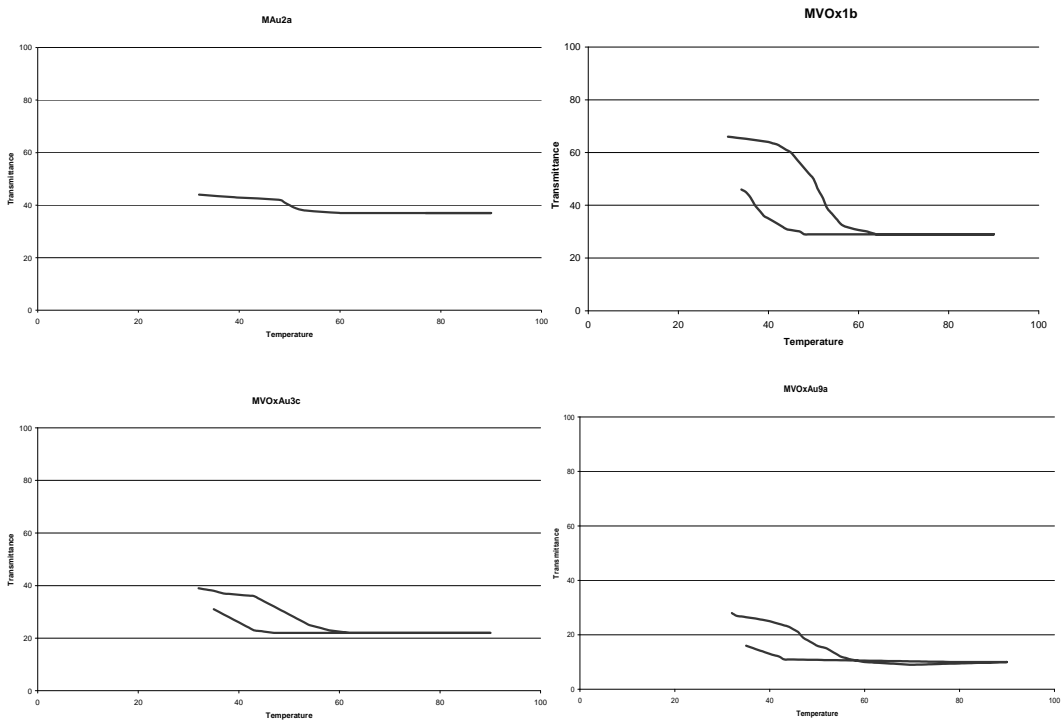


Fig. 5.11
Hysteresis of:
Left: MVoxAu-3c
Right: MVoxAu-9a

5.1.3 Raman Spectroscopy of MVOx, MAu and MVOxAu

As previously said, Raman Spectroscopy did not show any features on the Gold-doped Vanadium (IV) Dioxide films.

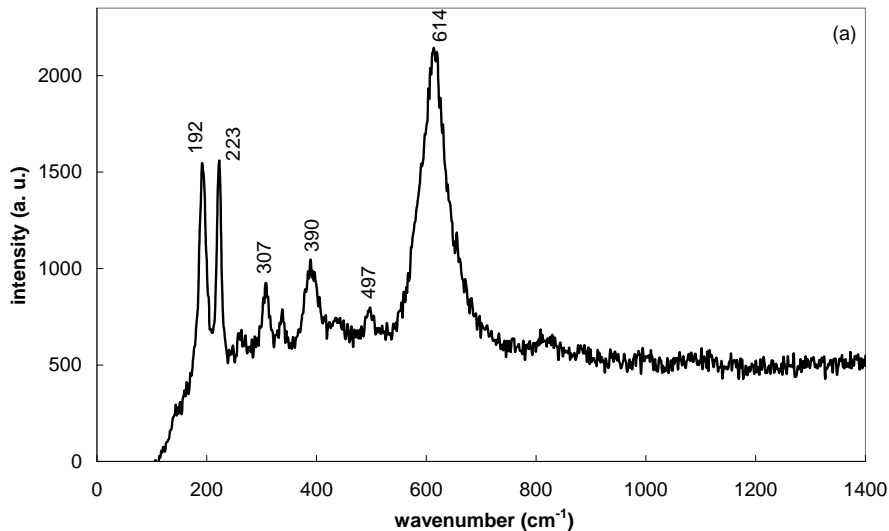


Fig. 5.12
Raman spectrum of VO₂ that shows the characteristic peaks of the composite.
(Source: spectrum supplied by Dr. Clara Piccirillo)

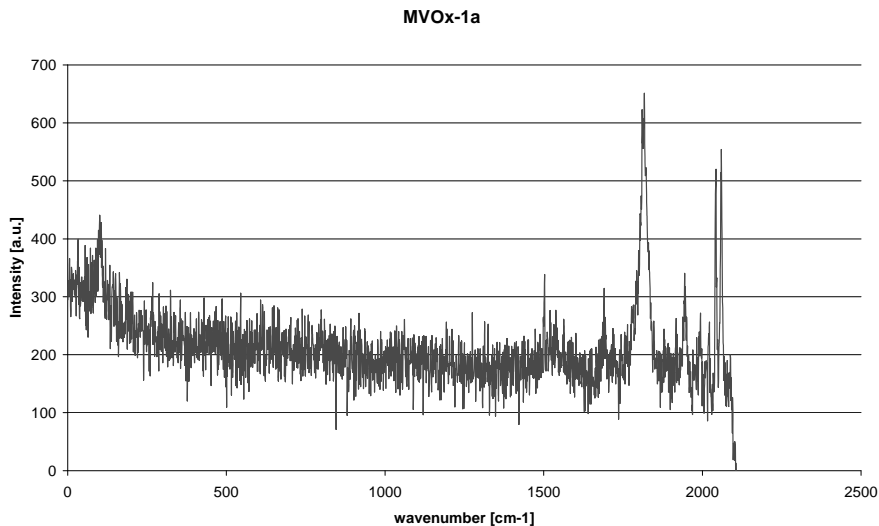


Fig. 5.12
Raman spectrum on carried on for just a few cycles.

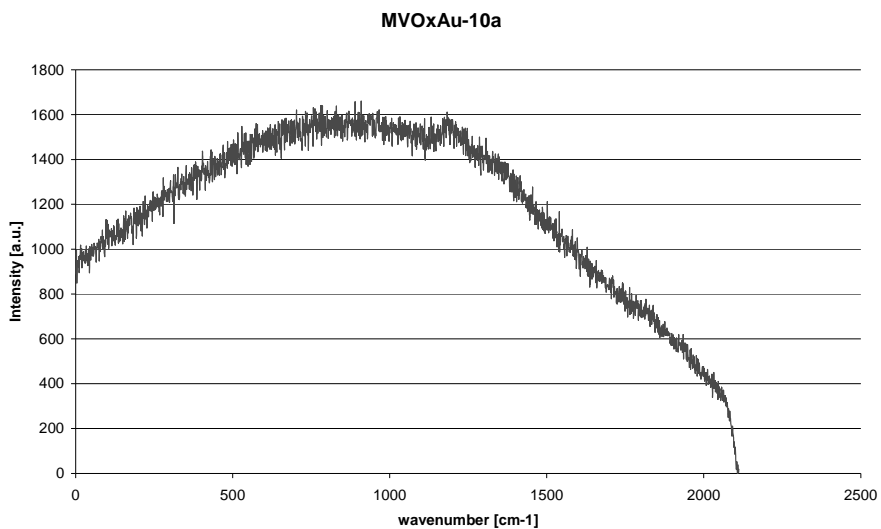


Fig. 5.13
Raman spectrum on
MVOxAu10a

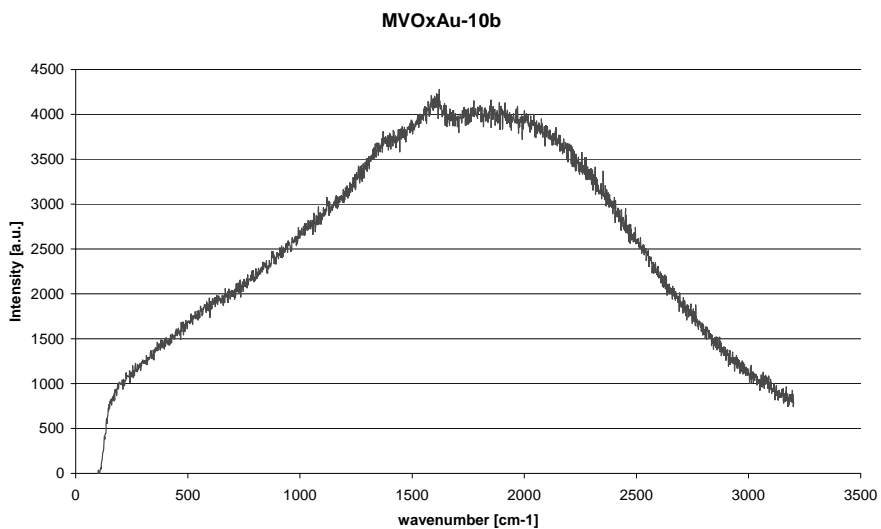


Fig. 5.14
Raman spectrum on
MVOxAu10b

Fig. 5.15 5.1.4 XRD of MVO, MAu and MVOxAu

XRD spectrum on
Left: MVOx1c;
Right: MAu2b showing
the main peak of
Gold.

XRD was also used to characterize the films and showed the production of monoclinic Vanadium (IV) Dioxide in all cases as shown in the following spectra. XRD spectrum on MVOx1c (Fig. 5.15 left) demonstrates that Vanadium (IV) Dioxide has been deposited in a monoclinic phase but the peaks are not very marked due to the bad crystalline structure.

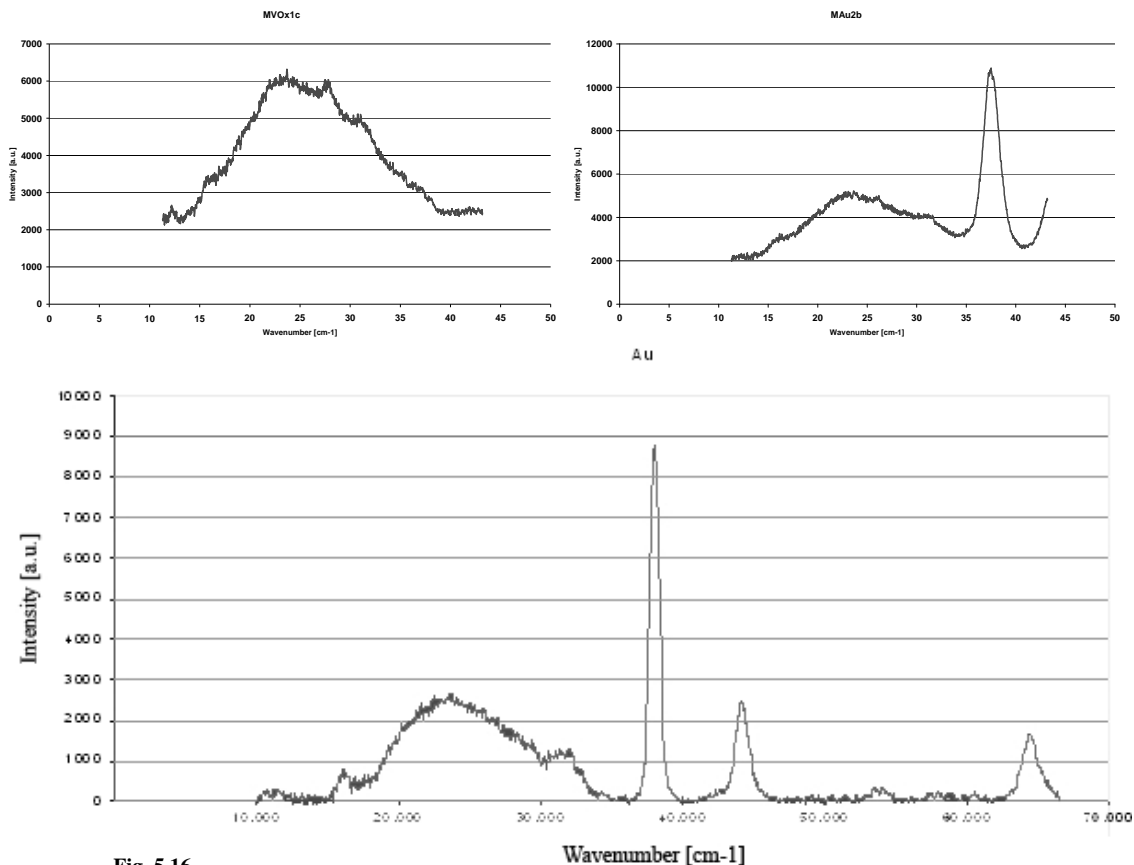


Fig. 5.16

XRD Spectrum on a Gold film on the whole range. It shows the three main peaks of Gold. In this case the film is very well crystallized. (Source: Spectrum supplied by Mr. Paolo Melgari)

XRD on MVOxAu samples showed that, in all the cases, Vanadium (IV) Dioxide has been deposited in the monoclinic phase, but it is never well crystallized, as well as Gold that is present in the structure.

To understand if the film can arrange in a more crystalline structure, some of the samples had been annealed and XRD was performed again, as shown in the next graphs. The blue graphs represent the non-annealed status while the purple one were recorded after the annealing process.

As it can be seen there was no improvement in the crystalline structure of the films and some of them turned from VO_2 to V_2O_5 . MVOxAu9a sample (Fig. 5.18 top right) is the only one that does not show a big change in the structure. MVOxAu6a (Fig. 5.17) shows that in the film there is a few of Vanadium (IV) Dioxide so the coating mainly consists of Gold.

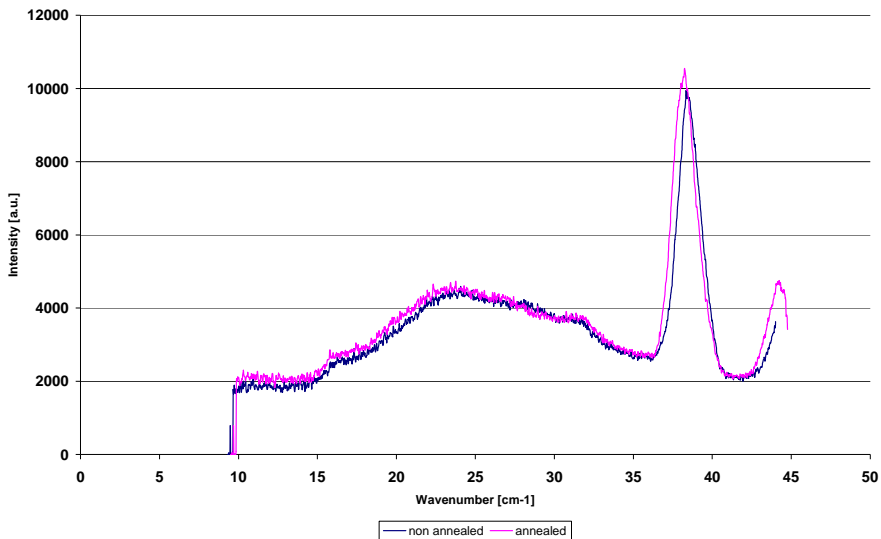


Fig. 5.17
XRD Spectrum on MVOxAu6a.

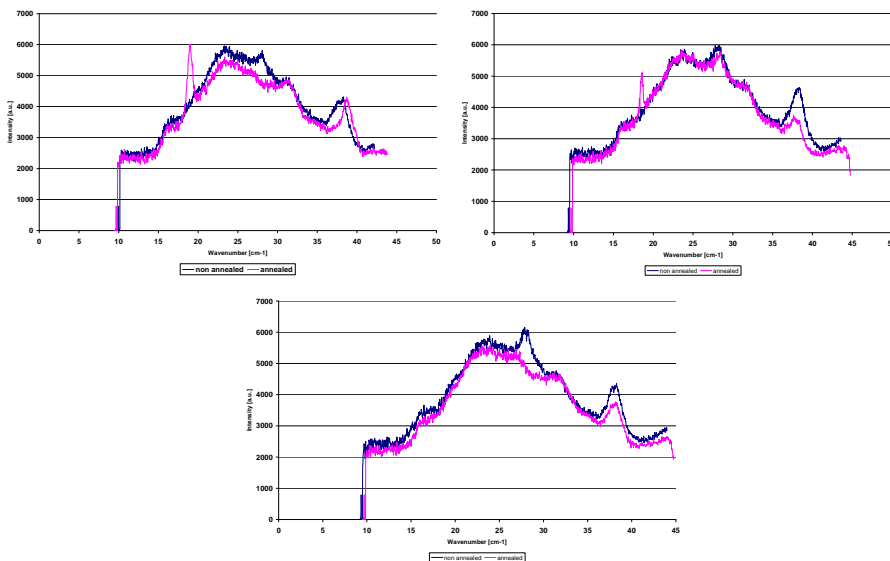


Fig. 5.18
XRD Spectrum on
Top left: MVOxAu3c
Top right: VOxAu9a
Bottom: MVOxAu11a

5.1.5 SEM/EDAX of MVO_x , MAu and MVO_xAu

SEM was used to record high resolution images of the sample surface taking back-scattered electrons (bs) images and secondary electrons (se) images. EDAX was used to quantify the amount of the chemical species in comparison to the Silica of the substrate, the glass with SiO_2 coating. Following there are some images taken using this technology to some differences in the films' structures. SEM of MAu2a (Fig. 5.19) show a coating with a good uniform coverage of the surface and Gold nanoparticles size of ~ 100 nm diameter. SEM of MVO_x1b (Fig. 5.20) show a coating with a good uniform coverage of the surface and Vanadium nanoparticles' size of about 50 nm wide.

Fig. 5.19

SEM on MAu-2a
Left: se - 2.500X
Middle: bs - 2.500X
Right: se - 100.000X

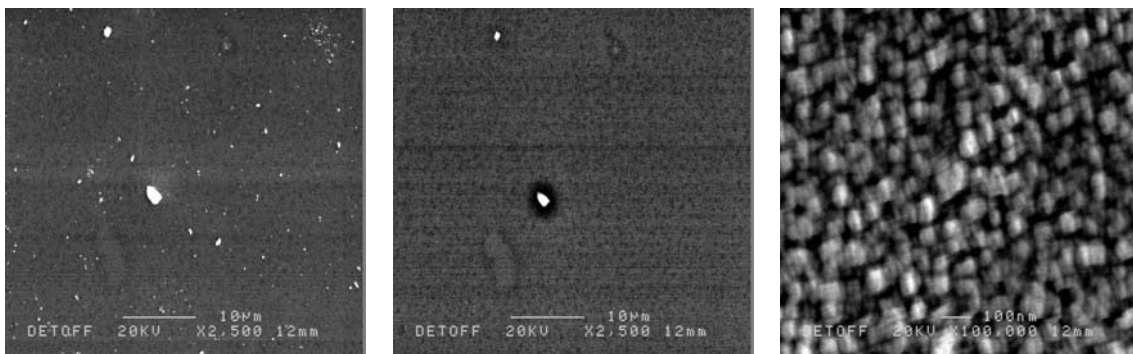
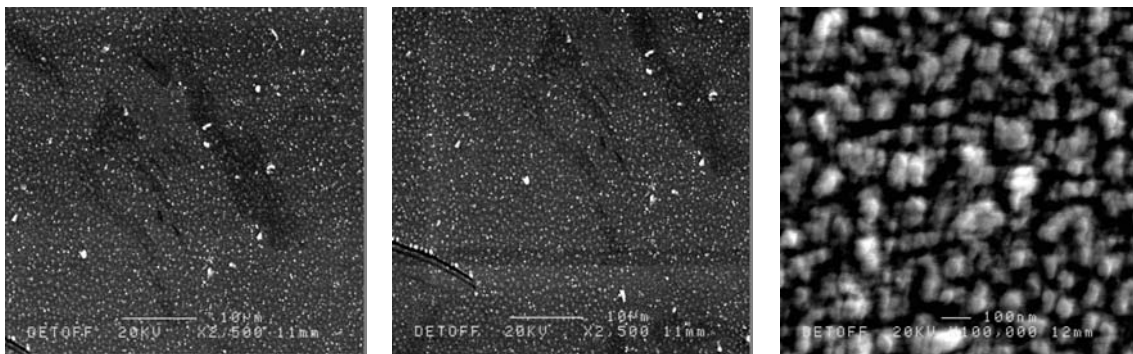
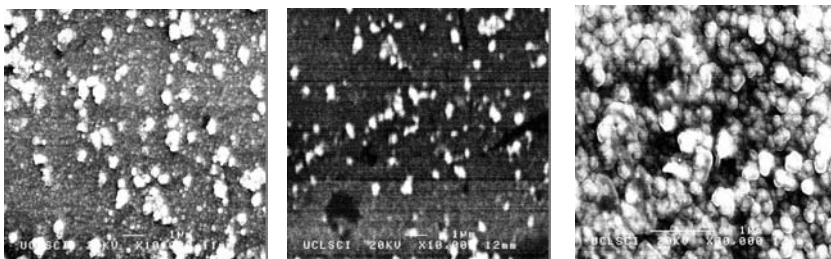


Fig. 5.20

SEM on MVO_x-1b
Left: se - 2.500X
Middle: bs - 2.500X
Right: se - 100.000X

Fig. 5.21

SEM on MVO_xAu13b
10.000X: se (left), bs (mid)
SEM on MVO_xAu14a
30.000X: se (right)



SEM on MVOxAu13b (Fig. 5.21 left and middle) show that Gold is almost present in the film matrix: the brighter spots in the right image. SEM on MVOxAu14a (Fig. 5.21 right) show nanoparticles with round shape.

SEM on MVOxAu2a (Fig. 5.22) show a particular way of film's growth (left) and the two enlargements of the matrix (middle and right) show a good uniformity in the coverage and a particle size of ~ 120 nm.

SEM on MVOxAu8a (Fig 5.23) show a different way of growth as the matrix doesn't seem regular and the nanoparticles have an lengthened shape.

Fig. 5.22

SEM on MVOxAu2a

Left: se - 3.000X

Middle: se - 9.000X

Right: se - 100.000X

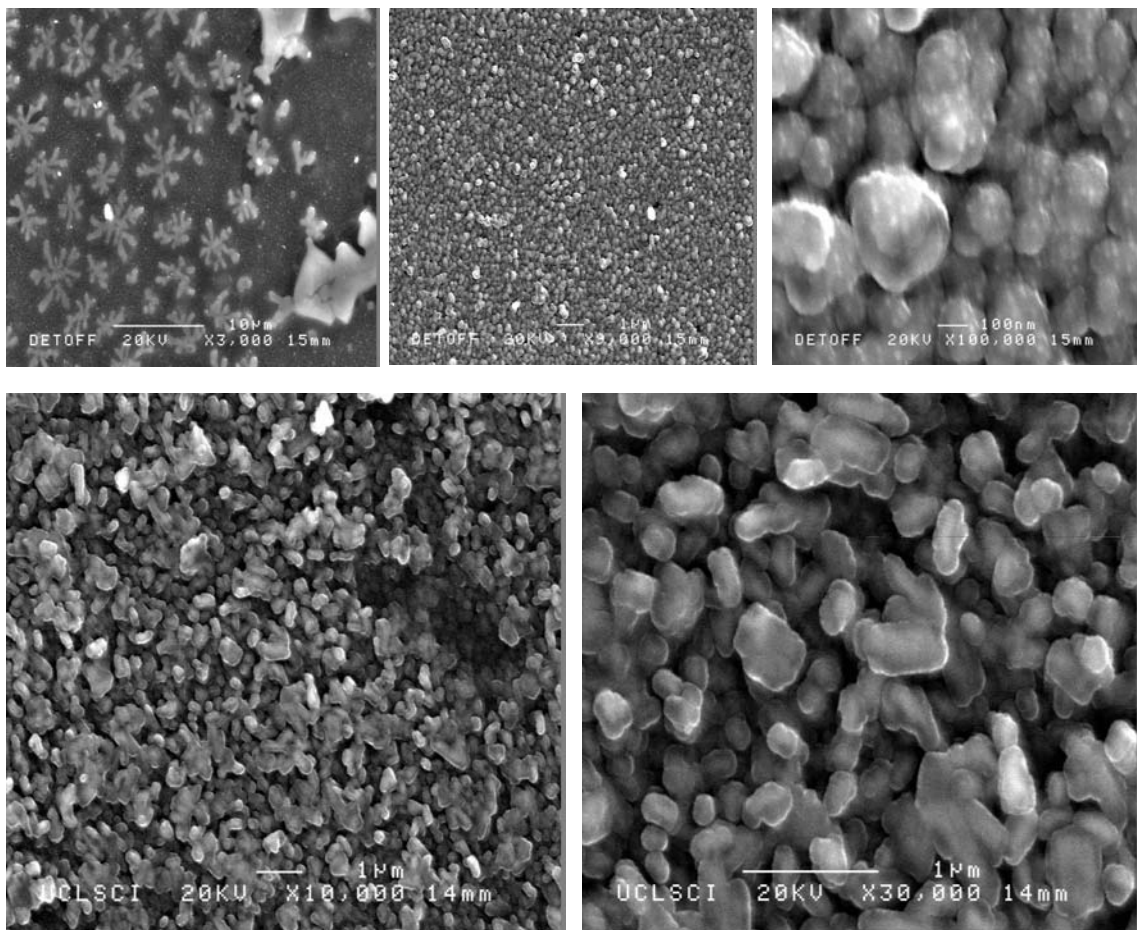


Fig. 5.23

SEM on MVOxAu8a

Left: se - 10.000X

Right: se - 30.000X

5.1.6 Thickness of MVOx, MAu and MVOxAu

Coatings' thickness has been calculated from EDAX analysis considering the amount (atomic weight %) of Vanadium (IV) Dioxide and Gold in comparison to the substrate of SiO₂-coated glass Silica's data. EDAX had been performed on both large areas and spots. Calculations were performed considering both 1) the large areas only and 2) all the areas (large areas and spots), thus achieving two different results for each film. When the two results are quite similar it can be said that the average value identifies films' thickness in a quite correct way.

Tab. 5.2 Different thickness calculated from EDAX analysis			
Sample	Thickness 1) [nm]	Thickness 2) [nm]	Average thickness [nm]
MVOxAu2a	141	143	142
MVOxAu3c	265	185	225
MVOxAu4a	44	43	43,50
MVOxAu8a	226	259	242,50
MVOxAu9a	177	190	183,50
MVOxAu11a	85	91	88
MVOxAu13b	37	47	42
MVOxAu14a	103	87	95

5.1.7 Colour of MVOx, MAu and MVOxAu

The films' colour is very important to identify the possible use of the coatings in the building market. Calculations were performed by Dr. Russell Binions, from Reflectance and Transmittance data achieved previously.

Tab. 5.3 Colour specifications.										
Sample	Transmission					Reflectance				
	lambda	Purity	L*	a*	b*	lambda	Purity	L*	a*	b*
MAu2a	480	4,6	63,6	-2,44	-2,65	577	22,4	50,33	4,44	12,5
MVOx1b	572	15,3	77,32	0,45	12,61	481	4,26	61,44	-2,78	-2,11
MVOxAu1b	562	15,6	62,64	-5,82	11,97	562	63,72	63,72	-6,27	13,04
MVOxAu2a	570	29,9	67,83	-1,42	22,71	575	8,83	50,03	1,16	4,67
MVOxAu3a	483	10,8	70,33	-9,48	-5,24	487	9,13	49,01	11,06	2,21
MVOxAu3c	567	23,1	57,72	-3,31	15,79	491	2,87	39,99	2,65	0,01
MVOxAu4a	488	10,8	65,15	-14,7	-1,71	494	11,05	57,03	12,56	-1,23
MVOxAu8a	570	40,3	54,89	-0,4	26,02	463	1,98	25,64	0,25	-0,96
MVOxAu9a	566	39,8	53,63	-6,08	26,11	568	8,02	62,26	-0,97	5,77
MVOxAu10a	570	43,1	52,66	-2,19	27,32	558	16,32	35,23	7,67	-10,2
MVOxAu11a	561	16	59,06	-5,92	11,75	547	8,54	50,4	6,14	-4,97
MVOxAu13a	561	3,6	90,43	-2,16	3,87	590	4,78	35,25	2,23	1,75
MVOxAu14a	567	7,5	80,63	-1,58	6,74	464	5,26	33,02	0,72	-2,99

5.2 Experiments 2: use of surfactant - MVOxAuT and MVOxT

Of all the films deposited previously, it was chosen the one that had showed the best optical properties, MVOxAu9a, and its flow rate conditions:

- Plain: 2 L/min⁻¹;
- Bubbler: 4 L/min⁻¹;
- Aerosol: 1 L/min⁻¹,

were used to continue the experiments adding a surfactant as discussed previously. Precursor solutions were made by dissolving 40 mg of HAuCl₄ in 25 ml of Methanol followed by the addition of Tetraoctylammonium Bromide (TOAB) at various concentrations as shown in the following table:

N°	HAuCl ₄ [g]	TOAB [g]	Methanol [ml]
1	0.040	1.0	25
2		0.5	
3		0.25	
4		0.12	
5		0.06	

The solution was stirred, as it is shown in the sequence below (Fig. 5.24), for 10 min, during which time the colour changed from pale yellow to dark orange, associated with the substitution of chloride for bromide ions in the gold coordination sphere:



As previously done, with each set of conditions two samples were produced to ensure that the technique can be considered reproducible and each sample had been given a name, MVOxAuT or MVOxT, followed by a number and a letter to identify the sample. The addition of TOAB to the precursor mix strongly affected the appearance of the deposited films, compared with the

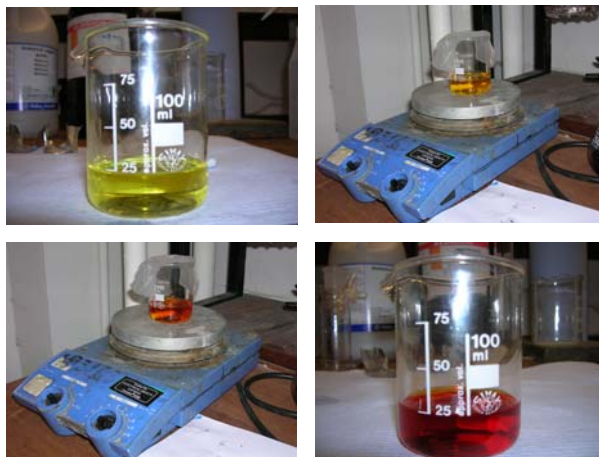


Fig. 5.24
From top left, clockwise: solution of HAuCl₄ with TOAB just added; stirring after 2 min; after 6 min; after 10 min.

previous depositions using $\text{VO}(\text{acac})_2 + \text{HAuCl}_4$; different portions of the film appeared either red, blue or green in transmission and in reflection, the films appeared metallic gold or green. Transition temperatures were higher than the T_c obtained without TOAB but the optical properties were improved a lot with a big shift between Transmittance and Reflectance. All the other analysis were performed and the film with the best properties proved to be $\text{MVO}_x\text{AuT}2c$ (0.5 g TOAB). It was also noted that the less TOAB had been added the darker the film appeared as it is shown in Fig. 5.25.

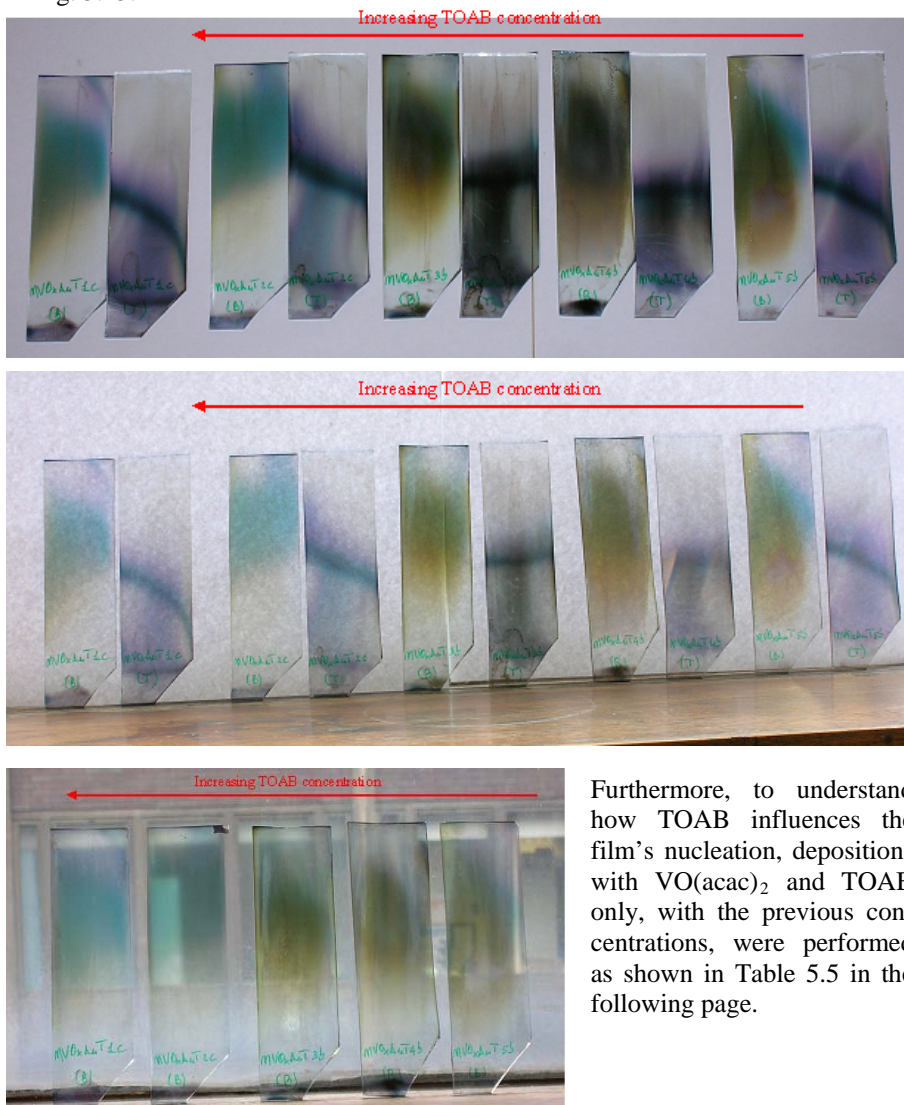


Fig. 5.25

Films of $\text{VO}(\text{acac})_2 + \text{HAuCl}_4 + \text{TOAB}$ where both the bottom and top plates are shown.

Top: reflected light;

Middle: transmitted light;

Bottom: bottom plates only. The different levels of coatings' transparency can be compared looking at the building outside the Chemistry Department's windows.

Furthermore, to understand how TOAB influences the film's nucleation, depositions with $\text{VO}(\text{acac})_2$ and TOAB only, with the previous concentrations, were performed as shown in Table 5.5 in the following page.

Tab. 5.5 Different conditions used to carry on depositions with $\text{VO}(\text{acac})_2 + \text{TOAB}$			
N°	Sample name	TOAB [g]	Methanol [ml]
1	MVOxT5	1.0	25
2	MVOxT1	0.5	
3	MVOxT3	0.25	
4	MVOxT2	0.12	
5	MVOxT4	0.06	

TOAB has shown a “dopant” effect on the films’ growth and that was completely unexpected. Transition temperatures are much lower than the previous T_c found out with Gold or Gold + TOAB. This fact suggests that TOAB influences the Vanadium

film’s growth and the nanocrystallites’ dimensions as demonstrated with the other analysis. As previously noted with the samples MVOxAuT, the less TOAB had been added the darker the film appeared as shown in the picture aside (fig. 5.26.).

There are shown coatings with 0,12 g and 0,50 g of TOAB, the one with the least quantity of TOAB was much darker than the other.

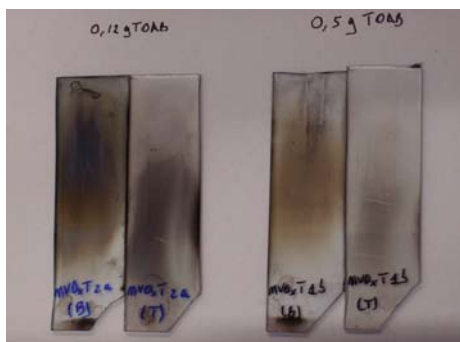


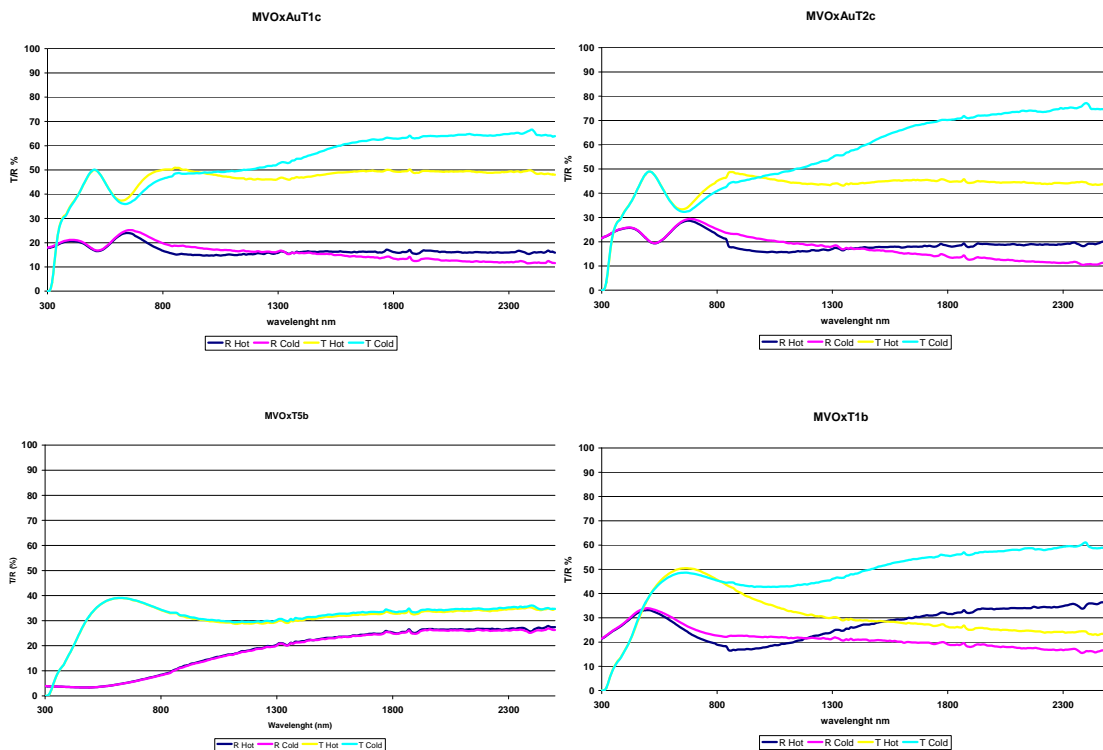
Fig. 5.26
 $\text{VO}(\text{acac})_2 + \text{TOAB}$ films, both the bottom and top plates are shown.
 Left: 0,12 g TOAB
 Right: 0,5 g TOAB

5.2.1 Reflectance and Transmittance of MVOxAuT and MVOxT

Following, there are some graphs showing the behaviours of Gold-doped Vanadium (IV) Dioxide + TOAB coatings. It can be reported that in the IR region Transmittance in the cold state is much higher, and Reflectance is much less, than what had been found without the use of the surfactant. The switch also between the hot state and the cold state is large ~ 35%, especially in the sample with 0,5 g of TOAB (fig. 5.27 right).

The same cannot be observed without the addition of Gold in the films, in fact the sample with 1 g of TOAB (fig. 5.28 left) doesn’t show any switch between the hot state and the cold one, behaviour that might be explained from the presence of Carbon within the matrix, as will be shown with the Raman analysis – or with the absence of VO_2 .

In the other sample (fig. 5.28 right), with 0,5 g of TOAB, the Transmittance is decreased in comparison to the analogous sample with Gold, the switch between the hot state and the cold one, in both transmittance and reflectance situation, still remains quite big.

**Fig. 5.27**

R/T of

Left: MVOxAuT1c
(TOAB = 1 g)
Right: MVOxAuT2c
(TOAB = 0,5 g)

Fig. 5.28

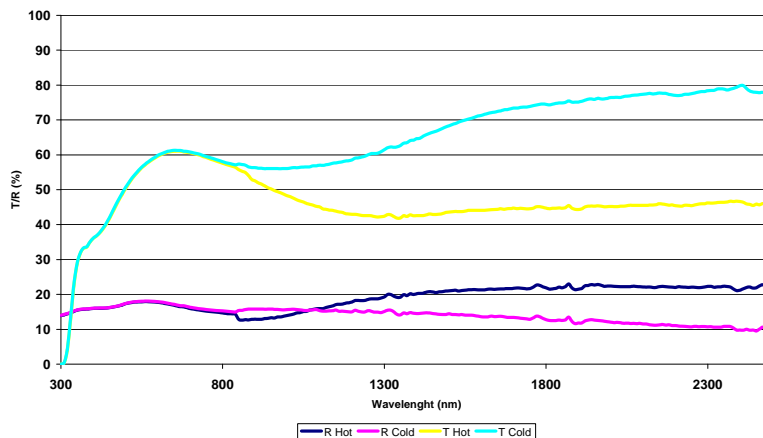
R/T of

Left: MVOxT5b
(TOAB = 1 g)
Right: MVOxT1b
(TOAB = 0,5 g)

Fig. 5.29

R/T of MVOxT3c
(TOAB = 0,25 g)

The following sample, MVOxT3c, with 0,25 g of TOAB added, optical properties seem to be improved quite a lot, showing a high value of Transmittance and a very low Reflectance in the cold state, while the switch remains significant.



5.2.2 Hysteresis and Tc of MVOxAuT and MVOxT

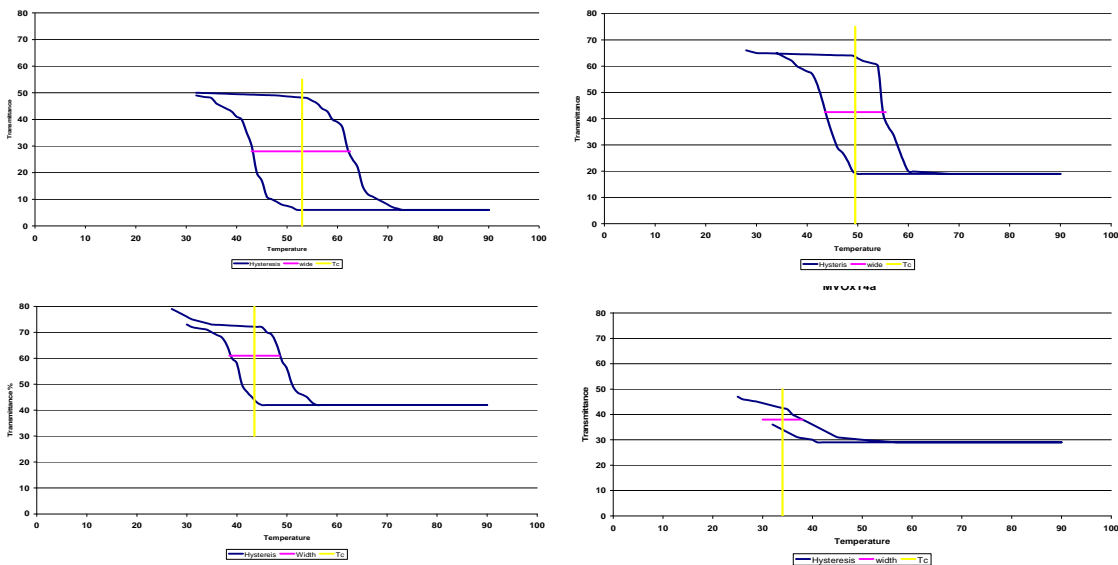
Hysteresis results for samples with gold show that the addition of TOAB in the [HAuCl₄ + Methanol] solution increases the size of the switch in comparison to the sample MVOxAu9a (T_c = 39 °C; %=19). For the sample MVOxAuT3b (fig. 5.30 left) a T_c of 53 °C with a 54 % switch was calculated, while for the MVOxAuT5b (fig. 5.30 right) T_c = 49,5 °C with a 47 % switch. Apparently, the less TOAB is added the bigger switch is shown while the T_c increases.

For the sample without Gold, but with Vanadium and TOAB only, it generally measured a lower T_c was measured, but the most surprising fact was that the T_cs are a lot lower than expected considering that no dopants had been used – thought carbon-doping may be occurring.

There are however no literature reports of this occurring.

- MVOxT3c (fig. 5.31 left) T_c = 43,5 °C %=38;
- MVOxT4a (fig. 5.31 right) T_c = 34 °C %=18.

Fig. 5.30
Hysteresis of
Left: MVOxAuT3b
(TOAB = 0,25 g)
Right: MVOxAuT5b
(TOAB = 0,06 g)



Tab. 5.6 Various Tc and % switch, with the different amount of TOAB				
TOAB [g]	With Gold		Without Gold	
	Tc	%	Tc	%
1,00	43,5	21	-	-
0,50	45,5	33	38,5	40
0,25	53	54	43,5	38
0,12	43	33	35	10
0,06	49,5	47	34	18

The sample MVOxT5b only (TOAB = 1,00 g) showed no Hysteresis, that happened because of the large amount of Carbon in the matrix, as it is observed with the Raman.

Fig. 5.31
Hysteresis of
Left: MVOxT3c
(TOAB = 0,25 g)
Right: MVOxT4a
(TOAB = 0,06 g)

5.2.3 Raman of MVOxAuT and MVOxT

Raman was performed on MVOxT samples only because it was noticed, as previously described, that transition temperatures are much lower than expected. What was searched for was the presence of Carbon that may affect the structure of the films and so their properties. Analysis showed that graphitic Carbon was present in almost every sample but MVOxT3c, as it is shown in the following figure.

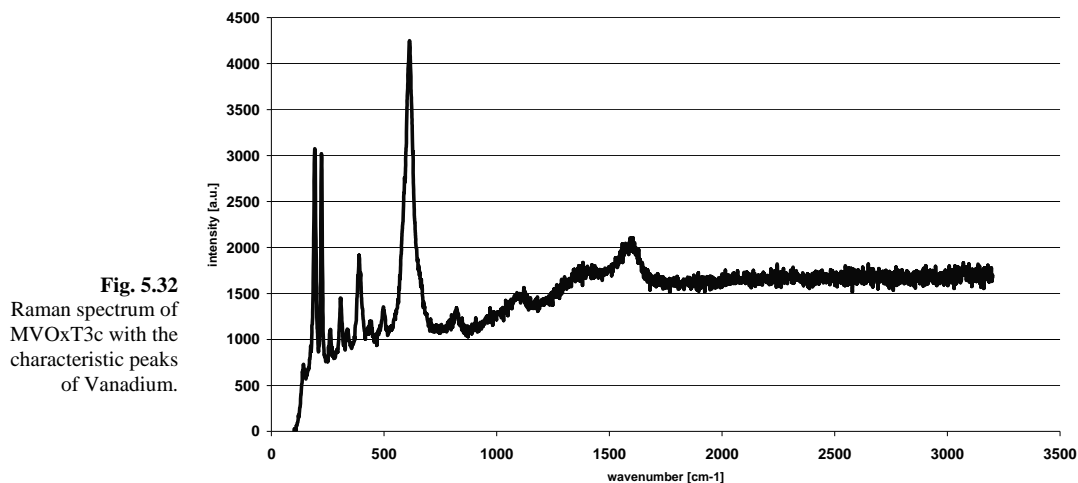


Fig. 5.32
Raman spectrum of MVOxT3c with the characteristic peaks of Vanadium.

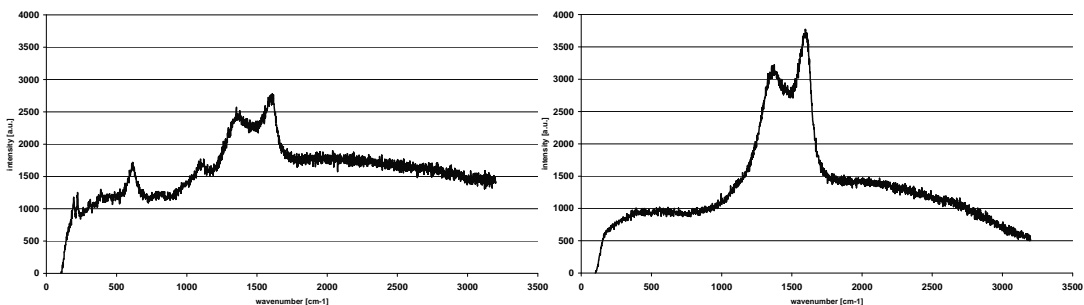


Fig. 5.33 a-b
Raman spectrum of
Left: MVOxT1b with both peaks of Vanadium (IV) Dioxide and Carbon.
Right: MVOxT5b with the characteristic peaks of Carbon.

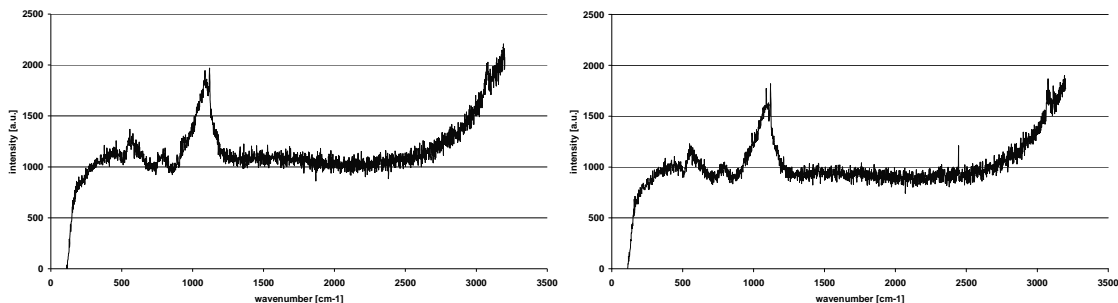
Raman analysis explained why MVOxT5b sample did not show neither switch nor hysteresis or differences in optical properties (Transmittance and Reflectance). The amount of Vanadium into the matrix is very low, almost absent, as it can be seen in fig. 5.32, so thermochromic properties are not very evident. As it can be seen in the spectra, there are no peaks referring to VO_2 , carbon related peaks only are present.

In the other sample MVOxT1b (fig. 5.33 left) Vanadium (IV) Dioxide and Carbon are both present and the two sets of peaks can be distinguished.

To understand the origin of Carbon into the matrix a further deposition with TOAB only, in a solution of 25 ml of Methanol, was carried on to interpret if it comes from

the surfactant or not. However, no film was deposited. At the deposition temperature used (525 °C) the surfactant is likely to be turned into CO₂ and other carbon species at the surface and be removed in the glass flow.

Fig. 5.34 a-b
Raman spectrum of
Left: MTOAB
Right: blank glass.



5.2.4 XRD of MVO_xAuT and MVO_xT

XRD analysis on MVO_xAuT showed that VO₂ and Gold had been deposited on the glass. The use of TOAB as surfactant made VO₂ more crystalline in comparison to the previous depositions made without the use of TOAB, as it is shown in the nearby graphs.

XRD spectra of MVO_xT showed a quite different result: VO₂ is still present but it is not very well crystallized as is demonstrated by the low intensity of the peaks. Sample MVO_xT5b showed almost no Vanadium peaks because, as previously discussed from the Raman analysis and optical properties, there is not so much Vanadium (IV) Dioxide as expected.

Following there are some spectra showing this fact:

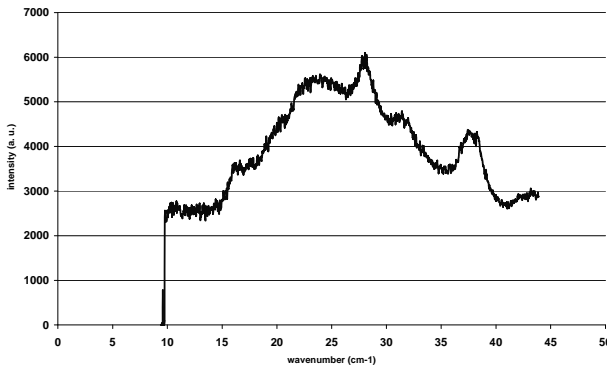


Fig. 5.35
Raman spectrum
MVO_xAuT4b that
shows the main peaks
of Vanadium (IV)
Dioxide and Gold.
VO₂ peaks resulted
more intense than
what obtained previ-
ously without the use
of TOAB.

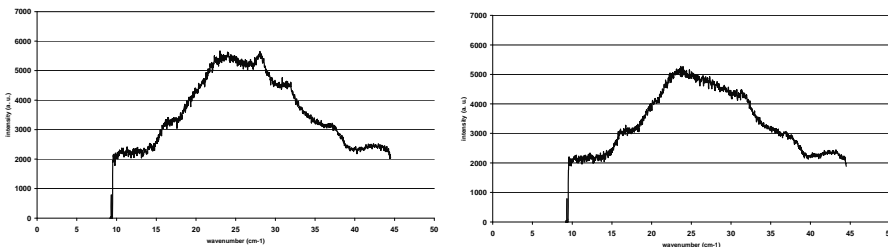


Fig. 5.36 a-b
Raman spectrum of
Left: MVO_xT1b
(TOAB = 0,50 g)
Right: MVO_xT5b
(TOAB = 1,00 g)

5.2.5 SEM/EDAX of MVOxAuT and MVOxT

Following there are some images taken using the SEM to show some differences in the films' structures.

Figure 5.37 a-b show the microstructure of MVOxAuT1c sample. It seems very compact with Gold nanoparticles in the matrix, the lighter areas in backscattered image.

Figure 5.38 a-b show the microstructure of MVOxAuT4b. It seems less regular and formed by round particles of 30 nm diameter with a lot of impurity.

It seems that the less TOAB is added to the precursor solution the less uniform the matrix is with the formation of round particles.

Figure 5.39 a-b show the microstructure of MVOxT1b where there is Vanadium (IV) Dioxide only with TOAB (0,50 g); the structure resulted to be quite irregular with different size-particles (20 ÷ 50 nm).

Fig. 5.37 a-b
SEM on
MVOxAuT1c

Left: se - 5.000X
Right: bs - 5.000X

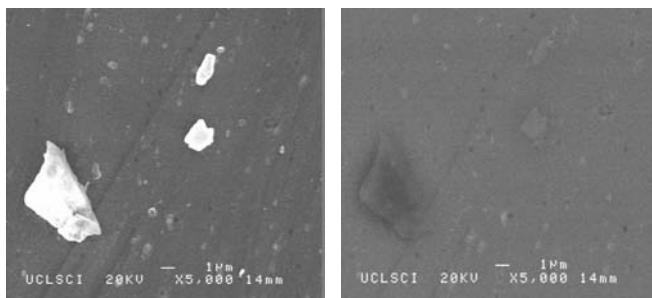


Fig. 5.38 a-b
SEM on
MVOxAuT4b

Left: se - 5.000X
Right: bs - 20.000X

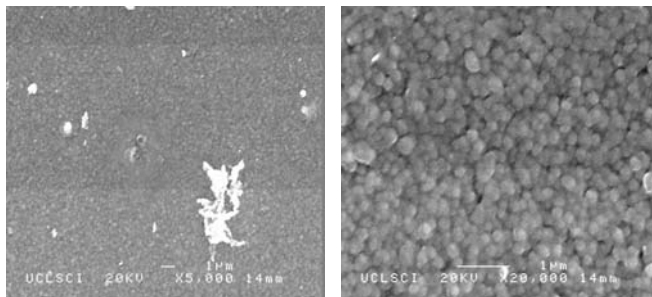
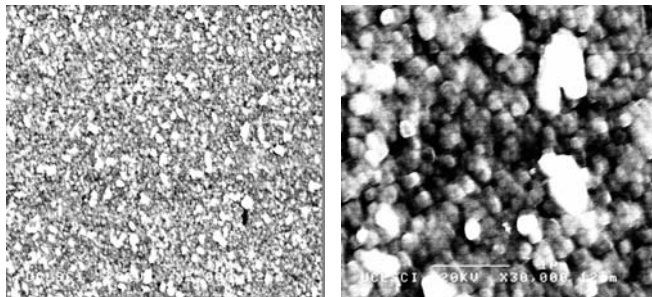


Fig. 5.39 a-b
SEM on MVOxT1b

Left: se - 5.000X
Right: se - 30.000X



Figures 5.40-42 show the microstructure of MVOxT3c (TOAB:0,25g), the structure was even more irregular with lots of holes surrounded by nanoparticles that result to be quite round but aggregated in a flower shape. A crack also on the sample surface is shown. It is interesting to notice the different way of the film growth on the glass with big differences in size and shape. The size of the particles in the crack (~ 50 nm) tends to be smaller than the particles in the other part of the film (~ 100 nm) and the coating in the crack seems to be more regular and uniform than the other part.

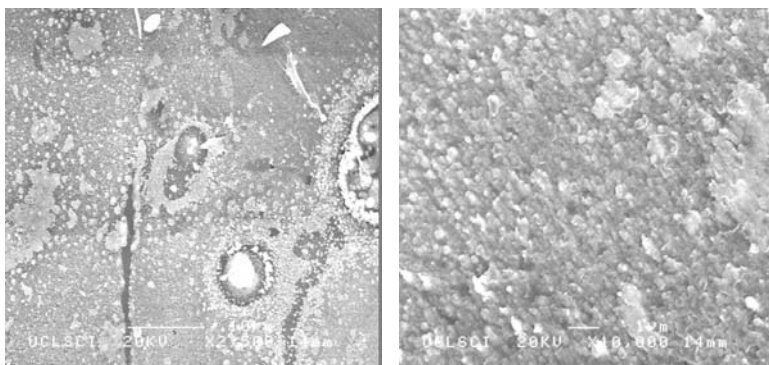


Fig. 5.40 a-b
SEM on MVOxT3c

Left: se - 2.500X
Right: se - 10.000X

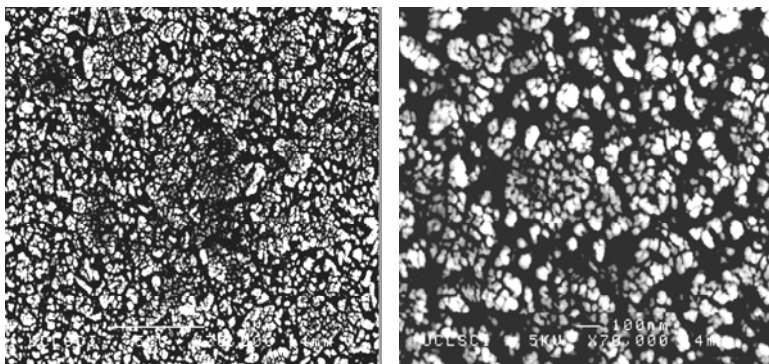


Fig. 5.41 a-b
SEM on MVOxT3c

Left: se - 30.000X
Right: se - 70.000X

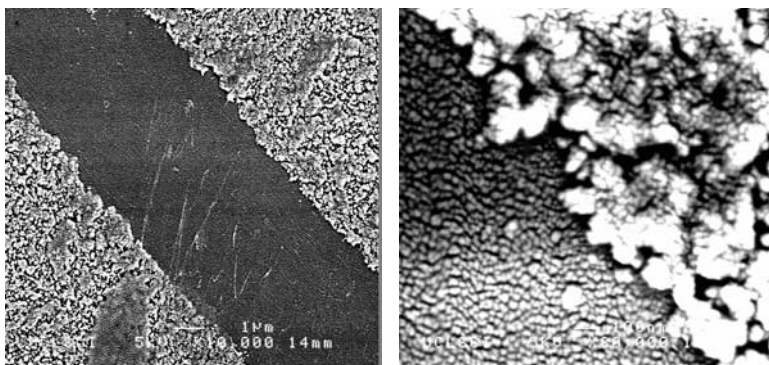


Fig. 5.42 a-b
SEM of a crack on
MVOxT3c surface

Left: se - 10.000X
Right: se - 80.000X

5.2.6 Thickness of MVOxAuT and MVOxT

Coating thickness has been calculated from EDAX analysis considering the amount (atomic weight %) of Vanadium (IV) Dioxide in comparison to Silica data coming from the substrate of SiO₂-coated glass. As previously done, EDAX had been performed on large areas and on spots so, to calculate the thickness of each film, calculations were performed considering both the large areas only and all the areas (large areas and spots) achieving two different results for each film. Often, the two results seem to be quite similar so it can be said that the average value is quite correct to identify films' thickness. In the table below MVOxAuT and MVOxT's average thicknesses are reported.

TOAB [g]	Sample	Average thickness [nm]	Sample	Average thickness [nm]
1,00	MVOxAuT1c	59	MVOxT5b	160
0,50	MVOxAuT2c	248	MVOxT1b	133,5
0,25	MVOxAuT3b	57	MVOxT3c	153,5
0,12	MVOxAuT4b	253	MVOxT2a	429
0,06	MVOxAuT5b	100,5	MVOxT4a	149

5.2.7 Colour of MVOxAuT and MVOxT

The films' colour is very important to identify the possible use of the coatings in the building market. Calculations were performed by Dr. Russell Binions, from Reflectance and Transmittance data achieved previously. Between the sample with Gold, a quite big shift can be noticed, that's because of the Gold nanoparticle that change the colour. The more Gold is present, the more blu the film appears.

Sample	Transmission					Reflectance				
	lambda	purity	L*	a*	b*	lambda	purity	L*	a*	b*
MVOxAuT1c	493	5,4	72,02	-10,4	0,6	495	8,72	51,15	8,94	-1,13
MVOxAuT2c	496	5,5	71,28	-12,1	1,8	530	10,29	53,85	8,88	-4,78
MVOxAuT3b	566	44,6	54,41	-6,37	29,67	559	6,58	47,91	3,55	-5,02
MVOxAuT4b	565	34,5	49,92	-6,65	21,59	545	9,61	46,18	6,66	-5,02
MVOxAuT5b	561	21,2	62,54	-8,1	16,25	596	1	60,17	0,87	0,51
MVOxT1b	570	25,4	71,48	-0,91	20,07	491	2,72	63,42	-4,3	0,01
MVOxT2a	569	36,6	60,97	-2,52	25,85	557	7,43	46,74	4,21	-5,24
MVOxT3c	571	16,4	79,37	0,19	13,86	565	4,76	49,19	-1,07	2,97
MVOxT4a	570	19,7	75,02	-1,07	16,17	500	1,87	55,95	-3,94	0,93
MVOxT5b	569	21	66,65	-1,7	15,77	591	9,6	23,15	3,5	2,69

6. THERMOCHROMIC GLASS BEHAVIOUR IN A BUILDING MODEL

6.1. Introduction

This simple home-made experiment was set up to validate the expected behaviour of the thermochromic glasses, produced previously, in a confined environment.

A simple model of a building room was built using polystyrene as walls; glazing were simulated using a float-produced blank glass and a Gold-doped Vanadium (IV) dioxide coated glass.

Then, the building model was irradiated by a IR light source and the inside temperature was measured in relation to the radiation time. Inside and outside glazing and radiated wall temperatures were also measured.

The analysis of the coated-glasses behaviours would make it easier to understand how these new coatings could work in a real situation since the only variable within the different models is the glass itself. In this way the increasing temperature in the confined environment – the model - could be directly related to glass optical properties.

6.2. Calculation of the model size

The Italian Decreto Ministeriale Sanità 5/7/1975 (ISO 10292) prescribes that the glazing area of a room in a civil building must be at least 1/8 of the floor area. One of the main problems was that the available coated glass samples (150 x 44 x 4 mm) are not very uniform in coverage so an area of 30 x 50 mm, that can be considered quite homogeneous in coverage, was used as glazing in the model.

The “room” size was calculated from this premise:

$$\begin{aligned} \text{Glazing area} &= 3 \times 5 \text{ cm} = 15 \text{ cm}^2 \\ \text{Floor area} &\leq 15 \text{ cm}^2 \times 8 = 120 \text{ cm}^2 \end{aligned}$$

So, imagining that a 1:50 scale model was planned, the real room would be 6 x 5 x 3 m with a 1,5 x 2,5 m window.

The walls' thickness of the model was calculated so that the polystyrene thermal conductivity would be as the same as a real masonry wall in order to simulate in a suitable way the exact materials behaviour in a building.

The calculation of the walls thickness was set up from the Fourier equation:

$$\frac{\Delta E}{\Delta t} = \lambda S \frac{\Delta T}{d} \quad (\text{eq. 6.1})$$

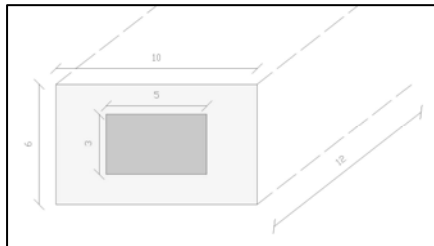


Fig. 6.1
Schematic model
dimensions in 1:50
scale.

where:

ΔE = heat quantity [Ws] crossing the walls in the time interval Δt [s];

λ = thermal conductivity $\left[\frac{W}{mK} \right]$;

S = wall surface [m²];

d = wall thickness [m];

ΔT = temperature difference between the two wall's surfaces [K].

Tab. 6.1 materials characteristics			
	$\lambda \left[\frac{W}{mK} \right]$	S [m ²]	D [m]
Brick wall	0,5	11,25	0,30
Limestone wall	1,3	11,25	0,30
Polystyrene	0,03	11,25	

$$1. \text{ Bricks wall: } \frac{\Delta E}{\Delta t} = \lambda S \frac{\Delta T}{d} = \frac{0,5 \times 11,25}{0,30} \Delta T = 18,75 \Delta T$$

$$2. \text{ Limestone wall: } \frac{\Delta E}{\Delta t} = \lambda S \frac{\Delta T}{d} = \frac{1,3 \times 11,25}{0,30} \Delta T = 48,75 \Delta T$$

$$3. \text{ Polystyrene: } \frac{\Delta E}{\Delta t} = \lambda S \frac{\Delta T}{d} = (0,03 \times 11,25) \frac{\Delta T}{d} = 0,3375 \frac{\Delta T}{d}$$

In order to have the same heat conductivity behaviour between a real masonry wall and a polystyrene one with the same initial conditions - ΔE , ΔT and Δt - it must result:

- Brick – polystyrene:

$$18,75 \Delta T = 0,3375 \frac{\Delta T}{d} \Rightarrow d(\text{polystyrene}) = 0,018m$$

- Limestone – polystyrene:

$$48,75 \Delta T = 0,3375 \frac{\Delta T}{d} \Rightarrow d(\text{polystyrene}) = 0,007m$$

Finally, to have an average behaviour and to have the model easier to build it was chosen to use 3 polystyrene sheets of 5 mm thick.

6.3 The experiment

The IR lamp used to radiate the model had a power of 150W and was produced by Osama. It was put at 70 cm and 50 cm above the model and the radiation last 50 minutes. By means of a 10 sensors thermocouple, some different temperatures were analyzed: internal temperature in two different points, internal and external wall temperature, internal and external glass temperature, surrounding environment temperature. All the data acquired were put into graphs, as shown below.

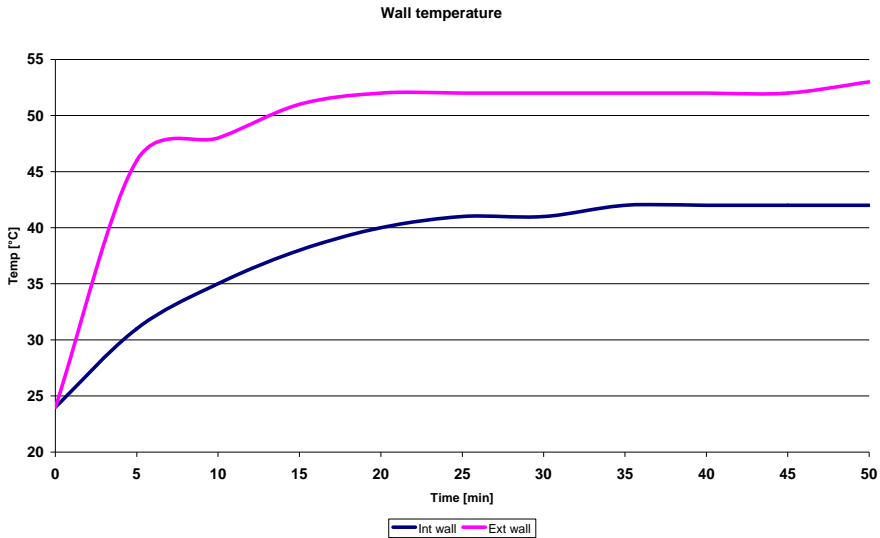


Fig. 6.2
Graph showing the internal and external temperature of the model's walls during the experiment.

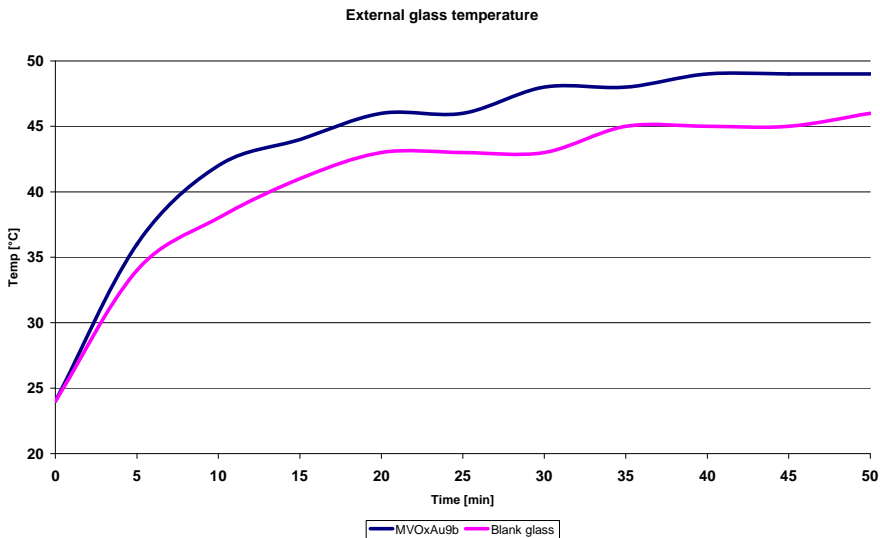
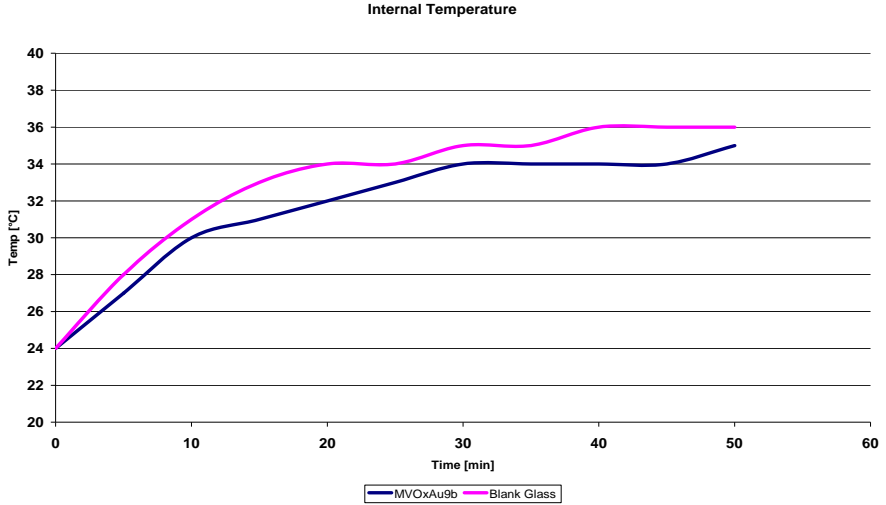
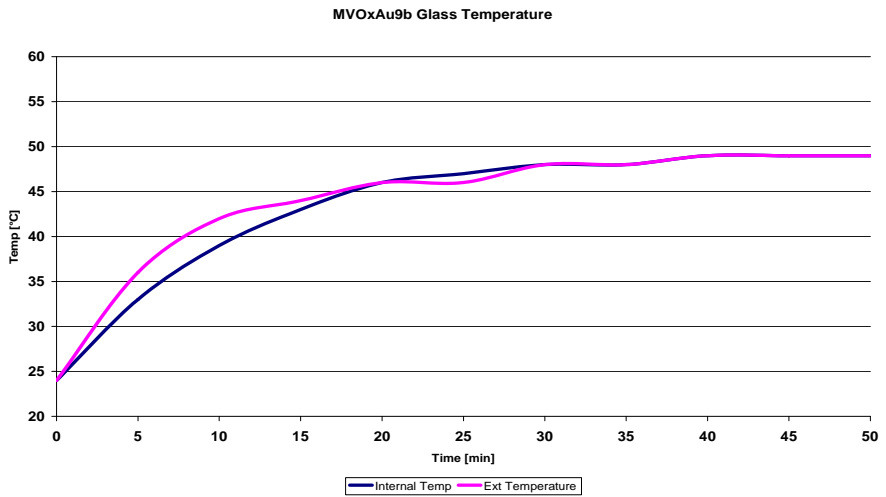


Fig. 6.3
Graph showing the external temperatures of both MV0xAu9b and blank glass during the experiment [50 cm].

**Fig. 6.4**

Graph showing the internal temperatures of the model with both MVOxAu9b and blank glass during the experiment [50 cm].

**Fig. 6.5**

Graph showing the internal and external temperature of the MVOxAu9b glass during the experiment [50 cm].

As expected, using the coated glass the internal temperature of the model increases more slowly than the one related to the non-coated glass. An interesting fact is that the coated glass is much hotter than the blank one but the heat transmitted by conduction is lower as the radiated wall transmits in the same way in both the experiment but the internal temperatures tend to be different. The polystyrene walls work quite well since the difference between the internal and external surfaces temperature is about 10 °C and so, the heat transmitted through them is not high.

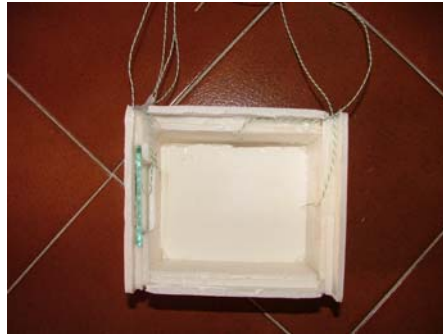
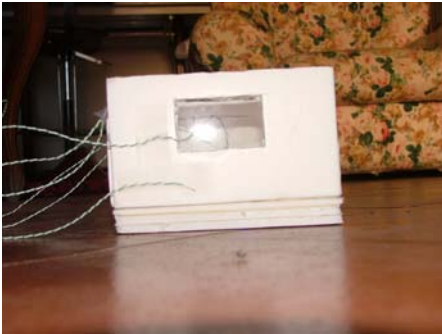


Fig. 6.6 a-b
The model with the blank glass, front view (left) and top view (right).



Fig. 6.7 a-b
The model with the thermocouple.



The effect seen in this experiment is not very evident since the metal-to-semiconductor transition temperature (T_c) of the coated glass sample used - MVO_xAu9b - is $39^\circ C$.

This fact means that from the starting point of analysis - which is the environmental temperature ($24^\circ C$) - to the working temperature $T_c = 39^\circ C$ the IR part of the spectrum is almost entirely transmitted and not reflected.

In other words, the high T_c of the sample lets a great quantity of heat enter through the glass by radiation just before the transition that makes the coating reflective to the IR radiation.

But, at the end, it can be said that this coating enhances, as expected, the glass properties in the way it should do.

Fig. 6.8
The experiment with the lamp placed 70 cm far from the model.

7. ENERGY MODELLING PERFORMANCE

7.1. Introduction

The easiest way to test the energy performance of the thermochromic glazing is to simulate the way they would respond if they were installed in a building.

These virtual simulations, due to the development of more powerful computers and software, allow us to predict the energy behaviour of various building components, either traditional or enhanced, under real internal and external conditions.

7.2 The simulation program – Energy Plus™

The software used in this work to perform simulations is Energy Plus™ which is one of the most advanced Building Energy Simulation Programs. It was mainly developed by Lawrence Berkeley National Laboratory with funds from the U.S. Department of Energy (DOE). Energy Plus™ is an energy analysis and thermal load simulation program. Based on a user's description of a building from the perspective of the building's physical make-up, associated mechanical systems, etc., the program will calculate the heating and cooling loads necessary to maintain thermal control set points, conditions throughout a secondary HVAC¹ system and coil loads,

and the energy consumption of primary plant equipment as well as many other simulation details that are necessary to verify that the model is performing as the actual building would.

Many of the simulation characteristics have been inherited from the legacy programs of BLAST (Building Load Analysis and System Thermodynamics) and DOE-2².

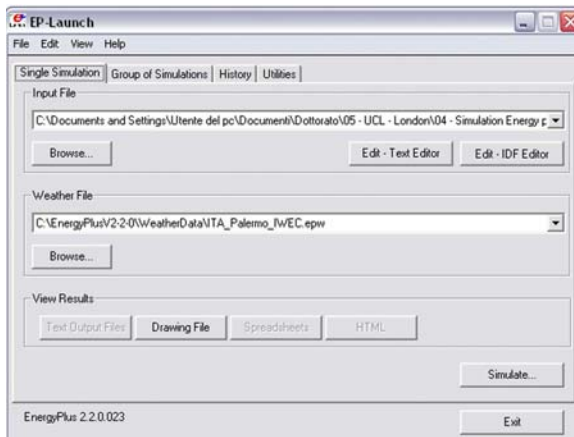


Fig. 7.1
Energy Plus,
Launch Program.

The main features of Energy Plus software are the following:

- **Integrated, simultaneous solution** where the building response and the primary and secondary systems are tightly coupled;
- **Sub-hourly, user-definable time steps** for the interaction between the thermal zones and the environment; variable time steps for interactions between the thermal zones and the HVAC systems;

¹ HVAC: Heating, Ventilation and Air Conditioning.

² DOE-2: freeware building energy analysis program that can predict the energy use and cost for all types of buildings.

- **ASCII text based weather, input, and output files** that include hourly or sub-hourly environmental conditions, and standard and user definable reports, respectively;
- **Heat balance based solution** technique for building thermal loads that allows for simultaneous calculation of radiant and convective effects at both in the interior and exterior surface during each time step;
- **Passing heat conduction** through building elements such as walls, roofs, floors, etc. using conduction transfer functions;
- **Improved ground heat transfer modelling** through links to three-dimensional finite difference ground models and simplified analytical techniques;
- **Combined heat and mass transfer model** that accounts for moisture adsorption/desorption either as a layer-by-layer integration into the conduction transfer functions or as an effective moisture penetration depth model (EMPD);
- **Thermal comfort models** based on activity, inside dry bulb, humidity, etc.;
- **Anisotropic sky model** for improved calculation of diffuse solar on tilted surfaces;
- **Advanced fenestration calculations** including controllable window blinds, electrochromic glazing, layer-by-layer heat balances that allow proper assignment of solar energy absorbed by window panes;
- **Day-lighting controls** including interior illuminance calculations, glare simulation and control, luminary controls, and the effect of reduced artificial lighting on heating and cooling;
- **Atmospheric pollution calculations** that predict CO₂, SO_x, NO_x, CO, particulate matter, and hydrocarbon production for both on site and remote energy conversion.

The simulation allows to more accurately investigations on the effect of undersizing fans and equipment and what impact may have on the thermal comfort of occupants within the building. The diagram below shows a basic overview of the integration of these important elements of a building energy simulation.

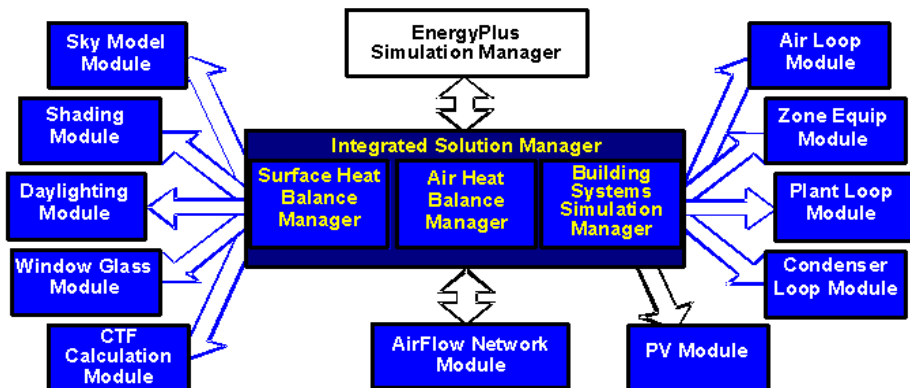


Fig. 7.2
Energy Plus
Internal elements.
(source: EP user
manual)

The greatest advantage of Energy Plus is the ability to input spectral distributions of new glazing units covering the spectrum from 300 nm to 2500 nm in 5 nm steps. This is particularly convenient in the investigation of performance of the thermochromic glass.

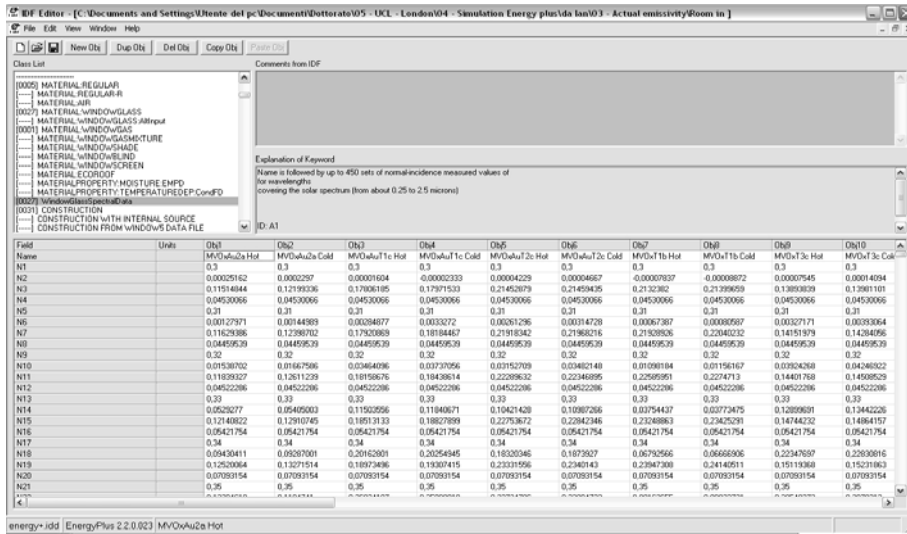


Fig. 7.3 Energy Plus IDF editor.

We are going to run a series of simulations³ with different configurations and settings in order to evaluate their performance through different weather sceneries. We will be looking into factors as annual heating load, cooling load, day lighting and artificial lighting load, glare discomfort and surface temperature of the glazing. The simulation set period is one year, having the results hour by hour for each day of the year.

7.3 Model

7.3.1 Geometry

In order to test the performance of the thermochromic glasses produced⁴ a very simple model of a room in a building was constructed in Energy Plus. As the model built for the home-made experiment of the previous chapter, the room has external dimensions 6 x 5 x 3 m (length x width x height) and it is placed so that the axis of every wall is perpendicular to one of the orientation North, South, West and East.

3 The initial model was developed by Dr. Ian Ridley – Lecturer, The Barlett School of Graduate Studies, UCL, London.

4 Analysis has been carried on samples previously produced in this work (look at previous chapters: MVOx, MVOxAu, MVOxAuT) as well as some samples produced by Dr. Russell Binions in a previous work.

The room is thought to be in the façade of a generic building so that just one wall is exposed to the external environment (weather, sun, wind, etc.); the remaining three walls are not affected by external conditions. In this work, the particular case of a room in the edge of a building – with two external exposed walls – has been omitted. The building is located in the northern hemisphere and the external wall is supposed to be exposed to the southern side. Two different sets of simulations were run with two different glazing widths: following the Italian regulation on building construction⁵ one model has a 1,5 x 2,5 m width window in the middle of the wall surface (fig. 7.4 a), that is to say the 25 % of the total surface; the other was carried out with a whole glazing wall (fig. 7.4 b), that is to say the 100 % of the surface. Thus to understand in which case thermochromic glasses work better in different extreme situations and how they perform.

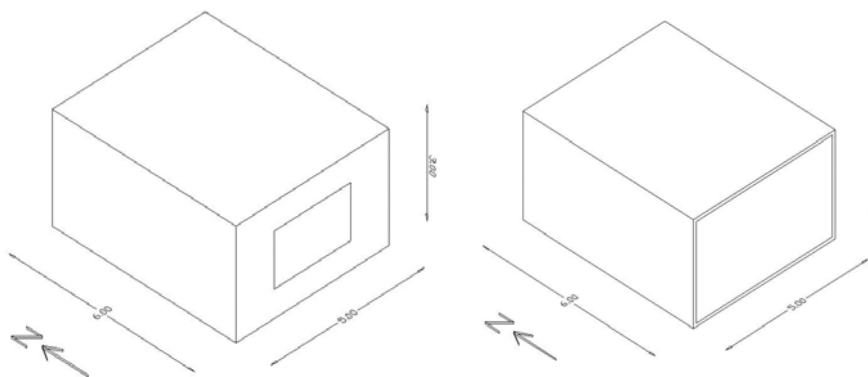


Fig. 7.4 a-b
The two room models: on the left – window 1,5 x 2,5 (25%); on the right - glazing wall (100%).

7.3.2 Location – Weather data

The simulations were run for different cities of Europe and one of Africa thus to cover a wide range of climates conditions through the northern hemisphere – from the South Europe-Mediterranean climate (hot summer, warm winter and high solar radiation), to the continental climate of the Centre of Europe (warm summer, cold winter and high solar radiation), to the North European climate (quite warm summer, very cold winter and low solar radiation).

In the images in the next page, the world climate chart by W. Köppen and the world surface temperature distribution are shown.

It was decided to perform simulations within European cities only to understand how thermochromic glasses work through different climate conditions in the northern hemisphere.

Further simulation could be performed for specific latitudes if required. All the weather data files were provided from the US Department of Energy (DOE) website.

⁵ Look at the previous chapter for more details about Italian regulation.

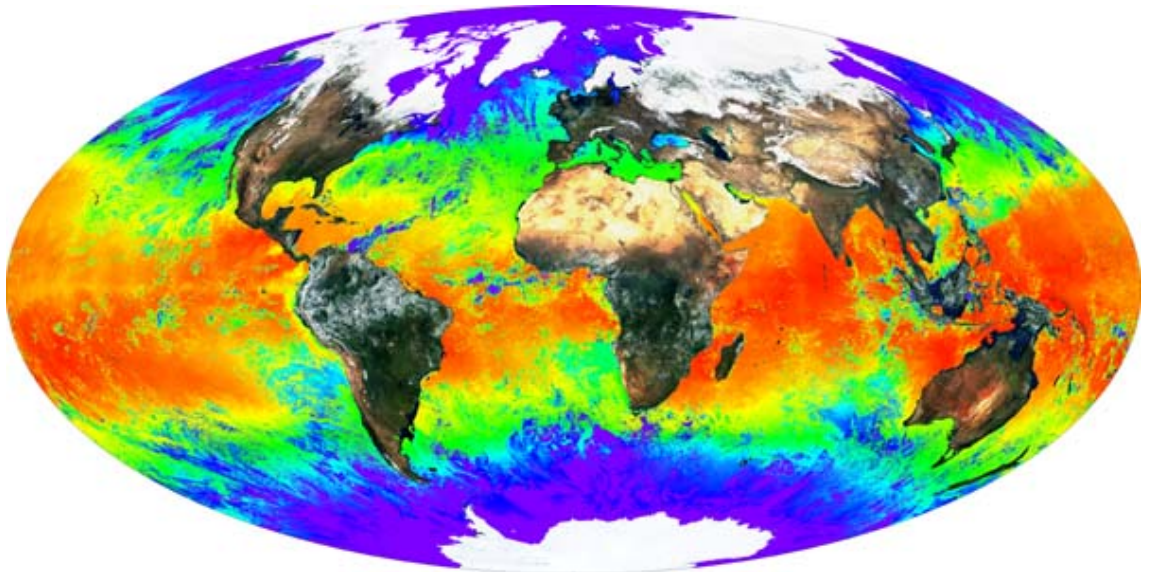
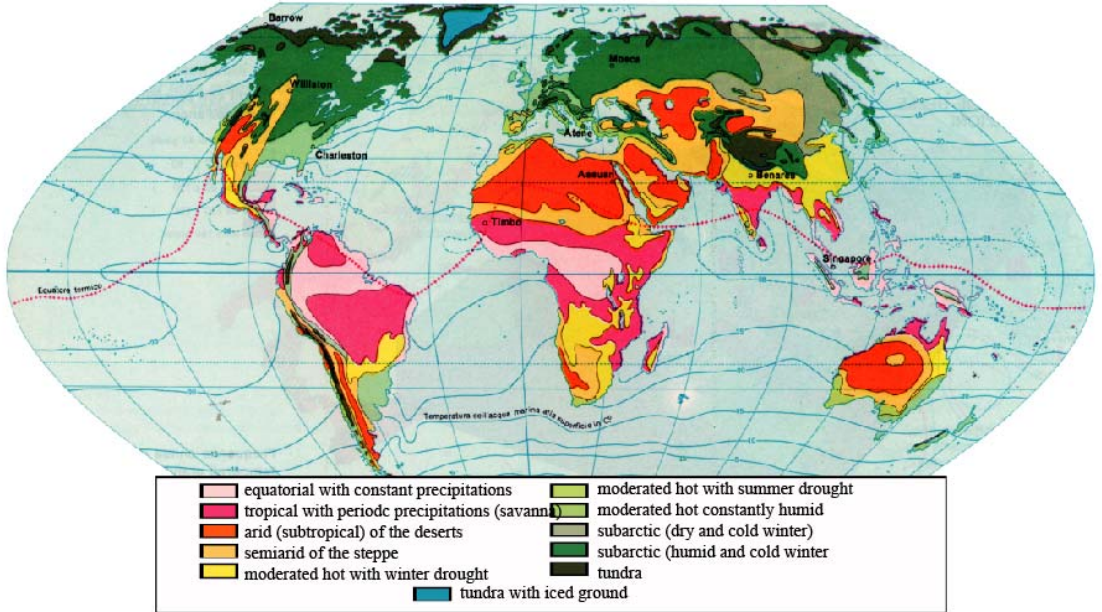


Fig. 7.5 a-b

Top: World climate chart by W. Köppen.

Bottom: World surface temperatures. Red stands for hot climate while white stands for snow and ice.

(Source: Fondazione Ammiraglio Michelagnoli Onlus, 2004)

Tab. 7.1 Geographical parameters of the locations used to carry on the simulations				
City	Latitude (deg)	Longitude (deg)	Elevation (m)	Time zone (hr)
Il Cairo, Egypt	30,13	31,4	74	+2
Palermo, Italy	38,18	13,1	34	+1
Roma, Italy	41,8	12,23	3	+1
Milano, Italy	45,62	8,73	211	+1
Paris (Orly), France	48,73	2,4	96	+1
London (Gatwick), UK	51,15	-0,18	62	0
Moscow, Russia	55,75	37,63	156	+3
Helsinki, Finland	60,32	24,97	56	+2



Fig. 7.6
Map with the locations where the simulations had been performed.

In the following pages, the outdoor dry bulb temperatures through a year are shown for each city. It is also shown the average minimum and maximum temperature for each month of the year.

Cairo - Egypt		
Month	T max	T min
January	23	7
February	26	8
March	28,4	9
April	39,3	11
May	41,2	13
June	42,6	17,9
July	36,1	21,6
August	37,2	21
September	36,9	18,5
October	34	16,4
November	28,1	9,3
December	22,8	8,9

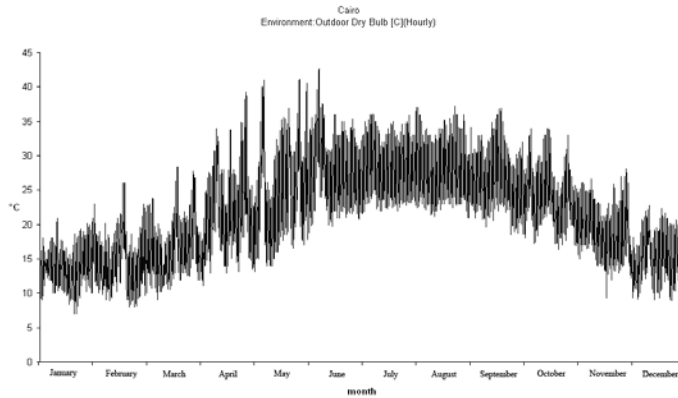


Fig. 7.7
Cairo, temperature flow over a year.

Palermo - Italy		
Month	T max	T min
January	16,6	7
February	17	5
March	21,9	8,6
April	27,7	7,9
May	29,9	13,9
June	29,7	15,4
July	32,7	19,2
August	30	21,2
September	29,9	16,5
October	28,6	15,4
November	24,3	12,6
December	21,6	7,8

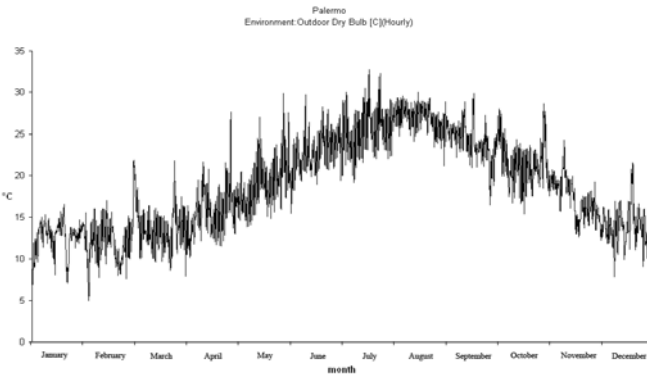


Fig. 7.8
Palermo temperature flow over a year.

Roma - Italy		
Month	T max	T min
January	17,4	-4
February	16,2	-1,9
March	18	-0,9
April	20,3	3,2
May	28,1	7,1
June	30,8	12,3
July	30,4	17,4
August	31,5	15,2
September	26,9	12,6
October	27,6	6,8
November	22,1	3,1
December	18,9	-0,4

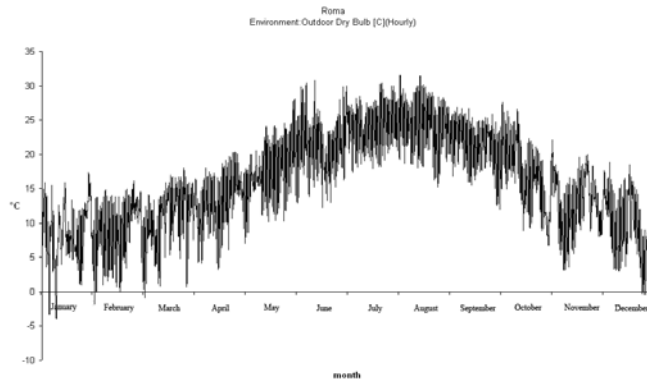
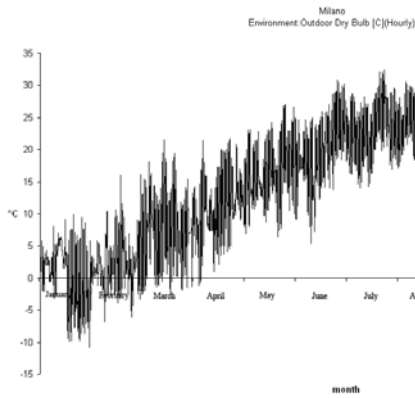


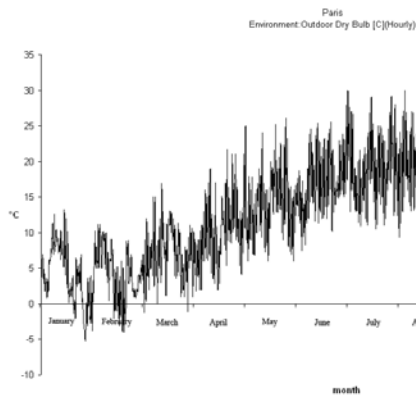
Fig. 7.9
Roma, temperature flow over a year.

Fig. 7.10
Milano, temperature
flow over a year.



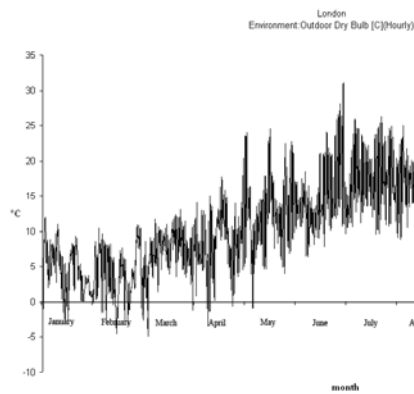
Milano - Italy		
Month	T max	T min
January	9,9	-10,8
February	16	-6,8
March	21,6	-3,2
April	21,7	-1,4
May	27	6,5
June	30,9	5,4
July	32,5	13,9
August	30,6	13,4
September	28,7	7,3
October	22,6	1,1
November	18,7	-3
December	12,5	-8,5

Fig. 7.11
Paris, temperature
flow over a year.



Paris - France		
Month	T max	T min
January	13,3	-5,2
February	11,2	-4
March	17	-1,3
April	21,7	0,9
May	26,1	6
June	25,6	7,5
July	30	10,6
August	30	9
September	27,1	6,9
October	22,5	1,3
November	14,6	-1
December	13,1	-5,5

Fig. 7.12
London, temperature
flow over a year.



London - UK		
Month	T max	T min
January	12	-2,8
February	10,9	-4,5
March	13	-4,9
April	17,7	-3,4
May	24,7	-0,9
June	31,1	6,4
July	26,2	9,6
August	28,7	7,2
September	21,2	3,6
October	19,3	-0,9
November	14,7	-4,9
December	12,4	-5,8

Moscow - Russia		
Month	T max	T min
January	2,6	-20,4
February	6,5	-25
March	11	-13,6
April	20,4	-3,1
May	24,9	1,9
June	29,4	7,4
July	30,5	9,1
August	28	4,7
September	22,3	1,4
October	14,3	-3,3
November	6,8	-19,9
December	3,5	-23,4

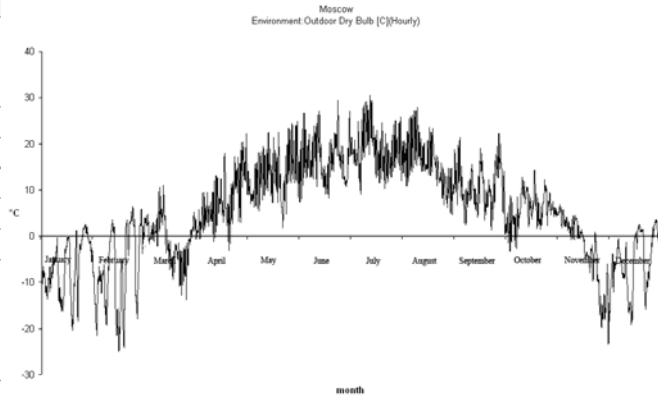


Fig. 7.13
Moscow, temperature
flow over a year.

Helsinki - Finland		
Month	T max	T min
January	2,8	-20
February	2,1	-21,4
March	5,1	-12,3
April	16,2	-4,4
May	24,1	-0,5
June	24,7	2,6
July	27,7	6,5
August	28,6	5,9
September	19,4	-1,1
October	11,6	-3,6
November	7,5	-14,8
December	3,6	-18,4

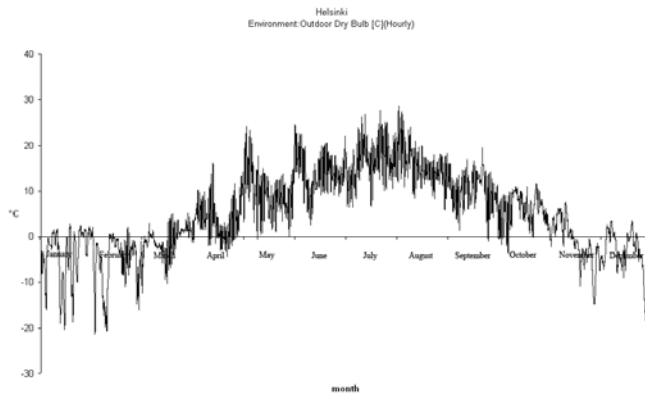


Fig. 7.14
Helsinki, temperature
flow over a year.

7.3.3 Construction of the model - Materials

The construction of the model of the building is simple and it respects the current building regulations. Materials data were taken from EP library.

Following, there is a list of building element materials:

- the external wall is made of 25 cm of heavyweight concrete on the exterior, 5 cm of expanded polyurethane as insulation and a 2 cm layer of plaster as interior finish;
- the internal walls are made of 12 cm of lightweight concrete on the exterior and a 2 cm layer of plaster as interior finishing;
- the roof is made of 25 cm of heavyweight concrete and a 2 cm layer of interior plaster;

Fig. 7.15
Details of construction materials.

- the floor is made of 25 cm of heavyweight concrete and a 3 cm layer of soft-wood as paving.

The details of the materials can be seen in the following figure (fig. 7.15).

Field	Units	Obj1	Obj2	Obj3	Obj4	Obj5
Name		HEAVYWEIGHT CONCRETE	EXPANDED POLYURETHANE	PLASTER · GYPSUM	WOOD · SOFTWOOD	lightweight concrete
Roughness		MediumRough	MediumRough	Smooth	MediumSmooth	MediumRough
Thickness	m	0,25	0,05	0,02	0,03	0,12
Conductivity	W/m-K	1,95	0,03	0,22	0,11	0,53
Density	kg/m ³	2240	40	720,83	512,59	1280
Specific Heat	J/kg-K	900	1210	830	1380	840
Absorptance: Thermal		0,9	0,9	0,9	0,9	0,9
Absorptance: Solar		0,65	0,5	0,78	0,78	0,65
Absorptance: Visible		0,65	0,5	0,78	0,78	0,65

Where:

- *Absorptance Thermal* represents the fraction of incident long wavelength radiation that is absorbed by the material. This parameter is used when calculating the long wavelength radiant exchange between various surfaces and affects the surface heat balances. Values for this field must be between 0,0 and 1,0 (with 1,0 representing “black body” conditions);
- *Absorptance Solar* represents the fraction of incident solar radiation that is absorbed by the material. Solar radiation includes the visible spectrum as well as infrared and ultraviolet wavelengths. This parameter is used when calculating the amount of incident solar radiation absorbed by various surfaces and affects the surface heat balances. Values for this field must be between 0,0 and 1,0.
- *Absorptance Visible* represents the fraction of incident visible wavelength radiation that is absorbed by the material. Visible wavelength radiation is slightly different than solar radiation in that the visible band of wavelengths is much more narrow while solar radiation includes the visible spectrum as well as infrared and ultraviolet wavelengths. This parameter is used when calculating the amount of incident visible radiation absorbed by various surfaces and affects the surface heat balances as well as the daylighting calculations. Values for this field must be between 0,0 and 1,0.

7.3.4 Construction of the model - Glazing

In both the cases analyzed, the single window and the glazed-wall, the window is always double glazed with a 12 mm air cavity. Simulations were carried on with 5 commercial Pilkington products and 11 different thermochromic glazing⁶.

7.3.4.1 Pilkington glazing

In this section the Pilkington glasses' properties will be discussed to have a better idea of their behaviour through the spectrum towards the visible light and the IR ra-

⁶ Thermochromic glasses were produced within different researches at the Christopher Ingold Laboratories – Chemistry Department – University College London (UCL) – London.

diation. That is quite useful to understand the differences between commercial glazing and glass with a thermochromic coating. The five Pilkington glasses analyzed here and used to carry on the simulations, are static glasses, that is to say that they do not change their optical properties from the cold state to the hot one. This is, maybe, the biggest difference between commercial products and thermochromic glazing.

As previously said, the window in the model is always double glazed. In the table below the different glazing configurations are shown for the Pilkington glazed window.

The outer pane is always the coated glass, with the coating positioned in surface 2, with the exception of the K Glass™ that must be put in surface 3, as suggested by the company itself.

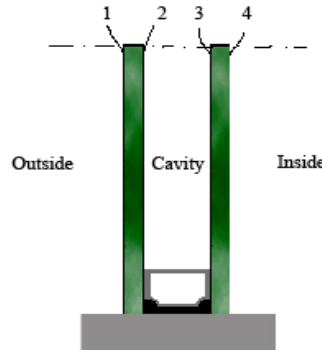


Fig. 7.16 Window surfaces.

Tab. 7.2 Pilkington glazing configurations

Case	Outer pane	Cavity	Inner pane
1	Optifloat™ Clear 4 mm (SiO ₂ coated)	12 mm	Optifloat™ Clear 4 mm (SiO ₂ coated)
2	Optifloat™ Clear 4 mm (SiO ₂ coated)	12 mm	K Glass™ 4 mm
3	Suncool™ Brilliant 66\33 4 mm	12 mm	Optifloat™ Clear 4 mm (SiO ₂ coated)
4	Arctic Blue™ 4 mm	12 mm	Optifloat™ Clear 4 mm (SiO ₂ coated)
5	Activ™ Blue 4 mm	12 mm	Optifloat™ Clear 4 mm (SiO ₂ coated)

In the image below the Pilkington products main properties are shown as they were edited in Energy Plus™ - IDF Editor.

Field	Units	Obj23	Obj24	Obj25	Obj26	Obj27
Name		Blank Glass	K Glass	Suncool Brilliant	Arctic Blue	Activ Blue
Optical Data Type		Spectral	Spectral	Spectral	Spectral	Spectral
Name of Window Glass Spectral Data Set		Blank Glass	K Glass	Suncool Brilliant	Arctic Blue	Activ Blue
Thickness	m	0,004	0,004	0,004	0,004	0,004
Solar Transmittance at Normal Incidence		0,83	0,664	0,36	0,453	0,801
Solar Reflectance at Normal Incidence: Front Side		0,082	0,111	0,502	0,054	0,122
Solar Reflectance at Normal Incidence: Back Side		0,082	0,092	0,374	0,054	0,117
Visible Transmittance at Normal Incidence		0,91	0,822	0,737	0,69	0,838
Visible Reflectance at Normal Incidence: Front Side		0,089	0,109	0,12	0,063	0,149
Visible Reflectance at Normal Incidence: Back Side		0,089	0,098	0,129	0,063	0,146
IR Transmittance at Normal Incidence		0	0	0	0	0
IR Hemispherical Emissivity: Front Side		0,837	0,17	0,03	0,837	0,833
IR Hemispherical Emissivity: Back Side		0,837	0,837	0,837	0,837	0,837
Conductivity	W/m-K	1	1	1	1	1
Dirt Correction Factor for Solar and Visible Transmittance						
Solar Diffusing						

We are going to analyze the typical spectra⁷ of the different glazing by Pilkington to understand their differences in properties and behaviour.

Fig. 7.17 Pilkington products properties from EP - IDF Editor¹.

7 www.pilkington.com

Optifloat™ Clear (SiO_2 coated) is the pane glass used for the previous depositions and has been discussed previously. Transmittance is very high through all the wavelength, especially in the visible part of the spectrum while the Reflectance is quite low ($< 10\%$) (Fig. 7.18).

K Glass™ is a low emissivity coated glass. It has a so-called low emissivity coating which is positioned on surface 3 (counting from the outside) of the Insulating Glass Unit (IGU). This coating reflects heat back into the room whilst also letting in free heat from the sun known as passive solar gain. The glass in the windows absorbs heat then radiates it again on the colder outside surface. The low emissivity coating is a poor radiator of heat. So the heat absorbed by the coated glass does not travel across the air gap to the outer pane and the cold outside world. Instead the coating reflects the heat back into the room. Transmittance is quite high ($> 80\%$) in the visible part of the spectrum, thus letting in light, while it lowers towards the IR part. Reflectance is about 10% in the visible and near IR part and it becomes higher in the far IR part reflecting over than 60% of the radiation (Fig. 7.19 top left).

Suncool™ Brilliant is a solar control product with high visible light transmittance and low emissivity. It is an off-line product offering a very high level of thermal insulation. It is suitable for any situation where excessive solar heat gain and heat loss are an issue, from building façades to large atria and glass linkways. It presents a high natural light transmission (80%) and very low total energy transmission providing an interior comfortable environment. Transmittance is quite high ($> 80\%$) in the visible part of the spectrum, thus letting in light, while it lowers a lot towards the near IR part of the spectrum going to almost zero towards the far IR. Thus preventing lot of the heat gain entering the building through the window. Reflectance is about 5% in the visible light increasing very fast in the near IR part reflecting over than 100% of the far IR radiation (Fig. 7.19 top right).

Arctic Blue™ is a body tinted float glass providing high daylight transmittance, good solar control and its blue colour creates a comfortable interior without sacrificing natural light. It has good solar and thermal performance with high visibility providing a crisp natural view from the interior. Transmittance is quite high ($\sim 80\%$) in the visible part of the spectrum, thus letting in light, while it lowers a lot towards the near IR part of the spectrum increasing again ($\sim 60\%$) towards the far IR. Reflectance is very low, about 5% through all the spectrum (Fig. 7.19 bottom left).

Activ Blue™ is a blue glass that combines self-cleaning properties with solar control performance. It uses daylight and rainwater to breakdown and wash away organic dirt from exterior surfaces. Its blue colour also helps keep internal temperatures cool whilst still maintaining excellent light transmittance. Activ™ spectrum is basically equal to the Activ Blue™ one. Transmittance is quite high ($\sim 80\%$) and constant through the spectrum, recalling the Blank Glass behaviour. Reflectance is about 10% with a higher value in the first part of the visible range (Fig. 7.19 bottom right).

Optifloat™ Clear

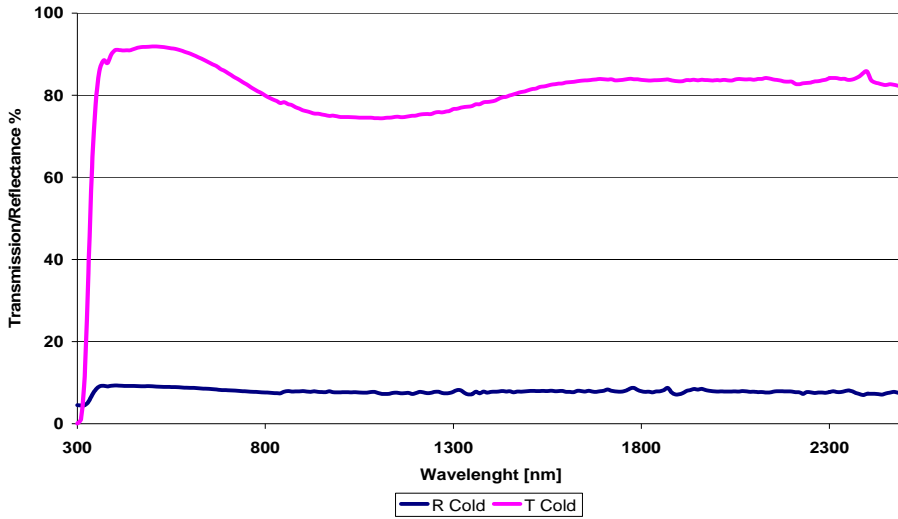
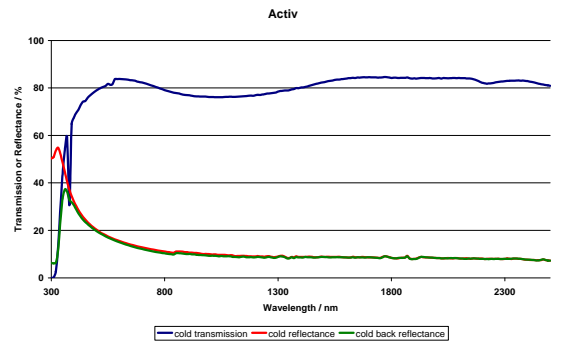
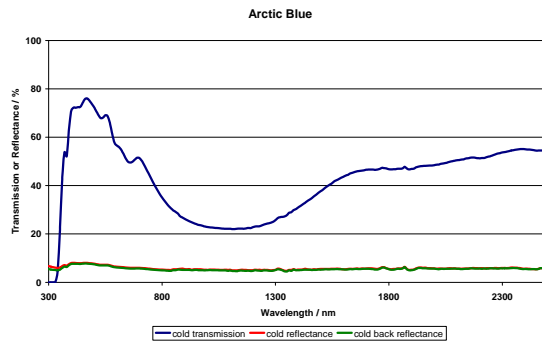
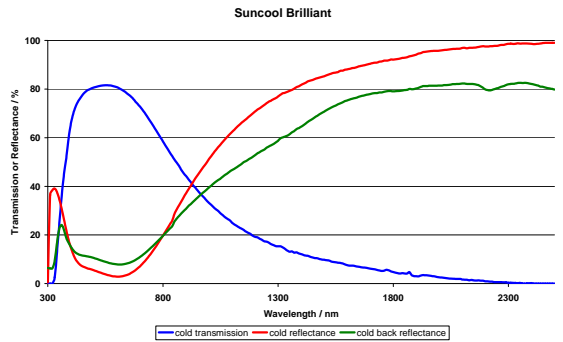
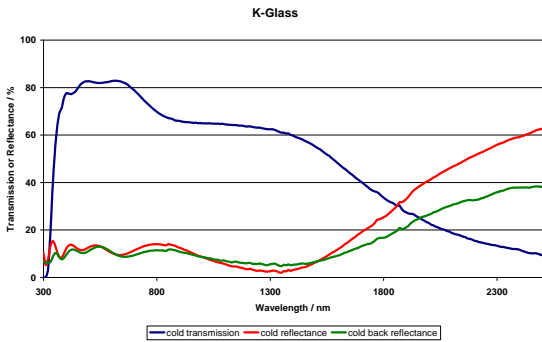
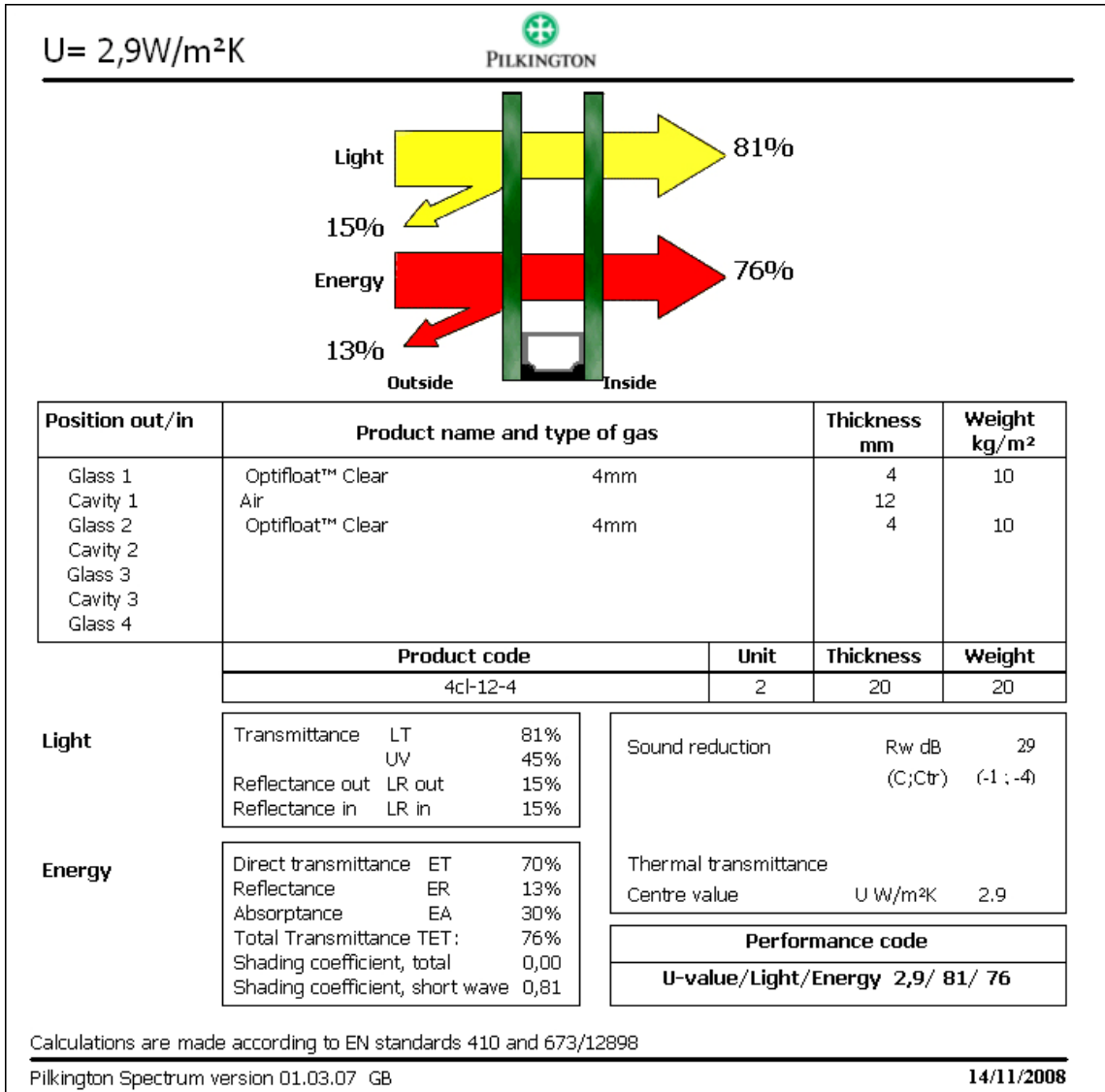


Fig. 7.18
Transmittance and Reflectance of a Blank glass

Fig. 7.19 a-d
Transmittance and Reflectance of
Top left: K-glass
Top right: Suncool Br
Bottom left: Arctic B.
Bottom right: Activ



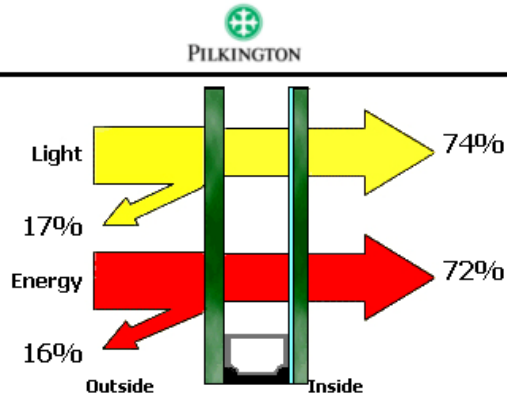
Below there are the main physical calculations of a Clear – Clear configuration⁸.



⁸ The software used to make these calculation is: Pilkington Spectrum.

Below there are the main physical calculations of a Clear – K Glass configuration.

$U = 1,9 \text{ W/m}^2\text{K}$



Position out/in	Product name and type of gas		Thickness mm	Weight kg/m ²
Glass 1	Optifloat™ Clear	4mm	4	10
Cavity 1	Air		12	
Glass 2	K Glass™	4mm	4	10
Cavity 2				
Glass 3				
Cavity 3				
Glass 4				
Product code			Unit	Thickness
4cl-12-K4			2	20
Unit			Thickness	Weight
			2	20

Light			
Transmittance	LT		74%
	UV		34%
Reflectance out	LR out		17%
Reflectance in	LR in		16%

Energy			
Direct transmittance	ET		60%
Reflectance	ER		16%
Absorptance	EA		40%
Total Transmittance	TET :		72%
Shading coefficient, total			0,00
Shading coefficient, short wave			0,70

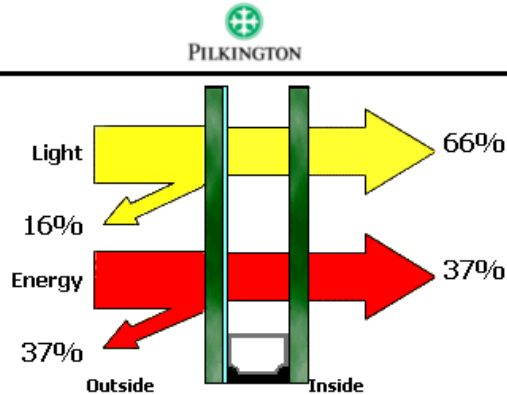
Sound reduction	Rw dB	29
	(C;Ctr)	(-1 ; -4)
Thermal transmittance		
Centre value	U W/m ² K	1,9

Performance code	
U-value/Light/Energy 1,9/ 74/ 72	

Calculations are made according to EN standards 410 and 673/12898

Below there are the main physical calculations of a Suncool™ Brilliant - Clear configuration.

$$U = 1,6 \text{ W/m}^2\text{K}$$

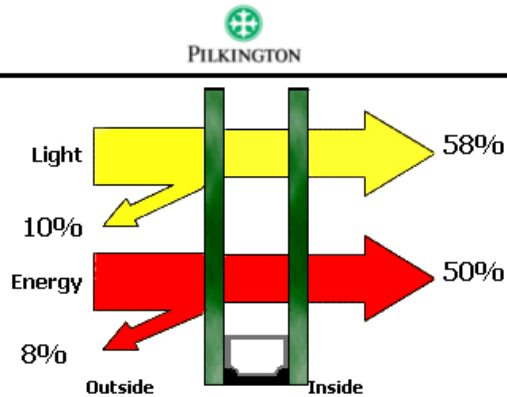


Position out/in	Product name and type of gas		Thickness mm	Weight kg/m ²
Glass 1	Suncool™ Brilliant 66/33	4mm	4	10
Cavity 1	Air		12	
Glass 2	Optifloat™ Clear	4mm	4	10
Cavity 2				
Glass 3				
Cavity 3				
Glass 4				
Product code			Unit	Thickness
4B(66)-12-cl4			2	20
Light	Transmittance	LT	66%	Sound reduction Rw dB 29 (C;Ctr) (-1 ; -4)
		UV	11%	
	Reflectance out	LR out	16%	
	Reflectance in	LR in	16%	
Energy	Direct transmittance	ET	34%	Thermal transmittance Centre value U W/m ² K 1.6
	Reflectance	ER	37%	
	Absorptance	EA	66%	
	Total Transmittance TET:		37%	
	Shading coefficient, total		0,00	
	Shading coefficient, short wave		0,40	
Performance code				
U-value/Light/Energy 1,6/ 66/ 37				

Calculations are made according to EN standards 410 and 673/12898

Below there are the main physical calculations of an Arctic Blue™ - Clear configuration.

$U = 2,9 \text{ W/m}^2\text{K}$

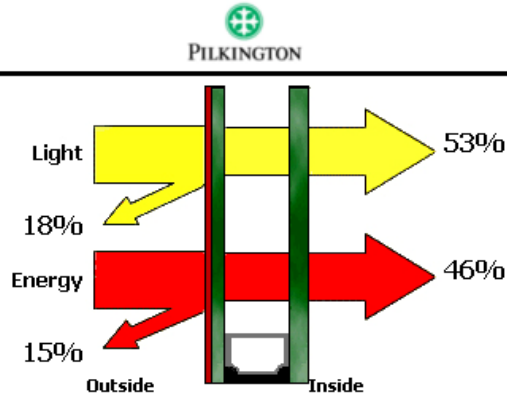


Position out/in	Product name and type of gas		Thickness mm	Weight kg/m ²
Glass 1	Arctic Blue™	4mm	4	10
Cavity 1	Air		12	
Glass 2	Optifloat™ Clear	4mm	4	10
Cavity 2				
Glass 3				
Cavity 3				
Glass 4				
Product code		Unit	Thickness	Weight
4ab-12-cl4		2	20	20
Light	Transmittance	LT	58%	Sound reduction Rw dB 29 (C;Ctr) (-1 ; -4)
		UV	20%	
	Reflectance out	LR out	10%	
	Reflectance in	LR in	13%	
Energy	Direct transmittance	ET	41%	Thermal transmittance Centre value U W/m ² K 2,9
	Reflectance	ER	8%	
	Absorptance	EA	59%	
	Total Transmittance	TET :	50%	
	Shading coefficient, total		0,00	
Shading coefficient, short wave		0,48		
Performance code				
U-value/Light/Energy 2,9/ 58/ 50				

Calculations are made according to EN standards 410 and 673/12898

Below there are the main physical calculations of an Activ Blue™ - Clear configuration.

$U = 2,9 \text{ W/m}^2\text{K}$



Position out/in	Product name and type of gas		Thickness mm	Weight kg/m ²
Glass 1	Activ™ Blue	4mm	4	10
Cavity 1	Air		12	
Glass 2	Optifloat™ Clear	4mm	4	10
Cavity 2				
Glass 3				
Cavity 3				
Glass 4				
Product code			Unit	Thickness
Aab4-12-cl4			2	20
Light	Transmittance	LT	53%	Sound reduction Rw dB 29 (C;Ctr) (-1 ; -4)
		UV	13%	
	Reflectance out	LR out	18%	
	Reflectance in	LR in	17%	
Energy	Direct transmittance	ET	38%	Thermal transmittance Centre value U W/m ² K 2,9
	Reflectance	ER	15%	
	Absorptance	EA	62%	
	Total Transmittance TET:		46%	
	Shading coefficient, total		0,00	
	Shading coefficient, short wave		0,44	
Performance code				
U-value/Light/Energy 2,9/ 53/ 46				

Calculations are made according to EN standards 410 and 673/12898

7.3.4.2 Thermochromic glazing

In this section the thermochromic glass properties will be briefly discussed to have a better idea of their behaviour through the spectrum towards the visible light and the IR radiation.

To learn more about their physical and chemical properties refer to the previous sections.

The thermochromic glasses, chosen to carry on the simulations, are listed in the table below. All of them show a transmittance in the visible range over the 50% thus to have enough visible light entering the room. The samples' switching temperatures are very different, varying from 34 °C to 62 °C, and depend on the physical\chemical properties of each film, as previously discussed. Samples listed as cases from 1 to 6 were produced and analysed in this work; the others, from 7 to 11, were produced and analysed in a preceding study.

Tab. 7.3 Thermochromic samples chosen to carry on the simulations

Case	Sample	Cold transmittance % max	Hot transmittance % max	Switching temperature (Tc) °C
1	MVOxAu2a	55,53	48,18	43
2	MVOxAuT1c	66,64	50,90	40
3	MVOxAuT2c	77,17	48,90	45,5
4	MVOxT1b	60,97	50,55	38,5
5	MVOxT3c	79,84	61,08	43,5
6	MVOxT4a	52,78	53,83	34
7	AAAP7b	69,28	58,89	56
8	AAAP8	77,23	54,39	62
9	VOx23	69,32	66,80	60
10	VOx23a	77,83	73,36	59
11	VOx26	64,31	63,16	62

Field	Units
Name	
Optical Data Type	
Name of Window Glass Spectral Data Set	
Thickness	m
Solar Transmittance at Normal Incidence	
Solar Reflectance at Normal Incidence: Front Side	
Solar Reflectance at Normal Incidence: Back Side	
Visible Transmittance at Normal Incidence	
Visible Reflectance at Normal Incidence: Front Side	
Visible Reflectance at Normal Incidence: Back Side	
IR Transmittance at Normal Incidence	
IR Hemispherical Emissivity: Front Side	
IR Hemispherical Emissivity: Back Side	
Conductivity	W/m.K
Dirt Correction Factor for Solar and Visible Transmittance	
Solar Diffusing	

In order to carry on the simulations the software Energy Plus requires some glasses' parameters listed in the picture on the left and the values of the spectrum in a range from 300 nm (visible light) to 2500 nm (IR). All the parameters had been calculated by means of the software "Window" by Dr. Russell Binions. The front side hemispherical emissivities were measured both in the hot and cold state with help from Dr. Troy

Fig. 7.20 Glasses Values required to perform simulations.

Manning from the Pilkington Technology Centre in Lathom (UK).

In the next table, the emissivity values are reported. The back emissivity was assumed to be equal to a glass with nothing deposited on it, a clear one, and is 0,837.

Tab. 7.4 Thermochromic samples' emissivity in both hot and cold state

Case	Sample	Front side emissivity Cold state	Front side emissivity Hot state
1	MVOxAu2a	0,800	0,752
2	MVOxAuT1c	0,829	0,779
3	MVOxAuT2c	0,828	0,797
4	MVOxT1b	0,827	0,789
5	MVOxT3c	0,828	0,801
6	MVOxT4a	0,829	0,793
7	AAAP7b	0,825	0,795
8	AAAP8	0,824	0,798
9	VOx23	0,829	0,793
10	VOx23a	0,825	0,795
11	VOx26	0,829	0,790

As previously said, the window in the model is always double glazed. The outer pane is always the coated thermochromic glass, with the coating positioned on surface 2. All the glasses are 4 mm thick.

In the next table the different glazing configurations are shown.

Tab. 7.5 Thermochromic glazing configurations

Case	Outer pane	Cavity	Inner pane
1	MVOxAu2a	12 mm	Blank glass
2	MVOxAuT1c	12 mm	Blank glass
3	MVOxAuT2c	12 mm	Blank glass
4	MVOxT1b	12 mm	Blank glass
5	MVOxT3c	12 mm	Blank glass
6	MVOxT4a	12 mm	Blank glass
7	AAAP7b	12 mm	Blank glass
8	AAAP8	12 mm	Blank glass
9	VOx23	12 mm	Blank glass
10	VOx23a	12 mm	Blank glass
11	VOx26	12 mm	Blank glass

In the next page, the cases 7 to 11 thermochromic samples' spectra are shown⁹ to understand better their optical properties..

⁹ For samples 1 – 6 spectra refer to the previous chapters.

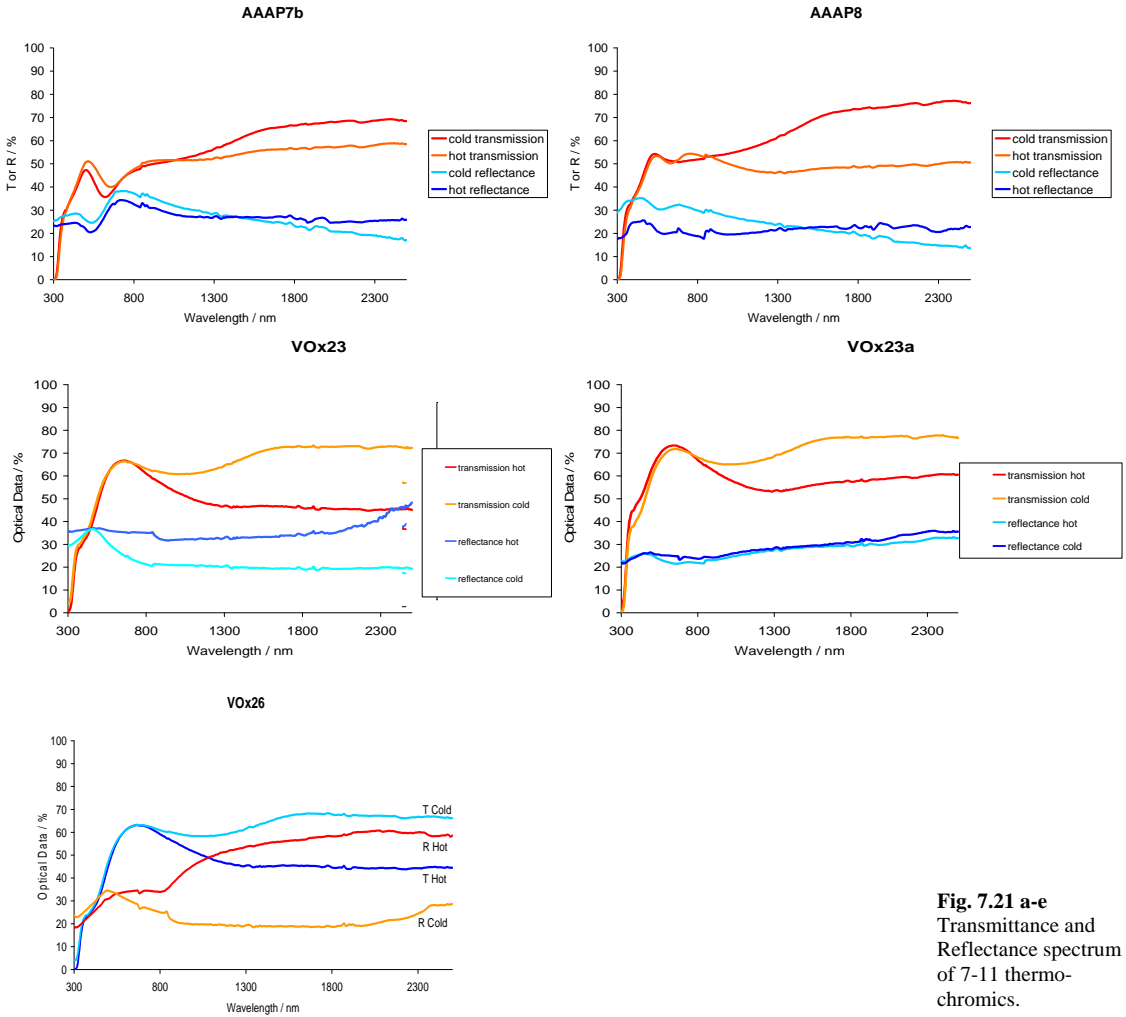


Fig. 7.21 a-e
Transmittance and Reflectance spectrum of 7-11 thermo-chromics.

7.3.5 Construction of the model - Internal conditions

In order to run the software it is necessary to set the internal conditions of the model such as lighting, electrical equipment, air flow rate, etc.. The building is supposed to be located in the suburbs, the ground temperatures are taken to be 18 °C throughout the year, as it remains constant after a small depth. The internal conditions were chosen to be air-conditioned between 19 – 26 °C to maintain the interior environment in a comfortable range.

7.3.5.1 Light

The required illuminance level in a general office-building is 500 lux. Using commercial lamps we need for a room in a commercial building about 400 W lighting load to have a comfortable illuminance level. The lights are fully dimmable: lowering their output when there is an adequate illuminance from the sun, in order to save energy. It is considered that they can be dimmed in the whole range from 0 to 100%. The software control is automatic and zoned. The illuminance measure is based on two reference points controlling half of the luminaries each: both the points are located on the working plane to insure a good illuminance level on it. The program calculates a daylight illuminance grid on the working plane height for every hour in each day of the year that there is natural light.

7.3.5.2 Casual gain

The equipment found inside an office room is assumed to be a personal computer per person, a fax machine and a desktop laser printer. The room is supposed to have 2-3 persons working. The total heat gain (persons + equipment) is supposed to be 500 W in total.

7.3.5.3 Ventilation rate

The infiltration rate (ir) is set to one air change per hour (ach). The volume of the room is:

$$V = 5 \times 6 \times 3 \text{ m} = 90 \text{ m}^3 \quad (\text{eq. 7.1})$$

$$\text{ir} = V \times \text{ach} = 90 \text{ m}^3 \times 1 \text{ h}^{-1} = 90 \text{ m}^3 / 3600 \text{ sec} = 0,025 \text{ m}^3/\text{s} \quad (\text{eq. 7.2})$$

7.3.6 Run period

The run period for every simulation is one year; the time step for the calculation procedure is a quarter of an hour.

7.3.7 Schedules

The occupancy of the place is supposed to be from 8:00 till 18:00, five days a week, as it usually is for an office. The weather files of the places used to carry on simulations have been built in the national holidays of the respective countries in order to be as close to reality as possible. All the internal conditions such as lighting, equipment, heating and cooling, etc. follow the occupancy schedule, as these things operate only if people are present in the building.

7.4 Running Energy Plus

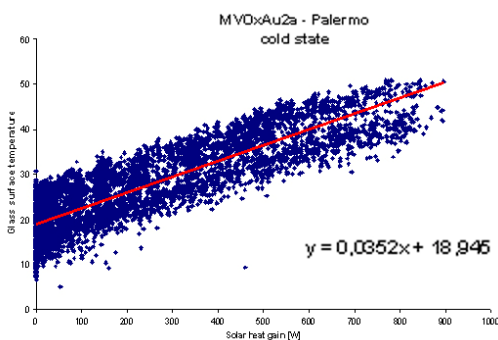
After feeding all the data into the program – Edit IDF Editor – we start simulating every case. The results are presented for each hour, day by day, for the whole year, that's to say 8760 hours for every aspect monitored. All the results are written in an Excel spreadsheet.

More particularly, the results given are:

- Environment: outdoor dry bulb temperature (°C);
- Environment: interior mean air temperature (°C);
- Window: solar gain on the window's surface (W/m²);
- Window: surface outside temperature (°C);
- Lighting electric power (W);
- Heating electric power (W);
- Cooling electric power (W).

Simulations carried on with the thermochromic glazing present a quite complicated procedure since it must be considered their switching behaviour through the cold and hot state depending on the glass surface temperature. The software deals with every glazing (or material in general) as having two different building elements. The first one is the window with the spectral characteristics of the thermochromic glass in the cold state while the second one is the window with the spectral characteristics of the glass in the hot state. The first one is the default glass and the second one replace the first as a certain condition is met. The software has some built in function to control the substitution automatically. These function are based on:

- Schedules;
- Solar gain on the window;
- Horizontal incoming radiation;
- Outside air temperature;
- Inside air temperature;
- Glare;
- Daylight illuminance;
- Controllers on the night time;
- Etc..



simulation having the glass in the cold state for the whole year, as a result we had, within the others, the glass surface temperature and the solar heat gain on the window. The values were related in a graph, as can be seen in the picture fig. 7.22 for the sample MVOxAu2a in the city of Palermo.

Unfortunately, the thermochromic glasses' switching mechanism is controlled by the surface temperature of the glass pane and there is no built-in function in the program to control this factor. To surpass the problem it was found a relationship between the surface window temperature and the solar heat gain for each glass and for each weather condition (city) doing the following: we run the

Fig. 7.22
Relationship between the glass surface temperature and the solar heat gain on it.

Then Excel was used to calculate the trend-line (in red in the image above) and to display the equation on the chart. Knowing what value the switching temperature (T_c) is and replacing it in the equation - as y value - we obtain the solar heat gain on the window that is necessary to make the thermochromic glass reach the transition temperature T_c and, thus, switching into the hot state.

This procedure had been run for every glass in each city (weather conditions) for both the models.

Tab. 7.6 Surface incident solar energy for the 25% glazing model

Case	Sample	T_c [°C]	Surface Incident Solar Energy [W/m ²]							
			Cairo	Palermo	Roma	Milano	Paris	London	Moscow	Helsinki
1	MVO _x Au2a	43	598	683	710	670	736	789	755	812
2	MVO _x AuT1c	40	569	664	696	660	728	785	756	809
3	MVO _x AuT2c	45,5	769	878	886	816	895	964	908	971
4	MVO _x T1b	38,5	563	664	697	662	730	791	761	817
5	MVO _x T3c	43,5	755	876	888	817	899	973	917	977
6	MVO _x T4a	34	392	479	529	524	580	631	623	672
7	AAAP7b	56	1330	1503	1438	1254	1373	1487	1345	1423
8	AAAP8	62	1756	1985	1845	1562	1715	1868	1653	1737
9	VO _x 23	60	1600	1808	1697	1455	1594	1733	1543	1630
10	VO _x 23a	59	1410	1584	1510	1315	1437	1553	1402	1485
11	VO _x 26	62	1344	1489	1434	1260	1377	1478	1342	1422

Tab. 7.7 Surface incident solar energy for the 100% glazing model

Case	Sample	T_c [°C]	Surface Incident Solar Energy [W/m ²]							
			Cairo	Palermo	Roma	Milano	Paris	London	Moscow	Helsinki
1	MVO _x Au2a	43	563	649	680	647	712	761	732	782
2	MVO _x AuT1c	40	528	624	661	633	699	752	727	774
3	MVO _x AuT2c	45,5	722	831	847	787	863	927	874	929
4	MVO _x T1b	38,5	522	622	661	636	702	759	733	781
5	MVO _x T3c	43,5	694	813	833	777	856	925	873	925
6	MVO _x T4a	34	355	441	496	500	556	603	600	642
7	AAAP7b	56	1258	1429	1374	1205	1315	1421	1289	1355
8	AAAP8	62	1641	1870	1749	1496	1626	1771	1570	1638
9	VO _x 23	60	1494	1702	1608	1388	1512	1644	1470	1534
10	VO _x 23a	59	1327	1504	1442	1262	1372	1484	1341	1407
11	VO _x 26	62	1271	1419	1373	1213	1320	1414	1288	1356

The so-calculated solar heat gain value was input in Energy Plus to control the substitution between cold and hot state glasses, as can be seen in the image in the next page.

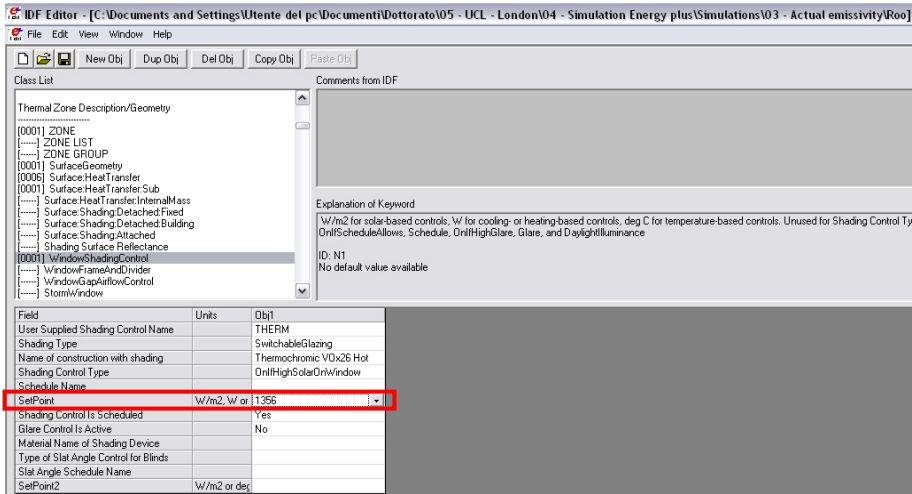
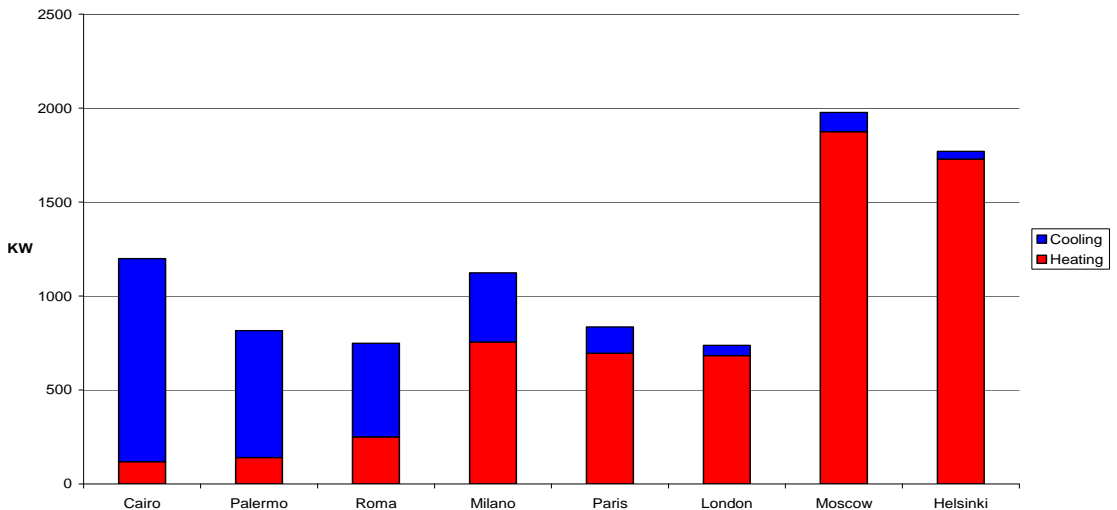


Fig. 7.23
Energy Plus – IDF Editor - Shading control.

7.5 Results

In the following pages some results are shown and discussed. The energy consumption for heating, cooling and lighting are always expressed in KW\year in order to compare the values in a more comprehensible way. It must be stressed out that the results are not completely representative of reality. Both the models are planned in a way that it is not possible to have a building suitable for almost all the climates and to enable the simulations to proceed faster. It is easily understandable that the model does not perform in the same way in all the climatic conditions.

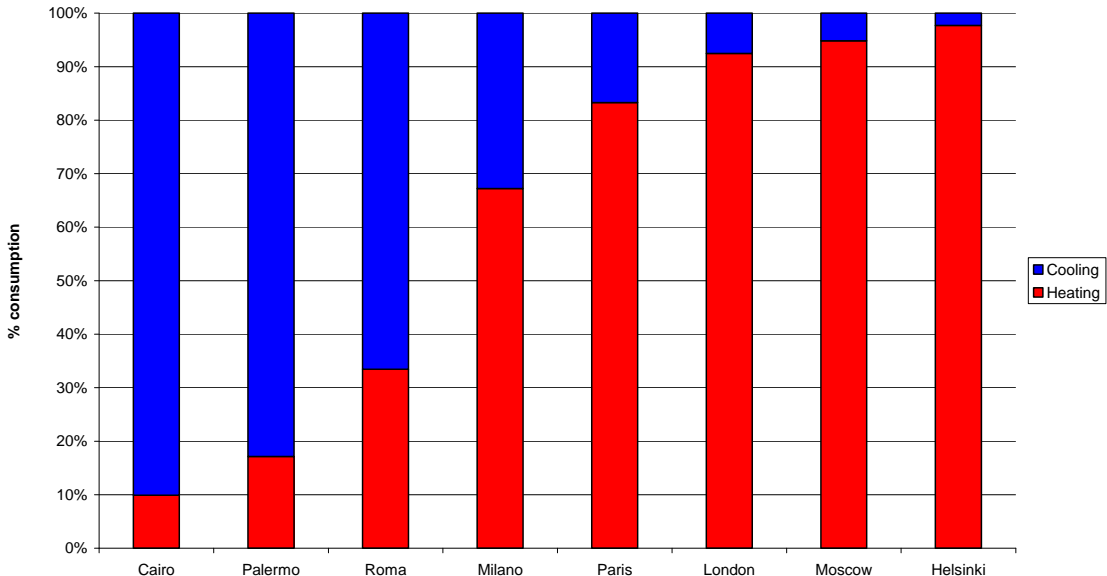
Fig. 7.24
Annual energy consumption for heating and cooling in the model with no windows.



For instance, in very cold, or very hot cities the insulation layer must be thicker than what had been planned (5 cm) and in each country there are different constructive technologies that deal better with the exterior conditions and building materials available in loco. This fact leads to different behaviours of the same model in the different climate conditions. A building model, analogous to the previously ones discussed, was modelled with no windows. The simulations were run through all the weather conditions to understand the amount of electric energy consumed by the building for heating and cooling and which climate is this model more suitable for. The results are shown in the following graph. The lighting energy consumption resulted 1.144KW/year in all the cities. An equal amount is quite obvious since the use of interior lights depends on the built environment and not on the exterior environment. As it can be seen, the model performs in a very different way from one city to another, that is to say from one weather condition to another. The percentage consumption for both heating or cooling depends on the exterior conditions and how the building materials work. For instance, in the coldest cities – Moscow and Helsinki – the model perform in the worst way consuming an amazingly high amount of energy in heating; in the hottest city – Cairo - there is a big amount of consumption for cooling. These conditions were almost expected and could have been solved using different building materials and architectural solutions.

In the graph below, the percentage consumption of energy for heating and cooling is shown for each city. It demonstrates that the model works as expected with an increasing energy consumption for heating towards the cold climate (towards the right) and, on the contrary, an increasing amount of energy for cooling towards the hot climate (towards the left).

Fig. 7.25
Percentage consumption for heating and cooling in the model.



Tab. 7.8 (b) Hours/year in the hot state										
Case	Sample	Tc [°C]	Paris		London		Moscow		Helsinki	
			25%	100%	25%	100%	25%	100%	25%	100%
1	MVOxAu2a	43	92	116	52	82	90	114	45	59
2	MVOxAuT1c	40	108	158	74	112	109	143	52	81
3	MVOxAuT2c	45,5	2	5	0	4	2	13	0	0
4	MVOxT1b	38,5	112	162	78	115	116	146	56	86
5	MVOxT3c	43,5	2	9	0	5	3	20	0	2
6	MVOxT4a	34	418	475	323	374	386	443	253	295
7	AAAP7b	56	0	0	0	0	0	0	0	0
8	AAAP8	62	0	0	0	0	0	0	0	0
9	VOx23	60	0	0	0	0	0	0	0	0
10	VOx23a	59	0	0	0	0	0	0	0	0
11	VOx26	62	0	0	0	0	0	0	0	0

Fig. 7.26
Hours in the hot state
in the 25 % to wall
window.

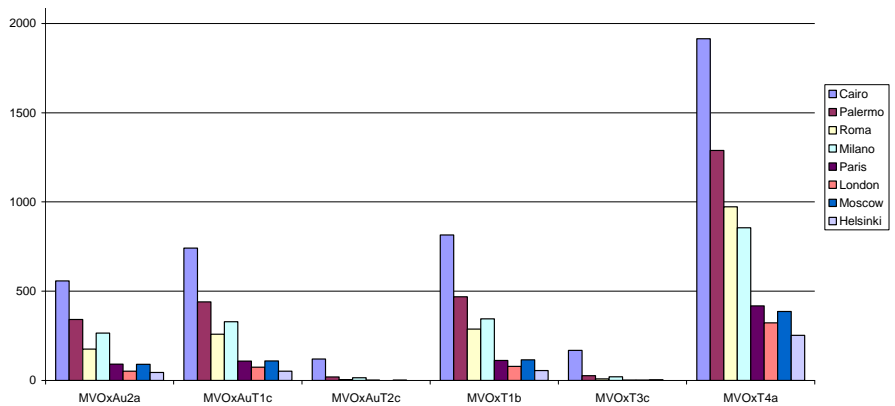
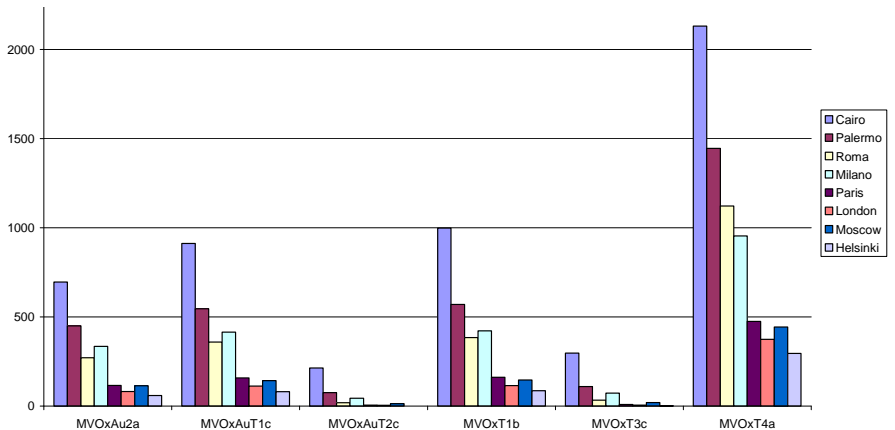


Fig. 7.27
Hours in the hot state
in the 100 % to wall
window.



As expected, the sample with the lowest switching temperature, MVOxT4a – 34 °C, has the greatest number of hours in the hot state. It is followed respectively by the others with a higher T_c . MVOxT1b (38,5 °C) than MVOxAuT1c (40 °C) and so on. For all the samples, the number of hot state hours in each city mostly depends on the climate conditions. In the hottest cities a warmer climate in combination with the more intense and frequent solar radiation rise the surface temperature of the samples above their T_c more often than in the cold climates. As a consequence, in the hottest cities the glasses are in their hot state more often than in the colder cities. Moreover we can notice that the number of hours in the hot state increases as the surface area of the window increases. An interested fact is that the last 5 samples never switch to the hot state because of their high switching temperature, even though they show a good behaviour in terms of consumption, as it will be discussed in the next paragraphs.

7.5.2 Annual heating and cooling loads

In this section we are going to look at the heating and cooling loads for the whole year. Each glazing performs in a very different way through the different cities. The results are expressed both in KW per year and in % to the clear - clear window to make some useful comparison.

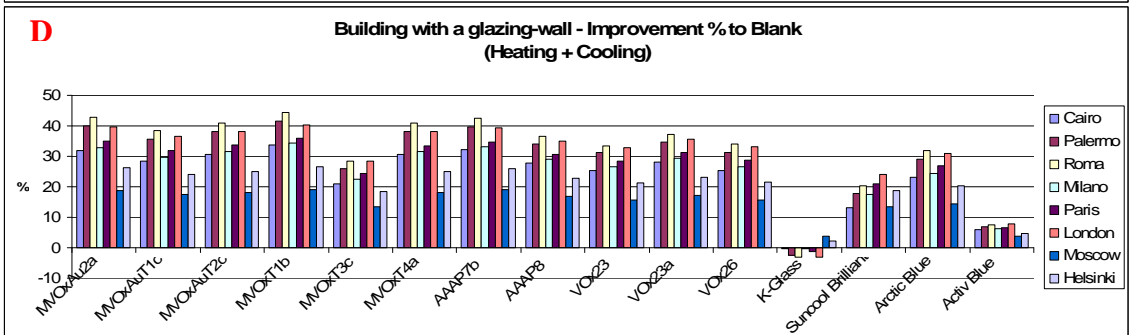
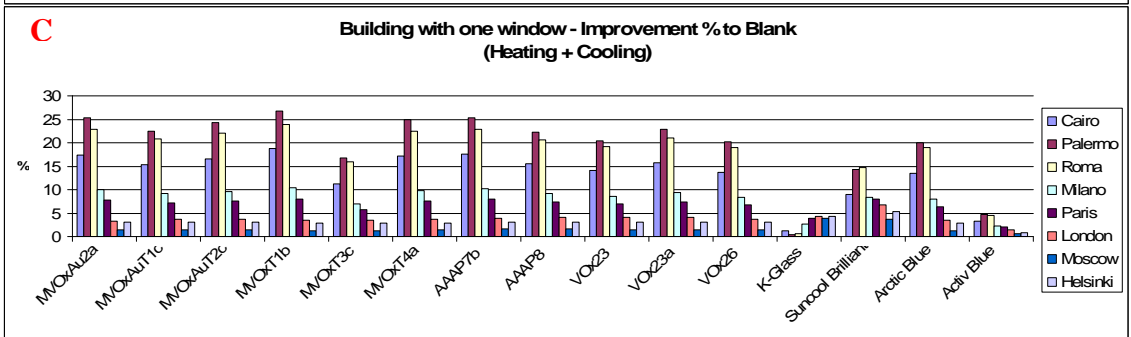
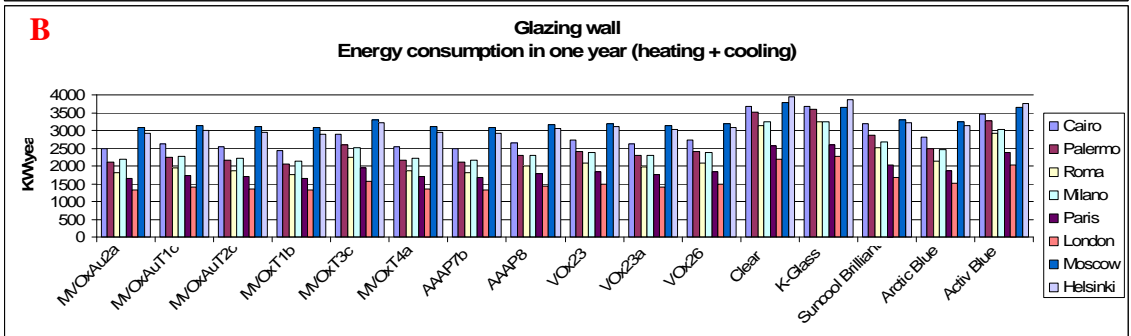
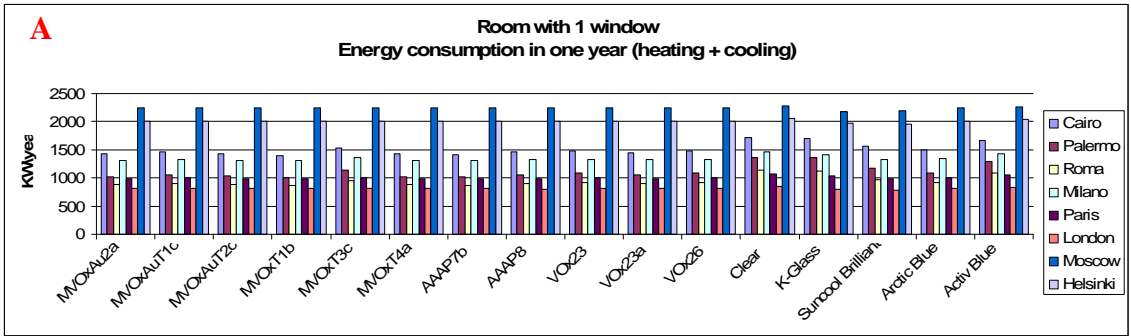
First of all we are going to look at the energy loads for heating and cooling through all the cities to have a general idea of the behaviour of the thermochromic glasses in comparison to the commercial ones.

As a general trend, it can be seen that in the coldest cities, Moscow and Helsinki, the energy consumption is much higher than the other cities. This fact is probably due to the model behaviour in general that, as discussed in the previous paragraph, is not suitable in an architectural-engineering way and so it consumes more in some climate conditions than in the colder ones.

Another point is that in the 100% glazing to wall model consumes more in terms of KW per year than the ones in the single 25% window model. However, if we look at the improvement % to the clear – clear window we have a much better behaviour than the 25% window. Again, this is because of the exterior wall that disperses a lot of energy through its surface as, previously said, it is not well insulated against some kind of weather conditions.

Anyway it can be easily noticed that, in general, thermochromic glazing performs better than the commercial products that have been analyzed in this work, especially in hot climate conditions.

The only one perplexity is on the K-Glass whose behaviour is not what had been expected, especially in some kind of climates like that for London.



As it can be seen in the last two graphs in figure 7.28, the improvement % to Blank (Clear – Clear window) is shown for both the models, 25% and 100% window to wall area. The Blank window is supposed to have an improvement equal to 0% as it is our base line. These two images show that all the glazing analyzed show a very good behaviour saving a lot of energy in comparison to a window with non-coated glasses. As previously told, the only perplexity is over the K-Glass behaviour which is negative¹⁰ in the 100% glazing model through all the cities but the coldest, Moscow and Helsinki.

A very interesting fact is that all the thermochromic samples behave better than the glasses produced by Pilkington. In the 25% glazing model the thermochromic's maximum improvement is 26,8% (MVOxT1b in Palermo) against a 19,9 % of the Pilkington's (Arctic Blue in Palermo). In the 100% glazing model the thermochromic's maximum improvement is 44,2% (MVOxT1b in Roma) against a 31,9% of the Pilkington's (Arctic Blue in Roma).

Fig. 7.28 a-d (prev. pg)

Energy consumption in one year for the 25% (A) and 100% (B) window model. Improvement % to Blank for the 25% (C) and 100% (D) window model.

Tab. 7.9 Improvement % to Blank in the 25% window to wall model

Glass	Cairo	Palermo	Roma	Milano	Paris	London	Moscow	Helsinki
	%	%	%	%	%	%	%	%
MVOxAu2a	17,37	25,29	22,77	9,98	7,69	3,33	1,36	2,99
MVOxAuT1c	15,35	22,54	20,76	9,10	7,18	3,61	1,39	3,01
MVOxAuT2c	16,61	24,20	22,05	9,68	7,59	3,62	1,43	3,01
MVOxT1b	18,69	26,83	23,80	10,48	7,93	3,38	1,32	2,88
MVOxT3c	11,18	16,67	15,88	6,98	5,77	3,46	1,32	2,78
MVOxT4a	17,05	24,82	22,49	9,79	7,55	3,61	1,36	2,95
AAAP7b	17,56	25,35	22,89	10,28	8,02	3,88	1,56	3,08
AAAP8	15,43	22,34	20,57	9,27	7,36	4,12	1,55	3,07
VOx23	14,05	20,48	19,09	8,59	6,88	4,03	1,51	3,01
VOx23a	15,65	22,76	20,97	9,32	7,37	3,99	1,51	3,05
VOx26	13,75	20,27	18,95	8,35	6,68	3,75	1,41	2,98
K-Glass	1,16	0,46	0,68	2,66	3,81	4,31	3,94	4,39
Suncool Brilliant	9,04	14,25	14,73	8,45	8,03	6,78	3,74	5,38
Arctic Blue	13,45	19,91	18,92	7,94	6,33	3,45	1,21	2,79
Activ Blue	3,25	4,66	4,55	2,29	2,00	1,47	0,57	0,90

N.B: in green the best performance between the thermochromic samples and the Pilkington's, in red the lowest.

¹⁰ A negative % behaviour means that the model consumes more energy than a model with the Clear-Clear window.

Tab. 7.10 Improvement % to Blank in the 100% window to wall model.

Glass	Cairo	Palermo	Roma	Milano	Paris	London	Moscow	Helsinki
	%	%	%	%	%	%	%	%
MVOxAu2a	31,92	39,89	42,88	32,94	34,99	39,55	18,77	26,23
MVOxAuT1c	28,45	35,57	38,43	29,73	31,89	36,45	17,36	24,00
MVOxAuT2c	30,53	38,00	40,84	31,58	33,62	38,21	18,22	25,14
MVOxT1b	33,73	41,61	44,26	34,30	35,88	40,40	19,16	26,45
MVOxT3c	20,87	25,99	28,31	22,40	24,34	28,30	13,39	18,46
MVOxT4a	30,63	38,07	40,78	31,52	33,37	38,07	18,00	24,92
AAAP7b	32,17	39,74	42,41	33,09	34,84	39,45	18,98	25,79
AAAP8	27,80	34,21	36,62	29,03	30,70	35,15	16,95	22,73
VOx23	25,31	31,21	33,55	26,67	28,37	32,68	15,72	21,11
VOx23a	28,12	34,76	37,34	29,34	31,16	35,67	17,11	23,19
VOx26	25,17	31,39	34,00	26,61	28,64	33,03	15,75	21,58
K-Glass	-0,31	-2,38	-3,25	-0,29	-1,10	-3,14	3,84	2,10
Suncool Brilliant	13,24	17,96	20,40	17,45	20,90	24,09	13,29	18,71
Arctic Blue	23,18	29,10	31,90	24,41	26,76	31,01	14,38	20,35
Activ Blue	5,80	6,92	7,36	6,36	6,64	7,79	3,83	4,81

In the following tables the energy consumption for heating and cooling in one year are shown for each sample and each city.

Tab. 7.11 Annual energy consumption for heating and cooling in the 25% window to wall model

Glass	Cairo	Palermo	Roma	Milano	Paris	London	Moscow	Helsinki
	KW	KW	KW	KW	KW	KW	KW	KW
MVOxAu2a	1420,74	1016,60	877,08	1309,53	991,14	814,13	2242,46	2003,81
MVOxAuT1c	1455,46	1053,98	899,87	1322,40	996,62	811,80	2241,64	2003,49
MVOxAuT2c	1433,76	1031,36	885,18	1313,94	992,22	811,71	2240,87	2003,37
MVOxT1b	1398,03	995,55	865,34	1302,31	988,52	813,77	2243,35	2006,11
MVOxT3c	1527,16	1133,88	955,34	1353,17	1011,76	813,09	2243,37	2008,26
MVOxT4a	1426,16	1022,96	880,23	1312,33	992,61	811,77	2242,33	2004,63
AAAP7b	1417,43	1015,74	875,73	1305,26	987,58	809,51	2237,85	2001,90
AAAP8	1454,16	1056,74	902,00	1319,89	994,72	807,53	2237,94	2002,22
VOx23	1477,74	1081,96	918,86	1329,74	999,81	808,22	2238,94	2003,40
VOx23a	1450,27	1050,99	897,48	1319,11	994,55	808,56	2238,92	2002,67
VOx26	1482,98	1084,81	920,38	1333,30	1001,97	810,60	2241,31	2004,13
Clear	1719,39	1360,65	1135,64	1454,75	1073,70	842,20	2273,29	2065,58
K-Glass	1699,42	1354,34	1127,86	1416,05	1032,76	805,92	2183,74	1974,98
Suncool Brilliant	1563,96	1166,78	968,36	1331,81	987,48	785,08	2188,38	1954,40
Arctic Blue	1488,11	1089,77	920,75	1339,23	1005,78	813,15	2245,78	2008,03
Activ Blue	1663,50	1297,17	1084,01	1421,49	1052,18	829,85	2260,30	2046,98

Tab. 7.12 Annual energy consumption for heating and cooling in the 100% window to wall model

Glass	Cairo	Palermo	Roma	Milano	Paris	London	Moscow	Helsinki
	KW	KW	KW	KW	KW	KW	KW	KW
MVOxAu2a	2494,66	2104,42	1797,38	2177,16	1662,14	1329,93	3083,55	2907,04
MVOxAuT1c	2621,56	2255,73	1937,29	2281,19	1741,31	1398,16	3137,27	2995,03
MVOxAuT2c	2545,38	2170,69	1861,50	2221,17	1696,99	1359,34	3104,61	2950,35
MVOxT1b	2428,06	2044,16	1753,99	2133,02	1639,21	1311,20	3068,61	2898,66
MVOxT3c	2899,20	2591,07	2255,91	2519,17	1934,29	1577,52	3287,68	3213,52
MVOxT4a	2541,79	2168,19	1863,27	2223,31	1703,49	1362,53	3112,74	2958,67
AAAP7b	2485,41	2109,55	1812,25	2172,08	1665,85	1332,20	3075,70	2924,71
AAAP8	2645,27	2303,49	1994,31	2304,15	1771,75	1426,74	3152,62	3044,99
VOx23	2736,65	2408,36	2090,83	2380,68	1831,36	1481,09	3199,49	3108,95
VOx23a	2633,65	2283,92	1971,69	2294,12	1759,85	1415,26	3146,53	3027,17
VOx26	2741,83	2402,22	2076,85	2382,70	1824,34	1473,45	3198,32	3090,45
Clear	3664,05	3501,03	3146,59	3246,47	2556,58	2200,05	3796,11	3940,91
K-Glass	3675,45	3584,25	3248,81	3255,73	2584,61	2269,09	3650,27	3858,24
Suncool Brilliant	3178,95	2872,16	2504,71	2680,10	2022,24	1670,04	3291,52	3203,43
Arctic Blue	2814,55	2482,34	2142,73	2453,87	1872,38	1517,73	3250,34	3138,79
Activ Blue	3451,42	3258,78	2915,11	3039,99	2386,73	2028,68	3650,86	3751,22

We are now going to analyze some results in a more detailed way for a couple of cities. More particularly we are going to look at Palermo and London’s results for the 100% wall to window model.

The two cities have very different climate conditions since Palermo has got a Mediterranean Climate while London a Moderate Marine West Coast Climate¹¹, as a consequence the models behaviour are quite different. Below, we can see the energy consumption for heating and cooling in the city of Palermo.

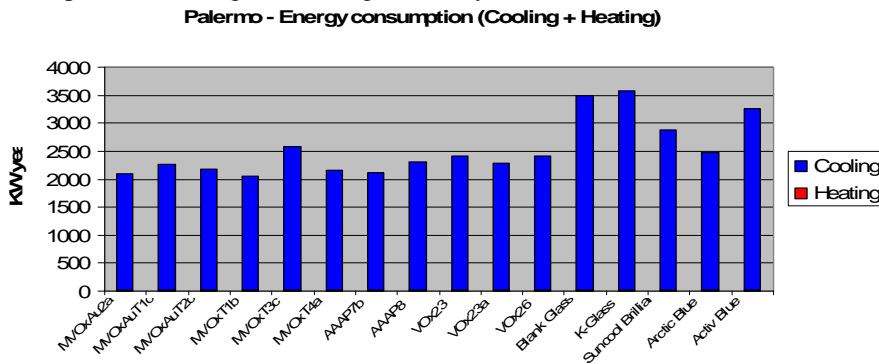


Fig. 7.29 Energy consumption for heating and cooling in Palermo.

¹¹ To learn more about climates refer to paragraph 7.3.2.

As it can be noticed the amount of energy used is almost correlated to cooling since the heating energy used is less than 5%. Below we are looking at the city of London.

London - Energy consumption (Cooling + Heating)

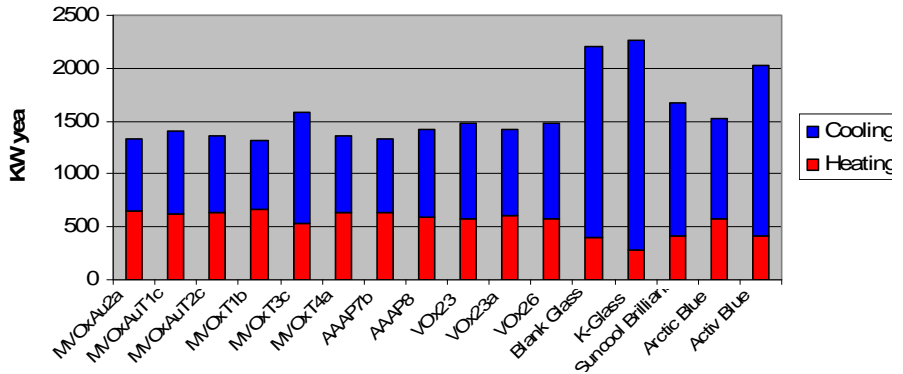


Fig. 7.30
Energy consumption
for heating and cooling
in London.

Tab. 7.13 Annual energy consumption for heating and cooling in the 100% window to wall model - Improvement % to Blank		
Sample	Palermo	London
MVOxAu2a	39,89129	39,54985
MVOxAuT1c	35,56957	36,44845
MVOxAuT2c	37,99854	38,21301
MVOxT1b	41,61244	40,40111
MVOxT3c	25,99107	28,29585
MVOxT4a	38,06985	38,06826
AAAP7b	39,74477	39,44686
AAAP8	34,20526	35,1494
VOx23	31,21	32,67902
VOx23a	34,76439	35,67148
VOx26	31,3851	33,0262
K-Glass	-2,37722	-3,13845
Suncool Brill.	17,96231	24,09069
Arctic Blue	29,09685	31,01392
Activ Blue	6,919207	7,789026

In this case the situation is completely different, as it can be easily noticed. The energy consumption is smaller than in Palermo.

Is interesting to notice that in both the cases the thermochromic samples show a much better behaviour in comparison to the Pilkington products. Looking at the improvement % to the Blank (Tab. 7.13) we notice that the improvements % are quite comparable.¹²

Looking at the graphs in the next page, as other times had been told, there are some perplexities on the K Glass behaviour especially for the city of London where its improvement % should be maximum.

¹² Every calculation refers to the Blank's behaviour in each city.

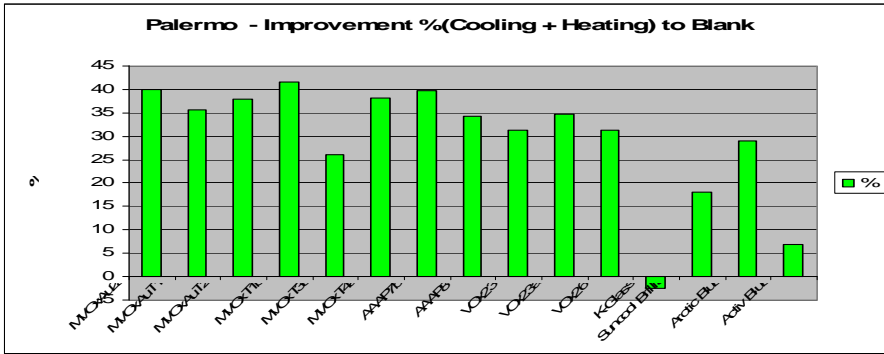


Fig. 7.31
Improvement % to Blank for heating and cooling in Palermo.

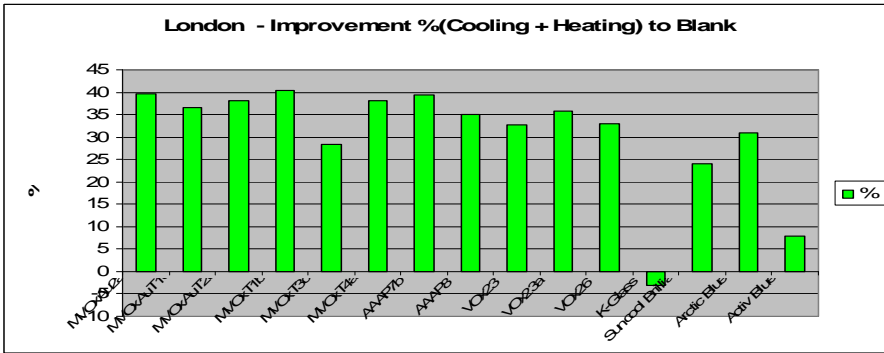


Fig. 7.32
Improvement % to Blank for heating and cooling in London.

7.5.3 Artificial lighting loads

The room model is divided into two zones that are controlled by the illuminance level of a reference point. If the illuminance drops below the set level of 500 lux, the artificial lights are switched on in order to provide the extra illuminance needed.

The division into two zones, one close to the window and one closed to the opposite wall – the northern one – was made to deliver a better uniform illuminance to the interior space and to save energy switching on only half of the total illuminance.

The first remark we can do is that the energy requirement is higher in the model with the 25% window since in the other model the lights are switched on for a shorter period of time due to the bigger glazing area. Another point is that, generally, the energy requirement is less in the cities in a low latitude (Cairo, Palermo, etc.) due to a longer day-light period and solar gain on windows.

Anyway, considering the Clear-Clear window as our base line, it is possible to notice that the use of all the glazing (thermochromic or by Pilkington) lead to a bigger consumption of energy. This fact is probably due to a lower transmission and higher reflection of the visible light in comparison to a Blank glass.

Below, the yearly energy consumption for lighting only are shown.

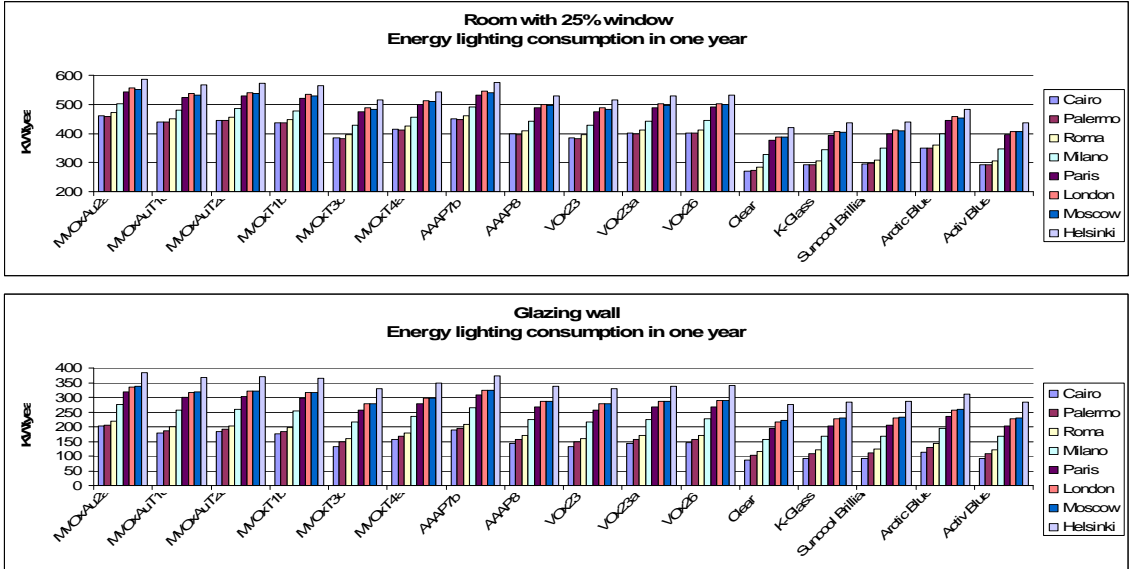
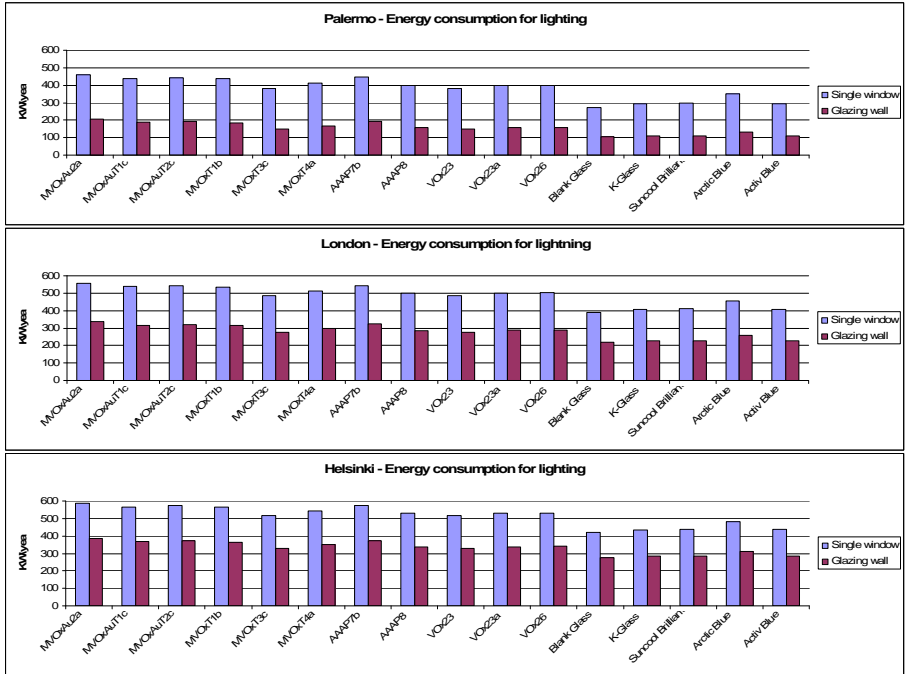


Fig. 7.33 a-b
Energy consumption for lighting in the 25% (top) and 100% (bottom) window model.

Fig. 7.34 a-b-c
Energy consumption for lighting in the city of Palermo (top), London (centre), Helsinki (bottom).

Blue: 25% window;
Purple: 100% window.



The three graphs in Fig. 7.34 show the energy consumption for lighting in the cities of Palermo, London and Helsinki. As previously said, the amount of energy used is bigger for cities located in higher latitudes and in the model with the 25% window. In the next page two tables show the KW consumption of energy through the different cities for all the glazing.

Unfortunately, the lighting energy consumption is the biggest amount of energy (between heating, cooling and lighting) used in all the models. As we will see in the next paragraph, this fact will bring to negative results, especially in the 25% window, as we will consider the whole energy amount required in the building.

Tab. 7.14 Model with the 25% window - Energy consumption for lighting (KW\year)

Glazing	Cairo	Palermo	Roma	Milano	Paris	London	Moscow	Helsinki
MVOxAu2a	459,95	459,42	471,43	501,57	542,40	555,84	551,33	586,61
MVOxAuT1c	440,51	438,77	451,11	481,58	523,58	536,80	532,52	567,02
MVOxAuT2c	445,67	444,12	456,26	486,63	528,13	541,31	537,00	571,67
MVOxT1b	437,44	435,78	448,33	478,87	521,26	534,55	530,27	564,71
MVOxT3c	384,87	382,69	395,72	428,85	474,78	487,75	483,44	515,31
MVOxT4a	413,94	411,57	424,69	456,15	500,39	513,64	509,49	542,81
AAAP7b	449,47	448,02	460,07	490,38	531,58	544,77	540,43	575,24
AAAP8	399,68	397,18	410,15	442,43	487,33	500,48	496,25	528,80
VOx23	385,04	382,94	395,97	429,08	474,99	487,97	483,67	515,55
VOx23a	400,51	397,99	410,96	443,19	488,03	501,19	496,97	529,55
VOx26	402,60	400,06	413,00	445,13	489,81	502,98	498,77	531,45
Clear	271,25	272,12	284,59	326,98	375,64	388,84	388,27	419,21
K-Glass	291,94	292,44	305,08	345,30	394,28	407,06	404,95	435,47
Suncool Brilliant	296,54	296,97	309,63	349,41	398,42	411,13	408,70	439,15
Arctic Blue	349,30	348,63	361,43	397,33	445,25	457,54	453,50	483,77
Activ Blue	292,53	293,02	305,72	345,89	394,94	407,70	405,57	436,08

Tab. 7.15 (a) Model with the 100% window - Energy consumption for lighting (KW\year)

Glazing	Cairo	Palermo	Roma	Milano	Paris	London	Moscow	Helsinki
MVOxAu2a	201,41	206,44	218,46	274,99	319,31	335,95	337,09	384,57
MVOxAuT1c	179,04	186,65	199,10	256,38	299,32	317,08	317,76	366,98
MVOxAuT2c	183,99	191,03	203,37	260,58	303,79	321,28	322,01	370,90
MVOxT1b	176,72	184,58	197,07	254,38	297,19	315,09	315,74	365,12
MVOxT3c	133,32	147,42	160,56	215,13	256,49	277,47	277,90	329,31
MVOxT4a	155,72	166,36	179,36	236,16	278,06	297,42	297,80	348,27
AAAP7b	187,95	194,50	206,77	263,89	307,32	324,61	325,40	374,02

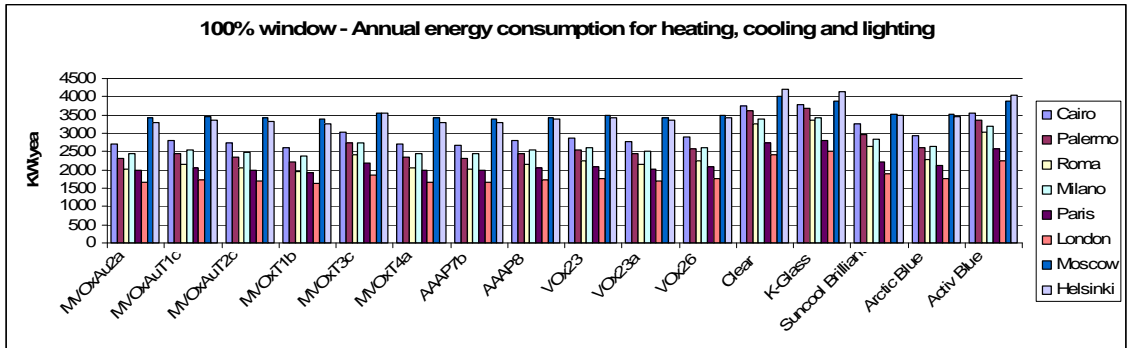
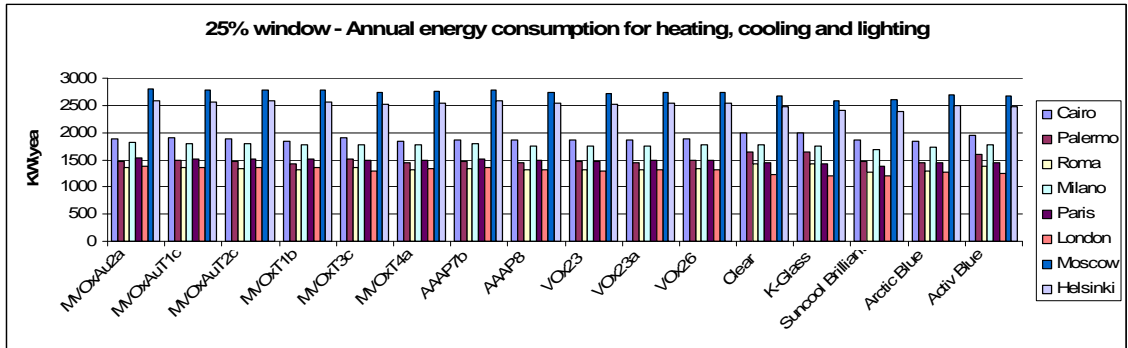
Tab. 7.15 (b) Model with the 100% window - Energy consumption for lighting (KW/year)

AAAP8	143,71	156,14	169,22	225,01	266,62	286,82	287,19	338,18
VOx23	133,48	147,56	160,70	215,29	256,66	277,63	278,05	329,46
VOx23a	144,34	156,65	169,73	225,58	267,20	287,36	287,73	338,69
VOx26	145,92	157,96	171,02	227,03	268,68	288,74	289,10	339,99
Clear	86,94	103,31	115,39	157,91	193,62	217,18	221,99	274,86
K-Glass	91,95	108,90	121,50	166,31	203,52	227,21	230,68	283,31
Suncool Brilliant	93,23	110,28	122,99	168,34	205,85	229,53	232,72	285,30
Arctic Blue	113,21	129,83	143,12	194,47	234,70	257,21	258,25	310,18
Activ Blue	92,02	108,98	121,60	166,46	203,70	227,39	230,85	283,48

7.5.4 Overall energy consumption

Fig. 7.35 a-b
Overall energy consumption in the 25% (top) and 100% (bottom) window model.

It is interesting to look at the overall energy consumption for our building for all cases. This would be the sum of heating, cooling and artificial lighting energy required in the whole year.



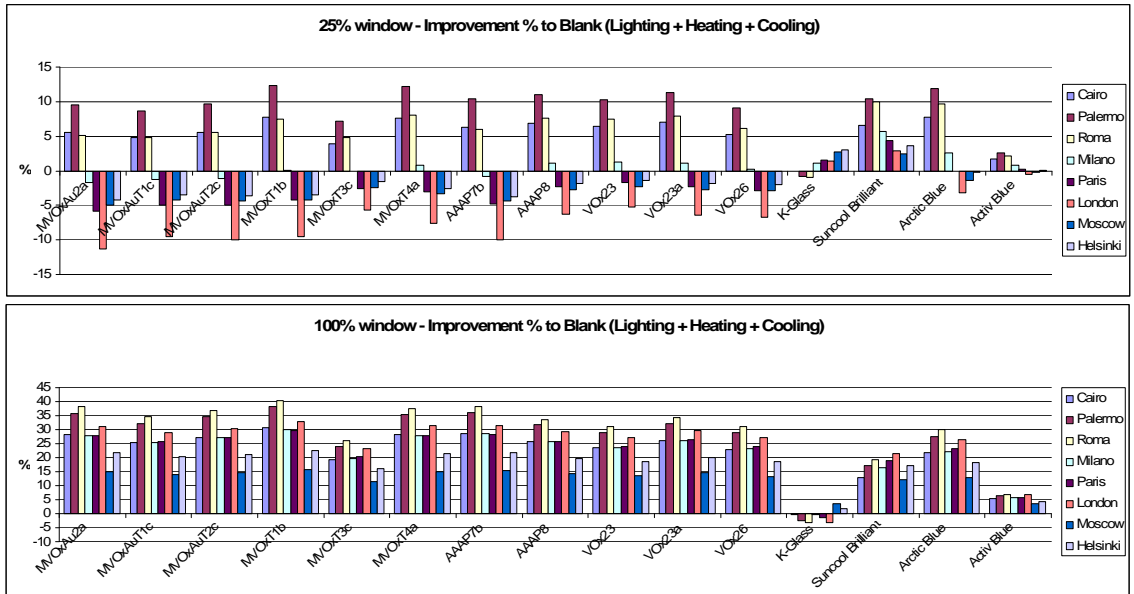


Fig. 7.36 a-b
Improvement to Blank in the 25% (top) and 100% (bottom) window model.

As it can be easily seen, the overall consumption of energy is bigger in the coldest cities. This fact was explained considering that the low average temperatures do not allow the thermochromic glazing to switch often into their hot state. Another explanation had been discussed before working on the model behaviour. As a first point, we can say that usually thermochromic glazing works in a very good way in comparison to a Clear – Clear glazing or to the Pilkington products. The best behaviour is shown in the city of Palermo for the 25% window model and in the city of Roma for the 100% window model. It is relevant to notice that in the model with a 25% window our sample work in a good way only in hot cities while in cold ones they show a bad behaviour, meaning that the model consumes more than the one with the Blank glazing. The best performance is shown in the 100% window model through all the cities where the % improvement is always positive, meaning the models consumes less than the same model with the Clear – Clear glazing. It is possible to say that the thermochromics would be a more favourable choice for large glazed areas. Large glazed surfaces, as the 100% window analyzed in this work, contribute to a greater percentage to the overall energy balance of the building, minimizing heat losses and controlling the incoming solar radiation. It is also interesting to notice that the last 5 samples (cases 7 – 11), even though they never switch in their hot state (par. 7.5.1) because of their high switching temperature T_c , they work as well in all the environmental conditions. This fact is easily explainable looking at their spectra: they show a high transmission in the visible part and high reflectance through the IR part. So we can say that they work as consequence of their optical properties and not of their smart properties.

Tab. 7.16 Overall annual energy consumption in the 25% window to wall model

Glass	Cairo	Palermo	Roma	Milano	Paris	London	Moscow	Helsinki
MVOxAu2a	1880,69	1476,02	1348,51	1811,10	1533,55	1369,97	2793,79	2590,42
MVOxAuT1c	1895,97	1492,75	1350,98	1803,98	1520,20	1348,60	2774,16	2570,51
MVOxAuT2c	1879,43	1475,48	1341,44	1800,57	1520,35	1353,02	2777,88	2575,04
MVOxT1b	1835,47	1431,34	1313,67	1781,18	1509,79	1348,32	2773,62	2570,83
MVOxT3c	1912,03	1516,57	1351,06	1782,02	1486,53	1300,83	2726,82	2523,57
MVOxT4a	1840,10	1434,54	1304,92	1768,47	1492,99	1325,41	2751,82	2547,44
AAAP7b	1866,90	1463,76	1335,80	1795,65	1519,16	1354,28	2778,28	2577,14
AAAP8	1853,84	1453,92	1312,15	1762,33	1482,05	1308,01	2734,20	2531,02
VOx23	1862,78	1464,90	1314,83	1758,82	1474,80	1296,19	2722,60	2518,95
VOx23a	1850,78	1448,99	1308,44	1762,30	1482,58	1309,75	2735,88	2532,22
VOx26	1885,58	1484,87	1333,38	1778,42	1491,78	1313,58	2740,08	2535,58
Clear	1990,64	1632,77	1420,23	1781,73	1449,34	1231,05	2661,56	2484,79
K-Glass	1991,35	1646,77	1432,95	1761,35	1427,04	1212,98	2588,70	2410,45
Suncool Brilliant	1860,50	1463,75	1278,00	1681,22	1385,91	1196,21	2597,08	2393,55
Arctic Blue	1837,42	1438,40	1282,18	1736,56	1451,03	1270,70	2699,28	2491,81
Activ Blue	1956,02	1590,19	1389,73	1767,38	1447,12	1237,55	2665,87	2483,07

Tab. 7.17 Improvement % to Blank on overall energy consumption - 25% window to wall model

Glass	Cairo	Palermo	Roma	Milano	Paris	London	Moscow	Helsinki
MVOxAu2a	5,52	9,60	5,05	-1,65	-5,81	-11,28	-4,97	-4,25
MVOxAuT1c	4,76	8,58	4,88	-1,25	-4,89	-9,55	-4,23	-3,45
MVOxAuT2c	5,59	9,63	5,55	-1,06	-4,90	-9,91	-4,37	-3,63
MVOxT1b	7,80	12,34	7,50	0,03	-4,17	-9,53	-4,21	-3,46
MVOxT3c	3,95	7,12	4,87	-0,02	-2,57	-5,67	-2,45	-1,56
MVOxT4a	7,56	12,14	8,12	0,74	-3,01	-7,67	-3,39	-2,52
AAAP7b	6,22	10,35	5,94	-0,78	-4,82	-10,01	-4,39	-3,72
AAAP8	6,87	10,95	7,61	1,09	-2,26	-6,25	-2,73	-1,86
VOx23	6,42	10,28	7,42	1,29	-1,76	-5,29	-2,29	-1,37
VOx23a	7,03	11,26	7,87	1,09	-2,29	-6,39	-2,79	-1,91
VOx26	5,28	9,06	6,11	0,19	-2,93	-6,70	-2,95	-2,04
Clear	-0,04	-0,86	-0,90	1,14	1,54	1,47	2,74	2,99
K-Glass	6,54	10,35	10,01	5,64	4,38	2,83	2,42	3,67
Suncool Brilliant	7,70	11,90	9,72	2,54	-0,12	-3,22	-1,42	-0,28
Arctic Blue	1,74	2,61	2,15	0,81	0,15	-0,53	-0,16	0,07
Activ Blue	5,52	9,60	5,05	-1,65	-5,81	-11,28	-4,97	-4,25

Tab. 7.18 Overall annual energy consumption in the 100% window to wall model								
Glass	Cairo	Palermo	Roma	Milano	Paris	London	Moscow	Helsinki
MVOxAu2a	2696,06	2310,86	2015,84	2452,15	1981,44	1665,88	3420,64	3291,61
MVOxAuT1c	2800,60	2442,38	2136,39	2537,57	2040,63	1715,24	3455,03	3362,01
MVOxAuT2c	2729,37	2361,72	2064,86	2481,75	2000,78	1680,62	3426,62	3321,25
MVOxT1b	2604,78	2228,74	1951,06	2387,40	1936,40	1626,29	3384,36	3263,78
MVOxT3c	3032,52	2738,49	2416,47	2734,30	2190,78	1855,00	3565,58	3542,84
MVOxT4a	2697,51	2334,55	2042,63	2459,47	1981,55	1659,95	3410,54	3306,93
AAAP7b	2673,35	2304,06	2019,02	2435,96	1973,17	1656,80	3401,10	3298,72
AAAP8	2788,98	2459,63	2163,53	2529,16	2038,36	1713,56	3439,81	3383,16
VOx23	2870,13	2555,92	2251,53	2595,97	2088,02	1758,72	3477,54	3438,41
VOx23a	2777,99	2440,56	2141,42	2519,70	2027,05	1702,62	3434,26	3365,86
VOx26	2887,76	2560,18	2247,87	2609,73	2093,01	1762,20	3487,42	3430,44
Clear	3750,99	3604,34	3261,98	3404,38	2750,20	2417,23	4018,10	4215,77
K-Glass	3767,40	3693,15	3370,31	3422,04	2788,13	2496,30	3880,95	4141,55
Suncool Brilliant	3272,19	2982,44	2627,70	2848,44	2228,09	1899,57	3524,24	3488,72
Arctic Blue	2927,75	2612,17	2285,85	2648,34	2107,07	1774,94	3508,59	3448,97
Activ Blue	3543,44	3367,76	3036,71	3206,45	2590,43	2256,07	3881,71	4034,70

Tab. 7.19 Improvement % to Blank on overall energy consumption-100% window to wall model								
Glass	Cairo	Palermo	Roma	Milano	Paris	London	Moscow	Helsinki
MVOxAu2a	28,12	35,89	38,20	27,97	27,95	31,08	14,87	21,92
MVOxAuT1c	25,34	32,24	34,51	25,46	25,80	29,04	14,01	20,25
MVOxAuT2c	27,24	34,48	36,70	27,10	27,25	30,47	14,72	21,22
MVOxT1b	30,56	38,16	40,19	29,87	29,59	32,72	15,77	22,58
MVOxT3c	19,15	24,02	25,92	19,68	20,34	23,26	11,26	15,96
MVOxT4a	28,09	35,23	37,38	27,76	27,95	31,33	15,12	21,56
AAAP7b	28,73	36,08	38,10	28,45	28,25	31,46	15,36	21,75
AAAP8	25,65	31,76	33,67	25,71	25,88	29,11	14,39	19,75
VOx23	23,48	29,09	30,98	23,75	24,08	27,24	13,45	18,44
VOx23a	25,94	32,29	34,35	25,99	26,29	29,56	14,53	20,16
VOx26	23,01	28,97	31,09	23,34	23,90	27,10	13,21	18,63
Clear	-0,44	-2,46	-3,32	-0,52	-1,38	-3,27	3,41	1,76
K-Glass	12,76	17,25	19,44	16,33	18,98	21,42	12,29	17,25
Suncool Brilliant	21,95	27,53	29,92	22,21	23,38	26,57	12,68	18,19
Arctic Blue	5,53	6,56	6,91	5,81	5,81	6,67	3,39	4,30
Activ Blue	28,12	35,89	38,20	27,97	27,95	31,08	14,87	21,92

7.6 Potential of thermochromic glazing

In the further paragraphs we are going to analyze the effect of switching temperature and infrared hemispherical emissivity on the thermochromic behaviour. We are going to run again the software Energy Plus by changing those parameters and looking at the effect they lead on the glazing behaviour.

7.6.1 Switching temperature

As previously discussed, thermochromic coatings are characterized by a switching temperature T_c . Above, or below, this parameter the coating alter its spectral attributes changing, as a consequence, its behaviour towards the radiation, both the visible and the IR.

We are going to run some energy simulation varying the T_c value for three sample in two different cities: Palermo, as a hot city, and London, as a cold one. We are going to look into cases with 25% window to wall ratio only since these are more common. In order to compare all the value, the spectral characteristics of every sample will not be changed. This is not completely correct from a physical/chemical point of view as different switching temperatures derive from different coatings. The samples' T_c and energy loads are summarized in the following table 7.20. The Clear-Clear window's energy loads are reported for comparison reason.

MVOxT1b was chosen because it showed the best performance in the previous analysis. The other two samples were chosen to look at glasses with gold nanoparticles, the first, and just Vanadium (IV) dioxide, the last.

Tab. 7.20 Thermochromic samples chosen for the analysis

Sample	Actual T_c [°C]	% improvement to Blank (%)		Heating load (KW/year)		Cooling load (KW/year)		Lighting load (KW/year)	
		Palermo	London	Palermo	London	Palermo	London	Palermo	London
MVOxAu2a	43	9,6	-11,28	53,14	680,04	963,46	134,09	459,42	555,84
MVOxT1b	38,5	12,34	-9,53	50,64	685,95	944,92	127,82	435,78	534,55
VOx26	60	9,06	-6,7	44,53	644,50	1040,28	166,10	400,06	502,98
Blank glass	-	-	-	30,85	531,23	1329,80	310,97	272,12	388,84

Looking at the Figure 7.37, it can be noticed that the increase of the T_c lead to higher consumption for all the three samples. On the contrary, a lower T_c lead to a decreasing consumption. This is quite expected since a higher T_c avoid the thermochromic glazing to switch in their hot state as often as they usually would. The sample showing the greatest gain is VOx26. However, looking at the Fig. 7.38, it can be reported that the percentage improvement is very small: about 5 points % for VOx26, about 2 points % for MVOxAu2a and MVOxT1b.

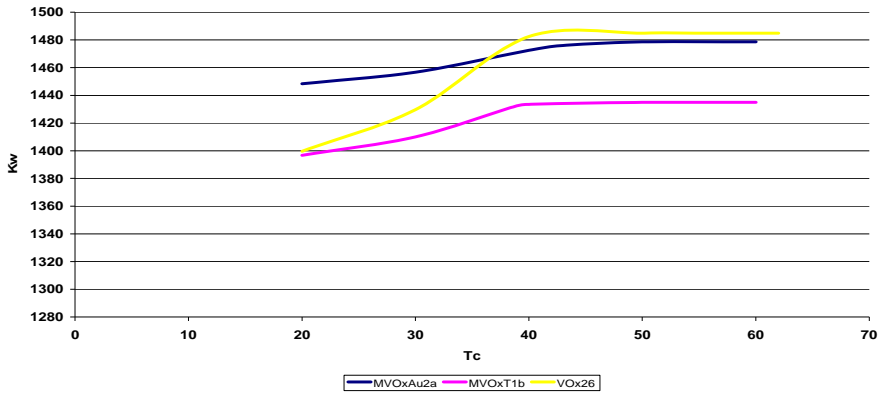


Fig. 7.37
Energy consumption in the 25% window model varying Tc in the city of Palermo.

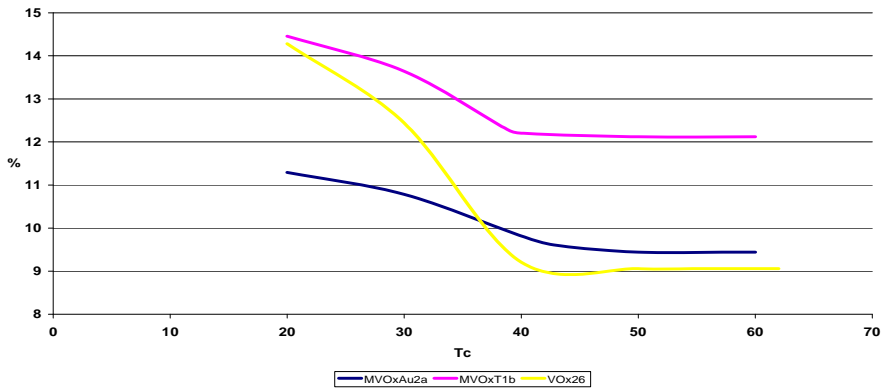


Fig. 7.38
Improvement to Blank in the 25% window model varying Tc in the city of Palermo.

Tab. 7.21 (a) Results varying the Tc for the city of Palermo. In green the real Tc

Sample	Tc (°C)	Improvement % to Blank	Heating load (KW/year)	Cooling load (KW/year)	Lighting load (KW/year)	Total load (KW/year)
MVOxAu2a	60	9,442	53,221	964,847	460,531	1478,598
	50	9,443	53,218	964,847	460,517	1478,582
	43	9,600	53,139	963,464	459,416	1476,018
	40	9,816	53,140	960,701	458,644	1472,485
	30	10,785	53,102	947,460	456,103	1456,664
	20	11,294	53,008	941,307	454,049	1448,365
MVOxT1b	60	12,119	50,558	947,771	436,559	1434,888
	40	12,119	50,558	947,771	436,559	1434,888
	40	12,205	50,613	946,827	436,052	1433,493
	38.5	12,337	50,635	944,916	435,784	1431,336
	30	13,642	50,859	924,991	434,178	1410,028
	20	14,455	50,973	912,916	432,854	1396,743

Tab. 7.21 (b) Results varying the Tc for the city of Palermo. In green the real Tc						
Sample	Tc (°C)	Improvement % to Blank	Heating load (KW\year)	Cooling load (KW\year)	Lighting load (KW\year)	Total load (KW\year)
VOx26	62	9,058	44,534	1040,279	400,056	1484,868
	55	9,058	44,534	1040,279	400,056	1484,868
	50	9,058	44,534	1040,279	400,056	1484,868
	40	9,208	44,547	1038,646	399,230	1482,424
	30	12,440	44,352	992,897	392,394	1429,643
	20	14,281	44,270	967,753	387,575	1399,598
Blank	-	-	30,85	1329,80	272,12	1632,77

In London we can report the same behaviour previously reported. The increase of the Tc lead to higher consumption while a lower Tc lead to a decreasing consumption. This time the switch is quite smaller. This is probably due to the climate conditions, a colder weather in general. However, the percentage improvement is: about 1 point % for VOx26, less than 1 point % for MVOxT1b and MVOxAu2a.

Tab. 7.22 (a) Results varying the Tc for the city of London						
Sample	Tc (°C)	Improvement % to Blank	Heating load (KW\year)	Cooling load (KW\year)	Lighting load (KW\year)	Total load (KW\year)
MVOxAu2a	60	-11,234	678,985	134,304	556,046	1369,335
	50	-11,234	678,985	134,304	556,046	1369,335
	43	-11,285	680,037	134,094	555,837	1369,967
	40	-11,290	681,014	133,443	555,574	1370,031
	30	-11,098	683,939	129,353	554,371	1367,662
	20	-11,005	686,945	126,653	552,947	1366,527
	15	-10,999	688,714	125,564	552,178	1366,455
	MVOxT1b	60	-9,435	684,422	128,112	534,661
40		-9,435	684,422	128,112	534,661	1347,195
40		-9,477	684,987	128,107	534,619	1347,713
38.5		-9,527	685,950	127,825	534,548	1348,323
30		-9,387	690,454	122,266	533,883	1346,603
20		-9,360	695,672	117,580	533,017	1346,269
15		-9,401	698,753	115,593	532,427	1346,774

Tab. 7.22 (b) Results varying the Tc for the city of London

Sample	Tc (°C)	Improvement % to Blank	Heating load (KW/year)	Cooling load (KW/year)	Lighting load (KW/year)	Total load (KW/year)
VOx26	62	-6,704	644,499	166,099	502,981	1313,580
	55	-6,704	644,499	166,099	502,981	1313,580
	50	-6,704	644,499	166,099	502,981	1313,580
	40	-6,757	645,187	166,099	502,934	1314,221
	30	-6,160	652,793	153,461	500,624	1306,877
	20	-5,693	660,888	142,902	497,334	1301,124
	15	-5,572	665,771	138,847	495,018	1299,636
Blank	-	-	531,23	310,975	388,841	1231,045

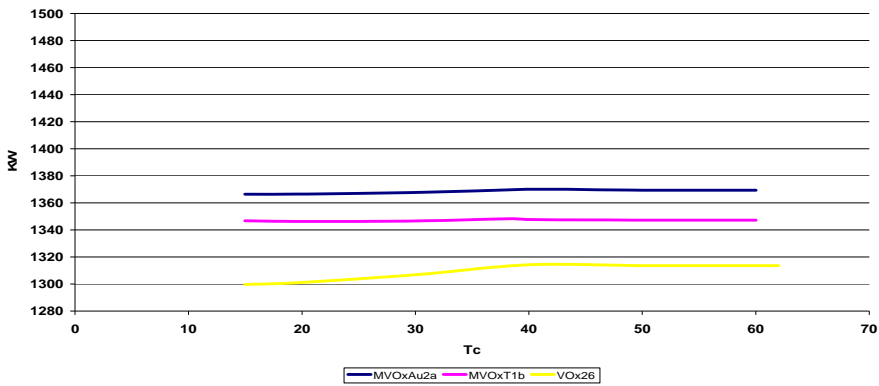


Fig. 7.39
Energy consumption in the 25% window model varying Tc in the city of London.

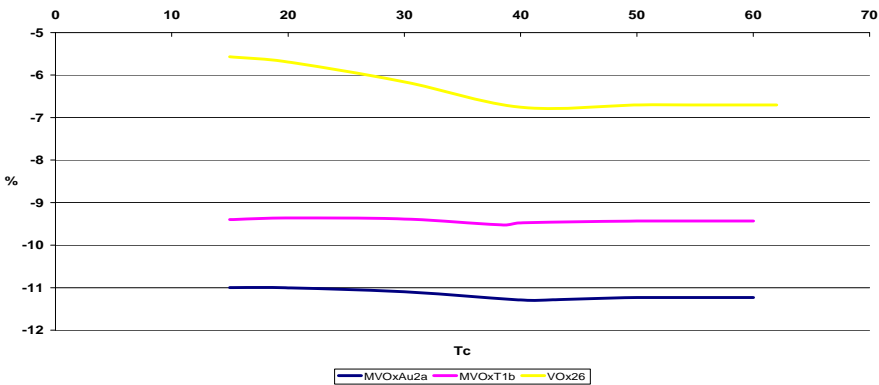


Fig. 7.40
Improvement to Blank in the 25% window model varying Tc in the city of London.

7.6.2 Infrared hemispherical emissivity

As previously discussed, all the glasses are characterized by a hemispherical emissivity, ϵ , which is the capacity of a material to radiate energy. We are going to run some energy simulations varying the emissivity values for three sample in two different cities, Palermo and London, as previously done with the switching temperature.

In order to compare all the values, the other spectral characteristics of every sample will not be changed. Following are shown the results of such simulations. The glasses behaviour does not change varying the glass emissivity. This fact is quite strange as the emissivity indicates, in a certain way, the amount of energy crossing the glass and, consequently, leaving the building. A change in the building behaviour should be recorded, even it was very little.

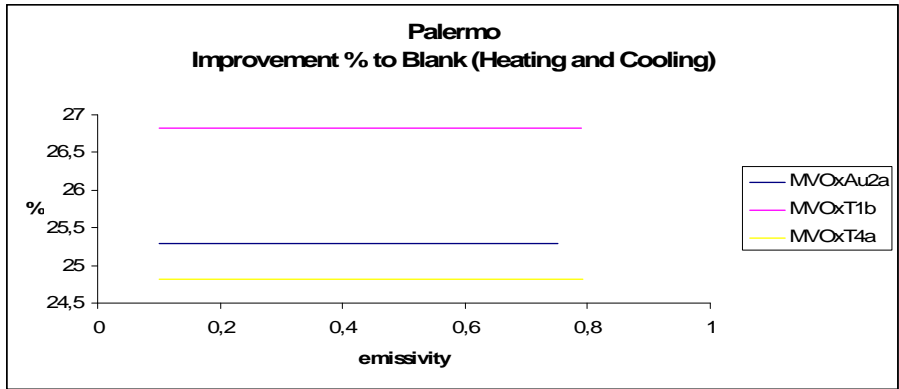


Fig. 7.41
Improvement to Blank in the 25% window model varying the emissivity in the city of Palermo.

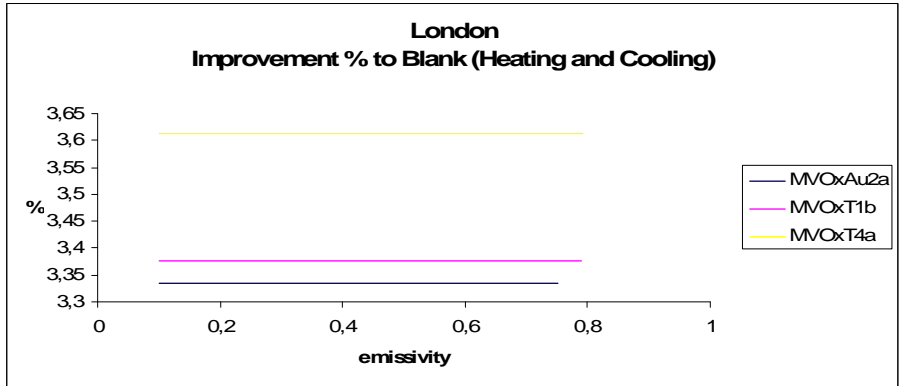


Fig. 7.42
Improvement to Blank in the 25% window model varying the Emissivity in the city of London.

To have a confirm of this result, another series of simulations were run for one sample only, MVOxT1b, keeping it in its cold state and hot state respectively, as it was a static glass. As it can be seen, this time a change in the building behaviour is recorded. The conclusion could be that the software Energy Plus can not succeed in recording the change in the behaviour as it switches from the cold state to the hot one and back.

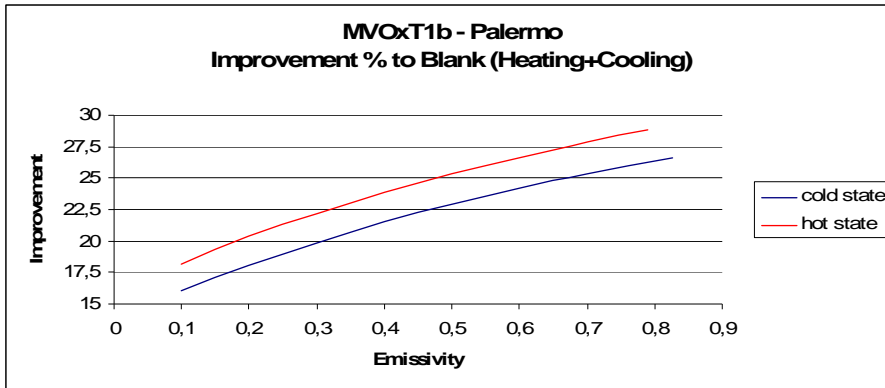


Fig. 7.43
Improvement to Blank in the 25% window model varying the Emissivity in the city of Palermo.

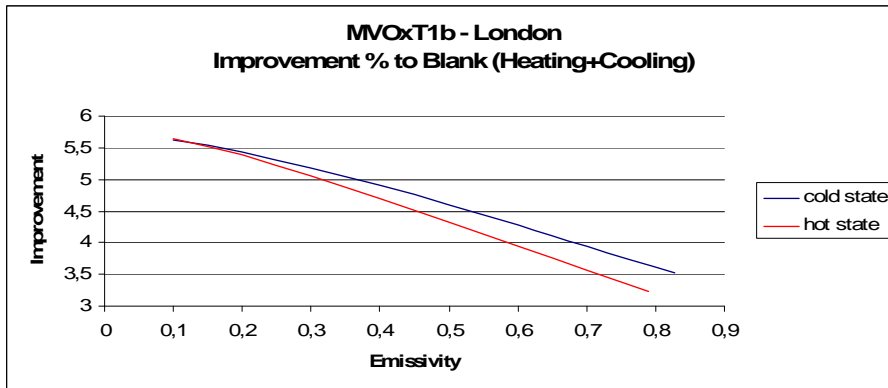


Fig. 7.44
Improvement to Blank in the 25% window model varying the Emissivity in the city of London.

8. IDEAL THERMOCHROMIC SPECTRUM

8.1 Introduction

In this section we are going to analyse the “ideal thermochromic spectrum” in order to understand the limit of this technology. As it was done in the previous chapter, some new simulations were carried on by means of the software Energy Plus™. The model is the room with a whole glazing window (100% window to wall ratio) in the city of Palermo since it was found out that thermochromics work best if applied in hot climates and if the building has got large windows (look at the results of Chapter 7). In this section, we are going to vary the thermochromic optical properties such as the transmittance and reflectance, both in the hot and cold states, over the IR range and the Visible range of the spectrum to understand how the ideal glazing behaviour changes. Furthermore, some comparisons with the Pilkington products will be made. To learn more about the model’s materials and configurations, as well as the software Energy Plus™, refer to Chapter 7.

8.2 Ideal thermochromic spectrum

The ideal thermochromic spectrum was designed considering the appropriate percentage of transmittance and reflectance, in both hot and cold state, over the spectrum to make the glazing work and perform in the best way. As we know from the previous experiments and analysis on the real glasses produced in our laboratory, there are no changes between the hot and the cold states in the visible part of the spectrum (300 – 750 nm); while there should be a quite big shift ($\approx 65\%$) in the IR part (750 – 2500 nm). From this assumption we designed the following:

1) Transmission in the cold state:

$$\lambda \text{ vis max}^1 (570 \text{ nm}) = 65 \%$$

$$\lambda \text{ vis } (700 \text{ nm}) = 55 \%$$

$$\text{IR transmission } (800\text{-}2500 \text{ nm}) = 80 \%$$

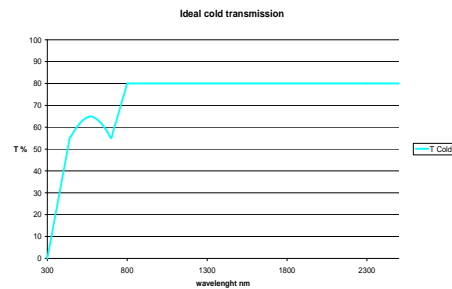
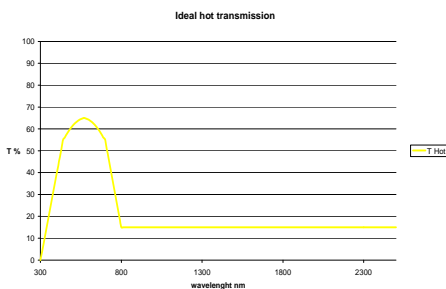


Fig. 8.1
Ideal cold transmission.

2) Transmission in the hot state:

$$\lambda \text{ vis max } (570 \text{ nm}) = 65 \%$$

$$\text{IR transmission } (800\text{-}2500 \text{ nm}) = 15 \%$$

Fig. 8.2
Ideal hot transmission.

¹ $\lambda \text{ vis max}$ = maximum value in the visible part of the spectrum.

3) Reflectance in the cold state:
 λ vis max (570 nm) = 17 %
 λ vis (750 nm) = 7 %
 IR reflectance (800-2500 nm) = 12 %

Fig. 8.3
Ideal cold reflectance.

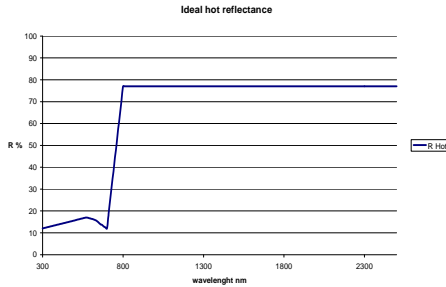
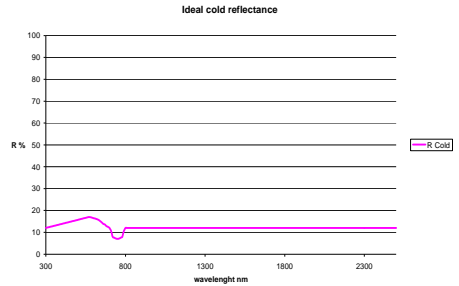


Fig. 8.4
Ideal hot reflectance.

4) Reflectance in the hot state:
 λ vis max (570 nm) = 17 %
 IR reflectance (800-2500 nm) = 77 %

The ideal spectrum designed in such a way should lead to the best thermochromic behaviour: while the glass is in its cold state – thus means during the cold season – the IR transmission is very high (80 %) and the IR reflectance is very low (12 %) to allow the thermal radiation – the IR – entering in the building. While the glass is in its hot state – thus means during the hot season – the IR transmission is quite low (15 %) and the IR reflectance is very high (77 %) thus preventing the thermal radiation entering in the building and reflecting it outside. Over the visible range the transmission should be quite high in both the hot and cold states while the reflectance should be quite low. The switch between the hot and cold transmission - $\delta(T)$ - had been designed to be at least 65 % as well as the switch between the hot and cold reflection $\delta(R)$.

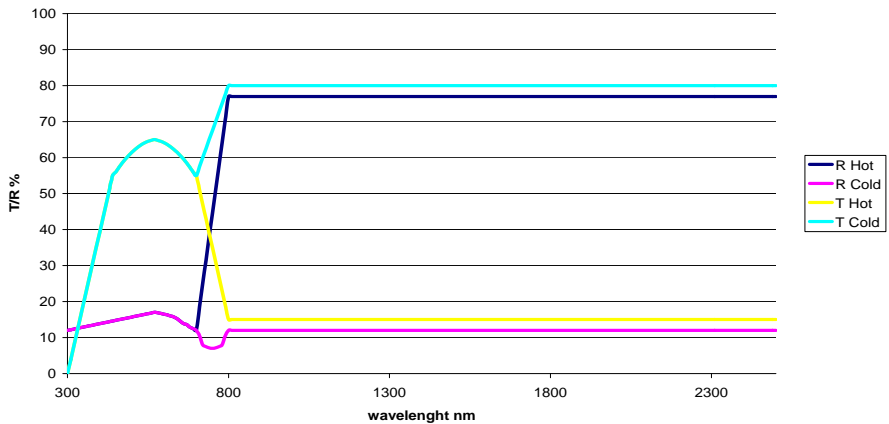


Fig. 8.5
Ideal thermochromic spectrum

Some energy modelling simulations were carried out to calculate the energy consumption for heating, cooling and lighting in the 100 % window to wall ratio in the city of Palermo and to understand how the ideal thermochromic glass behaves in comparison to the commercial glazing produced by Pilkington. The simulations were carried out with the ideal thermochromic glazing’s switching temperature changing between 35°C to 20°C which is the minimum value physically reachable by our configuration. As previously done, the results are shown in terms of electrical energy [KW] per year consumed by the building for heating, cooling and lighting and in terms of improvement percentage to a Clear-Clear glazing configuration. Following, graphs concerning the energy consumption and the improvement percentage are shown for the $\delta(T,R)=65\%$ ideal thermochromic glass.

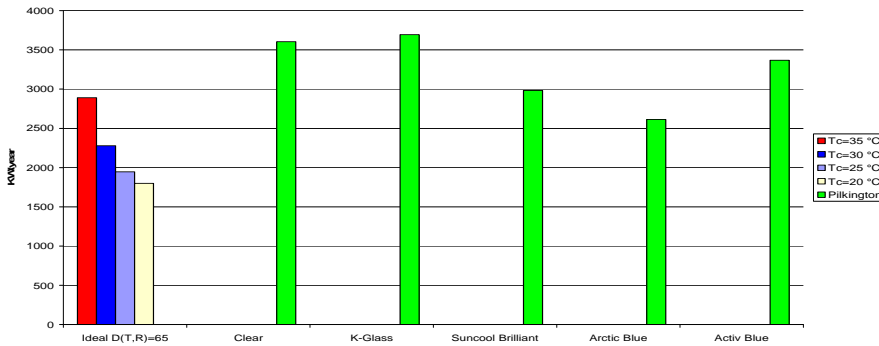


Fig. 8.6 Energy consumption [KW/year] of the ideal thermochromic glazing in comparison to the Pilkington products for the city of Palermo and with 100% window to wall ratio.

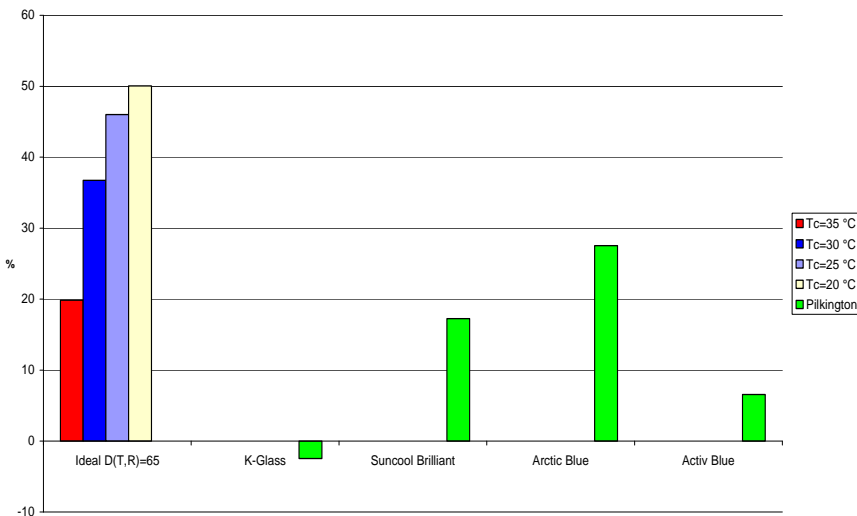


Fig. 8.7 Improvement percentage of the ideal thermochromic glazing in comparison to the Pilkington products for the city of Palermo and with 100% window to wall ratio.

As it can be easily seen from the graphs in the previous page, the energy consumption for heating, cooling and lighting in one year for our ideal glazing is lower than the standard Pilkington products. Moreover, it is interesting to notice that the transition temperature T_c influences a lot the glass behaviour, more particularly the lower the T_c the lower the energy consumption.

The minimum sensible value of T_c is about 20 °C. This fact is due to the way the simulations are performed: to run them a relationship between the surface outside temperature (\approx coating temperature) and the solar gain on the glass surface (W/m^2) is found out running a simulation where the glass never switches in its hot state.

In the following image this relationship is shown.

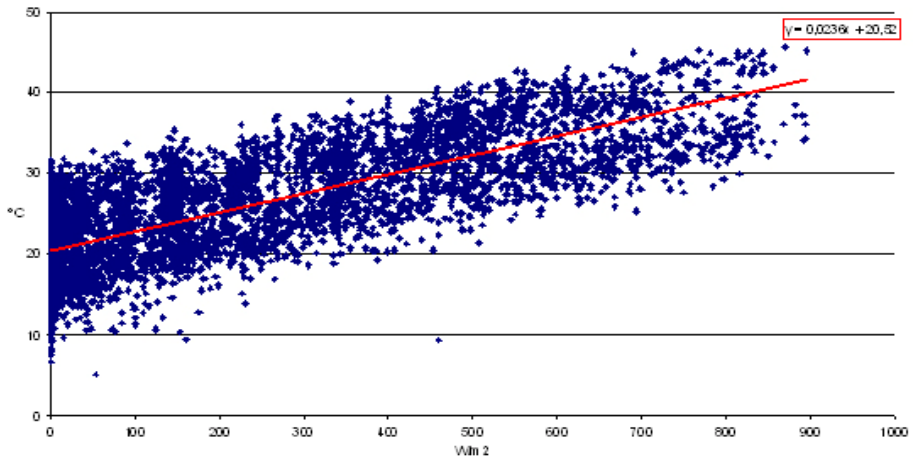


Fig. 8.8
Relationship between the glazing surface external temperature and the incident solar energy.

Then, Excel was used to calculate the trend-line (in red in the image above) and to display the equation on the chart. Setting the value we want the switching temperature (T_c) would be and replacing it in the equation - as y value - we obtain the solar heat gain on the window that is necessary to make the thermochromic glass reach the set transition temperature T_c and, thus, switch into its hot state. In this particular case:

$$y = 0,0236 x + 20,52 \quad (\text{eq. 8.1})$$

$$y = T_c; x = \text{solar gain} \quad (\text{eq. 8.2; eq. 8.3})$$

$$\text{solar gain} = (T_c - 20,52) / 0,0236 \quad (\text{eq. 8.4})$$

The solar gain so calculated is set into Energy Plus™ to perform the complete simulations (with the glazing switching into their hot state) but, as a mathematical/physical consequence, the minimum value settable is $T_c = 20,52 \text{ °C} \approx 20 \text{ °C}$.

Tab 8.1 Relationship T_c – Solar gain for a $\delta(T,R) = 65\%$ ideal thermochromic coatings	
T_c [°C]	Solar gain [W/m ²]
35	614
30	402
25	190
20	The glass is always in its hot state

In the tables below all the results in terms of energy consumption for lighting, heating, cooling – all expressed in KW/year - and the percentage improvements are summarized.

Tab 8.2 Ideal thermochromic $\delta(T,R) = 65\%$ energy consumption [KW/year]			
T_c [°C]	Heating	Cooling	Lighting
35	20,58622424	2735,784692	132,9671273
30	20,54815304	2126,511895	132,9671273
25	20,80346232	1792,474174	132,9684553
20	21,47525742	1645,176159	132,9758123

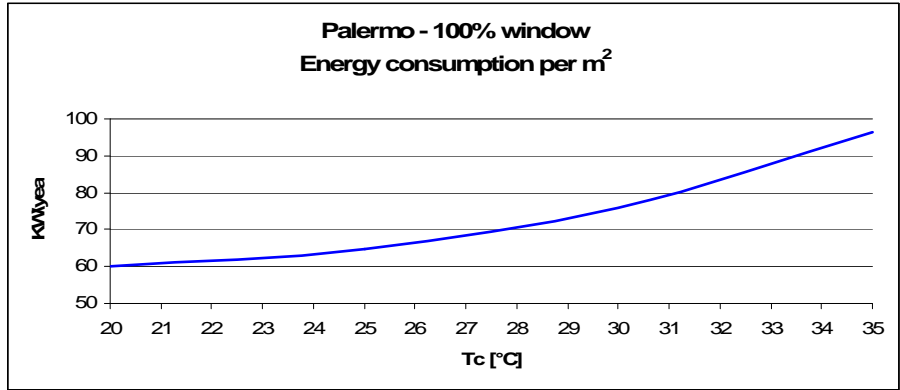
Tab 8.3 Clear – Clear glazing energy consumption [KW/year]			
T_c [°C]	Heating	Cooling	Lighting
static	17,69894218	3483,326255	103,3138466

Tab 8.4 Ideal thermochromic $\delta(T,R) = 65\%$ total energy consumption [KW/year] and improvement % to a Clear-Clear				
T_c [°C]	H + C	H + C (%)	H + C + L	H + C + L (%)
35	2756,370917	21,26961	2889,338044	19,837229
30	2147,060048	38,67339	2280,027175	36,742156
25	1813,277636	48,20724	1946,246091	46,002691
20	1666,651416	52,39533	1799,627228	50,070534

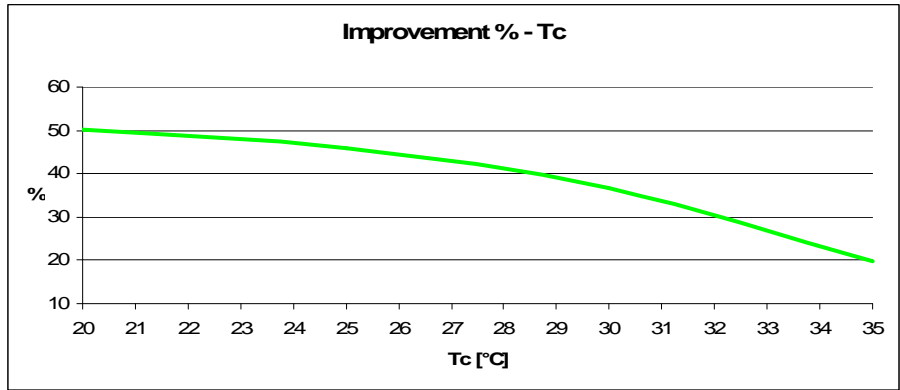
An interesting consequence of these simulations is that we are able to create a chart where it can immediately be read that the energy consumption per m² (Fig. 8.9) - or the improvement % (Fig. 8.10) - of a building with 100% window to wall ratio in the city of Palermo depending on the real transition temperature of the thermochromic film we are going to apply in that particular building, as it shown in the graphs below.

Fig. 8.9

Relationship between the transition temperature and the energy consumption per m^2 in a building with a 100% window to wall ratio in Palermo.

**Fig. 8.10**

Relationship between the transition temperature and the improvement percentage in a building with a 100% window to wall ratio in Palermo.



What these graphs tell us, in this particular case, is the following:

1. the lower T_c , the lower energy consumption (or the higher improvement percentage) for heating, cooling and lighting (as we saw in the graphs 8.6 and 8.7);
2. if we have a real thermochromic glazing with a switch of 65% between the hot and the cold transmission and between the hot and the cold reflection - $\delta(T,R) = 65\%$ - and we know its transition temperature T_c , we can immediately know the energy consumption per m^2 in our particular building.

8.3 Varying $\delta(T,R)$ through the IR region

We are now going to run some simulations using ideal thermochromic spectra where the switch between the hot and the cold transmission and the hot and the cold reflection vary from 65% to 0% in the IR region only. Thus to understand which is the best switch in a thermochromic coating and what consequence this change leads to in terms of energy consumption in a building.

Tab. 8.5 Relationship between Tc and solar gain

$\delta(T;R)$ [%]	Tc [°C]			$\delta(T;R)$ [%]	Tc [°C]			$\delta(T;R)$ [%]	T [°C]		
	35	30	25		35	30	25		30	25	20
65	614	402	190	50	619	407	196	20	610	406	201
60	615	404	192	45	621	409	197	10	617	411	205
55	617	405	194	40	623	411	199	0	623	417	210

N.B. for Tc=20°C the glass is always in its hot state

In the following graphs some ideal spectra, where the optical properties in the visible region never change, are shown.

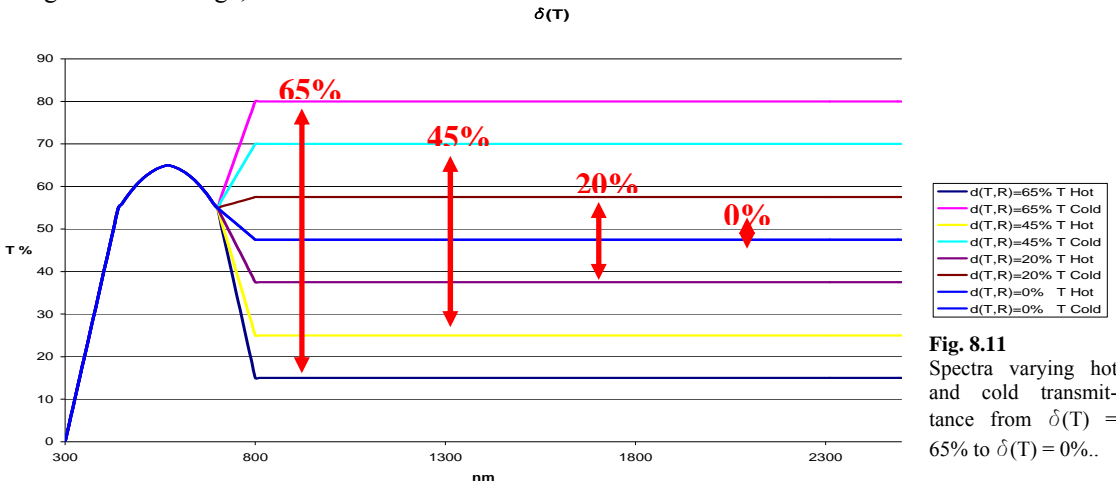


Fig. 8.11
Spectra varying hot and cold transmittance from $\delta(T) = 65\%$ to $\delta(T) = 0\%$.

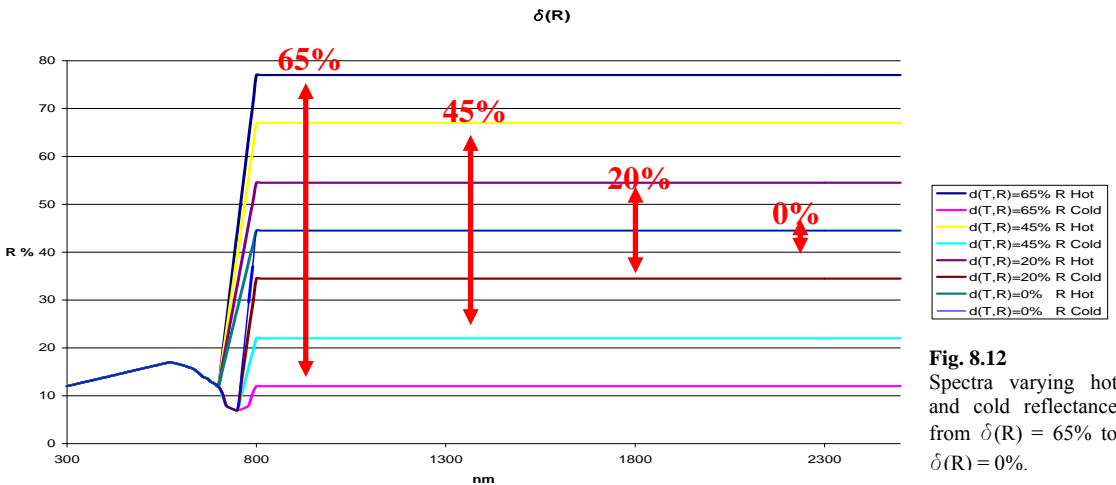


Fig. 8.12
Spectra varying hot and cold reflectance from $\delta(R) = 65\%$ to $\delta(R) = 0\%$.

As previously done, we are going to show the results of the simulations where the energy consumption for heating, cooling and lighting are shown for each transition temperature.

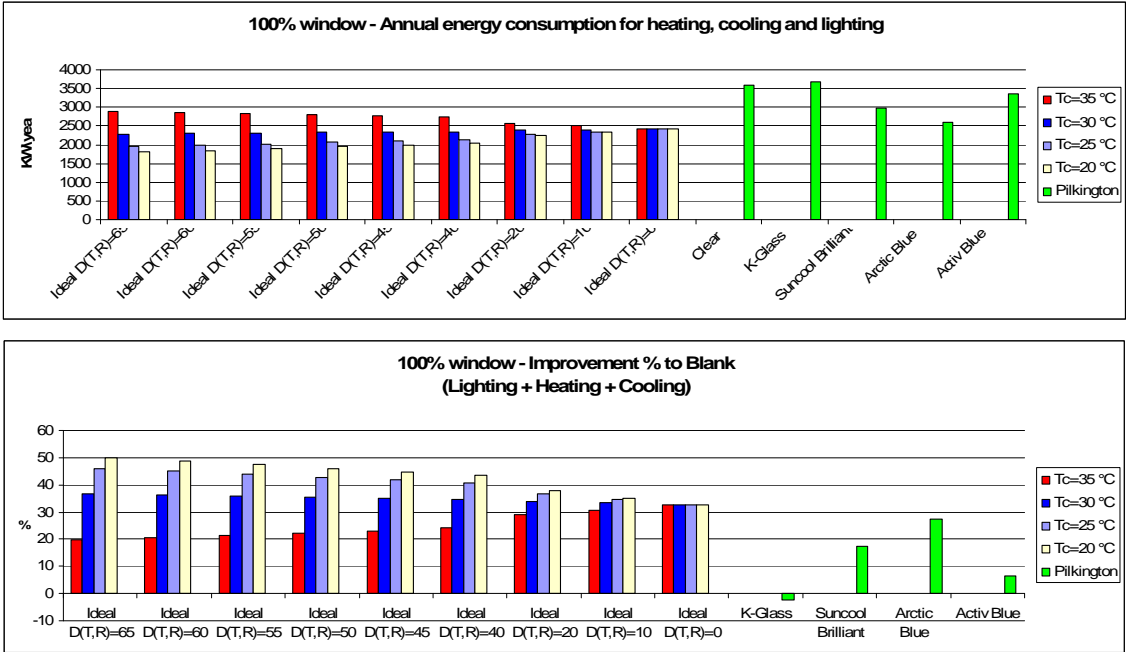


Fig. 8.13 a-b
 Top: Energy consumption for heating, cooling and lighting.
 Bottom: Improvement percentage for heating, cooling and lighting.

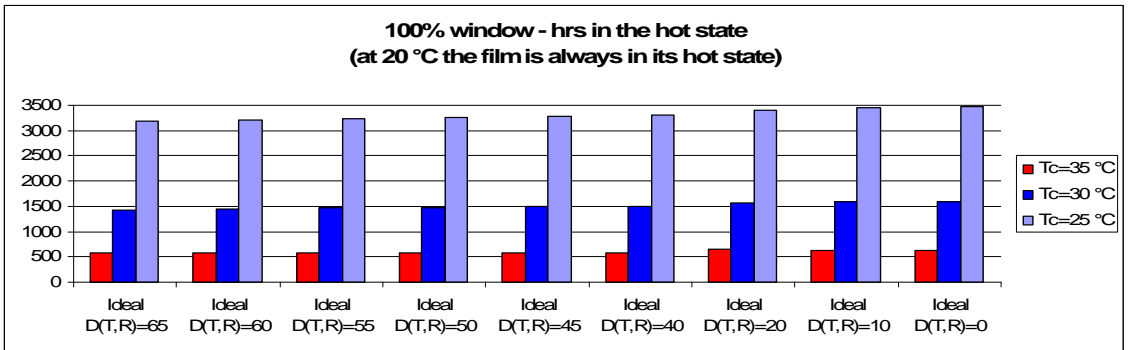
Tab. 10.6 Ideal thermochromic coatings, total energy consumption [KW/year] for heating, cooling and lighting

$\delta(T,R)$	Heating + Cooling + Lighting			
	35°C	30°C	25°C	20°C
65 %	2889,338044	2280,027175	1946,246091	1799,627228
60 %	2856,998372	2295,233408	1985,125311	1847,881305
55 %	2829,147216	2308,43865	2023,879829	1896,341851
50 %	2799,924401	2323,345758	2062,070385	1944,934191
45 %	2770,309636	2337,096193	2098,865477	1993,554192
40 %	2736,827971	2350,133511	2136,202526	2042,281572
20 %	2564,142204	2380,961653	2277,967921	2237,924599
10 %	2502,119968	2405,009614	2349,704865	2335,95565
0 %	2434,428554	2425,620563	2420,513934	2434,071275

Again, the energy consumption for all our ideal thermochromic glazing are lower than the one of the standard products by Pilkington. More particularly:

1. the bigger switch between hot and cold transmission and hot and cold reflection – that is to say $\delta(T,R) = 65\%$ – the lower energy consumption or the maximum improvement percentage to a Clear-Clear configuration;
2. in all the cases, the lower T_c (the white rectangles), the lower energy consumption, the higher improvement percentage;
3. in the case $\delta(T,R) = 0\%$ (the last on the right) the four energy consumptions calculated tend to be almost the same. This fact is explainable with the assumption that the coating tends to become static rather than a dynamic one as it should be;
4. the transition temperature T_c plays an important role in the thermochromics' behaviour (30% improvement is recorded for the $\delta(T,R) = 65\%$ case from $T_c = 35^\circ\text{C}$ to $T_c = 20^\circ\text{C}$) while with the simulation run in the previous chapter on real thermochromic coatings it did affect for no more than 2 %.

In the following pages we are going to look at some graphs to compare the ideal thermochromics only with the aim to understand more clearly what the differences are between the various ideal designed spectra:



A consequence of the different transition temperatures is the different amount of hours in which the ideal thermochromic coatings switch in their hot state. As it can be seen above (fig. 8.14), for all the cases the lower transition temperature the bigger number of hours in the hot state, while there are almost no differences between the different $\delta(T,R)$. The columns relative to the $T_c = 20^\circ\text{C}$ are not reported since, as previously discussed, the films are always in their hot state.

Fig. 8.14
Numbers of hour in a year the thermo-chromics are in the hot state.

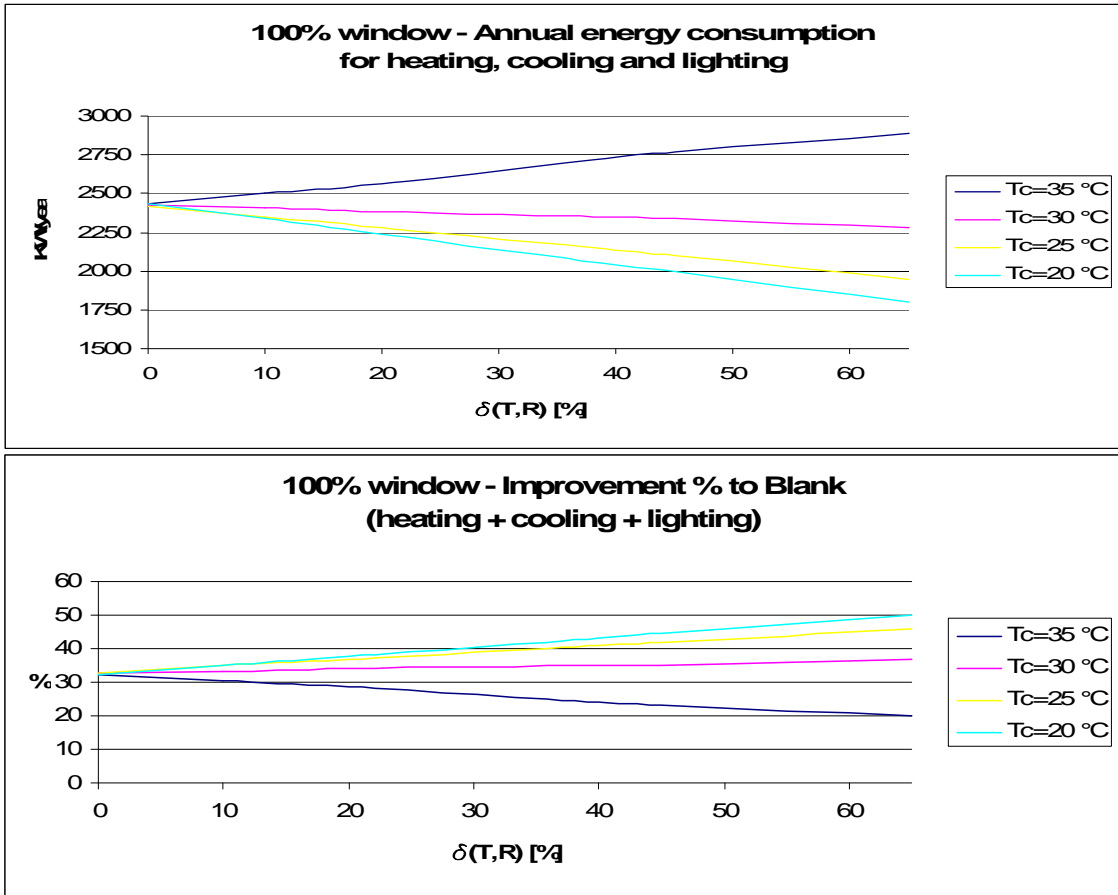
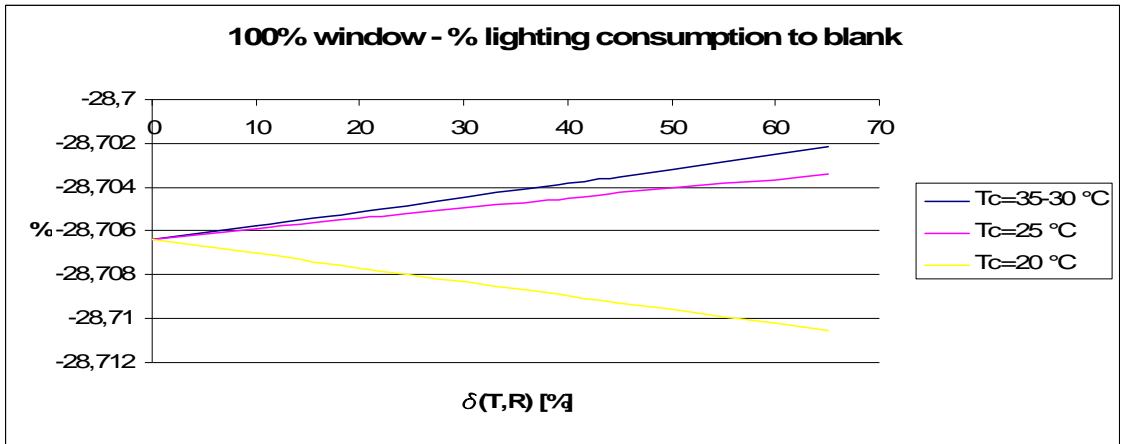


Fig. 8.15 a-b
 Top: Annual energy consumption.
 Bottom: Improvement %.

In the images above, the total energy consumption for one year is reported. Looking at these graphs, it is more clear that moving toward $\delta(T,R)=0\%$ - on the left side of the graphs - the glass tends to become static since there is no switch between the hot state and the cold one. Once again, this is even more clear how important is the transition temperature in the whole thermochromic behaviour, the difference between 20°C and 35°C is more than 30%, as previously said.

Furthermore if we consider the glass as a static one - $\delta(T,R) = 0\%$ - the energy improvement to a Clear-Clear configuration is more than 30 %.

It is important to notice that the consumption for lighting does not influence the total amount since the improvement between the two opposite ideal spectra is $0,003 \div 0,004\%$, as shown in the following graph.



Using the results achieved, it would be possible to draw a chart for each weather condition and for each window-to-wall-ratio where it can be read the energy consumption per m^2 (or the energy improvement to a Clear-Clear configuration) of an ideal thermochromic glazing depending on the switch between the hot and the cold transmittance and reflectance, $\delta(T,R)$, and the transition temperature T_c .

Fig. 8.16
Percentage consumption for lighting to a Clear-Clear configuration.

In this work the chart is drawn for the city of Palermo with a 100% window to wall ratio as the simulations had been performed with this settings only. The graphs in the next page show which is the best ideal thermochromic configuration: high $\delta(T,R)$ and low T_c .

It is interesting to notice that there are two singular points at $31,4^\circ\text{C}$ and $31,85^\circ\text{C}$, depending on the $\delta(T,R)$, where the energy consumptions tend to be almost the same as the glass is becoming more and more static reaching those values of T_c .

Furthermore it can be easily noticed that all the analysis previously done are confirmed:

1. the bigger switch between hot and cold transmission and reflection – that is to say $\delta(T,R) = 65\%$ - the lower energy consumption, the maximum improvement percentage to a Clear-Clear Pilkington configuration;
2. the lower T_c the lower energy consumption, the higher improvement percentage, showing that the T_c plays an important role in the thermochromics' behaviour;

in the case $\delta(T,R) = 0\%$ the energy consumptions tend to be almost constant, as the coating tends to become a static film.

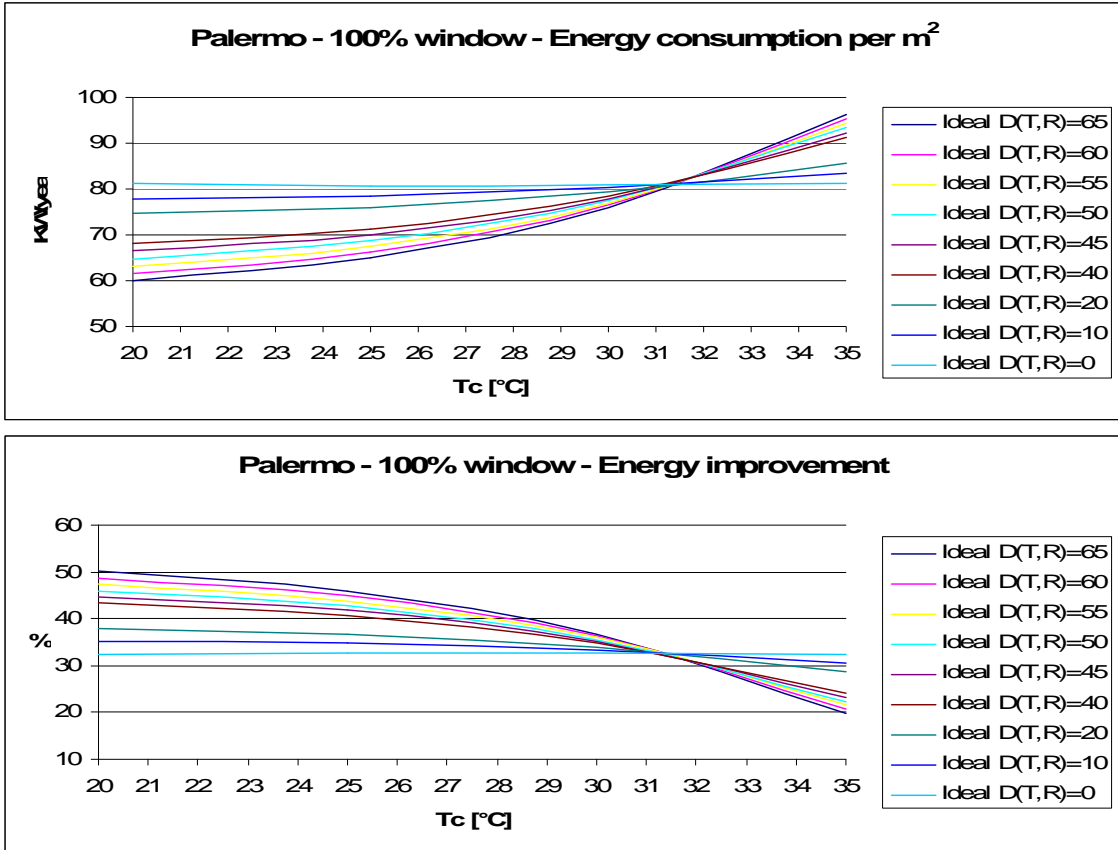


Fig. 8.17 a-b
 Top: Thermochromic energy consumption chart.
 Bottom: Ideal thermochromic energy improvement chart.

8.4 Varying $\delta(T)$ through the visible region

We are now going to run some simulations using the ideal thermochromic spectra where the transmittance through the visible range varies. More particularly, $\lambda_{\text{vis max}} = 65\%$ and its position varies from 570 nm to 470 nm leading to a change in the film visible transmittance as well as its colour from red/orange to blue/violet.

The switch between the hot and the cold transmittance and the hot and the cold reflectance is constant through the IR range, $\delta(T,R) = 65\%$, since the simulations with this setting lead to the best results².

In the following graphs the two border ideal thermochromic spectra, where the optical properties in the visible region change, are shown.

² Refer to paragraph 8.3 "Varying $\delta(T,R)$ through the IR region".

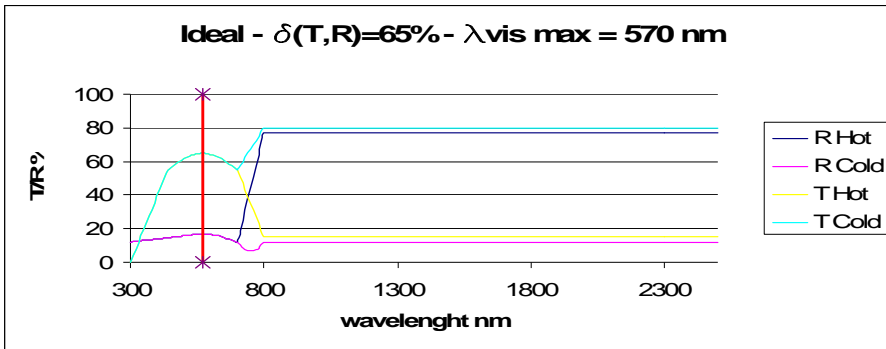


Fig. 8.18
Spectrum with λ_{vis} max at 570 nm.

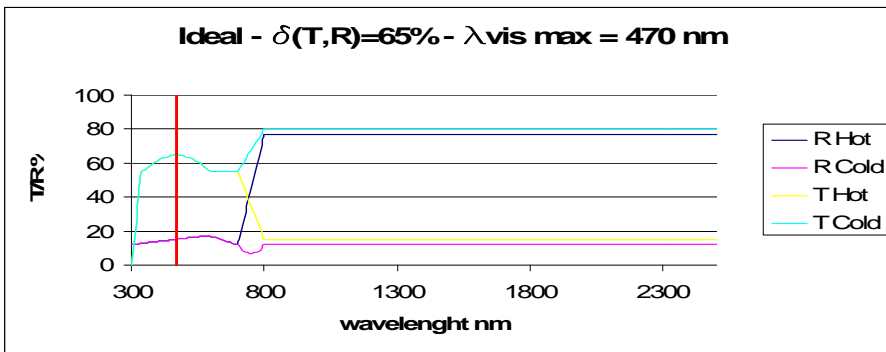
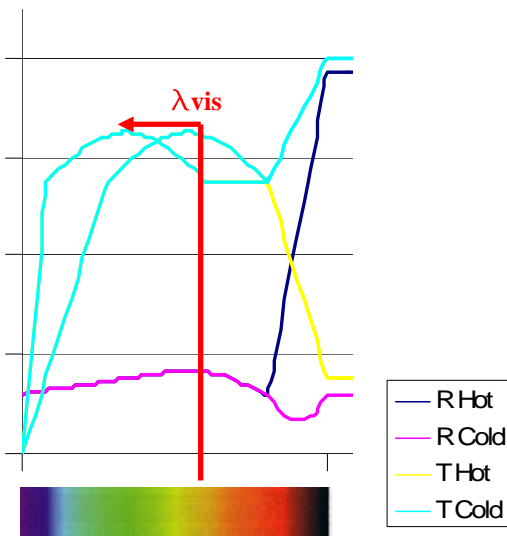


Fig. 8.19
Spectrum with λ_{vis} max at 470 nm.



Tab. 10.7 Visible spectrum range.	
Color	Wavelength [nm]
Violet	380 – 450
Blue	450 – 495
Green	495 – 570
Yellow	570 - 590
Orange	590 - 620
Red	620 - 750

The simulations were carried out considering a fixed $T_c = 25 \text{ }^\circ\text{C}$, as it was considered an acceptable value for a thermochromic glazing for architectural applications.

Fig. 8.20
Enlargement of the visible range of the two border thermochromic spectra, with the graphical indication of the λ_{vis} max shift and the colours range.

Tab. 8.8 Solar gain on the window external surface necessary to make the coatings change into their hot state

$\lambda_{vis\ max}$ [nm]	Surface solar gain [W/m^2]
470	194,69
480	194,74
490	194,78
500	194,06
510	194,15
520	193,49
530	192,81
540	193,07
550	191,67
560	191,11
570	189,83

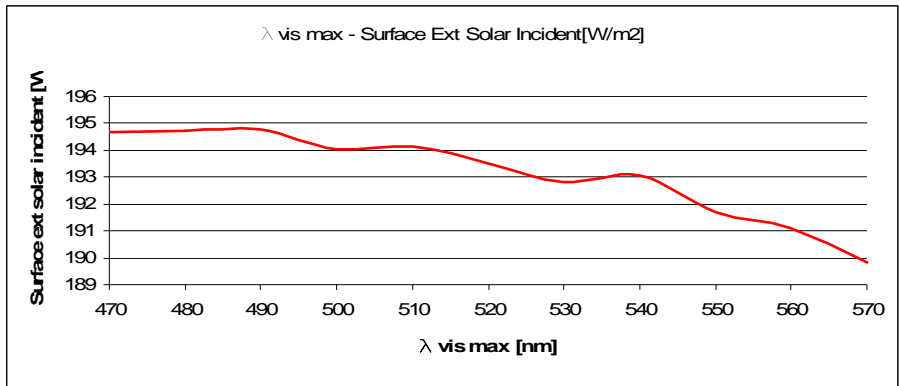


Fig. 8.21
Relationship between the external solar gain and the $\lambda_{vis\ max}$.

Following, it is possible to see the energy consumption in one year. It is important to notice that all the spectra analysed perform better than the Pilkington standard products.

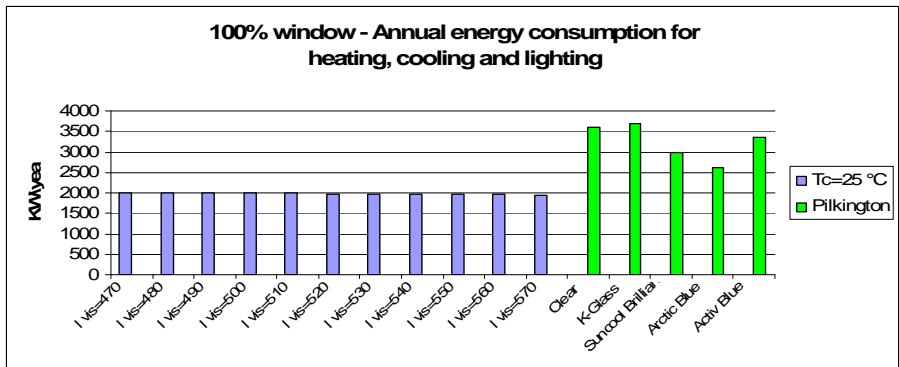


Fig. 8.22
Energy consumption in one year for heating, cooling and lighting.

The total energy consumption value (≈ 2000 KW/year) is almost equal to the previous simulation carried out with the spectrum $\delta(T,R) = 65\%$ where there was no change in the visible range of the spectrum. This fact means that a shift in the visible part of the spectrum does not influence the total glazing behaviour in a sensible way.

Looking at the enlargements below, it is possible to notice that the better configuration is $\lambda_{vis\ max} = 570$ nm with a 46% improvement since it shows the lowest energy consumption per year. Anyway, the difference between the two opposite configuration is about 1,5 % which is almost negligible.

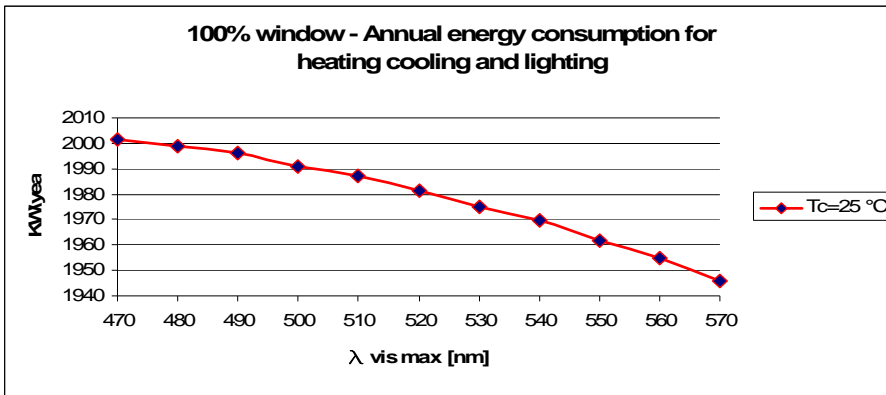


Fig. 8.23
Detailed energy consumption in one year for heating, cooling and lighting.

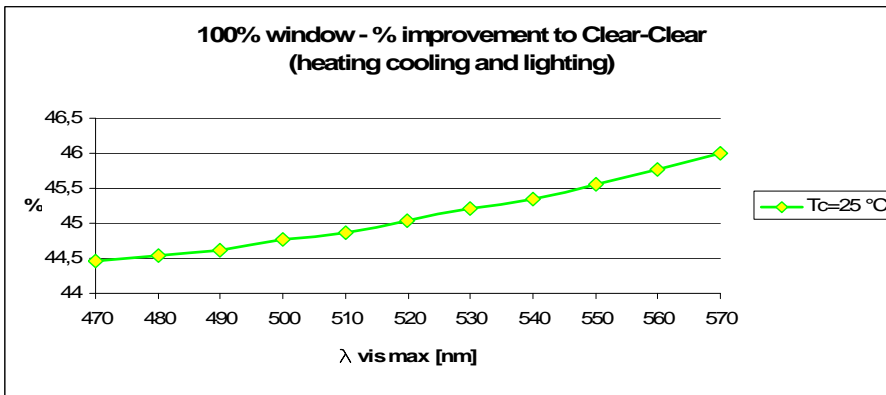


Fig. 8.24
Improvement % for heating, cooling and lighting.

The lighting energy consumption is a bit bigger than what had been recorded in the previous simulations, as it can be seen in the graphs below. Again, we notice that the better configuration is close to $\lambda_{vis\ max} = 570$ nm, more particularly the best value is $\lambda_{vis\ max} = 560$ nm. The difference between the two opposite configurations is about 8 %.

Fig. 8.25
Detailed energy consumption in one year for lighting in the city of Palermo.

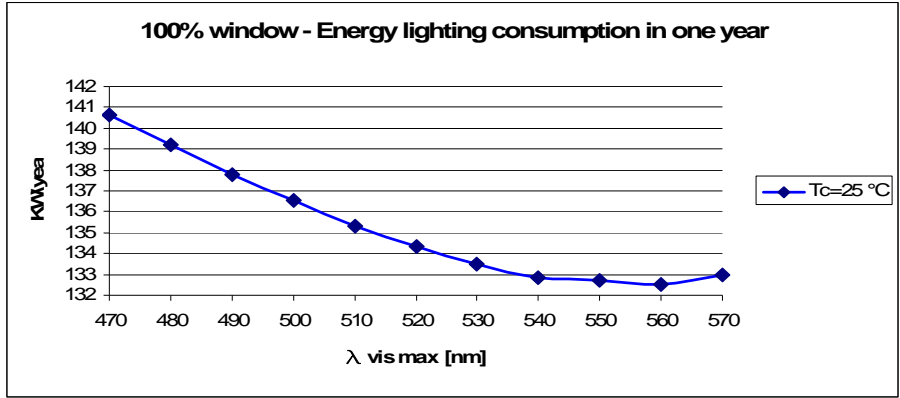
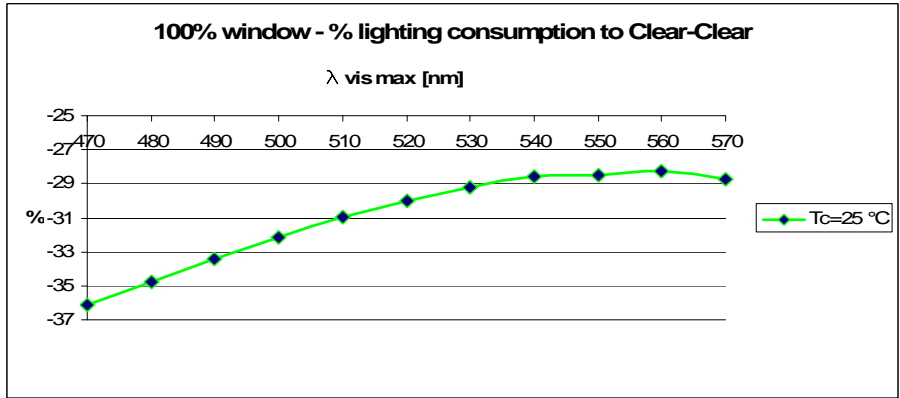
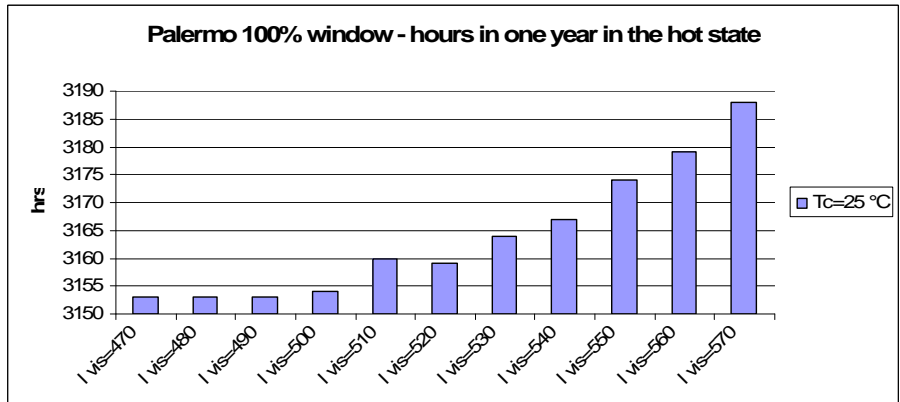


Fig. 8.26
Improvement % for lighting in the city of Palermo.



The last thing we want to look at is the number of hours in which these ideal thermochromic coatings switch into their hot state.

Fig. 8.27
Number of hours in the hot state.



As it can be seen in the previous graph, the biggest amount of hours in which the coatings switch into their hot state is red-shifted ($\lambda_{\text{vis max}}=570$ nm). Anyway, it must be noticed that the different number of hours is not so dissimilar between the various sample.

Tab. 10.9 Number of hours in one year the glazing switch into their hot state.

$\lambda_{\text{vis max}}$ [nm]	hrs
470	3153
480	3153
490	3153
500	3154
510	3160
520	3159
530	3164
540	3167
550	3174
560	3179
570	3188

9. CONCLUSIONS AND FURTHER WORKS

The new thermochromic coatings of gold-doped vanadium (IV) dioxide produced by the hybrid Aerosol Assisted Atmospheric Pressure Chemical Vapour Deposition (AA/AP CVD) technique studied and analysed in this work, represent a new frontier in the construction sector for energy control.

Vanadium (IV) dioxide films doped by gold nanoparticles showed a great applicability in architectural glazing since they increase - or obstruct - the passage of radiation through them - the IR in particular - depending on the surface temperature. Some of the problems related to the VO₂ coatings market development seems to be more easily surmountable than what previously thought. The unpleasant brown/yellow colour of pure VO₂ can be changed adding gold nanoparticles in the oxide matrix as well as lowering the metal-to-semiconductor transition temperature (T_c). By varying the initial flow rate conditions different kinds of coatings can be produced. Each coating has got different chemical/physical properties and colours depending on the initial conditions but the technique can be considered reproducible. Adding TOAB to the gold solution makes it easier to control the gold nanoparticle size in the coatings' matrix. Furthermore, TOAB has shown a "dopant" effect on the films' growth opening a new field of research.

We built a room model made of polystyrene to test our thermochromic samples in an artificial scaled model and we observed that the internal temperature increased much more slow compared to the clear glass but we recognized that simulating a real building and analysing its behaviour under different climates is quite expensive and difficult. So, simulating building behaviour and response to external different stimulus by means of energy modelling software, such as Energy Plus™, is a very easy and inexpensive way to manage these tests.

We have run a lot of energy simulations for two different building models (25 % and 100 % glazing to wall ratio) with eleven different glazing configurations in eight different climate conditions to understand how and when thermochromic glazing influence the energy consumption of a building in comparison to the use of some commercial "static" glazing produced by NSG/Pilkington.

The model's material choice is just a hypothesis and it can influence the total energy behaviour of the model as we had discussed. Dedicated simulations can be done by choosing appropriate materials and constructive technologies to deal better with the different weather conditions. This could lead to more realistic results for a regional area analysis.

We have found out that there is a great potential for these enhanced glasses since all the samples showed an energy improvement over the standard Pilkington products. The greatest energy reduction came in the cases with the 100 % window to wall as the energy transmitted is more and a switchable glazing may have a greater impact

on it, even though the 25 % model's construction and materials influence the performance.

All the thermochromic samples show a better behaviour towards the IR radiation compared to a Clear glass or simply coloured glasses even though they have a comparable emissivity factor. It could be reported that they have comparable emissivity to the low-e glazing (K-glass and Suncool Brilliant).

In all the simulations we noticed that our glasses switch from their cold state to their hot one depending on the switching temperature T_c . The lower the T_c the greater number of hours in the hot state, as expected. The last five samples never switch due to their high T_c in comparison to the average external temperature. The greatest number of hours in the hot state is recorded in the hottest cities, Cairo and Palermo, for the samples with the lowest T_c .

The annual heating and cooling load is much smaller in comparison to the standard products, especially in hot climates. We record a maximum of ~ 27 % improvement for the 25 % window model and of ~ 44 % improvement for the 100 % window model. This is a very big improvement as we are looking at one room only of a building and considering that the maximum improvement values with standard products are ~ 20 % for the 25 % window model and ~ 32 % for the 100 % window model. Furthermore, the best improvement is shown for Arctic Blue, which is a coloured glass and not a low-e one as expected.

The artificial lighting load is quite high for all the thermochromic samples, higher than the standard product. This fact is due to the dark colour of the glasses that influences a lot the overall energy consumption of the building.

Anyway we can record, as a general trend, a big improvement percentage with the total energy consumption.

Making the sensitivity analysis, we record that T_c and hemispherical emissivity do not influence a lot our glasses behaviour. As expected, a lower T_c lead to a larger number of hours in the hot state with an improvement in the building behaviour. Unfortunately, this improvement is less than 5 %. On the contrary, no improvement is shown on changing the emissivity factor but this is probably due to the software issue since we notice a variation keeping the glass in its cold or hot state only if it performed as a static glass.

We conclude that thermochromic glasses work better than the standard products analyzed due to their spectral properties rather than their smart behaviour. Their colour influences a lot the energy transmittance. Their metallic nature helps in reflecting a part of the near IR radiation. Their spectra show a big transmittance of the visible light even though they appear quite dark in colour; a high reflectance in the IR part of the spectrum prevents heat from entering the building when the glazing is hot, that's to say as the exterior temperature is high. Additionally they keep the heat inside the building when the exterior temperature is low reflecting the interior heat back to the interior preventing its dispersion.

We finally design the “ideal” thermochromic spectrum to understand the limit of our technology. We run again a series of energy simulations to understand how different percentages of transmittance and reflectance, over the visible and the IR range of the spectrum, can influence the glazing behaviour. We also varied the switch between the hot and the cold state for both the optical properties. The following conclusion are reported:

1. the bigger the switch between hot and cold transmission and reflection – that is to say $\delta(T,R)=65\%$ - the lower the energy consumption and the maximum improvement percentage compared to a Clear-Clear Pilkington configuration;
2. the lower the T_c the lower the energy consumption, the higher improvement percentage, showing that the T_c plays a very important role in thermochromics’ behaviour – an observation that did not appear with the previous simulations run with real lab glasses;
3. in the case $\delta(T,R)=0\%$ the energy consumptions tend to be almost constant, as the coating tends to become a static film.

Further investigations could be undertaken into producing and analysing new materials coatings. New samples with better properties should be created and tested to achieve better results and simulations should be carried on to verify when and where these new enhanced materials show the best performance in order to save energy efficiently in a building.

SECTION 3

Polyurea-based nanocomposite for civil applications

1. CARBON NANOTUBES (CNTs)

1. Introduction

Since their discovery in 1991 made by Iijima, a Japanese electron microscopist, carbon nanotubes (CNT) have been the subject of intensive research due to a very wide range of potential applications.

Below there is a list with such applications, just to report a few:

- as light-weight structural material with extraordinary mechanical properties;
- in nano-electronic components as the next-generation of nano-transistors, semi-conductors and nanowires;
- as probes in scanning probe microscopy (SPM) and atomic force microscopy (AFM) with the added advantage of a chemically-functionalized tip;
- as high-sensitivity microbalances;
- as gas and molecule sensors or nanostrain sensors;
- in hydrogen storage devices by using their high surface-volume ratio;
- as field-emission type displays;
- as electrodes in organic light-emitting diodes;
- as tiny tweezers for nanoscale manipulation;
- as nano-fluidic components and nano-valves;
- as actuators such as artificial muscles;
- as energy absorption and storage devices.

1.2. The discovery

In 1952 L. V. Radushkevich and V. M. Lukyanovich published some images of 50 nanometre diameter tubes made of carbon in the Soviet Journal of Physical Chemistry. This discovery was largely unnoticed, as the article was published in Russian, and Western scientists' access to Soviet press was limited during the Cold War. It is likely that carbon nanotubes were produced before this date, but the invention of the transmission electron microscope allowed the direct visualization of these structures. Carbon nanotubes have been produced and observed under a variety of conditions prior to 1991. A paper by Oberlin, Endo, and Koyama published in 1976 clearly showed hollow carbon fibers with nanometre-scale diameters using a vapor-growth technique. Furthermore, in 1979, John Abrahamson presented evidence of carbon nanotubes at the XIV Biennial Conference of Carbon at Penn State University. The conference paper described carbon nanotubes as carbon fibres which were produced on carbon anodes during arc-discharge.

In 1981 a group of Soviet scientists published the results of chemical and structural characterization of carbon nanoparticles produced by a thermocatalytical disproportionation¹ of carbon monoxide. Using TEM images and XRD patterns, the authors

¹ Disproportionation or dismutation is used to describe two particular types of chemical reaction: [to follow in the next page]

suggested that their “*carbon multi-layer tubular crystals*” were formed by rolling graphene layers into cylinders. Additionally, they speculated that during rolling graphene layers into a cylinder, many different arrangements of graphene hexagonal nets are possible. They suggested two possibilities of such arrangements: circular arrangement (armchair nanotube) and a spiral, helical arrangement (chiral tube).

In 1987, Howard G. Tennent of Hyperion Catalysis was issued a U.S. patent for the production of “*cylindrical discrete carbon fibrils*” with a “*constant diameter between about 3.5 and about 70 nanometers..., length 10^2 times the diameter, and an outer region of multiple essentially continuous layers of ordered carbon atoms and a distinct inner core [...]*”.

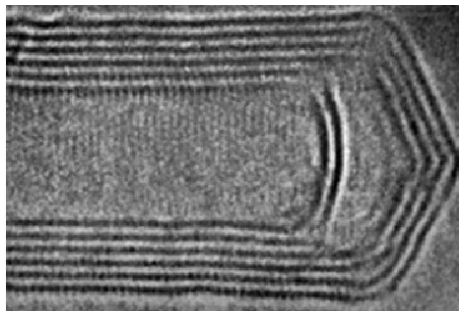


Fig. 1.1
HRTEM image of a
MWCNT
(Iijima, 1991).

Anyway, Iijima is claimed around the world to have discovered carbon nanotubes in 1991 using a high-resolution transmission electron microscopy (HRTEM) and electron diffraction. He observed a multi-walled carbon nanotubes (MWNTs) in carbon soot made by arc-discharge method.

Subsequently, in 1992 Ebbesen and Ajayan studied the bulk synthesis of CNTs, obtaining gram quantities of

them by electric-arc discharge in He atmosphere at optimum current and pressure conditions. Then, in 1993, Iijima and Ichihashi made the observation of another type of carbon nanotube, that is the single-walled nanotubes (SWNT).

Since then on a significant amount of work has been done to understand the unique properties of these structures such as the electrical, optical, mechanical, magnetic and thermal properties as well as their many potential applications in almost all the scientific fields.

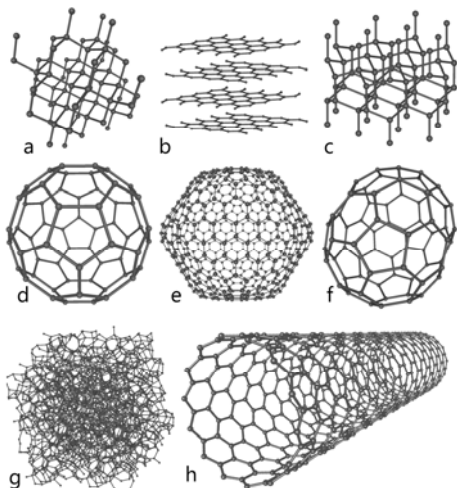
In 2000, professors Tang Zikang and Wang Ning successfully created the smallest stable carbon nanotube in the world, measuring at just 0.4 nanometres in diameter.

1.3. What a carbon nanotube is

Carbon nanotubes are allotropes of carbon² with a nanostructure that can have a length-to-diameter ratio greater than 1,000,000.

-
1. a chemical reaction of the type: $2A \rightarrow A' + A''$ where A, A' and A'' are different chemical species. While the most common type is a redox reaction, other types are possible. For example: $2H_2O \rightarrow H_3O^+ + OH^-$ is a disproportionation but is not a redox reaction.
 2. a chemical reaction (reversible or irreversible) in which a species is simultaneously reduced and oxidized so as to form two different products.

2 Allotropes: different forms in which a chemical element or molecule may exist. These are known as allotropes of that element. I.E. carbon has got two allotropes: diamond, where the carbon atoms are bonded together in a tetrahedral lattice arrangement, and graphite, where the carbon atoms are bonded together in sheets of a hexagonal lattice.



Nanotubes are members of the fullerene structural family, which also includes the spherical buckyballs. The cylindrical nanotube usually has at least one end capped with a hemisphere of the buckyball structure. Their name is derived from their size, since the diameter of a nanotube is in the order of a few nanometres (approximately 1/50,000th of the width of a human hair), while they can be up to several millimetres in length. Nanotubes are categorized as single-walled nanotubes (SWNTs) and multi-walled nanotubes (MWNTs).

Fig. 1.2

Eight different allotropes of carbon: a) diamond, b) graphite, c) Lonsdaleite, d) C_{60} (buckminsterfullerene or buckyball), e) C_{540} , f) C_{70} , g) amorphous carbon, h) single wall carbon

The nature of the bonding of a nanotube is described by applied quantum chemistry, specifically, orbital hybridization. The chemical bonding of nanotubes is composed entirely of sp^2 bonds, similar to those of graphite. This bonding structure, which is stronger than the sp^3 bonds found in diamond, provides the molecules with their unique strength. Nanotubes naturally align themselves into "ropes" held together by Van der Waals forces. Under high pressure, nanotubes can merge together, trading some sp^2 bonds for sp^3 bonds, giving the possibility of producing strong, unlimited-length wires through high-pressure nanotube linking.

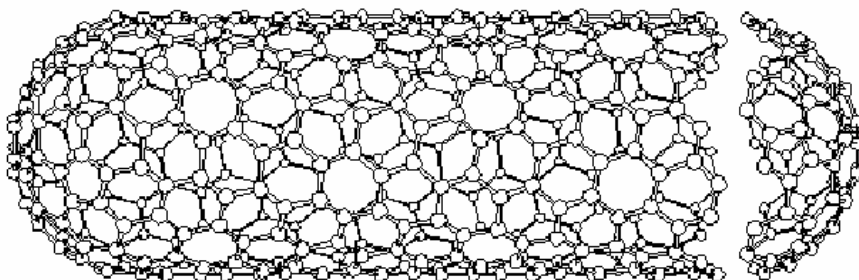


Fig. 1.3

An end-capped single wall nanotube.

1.4. SWCNT and MWCNT

In general, a single-walled carbon nanotube (SWCNT) can be regarded as a roll of graphene sheet, and different chiralities arise by varying the rolling (chiral) vector. The atomic structures of the zigzag, armchair, and chiral SWCNTs are shown in figure 1.4. The chirality (m_n) is the chiral vector with m and n as number of unit vectors along two directions of the honeycomb lattice of a graphene sheet, and along such rolling direction a SWCNT can be made. The multi-walled CNTs (MWCNTs)

are assemblies of coaxial SWCNTs where the neighboring layers are separated by the Van der Waals equilibrium distance (~0.34 nm).

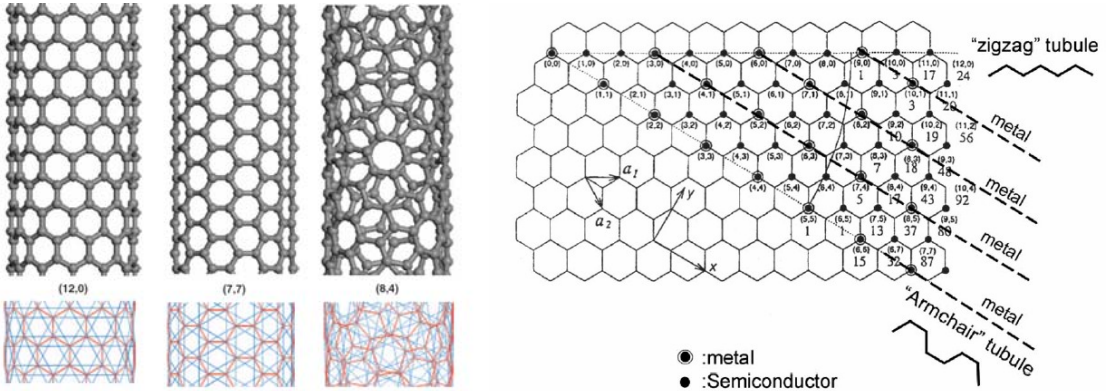


Fig. 1.4 (left) The atomic structures of zigzag (12,0), armchair (7,7), and chiral (8,4) SWCNTs, all have similar radii. The chirality is a key factor governing the mechanical properties of CNTs. Their corresponding space frame models are shown in the lower half, where the dark solid lines represent primary beams and light dash lines are secondary virtual beams.

Fig. 1.5 (right) Graphene sheet and different chirality

Mathematically, tube chirality can be defined in terms of a chiral vector:

$$Ch = ma_1 + na_2 \tag{eq.1.1}$$

a_1 and a_2 are unit vectors; m and n are the translation indices of the graphene sheet and determine the diameter of the nanotube. The chiral vector establishes the direction of rolling of the graphene sheet, in which a point (m,n) is superimposed with an origin defined as $(0,0)$.

The chiral angle, q , is the angle between the chiral vector and the zig-zag direction $(m,0)$. To determine the armchair and zigzag structure in terms of (m,n) and the chiral angle, q , it is necessary to have the following conditions:

- armchair: $\theta = \pm 30^\circ$; $(m,n) = (2p, -p)$ or (p,p) with p integer (eq. 1.2)
- zig-zag: $\theta = 0$; $(m,n) = (p,0)$ (eq. 1.3)

Theoretical studies on the electronic properties of carbon nanotubes indicate that all armchair configurations are metallic, whereas only zig-zag cylinders exhibiting values of m that are multiples of three are metallic. However, for all the other configurations (m,n) when $m - n = 3p$, the nanotubes are expected to be metallic and when $m - n \neq 3p$ the carbon nanotubes are predicted to be semiconducting material. Thus, the electrical properties of CNTs are mainly dependent upon their diameter and chirality.

1.5. Properties

The mechanical properties of a solid depend on different factors such as the crystallinity of the material, the number of defects present within the structure and the

strength of inter-atomic bonds. Macroscopic stiffness is directly connected to the stiffness of the atomic bonds. Because the carbon-carbon bond observed in graphite is one of the most rigid in nature, CNTs are among the stiffest materials ever synthesized. Nevertheless, the experiments at nanoscale are very difficult to perform and are prone to uncertain fluctuations. Therefore, theoretical and numerical studies have emerged as a powerful tool for studying the intrinsic mechanical properties of CNTs. These studies provide critical insights on the deformation and strength of materials and structures made by the CNTs. For example, the effects of waviness, weak bonding, and agglomeration of the CNTs have limited the strength of the CNT reinforced composite, the presence of geometrical imperfections and defects may significantly reduce their buckling strength, and thermal vibration causes apparent thermal contraction of these compliant quasi-one dimensional structures.

1.5.1 Strength

Carbon nanotubes are the strongest and stiffest materials known, in terms of tensile strength and elastic modulus respectively. This strength results from the covalent sp^2 bonds formed between the individual carbon atoms.

In 2000, a multi-walled carbon nanotube was tested to have a tensile strength of 63 GPa. Since carbon nanotubes have a low density for a solid of $1.3\text{-}1.4\text{ g}\cdot\text{cm}^{-3}$, its specific strength of up to $48,000\text{ kN}\cdot\text{m}\cdot\text{kg}^{-1}$ is the best of known materials, compared to high-carbon steel's $154\text{ kN}\cdot\text{m}\cdot\text{kg}^{-1}$. Under excessive tensile strain, the tubes will undergo plastic deformation, which means the deformation is permanent. This deformation begins at strains of approximately 5 % and can increase the maximum strain the tube undergoes before fracture by releasing strain energy.

CNTs are not nearly as strong under compression. Because of their hollow structure and high aspect ratio, they tend to undergo buckling when placed under compressive, torsional or bending stress.

Tab. 1.1 Typical Young modulus, tensile strength and density for some materials.

Material	Young modulus (GPa)	Tensile strength (GPa)	Density (g/cm^3)
SWNT	1000	150	0.8
MWNT	300-1000	10-60	1.8
Graphite (in plane)	1000	96	2.26
Diamond	1000	>1.2	3.52
Carbon fibres	750	5	1.8-1.9
Steel	215	0.9	7.8
High density polyethylene (HDPE)	26-33	37	0.95
Carbon fibre	-	5.65	1.75

1.5.2 Electrical properties

Graphite possesses excellent capacities of electric conduction in planar direction (resistivity of 5×10^{-5} W cm), therefore similar behaviour could be expected for CNTs. Carbon nanotubes, in contrast, show unique electronic properties dependent on their geometric differences (e.g. defects, chirality, diameter, etc.). Conductivity measurements on individual MWNTs established that each multi-walled carbon nanotube exhibits an exceptional electronic nature, ranging from semiconducting to high conductivity metallic behaviour (resistivities at 300 K of $1.2 \cdot 10^{-4}$ - $5.1 \cdot 10^{-6}$ W cm). It was experimentally proved the possibility of superconductivity in CNTs as ropes of SWNTs, attached between two superconducting electrodes, exhibit superconductivity below 1 K. In addition, due to their very low energy dissipation, nanotubes could carry elevated current densities, higher than 100 MA/cm² for MWNTs. The CNTs electronic properties could be modified by introducing defects, such as additional pentagons and heptagons, in the predominantly hexagonal tubule.

1.5.3 Thermal properties

The thermal conductivity of CNTs is highly anisotropic, diamond-like along the tube axis and insulating in the transverse direction. Because the thermal conductivity of the diamond and graphite (in-plane) is extremely high (~ 2000 W/m·K), the thermal conductivity of CNTs, over the length of the tube, may be much more elevated than that of other materials. Theoretical studies predicted a room-temperature thermal conductivity of 3000 W/(m·K) for individual MWNTs, while experimental values for an isolated SWNT were around 200 W/(m·K). In addition, CNTs have a high thermal stability, > 700 °C in air and 2800 °C in vacuum.

1.6 Synthesis of CNT

Carbon nanotubes can be produced with different techniques. Some are based on vaporization of a graphite block (therefore requiring very high temperatures); others are based on the decomposition of a gaseous precursor. All these techniques require the presence of a carbon source.

1.6.1 Arc discharge

Nanotubes were observed in 1991 in the carbon soot of graphite electrodes during an arc discharge, by using a current of 100 amps, that was intended to produce fullerenes. However the first macroscopic production of carbon nanotubes was made in 1992 by two researchers at NEC's Fundamental Research Laboratory. This technique consists of the passage of direct current (80 - 100 A) through two high-purity graphite electrodes separated by ~ 1 - 2 mm, in a He atmosphere (500 tor).

The high energy generated during this process produces temperatures between the two electrodes that can reach about 4000°C and part of the carbon positive electrode (anode) sublimates. The generated carbon gas recondenses, at a rate of 1 mm/min on the negative electrode (cathode) and on the walls of the reactor. The material deposited on the cathode shows a cigar-like structure, made up of a hard grey which is ex-

ternal shell containing curved and dense graphene layers, and an inner core, dark and soft, with CNTs and graphene particles inside.

Because nanotubes were initially discovered using this technique, it has been the most widely used method of nanotube synthesis. The yield for this method is up to 30 percent by weight and it produces both single- and multi-walled nanotubes with lengths of up to 50 microns.

Currently, SWNTs can be produced using the electric arc discharge method with different metals: Gd, Co-Pt, Co-Ru, Ni-Y, Co-Ni-Fe-Ce, etc.

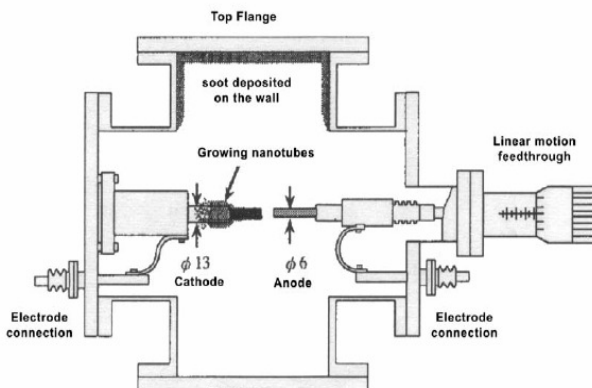


Fig. 1.6
Schematic arc discharge apparatus for CNT production. (source: Ebbesen and Ajayan, 1992)

1.6.2 Pulsed laser vaporization / laser ablation

This technique involves laser vaporization of pure graphite targets inside a furnace at 1200 °C, in an inert gas (e.g. Ar) atmosphere. The nanotubes develop on the cooler surfaces of the reactor, as the vaporized carbon condenses. A water-cooled surface may be included in the system to collect the nanotubes.

This technique was invented by Richard Smalley and co-workers at Rice University, who at the time of the discovery of carbon nanotubes, were blasting metals with the laser to produce various metal molecules. When they heard of CNT discovery, they substituted the metals with graphite to create multi-walled carbon nanotubes. Later that year, the team used a composite of graphite and metal catalyst particles (the best yield was from a cobalt and nickel mixture) to synthesize single-walled carbon nanotubes.

This method has a yield of around 70% and produces primarily single-walled carbon nanotubes with a controllable diameter determined by the reaction temperature. However, it is more expensive than either arc discharge or chemical vapour deposition.

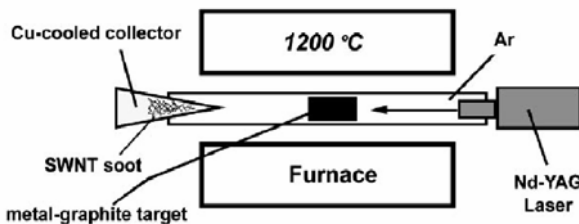


Fig. 1.7
Schematic pulsed laser vaporization apparatus for CNT production. (source: Gao et al. 1995)

1.6.3 Chemical vapour deposition (CVD)

During CVD, a substrate is prepared with a layer of metal catalyst particles, most commonly nickel, cobalt, iron, or a combination. The metal nanoparticles can also be produced by other ways, including reduction of oxides or oxides solid solutions. The diameters of the nanotubes that are to be grown are related to the size of the metal particles. This can be controlled by patterned (or masked) deposition of the metal, annealing, or by plasma etching of a metal layer. The substrate is heated to approximately 700 °C. To initiate the growth of nanotubes, two gases are bled into the reactor: a process gas (such as ammonia, nitrogen, hydrogen, etc.) and a carbon-containing gas (such as acetylene, ethylene, ethanol, methane, etc.).

Nanotubes grow at the sites of the metal catalyst; the carbon-containing gas is broken apart at the surface of the catalyst particle, and the carbon is transported to the edges of the particle, where it forms the nanotubes.

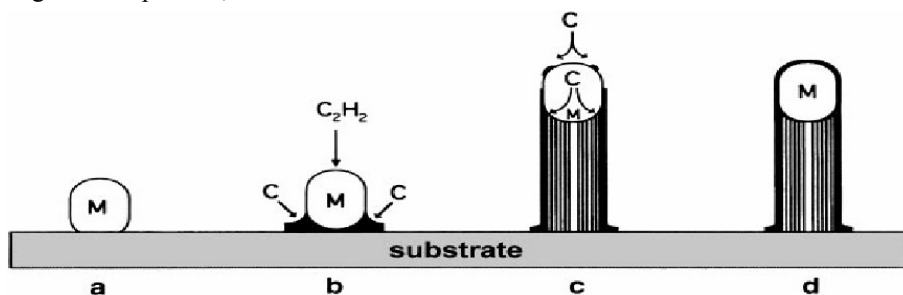


Fig. 1.8
Growth mechanism.
(source: Baker et al.
1978)

This mechanism is still under discussion. The catalyst particles can stay at the tips of the growing nanotube during the growth process, or remain at the nanotube base, depending on the adhesion between the catalyst particle and the substrate. If a plasma is generated by the application of a strong electric field during the growth process (plasma enhanced chemical vapour deposition), then the nanotube growth will follow the direction of the electric field. By properly adjusting the geometry of the reactor it is possible to synthesize vertically aligned carbon nanotubes (i.e., perpendicular to the substrate), a morphology that has been of interest to researchers interested in the electron emission from nanotubes. Without the plasma, the resulting nanotubes are often randomly oriented, resembling a bowl of silicon-spaghetti.

CVD shows the most promise for industrial scale deposition in terms of its price/unit ratio. There are additional advantages to the CVD synthesis of nanotubes. Unlike the above methods, CVD is capable of growing nanotubes directly on a desired substrate, whereas the nanotubes must be collected in the other growth techniques. The growth sites are controllable by careful deposition of the catalyst. Additionally, no other growth methods have been developed to produce vertically aligned nanotubes. CVD is a common method for the commercial production of carbon nanotubes. For this purpose, the metal nanoparticles will be carefully mixed with a catalyst support (e.g., MgO, Al_2O_3 , etc.) to increase the specific surface area for higher yield of the catalytic reaction of the carbon feedstock with the metal particles.

1.7 Toxicity

Determining the toxicity of carbon nanotubes has been one of the most pressing questions as some studies reported that CNT may lead to cancer. Results from various scientific tests on cells have so far proven confusing, with some results indicating it to be highly toxic and others showing no signs of toxicity. Some CNTs contain measureable levels of impurities such as cobalt and nickel which have documented toxicity and which may be the true causes of the effects. Additionally CNTs have a range of physical and chemical properties (e.g., surface area, zeta potential³) that are not often controlled for in toxicology studies.

A study led by Alexandra Porter from the University of Cambridge shows once CNTs are inside the cell, they accumulate in the cytoplasm and cause cell death, but without rigorous CNT/impurity characterization it is difficult to interpret this result or determine its significance.

A more recent study reveals that carbon nanotubes, when injected in the lungs of mice, are incapable of being disposed of by specialized cells in the lung as these tubes are too large for the cells to engulf, thus leading to constitutive inflammation, a hallmark, precancerous symptom. However, the doses required to achieve this response are also considered high or even extreme.

Anyway, it is suggested to follow some basic rules when dealing with CNTs such as wearing safety glasses, laboratory coat and latex gloves and work in a fume cupboard.

1.8 CNTs producers

All around the world, the industrial production of carbon nanotubes is increasing very fast due to the great numbers of applications they are suitable for. Also their price is decreasing a lot making their use more frequent and accessible to researchers.

More particularly, SWCNTs price decreased from 1,500 USD per gram of the 2000 to 100 USD per gram of the 2007 and the price now are quite stable.

In the next page, an image with the main CNTs' producers worldwide.

³ Zeta potential is an abbreviation for electrokinetic potential in colloidal systems. From a theoretical viewpoint, zeta potential is electric potential in the interfacial double layer (DL) at the location of the slipping plane versus a point in the bulk fluid away from the interface. In other words, zeta potential is the potential difference between the dispersion medium and the stationary layer of fluid attached to the dispersed particle.

The significance of zeta potential is that its value can be related to the stability of colloidal dispersions. For molecules and particles that are small enough, a high zeta potential will confer stability, i.e. the solution or dispersion will resist aggregation. When the potential is low, attraction exceeds repulsion and the dispersion will break and flocculate. So, colloids with high zeta potential (negative or positive) are electrically stabilized while colloids with low zeta potentials tend to coagulate or flocculate as outlined in the table.

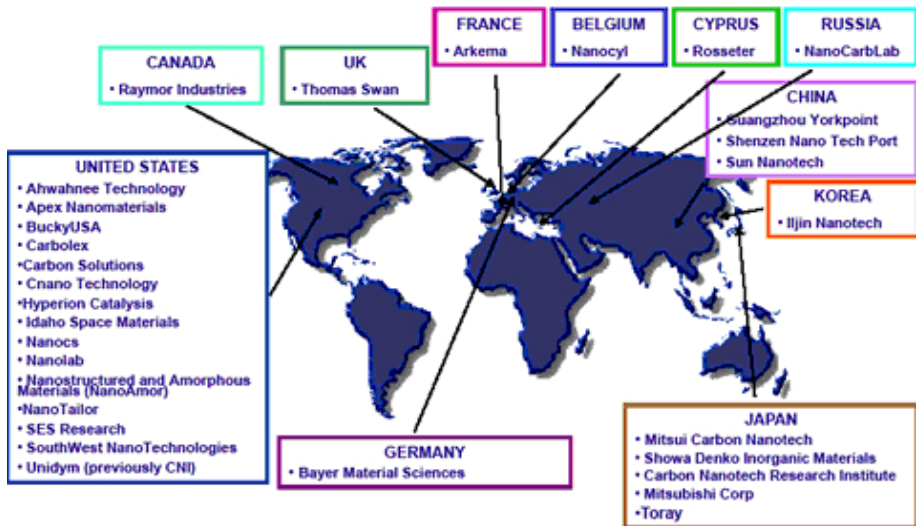


Fig. 1.9
CNTs producers
around the world.

2. POLYUREA: THE MATERIAL

2.1 Introduction

Polyurea is a fast reacting bi-component polymer system that contains 70% of amine. The first component is isocyanate¹, a $-NCO$ group, while the other part is a resin blend component. The reaction between the two components yields a urea linkage that makes the polymer solid. It is a 100% solids elastomer sprayed under high pressure to produce a thick, strong, seamless, waterproof coating with incredible abrasion, corrosion and chemical resistance.

2.2. Discovery and applications

Polyurea was used for the very first time in 1970 for the construction of Reaction Injection Molding (RIM) of the cars components since the different parts could be take away from the moulds in a very short time. RIM polyurea was used for a long period for the construction of parts requiring a particular strength such as bumpers. The only biggest problem in its development was the high velocity of polymerization that forced industries in working with chemistry of materials and inventing new production systems and machines.

During the '80s it was invented a hybrid product made of polyurea and polyurethane, this fact lead to a never-ending confusion between the two products, as it will be discussed later.

Many are the advantages of using polyurea in civil engineering:

1. extraordinary toughness and flexibility;
2. application thickness from 20 to 375 mils or greater;
3. snap cure, 3 – 8 seconds;
4. can be sprayed on a slope or vertical surfaces up to 275 mils with no sags or runs;
5. foot traffic can resume within 30 seconds on horizontal surfaces;
6. outstanding corrosion resistances;
7. increased structural strength;
8. return to service in several hours.

Furthermore, it can be used in several applications such as steel or concrete water tanks, secondary containments, concrete reservoirs, process piping, storm drains, natural gas piping, sanitary sewer piping, manholes, cooling water piping, building and bridge structures, brine tanks, etc..

¹ Isocyanate is the functional group of atoms $-N=C=O$ (1 nitrogen, 1 carbon, 1 oxygen). An isocyanate may have more than one isocyanate group. An isocyanate that has two isocyanate groups is known as a diisocyanate. Diisocyanates are manufactured for reaction with polyols in the production of polyurethanes.



Fig. 1.1. a-b-c-d.

Different applications of the Polyurea system. It can be sprayed on horizontal or vertical surfaces as well as in very humid environments.



Fig. 1.2. a-f. Polyurea used as concrete coating in a secondary containment: primed (top left) and sprayed the same day (top right). Polyurea used as Manhole rehabilitation: the primed pipe (centre left) and sprayed the same day (centre right). The high pressure spray gun to spray polyurea (bottom). (source: CSI Construction Solution Inc.: Polyurea, 2006)

2.3. Two systems in comparison: polyurea and polyurethane

Polyurea is often confused with another similar product, polyurethane, but there are some differences between the two materials.

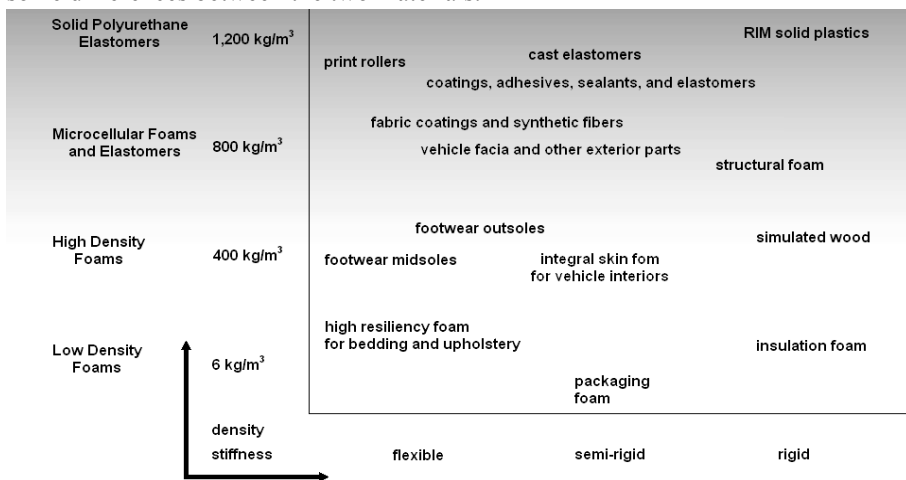


Fig. 1.3
Industrial application
of polyurethane and
its derivatives.

First of all in a polyurea the amine percentage must be at least 80% (or more) while in a Polyurethane the hydroxyl²-polio percentage must be at least 80% (or more).

The system polyurethane (characterized by polyeter or polyester³) requires a catalyst that can usually be measured and varies depending on the specific application. The consequence is a different length of the gel phase. The reaction time varies a lot depending on the catalyst quantities: from a few seconds to hours; the gel could interact with the environmental humidity leading often to the production of CO₂.

The system polyurea (characterized by polyeter-amine⁴ or amine-composites) is highly reactive and it does not need a catalyst. Polyols⁵ are switched with amine molecules (functional group -NH₂) resulting in polymers with urea bonding, -(NH)(CO)(NH). The reaction lasts between 5 and 15 seconds and it usually cannot react with the water present on the surface of application. This fact lead to the conclusion that polyurea may be also sprayed on iced or wet surfaces.

The application temperature range vary between -1°C to -6°C, that is particularly useful when it is applied on steel due to its great heat absorption and the service temperature range from -50°C to 150°C.

² Hydroxyl in chemistry stands for a molecule consisting of an oxygen atom and a hydrogen atom connected by a covalent bond (single bond).

³ Polyester is a category of polymers.

⁴ Amines are organic compounds and functional groups that contain a basic nitrogen atom with a lone pair. Amines are derivatives of ammonia, where in one or more hydrogen atoms have been replaced by a substituent such as an alkyl or aryl group. Important amines include amino acids, biogenic amines, trimethylamine and aniline.

⁵ Polyols are alcohols containing multiple hydroxyl groups.

Both the products have a good colour-resistance, bad-weather resistance and resistance to acids, alkali and salts and polyurea is usually 1,5 ÷ 2 times more expensive than polyurethane.

Today polyurea is frequently used on metallic substrates where it provides corrosion and abrasion resistance in harsh environments. Applications include transportation vehicles, pipelines, steel buildings or marine constructions. More recently, polyurea is also considered for the blast protection of transportation vehicles because of its high toughness-to-density ratio, in particular at high strain rates.

In 2007, the global consumption of polyurethane raw materials was above 12 million metric tons, the average annual growth rate is about 5%.

Tab. 1.1 Polyurethane usage in USA in 2004.

Application	Amount of polyurethane used (millions of Kg)	Percentage of total
Building & Construction	661,79	26,8%
Transportation	588,76	23,8%
Furniture & Bedding	511,20	20,7%
Appliances	126,10	5,1%
Packaging	113,85	4,6%
Textiles, Fibres & Apparel	82,10	3,3%
Machinery & Foundry	80,74	3,3%
Electronics	34,02	1,4%

2.4. Physical and chemical properties: state of art of the researches

Polyurea is a polymer so is characterized by utilizing a urethane linkage to covalently bond hard segments with soft segments. This linkage is typically formed from the reaction between the isocyanate functionality of one component with the hydroxyl group of another component. By controlling the composition of each component, two solid-state phases are expected.

Tab. 1.2. Comparison between Polyurea and HDPE physical properties

Properties	Polyurea	High Density Polyethylene (HDPE)
Hardness [shore "A"]	60 ÷ 85	65 ÷ 85
Tensile strength [MPa]	23 ÷ 48	22 ÷ 31
Elongation [%]	35 ÷ 403	20 ÷ 800
Flexural modulus [MPa]	331 ÷ 2517	1000 ÷ 1517
Adhesion test	-	-
Concrete bond	500	-
Metal bond	1750	-
Wood bond	500	-

This two-phase morphology provides the key in controlling the performance of the final product and gives the manufacturer versatility in tuning properties as desired by varying the composition or content of one or the other phases.

One phase of typical water-blown foam systems is based upon the reaction of water with a diisocyanate - such as toluene diisocyanate (TDI). The reaction initially produces a carbamic acid⁶ which then decomposes yielding heat, carbon dioxide, and an amine functionality. The heat and carbon dioxide contribute to the expansion of the gas bubbles in the reactive mixture and so play important roles in the development of the foam's cellular structure.

On the other hand, a disubstituted urea product results from the reaction of the amine with other isocyanate groups. A "hard segment" results from several isocyanate groups covalently bonding through the urea linkages, and solid state phase separation in typical systems arises from the precipitation of these segments into "hard domains".

An additional structure is also sometimes observed as the urea precipitating can aggregate further to form what have been termed "urea balls" or urea-rich aggregates, which may be considered a macrophase aggregation. Their dimension resulted to be about (7–11 nm) when observed via small-angle X-ray scattering (SAXS) with an anisotropic structures on the order of 1 nm across with length 4–6 nm. Via TEM was observed a macro-phase separation of about 50–200 nm.

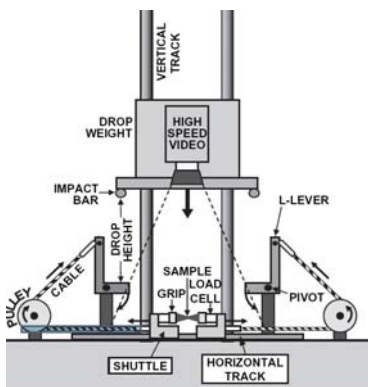


Fig. 1.4
Schematic of the
high-speed tensile
test instrument.
(source : Roland
C.M. et al., 2007)

In examining how these materials behave during mechanical deformation by using FTIR linear dichroism techniques, it was shown an initial hard segment orientation transverse to the direction of elongation in flexible slab stock foams followed by transformation to parallel orientation parallel to the stretch direction at higher uniaxial deformations.

Different researches have been carried on to understand the actual properties of polyurea.

A study, for instance, focused on the stress-strain measurement in uniaxial tension of an elastomeric polyurea as the typical dynamic

mechanical spectrometers are limited to frequencies below ca. 100 Hz. Atomic force microscopes ("nano-indenters") operate as high as 1 MHz but only probe the surface. While time-temperature super-positioning is often invoked to extend the effective frequency range of test data, the results are inaccurate for measurements in the glass transition zone.

A new drop weight tensile test instrument, show in figure 1.4, was used to obtain extensional stress-strain measurements at rates up to 480 s⁻¹.

⁶ Carbamic acid: CH₃NO₂. The carbamic acid is a compound that is instable under normal circumstances.

In the instrument illustrated, a 100 kg mass is dropped down a vertical track to engage L-levers, which displace shuttles to which the test specimen is attached. Equilibrium was ensured - and subsequently verified - by equal displacement of each end of the sample. Shuttle speeds as high as 26 m/s are achievable, corresponding to strain rates equal to 103 s^{-1} .

The material initially exhibits a high modulus, defined as the slope of the engineering stress vs. strain curve (strain, ϵ , defined as the change in length over the initial length) = 27 MPa. Following this initial linear region the material yields at $\epsilon \sim 70\%$ elongation, with a subsequent slow rise in stress to failure at 620 % elongation. These are very good mechanical properties, i.e., high stiffness and elongation, associated with a tough elastomer.

Interestingly, when the chemistry of the polyurea is altered by 5 - 10 %, there is an enormous change in the mechanical properties. The yield stress varies inversely with stoichiometry, while the failure strain increases with increasing curative. These results show that increasing the amount of diisocyanate is necessary to drive the cross-linking reaction toward completion.

Shim J. et al. tried to characterize the mechanical properties of polyurea at low, intermediate and high strain rates due to the possible use against blast. A hydraulic testing machine was used to perform compression tests on polyurea with a mass density of 1.0 g/cm^3 and an elastic modulus of about 100 MPa.

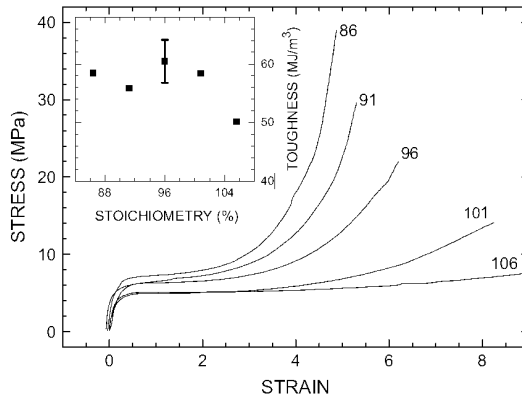


Fig. 1.5 Stress-strain curves obtained using an Instron for polyureas prepared with the indicated % stoichiometry. The strain rate for all tests was 0.06 s^{-1} . The inset shows the toughness (integral of stress-strain curve); error bars are one standard deviation. (source : Roland C.M. et al., 2007)

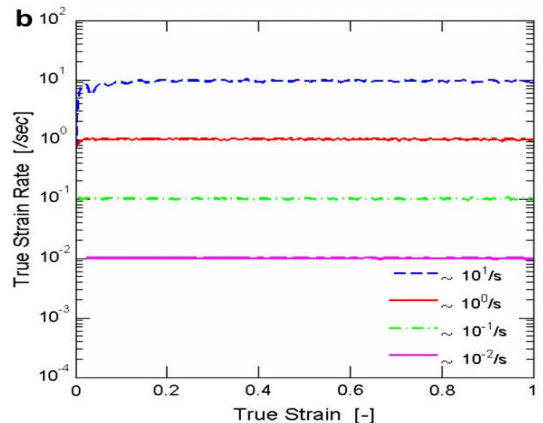
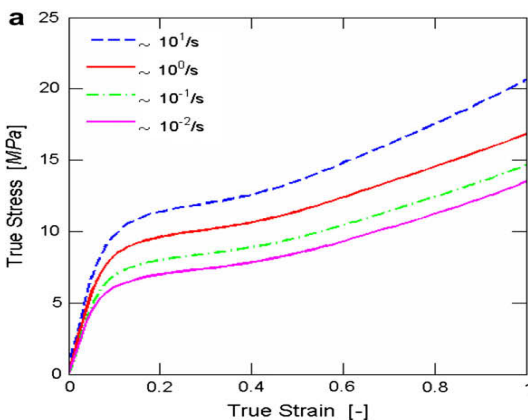


Fig. 1.6 a-b. Test results from the universal testing machine: (a) True stress-strain curves, (b) True strain versus true strain curves. (source: Shim J. et al., 2009)

3. CNT-DOPED POLYMERS: STATE OF ART

3.1 Introduction

Around the world several researches have been done, in both academia and industry, to enhance polymers properties and the most of the studies involve carbon nanotubes in order to produce a hybrid nano-material. Attention in CNT has developed due to their unique mechanical properties, surface and multifunctional properties, strong filler/matrix interaction, extremely large interfacial area as well as their nano and micro scale structure. The main limitation, which is in the same time the most important point, is the reaction of existing polymers containing terminal functional groups (e.g. -OH and -NH₂) with the anterior functional groups (e.g. -COOH and -COCl) on CNTs, either in solution or by melt-compounding.

Industry, in particular, recognizes many potential applications such as their use to produce electrostatically dissipative materials and aerospace structural materials.

Currently, the two main obstacles to a more widespread use of nanotubes as polymer fillers are their cost (USD 100 per gram) and difficulty in controlling their dimensions (length and diameter), as well as the chirality of the tubes (which is related to conductivity). However, much progress has been made and both their quantity and quality continue to improve rapidly.

3.2 Preliminary treatment of CNTs

Carbon nanotube can't be utilized as furnished by companies: a chemical modification is necessary to achieve an adequate interfacial adhesion and, consequently, a good load transfer, in order to take advantage of the very high Young's modulus and strength of the nanotubes. Furthermore, their utilization as effective reinforcements in high strength composites depends on the ability to disperse them individually and uniformly in the matrix without destroying their integrity or reducing their aspect ratio.

3.2.1 CNT purification

Synthesized carbon nanotubes are often contaminated by unwanted elements such as carbonaceous particles (fullerenes, amorphous carbon, graphite), encapsulated metal particles or substrate granules.

Currently, there are many different techniques of purification but they tend to reduce the amount of mass material by approximately 50 % and to damage the morphological properties of the CNTs. The most common methods of purification include thermal annealing at about 700 °C in air or oxygen to remove carbonaceous by-products and acid treatment (e.g. nitric acid aqueous solutions) to eliminate catalyst residues. Mechanical techniques such as filtration, centrifugal separation and ultra-sonic microfiltration may also be applied. If the CNTs are produced by chemical vapour deposition (CVD), the substrate granules can be removed by acid solution treatment with HNO₃ or HF followed by filtration and drying.

3.2.2 CNT functionalization

The surface of CNTs needs to be chemically functionalized to realize a good dispersion of the nanotubes in the matrix and a strong interfacial adhesion between CNTs and the surrounding polymer chains.

The first types of chemical functionalization were based on oxidation of carbon nanotubes in air (or CO_2 , N_2O , NO , O_3 , ClO_2) for 10 minutes at a temperature above $700\text{ }^\circ\text{C}$ that resulted in the opening of the hemispherical end caps, which are more reactive than the graphite sidewall.

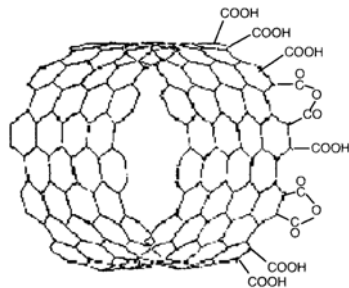


Fig. 3.1
Functional groups at
the open end of CNT.

An other way is the acid oxidation (HNO_3 , $\text{HNO}_3 + \text{H}_2\text{SO}_4$, HClO_4 , etc.) of the CNTs.

In general, carboxylic acid (COOH) and hydroxyl (OH) groups could be formed at the opened ends or defect sites on the side-walls of the CNTs during the oxidation process by oxygen, air, and acids. As shown in figure 3.1, COOH and OH groups can be used to generate covalent connections with the molecules of the polymer.

Many high molecular weight polymers (especially conjugated polymers) can be non-covalently wrapped around the surface of carbon nanotubes. The wrapping of polymer chains around SWNTs could reduce the intertube Van der Waals interaction and hence enhances the solubility of the CNTs.

In any case the functionalized CNT must be compatible with the polymer matrix to avoid microscopic phase separation in the nanocomposite.

3.3 Dispersion of functionalized CNTs in the polymer

Presently, three methods are commonly used to incorporate nanotubes into polymers:

1. polymerization of nanotube-polymer monomer mixtures;
2. film casting of suspensions of nanotubes in dissolved polymers;
3. melt mixing of nanotubes with polymers.

The last method is usually the most preferred for polymer/CNT nanocomposites formation. Sometimes the tendency of CNTs to form aggregates may be minimized by appropriate application of shear during melt mixing.

3.3.1 In situ polymerization

This method is principally used with conducting and conjugated polymers for improving dispersion and integration between the phases. It is a chemical encapsulation technique very similar to interfacial coating. The distinguishing characteristic of in situ polymerization is that no reactants are included in the core material. All polymerization occur in the continuous phase, rather than on both sides of the interface between the continuous phase and the core material.

3.3.2 Solution processing

Solution-based methods are very often used to make CNT/polymer composites because of low viscosity that facilitate CNTs mixing and dispersion.

Some researcher dissolve polystyrene in either tetrahydrofuran (THF) or toluene, then add carbon nanotubes and finally evaporate the solvent.

Others prepare CNT/polypropylene composites via a solution-based method: octadecylamine-functionalized SWNTs are dispersed into the polymer matrix exploiting the common solubility of the functionalized nanotubes and the polymer in the same selected solvent. As previously mentioned, carbon nanotubes can be solubilised through functionalization with the polymer matrix and then be used for the preparation of polymeric nanocomposites by solution based methods. This procedure ensures the compatibility of the functionalized carbon nanotubes with the polymer, avoiding any potential microscopic phase separation in the nanocomposites.

3.3.3 Melt mixing

Melt-mixing of CNTs into thermoplastic polymers can be realized by common processing techniques such as extrusion, internal mixing, injection molding or by a combination of the above techniques. These methods are particularly advantageous because of their speed and simplicity. Moreover, they are also free of solvents and contaminants, which are present in solution processing methods and in-situ polymerization.

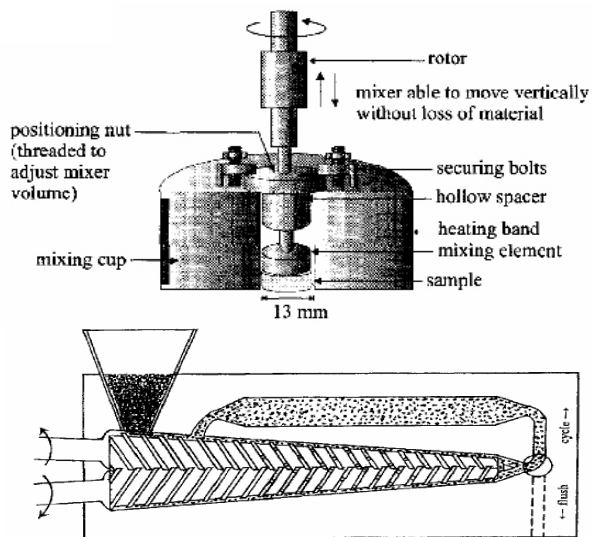


Fig.3.2 a-b

Top: mixer machine “MiniMax” mixer has a rotor, which can be submerged into a heated cup containing the material (~ 0.5 g). Mixing is imparted by the rotor, and some reorientation may also be obtained if the rotor is raised and lowered manually. (source: Maric and Macosko, 2001)

Bottom: extruder machine “Haake MiniLab” is a co-rotating twin screw extruder, where a recirculation channel is used to recycle the melt sample. Small quantities (≤ 5 g) of material are fed into the extruder; a mixing time of 5-15 minutes and a screw rotation rate of 50-100 rpm are generally applied.

3.4 CNT/polymers composite - State of art

There are lots of researches dealing with incorporating carbon nanotubes in a polymer matrix. We are now going to analyze some works and some results.

3.4.1 Interfaces

Increasing attention has been focused on the interface between the CNT and polymer matrix because as the weaker the interfacial adhesion is, the worse nanotubes behave, inducing local stress concentrations, and the benefits of the CNT properties are lost. The strength of the interface could be a function of nanotube geometry (e.g.

wall thickness, chirality, etc.) and of the chemistry of the external graphene surface. Although the very high aspect ratio of nanotubes implies very large interfacial areas, their intrinsic chemical nature could cause weak interfacial adhesion. In fact, the surface of a CNT may be considered essentially as an exposed graphene sheet and it is well known that, because of its weak inter-planar interactions, graphite shows solid lubricant quality and resistance to matrix adhesion. For this reason, chemical functionalization of the CNTs surface is essential for improving nanotube-matrix interactions.

In addition, there are three main load transfer mechanisms that control stress transfer, as follows:

1. micromechanical interconnection (typically not so important, as the surface of the CNTs appears atomically smooth);
2. chemical bonding;
3. weak Van der Waals attractive force.

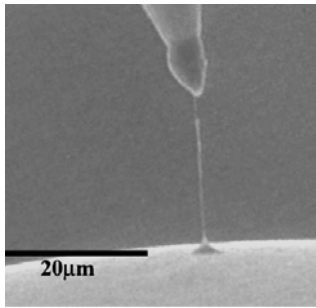


Fig. 3.3
CNT pull-out from a
polymer surface.
(Source: Barber et
alt., 2003)

Barber et al. (2003) did an experiment during which a single MWNT, directly attached to an AFM tip, was pulled out from a polymer surface (fig. 3.3). The forces acting on the nanotubes were recorded from the deflection of the AFM tip and an interfacial strength of about 50 MPa was recorded. This value is about ten times larger than the adhesion level between the same type of polymer and carbon fibres.

Another research studied how to disperse in a uniform way SWCNT in a polymer substrate. The adhesion between the two phases is fundamental to

achieve a good strength and avoid the loss of CNT as the hybrid material is exposed to the external environment. It was reported that microwave radiation and a subsequent ultrasonic bath enhance the adhesion. Experiments were carried on polyethylene (PET): SWNTs theoretically have very high dielectric constants so they can release heat at around 2000 °C under microwave irradiation. Therefore, SWNTs can be heated selectively under microwave irradiation to higher temperatures than can polymer substrates. For this reason, SWNTs can be locally welded onto the surface of polymer substrates or penetrated into the polymer matrix, because heated SWNTs instantly begin to release heat around the polymer matrix. Microwaves irradiation was 2,45 GHz and 800 W for 10 - 300 s. The procedure to disperse CNT on the polymer was: the SWNT samples were purified and well dispersed in distilled water with 1 wt.% sodium dodecyl sulfate as a surfactant. For the uniform deposition of the SWNTs onto the PET substrate, 200 ml of the SWNTs solution was diluted and vacuum filtered through a porous alumina filtration membrane (Whatman, 200 nm pore size) until the surfactant around the SWNTs was washed out. As a result of this process, the SWNTs were trapped on the membrane filter and formed a homogeneous layer of SWNTs. Next, the SWNT layer-membrane filter was floated onto 3 M of sodium hydroxide (NaOH) to eliminate the membrane filter. After the complete

melting of the membrane filter, the aqueous surroundings (distilled water + NaOH) of the SWNT layer were neutralized using circulated distilled water. Finally, the SWNT film was transferred to a PET and polycarbonate (PC) substrate and was dried at 60 °C for 30 min. Film samples were prepared after cooling the film to room temperature, and microwave energy of 800 W at 2.45 GHz was applied to the SWNT films. The SWNT films were heated in a microwave furnace for 10–300 s. Finally, the SWNTs and the polymer composite were washed in an ultrasonic bath with ethanol for 10 min to eliminate residual SWNTs not attached to the polymer substrate. It was observed that SWCNT with small diameters (0,84 – 1,45 nm) could be easily damaged or destroyed by microwave irradiation and the lost of some of them may influence the sheet resistance. The sheet resistance was measured on the samples, after 10 s microwave treatment and a ultrasonic bath, showed over 500 % increase in sheet resistance value. In conclusion, at least 2 min is required to effectively fuse SWNTs into the polymer substrate. This method is simple, fast and can be applied to fabricate a SWNT and polymer composite. For the fabrication of a SWNT and polymer composite, the proper temperature and fabrication time are very important, because the polymer materials are more easily damaged or deformed by heat than the SWNTs. The short period of microwave irradiation used in this paper could minimize the deformation of the polymeric matrices.

3.4.2 Mechanical properties

Incorporation of CNTs into a polymer can dramatically increase the modulus and strength of the matrix.

For instance, some reported that by adding 1wt % MWNTs into polystyrene matrices, the tensile modulus and strength of the composites increased by 42 % and 25 %, respectively. These researchers also showed that nanotubes aligned perpendicularly to a crack, are able to slow down its propagation by bridging the crack surfaces. In general, the addition of CNTs in polymer matrices reduces the toughness (area under tensile stress-strain curve) of composites. However, opposite effects, i.e. improvement in toughness, are also reported. For example, it was showed that in ultra-high molecular weight polyethylene (UHMWPE) with 1wt % MWNTs, the toughness and ductility increased by 150 % and 104 % respectively, possibly due to the better mobility of the polymer chains induced by MWNTs.

Ren et al. (2003) conducted it was mixed 8-15 layer CNT (hollow of 5 nm core) with a typical diameter ranging from 10 to 15 nm and 1 – 10 mm length. The density was approximately 1.75 g/cm³. the masterbatch, delivered in pellet form, was diluted with a polycarbonate. The materials were dried for 16 hrs at 80 °C in a vacuum oven and then extruded to obtain concentrations of 0.5, 1, 2, 5 wt % nanotubes in polycarbonate.

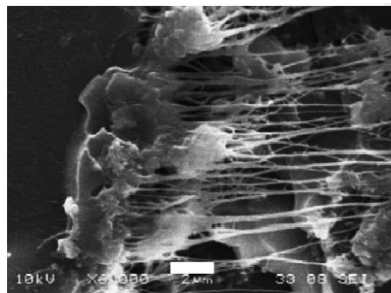


Fig.3.4
SWCNT bridging the fracture surface in an epoxy matrix.
(Source: Ren et al., 2003)

To make some analysis, and especially to study the uniformity of the dispersion, the nanocomposites were dissolved in tetrahydrofuran (THF). A small pellet of the masterbatch (8 mg, corresponding to 1,2 mg nanotubes) and corresponding weights of the diluted materials were immersed in approximately 50 ml of THF for about two weeks at room temperature. The solutions were formulated to have an equal amount of nanotubes in each vial. Under these conditions, polycarbonate was dissolved thereby leading to a suspension of the nanotubes in the solvent-PC solution.

In an other study, conducted at NASA in 2004, it was reported the following table, showing that a small amount of CNTs (5 wt %) into a polymer is enough to strongly improve the thermal conductivity, electrical and mechanical properties of the matrix.

Tab. 3.1 Mechanical properties of extruded SWCNT nanocomposite.			
SWCNT [Wt%]	Tensile modulus [Gpa]	Ultimate strength [Mpa]	Yield stress [Mpa]
0,0	2,2 ± 0,3	105 ± 7	74 ± 5
0,1	2,6 ± 0,3	105 ± 10	86 ± 6
0,3	2,8 ± 0,2	105 ± 7	94 ± 5
1,0	3,2 ± 0,2	105 ± 5	100 ± 5

3.4.3 Electrical properties

One of the major commercial applications of CNTs is their use as electrically conducting components in polymer composite. Many studies have revealed that electric conductivity can be obtained in a CNT/polymer composite at extremely low quantities of CNTs, due to their tendency to form a three dimensional, interconnecting network in the molten plastic.

3.4.4 Thermal properties

The incorporation of CNTs could improve the thermal transport properties of polymer composites, due to the excellent thermal conductivity of the nanotubes. For instance, in a study it was found out that the thermal conductivity of the SWNT/PMMA nanocomposite increased more than 100 % with 10 wt % nanotube loading. The CNTs could also modify matrix glass transition, melting and thermal decomposition temperatures of the matrix, because of their effect on the mobility and crystallization of the polymer chains. It was showed that the presence of CNTs in a polymer matrix increases the glass transition temperature.

3.5 CNT/Polyurea composite – State of art

Just a few works were carried on nanocomposites of carbon nanotubes and polyurea. Now, we are going to analyze some of the results achieved.

Chao Gao et al. (2005) followed the poly-condensation approach using, as precursors, bonding linear polyurea, polyurethane, and hyperbranched poly-(urea-urethane) on amino-functionalized MWNTs (MWCNT-NH₂). The relative quantities were: 400 mg polyurea/other polymer matrix and 40 mg of MWCNT-NO₂ To

have one only homogenous phase, the mixture was stirred for 24 hrs at room temperature. Then polyurea was washed away and from the analysis it was shown that CNTs resulted well coated by the polymer. Thus to understand the inter-phase polyurea/CNTs.

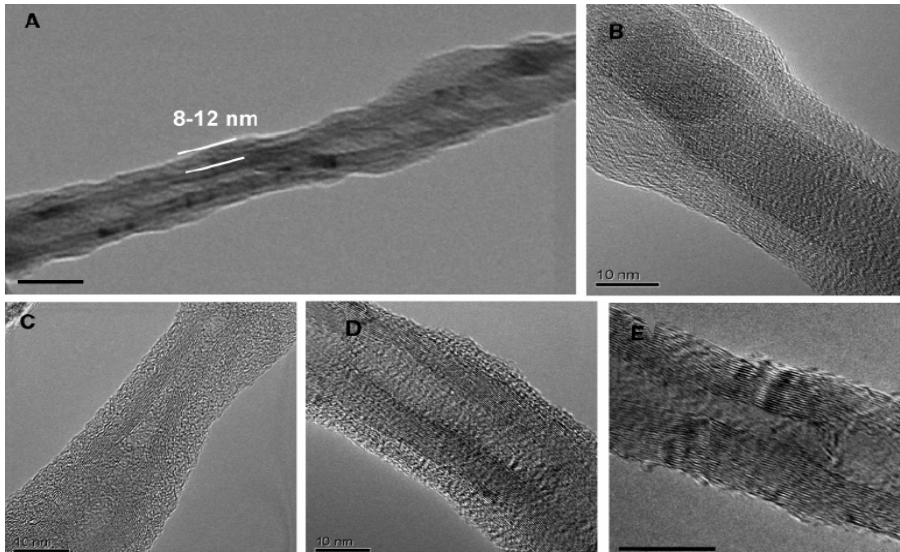


Fig.3.5 a-e Representative TEM images of different samples of CNTs coated by polyurea. Figure E pictures a crude MWNT. The scale bar represents 25 (in panel A) and 10 nm (in panels B-E), respectively. (Source: Chao Gao et al., 2005).

Hang-Lang Wu et al. (2006) investigated how CNTs improve polyurea properties using different types of carbon nanotubes dispersed in a poly (urea urethane) system:

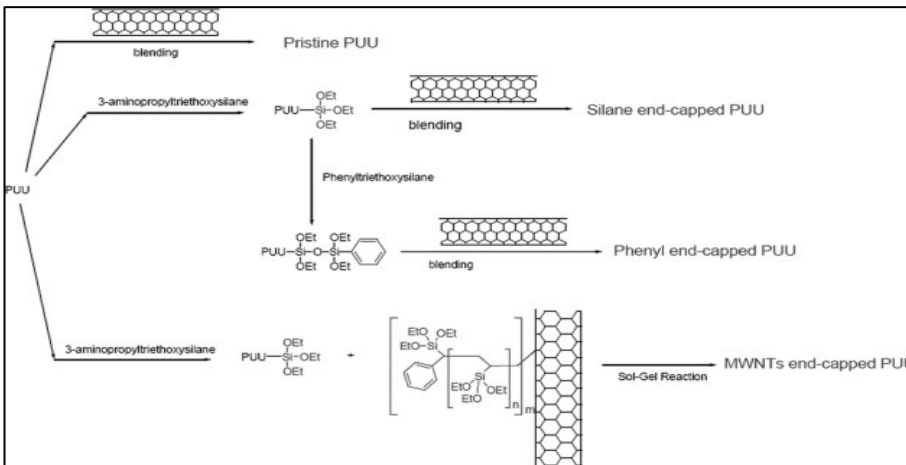
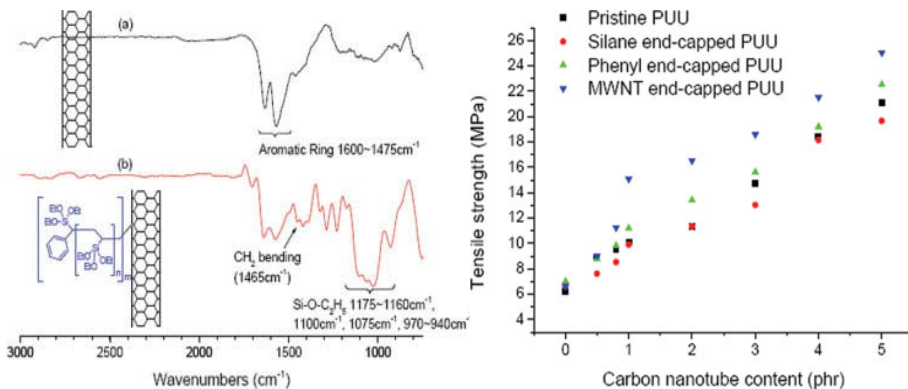


Fig.3.6 Flow chart of the fabrication of PUU/MWNT nanocomposites. (Source: Hang-Lang Wu et al., 2006)

Following there are the different composites produced:

- Pristine PUU: Pristine MWNT was first dissolved in THF¹, and then added to PUU solution for 30 min in an ultrasonic vibration bath.
- Silane end-capped PUU: A-silane was dissolved in THF by 10 % w/v, and then reacted with PUU at 40 °C for 8 hrs to obtain A-silane end-capped PUU. The functionalized MWNT was added into A-silane end-capped PUU solution for 30 min in an ultrasonic vibration bath.
- Phenyl End-capped PUU: The A-silane end-capped PUU was further reacted with P-silane via sol-gel reaction. MWNT/THF solution was added into phenyl end-capped PUU solution for 30 min in an ultrasonic vibration bath.
- MWNT end-capped PUU: The functionalized MWNT and HCl were added into A-silane end-capped PUU solution for 2 h. Aforementioned MWNT/PUU nanocomposites solutions were kept under high shear stirring at room temperature for 1 h. The solutions were cast onto the mold (150 x 150 mm²) and vacuum dried at 80 °C for 10 h.

Fig.3.7 a-b
Left: FTIR spectra of
(a) pristine CNT and
(b) functionalized
CNT.
Right: Tensile
strength of various
MWNT/PUU nano-
composites.
(Source: Hang-Lang
Wu et al., 2006)



It was found out that the surface electrical resistance decreases with the increasing MWNT content even though their dispersion in PUU matrix plays a fundamental role. Regarding the tensile strength, for all CNT/PUU systems, it increased 3 – 4 times as the content of MWNT increased from 0 to 5 phr. On the other hand, the tensile strength of MWNT/PUU sheets is greatly associated with the interfacial adhesion between MWNT and PUU. It was found that the higher the interfacial interaction, the higher the tensile strength. The A-silane functionalized MWNT and PUU and the Psilane end-capped PUU may increase the interfacial interaction between MWNT and PUU, thus, leading to the increase of the tensile strength. Consequently, both P-silane end-capped PUU and MWNT end-capped PUU showed higher tensile strength than that of the pristine PUU.

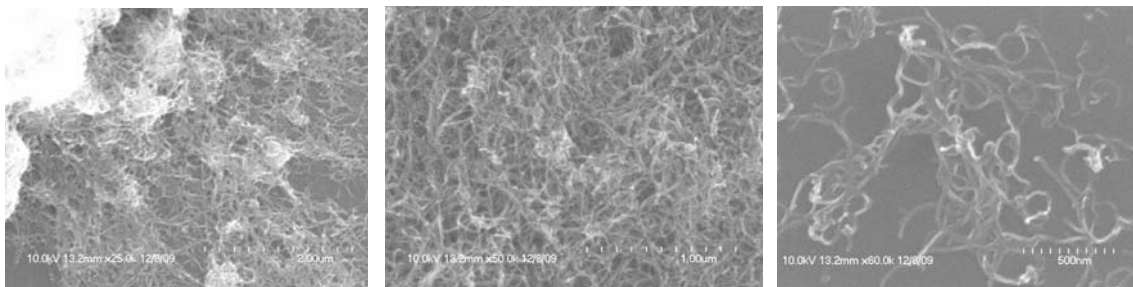
¹ Tetrahydrofuran (THF) is a colorless, water-miscible organic liquid with low-viscosity at standard temperature and pressure. It is a heterocyclic compound with a chemical formula C₄H₈O, and is the fully hydrogenated analog of the aromatic organic compound furan. It is one of the most polar of the organic functional class of ethers, and has a relatively low freeze point, and so is a commonly used modern organic chemical laboratory solvent across a range of temperatures.

4. MATERIALS AND SPECIMEN PRODUCTION

4.1 Materials used

4.1.1 Carbon nanotubes

The Carbon nanotubes (CNTs) used in this work were purchased from Sigma Aldrich Inc.. The product purchased is: Multiwalled Carbon Nanotubes (MWCNTs) >90% carbon basis, O.D. x I.D. x L = 10-15 nm x 2-6 nm x 0.1-10 μm. Density of 2.1 g/mL (25 °C). Synthesized by Catalytic Chemical Vapour Deposition (CCVD).



4.1.2 Polyurea

Polyurea was purchased from ITW Futura Coatings, 1685 Galt Industrial Boulevard, St. Louis, MO (USA). The product purchased is Aqualine 300® that is a two component, 100% solids, ambient temperature cure polyurea. It is designed to provide an excellent resistance to both corrosion and erosion in a large number of different environments forming a flexible membrane over both concrete and steel substrates. This material is characterized by a quite long pot life¹, about 30 minutes, that makes it suitable for applications by brush, roller, trowel or squeegee.

Fig. 4.1 a-b-c Secondary electron micrographs of the multiwalled carbon nanotubes that we used in our work. The enlargements are 2 mm, 1 mm, 500 nm.

Solids by volume	100%	Elongation	400%
Volatile organic compounds	0.0 lb/gal (0 g/l)	Adhesive tensile shear (ASTM D-1002)	2000 psi
Theoretical coverage	1604 ft ² /gal @ 1 mil	Tensile strength	1300 psi
Recommend DFT	60 mils	Tear strength	250 pli
Number of coats	1 or more	Hardness (ASTM D-2240)	90 Shore A
Mix ratio	21 curative : 79 resin	Pot life @ 75 °F (24 °C)	35 minutes
Operating temperature	-70 to 180 °F (-56 to 82 °C)		

¹ Pot life: the length of time that a catalyzed resin system retains a viscosity low enough to be used in processing.

4.1.3 Tetrahydrofuran (THF)

Tetrahydrofuran (THF) anhydrous was purchased from Sigma Aldrich. It is an organic solvent characterized by low viscosity at standard temperature and pressure. Its chemical formula is C_4H_8O and it is often used as precursor for polymers. As it will be discussed, the solvent has a strong effect on the Polyurea mechanical resistance but its use was necessary to disperse CNTs in the polymer matrix.

4.2 Specimen production

To perform the mechanical tests, two different kinds of specimen had been prepared. One kind is made of Polyurea + CNTs to analyze the mechanical performance of the polymer due to the addition of nanometric particles. The other kind is the composite steel + Polyurea + CNTs to analyze the mechanical behavior of the steel plates when coated by these new nanocomposite.

In both cases, the nanocomposites have been prepared by adding different quantities in weight percentage [wt %] of CNTs, as following described:

1. polyurea + 0 wt % CNTs (pure polyurea);
2. polyurea + 1 wt % CNTs;
3. polyurea + 5 wt % CNTs;
4. polyurea + 10 wt % CNTs.

Tab. 4.2 Materials quantities needed to produce the specimen				
		1 wt % CNTs	5 wt % CNTs	10 wt % CNTs
100 g				
CNT [g]		1	5	10
Curative [g]	21 part	20,79	19,95	18,9
Resin [g]	79 part	78,21	75,05	71,1
150 g				
CNT [g]		1,5	7,5	15
Curative [g]	21 part	31,185	29,925	28,35
Resin [g]	79 part	117,315	112,575	106,65
200 g				
CNT [g]		2	10	20
Curative [g]	21 part	41,58	39,9	37,8
Resin [g]	79 part	156,42	150,1	142,2

Carbon Nanotubes have been previously dissolved in 50 ml of Tetrahydrofuran (THF) and stirred for 30 minutes to homogeneously disperse them. Then, the curative part is added and stirred for another 30 minutes until the mixture becomes homogeneous. Finally, the resin is added to proceed with the polymerization process. The mixture is mixed for about 5 minutes with a wooden spatula and then poured into a paper box in order to have a homogeneous 6 mm thick sheet of nanocomposite. The pot life of this compound is considered to be about 30 minutes as suggested by the product producer.



Fig. 4.2 a-b
 Left: Aqualine 300® resin.
 Right: CNT dissolved in THF has been stirring for 30 min with the curative.

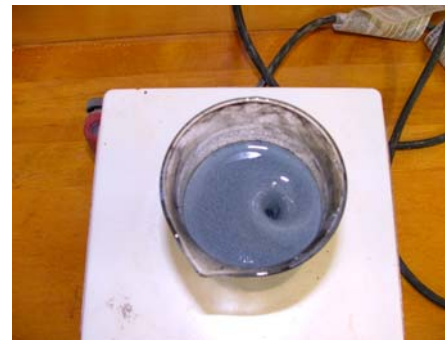
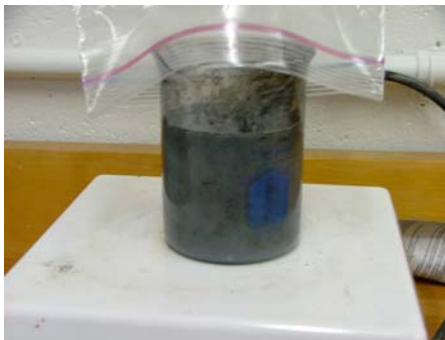


Fig. 4.3 a-b
 CNT dissolved in THF has been stirring for 30 min with the curative.



Fig. 4.4
 The solution is put in the container to have a sheet of nanocomposite.

The boxes are then stored for about 24 hours at room temperature to let the polymerization process cure and obtain a hard sheet of nanocomposite.

At the end, the sheets are cut in stripes and shaped according to the ATSM D-412 Die C to obtain the specimen suitable to perform the mechanical tests.



Fig. 4.5 a-b
The nanocomposite is placed for 24 hours at room temperature to polymerize.



Fig. 4.6 a-b
The four kind of specimen produced. (Plane and cross section views)

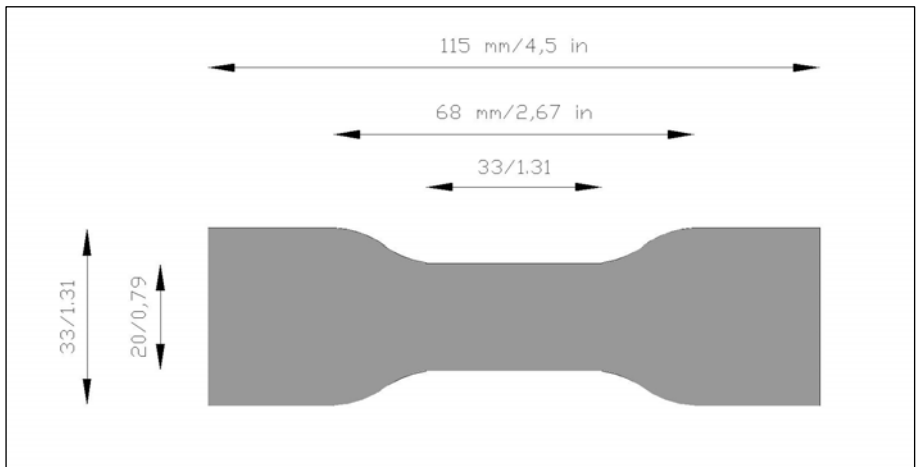


Fig. 4.7
Specimen dimensions quoted both in mm and inches.

To obtain the specimen for the composite system steel + polyurea + CNTs, the new nanocomposite is applied by brush on the steel plates that had been previously cut according to ASTM standard. This system was not tested.



Fig. 4.8 –a-b-c

Top left: Steel specimens coated by a layer of nanocomposite and, top right, an enlargements of two samples.

Bottom: Top view of two steel specimen coated by two different layer of composite: on the top pure polyurea, on the bottom polyurea + 1wt % of CNT. It is possible to notice a big difference in roughness in the coating surface.

5. TENSION TESTS

5.1 Introduction

The Tension tests of the new material CNT-enhanced Polyurea were performed in accordance to the ASTM D-412: “Standard test methods for vulcanized rubber and thermoplastic elastomers – Tension” that covers the procedures used to evaluate the tensile (tension) properties of rubbers. Tensile properties depend both on the material and the conditions of the test (extension rate, temperature, humidity, specimen geometry, etc.); therefore materials should be compared only when tested under the same conditions. The determination of these properties starts with test pieces taken from the sample material and includes the preparation of the specimen and the testing of the specimen that may be in the shape of dumbbells, rings or straight pieces of uniform cross-sectional area¹.

5.2 Elements of solid mechanics and some definitions

In solid mechanics, solids generally have three responses to force, depending on the amount of force and the type of material:

1. elasticity — the ability of a material to temporarily change shape, but return to the original shape when the pressure is removed;
2. plasticity — the ability to permanently change shape in response to the force, but remain in one piece. The yield strength is the point at which elastic deformation gives way to plastic deformation. Deformation in the plastic range is non-linear, and is described by the stress-strain curve. This response produces the observed properties of scratch and indentation hardness, as described and measured in materials science. Some materials exhibit both elasticity and viscosity when undergoing plastic deformation; this is called viscoelasticity;
3. fracture — split into two or more pieces. The "ultimate strength" or toughness of an object is the point at which fracture occurs.

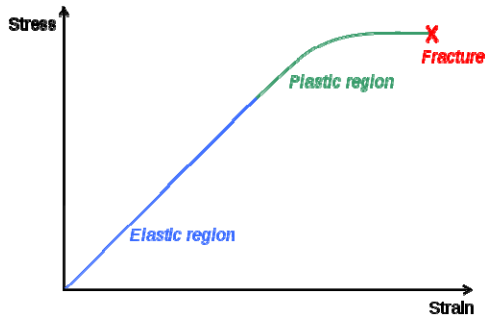
Strength is a measure of the extent of a material's elastic range, or elastic and plastic ranges together. This is quantified as compressive strength, shear strength, tensile strength depending on the direction of the forces involved. Ultimate strength is measure of the maximum strain a material can withstand.

Brittleness, in technical usage, is the tendency of a material to fracture with very little or no detectable deformation beforehand. Thus in technical terms, a material can be both brittle and strong.

In everyday usage, the word *brittleness* usually refers to the tendency to fracture under a small amount of force, which exhibits both brittleness and a lack of strength (in the technical sense). For brittle materials, yield strength and ultimate strength are the same, because they do not experience detectable plastic deformation. The opposite of brittleness is ductility.

¹ The preparation of the specimen has been discussed in Chapter 4.

Fig. 5.1
Diagram of a typical stress-strain curve that shows the relationship between stress (force applied per unit area) and strain or deformation of a ductile material.



The toughness of a material is the maximum amount of energy it can absorb before fracturing, which is different than the amount of force that can be applied. Toughness tends to be small for brittle materials, because it is elastic and plastic deformations that allow materials to absorb large amounts of energy.

Tensile strength is the maximum tensile stress reached in stretching a

test piece of a particular material and is usually stated in Metric units, MegaPascals (MPa) or in English units, pounds-per-square inch (psi).

Below, the metric conversion is shown:

$$1 \text{ psi} = 0,0068948 \text{ MPa} = 0,6894757 \text{ N/cm}^2 \quad (\text{eq. 5.1})$$

The test methods allowed by the standards for the measurement of tensile properties may not directly relate to the total end use performance of the product, if considered alone. Tensile set represents residual deformation which is partly permanent and partly recoverable after stretching and retraction. For this reason, the periods of extension and recovery (and other conditions of test) must be controlled to obtain comparable results.

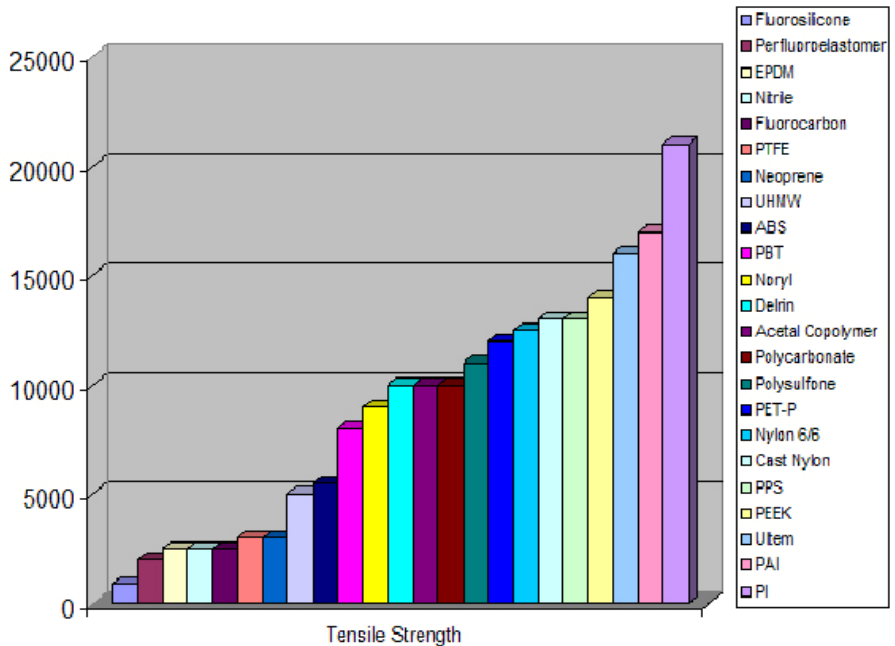


Fig. 5.2
Tensile strength comparison [PSI]

The ASTM D - 412 1.1 reports two test methods that cover procedures used to evaluate the tensile (tension) properties of vulcanized thermoset rubbers and thermoplastic elastomers. These methods are not applicable to low elongation materials. The methods usually used are:

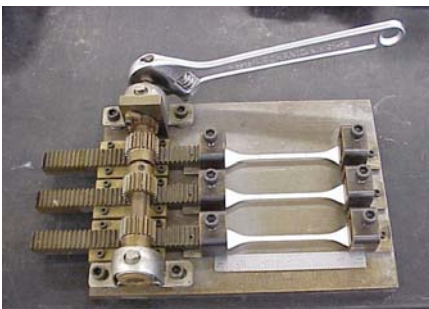
- Test method A: Dumbbell and Straight section specimens;
- Test method B: Cut ring specimen.

These methods cover the tension testing at various temperatures and include measurements of tensile stress at given elongations, tensile strength, ultimate elongation and tensile set.



Fig. 5.3
An instrument generally used to measure tensile properties.

The methods start with a piece taken from the sample and include: the preparation of the specimen and the testing of the specimen.



Measurements of tensile stress, tensile strength, and ultimate elongation are made on specimens that have not been pre-stressed. Tensile stress and tensile strength are based on the original cross sectional area of a uniform section of that specimen. Measurement of tensile set is made after a specimen has been extended and allowed to retract by a prescribed procedure without pre-stressing. The tensile properties of rubber are not intrinsic characteristics but depend on both the material and the conditions of test such as rate of extension, temperature, humidity, geometry of specimen, inertia of dynamometer in tester, and environmental or mechanical preconditioning. Modest changes in rate of extension caused by type of tester (pendulum versus inertia-less) have little or no effect on the tensile properties of most rubbers. As temperature may have a signifi-

Fig. 5.4
An instrument generally used to measure elongation.

As temperature may have a signifi-

cant effect on tensile properties, it should be controlled. For most rubbers, humidity has a small effect that can be neglected. Tensile strength and ultimate elongation depend on the volume of the specimen and stress concentrations due to shape of specimens. Inertia type dynamometers may give erroneous results if the load capacity of the tester is too high - or too low - for the material being tested. The periods of extension and recovery and the other conditions of testing need to be controlled in order to obtain comparable results. Tensile set testing of a rubber or thermoplastic elastomer evaluates the residual elongation of a test sample after being stretched and allowed to relax in the specified manner. This elongation consists of both permanent and recoverable components - thus the time for stretching and recovery are important factors, and are both specified by the standard ASTM D - 412.

ASTM D - 412 also specifies a dumbbell shaped specimen: the specification describes 6 options for the sample dimensions, but the preferred sample is called "Die C". Die C has an overall length of 115 mm (4.5 inches) with a narrow section 33 mm (1.31 inches) long. This provides a gauge length (benchmark) 25 mm (1 inch) long and a gauge width of 6 mm (0.25 inch).

Tensile set is expressed in percent and is calculated by dividing the change in length of the test sample by the initial length. Below there are some definitions, as stated by standard, to avoid any misunderstandings:

- *Tensile set*: the extension remaining after a specimen has been stretched and allowed to retract in a specific manner, expressed as a percentage of the original length.
- *Tensile strength*: the maximum tensile stress applied in stretching a specimen to rupture.
- *Tensile stress*: a stress applied to stretch a test piece.
- *Tensile stress at a given elongation*: the stress required to stretch the uniform cross section of a test specimen to a given elongation.
- *Ultimate elongation*: the elongation at which rupture occurs in the application of continued tensile stress.
- *Yield point*: that point on the stress-strain curve, short of ultimate failure, where the rate of stress with respect to strain, goes through a zero value and may become negative. (That particular point at which the material strain changes from elastic deformation to plastic deformation) At the yield point the yield strain (level of strain at the yield point) and the yield stress (level of stress at the yield point) are defined.

5.3 Apparatus and procedure

The testing machine used to perform the tests was an Instron 4260 that may apply a maximum load of 30.000 lb ~ 15.000 Kg ~ 150 KN².

The software used to acquire the data was LabView 8.5 developed by the National Instrument, 2007.

2 1 lb = 0,454 Kg

In order to perform the tests, the specimens are placed in the grips of the testing machine using care to adjust them symmetrically so that the tension is distributed uniformly over the cross section. The loading rate was set to be 2.00 inch/min, which equal to 50 mm/min, and may be considered quasi-static. At every stopping point of the machine the distance between the grips is recorded.



Once the final load is reached, the specimens are held at the specified elongation for 10 minutes and then released quickly. Then it is made them rest for 10 minutes. At the end of the 10 min rest period the distance between the bench marks has been measured. To determine cycling loading, the residual elongation and the strength lost at each cycle (hysteresis) the specimens are held at the maximum permitted elongation for 10 minutes, then they are released until the load comes to zero and make them rest for 10 minutes. At the end of the 10 min rest period they are pulled again. This operation has been repeated for 5 cycles.

Fig. 5.5 a-b-c
Left: the apparatus controller
Centre: the software recording a test
Right: testing machine - the grips used to hold the specimen.



Fig. 5.6
The tension test: the specimen (in this case Polyurea + THF) is placed between the grips and the bench marks are marked on the material (left). Then, the specimen is pulled (centre) until it breaks (right). The machine has got some sensors that make the software records the elongation and the load applied.

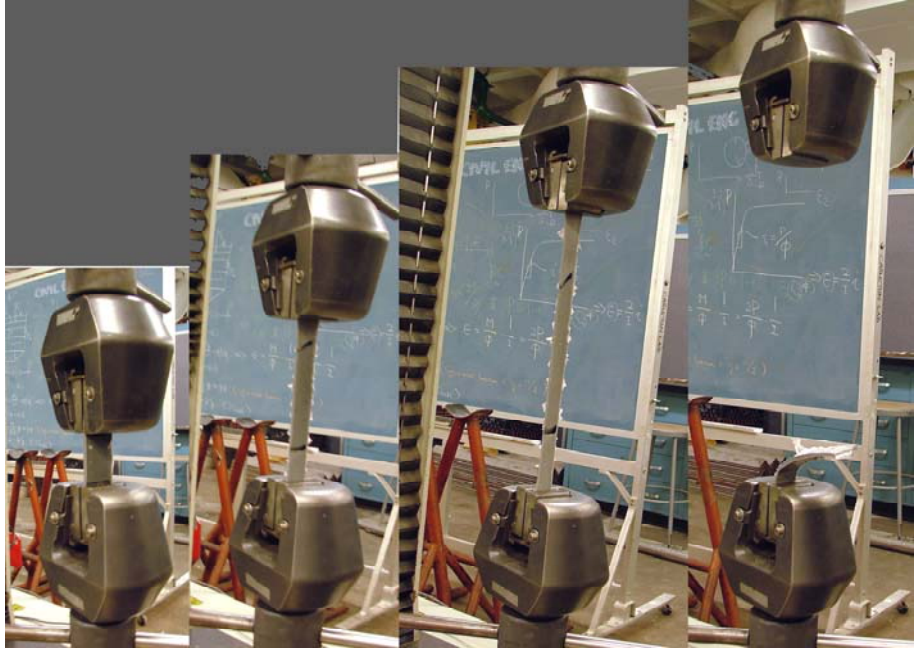


Fig. 5.7

An other tension test performed on a sample of Polyurea + THF+ 5 wt % of CNT. In this case the specimen has a larger elongation if compared to the picture above.

5.4 Calculations

The **tensile stress** at any specified elongation is calculated as follows:

$$T_{(xxx)} = F_{(xxx)} / A \quad \text{eq. 5.2}$$

where:

$T_{(xxx)}$ = tensile stress at (xxx) % elongation, MPa or lbf/in²,

$F_{(xxx)}$ = force at specified elongation, MN or lbf,

A = cross sectional area of unstrained specimen, m² or in².

The **yield stress** is calculated as follows:

$$Y_{(stress)} = F_{(y)} / A \quad \text{eq. 5.3}$$

where :

$Y_{(stress)}$ = yield stress, that stress level where the yield point occurs, MPa or lbf/in²,

$F_{(y)}$ = magnitude of force at the yield point, MN or lbf,

A = cross sectional area of unstrained specimen, m² or in².

The **tensile strength** is calculated as follows:

$$TS = F_{(BE)} / A \quad \text{eq. 5.4}$$

where:

TS = tensile strength, the stress at rupture, MPa or lbf/in²,

$F_{(BE)}$ = the force magnitude at rupture, MN or lbf,

A = cross sectional area of unstrained specimen, m² or in².

The **elongation** at any degree of extension is calculated as follows:

$$E = 100 [L - L_0] / L_0 \quad \text{eq.5.5}$$

where:

- E = the elongation in percent (of original bench mark distance),
 L = observed distance between bench marks on the extended specimen,
 L₀ = original distance between bench marks (use same units for L and L₀).

A test result is the median of three individual test measurement values for any of the measured properties as described above, for routine testing.³

5.5 Results and discussion – Influence of THF

First, we want to compare the mechanical behaviour of pure Polyurea with those of Polyurea + THF prepared in the Carleton Laboratory at Columbia University. More particularly, the tension tests were performed at a crosshead displacement of 50.8 mm/min and at controlled temperature and humidity ($24 \pm 2^\circ\text{C}$, $50 \pm 5\%$ RH).

The aim of this comparison is to evaluate the influence of THF on the polymer matrix. Figure 5.8 and Figure 5.9 show the stress-strain curves of the two different Polyurea specimens as obtained in the experiments while the values of the tensile strength and elongation were previously reported in Table 5.1.

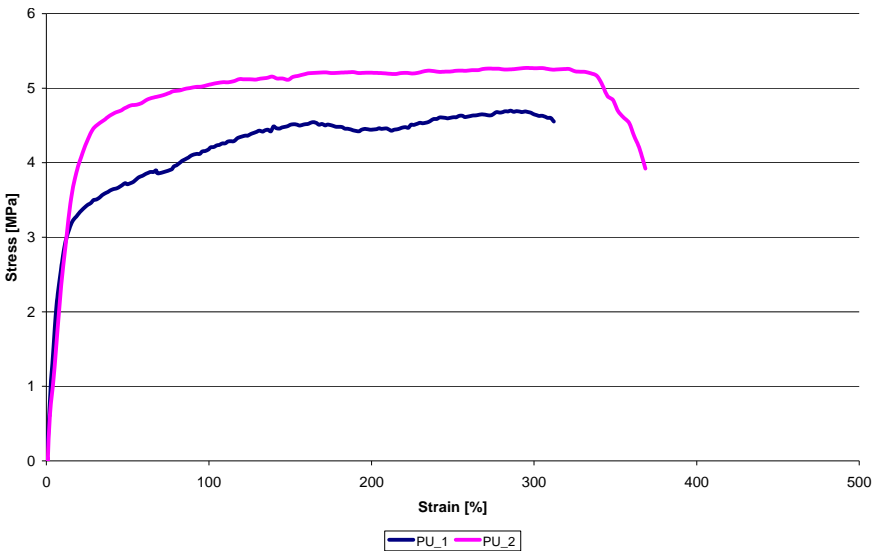


Fig. 5.8
 Stress – Strain curve for Polyurea without THF. The average tensile strength is about 5 MPa while the maximum elongation percentage at breakage is about 290%.

³ There are two exceptions to this and for these exceptions a total of five (5) specimens (measurements) shall be tested and the test result reported as the median of five:

exception 1: if one or two of the three measured values do not meet specified requirement values when testing for compliance with specifications;

exception 2: if referee tests are being conducted.

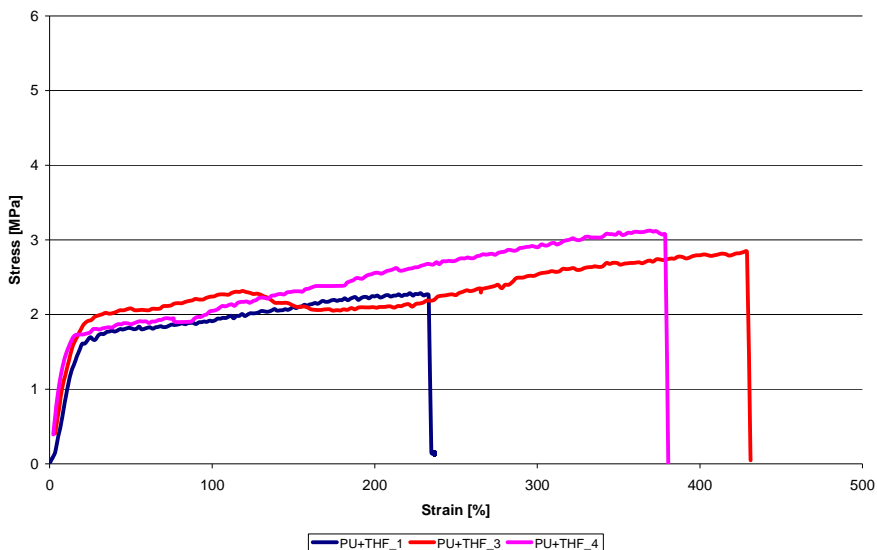


Fig. 5.9
Stress – Strain curve obtained for Polyurea with THF. The average tensile strength is about 2,75 MPa while the maximum elongation percentage at breakage is about 370%.

As expected, adding THF has a very negative effect on the polymer behaviour as the maximum stress shown by the material with THF is about half of the original value for the polymer without THF. However, there are substantially no effects on the maximum elongation (strain) recorded at breakage of the specimen, value that tends to be close to the elongation of the original product (the polyurea used in this study should have shown a 400% elongation as stated by the company data sheet).

The values of the tensile strength and elongation for the specimens with and without THF, and the hypothetical values for virgin Polyurea, are reported in Table 5.1 and Figure 5.10.

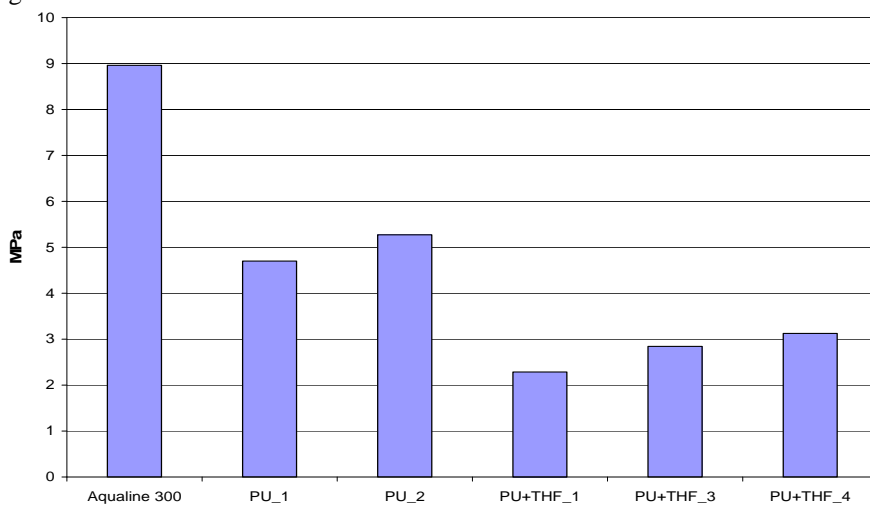


Fig. 5.10
Graphical visualization of the different tensile strengths.

Tab. 5.1
Comparison between Aqualine 300, polyurea without THF and polyurea + THF

Sample	Tensile Strength (MPa)	Tensile Strength (psi)	Max elongation (m)	Elongation %
Aqualine 300 ⁴	8,96	1300	-	400
Polyurea sample 1	4,70	681,68	0,138	285,49
Polyurea sample 2	5,27	764,35	0,075	295,15
Polyurea + THF sample 1	2,29	332,14	0,113	221,65
Polyurea + THF sample 3	2,84	411,91	0,163	428,93
Polyurea + THF sample 4	3,12	452,52	0,164	369,31

5.6 Results and discussion – Influence of CNT

In this section, we analyse the influence of different amounts of CNTs with 0, 1, 5 and 10 wt %, on the Polyurea matrix, as shown in the stress strain curves in Figures 5.11 – 5.14, respectively.

As illustrated, the addition of carbon nanotubes improves the tensile strength of all the samples. All the specimens show an initial linear behaviour, with a high value of Young's modulus, up to a stress level that ranges between 3.5 – 4 MPa. After this value, the stress-strain behaviour remain linear but with a slope that depends on the amount of CNTs used. The best performance is recorded for the sample with 1 wt % of added CNTs: all 1 wt % CNT doped-Polyurea specimens did not break during the tensile test, reaching a maximum elongation of 30.48 cm (this is the maximum elongation allowed by our universal testing machine). The elongation resulted in an almost 800%, which indicates an increase of more than twice as compared to either the base material (Polyurea + THF) or the commercial one (both reach elongation of about 400 %).

The tensile strength of the new material resulted in about 3 times the value of the base material (Polyurea + THF) which is a clear enhancement in the mechanical strength and toughness.

The specimens with 5 wt % CNT showed a behaviour similar to the one of the base material in terms of maximum stress. However, the elongation percentage resulted to be quite smaller.

The specimens with 10 wt % CNT added showed the worst behaviour as they broke almost immediately under small loads and small elongations, presenting a brittle-type behaviour. The results are summarized in Table 5.2.

⁴ Data taken from the Technical Data sheet of Aqualine 300® by ITW Futura Coating.

Polyurea + THF + 0 wt % CNT

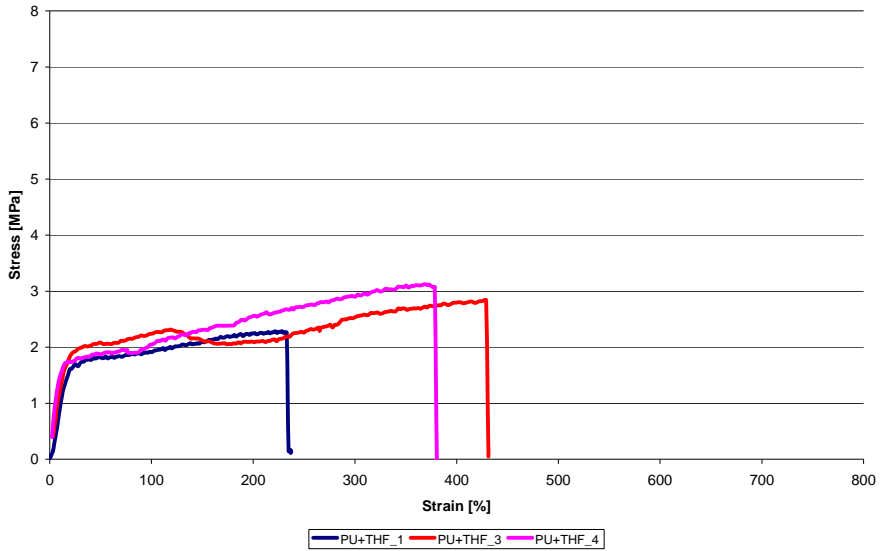


Fig. 5.11

Stress – Strain curve for Polyurea + THF + 0 wt % CNT. The lines represent the mechanical behaviour of the specimens tested. The average tensile strength is about 2,75 MPa while the maximum elongation percentage at breakage is about 370%.

Polyurea + THF + 1 wt % CNT

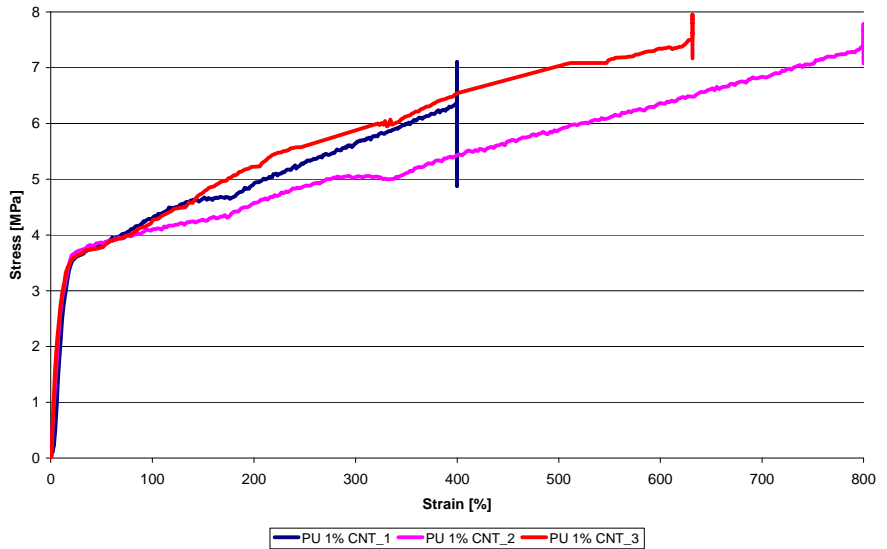


Fig. 5.12

Stress – Strain curve for Polyurea + THF + 1 wt % CNT. The lines represent the mechanical behaviour of the specimens tested. The average tensile strength is about 7 MPa while the maximum elongation percentage at breakage is about 610%.

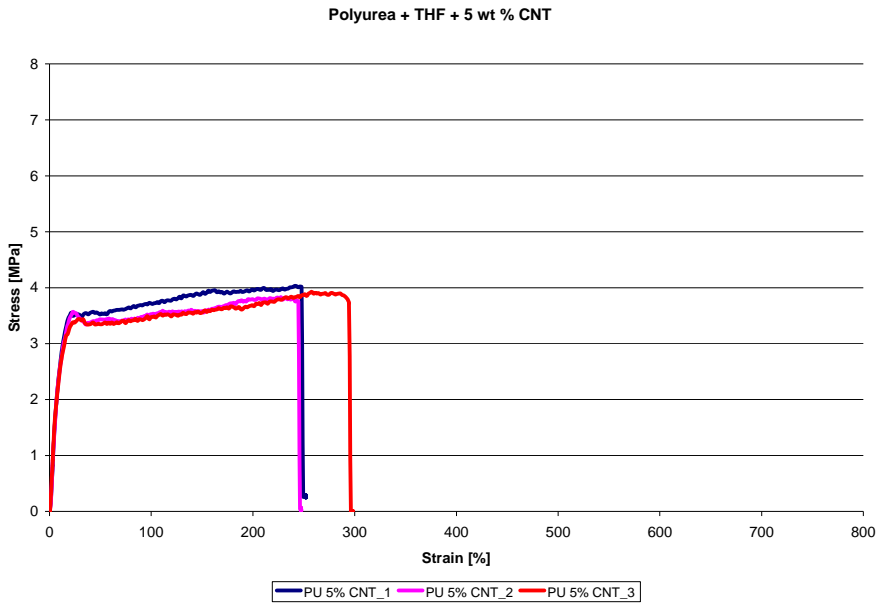


Fig. 5.13
 Stress – Strain curve for Polyurea + THF + 5 wt % CNT. The lines represent the mechanical behaviour of the specimens tested. The average tensile strength is about 4 MPa while the maximum elongation percentage at breakage is about 242%.

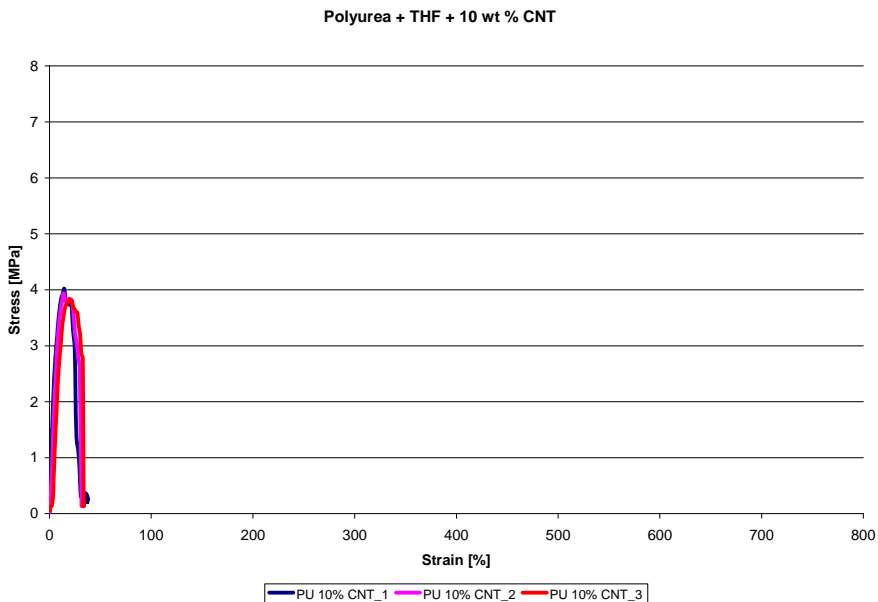


Fig. 5.14
 Stress – Strain curve for Polyurea + THF + 10 wt % CNT. The lines represent the mechanical behaviour of the specimens tested. The average tensile strength is about 4 MPa while the maximum elongation percentage at breakage is about 16%.

CNT wt %		Tensile Strength (MPa)	Max elongation (m)	Elongation %
0	Sample 1	2,29	0,113	221,65
	Sample 2	2,84	0,163	428,93
	Sample 3	3,12	0,164	369,31
1	Sample 1	6,36	0,253	398,86
	Sample 2	7,37	0,304	797,75
	Sample 3	7,51	0,305	631,52
5	Sample 1	4,03	0,123	241,18
	Sample 2	3,83	0,124	227,53
	Sample 3	3,93	0,131	257,78
10	Sample 1	4,02	0,0082	14,47
	Sample 2	3,94	0,0074	13,87
	Sample 3	3,84	0,0123	19,38

Figures 5.15 and 5.16 show the average tensile strength and the average maximum elongation as a function of the carbon nanotubes content.

In these figures, it can be seen that the best result is achieved when adding 1 wt % of CNT into the Polyurea + THF matrix, even though there are some uncertainties in the test data denoted by a certain scattering of them. From Figure 5.16, it is noteworthy to highlight the fact that adding larger quantities of CNT makes the material more brittle lowering the maximum elongation percentage.

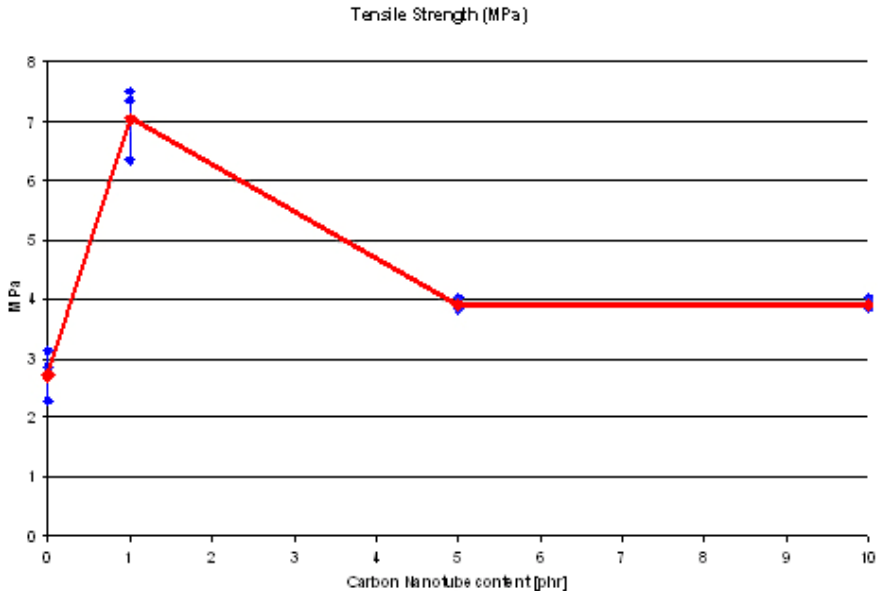


Fig. 5.15
Tensile strength as function of CNTs content. The red line represents the average values, the blue dots the exact values.

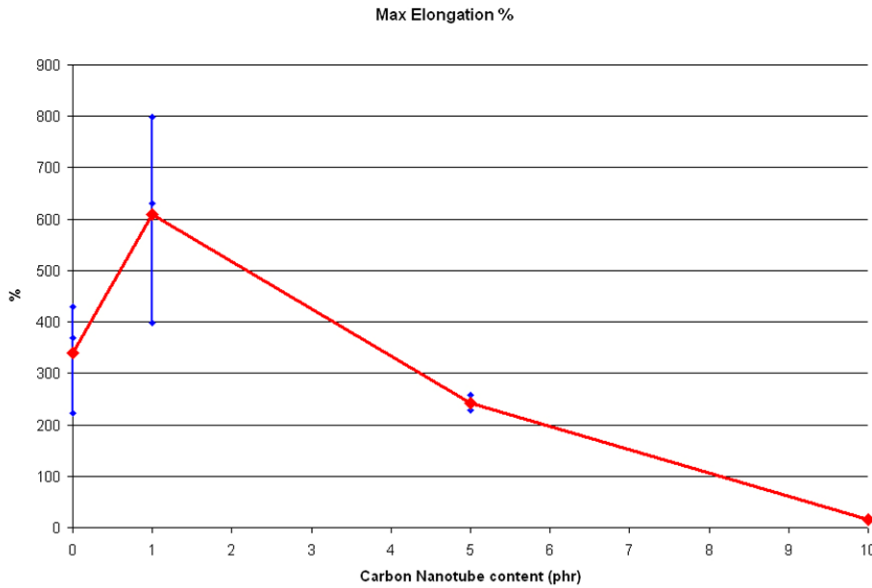


Fig. 5.16 Ultimate elongation percentage as function of CNTs content. The red line represents the average values while the blue dots indicate the values from each test.

5.7 Results and discussion – Tensile set

For the 1 wt % CNT doped-Polyurea specimens we measured the tensile set, which, according to the Standard ASTM D-412, is the extension remaining after a specimen has been stretched and allowed to retract for 10 min.

The results of this analysis, shown in Table 5.3, indicate an average tensile set of about 60 %.

Table 5.3 Tensile set for 1 wt % CNT doped-Polyurea + THF specimens.				
Sample	Distance between the bench marks		Residual elongation [cm]	Tensile set [%]
	Before the test [cm]	After 10 min [cm]		
Sample 1	6,35	9,53	3,18	50
Sample 2	3,81	6,60	2,79	73
Sample 3	4,83	7,72	2,89	60
Average tensile set [%]				61

5.8 Results and discussion – Load and Unload Test

Loading and unloading tests were performed in order to evaluate the material response to repeated loading cycles. Specifically, five cycles were performed for each CNT + Polyurea material, and recorded in Figures 5.17 – 5.19.

Each test cycle was performed in the following way: each specimen was strained to half of the maximum expected elongation and kept under constant load for 10 min. Then, the load was slowly removed (quasi-statically) until it became nearly zero and kept at this value for another 10 min. Then a new cycle began, repeating the same procedure.

The Stress – Strain curves illustrated in Figures 5.17 – 5.19 show a typical hysteresis loop of loading cycles. The tensile strength decreases at every cycle while the residual strain increases. The test was not performed for the 10 wt % CNT doped-Polyurea as the material was too brittle and the maximum elongation was too small. Figures 5.20 – 5.21 summarize the maximum tensile stress and the loss percentage recorded at each cycle for 0, 1 and 5 wt % of CNTs added into the polymer matrix, respectively.

It is noteworthy that the 1 wt % CNT doped-Polyurea shows better performance at every cycle, handling a higher stress in comparison to the 0 and 5 wt % CNT doped-nanocomposites. In addition, this mixing shows to have the largest loss per cycle, as presented in Figure 5.21. In this figure, it is also interesting to notice that, after 4 cycles, the mechanical loss tends to be almost the same for all the materials.

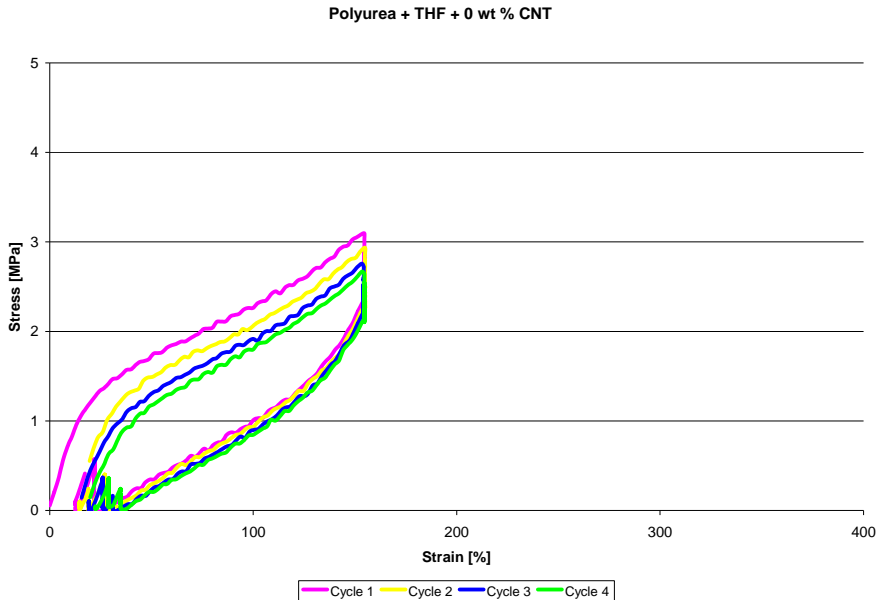


Fig. 5.17
Load and unload cycles on 0 wt % CNT doped-Polyurea.

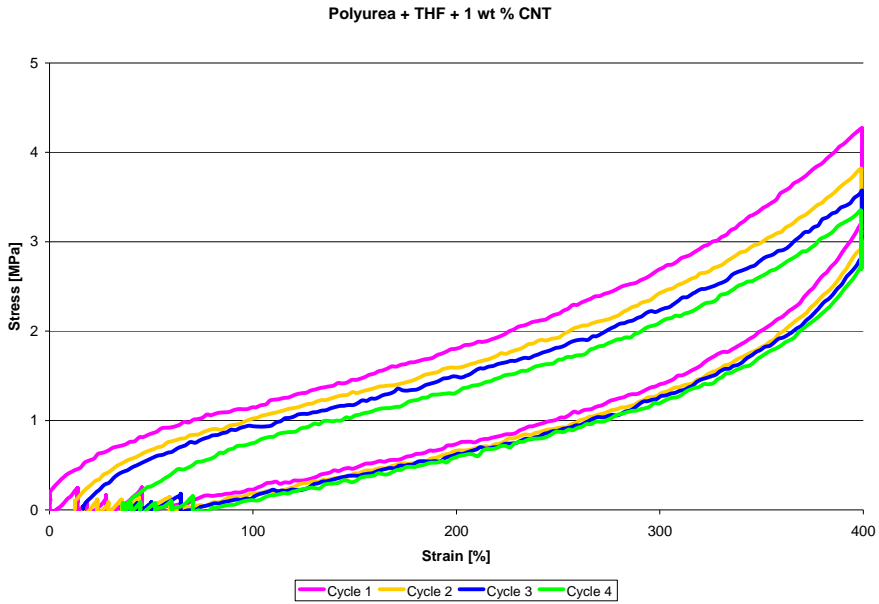


Fig. 5.18 Load and unload cycles on 1 wt % CNT doped-Polyurea.

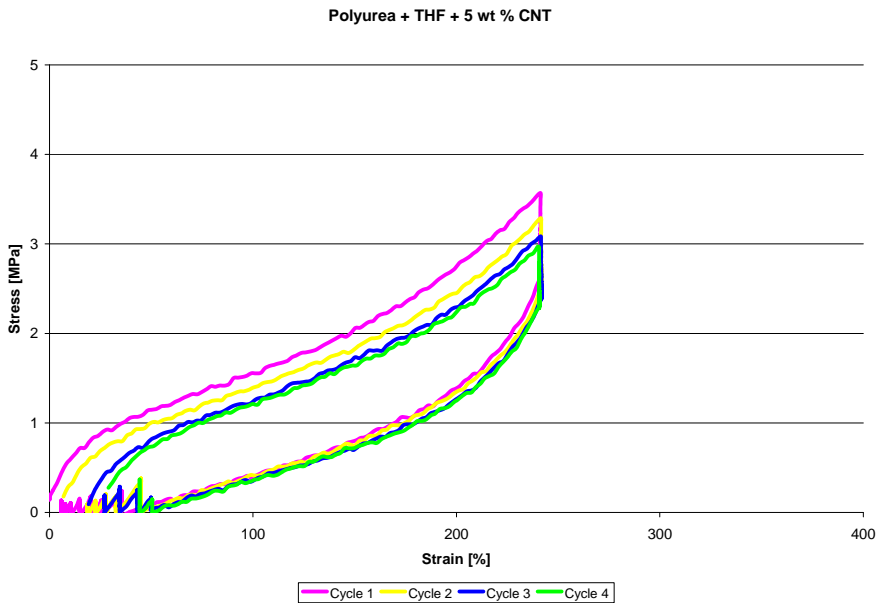


Fig. 5.19 Load and unload cycles on 5 wt % CNT doped-Polyurea.

Max tensile stress per cycle

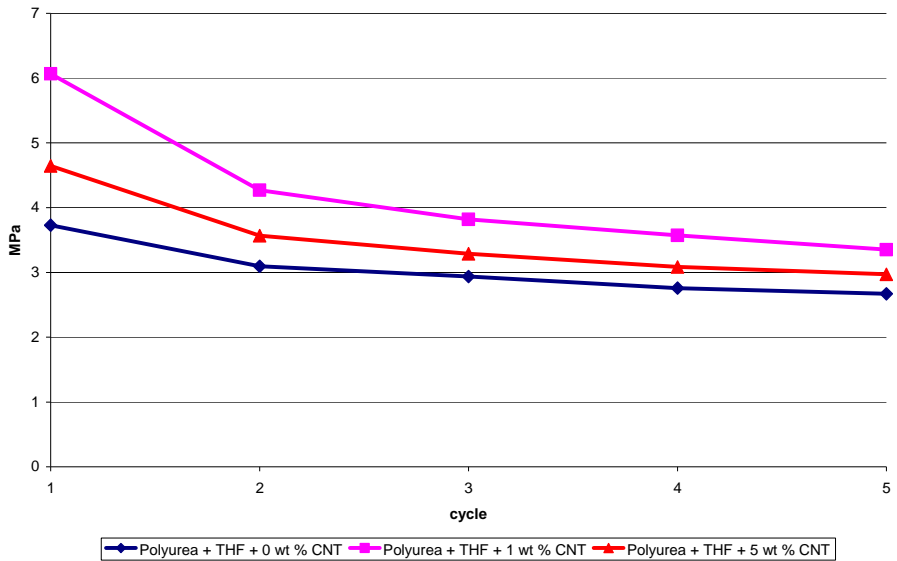


Fig. 5.20
Maximum tensile stress recorded at each cycle for 3 different CNT quantities.

Max tensile stress loss percentage per cycle

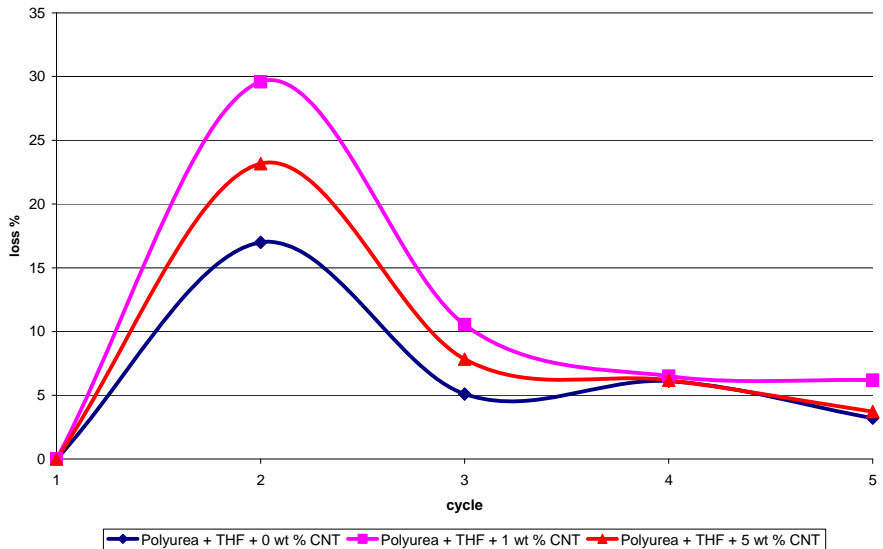


Fig. 5.21
Maximum tensile stress loss percentage at each cycle.

Tab. 5.4 Load and Unload test on Polyurea + THF + 0 wt % CNT – Tensile Strength and loss %		
	Tensile Strength [MPa]	Loss % per cycle
Cycle 1	3,73	
Cycle 2	3,10	15,96
Cycle 3	2,94	5,10
Cycle 4	2,76	6,11
Cycle 5	2,67	3,21
		Total loss % after 5 cycles
		28,41

Tab. 5.5 Load and Unload test on Polyurea + THF + 1 wt % CNT – Tensile Strength and loss %		
	Tensile Strength [MPa]	Loss % per cycle
Cycle 1	6,07	
Cycle 2	4,27	29,6
Cycle 3	3,82	10,5
Cycle 4	3,57	6,5
Cycle 5	3,35	6,2
		Total loss % after 5 cycles
		44,8

Tab. 5.6 Load and Unload test on Polyurea + THF + 5 wt % CNT – Tensile Strength and loss %		
	Tensile Strength [MPa]	Loss % per cycle
Cycle 1	4,65	
Cycle 2	3,57	23,17
Cycle 3	3,29	7,84
Cycle 4	3,09	6,18
Cycle 5	2,97	3,72
		Total loss % after 5 cycles
		36,04

5.9 Results and discussion - Scanning Electron Micrograph (SEM) imaging.

Figures 5.22 – 5.23 show SEM images taken at the top surface and at the cross section of the CNT + Polyurea specimens, respectively. The images reveal that when more CNTs are added to the mixture, the surface becomes rougher. Furthermore, the specimen with the 10 wt % of CNT is shown to have lots of cracks all over the surface and CNTs appear at many locations. For all cases, very few CNTs are actually observed, which suggest that the polymer matrix has thoroughly coated the nanoparticles, making strong bonds and increasing the interface Polyurea/CNTs.

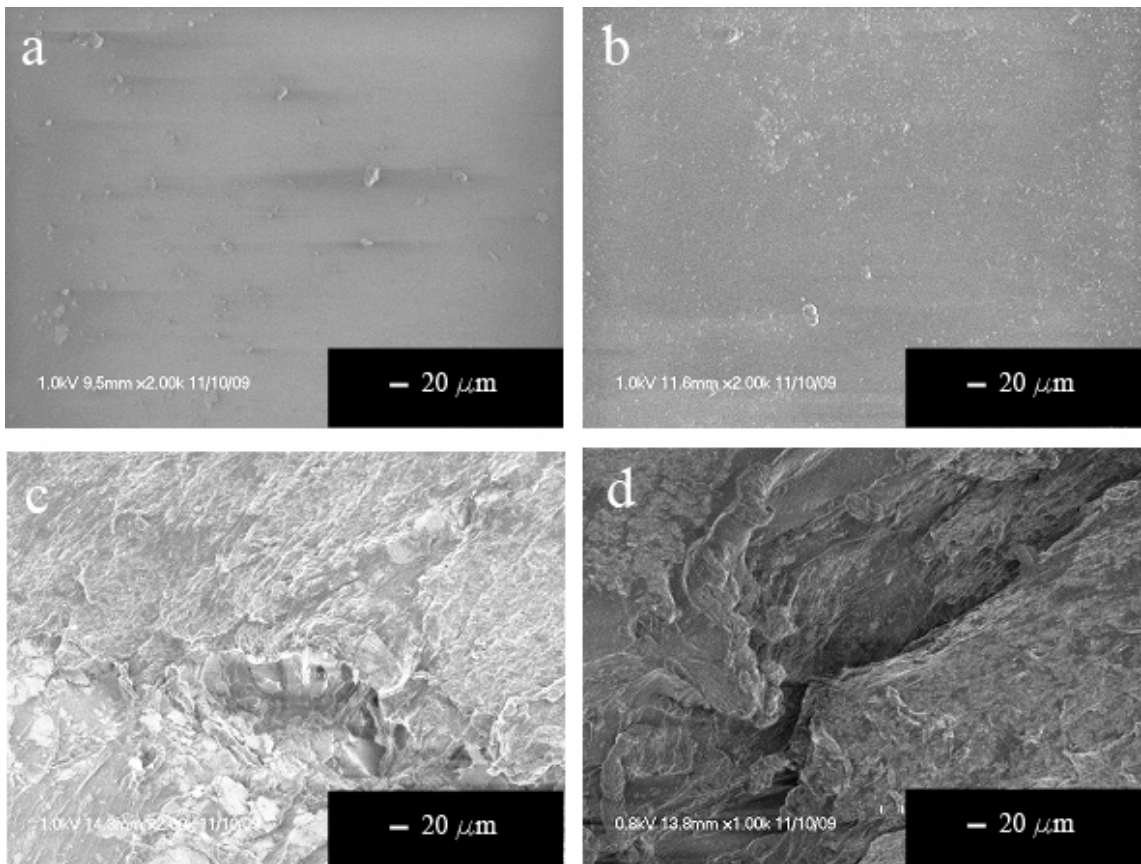
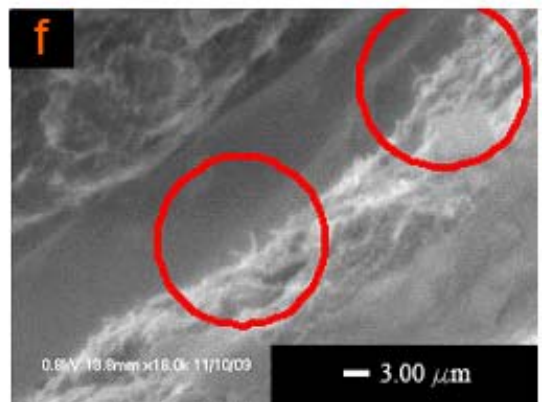
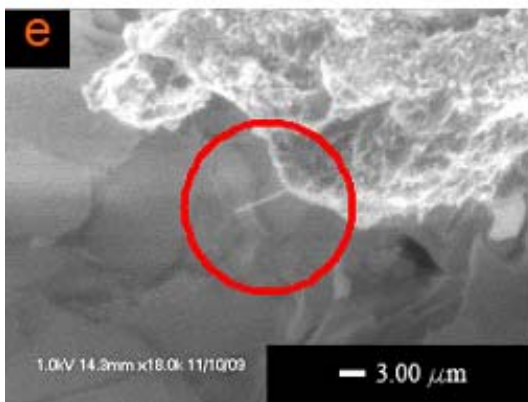
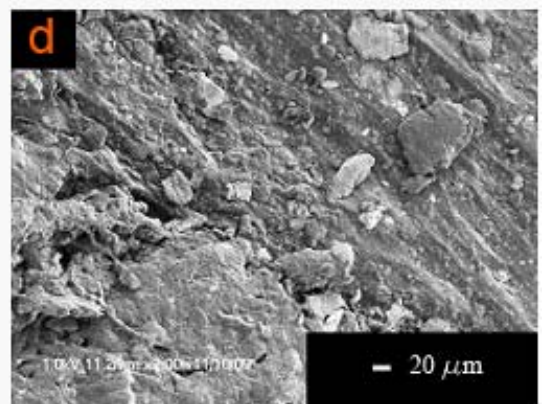
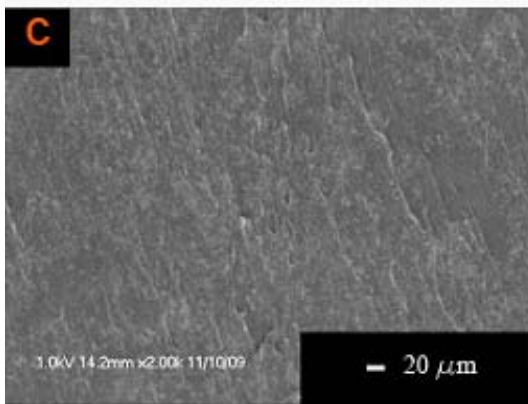
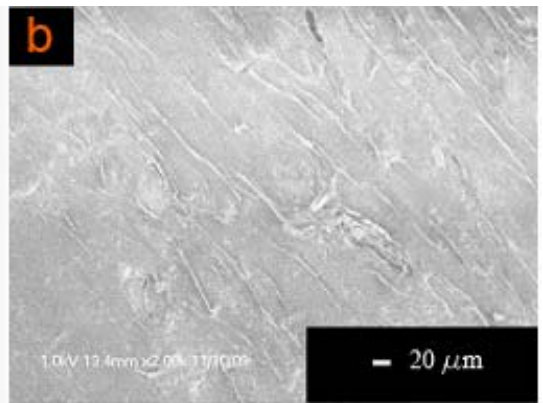
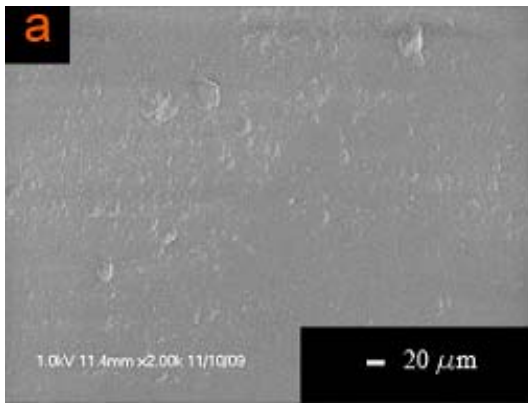


Fig. 5.22 (This page) Secondary electron micrograph (SEM) of the samples top surface. (a) Polyurea + THF + 0% wt CNT; (b) Polyurea + THF + 1% wt CNT; (c) Polyurea + THF + 5% wt CNT; (d) Polyurea + THF + 10% wt CNT.

Fig. 5.23 (Next page) Secondary electron micrograph (SEM) of the samples cross section areas. (a) Polyurea + THF + 0% wt CNT; (b) Polyurea + THF + 1% wt CNT; (c) Polyurea + THF + 5% wt CNT; (d) Polyurea + THF + 10% wt CNT; (e) Free carbon nanotubes in cracks surface in Polyurea + THF + 5% wt CNT; (f) Free carbon nanotubes in cracks surface in Polyurea + THF + 10% wt CNT.



6. DETERIORATION AND ACCELERATED AGING

6.1 Introduction

The service life of new materials in a real application is a very tricky problem, especially in harsh environments where the natural aging could be very fast. However, determining the influence of different factors - such as elevated temperature or presence of acid smog in the atmosphere - on the physical properties of a rubber is quite difficult as the results of the tests may not give an exact correlation with service performance as the real conditions vary widely.

Furthermore, a composite material is formed by two or more different compounds and everyone has got its own mechanical properties and behaviour. In a real environment, a composite may incur in some problems related to this various and often inhomogeneous nature that may cause disaggregation of the different grains.

The only way we have to predict how a material will perform in a real situation is performing tests of accelerated aging. Standard tension tests should be performed on the aged samples and comparison can be made to non-aged samples so that the main properties are measured prior to and after the exposure. Values represent a percentage change in properties.

The procedure of aging investigation is very complicated as it includes chemical and physical aspects as well as mathematical ones.

6.2 Polymer aging

The properties of polymers are not determined only by their composition. Even a simple polymer may have molecules of different lengths and nature. Besides, these molecules may cooperate with each other forming more complex structures. All these lead to a non-reproduction of the material properties. For instance, the same plastic made under different conditions demonstrates completely different properties. Polymers are in a state of thermodynamic non-equilibrium below their glass transition temperature (T_g) and their structure and properties change in the course of time even in absence of external influences. Besides, many polymers are rather sensitive to the external environment. Oxygen, light and high temperature may affect their behaviour in different ways. It's therefore important to stress out that aging does not always involve degrading of the mechanical properties. There are different aging mechanisms which vary a lot depending on the polymer, the aging conditions and the structure (geometry) of the material.

6.3 Accelerated aging testing - Theory

It is well known that the rate of chemical reaction changes depending on the conditions in which the reaction proceeds. More particularly, the temperature dependence of reaction rate constant k is described by the Arrhenius law:

$$k = k_0 \exp\left(-\frac{E}{RT}\right) \quad (\text{eq. 6.1}) \quad \text{where:}$$

k_0 = entropy factor,
 E = activation energy,
 T = temperature (°K),
 R = gas constant.

From this equation, it follows that the process proceeds really faster under increased temperature. In literature, there are similar ideas about the influence of other factors of external environment - such as light, loading, etc. - on the process of aging. Founded on these assumptions, it is possible to design the experiment in which, during a reasonable time, polymer aging reaches deep degrees of transformation. Such technique of testing is called accelerated aging test and is widely used in practice. However, while planning such tests, it is necessary to keep in mind that conditions of experiment should be such that mechanism of accelerated and natural aging are similar. Only under these conditions a useful extrapolation is possible.

The American Society for Testing Materials (ASTM) has established guidelines to contribute to the reliability of materials. Accelerated aging testing is done based on ASTM D 573 - 04 "Standard Test Method for Rubber - Deterioration in an Air Oven" and ASTM D 1349 - 09 "Standard Practice for Rubber - Standard Temperatures for Testing" as rubber and rubber products must resist the deterioration of physical properties with time caused by oxidative and thermal aging.

Testing is performed in air using an oven aging for a specified period at a specified temperature. Standard testing can be performed on the aged samples and comparison can be made to non-aged samples so that the main properties are measured prior to and after high temperature exposure. The values recorded represent a percentage change in properties.

6.4 Aging conditions (New York City temperature)

To simulate the real conditions under which a real CNT doped- polyurea would work, we plot by means of the software Energy Plus[®] the average climate conditions in New York City and, more particularly, in Central Park, JFK and La Guardia airports (NY - USA).

More particularly, under the Köppen climate classification, New York City has a humid subtropical climate and enjoys an average of 234 sunshine days annually. Summers are typically hot and humid with average high temperatures of 79 - 84 °F (26 - 29 °C) and lows of 63 - 69 °F (17 - 21 °C), however temperatures exceed 90 °F (32 °C) on average of 16 - 19 days each summer and can exceed 100 °F (38 °C) every 4-6 years. Winters are cold, and prevailing wind patterns that blow offshore somewhat minimizes the influence of the Atlantic Ocean. Yet, the Atlantic Ocean keeps the city warmer in the winter than inland North American cities located at similar latitudes such as Chicago, Pittsburgh and Cincinnati. New York City receives 1,260 mm of precipitation annually and the average winter snowfall is about 62 cm.

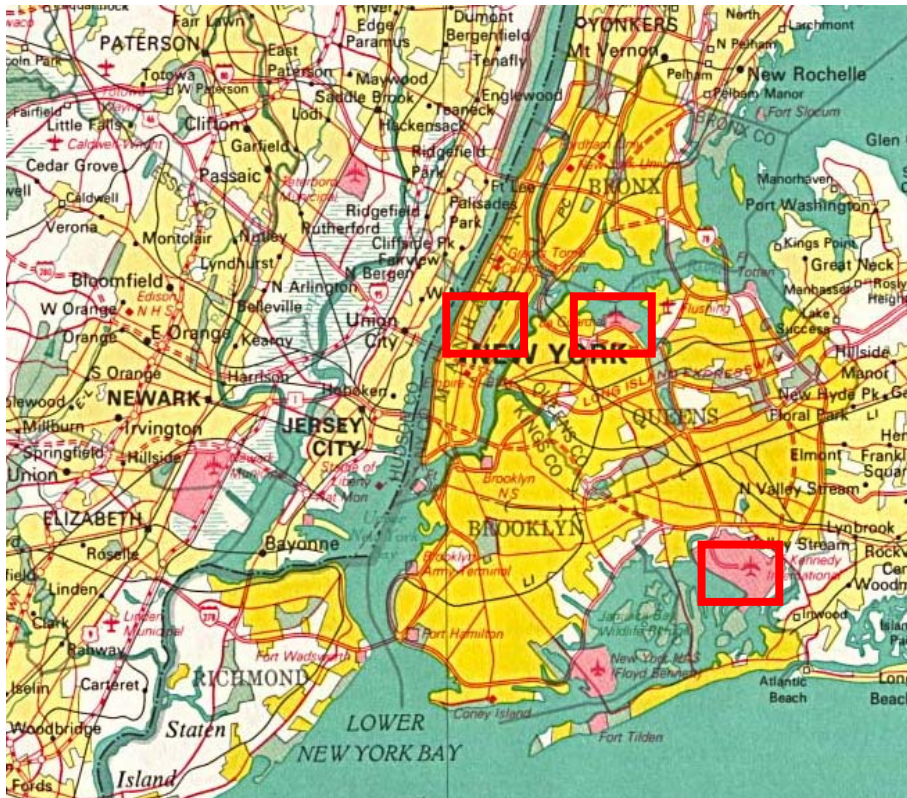


Fig. 6.1 New York City map with the indication of the point of interests.

Tab. 6.1 Average temperature in NYC district

Month	Average temp. [°C] in:			→	Average temp. [°C] NYC
	JFK	La Guardia	Central Park		NYC
January	1,17	1,87	-1,72		- 1,72
February	-0,18	0,05	1,54		1,54
March	5,58	6,84	6,48		6,48
April	10,94	12,72	11,26		11,26
May	16,05	16,44	17,22		17,22
June	21,71	22,21	22,20		22,20
July	25,05	26,52	25,01		25,01
August	24,79	25,04	23,18		23,18
September	19,96	20,34	20,23		20,23
October	14,02	15,39	13,00		13,00
November	7,31	11,17	8,86		8,86
December	3,33	3,64	1,88		1,88

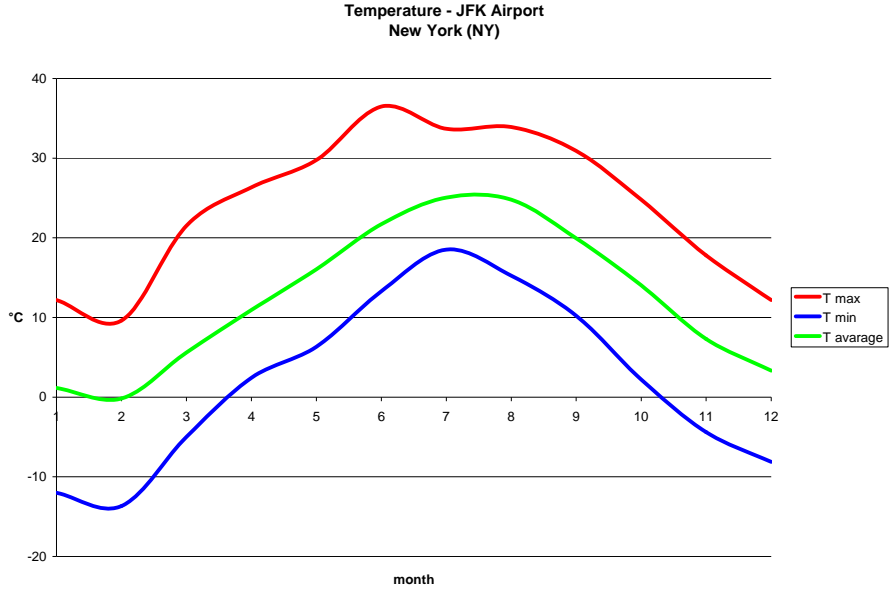


Fig. 6.2
Weather conditions in
JFK Airport, New
York City (NY).

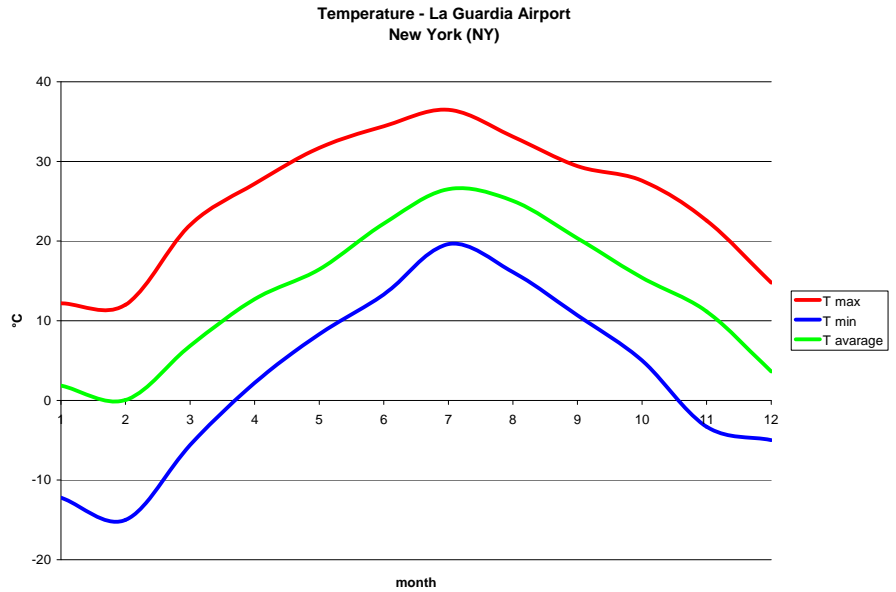


Fig. 6.3
Weather conditions in
La Guardia Airport,
New York City (NY).

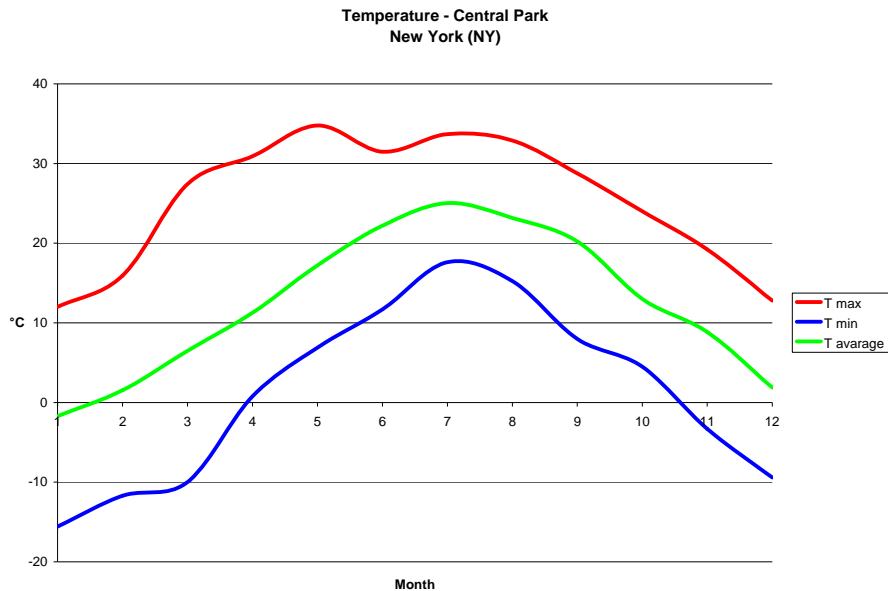


Fig. 6.4 Weather conditions in Central Park, New York City (NY).

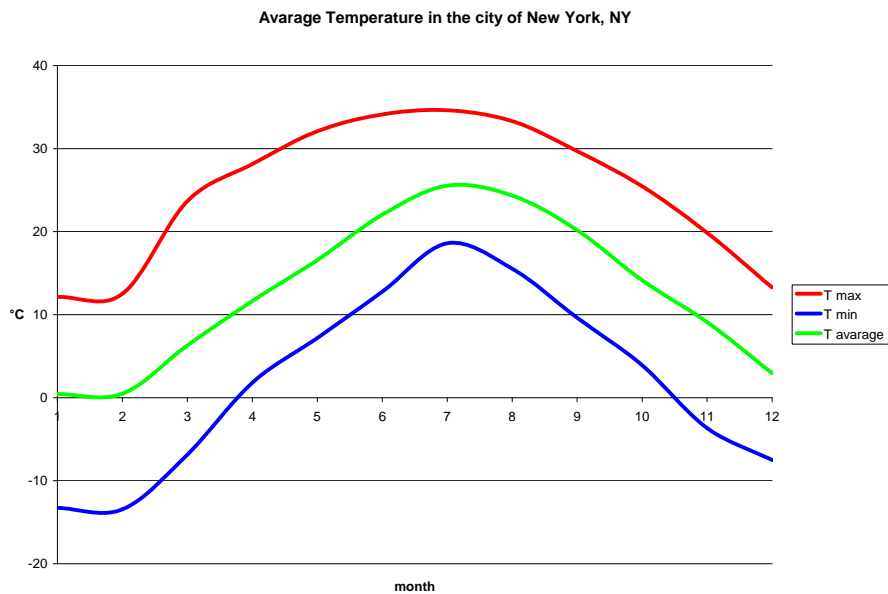


Fig. 6.5 Average weather conditions in New York City (NY).

6.5 Laboratory procedure

Nothing was found in literature about aging polyurea specimens, moreover, the length of time and the testing temperature depends on the specific material analysed. In our case, the temperature chosen to heat the specimens was 140° F (60° C) for different hours cycle duration. Polyurea operating temperature is between -70° to 180° F (-56° to 82° C) and the maximum temperature recorded in New York during a year is 35° C. Furthermore, in some experiments performed on similar materials an aging cycle of about 2 hours is intended to correspond to 12 simulated months.

To perform accelerated aging, the specimens were placed in the oven after it has been heated to the operating temperature. At the termination of each aging interval (2, 4, 6, 12 and 20 hours), they were removed from the oven and cooled down to room temperature on a flat surface.

The tension tests were performed after about 20 hours (the standard ASTM D 573 – 04 prescribes a length of time between 16 and 96 hours to perform the tests after the aging) and data were compared to the unaged samples' results.

6.6 Discussion and Results

We defined 6 different aging intervals (2, 4, 6, 12, 20 and 50 hours). At the end of each interval, some specimens were removed out of the oven and cooled down to room temperature on a flat surface. After approximately 20 hours of cooling off, tension tests were performed and the results were compared to the unaged samples. Figure 6.6 and Figure 6.7 summarize the average ultimate tensile stress and average maximum elongation, respectively.

The points in the figures were obtained by loading the specimens up to their breaking point. The results obtained are interesting and counterintuitive. From Figure 6.6, it is clear that the ultimate stress varies significantly for all models, as aging continues. Furthermore, three general trends can be seen in the figures: the short (0-4 hours), medium (4-20 hours) and long (20-50 hours) time periods.

In the short time period, Polyurea + 1 wt % CNT shows the best performance and all the materials are quickly enhancing their performance. In the medium period, all nanocomposites are starting to age, and their performance deteriorates while the virgin Polyurea keeps performing better. It is also interesting that Polyurea + 1 wt % CNT which gave the best results in the short term, now gives the worst performance. In the long period, the best performance is obtained by the virgin Polyurea. Nonetheless, performance of the nanocomposites are stabilized with slow increase in performance.

From Figure 6.7, similar three trends (time intervals) are observed. The maximum elongation of 1 wt % CNT decreases from about 600 % to 80 % during the initial aging stage. Thereafter, the maximum elongation is stabilized and shows an increase when exposed to long aging. Similar trend is shown for the 5 wt % CNT sample while the 10 wt % does not show significant changes in elongation with aging. Once again, the virgin polyurea with 0 wt % CNT shows the optimal performance. A simple analysis and interpretation of the aging results suggest that while nanotubes are

strong and stiff initially they cause the polyurea to brittle much faster leading to suboptimal results as compared with the pure polyurea.

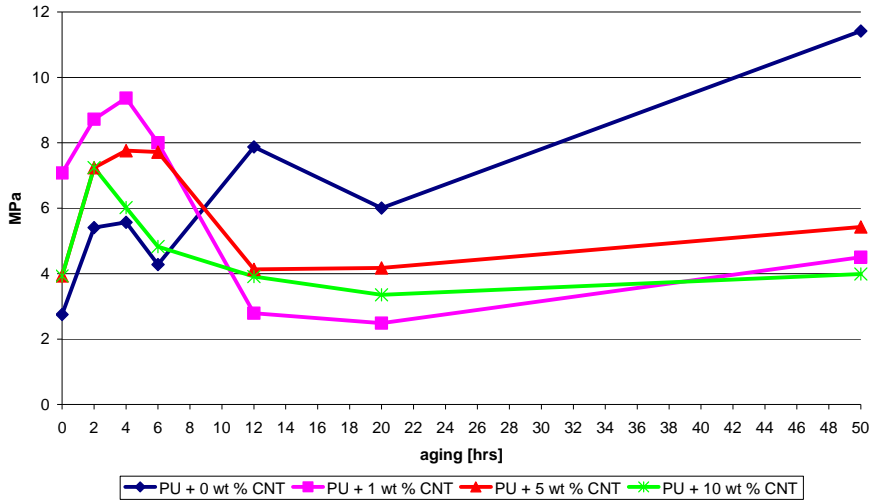


Fig. 6.6
Average ultimate tensile stress of the specimens after extended aging in an air oven.

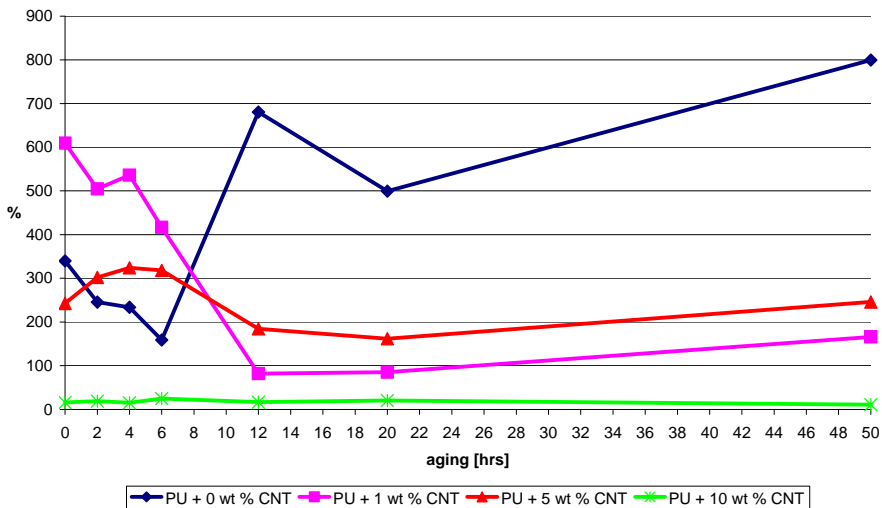


Fig. 6.7
Average maximum elongation of the specimens after extended aging in an air oven.

6.7 Scanning Electron Micrograph (SEM) imaging.

Figures 6.8 – 6.11 show the secondary electron scanning electron microscopy images taken at the cross section of the unaged and aged specimens, respectively. For the 0 % and 1 % CNT specimens, the pictures reveal that there are almost no apparent differences in the matrix structure between the two different states, unaged and aged. However, the SEM images of 5 % and 10 % enriched specimens show that accelerated aging has a huge effect on the structure of the polymer matrix as it looks more compact and smooth.

Fig. 6.8
Secondary electron
micrograph of Poly-
urea + THF + 0 % wt
CNT cross section
area. (left) Unaged;
(right) Aged.

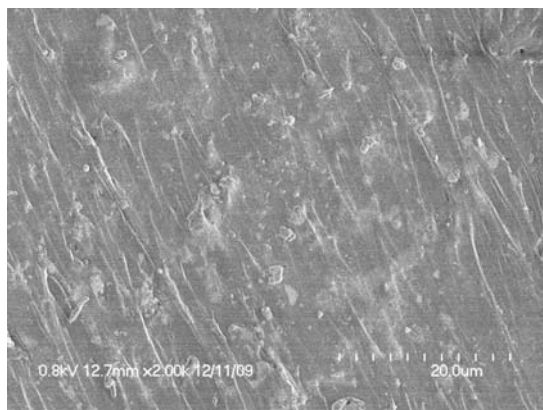
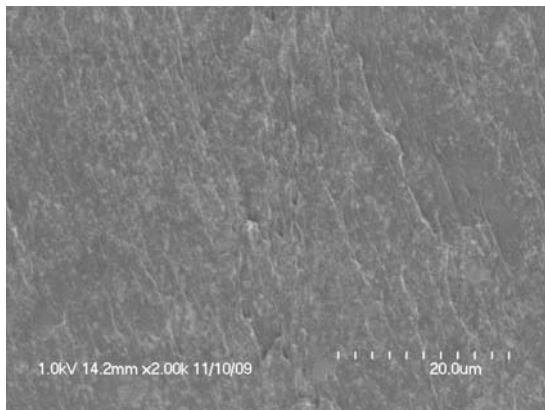
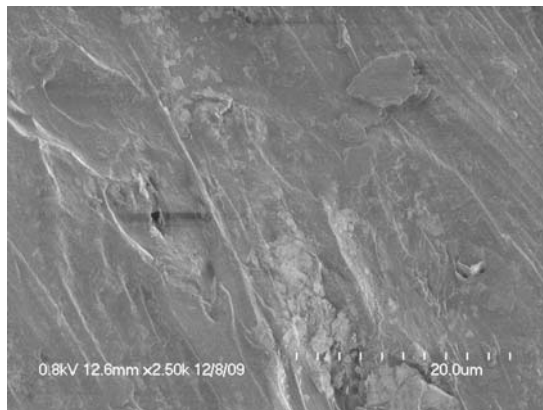
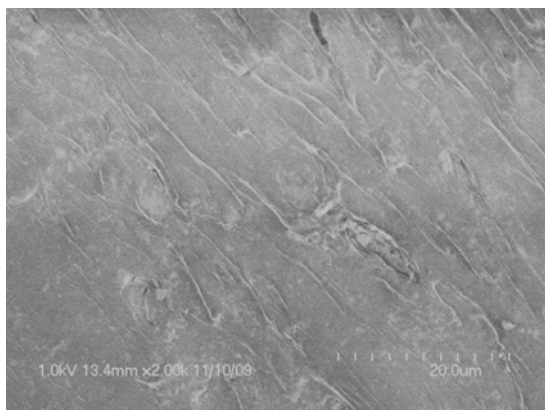


Fig. 6.9
Secondary electron
micrograph of Poly-
urea + THF + 1 % wt
CNT cross section
area. (left) Unaged;
(right) Aged.

Fig. 6.10
Secondary electron micrograph of Polyurea + THF + 5 % wt CNT cross section area. (left) Unaged; (right) Aged.

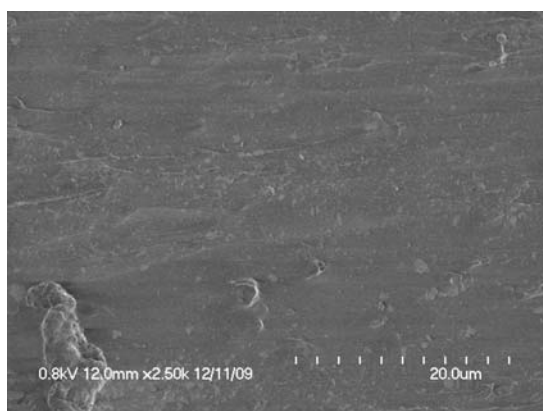
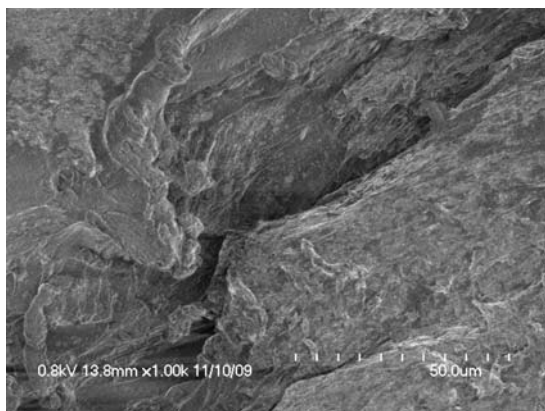
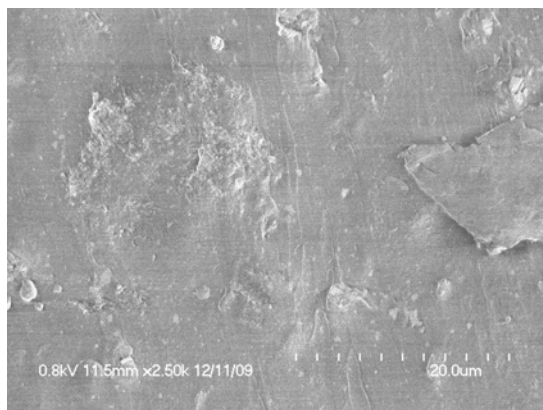


Fig. 6.11
Secondary electron micrograph of Polyurea + THF + 10 % wt CNT cross section area. (left) Unaged; (right) Aged.

REFERENCES

SECTION 1

Chapter 1

- Bhushan B., *Springer handbook of nanotechnology*, Springer, 2007
- Brown L. M., J. S. Rigden, *Most of the good stuff. Memories of Richard Feynman*, New York, 1993
- Cao Guozhong, *Nanostructures & nanomaterials - synthesis, properties & applications*, Imperial College Press, London, 2004
- Drexler K.E., *Engines of creation – the coming era of nanotechnology*, Anchor Books, 1986.
- Drexler K.E., *Engines of creation 2.0 – the coming era of nanotechnology – updated and expanded*, 2006
- Drexler K.E., *Molecular engineering: an approach to the development of general capabilities for molecular manipulation*, Proc. Natl. Acad. Sci. USA 78 (1981), pp. 5275–5278.
- Feynman Richard, *There's Plenty of Room at the Bottom*, Engineering & Science Vol.23, No. 5 (February 1960).
- Gribbin J., Gribbin M., *Richard Feynman: a life in science*, 1994
- Li X, Chang W, Chao Y, Wang R, Chang M., *Nanoscale structural and mechanical characterization of a natural of a natural nanocomposite material: the shell of red abalone*. Nano Lett. 4 (2004), pp. 613–617
- Meyers M., Lim C., Nizam B., Tan E., Seki Y., Mc Kittrick J., *The role of organic intertile layer in abalone nacre*. Material Science Eng. C29 (2009), pp. 2398-2410
- Poole Charles P. Jr., Owens Frank J., *Introduction to nanotechnology*, John Wiley & Sons, Inc., New Jersey, 2004
- Sitti M., Fearin R.S., *Synthetic Gecko Foot-Hair Micro/Nano-Structures for Future Wall-Climbing Robots*, University of California at Berkeley, USA
- <http://users.physik.fu-berlin.de/~kleinert/feynman/feynmanpub.htm>
- http://www.100interior.de/index_en.htm
- <http://www.architectmagazine.com/industry-news.asp?sectionID=1006&articleID=492836&artnum=1> (accessed 19-08-09)
- <http://www.azonano.com/>
- <http://www.caltech.edu/>
- <http://www.cordis.lu/nanotechnology>
- <http://www.e-drexler.com>
- <http://www.feynman.com>
- <http://www.feynmanlectures.info/>

- <http://www.inm-gmbh.de/en/news/press/>
- <http://www.nanofab.it/it/>
- <http://www.nanorobotdesign.com>
- <http://www.nature.com/>
- http://www.nobel-winners.com/Physics/richard_phillips_feynman.html
- <http://www.sciencedaily.com/>
- <http://www.solgel.com/>
- <http://www-groups.dcs.st-and.ac.uk/~history/Mathematicians/Feynman.html>

Chapter 2

- Barroso José Manuel, *Political guidelines for the next commission*, Brussels, 2009
- European Commission - *Communication from the commission to the council, the European parliament and the European economic and social committee: Nanosciences and Nanotechnologies: An action plan for Europe 2005-2009. First Implementation Report 2005-2007*, Brussels, 2007
- European Commission, *Communication from the commission to the council, the european parliament and the European economic and social committee: Nanosciences and Nanotechnologies: An action plan for Europe 2005-2009. Second Implementation Report 2007-2009*, Brussels, 2009
- European Commission, Directorate-General for Research - *Communication from the commission: Towards a European Strategy for Nanotechnology*, Belgium, 2004
- European Commission, Directorate-General for Research – *Communication: Nanosciences and nanotechnologies: An action plan for Europe 2005-2009*, Belgium, 2005
- European Commission, Directorate-General for Research – *Communication from the Commission COM (2004) 338: Towards a European Strategy for Nanotechnology*, Brussels, 2004
- European Commission, Directorate-General for Research - *EuroNanoForum 2003, European and International Forum on Nanotechnology*, Trieste, 9-12 December 2003
- European Commission, Directorate-General for Research - *EuroNanoForum 2005, Nanotechnology and the health of EU citizen in 2020*, Edimburgh, 5-9 September 2005
- European Commission, Directorate-General for Research - *EuroNanoForum 2007, Nanotechnology in Industrial Applications European and International Forum on Nanotechnology*, Düsseldorf, 19-21 June 2007
- European Commission, Directorate-General for Research - *EuroNanoForum 2009 Nanotechnology for Sustainable Economy European and International Forum on Nanotechnology*, Prague, 2-5 June 2009

- European Commission, *Looking small, thinking big – keeping Europe at the forefront of nanotechnology*, Brussels, 2005
- National Science and Technology Council – Committee on Technology – Subcommittee on Nanoscale Science, Engineering and Technology, *The National Nanotechnology Initiative, Supplement to the President's 2010 budget*, USA, May 2009
- National Science and Technology Council – Committee on Technology – Subcommittee on Nanoscale Science, Engineering and Technology, *The National Nanotechnology Initiative, Strategic Plan*, USA, December 2007
- National Science and Technology Council – Committee on Technology – Subcommittee on Nanoscale Science, Engineering and Technology, *Nanotechnology and Environment Report of a national nanotechnology initiative workshop*, USA, May 2003
- European Commission - *Commission recommendation of 07/02/2008 on a code of conduct for responsible nanosciences and nanotechnologies research*, Brussels, 2008
- <http://cordis.europa.eu/nanotechnology>
- <http://ec.europa.eu/environment> (accessed 6-07-10)
- <http://www.nano.gov/>
- <http://www.rparts.com/> (accessed 6-07-10)

Chapter 3

- Fouad El-Samny, *NanoArchitecture – Nanotechnology and Architecture*, Thesis of Master of science in Architecture, Department of Architecture, Faculty of Engineering, University of Alexandria (Egypt), October 2008
- Johansen John, *Nanoarchitecture: a new species of architecture*, M. Princeton Architectural Press, New York, 2002
- <http://www.metropolismag.com/story/20030201/carbon-fiber-future> (accessed 29-03-10)
- http://archrecord.construction.com/innovation/2_features/0310carbonfiber.asp (accessed 29-03-10)
- <http://span.vox.com/library/post/a-conversation-with-peter-testa.html> (accessed 29-03-10)
- <http://yatin.wikidot.com/nanotechnology-in-architecture> (accessed 29-03-10)
- <http://dsc.discovery.com/convergence/engineering/pyramidcity/interactive/interactive.html> (accessed 8-04-10)
- http://www.absoluteastronomy.com/topics/Shimizu_Mega-City_Pyramid (accessed 8-4-10)
- <http://heritage-key.com/blogs/ann/shimizu-project-giant-modern-day-pyramid-living> (accessed 8-04-10)
- <http://www.nano.uts.edu.au/about/australia.html> (accessed 23-03-10)

- <http://www.hindu.com/2007/10/18/stories/2007101853840400.htm> (accessed 26-04-10)
- http://www.consulenzaimmobiliare.org/wp-content/uploads/2008/07/shimizu_mega_city_pyramid03.jpg (accessed 8-04-10)
- <http://www.sfgate.com/cgi-bin/article.cgi?f=/c/a/2008/08/10/MN9S120S1G.DTL> (accessed 26-04-10)
- <http://www.nanohouse.nl> (accessed 24-03-10)
- <http://daheadley.iweb.bsu.edu/NanoStudio2> (accessed 24-03-10)
- <http://www.peter-testa.com> (accessed 29-03-10)
- <http://www.l-a-v-a.net> (accessed 7-04-10)
- <http://www.mswct.com> (accessed 7-04-10)
- <http://www.binisystems.com> (accessed 8-04-10)
- <http://www.shimz.co.jp/english/index.html> (8-04-10)
- <http://www.nanocity.in> (accessed 26-04-10)

Chapter 4

- Bartos P. J. M., Hughes J.J., Trtik P., Zhu W., *Nanotechnology in construction*, The Royal Society of Chemistry, Cambridge, 2004
- Campillo I. et al., *High-performance nanostructured materials for construction* in Proceedings of the 1st International Symposium on Nanotechnology in Construction, June 2003, University of Paisley, Scotland (UK), pgg 215-225
- Davies S.R., *How we talk when we talk about nano: The future in lay-people's talk*, Futures (2010) article in press, doi:10.1016/j.futures.2010.07.003
- Miyazaki K., Islam N., *Nanotechnology systems of innovation—An analysis of industry and academia research activities*, Technovation 27 (2007), pp. 661–675
- Nikulainen T., Palmberg C., *Transferring science-based technologies to industry—Does nanotechnology make a difference?*, Technovation 30 (2010), pp. 3–11
- Pacheco-Torgal F., Jalali S., *Nanotechnology: Advantages and drawbacks in the field of construction and building materials*, Construction and Building Materials (2010) article in press, doi:10.1016/j.conbuildmat.2010.07.009
- Rebolj D., Fischer M., Endy D., Moore T., Šorgo A., *Can we grow buildings? Concepts and requirements for automated nano- to meter-scale building*, Advanced Engineering Informatics (2010) article in press, doi:10.1016/j.aei.2010.08.006
- Yeadon Peter, *Smarticles: nanotechnology materializes*, ab Architecture Boston, July-August 2008

- Zhu W. et al., *Application of nanotechnology in construction – current status and future potential* in Proceedings of the 1st International Symposium on Nanotechnology in Construction, June 2003, University of Paisley, Scotland (UK), pgg 31-45
- <http://en.percenta.com/>
- <http://www.building.co.uk/>
- <http://www.kaelintaefer.ch/>
- <http://www.labein.es/labeinWeb/home.nsf/fwhome?openform>
- <http://www.nanosysinc.com>
- <http://www.slideshare.net/Colloquium/nanotechnology-in-civil-engineering>

Chapter 5 (Thin films for architectural glazing)

– Solar protection coatings

- Leydecker S., *Nanomaterials in architecture, interior architecture and design*, Birkhäuser Verlag AG, Germany, 2008, pp. 144-145
- <http://gizmodo.com/190931/electrochromic-glass-instant-darkening> (accessed 9-07-10)
- <http://www.julbousa.com/performance/race> (accessed 9-07-10)

– IR protection coatings

- Leydecker S., *Nanomaterials in architecture, interior architecture and design*, Birkhäuser Verlag AG, Germany, 2008

– UV protection coatings

- ISO 21348:2004 “Definitions of solar irradiance spectral categories”
- Leydecker S., *Nanomaterials in architecture, interior architecture and design*, Birkhäuser Verlag AG, Germany, 2008, pp. 142-143

– Anti-fogging coatings

- Leydecker S., *Nanomaterials in architecture, interior architecture and design*, Birkhäuser Verlag AG, Germany, 2008, pp. 118-119
- US Patent n° 5804612 – 8 September 1998
- http://www.anti-fog-coating.com/anti_fog_coatings.asp (accessed 23-06-10)
- <http://www.filmspecialities.com> (accessed 23-06-10)
- <http://www.nanotechweb.org/cws/article/tech/23086> (accessed 23-06-10)
- <http://www.nanowerk.com/news/newsid=1157.php> (accessed 28-07-09)
- <http://www.newscientist.com/article/dn7921-antifog-glasscoating-has-clear-applications.html> (accessed 23-06-10)

- <http://www.scientificamerican.com/article.cfm?id=multilayer-technology-antifogging> (accessed 23-06-10)
- <http://www.web.mit.edu/cohengroup/index.html> (accessed 23-06-10)
- <http://www.web.mit.edu/dmse/rubner> (accessed 23-06-10)

– Anti-reflective coatings

- Leydecker S., *Nanomaterials in architecture, interior architecture and design*, Birkhäuser Verlag AG, Germany, 2008, pp. 160-161
- Miller F., *Nanostructured surfaces*, Fraunhofer Magazine – Special Issue, 2 (2005), pp. 8-12
- Päivänranta B., Saastamoinen T., Kuittinen M., *A wide-angle antireflection surface for the visible spectrum*, Nanotechnology 20(2009), doi:10.1088/0957-4484/20/37/375301
- <http://nanotechweb.org/cws/article/tech/40867> (accessed 06-10-10)
- <http://www.azonano.com/news.asp?newsID=5204> (accessed 06-10-10)
- http://www.bowmanconstructionsupply.com/architectural_schott.htm (accessed 06-10-10)
- <http://www.foresight.org/nanodot/?p=2880> (accessed 06-10-10)
- <http://www.fraunhofer.de/en/index.jsp> (accessed 06-10-2010)
- <http://www.reflexite.com/> (accessed 06-10-10)

– Anti-fingerprints coatings

- Block S. et al., *New anti-fingerprint coatings*, Dow Corning Corporation, 2008
- Leydecker S., *Nanomaterials in architecture, interior architecture and design*, Birkhäuser Verlag AG, Germany, 2008, pp. 172-175
- <http://www.nanomatetech.com/NanoMate-Product-NanoSolution-Feature.html>
- <http://www.infolink.com.au/c/Nanokote/Nanokote-Anti-Fingerprint-coating-for-glass-n843872> (accessed 11-10-10)
- <http://www.specialchem4coatings.com/resources/articles/article.aspx?id=10300>
- <http://www.freshpatents.com/Anti-fingerprint-coating-construction-dt20060525ptan20060110537.php> (accessed 11-10-10)
- <http://www.nanogate.de/en/product-enhancement/functions/nanotension/anti-fingerprint.php> (accessed 11-10-10)
(accessed 11-10-10)
- <http://www.dowcorning.com/default.aspx?bhcp=1> (accessed 11-10-10)
(accessed 11-10-10)

– Scratchproof and abrasion resistant coatings

- Leydecker S., *Nanomaterials in architecture, interior architecture and design*, Birkhäuser Verlag AG, Germany, 2008, pp. 176-177
- Nogarole Marco, *Nanocomposite for abrasion-resistant finishes*, *Tecnologie conciarie* 218 (2008), pp. 90-100

Chapter 6 (Cement based materials)

- Brouwers H.J.H., *The role of nanotechnology for the development of sustainable concrete*. Proceedings of ACI session on “Nanotechnology of concrete: recent developments and future perspectives”, 7 November 2006, Denver (USA).
- Byung-Wan J., Chang-Hyun K., Ghi-Ho T., Jong-Bin P.. *Characteristics of cement mortar with nano-SiO₂ particles*. *Construction and Building materials*, 21:2007.
- Chen J., Poon C.. *Photocatalytic construction and building materials: from fundamentals to applications*. *Building and Environment* 44:2009.
- Féret R., *Sur la compacité des mortiers hydrauliques*, *Ann. Ponts Chaussée, mémoires et documents, Série 7, No. IV, 1892*, pp. 5-164
- Italcementi Group. *TX Active®: presentation of the first active solution to the problem of pollution*, Milano (Italy) 2006.
- Maile A. *The chemistry and physics of nano-cement*. Thesis submitted to University of Delaware (USA), 2006.
- Mehta P., Ranka A.. *Nanotechnology in water proofing of building materials (long life, economical & eco-friendly)*.
- Perera Y., Cano J., Martinez S., Quercia G., Blanco A., *Characterization of nano-cement phases by Field Emission Scanning Electron Microscopy (FESEM)*, *Acta microscopica*, Vol. 16 n. 1-2, 2007.
- Rouainia G., Djeghaba K., *Evaluation of Young’s modulus of single walled carbon nanotube (SWNT) reinforced concrete composite*. *Journal of Engineering and Applied Sciences*, 3 (6): 2008.
- Shah S. P., *Application of nanotechnology in concrete*. Seminar at Columbia University, Department of Civil Engineering and Engineering Mechanics, October 2008.
- Shah S. P., *Application of nanotechnology to concrete*. Seminar at The Hong Kong Polytechnic University, Department of Civil and Structural Engineering, October 2008.
- Sobolev K., Gutiérrez M.F., *How nanotechnology can change the Concrete world*. *American Ceramic Society Bulletin*, Vol. 84, n 11, 2005.
- Taylor P., Rajan K., Birgisson B., Cackler T.. *Report of the Workshop on Nanotechnology for Cement and Concrete*, sponsored by The National Concrete Pavement Technology Center and The National Science Foundation, 5 September 2007, Arlington (VA).

- Yakovlev G., Kerienè J., Gailius A., Girnienè I., *Cement based foam concrete reinforced by carbon nanotubes*, Materials Science Vol. 12, n. 2, 2006, pp.147-151.

Chapter 7 (Steel-based materials)

- Alves V.A., Chiorcea Paquim A.M., Cavaleiro A., Brett C.M.A., *The nanostructure and microstructure of steels: Electrochemical Tafel behaviour and atomic force microscopy*, Corrosion Science 47 (2005), pp.2871–2882
- Suh C.M., Song G.H., Suh M.S., Pyoun Y.S., *Fatigue and mechanical characteristics of nano-structured tool steel by ultrasonic cold forging technology*, Materials Science and Engineering A 443 (2007), pp.101–106
- US Patent n° US20100101686 A1 – 29 April 2010
- Xu Y.H., Peng J.H., Fang L., *Nano-crystallization of steel wire and its wear behaviour*, Materials Science and Engineering A 483–484 (2008), pp.688–691
- <http://www.almatis.com/refractory/global-steel-production.aspx> (accessed 09-11-10)
- <http://nextbigfuture.com/2008/01/nanotechnology-enhanced-steel-and.html>
- <http://davidkirkpatrick.wordpress.com/2008/10/20/nanotech-making-steel-even-stronger/> (accessed 04-11-10)
- <http://www.nanovations.com.au/metal.htm> (accessed 04-11-10)
- <http://www.worldsteel.org> (accessed 09-11-10)
- <http://www.azonano.com/details.asp?ArticleID=338> (accessed 04-11-10)
- <http://www.nanowerk.com/spotlight/spotid=2827.php> (accessed 04-11-10)

Chapter 8 (Wood-based materials)

- Cristea M.V., Riedl B., Blanchet P., *Enhancing the performance of exterior waterborne coatings for wood by inorganic nanosized UV absorbers*, Progress in Organic Coatings 69 (2010), pp. 432–441
- Dányádi L., Móczó J., Pukánszky B., *Effect of various surface modifications of wood flour on the properties of PP/wood composites*, Composites: Part A 41 (2010), pp. 199–206
- Kopač J., Šali S., *Wood: an important material in manufacturing technology*, Journal of Materials Processing Technology 133 (2003), pp. 134-142
- Landry V., Blanchet P., Riedl B., *Mechanical and optical properties of clay-based nanocomposites coatings for wood flooring*, Progress in Organic Coatings 67 (2010), pp.381–388
- Landry V., Riedl B., Blanchet P., *Alumina and zirconia acrylate nanocomposites coatings for wood flooring: Photocalorimetric characterization*, Progress in Organic Coatings 61 (2008), pp. 76–82

- Lin Z., Rennecker S., *Nanocomposite-based lignocellulosic fibers 2: Layer-by-layer modification of wood fibers for reinforcement in thermoplastic composites*, Composites: Part A (2010) article in press. doi:10.1016/j.compositesa.2010.10.011
- Lua Z., Eadula S., Zheng Z., Xua K., Grozdits G., Lvov Y., *Layer-by-layer nanoparticle coatings on lignocellulose wood microfibers*, Colloids and Surfaces A: Physicochem. Eng. Aspects 292 (2007), pp. 56–62
- Shafizadeh, F., *The chemistry of pyrolysis and combustion*, in: Rowell, R. (Ed.), *The Chemistry of Solid Wood*. American Chemical Society, Washington, D.C., 1984, pp. 489–529.
- Xie X., Goodell B., Daniel G., Qian Y., Jellison J., Peterson M., *Carbonization of wood and nanostructures formed from the cell wall*, International Biodeterioration & Biodegradation 63 (2009), pp. 933–935
- <http://www.federica.unina.it/architettura/laboratorio-di-restauro/strutture-lignee-edifici-storici/> (accessed 09-11-10)
- <http://www.woodworks.org/publicationsResources/Presentations.aspx> (accessed 15-11-10)

Chapter 9 (Quality and comfort)

– Self-cleaning coatings

- Jones Anthony C., Hitchman Michael L., *Chemical Vapour Deposition – Precursors, processes and applications*, Royal Society of Chemistry, 2009. ISBN: 978-0-85404-465-8.
- Leydecker S., *Nanomaterials in architecture, interior architecture and design*, Birkhäuser Verlag AG, Germany, 2008, pp. 58-91
- Mills A., Le Hunte S., *An overview of semiconductor photocatalysis*, Journal of photochemistry and photobiology, A: Chemistry 108 (1997), pp. 1-35
- Parkin I. P., Palgrave R. G., *Self-cleaning coatings*, Journal of Material Chemistry, 15:2005, ppg.1689-1695
- <http://biodsign.wordpress.com/2008/08/27/lotus-effect-efecto-lotus/>
- <http://www.advancedphysics.org/forum/showthread.php?t=1546>
- <http://www.arapacis.it>
- <http://www.cardinalcorp.com>
- <http://www.corporateportal.ppg.com>
- <http://www.flickr.com/photos/40094136@N00/339733266/>
- <http://www.italcementi.it>
- <http://www.italcementigroup.com>
- http://www.kaelintaefer.ch/global/prod_nanotech.html
- <http://www.lotusan.de>
- http://www.paintpro.net/Articles/PP804/PP804-Product_Profile.cfm

- <http://www.pilkington.com>
 - <http://www.ramehart.com/contactangle.htm>
 - <http://www.saint-gobain.com>
 - <http://www.selfcleaningglass.com>
 - <http://www.sto.com>
 - <http://www.stocorp.com/allweb.nsf/lotusanpage>
 - <http://www.toto.co.jp/en/>
 - www.kaldewei.com
- **Easy-to-clean coatings**
- CD Nano, L'innovation du 21^{ème} siècle, catalogue.
 - Leydecker S., *Nanomaterials in architecture, interior architecture and design*, Birkhäuser Verlag AG, Germany, 2008, pp. 92-107
 - <http://www.aerosil.com/product/aerosil/en/Pages/default.aspx>
 - <http://www.teg.fraunhofer.de/en>
 - http://www.rsnano.com.my/?page_id=56 (accessed 28-07-09)
- **Air-purifying materials**
- Bayer, *The world's tiniest perfume bottles*, Bayer Research 15.
 - Leydecker S., *Nanomaterials in architecture, interior architecture and design*, Birkhäuser Verlag AG, Germany, 2008, pp. 108-117, 120-121
 - <http://www.bio-medicine.org/biology-news-1/Air-purifying-church-windows-early-nanotechnology-4562-1> (accessed 28-07-09)
 - <http://www.deccanherald.com/Content/Jan62008/national2008010645193.asp?section=updatenews>
 - <http://www.freepatentsonline.com/4952400.html> (accessed 21-06-10)
 - http://www.research.bayer.com/edition_15/15_microcapsules.pdf (accessed 21-06-10)
- **Anti-bacterial materials**
- Kandelbauer A., Widsten P., *Antibacterial melamine resin surfaces for wood-based furniture and flooring*, Progress in Organic Coatings 65 (2009), pp. 305–313
 - Leydecker S., *Nanomaterials in architecture, interior architecture and design*, Birkhäuser Verlag AG, Germany, 2008, pp. 162-171
 - Wu Y. et al., *Multi-action antibacterial nanofibrous membranes fabricated by electrospinning: an excellent system for antibacterial applications*, Nanotechnology 20(2009), doi:10.1088/0957-4484/20/24/245101
 - <http://www.nanoprotect.co.uk/>
 - <http://www.silvernanoparticles.info/Silver-Nanoparticles-Antibacterial-Properties.html> (accessed 07-10-10)

- <http://www.nanowerk.com/spotlight/spotid=10951.php> (accessed 07-10-10)

– Anti-graffiti coatings

- Leydecker S., *Nanomaterials in architecture, interior architecture and design*, Birkhäuser Verlag AG, Germany, 2008, pp. 152-159
- <http://ita.archinform.net/projekte/10262.htm> (accessed 05-10-10)
- <http://www.ethicalcoatings.org.uk/> (accessed 05-10-10)
- http://www.nanokote.com.au/anti_graffiti.html (accessed 05-10-10)
- <http://www.nanoprotect.co.uk/anti-graffiti-system.html> (accessed 05-10-10)

– Fire-protection and detection

- Leydecker S., *Nanomaterials in architecture, interior architecture and design*, Birkhäuser Verlag AG, Germany, 2008, pp. 146-151 (accessed 29-09-10)
- U.S. Patent 7647957, 19 January 2010
- <http://bamboopanama.com/fire-retardant-bamboo-patent-using-nanotechnology>
- <http://nanopatentsandinnovations.blogspot.com/2010/01/bamboo-nanotechnology-total-green.html> (accessed 29-09-10)
- <http://news.softpedia.com/news/Nanotechnology-Creates-Fireproof-Paint-61208.shtml> (accessed 21-09-10)
- <http://news.softpedia.com/news/Nanotechnology-Creates-Fireproof-Paint-61208.shtml> (accessed 28-09-10)
- <http://waverleygate.co.uk> (accessed 28-09-10)
- http://www.associatedcontent.com/article/2689213/nanotechnology_bambo_o_virtually_fireproof.html (accessed 29-09-10)
- <http://www.csiro.au/science/Geopolymers-Overview.html> (accessed 28-09-10)
- <http://www.gizmag.com/hips-fire-proof-coating/12090/> (accessed 28-09-10)
- <http://www.glassonweb.com/directory/details.php?id=2643> (accessed 27-09-10)
- <http://www.interver.ch> (accessed 27-09-10)
- <http://www.nano.org.uk/news/356/> (accessed 29-09-10)
- <http://www.physorg.com/news167306601.html> (accessed 28-09-10)
- http://www.thaindian.com/newsportal/health/new-fireproof-coatings-can-withstand-temperatures-of-over-1000-degrees-celsius_100220907.html (accessed 28-09-10)
- http://www.vetrotech.com/cp/eng/CONTRA_504.asp (accessed 28-09-10)

– **Anti-icing materials**

- Cao L. et al., Anti-Icing *Superhydrophobic Coatings*, *Langmuir* 2009, 25(21) pp.12444–12448.
- <http://www.gizmag.com/anti-ice-coating/13231/> (accessed 30-09-10)

Chapter 10 (Energy control and saving)

– **Phase-changing materials**

- Cabeza L.F. et al., *Use of microencapsulated PCM in concrete walls for energy savings*, *Energy and Buildings*, 39 (2007), pp. 113-119
- Castell A. et al., *Experimental study of using PCM in brick constructive solutions for passive cooling*, *Energy and Buildings*, 42 (2010), pp. 534–540
- Castellón C. et al., *Use of microencapsulated phase change materials in building applications*, in *Proceedings of Thermal Performance of the Exterior Envelopes of Whole Buildings X International Conference*, December 2007, Florida
- Hawes D. W. et al., *Latent heat storage in building materials*, *Energy and Buildings*, 20-1 (1993), pp. 77-86
- Khudhair A.M., Farid M.M., *A review on energy conservation in building applications with thermal storage by latent heat using phase change materials*, *Energy Conversion and Management* 45 (2004), pp. 263-275
- Leydecker S., *Nanomaterials in architecture, interior architecture and design*, Birkhäuser Verlag AG, Germany, 2008, pp. 136-141
- US Patent n° 5755216 – 26 May 1998
- Zhang Y. et al., *Application of latent heat thermal energy storage in buildings: state-of-the-art and outlook*, *Building and Environment*, 42 (2007), pp. 2197–2209
- <http://www.ecnmag.com/Blogs/ECN-Blog/Wozniak-s-New-Goal-is-Efficient-Housing> (accessed 22-06-10)
- <http://www.nationalgypsum.com/about/news/2009/news137.aspx> (accessed 22-06-10)
- <http://www.greenbuildingadvisor.com/blogs/dept/energy-solutions/storing-heat-walls-phase-change-materials> (accessed 23-06-10)
- <http://www.barackobamavideos.net/infinite-r-wmv> (accessed 21-06-10)
- <http://www.basf.com/group/pressrelease/P-05-369> (accessed 22-06-10)
- <http://www.freepatentsonline.com/5755216.html> (accessed 21-06-10)
- <http://www.thermalcore.info> (accessed 22-06-10)
- <http://www.pcmenergy.com> (accessed 23-06-10)
- <http://www.entropysolutionsinc.com> (accessed 23-06-10)
- <http://www.goodfellow.com> (accessed 23-06-10)
- <http://www.futurepundit.com/archives/006926.html> (accessed 21-06-10)

– Vacuum-insulation panels

- Caps Roland, *Vacuum Insulation Panels for Buildings and Technical Applications*
- Leydecker S., *Nanomaterials in architecture, interior architecture and design*, Birkhäuser Verlag AG, Germany, 2008, pp. 122-127
- Mukhopadhyaya Phalguni, *High Performance Vacuum Insulation Panel – Research Update from Canada*, Global Insulation Magazine, Oct.2006, pp. 9-15.
- Pool M., *Insulation of a mixed use building with 7 storeys in Munich with VIP*. Pool Architekten
- <http://www.enob.info/en/new-technologies/projects/details/precast-concrete-units-with-vacuum-insulation> (accessed 6-07-10)
- <http://www.toolbase.org/Technology-Inventory/Interior-Partitions-Ceilings/vacuum-insulation-panel> (accessed 6-07-10)

– Aerogel

- At:Length, *Introducing nanogel*.
- Leydecker S., *Nanomaterials in architecture, interior architecture and design*, Birkhäuser Verlag AG, Germany, 2008, pp. 128-134
- <http://www.cabot-corp.com/aerogel> (accessed 8-07-10)
- <http://www.milwaukeezo.org> (accessed 8-07-10)
- <http://www.kalwall.com/rcntproj/40.htm> (accessed 8-07-10)

– Photovoltaic

- Ertex Solar, Laminated safety glass modules
- ISO 21348:2004 “*Definitions of solar irradiance spectral categories*”
- John Perlin, *From space to earth, the story of solar electricity*, 2002, Harvard University Press
- John Perlin, *The silicon solar cell turns 50*, 3rd World Conference on PV Energy Conversion, Osaka, Japan May 11 – 16 2003
- US Patent n° 7647957 – 19 January 2010
- <http://inventors.about.com/od/timelines/a/Photovoltaics.htm> (accessed 15-06-10)
- <http://link.aps.org/doi/10.1103/PhysRev.96.1708> (accessed 16-06-10)
- http://photochemistry.epfl.ch/EDEY/PV_history.pdf (accessed 16-06-10)
- http://sunearth.gsfc.nasa.gov/sunearthday/media_viewer/flash.html (accessed 9-07-10)
- http://techon.nikkeibp.co.jp/english/NEWS_EN/20090226/166366 (accessed 14-06-10)
- <http://www.building.co.uk/sustainability/3059164.article> (accessed 7-07-10)

- http://www.edilportale.com/news/2009/08/risparmio-energetico/fotovoltaico-in-italia-900-mw-installati-entro-il-2009_15984_27.html (accessed 16-06-10)
- http://www.edilportale.com/news/2010/04/risparmio-energetico/fotovoltaico-verso-l-integrazione-architettonica-totale_18340_27.html (accessed 16-06-10)
- http://www.edilportale.com/news/incentivi_fotovoltaico (accessed 16-06-10)
- http://www.eere.energy.gov/solar/pv_systems.html (accessed 14-06-10)
- <http://www.enerpoint.it/operatori/fotovoltaico-italia.php> (accessed 16-06-10)
- <http://www.ertex-solar.at>
- <http://www.ertex-solar.at/cms/startseiteeng> (accessed 14-06-10)
- <http://www.green-planet-solar-energy.com/CIS-tower.html> (accessed 16-06-10)
- http://www.madamaoliva.it/index.php/ita/news_events/impianto_fotovoltaico_integrato (accessed 16-06-10)
- http://www.pvdatabase.org/projects_view_details.php?ID=324 (accessed 7-07-10)
- <http://www.solarroadways.com> (accessed 15-06-10)
- http://www.youtube.com/watch?v=J3PeSm6_hTE (accessed 15-06-10)
- www.scribd.com/doc/7370648/Solar-stree-t-rack-module (accessed 16-06-10)

Chapter 11 (Sensing)

- Adey R.A., Lahrman A., Lessmoelman C., *Simulation and Design of Microsystems and Microstructures*, WIT Press, Southampton, 1995
- Aldraihem O.J., Akl W.N., Baz A.M., *Nanocomposite functional paint sensor for vibration and noise monitoring*, Sensors and Actuators A 149 (2009), pp. 233–240
- Beltrame M., *Sviluppo di una rete wireless di sensori per il monitoraggio di strutture in tempo reale*, Tesi di Laurea, Università degli Studi di Pavia, Facoltà di Ingegneria, Corso di Laurea specialistica in Ingegneria Informatica, A.A. 2007-2008
- Bhushan B., *Springer handbook of nanotechnology*, Springer, 2007, pp. 415-436
- Chen Lung-Tai, Lee Chia-Yen, Cheng Wood-Hi, *MEMS-based humidity sensor with integrated temperature compensation mechanism*, Sensors and Actuators A 147(2008), pp.522–528
- Consales M., Crescitelli A., Penza M., Aversa P., Delli Veneric P., Giordano M., Cusano A., *SWCNT nano-composite optical sensors for VOC and gas trace detection*, Sensors and Actuators B 138 (2009), pp.351–361

- Egusa S., Iwasawa N., *Piezoelectric paints as one approach to smart structural materials with health-monitoring capabilities*, Smart Materials and Structures 7 (1998), pp. 438–445
- Goel M., *Recent developments in electroceramics: MEMS applications for energy and environment*, Ceramics International 30 (2004), pp. 1147–1154
- Gong J., Chen Q., Fei W., Seal S., *Micromachined nanocrystalline SnO₂ chemical gas sensors for electronic nose*, Sensors and Actuators B 102 (2004), pp. 117–125
- Lynch J.P., Wang Y., Loh K.J., Yi J., Yun C-B, *Wireless Structural Monitoring of the Geumdang Bridge using Resolution Enhancing Signal Conditioning*, Proceedings of the 24th International Modal Analysis Conference (IMAC XXIV), St. Louis, MO, 30/01-2/02, 2006
- Middelhoek S., *Celebration of the tenth transducers conference: The past, present and future of transducer research and development*, Sensors and Actuators 82 (2000), pp. 2–23
- Norris Ashley, Saafi Mohamed, Romine Peter, *Temperature and moisture monitoring in concrete structures using embedded nanotechnology/microelectromechanical systems (MEMS) sensors*, Construction and Building Materials 22 (2008), pp. 111–120
- Riu J., Maroto A., Rius F.X., *Nanosensors in environmental analysis*, Talanta 69 (2006), pp. 88–301
- Stajano F., Hoult N., Wassell I., Bennett P., Middleton C., Soga K., *Smart bridges, smart tunnels: Transforming wireless sensor networks from research prototypes into robust engineering infrastructure*, Ad Hoc Networks 8 (2010), pp. 872–888
- Vermaas G., Betti R., Barton S.C., Duby P. West A.C., *Corrosion and embrittlement of high-strength bridge wires*, Proceedings of the Durability Workshop, Berkeley (CA), 26–27 October 2000-2001, pp. 85-96 doi:10.1016/B978-008043890-0/50009-2
- Wang L., Ma W., Xu L., Chen W., Zhu Y., Xu C., Kotov N.A., *Nanoparticle-based environmental sensors*, Materials Science and Engineering R, 2010 doi:10.1016/j.mser.2010.06.012
- Yamazoe N., Shimanoe K., *New perspectives of gas sensor technology*, Sensors and Actuators B 138 (2009), pp. 100–107
- Zhang Y., *Piezoelectric paint sensor for real-time structural health monitoring*, in: M. Tomizuka (Ed.), Sensors and Smart Structures Technologies for Civil, Mechanical and Aerospace Systems Conference, San Diego, CA, 7–10 March, 2005
- <http://ondamultimediale.blogosfere.it/2008/08/torcia-olimpica-e-iphone-sapete-che-coshanno-in-comune.html> (accessed 14-10-10)
- <http://www.cavachanger.fr/une-histoire-de-mems> (accessed 14-10-10)
- <http://www.scienceprog.com/what-are-mems> (accessed 14-10-10)

- <http://www.memx.com/products.htm> (accessed 14-10-10)

Chapter 12 (Preservation and archaeology practice)

- Ambrosi M., Dei L., Giorgi R., Neto C., Baglioni P., *Colloidal Particles of Ca(OH)₂: Properties and Applications to Restoration of Frescoes*, Langmuir 17 (2001), pp. 4251-4255
- Baglioni P., Carretti E., Dei L., Ferroni E., Giorgio R., *Elisirs di lunga vita per le opere d'arte*, Darwin, pp.26-33
- Baglioni P., Giorgi R., Dei L., *Soft condensed matter for the conservation of cultural heritage*, C. R. Chimie 12 (2009), pp.61-69
- Bernardi A., *Conservare opera d'arte, il microclima negli ambienti museali*, Ed. Il Prato
- Camuffo D., *Microclimate for Cultural Heritage*, Elsevier.
- Carretti E., Dei L., Baglioni P., *Solubilization of Acrylic and Vinyl Polymers in Nanocontainer Solutions. Application of Microemulsions and Micelles to Cultural Heritage Conservation*, Langmuir 19 (2003), pp.7867-7872
- Carretti E., Dei L., Weiss R.G., Baglioni P., *A new class of gels for the conservation of painted surfaces*, Journal of Cultural Heritage 9 (2008), pp.386-393
- Cass G. R., Druzik J. R., Grosjean D., Nazaroff W. W., Whitmore P. M., Wittman C. L., *Protection of works of art from atmospheric ozone*, Research in Conservation, The Getty Conservation Institute, USA, 1989
- Chelazzi D., Giorgi R., Dei L., Baglioni P., *Nanotecnologie per la conservazione del patrimonio culturale*, La Chimica e l'Industria 10 (2005), pp.78-82
- D'Arienzo L., Scarfato P., Incarnato L., *New polymeric nanocomposites for improving the protective and consolidating efficiency of tuff stone*, Journal of Cultural Heritage 9 (2008), pp. 253-260
- De Lisi R., Lazzara G., Milioto S., Muratore N., *Nanostructured systems functional to the recover and conservation of cultural heritage*, in Proceedings of the 1st International Conference "Nanotech for Architecture", Palermo 26-28 March 2009, p.251-263
- Dei L, Mauro M., Bitossi G., *Characterisation of salt efflorescences in cultural heritage conservation by thermal analysis*, Thermochemica Acta 317 (1998), pp.133-140
- Dei L., Salvadori B., *Nanotechnology in cultural heritage conservation: nanometric slaked lime saves architectonic and artistic surfaces from decay*, Journal of Cultural Heritage 7 (2006), pp.110-115
- Giorgi R., Chelazzi D., Fratini E., Langer S., Niklasson A., Rådemar M., Svensson J.E., Baglioni P., *Nanoparticles of calcium hydroxide for wood*

deacidification: Decreasing the emissions of organic acid vapors in church organ environments, Journal of Cultural Heritage 10 (2009), pp. 206–213

- Grassi S., Favaro M., Tomasin P., Dei L., *Nanocontainer aqueous systems for removing polymeric materials from marble surfaces: A new and promising tool in cultural heritage conservation*, Journal of Cultural Heritage 10 (2009), pp.347–355
- Liua B., Chen X., Fang D., Perrone A., Pispas S., Vainos N.A., *Environmental monitoring by thin film nanocomposite sensors for cultural heritage preservation*, Journal of Alloys and Compounds (in press 2010)
- Nanni A. Dei L., *Ca(OH)₂ Nanoparticles from W/O Microemulsions*, Langmuir 19 (2003), pp. 933-938
- Valentini F., Diamanti A., Palleschi G., *New bio-cleaning strategies on porous building materials affected by biodeterioration event*, Applied Surface Science 256 (2010), pp.6550–6563

SECTION 2

Chapter 1 (Notes on glass for architectural glazing)

- Schittich, S., Balkow, Schuler, Sobek, *Atlante del vetro*, UTET, 2000, Torino
- Scholze H., *Glass - Nature, Structure, and Properties*, Springer, 1991
- UNI EN 1096-1:2000 – Vetro per edilizia, vetri rivestiti, definizione e classificazione. (Glass in building, coated glass, definition and classification)
- UNI EN 1745:2005 - Marcatura e prodotti per muratura - Metodi per determinare i valori termici di progetto
- UNI EN 410:2000 – Vetro per edilizia, determinazione delle caratteristiche luminose e solari delle vetrate. (Glass in building, determination of luminous and solar characteristics of glazing)
- UNI EN 572-1:1996 – Vetro per edilizia. Prodotti a base di vetro di silicato sodio-calcico. Definizione e proprietà generali fisiche e meccaniche. (Glass in building. Basic soda lime silicate glass products. Definitions and general physical and mechanical properties)
- UNI EN 572-2:1996 - Vetro per edilizia. Prodotti a base di vetro di silicato sodio-calcico. Vetro float (Glass in building. Basic soda lime silicate glass products. Float glass)
- UNI EN 7345:1999 – Isolamento termico – Grandezze fisiche e definizioni (Thermal insulation, physical quantities and definitions)
- UNI EN ISO 6946:1999 - Componenti ed elementi per edilizia - Resistenza termica e trasmittanza termica - Metodo di calcolo
- Various authors, *Il nuovissimo manuale dell'architetto*, 2006, Roma
- Various authors, *Manuale dell'ingegnere*, Hoepli, 2007, Milano

- <http://www.efficientwindows.org/lowe.cfm>
- http://www.energymanager.net/index.php?option=com_content&task=view&id=79&Itemid=95

Chapter 2 (Thermochromic coatings)

- Binions R., Blackman C.S., Manning T.D., Parkin I.P., Piccirillo C., *Thermochromic coatings for intelligent architectural glazing*, Journal of Nano Research, Vol II (2008), pp. 1-20
- Binions R., Palgrave R.G., Parkin I.P., Piccirillo C., *Hybrid aerosol assisted and atmospheric pressure CVD of gold-doped vanadium dioxide*, Chemical Vapor Deposition 14 (2008)
- Manning T. D., *Atmospheric pressure chemical vapour deposition of vanadium oxides*. Thesis (PhD). University of London, 2004
- Manning T.D., Parkin I.P., Pemble M.E., Sheel D., Vernardou D., *Intelligent window coatings: atmospheric pressure chemical vapor deposition of tungsten-doped vanadium dioxide*, Chem. Mater., 16 (2004)
- McMillan, P.F. Journal of Materials Chemistry, 14 (2004), pp. 1506-1512
- Palgrave R., *Chemical Vapor Deposition of Nanoparticulate and Nanocomposite thin film* (Thesis of Ph.D. in Chemistry), UCL, London, 2007
- Saeli M., *New thermochromic coatings for architectural glazing*, Thesis of M.Sci.: "Nanotechnology for Cultural Heritage", Università degli Studi di Palermo, 2008
- Vernardou D., *The growth of thermochromic vanadium dioxide films by chemical vapour deposition*. Thesis (PhD). University of Salford, 2005
- White M.A., LeBlanc M., *Thermochromism in Commercial Products*, Journal of Chemical Education 76-9 (1999)
- <http://www.azom.com/details.asp?ArticleID=2587>
- <http://www.thermochromic-polymers.com/>
- Jin P., *Demonstration of thermochromic coating*, <http://www.aist.go.jp/NIRIN/People/pjin/GIF/tc.gif>, 2000

Chapter 3 (Theory on thin films and chemical vapour deposition (CVD))

- Bruno T.J, Svoronos D.N., *CRC - Handbook of fundamental spectroscopic correlations chart*, CRC Press, 2005
- Choy K.L., *Chemical vapor deposition of coatings*, Progress in Materials Science 48 (2003)
- Dobkin M.D., Zuraw M., *Principles of Chemical Vapor Deposition – What's going on inside the reactor*, Kluwer Academic Publisher, The Netherlands, 2003
- Palgrave R., *Chemical Vapor Deposition of Nanoparticulate and Nanocomposite thin film* (Thesis of Ph.D. in Chemistry), UCL, London, 2007

Chapter 4 (Analysis technique)

- Palgrave R., *Chemical Vapor Deposition of Nanoparticulate and Nanocomposite thin film* (Thesis of Ph.D. in Chemistry), UCL, London, 2007
- <http://www.cie.co.at>

Chapter 7 (Energy modelling performance)

- Diamantouros P., *The energy performance of the thermochromic glazing* (Thesis of M.Sci. Built Environment: Environmental Design and Engineering), UCL - The Barlett School of Graduate Studies, London, 2006
- Fondazione Ammiraglio Michelagnoli Onlus, *Il Clima*, 2004
- KlimaHaus, *Conduttività termica di materiali da costruzione*, Provincia autonoma di Bolzano–Alto Adige, Agenzia per l'ambiente, Ufficio Aria e Rumore
- Energy Plus users' manual (Vers. 2.2 – April 2008)
- <http://digilander.libero.it/digitalrino/serbatoio%20termico%20-%20Marcello%20Vespa.htm>
- http://servizi.lifegate.it/newimpattozero/ecoconsigli/come/edif/ed_1_05.htm
- <http://www.architetturaesostenibilita.it/Laterizi.htm>
- <http://www.cedisgroup.it/public/doc/32410052004145702.pdf>
- http://www.ediliziainrete.it/norme_sostenibilita.asp
- <http://www.efficientwindows.org/lowe.cfm>
- http://www.enviport.com/index_it.html
- http://www.ilfarodellamente.it/FRMNT_A/FISICA/II%20calore%20specifico.htm
- <http://www.pilkington.com>
- http://www.saecollege.de/reference_material/pages/Coefficient%20Chart.htm
- http://www.sequoien.com/view_news_and_articles/waterhogs_improve_the_rmal_mass_performance
- [http://www.solarenergynews.net/BioClimaticDesign/Mass/Thermal.ppt#256,1,Thermal Mass](http://www.solarenergynews.net/BioClimaticDesign/Mass/Thermal.ppt#256,1,Thermal%20Mass)
- <http://www.solarmirror.com/fom/fom-serve/cache/43.html>
- <http://wwwusers.ts.infn.it/~milotti/Didattica/LabTermodinamica/Calore%20specifico.pdf>
- www.casaclima.info

SECTION 3

Chapter 1 (Carbon Nanotubes)

- Bhushan B., *Springer handbook of nanotechnology*, Springer, 2007, pp. 364-366
- Chen X., Cao G. *Atomistic studies of mechanical properties of carbon nanotubes*. Journal of computational and theoretical nanoscience, Vol. 4, 2007. pp. 1-17
- Baker R.T.K., Harris P.S., *Chemistry and physics of carbon*, Marcel Dekker, New York, 1978.
- Chen X., Huang Y. *Nanomechanics modelling and simulation of carbon nanotubes*. Journal of engineering mechanics. March 2008, pp. 211-216
- Iijima S., *Helical microtubules of graphitic carbon*, Nature 354 (1991), pp. 56–58

Chapter 2 (Polyurea: the material)

- Amirkhizi A.V., Isaacs J., McGee J., Nemat-Nasser S., *An experimentally-based viscoelastic constitutive model for polyurea, including temperature and pressure effects*. Philosophical Magazine, Vol. 86, No 36 (2006), pp. 5847-5866
- Amirkhizi A.V., Isaacs J., Nemat-Nasser S., *Experimentally-based viscoelastic model for Polyurea, including pressure and temperature effects*. Proceedings of the 2006 SEM annual conference and exposition on experimental and applied mechanics, St. Louis (MO), June 4-7, 2006
- CSI Construction Solution Inc.: Polyurea, 2006
- Futuracoating Inc. St. Louis, MO, USA, *Miti e verità della poliurea*.
- Li C., Lua J., *A hyper-viscoelastic constitutive model for polyurea*. Materials letters, 63 (2009), pp. 877-880
- Nemat-Nasser S., Amirkhizi A.V., *Finite-amplitude shear wave in pre-stressed thin elastomer*, Wave Motion 43 (2005), pp. 20-28
- Roland C.M., Casalini R., *Effect of hydrostatic pressure on the viscoelastic response of polyurea*, Polymer 48 (2007), pp. 5747-5752
- Roland C.M., Twigg J.M., Vu Y., Mott P.H., *High strain rate behaviour of polyurea*. Polymer 48 (2007), pp. 574-578
- Shim J., Mohr D., *Using split Hopkinson pressure bars to perform large strain compression tests on polyurea at low, intermediate and high strain rates*. International Journal of Impact Engineering, 36(2009), pp.1116-1127
- Sarva S.S., Hsieh A.J., *The effect of microstructure on the rate-dependent stress-strain behaviour of poly(urethane urea) elastomers*. Polymer 50 (2009), pp. 3007-3015

- Tekalur S.A., Shukla A., Shivakumar K., *Blast resistance of polyurea based layered composite materials*, Composite Structures 84 (2008), pp. 271-281
- Yi J., Boyce M.C., Lee G.F., Balizer E., *Large deformation rate-dependent stress-strain behaviour of polyurea and polyurethanes*, Polymer 47 (2006), pp. 319-329
- Zhu Y., Liechti K.M., Ravi-Chandar K., *Direct extraction of rate-dependent traction-separation laws for polyurea/steel interfaces*. International Journal of Solids and Structures, 46 (2009), pp. 31-51

Chapter 3 (CNT-doped polymers: state of art)

- Gao C. et al. *Polyurea functionalized multiwalled carbon nanotubes: synthesis, morphology and Raman spectroscopy*, J. Phys. Chem. B. 109 (2005), pp. 11925-11932
- Barber A.H., Cohen S.R., Wagner H.D., *Measurement of carbon nanotube-polymer interfacial strength*, Appl. Phys. Lett. 82 (2003), pp. 4140-4142
- Kaushiva B.D., Wilkes G.L., *Uniaxial orientation behaviour and consideration of the geometric anisotropy of polyurea hard domain structure in flexible polyurethane foam*. Polymer, 41 (2000), pp. 6987-6991
- Lillehei P.T., *Characterization of Carbon Nanotube polymer composites*, NASA tech report, 2004.
- Peng H., *Aligned carbon nanotube/polymer composite films with robust flexibility, high transparency, and excellent conductivity*. J. Am. Chem. Soc. 130 (2008), pp. 42-43
- Pötsche P., Fornes T.D., Paul D.R., *Rheological behaviour of MWCNT-polycarbonate composites*, Polymer 43 (2002), pp. 3247-3255
- Ren Y., Li F., Cheng H.M., Liao K., *Tension-tension fatigue behavior of unidirectional single-walled carbon nanotube reinforced epoxy composite*, Carbon 41 (2003), pp. 2159-2179
- Wu H. et al.. *Morphology, electrical resistance, electromagnetic interference shielding and mechanical properties of functionalized MWNT and Poly (urea urethane) nanocomposites..* (publishing on-line on Wiley Inter-Science, 2006). Journal of Polymer Science, part B, polymer physics

Chapter 4 (Materials and specimen production)

- Shim H.C. et al.. *Enhancement of adhesion between carbon nanotubes and polymer substrates using microwave irradiation*. Scripta Materialia, 61(2009), pp. 32-35
- Valentino O., *The effect of surface treatment and matrix properties on CNT/polymer composites*. PhD thesis, Università degli Studi di Salerno, 2007

Chapter 5 (Tension tests)

- ASTM D 412 – 06a “Standard test methods for vulcanized rubber and thermoplastic elastomers – Tension”

Chapter 6 (Deterioration and accelerated aging)

- ASTM D 1349 – 09 “Rubber – Standard temperatures for testing”
- ASTM D 573 – 04 “Rubber – Deterioration in an air oven”
- Boubakri A., Elleuch K., Guermazi N., Ayedi H.F., *Investigations on hygrothermal aging of thermoplastic polyurethane material*. Materials and Design, 30 (2009), pp. 3958-3965
- Bystritskaya E.V., Pomerantsev A.K., Rodionova O. Ye., *Prediction of the aging of polymer materials*. Chemometrics and Intelligent Laboratory Systems, 47 (1999), pp. 175-178
- Davies P., Evrard G., *Accelerated ageing of polyurethanes for marine applications*. Polymer degradation and stability, 92 (2007), pp. 1455-1464
- Gorokhov V.I., Fedotova O. Ya., Korshak V.V., *Investigation of the thermooxidative degradation of aromatic polycarbamides*. A16: No. 2 (1974), pp. 359-364
- Jianwen Hu, Xiaogang Li, Jin Gao, Quanlin Zhao, Ageing behaviour of acrylic polyurethane varnishing coating in artificial weathering environments. Progress in organic Coatings, 65 (2009), pp. 504-509
- Kovačević V., Hace D., Bravar M., Stanojević D., Mudri I., *Correlation between mechanical and chemical properties of polyurethane compounds under ageing conditions*. Polymer Degradation and Stability, 24 (1989), pp. 349-360
- Lévêque D., Schieffer A., Mavel A., Maire J.F., *Analysis of how thermal aging affects the long-term mechanical behaviour and strength of polymer-matrix composites*. Composites Science and Technology, 65 (2005), pp. 395-401
- Medical device Ink., Accelerated aging in www.decicelink.com (accessed 30/09/09)
- Ostrogorsky A.G., Glicksman L.R., Reitz D.W., *Aging of polyurethane foams*. Int. J. Heat Mass Transfer, Vol. 29, No.8 (1986), pp. 1169-1176
- SGS, *Accelerated aging reference chart* in <http://www.sgs.com> (accessed 30/09/09)

LIST OF PUBLICATIONS

About the topic “Nanotechnology in Construction”

- Saeli Manfredi, *Nanotechnologies in construction: new materials and high performance buildings*, L'attività di ricerca nel dottorato (atti CODAT Roma 2011 - VI Congresso internazionale Ar.Tec. – Università degli Studi di Roma “La Sapienza”, Roma (Italy), 18 February 2011 (submitted Jan, 2011)
- Saeli Manfredi, *Nanotechnologies for Architecture*, Poster OSDOTTA 2010 VI Seminario Estivo Rete Nazionale dei Dottorati in Tecnologia dell'Architettura, Palermo 15/17 September 2010
- Saeli Manfredi, *Nanotechnologies for Architecture*, OSDOTTA 2010 VI Seminario Estivo Rete Nazionale dei Dottorati in Tecnologia dell'Architettura, Palermo 15/17 September 2010 (submitted)

About UCL research

- Saeli Manfredi, Piccirillo Clara, Parkin Ivan P., Binions Russell, Ridley Ian, *Optimization of thermochromic thin films on glass; design of intelligent windows*, Advances in Science and Technology Vol. 75 (2010) pp 79-90, doi:10.4028/www.scientific.net/AST.75.79
- Saeli Manfredi, Piccirillo Clara, Parkin Ivan P., Binions Russell, Ridley Ian. Energy modelling studies of thermochromic glazing. Energy and Buildings Volume 42, Issue 10, October 2010, doi: 10.1061/j.enbuild.2010.04.010
- Saeli Manfredi, Piccirillo Clara, Parkin Ivan P., Ridley Ian, Binions Russell. Nano-composite thermochromic thin films and their application in Energy-efficient glazing. Solar Energy Materials & Solar Cells 94 (2010), pp. 141-151 doi: 10.1016/j.solmat.2009.08.010
- Saeli Manfredi. *Nuovi vetri termocromici: analisi dei consumi elettrici nel modello di un edificio (New thermochromic glazing: Energy consumption analysis in a building model)*. L'attività di ricerca nel dottorato (atti CODAT Messina 2009 - V Congresso internazionale Ar.Tec. - Università degli Studi di Messina (Italy), 18 November 2009. pp. 163-166 ISBN: 978-88-6055-459-8
- Binions Russell, Saeli Manfredi, Piccirillo Clara, Parkin Ivan P.. Hybrid aerosol assisted atmospheric pressure Chemical Vapour Deposition: a facile route toward nano-composite thin films? In ECS Transactions 25(8) 2009 pp. 773-780. Proceedings of Euro CVD 17 and CVD 17 (216th meeting of the Electrochemical Society), Vienna (Austria), 4-9 October 2009
- Saeli Manfredi, Binions Russell, Piccirillo Clara, Hyett G., Parkin Ivan P.. *Templated Growth of Smart Nanocomposite Thin Films: Hybrid Aerosol Assisted and Atmospheric Pressure Chemical Vapour Deposition of Vanadyl Acetylacetonate, Auric Acid and Tetraoctyl Ammonium Bromide*. Polyhedron, Volume 28, Issue 11 (July 2009), pp. 2233-2239. Available on-line 31 March 2009 - DOI: 10.1016/j.poly.2009.03.025. ISSN: 0277-5387

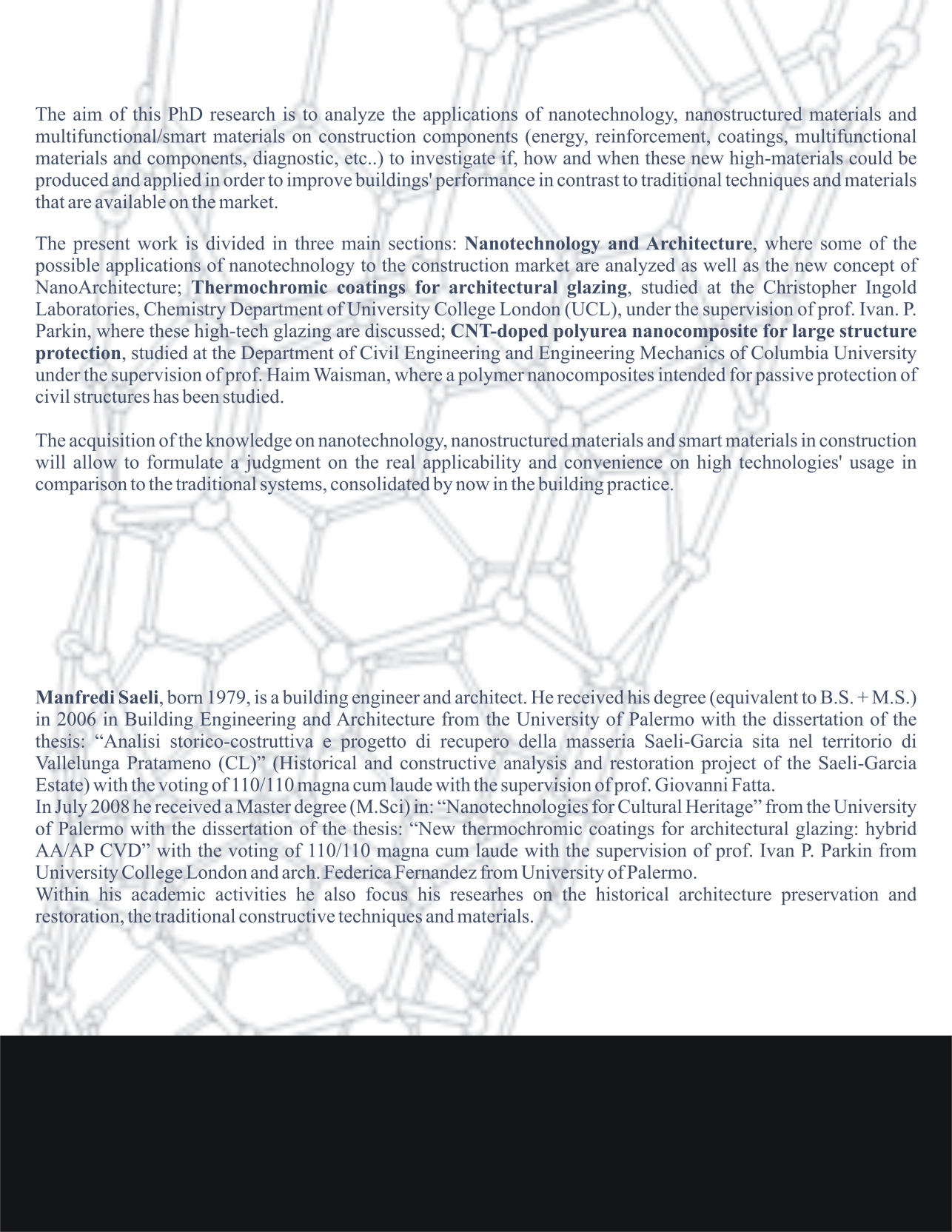
- Binions Russell, Saeli Manfredi, Piccirillo Clara, Parkin Ivan P.. *Hybrid Chemical Vapour Deposition: Gold and Vanadium Dioxide Nano-composites for Smart Windows*. Proceedings of the 2nd International Networking Meeting for Young Scientists. National University of Taiwan, Taipei, Taiwan ROC, 2009 (Abstract).
- Binions Russell, Parkin Ivan P., Saeli Manfredi, Piccirillo Clara. *Vanadium dioxide and gold nanocomposite films for glazing applications*. In Proceedings of the 1st International Conference “Nanotech for Architecture”. Palermo, 26-28 March 2009. pp. 163-174. ISBN: 88-6026-096-5.
- Parkin Ivan P., Binions Russell, Saeli Manfredi, Piccirillo Clara. *Functional thin films for glazing application*. In Proceedings of the 1st International Conference “Nanotech for Architecture”. Palermo, 26-28 March 2009. pp. 129-140. ISBN: 88-6026-096-5.
- Saeli Manfredi, Parkin Ivan P., Binions Russell, Piccirillo Clara, Ridley Ian. *Energy modelling studies of enhanced glazing*. Poster at the 1st International Conference “Nanotech for Architecture”. Palermo, 26-28 March 2009.
- Saeli Manfredi, Parkin Ivan P., Binions Russell, Piccirillo Clara, Ridley Ian. *Energy modelling studies of enhanced glazing*. In Proceedings of the 1st International Conference “Nanotech for Architecture”. Palermo 26-28 March 2009. pp. 199-212. ISBN: 88-6026-096-5.
- Saeli Manfredi, Binions Russell, Piccirillo Clara, Parkin Ivan P.. *Templated Growth of Smart Coatings: Hybrid Chemical Vapour Deposition of Vanadyl Acetylacetonate with Tetraoctyl Ammonium Bromide*. Applied Surface Science, Volume 255, No. 16 (2009), pp. 7291-7295. ISSN: 0169-4332
- Saeli Manfredi, *Nuovi rivestimenti termocromici a scala nanometrica per vetrate architettoniche depositati tramite la tecnica AA/AP CVD (New nanometric thermochromic coatings for architectural glazing carried out by the hybrid A-A/AP CVD)* – Research in PhD, topics methods perspectives - IV Congresso internazionale Ar.Tec. - Università degli Studi di Pavia – Via Ferrata, 1 – 27100 Pavia (Italy), 17 September 2008, pgg. 117-121. ISBN: 978-88-86719-65-0.

About Columbia research

- Saeli Manfredi, Waisman Haim, Betti Raimondo. *Nanocomposite, an innovative route to large structure and infrastructure protection. A case of study: CNT-doped polyurea*. Proceedings of 34th IABSE Symposium 2010 “Large structures and infrastructures for environmentally constrained and urbanised areas. Venezia (Italy), 22/24 September 2010
- Saeli Manfredi, Waisman Haim, Betti Raimondo. *Nanocomposite, an innovative route to large structure and infrastructure protection. A case of study: CNT-doped polyurea*. Poster at 34th IABSE Symposium 2010 “Large structures and infrastructures for environmentally constrained and urbanised areas. Venezia (Italy), 22/24 September 2010

Other publications

- Saeli Manfredi, Saeli Enrico. *La masseria Saeli-Garcia: da casale saraceno ad impresa agricola*. Kalòs, arte in Sicilia (submitted Dec, 2010)
- Saeli Manfredi, *Bagli e masserie della Sicilia centro-occidentale, casi di studio a confronto*, OSDOTTA 2010 VI Seminario Estivo Rete Nazionale dei Dottorati in Tecnologia dell'Architettura, Palermo 15/17 September 2010 (submitted Sept, 2010)
- Saeli Manfredi. *Interventi di lotta contro le termiti nella cinquecentesca villa Naselli di Gela Amblers a Palermo*. Proceedings of the XXV Convegno Internazionale Scienza e Beni Culturali: conservare e restaurare il legno. Bressanone, 23-26 Giugno 2009. Edizioni Arcadia Ricerche. pp 909-918. ISBN: 978-88-95409-13-9



The aim of this PhD research is to analyze the applications of nanotechnology, nanostructured materials and multifunctional/smart materials on construction components (energy, reinforcement, coatings, multifunctional materials and components, diagnostic, etc..) to investigate if, how and when these new high-materials could be produced and applied in order to improve buildings' performance in contrast to traditional techniques and materials that are available on the market.

The present work is divided in three main sections: **Nanotechnology and Architecture**, where some of the possible applications of nanotechnology to the construction market are analyzed as well as the new concept of NanoArchitecture; **Thermochromic coatings for architectural glazing**, studied at the Christopher Ingold Laboratories, Chemistry Department of University College London (UCL), under the supervision of prof. Ivan. P. Parkin, where these high-tech glazing are discussed; **CNT-doped polyurea nanocomposite for large structure protection**, studied at the Department of Civil Engineering and Engineering Mechanics of Columbia University under the supervision of prof. Haim Waisman, where a polymer nanocomposites intended for passive protection of civil structures has been studied.

The acquisition of the knowledge on nanotechnology, nanostructured materials and smart materials in construction will allow to formulate a judgment on the real applicability and convenience on high technologies' usage in comparison to the traditional systems, consolidated by now in the building practice.

Manfredi Saeli, born 1979, is a building engineer and architect. He received his degree (equivalent to B.S. + M.S.) in 2006 in Building Engineering and Architecture from the University of Palermo with the dissertation of the thesis: “Analisi storico-costruttiva e progetto di recupero della masseria Saeli-Garcia sita nel territorio di Vallelunga Pratameno (CL)” (Historical and constructive analysis and restoration project of the Saeli-Garcia Estate) with the voting of 110/110 magna cum laude with the supervision of prof. Giovanni Fatta.

In July 2008 he received a Master degree (M.Sci) in: “Nanotechnologies for Cultural Heritage” from the University of Palermo with the dissertation of the thesis: “New thermochromic coatings for architectural glazing: hybrid AA/AP CVD” with the voting of 110/110 magna cum laude with the supervision of prof. Ivan P. Parkin from University College London and arch. Federica Fernandez from University of Palermo.

Within his academic activities he also focus his researches on the historical architecture preservation and restoration, the traditional constructive techniques and materials.